AD-A181 731

Balancing of Rigid and Flexible Rotors

Alphabetical List of Units and Their SI
Conversion Factors

To Convert	Into	Multiply By
atmospheres	pascals (Pa)	1.0133 E+05
atmospheres	pounds per square inch (lb/in.^{2})	1.4696 E+01
centimeters (cm)	inches (in.)	3.9370 E−01
feet (ft)	meters (m)	3.0480 E−01
feet (ft)	millimeters (mm)	3.0480 E+02
grams (g)	ounces (oz)	3.5274 E−02
grams (g)	pound seconds squared per inch (lb · s^2/in.)	5.7100 E−06
gram inches (g · in.)	ounce inches (oz · in.)	3.5274 E−02
gram millimeters (g · mm)	ounce inches (oz · in.)	1.3887 E−03
gram square millimeters (g · mm^2)	pound inch seconds squared (lb · in. · s^2)	8.8511 E−09
grams per cubic centimeter (g/cm^3)	pounds per cubic inch (lb/in.^{3})	3.6127 E−02
horsepower	kilowatts (kW)	7.4570 E−01
inches (in.)	centimeters (cm)	2.5400 E+00
inches (in.)	meters (m)	2.5400 E−02
inches (in.)	millimeters (mm)	2.5400 E+01
kilograms (kg)	pounds (lb)	2.2046 E+00
kilograms (kg)	newtons (N)	9.8067 E+00
kilograms (kg)	pound seconds squared per inch (lb · s^2/in.)	5.7100 E−03
kilogram square centimeters (kg · cm^2)	pound inch seconds squared (lb · in. · s^2)	8.8511 E−04
kilograms per cubic meter (kg/m^3)	pounds per cubic inch (lb/in.^{3})	3.6127 E−05
kilowatts (kW)	horsepower	1.3410 E+00
meters (m)	feet (ft)	3.2808 E+00
meters (m)	inches (in.)	3.9370 E+01
microinches (µin.)	millimeters (mm)	2.5400 E−05
microinches (µin.)	microns (µm)	2.5400 E−02
microns (µm)	microinches (µin.)	3.9370 E+01
millimeters (mm)	feet (ft)	3.2808 E−03
millimeters (mm)	inches (in.)	3.9370 E+02
millimeters (mm)	microinches (µin.)	3.9370 E+04

Alphabetical List of Units and Their SI
Conversion Factors (Continued)

To Convert	Into	Multiply By
newtons (N)	kilograms (kg)	1.0197 E+01
newtons (N)	pounds (lb)	2.2480 E−01
newton seconds per meter (N · s/m)	pound seconds per inch (lb · s/in.)	5.7100 E−03
newtons per meter	pounds per inch (lb/in.)	5.7100 E−03
ounces (oz)	grams (g)	2.8350 E+01
ounce inches (oz · in.)	gram inches (g · in.)	2.8350 E+01
ounce inches (oz · in.)	gram millimeters (g · mm)	7.2010 E+02
pascals (Pa)	atmospheres	9.8692 E−06
pascals (Pa)	pounds per square inch (lb/in.^{2})	1.4504 E−04
pascal seconds (Pa · s)	pound seconds per square inch (lb · s/in.^{2})	1.4504 E−04
pounds (lb)	kilograms (kg)	4.5360 E−01
pound inch seconds squared (lb · in. · s^2)	gram square millimeters (g · mm^2)	1.1298 E+08
pound inch seconds squared (lb · in. · s^2)	kilogram square centimeters (kg · cm^2)	1.1298 E+03
pound seconds per inch (lb · s/in.)	newton seconds per meter (N · s/m)	1.7513 E+02
pound seconds per square inch (lb · s/in.^{2})	pascal seconds (Pa · s)	6.8948 E+03
pound seconds squared per inch (lb · s^2/in.)	grams (g)	1.7513 E+05
pound seconds squared per inch (lb · s^2/in.)	kilograms (kg)	1.7513 E+02
pounds per inch (lb/in.)	newtons per meter (N/m)	1.7513 E+02
pounds per square inch (lb/in.^{2})	atmosheres	6.8046 E−02
pounds per square inch (lb/in.^{2})	pascals (Pa)	6.8948 E+03
pounds per cubic inch (lb/in.^{3})	grams per cubic centimeter (g/cm^3)	2.7680 E+01
pounds per cubic inch (lb/in.^{3})	kilograms per cubic meter (kg/m^3)	2.7680 E+04

SVM-12

Balancing of Rigid
and
Flexible Rotors

DTIC
ELECTE
JUN 1 8 1987

S

D

A

THE SHOCK AND VIBRATION MONOGRAPH SERIES

SVM-1 Random Noise and Vibration in Space Vehicles —
       Lyon

SVM-2 Theory and Practice of Cushion Design — *Mustin*

SVM-3 Programming and Analysis for Digital Time Series
       Data — *Enochson and Otnes*

SVM-4 Dynamics of Rotating Shafts — *Loewy and Piarulli*

SVM-5 Principles and Techniques of Shock Data Analysis —
       Kelly and Richman

SVM-6 Optimum Shock and Vibration Isolation — *Sevin and
       Pilkey*

SVM-7 Influence of Damping in Vibration Isolation —
       Ruzicka and Derby

SVM-8 Selection and Performance of Vibration Tests —
       Curtis, Tinling, and Abstein

SVM-9 Equivalence Techniques for Vibration Testing —
       Fackler

SVM-10 Shock and Vibration Computer Programs: Reviews
       and Summaries — *Pilkey and Pilkey*

SVM-11 Calibration of Shock and Vibration Measuring
       Transducers — *Bouche*

SVM-12 Balancing of Rigid and Flexible Rotors — *Rieger*

Balancing of Rigid
and
Flexible Rotors

Neville F. Rieger

Stress Technology, Inc.

1986

THE SHOCK AND VIBRATION INFORMATION CENTER

Naval Research Laboratory
Washington, DC

J. Gordan Showalter, *Acting Director*

Rudolph H. Volin

Elizabeth A. McLaughlin

Mary K. Gobbett

PREFACE

This monograph has been written to meet the need for a comprehensive treatise on the balancing of rotating equipment. The subject of rotor balancing is a broad topic which involves many skills and disciplines. It has recently evolved from what was previously a mechanical engineering operation into an electromechanical technology. This has resulted from the intensive application of the minicomputer to coordinate the required balancing operations. Indeed, the entire subject of rotor balancing has recently experienced an era of growth and development in which technological changes have occurred in many fundamental areas. These changes have resulted from balancing requirements associated with the rapid development of advanced high-speed rotating machinery during the two previous decades. The continued demand for greater power output per unit weight in rotating equipment has led to the acceptance of more flexible rotor balancing techniques. These techniques and the associated equipment are now being used to balance advanced, flexible rotor equipment, and they are also replacing the older, established rigid rotor balancing procedures.

In use, this book is directed toward the professional engineer with no significant prior experiences in rotor balancing. It is hoped that such engineers may obtain from it an introduction to the principles of balancing, certain basic balancing procedures, and some acquaintance with the hardware involved in rotor balancing. Sufficient advanced material has been included so that further in-depth study may be conveniently pursued on specific state-of-the-art topics using the literature sources specified at the end of each chapter.

The author will appreciate advice and comments from readers concerning other important topics and related material that might be included in future editions of this monograph. Advice on publications of importance that have been inadvertently overlooked is also welcome. Careful efforts have been made during preparation to eliminate textual errors, but advice will be appreciated to any error that may remain, for which the author accepts all responsibility.

Gratitude is expressed both to Henry C. Pusey, former Director of the Shock and Vibration Information Center at NRL and Dr. J. Gordan Showalter, the acting director for their supportive recognition of the importance of this subject, and for much encouragement and friendly advice given during the preparation of the manuscript. Special gratitude is also expressed to Sara Curry for her patient care, editing, and guidance in the preparation of the manuscript, and to Dr. Ronald L. Eshelman of the Vibration Institute and to Shixiang Zhou, Visiting Scholar, Hupei Province, Peoples Republic of China, for their helpful review of the material herein. A special note of thanks goes to the Computerized Technical Composition Section of NRL's Technical Information Division, especially Mrs. Deborah Blodgett and Mrs. Dora Wilbanks. Without their patience and help this book would never have been put in the excellent shape that it is now in.

Rochester, New York Neville F. Rieger

v

FOREWORD

Rotor unbalance is a basic concern in the design and operation of machinery because it is a major cause of excessive vibration.

The classical balancing procedures available today are deceptively simple: balancing can be difficult due to the number of interacting phenomena present. The entire area of rotor dynamics plays a role in many balancing problems. Critical speeds are influenced by rotor and bearing flexibilities; the weight, flexibility, and position of couplings as well as casing and foundation properties are often integral parts of balancing techniques and strategies. Because critical speeds involve phase changes—between mass unbalance forces and vibration—they always affect the sensitivity of the balancing process. Balancing techniques for high-speed equipment are thus intimately involved with rotor dynamics. And because mass unbalance is sensitive to thermal changes, which cause changes in rotor shape, balancing procedures must also account for thermal effects. The fact that such phenomena as misalignment cause once-per-revolution frequency vibration—as does mass unbalance—is one reason for the misapplication of balancing procedures. It is obvious that many factors are involved in applying balancing procedures to rotors.

Balancing techniques and rotor dynamics have evolved with the development of machinery, particularly as operating speeds have increased. The development of balancing technology began in the industrial revolution of the 19th century; the first balancing machine was developed and patented by Martenson in 1870. At that time and in the early 20th century balancing accuracy was severly limited by the lack of vibration transducers and analyzers. A chalk mark of the high spot of the rotor was used to identify the heavy spot (location of mass unbalance). Balancing procedures were not formalized until the 20th century when Thearle in 1934 developed a two-plane influence coefficient method. From that time to the present balancing procedures have closely followed developments in various areas: the theory of rotor dynamics, transducers and analyzers for measuring vibration, and computers. All of these ingredients were essential to the evolution of the sophisticated flexible-rotor balancing techniques available today.

One early flexible-rotor balancing technique, traceable to Lynn in 1928, was based on mode shapes (modal method). In England the theory of the modal method was developed by Bishop, Gladwell, and Parkinson in the 1960s; Moore demonstrated the practical application of the method to heavy rotating equipment. At the same time in Europe

vii

Federn developed a comprehensive modal balancing method that encompassed a wide range of rotors. The simultaneous development of these modal methods was not without controversy—specifically, with whether the so-called rigid body modes should or should not be eliminated in the balancing process. Even greater was the controversy between modal and influence coefficient methods which began with Goodman's formulation in 1962 of the influence coefficient method of Thearle for flexible rotors.

The exact-point speed method, which was developed for multiple planes and speeds, evolved into the least squares method; major contributions were made by Lund. This method depends heavily on computers, good measurements, and rigid procedures whereas the modal approach involved physical insight.

The merits of the modal and influence coefficient methods were discussed with eloquence and emotion at major vibration meetings for a decade. Finally in the late 1970s, the opposing factions, represented by Parkinson of the U.K., an advocate of the modal method, and Smalley of the U.S., an advocate of the influence coefficient method, worked together to develop the unified method of flexible rotor balancing. This method includes aspects of both the modal and influence coefficient methods. About the same time Dreschler of West Germany evolved a similar general method.

Even though a huge body of literature exists in rotor dynamics and balancing, few books have been written—and until now, no comprehensive book has been published. Dr. Rieger has written the first classical, complete work on balancing with a strong emphasis on rotor dynamics. And because rotor dynamics provides much of the theoretical basis for balancing, it is fitting that a major portion of the text be devoted to it. This exhaustive coverage of the field is reminiscent of Ker Wilson's books on torsional vibration.

Dr. Rieger's book is well organized and contains many illustrations, worked examples, and documented experiments. The historical coverage of the field is accurate and comprehensive. It shows how and why the rapid development of this field occurred.

Dr. Rieger is to be congratulated for completing this well-written work. It will provide guidance for many engineers who want to learn balancing techniques together with a necessary understanding of rotor dynamics.

Ronald L. Eshleman
Vibration Institute
Clarendon Hills, Illinois
April 1984

CONTENTS

CONTENTS (Cont.)

CONTENTS (Cont.)

CONTENTS (Cont.)

CHAPTER 1
FUNDAMENTAL CONCEPTS

1.1 Introduction

Rotor balancing is now accepted as a fundamental requirement for the smooth operation of rotating machinery. Its objective is the effective elimination of the centrifugal force components that arise from the eccentric rotation of the rotor center of gravity (c.g.) about its axis of rotation. If such an eccentric condition exists, the rotor is said to be unbalanced. An unbalanced rotor experiences an overall centrifugal force that causes it to deflect in a radial direction. This centrifugal force is transmitted to the bearings and to the structure of the machine as a harmonically varying force. Such forces may cause problems ranging from an irritating noise level or foundation vibration to the failure of a bearing or other structural components by fatigue. Unbalance is therefore recognized as an important potential cause of machinery failure.

A number of practical causes of rotor unbalance are listed in Table 1.1. Each cause has the same net effect: to displace the rotor c.g. off the axis of rotation. Even with careful machining, single-component rotors will experience some residual unbalance from dimensional inaccuracy and material inhomogeneity. Rotors constructed from many separate components (e.g., jet-engine rotors, multistage pump rotors) are susceptible to greater inherent unbalance because of construction difficulties in achieving a concentric and uniform distribution of mass along the rotor axis. Most high-speed rotors are therefore manufactured to production tolerances and are then trim balanced, by some suitable procedure, to compensate for any remaining eccentric mass distribution.

The balancing of rotors is clearly an important aspect of modern machine construction of the and maintenance process. Without balancing, very few rotating assemblies could function smoothly. This is especially true of high-precision machinery, such as Brayton-cycle space power systems, aircraft jet engines, large turbine-generator sets, and pump assemblies for nuclear reactor service.

The importance of balancing is now recognized in the codes of various qualifying agencies, such as the Nuclear Regulatory Commission and the Department of Defense. Its importance in advanced rotating machinery has been widely recognized by agencies such as the National Aeronautics and Space Administration and many branches of the Department of Defense in their continuing support of balancing-technology programs over the past decade.

1

Table 1.1. Possible causes and signs of rotor unbalance

Cause of unbalance	Observable signs*
Disk or component eccentric on shaft	Detectable runout on slow rotation (e.g. runs to bottom on knife edges)
Dimensional inaccuracies	Measurable lack of symmetry
Eccentric machining or forming inaccuracies	Detectable runout
Oblique angled component	Detectable angular runout; measured with dial gage on knife edges
Bent shaft; distorted assembly; stress relaxation with time	Detectable runout on slow rotation, often heavy vibration during rotation
Section of blade or vane broken off	Visually observable; bearing vibration during operation; possible process pulsations
Eccentric accumulation of process dirt on blade	Bearing vibration
Differential thermal expansion	Shaft bends and throws c.g. out; source of heavy vibration
Nonhomogeneous component structure; subsurface voids in casting	Rotor machined concentric, bearing vibration during operation; c.g. runs to bottom on knife edges
Nonuniform process erosion	Bearing vibration
Loose bolt or component slip	Vibration reappears after balancing because of component angular movement; possible vibration magnitude and phase changes
Trapped fluid inside rotor, possible condensing or vaporizing with process cycle	Vibration reappears after balancing; apparent c.g. angular movement occurs; possible vibration magnitude and phase changes
Ball-bearing wear	Bearing vibration; eccentric orbit with possible multiloops; frequency of vibration is one, two, or more per revolution

*Unless otherwise indicated, the frequency of vibration is one per revolution.

The need for written guidelines, quality criteria, and tolerance values for the balancing of rotating machinery has received attention in recent years from the International Organization for Standardization (ISO) and from various professional groups, such as the American Society of Mechanical Engineers and the Vereines Deutsche Ingenier. Various manufacturers' organizations (e.g., the American Gear Manufacturers Organization, the National Electrical Manufacturers Association, the American Pump Manufacturers Association) have also published their own industry standards and guidelines for improving the balance quality of specific rotating machinery. In each instance the objective is to specify balancing procedures, guidelines, and criteria that will enable manufacturers to design and construct rotating equipment that is not prone to failure by fatigue, is smooth running, and has a low inherent noise level during operation. Adequate rotor balancing begins at the equipment design phase and is an essential part of modern machinery development and operation.

This monograph discusses the problem of rotor unbalance, its effects on the dynamics of rotating machinery, and practical procedures for reducing unbalance levels. Its objective is to consolidate present knowledge on balancing principles and procedures into a single-volume, general reference on rotor balancing. Chapters 1 through 4 discuss the balancing of rigid-rotor systems, which represent the largest segment of all rotors manufactured and balanced. The dynamics of rigid-rotor systems are discussed first to provide a theoretical basis for the practical balancing of such rotors. Rigid rotor dynamics is simpler than the dynamics of flexible-rotor systems, and so this section also provides a convenient introduction to the general principles of rotor-bearing dynamics, which are discussed in Chapter 5. The various types of balancing machines now available are described in Chapter 3. The procedures for balancing rigid rotors are discussed in Chapter 4, using the theory and the practical concepts presented in the two preceding chapters. Criteria for rigid-rotor balancing from several sources are discussed, although emphasis is placed on ISO Document 1940–1973(E), "Balance Quality of Rotating Rigid Bodies," which is now the basic reference on this topic. Flexible-rotor-bearing dynamics are discussed in Chapter 5. The flexible-rotor balancing procedures described in Chapter 6 are based on the principles discussed in Chapter 5, with emphasis on the modal methods and on the influence coefficient method, now the most widely used balancing procedures for flexible rotors. Experiences with the application of each method for the balancing of flexible rotors are described in Chapter 7, which also discusses recent ISO publications on flexible-rotor balancing procedures and criteria. Chapter 8 contains a review of important trends in balancing technology.

The appendix is a review of static and dynamic data for fluid film bearings, which are widely used in rotating machinery. Such bearings exert an important effect on the dynamic behavior of rotor-bearing systems, and their properties are frequently referred to in the text. The appendix is followed by a comprehensive bibliography on balancing.

1.2 Standard Terms for Balancing and Mechanical Vibration

The nomenclature of balancing and mechanical vibration has been standardized in recent years under the auspices of the ISO. The ISO documents [1-3]* are fundamental references on balancing technology and procedures, and they contain balance quality criteria information that is referred to throughout this volume. Standardized terms have been used wherever possible in this monograph.

1.3 Nature of Unbalance

A rotor is in a state of unbalance when its principal axis of inertia does not coincide with its axis of rotation. This causes vibratory motion to be transmitted to the bearings in which the rotor operates, as the result of centrifugal forces generated by the eccentricity of the principal inertia in question. This condition is demonstrated in Fig. 1.1, where the c.g. of the rigid rotor is eccentric from the rotor axis by a distance a. The bearings have no flexibility in directions normal to the rotor axis; they are radially rigid. As the rotor spins about its axis of rotation under these conditions, a centrifugal force will be caused by the eccentricity of the c.g., and the magnitude of this force can be calculated from the equation

$$F = \frac{W}{g} \omega^2 a$$

where

F = centrifugal force of disk, lb
W = disk weight, lb
g = gravitational acceleration, in./s^2
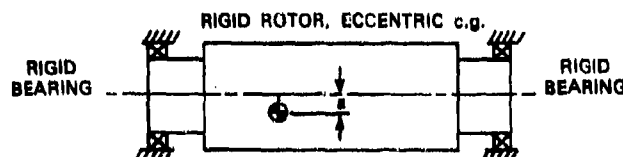
Fig. 1.1. Simple rigid rotor in rigid bearings

*Numbers in parenthesis correspond to references listed in Section 1.9

ω = disk velocity about the axis of rotation, rad/s (= rpm/9.55)

a = eccentricity of the disk c.g. from the disk axis of rotation, in.

This force is transmitted to the bearings during rotation. A practical example of such a "rigid" rotor in "rigid" bearings is a slow-speed bull gear mounted in spherical roller bearings. The bull gear is functionally rigid because of its large size. The shaft on which the bull gear is mounted is very stiff because of its short length. The bearings are rigid by design to provide high-quality smooth power transmission.

The effect of unbalance on a flexibly supported rotor is shown in the washing-machine schematic of Fig. 1.2: the rotor shaft deflects in a radial direction under the influence of bowl unbalance. The upper bearing is flexibly restrained in the radial direction; the lower bearing is rigidly constrained in the radial direction. Sources of unbalance during operation are the eccentricity of the washload, which may vary with location in the bowl, and the residual unbalance of the rotor bowl. At slow rotational speeds the centrifugal force developed from both sources is usually insignificant, but much greater loads may be developed when the machine is centrifuging water from the wash at about 300 to 400 rpm. Highly eccentric loads may even render the machine unable to spin up to centrifuging speed, because all available machine power is consumed in the work done by the washload on the dampers.
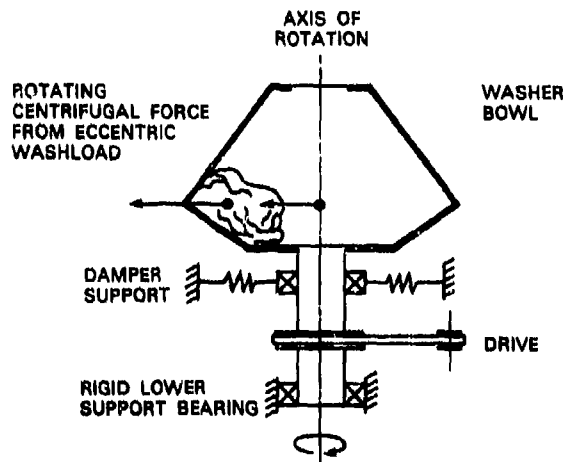
Fig. 1.2. Washing machine with washload unbalance and bowl unbalance

An example of a rigid rotor in radially flexible bearings is the locomotive diesel turbocharger unit shown in Fig. 1.3a. Such rotors are usually assembled by mounting the compressor disks onto the shaft. Disks and shaft may possess some residual unbalance, and this unbalance will not generally lie in the same radial plane or even be symmetrically located between the bearings (Fig. 1.3b). If the rotor remains rigid during operation, the total unbalance will act as a single resultant force vector (Fig. 1.3c),

$$F = \sum_{i=1}^{n} F_i,$$

which is the sum of the individual unbalance force vectors F_i acting at the rotor c.g. and a single resultant moment vector (Fig. 1.3d),

$$M = \sum_{i=1}^{n} M_i = \sum F_i \times S_i,$$

(a) Rigid rotor with unbalance

(b) Unbalance force vector arrangement

(c) Axial view of vectors with resultant

(d) Vector diagram for resultant unbalance force
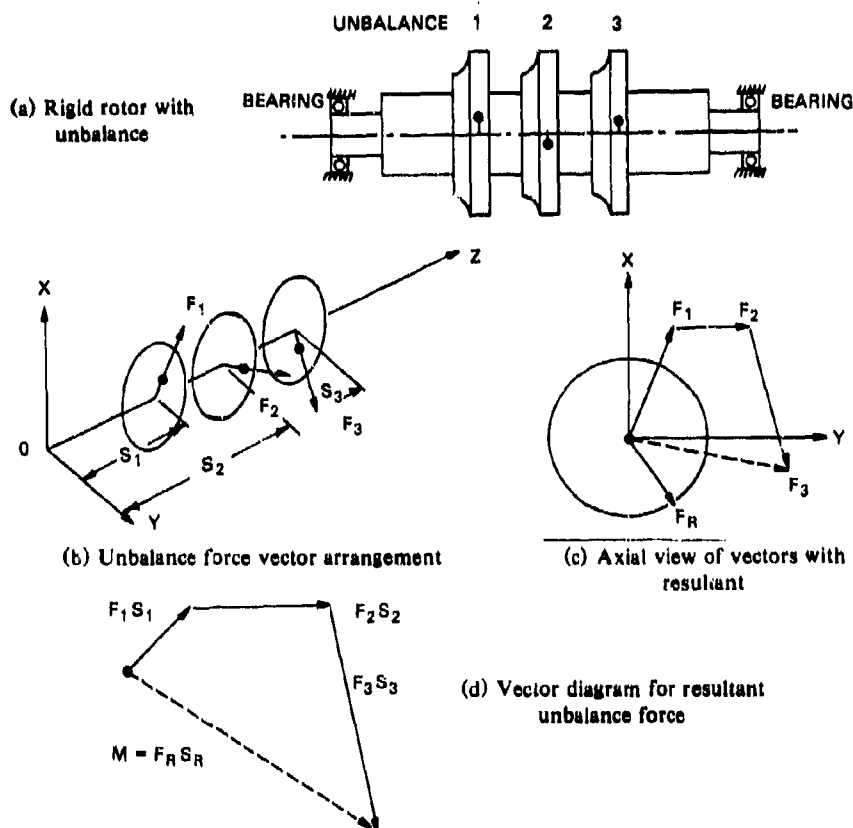
Fig. 1.3. Rigid rotor with nonuniform axial distribution of unbalance

acting about the rotor c.g., where M_i are the individual unbalance moments acting on the rotor as products of the F_i times their distances S_i from the origin (Fig. 1.3d). Such rigid rotors may then be balanced to operate smoothly in their bearings by the addition of balance weights in *any two separate planes* along the rotor length. The need for only two balancing planes is a direct result of the unbalance consisting of two basic components, a force and a moment. In practice, the balancing planes are situated near the bearings for convenient access and for good balance effectiveness (long moment arms).

The effect of unbalance on a flexible rotor consisting of a thin rigid disk, of weight W, mounted at midspan on a weightless flexible shaft in rigid end bearings, is shown in Fig. 1.4a. The disk c.g. is situated in a transverse plane, slightly eccentric by distance a from the elastic axis of the shaft. The centrifugal force that acts on the disk from rotation at speed ω is given by

$$F = \frac{W}{g} \omega^2 a.$$

This force causes the shaft to deflect in the radial direction by a distance r, as shown in Fig. 1.4b. In Chapter 5 it is shown that the magnitude of the radial deflection r is given by

$$r = \frac{(W/g) \omega^2 a}{K - (W/g) \omega^2}$$

where K is the radial stiffness of the shaft, considered as a flexible beam. It is evident from this expression that in any given instance the radial deflection will increase greatly as $[K - (W/g) \omega^2]$ approaches zero—that is, as the condition

$$\omega = \left(\frac{Kg}{W}\right)^{1/2}$$

is approached. This expression corresponds to the transverse natural frequency of the disk—shaft system, and the large amplitude buildup evidently represents a condition of resonance for this system.

The single-disk flexible rotor shown has a single unbalance force where the disk is mounted in a plane transverse to the shaft. If the disk also has a small angular misalignment to the transverse plane (Fig. 1.4c), moment unbalance effects will arise in addition to the force unbalance effects discussed above. Removing moment unbalance as well as force unbalance requires balancing the rotor in two planes, in the same manner as described for the turbocharger example.

Two-plane balancing frequently gives rise to considerable improvement in the overall balance quality. Rigid cylindrical rotors such as

(a) Simple flexible rotor in rigid bearings with disk unbalance

(b) Effect of rotation causing shaft to whirl with bending

(c) Transverse twisting couple caused by oblique mounting of disk on shaft
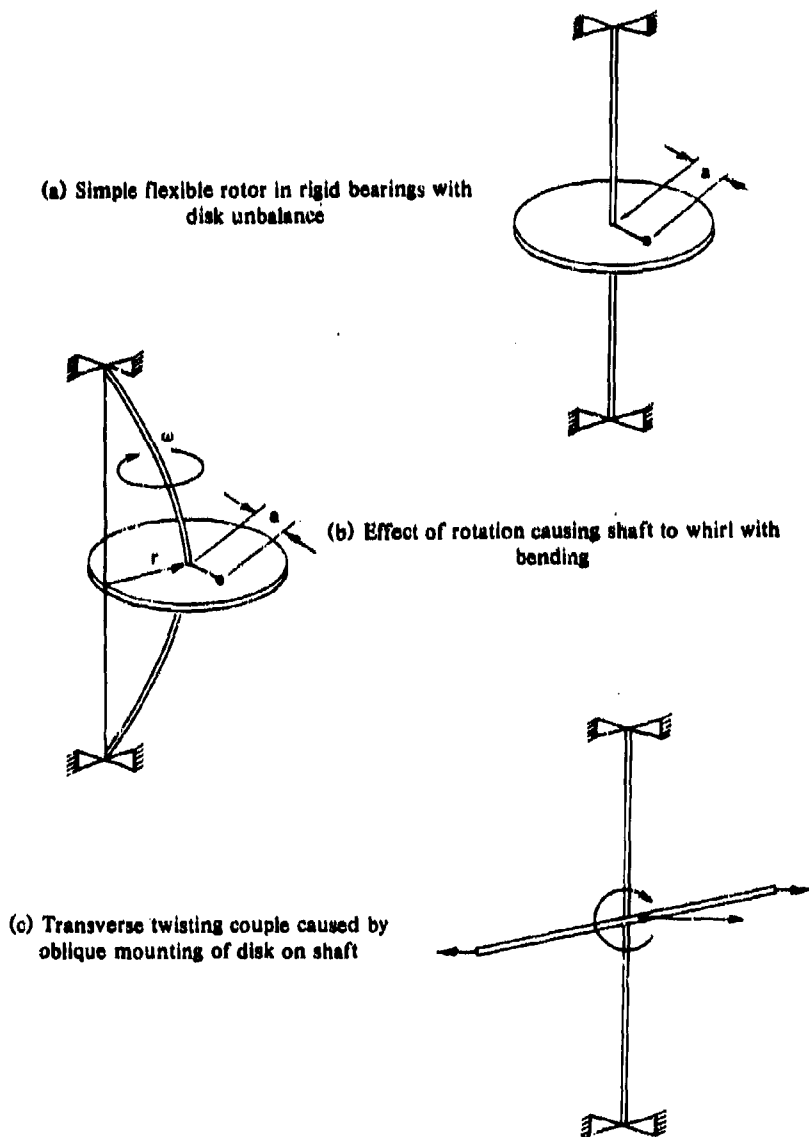
Fig. 1.4. Unbalance properties of a simple elastic rotor in rigid end bearings

motor armatures are routinely balanced in two planes. It is also becoming more common to balance disk-type rotors in two planes; for example, increasing numbers of automotive wheels and gears that operate at moderately high speeds (typically, automobile wheels at 500 to 800 rpm, gears at 200 to 800 rpm) are being balanced in two planes.

These examples illustrate the nature of unbalance and how its effects are felt in several practical applications. Where the rotor is rigid, the resultant unbalance acts as a force in, and as a moment normal to, the plane of the rotor c.g. Under conditions where unbalance forces are influenced by rotor flexibility, the balancing procedure is usually more complicated.

1.4 Classification of Rotors

It is common practice to classify rotors as either rigid or flexible, according to their observed, or anticipated, dynamic behavior during operation. Rigid rotors are those that may be balanced by the addition of suitable correction masses in two axial planes along the rotor.* Where balancing in more than two planes is required to achieve an acceptable condition throughout the operating-speed range, the rotor must be balanced as a flexible rotor. In practice, it is frequently not evident from inspection as to whether a given rotor will behave in a rigid or a flexible manner. The required information can be obtained by calculating the rotor behavior or by measuring it during operation. If such data are not available e.g., during design, the following ISO classification of rotors may be used to prescribe the type and quality of balance needed in a given situation.

Class 1. *Rigid rotors:* Rotors that can be balanced in any two arbitrarily selected axial planes and will remain in balance throughout the operating-speed range.

Class 2. *Quasi-flexible rotors:* Rotors which cannot be considered rigid but which can be adequately balanced in a low-speed balancing machine for smooth operation throughout the operating-speed range.

Class 3. *Flexible rotors:* Rotors that cannot be balanced in a low-speed balancing machine and which require some high-speed balancing procedure.
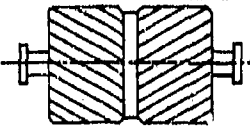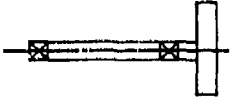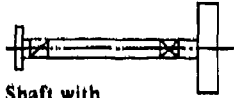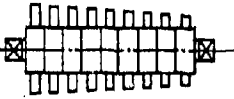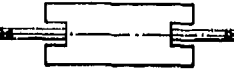
Class 4. *Flexible-attachment rotors:* Rotors which can be categorized as class 1, class 2, or class 3 rotors but which have components that are either flexible within themselves or are flexibly attached.

Class 5. *Single-speed flexible rotors:* Rotors that could fall into class 3 but for some reason (e.g., economy) are balanced for operation at one speed only.

Table 1.2 illustrates the types of rotors in each of the above categories. As shown, many subcategories for class 2 rotors have also been developed. The balancing of class 1 and class 2 rotors is discussed in detail in Chapters 3 and 4, respectively; the balancing of class 3 rotors is discussed in Chapters 6 and 7.

---

*For precise definitions of the terms *rigid rotor* and *flexible rotor* see Ref. 1 and Table 1.2.

Table 1.2. ISO classification of rotors*
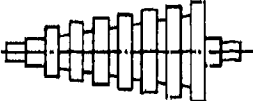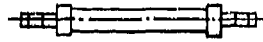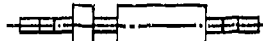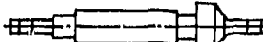
Class	Description	Example
1	Rigid rotor: unbalance can be corrected in any two (arbitrarily selected) planes and, after that correction, unbalance does not significantly change at any speed up to maximum service speed	Gear wheel
2	Quasi-flexible rotors: rotors that cannot be considered rigid but can be balanced in a low-speed balancing machine	
2A†	A rotor with a single transverse plane of unbalance (e.g., single mass on a light shaft whose unbalance can be neglected)	Shaft with grinding wheel
2B†	A rotor with two axial planes of unbalance (e.g., two masses on a light shaft whose unbalance can be neglected)	Shaft with grinding wheel and pulley
2C†	A rotor with more than two transverse planes of unbalance	Jet-engine compressor rotor
2D†	A rotor with uniformly distributed unbalance	Printing-press roller
2E‡	A rotor consisting of a rigid mass of significant axial length supported by a flexible shaft whose unbalance can be neglected	Computer memory drum

*Adapted from ISO Draft Document TC108/SC 1 WG2/N16.
†Rotors where the axial distribution of unbalance is known.
‡Rotors where the axial distribution of unbalance is not known.

Table 1.2 (Continued)

Class	Description	Example
2F‡	A symmetrical rotor, with two end correction planes, whose maximum speed does not significantly approach second critical speed, whose service speed range does not contain first critical speed, and with a controlled initial unbalance	Five-stage centrifugal pump
2G‡	A symmetrical rotor with two end correction planes and a central correction plane whose maximum speed does not significantly approach second critical speed and with a controlled initial unbalance	Multistage pump impeller
2H‡	An asymmetrical rotor with controlled initial unbalance treated in a similar manner as class 2F rotors	Impeller pump. Steam trubine rotor
3	Flexible rotors: rotors that cannot be balanced in a low-speed balancing machine and require high-speed balancing	Generator rotor
4	Special flexible rotors: rotors that could fall into classes 1, 2, or 3 but have in addition one or more components that are themselves flexible or are flexibly attached	Rotor with centrifugal switch
5	Single-speed flexible rotors: rotors that could fall into class 3 but for some reason (e.g., economy) are balanced only for a single service speed	High-speed motor

The ISO rotor classification is based mainly on practical experience with many types of rotors in each category. Its purpose is to serve as a preliminary guide to balancing and to indicate possible next steps if a rotor fails to balance by the first procedure tried. However, no mention is made of the typical speed ranges for which the ISO guidelines will apply, and evaluation of the applicable category is left to the user in each instance. If further guidance is required, the next step will be to calculate the dynamic properties of the rotor in its supports or to spin test the rotor in an environment that simulates operating conditions as closely as possible. Modern design procedure would include the calculation step as part of the rotor-system design process, and virtually all rotor construction firms would spin test the rotor on preliminary assembly. Practical rotor balancing is usually part of this initial rotation checkout.

1.5 Scope of the Balancing Problem

Rotors are balanced for a variety of practical reasons. The process of balancing reduces the net effect of the unbalance forces on the rotor. This reduced unbalance leads to lower vibration levels being transmitted to the bearings and foundations. Balanced machinery operates more smoothly and quietly than unbalanced machinery, and longer periods between overhauls can usually be scheduled with no decrease in reliability. In general, a well-balanced machine gives the impression of superior quality and greater safety. Further, in many process industries such as papermaking, newsprint production, and office copiers, product quality improvement is closely related to the reduction of machine vibration levels. Much machine structural vibration, torsional vibration, and rotating-shaft vibration can be traced to unbalanced rotating equipment. Poor product quality is often correctly associated with any observed structural vibration and noise generation.

Rotating industrial equipment is commonly categorized as low-, medium-, and high-speed machinery. Low-speed equipment is often large and massive and may have relatively low natural frequencies. Water-wheel turbine units, man-centrifuges, ship propellers, windmills, and communications satellites commonly operate in the speed range of 10 to 300 rpm, and each component or system is balanced by some suitable procedure before being put into service (see Table 1.3). Special purpose balancing machines have been developed for satellites, ship propellers, and other types of low-speed components. Medium- and high-speed rotating machinery must always be balanced to operate smoothly. The choice of balancing procedure is made on the basis of effectiveness and economics. The ISO classification of rotors, described in the preceding section, provides guidance as to the most

Table 1.3. Typical operating conditions for various low-speed machines

Type of machine	Speed range (rpm)	Power (W)	Size range
Aerospace man-centrifuge	20—100	300—500	50-ft arm
Office building fans	400—1800	30,000—200,000	5—12 ft
Marine propellers	80—300	100—50,000	3—25 ft
Large marine diesel engine	80—300	6000—15,000	8-ft-dia. cylinders
Power windmill	60—300	30—200 kW	60-ft-dia. blades
Mineshaft pulleys	50—240	100—300	12—20-ft diameter
Francis water turbine	80—450	5000—30,000	10—35 ft
Salient-pole generator	80—450	5000—30,000	10—60 ft
Watches, clocks	60	10^{-4}—10^{-2}	0.1—3.0 in.
Hospital washing machines	120—300	7—20	5—15 ft

suitable balancing procedure for a given case. Additional guidance can be obtained by calculating the dynamic properties of the machine system, to determine at the design stage whether the rotor is rigid (class 1) or flexible (class 3), or otherwise, under operating conditions. Accurate computer procedures for calculating the critical speeds and the unbalance response characteristics of rotating machine systems have been developed in recent years. When the dynamic properties of the unit are known, the class of rotor will be evident from the mode shapes (rigid or flexible) that occur within the operating-speed range. A suitable balancing technique can then be selected, and the required number of balancing planes can be designed into the rotor/stator structure where the addition of correction weights will be most effective.

The design of rotors for effective balancing is becoming recognized as an important part of the overall design process. If a given rotor does not deform but remains rigid throughout its speed range, it may be balanced as a class 1 rotor, usually with balance correction planes near its ends. If the speed range includes a strong bending critical speed, a midspan correction plane will also be desirable (and possibly essential) for efficient balancing. It is obviously easier to include such a plane during the design stage than to make room for it during manufacture.

The range of machinery for which special balancing facilities have been developed is indicated in Figs. 1.5 through 1.8. For example, the high production requirements of the automotive industry have led to the development of self-contained automatic balancing facilities incorporating conveyors, automatic handling and inspection equipment, automatic indexing, unbalance measurement and evaluation instruments, and precise correction-hole drilling operations. Crankshaft and clutch housing assemblies are balanced in this manner in many

Fig. 1.5. Facility for automatic motor armature balancing. (Courtesy of Schenck Trebel Corporation.)

Fig. 1.6. Medium-size double-flow turbine rotor being balanced in a hard-pedestal machine. (Courtesy of Schenck Trebel Corporation.)

Fig. 1.7. Vacuum-spin-pit balancing facility. (Courtesy of Schenck Trebel Corporation.)

Fig. 1.8. Semi-automated balancing facility for rigid and flexible rotors for speeds up to 9000 rpm and transmitting up to 4000 hp. (Courtesy of Mechanical Technology Inc.)

engine plants to within precise, repeatable limits. Similar equipment is available for automatic wheel-tire assembly balancing in two planes and for balancing of railroad axle sets.

Armature production is another high-volume industry. Figure 1.5 shows an automatic armature-balancing facility. Automated balancing is attractive in high-volume industries because the installation cost of an automatic balancing facility is frequently less than the overall costs of manually operated facilities capable of the same skilled work. For example, an automatic armature-balancing facility can balance 100 armatures per hour to within 0.01 oz-in. For an equivalent production, the comparable ongoing annual cost of semiskilled labor using nonautomated equipment could be a sizeable portion of the capital cost of the automated facility.

The specific balancing needs of many other industries have also led to the development of special purpose equipment. The balancing of steam turbine generators has become more complex as the size of the average turbine has increased; turbine balancers now range from the conventional hard-pedestal units shown in Fig. 1.6 to the large vacuum

spin-test balancing facility shown in Fig. 1.7. Further details of turbine-generator balancing facilities now in operation throughout the world are given in Section 3.5.

Ultra-high-speed power-shaft balancing is being investigated at Mechanical Technology Inc., Latham, New York; where an installation has been developed to balance shafts operating at speeds of up to 9000 rpm and transmitting up to 4000 hp. This problem involves complex shaft dynamics and sophisticated balancing technology. A semiautomated rotor balancing facility is shown in Fig. 1.8.

The use of lasers to remove metal for automatic balancing has been attempted by several industrial firms: Avery (United Kingdom) in 1964, Schenck Trebel (who marketed a laser-removal balancer in 1972), and by Mechanical Technology Inc. in 1974. At present, it is a potentially useful development for future application in industry. Removal of metal by the Schenck Trebel laser balancer is shown in Fig. 1.9.

Fig. 1.9. Equipment for metal removal by laser. It is not necessary, in the balancing process, to stop the workpiece from rotating. The volume of metal removed per laser pulse is presently small, making the cycle time longer. Rotational speed is the range of 100 to 400 rpm. (Courtesy of Schenck Trebel Corporation.)

1.6 Whirl Orbits

Unbalance is a major cause of vibration in rotating machinery, but it is not the only cause. Bearing instability, seal instability, mechanical rubbing, thermal instability, and externally applied vibrations are other known causes of rotor vibration. When a rotor is undergoing initial balancing in the manufacturer's plant, most of these additional sources of vibration are likely to be absent; however, when the rotor is installed in its own bearings and casing, and is operating under process load and flow conditions, the above sources other than residual unbalance can give rise to undesirable unit vibrations. For corrective action, accurate diagnosis of the cause of any such vibrations is an essential first step.

Whirl orbits are customarily obtained by means of displacement sensors mounted on the casing to observe the orbit of the shaft. The displacement sensors are arranged 90° apart, as shown in Fig. 1.10. A vibration signal is obtained from variations occurring in the gap clearance as the shaft rotates. This signal is then filtered and displayed on an oscilloscope screen. Typically, a machine on the test stand or a unit that is giving trouble in the field will be instrumented with shaft sensors situated near the bearings, to obtain details of the whirl orbit shape. Extensive experience with the orbit types shown in Figs. 1.11 through 1.15 has indicated that frequently there is a correlation between the types of orbits shown and the sources of rotor vibrations discussed below.

Irregular Orbits

Rotor whirl orbits are frequently irregular in shape. This irregularity arises from the presence of several simultaneous sources of excitation acting on the rotor. Rotor unbalance, magnetic field effects, externally transmitted vibration, hysteretic whirling, and stator–rotor fluid

SENSORS MOUNTED
   ON CASING

AIR GAP

SIGNALS PROCESSED BY
TRACKING FILTERS AND
TIME-AVERAGED TO
IDENTIFY PRINCIPAL
FREQUENCY COMPONENTS
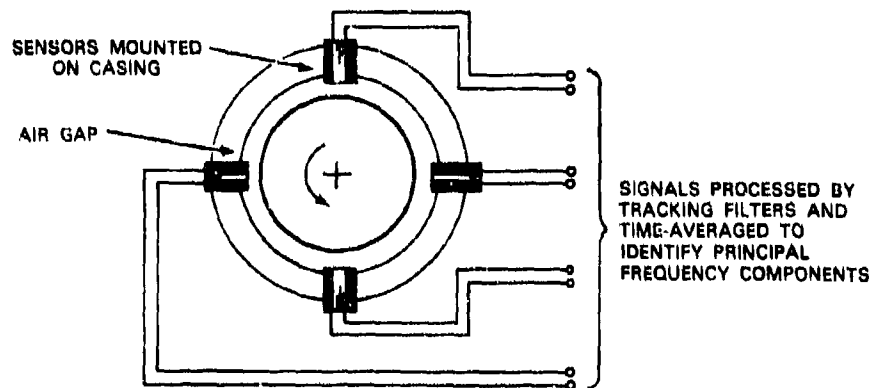
Fig. 1.10. Noncontacting probe arrangement for shaft orbit measurements
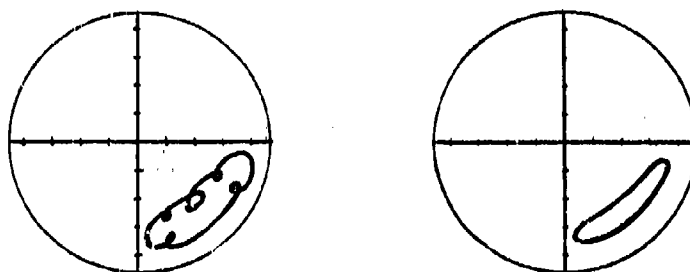
(a) Orbit of shaft with several con-
current whirls at different frequencies
(unfiltered response)

(b) Synchronous unbalance whirl orbit
obtained by filtering out nonsynchro-
nous frequencies from above orbit
(synchronous filtered response)

Fig. 1.11. Typical whirl orbits for a shaft in fluid-film bearings

interaction are all possible sources that can contribute at different fre-
quencies to the total orbit. Where one source of excitation (e.g.,
unbalance) predominates, the other excitations will be superimposed on
the primary orbit (Fig. 1.11a).

Elliptical Orbit at Shaft Synchronous Frequency

An orbit such as that shown in Fig. 1.11b can result when all non-
synchronous components of the shaft vibration are absent or have been
filtered out of sensor signals similar to those shown in Fig. 1.11a. This
filtered synchronous orbit is the response of the shaft to residual unbal-
ance at its speed of rotation. The ellipticity of the orbit represents the
difference in bearing stiffness in the two principal stiffness directions.
The angular orientation of the orbit is the result of coupling between
the bearing radial stiffness properties in the x- and y-directions. Bearing
properties can influence the unbalance orbit in the following ways:

Property	Effect on orbit
Identical stiffness in the x- and y-directions	Circular orbit (Fig. 1.12a); vertical displacement due to gravity
Different stiffnesses, no coupling between the x- and y-directions	Elliptical orbit (Fig. 1.12b); the x- and y-directions coincide with orbit principal axes
Different stiffnesses, cross-coupling between the x- and y-directions; fluid-film bearings	Elliptical orbit (Fig. 1.12c); orbit principal axes oriented between the x- and y-directions; x-y offset due to static fluid properties
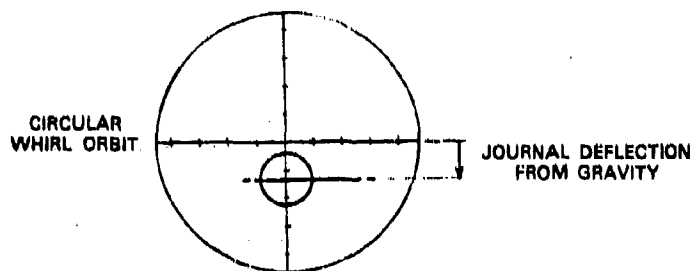
CIRCULAR
WHIRL ORBIT

JOURNAL DEFLECTION
FROM GRAVITY

(a) Shaft in bearings with identical stiffnesses in both coordinate direc-
tions and no cross-coupling effects

ELLIPTICAL
WHIRL ORBIT

JOURNAL DEFLECTION
BY GRAVITY
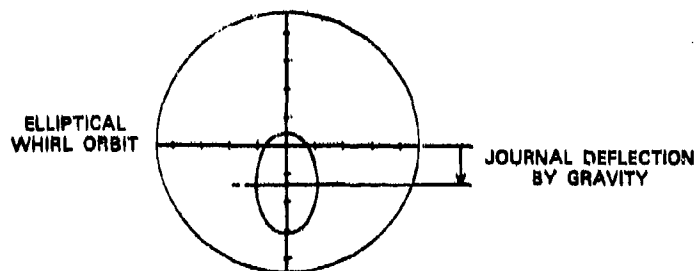
(b) Shaft in bearings with dissimilar stiffnesses in both coordinate
directions, and no cross-coupling effects

STEADY-STATE JOURNAL
ECCENTRICITY

RADIUS OF
WHIRL ORBIT
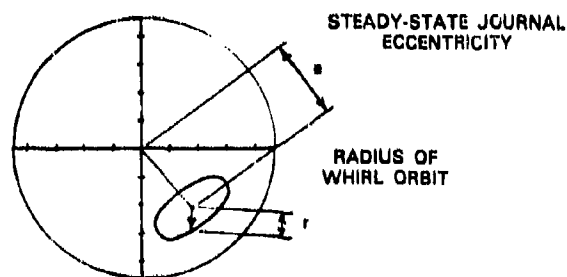
(c) Shaft in fluid-film bearings with dissimiliar stiffnesses
and cross-coupling effects

Fig. 1.12. Effect of several bearing stiffness conditions on the journal whirl orbit

Rotors that operate in rolling-element bearings tend to show a
small gravity offset in the whirl orbit; the orbit itself is usually quite
circular. Both characteristics are due to the high radial stiffness and
isotropic bearing stiffness. High-frequency components may also be

present at the ball-passing frequency. Unbalance whirling in fluid-film bearings usually occurs in an elliptical orbit, at synchronous frequency. The presence of a strong filtered synchronous response signal suggests that rotor unbalance is a possible cause of the observed whirling. Nonsynchronous whirling at some multiple of the running speed is seldom due to residual unbalance.

Orbits with Loops

An orbit with internal loops (Figs. 1.13—1.15) indicates the presence of two or more separate excitations with different frequencies. The examples given below illustrate how this may occur in practice.

A half-frequency whirl often has a characteristic orbit, as shown in Fig. 1.13a. The shape of the orbit is due to the action of a bounded whirl that has a frequency about half the rotational frequency of the shaft and is superimposed on the shaft unbalance whirl occurring at synchronous frequency. It should be noted, however, that not all half-frequency whirls are stable or bounded.

Forced whirling of a floating sun gear between three epicyclic planetary gears is shown in Fig. 1.13b. The planetary gears give a "three-per-revolution" excitation to the shaft at their rotational frequency; the shaft has its own synchronous whirl caused by unbalance. The net effect is a three-lobe epicyclic orbit.

Light rubs of a shaft against a bearing wall, seal face, or other stator component may cause the looped orbits shown in Fig. 1.14a. The details of the orbit depend on the speed of the shaft and its relation to the critical speed of the system; for example, at near twice the critical speed, the orbit may look like a bearing-induced half-frequency whirl as the shaft responds to a light rub with a forward whirl at its natural frequency, on which is superimposed the shaft unbalance whirl. Many loops may indicate continuous intermittent light rubbing in a well-balanced shaft (Fig. 1.14b).

Heavy occasional rubs may also induce very high speed backward whirls, as shown in Fig. 1.14c. The shaft responds by whirling backward at its natural frequency in a decaying transient whirl, at speeds below the natural frequency. Where the contact is sustained along the bearing or seal surface, the shaft will rotate backward with some slipping. High whirl frequencies can be generated in this manner, causing high centrifugal forces that maintain the contact between shaft and casing, as shown in Fig. 1.14d. This type of rubbing can cause extreme wear and possible seizure of the shaft in its bearings. For a discussion of the properties of orbital rub motion, see Ref. 4.

Shaft misalignment may be recognized by a characteristic two-per-revolution whirl pattern (Fig. 1.15a) superimposed on the shaft unbal-

ance whirl at synchronous speed. Another indication of shaft misalign-
ment occurs when the whirl orbits in adjacent fluid-film bearings lie in
opposite halves of the bearing clearance (Fig. 1.15b). Banana-shaped
orbits and "figure-eight" orbits both contain twice-per-revolution fre-
quency components for the reasons indicated in Fig. 1.15.
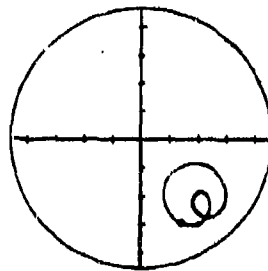
(a) Bounded half-frequency whirl pat-
tern arising from bearing fluid-film
effects

(b) Floating sun gear whirling between
three planetary gears
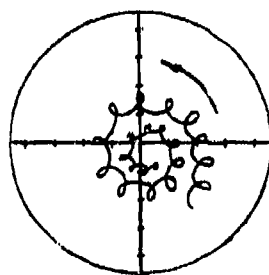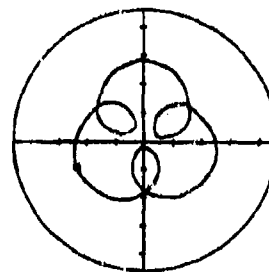
(c) Effect on original orbit as in Fig.
1.12 of sudden light rub against the
bearing   (typical,   not   necessarily
characteristic)

(d) High-frequency backward whirl
induced by heavy transient rubbing
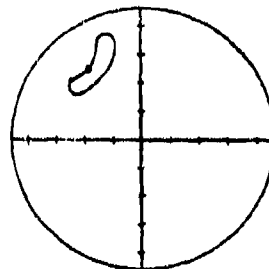
Fig. 1.13. Shaft whirl patterns arising from various causes

(a) Light sustained rubbing of shaft against bearing wall

(b) Intermittent rubbing of shaft against stator

(c) Shock-induced rubbing of rotor against stator; high-frequency transient at shaft natural frequency decays with transient

(d) Continuing skidding within rolling-element bearing (excluding noise components)
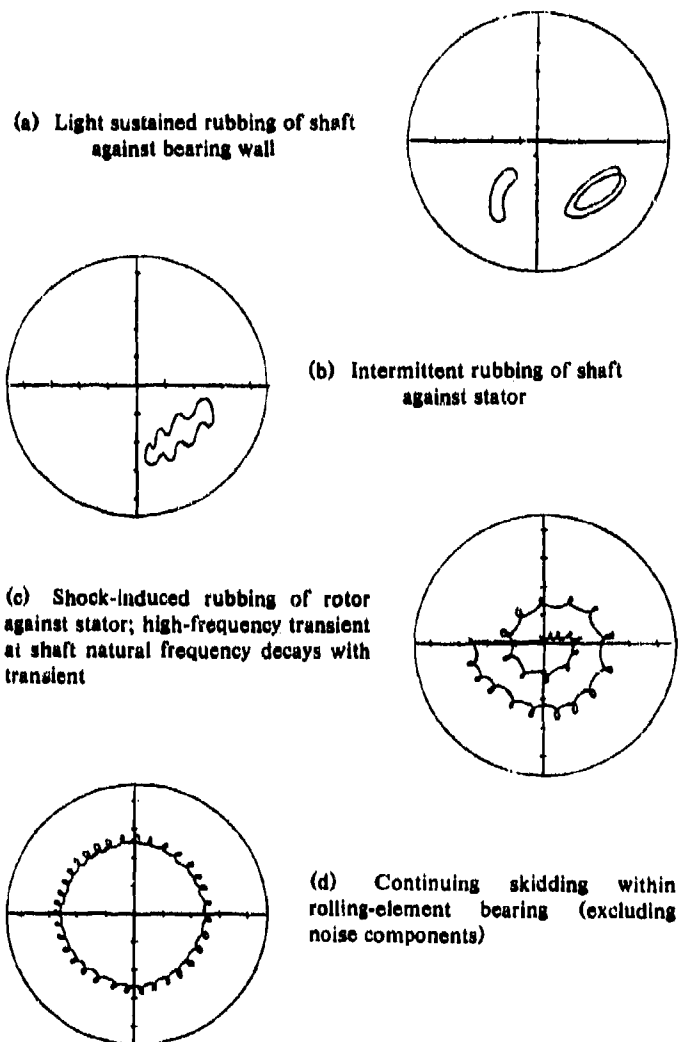
Fig. 1.14. Typical rubbing patterns induced by various types of contact between shaft and wall

MAIN SIGNAL

MISALIGNMENT
SIGNAL

ELLIPSE ORBIT
WITH MISALIGNMENT

(a) Orbit indication of misalignment

RIGHT-HAND
BEARING

LEFT-HAND
BEARING
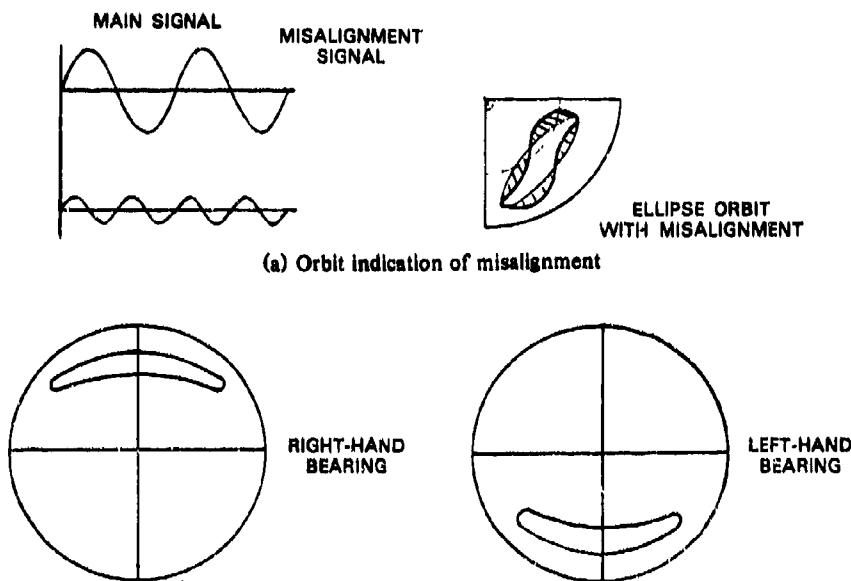
(b) Effect of misaligned coupling of orbits at adjacent bearings

Fig. 1.15. Effects of misalignment on shaft orbits

External Vibration Effects

There are many possible causes of external vibration. External vibration components (usually nonsynchronous) can appear in the whirl orbit superimposed on the unbalance whirl motion. Possible sources are again suggested by the shape of the orbit and by any integer loops. For example, magnetic unbalance excitation from an ac generator could be indicated by the number of loops being equal to the number of pole faces (Fig. 1.16a). Vortex excitation from a pump impeller or from turning vanes in a fan might induce high-frequency compone ..s at the shedding frequency of the impeller or vanes (Fig. 1.16b). I teresting vortex-shedding problems in hydraulic turbine sets have been discussed by Parmakian [5]. Screw compressors or pumps that use lobed rotors may generate forced vibrations at the frequency of the escaping fluid (i.e., lobe-passing frequency), which is commonly two or four times the rotational speed. This could give orbits of the type shown in Fig. 1.16c.

External vibrations consisting of regular impulses will generate regular, repeated loops in the unbalance orbit only if the impulses are integer harmonics of the unbalance frequency; if not, the multirevolution pattern will be irregular. Intermittent impulses cause the rotor to respond at its natural frequency or frequencies. The vibration orbit

from such sources is commonly a rapidly decaying transient for rotors in fluid-film bearings (Fig. 1.16d).

Early diagnosis of whether rotor vibrations are due to unbalance or to some other source is of major importance in machine problem solving. Unbalance vibrations can be eliminated by the techniques described in this monograph. However, shaft whirls that are due to instability or externally imposed vibrations *cannot* be removed by balancing. Unstable whirls must be treated by other techniques, which frequently involve modifications to the bearings, seals, or casing [6]. Similarly, vibrations affecting the rotor from external sources must also be treated by other means, e.g., by isolation of the unit.

(a) Unbalanced magnetic field causes four pulses per revolution in rotor with residual unbalance (sustained orbit)
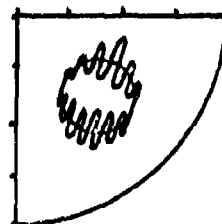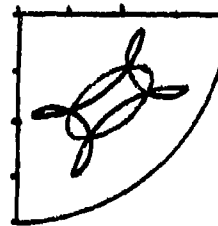
(b) High-frequency vortex shedding transmitted to casing and rotor with residual unbalance. Sustained orbit with stochastic high-frequency component.

(c) Four-lobed rotor causes vibration at four pulses per revolution superimposed on residual unbalance. Sustained orbit.
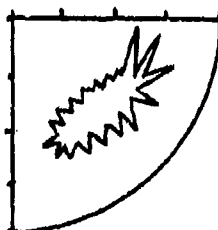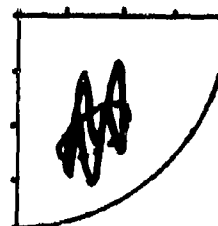
(d) External impulse causes rotor to vibrate at its natural frequency during rotation. Vibrations decay rapidly in fluid-film bearings. Transient orbit decays to synchronous unbalance orbit.

Fig. 1.16. Effect of externally induced vibration on rotor orbits

1.7 Literature Sources on Balancing

The general subject of rotor balancing includes rigid-rotor balancing, flexible-rotor balancing, and balancing machines. The balancing of all classes of rotors requires a knowledge of rotor dynamics, which in turn involves shaft dynamics, bearing dynamics, and system dynamics. The subject of balancing machines includes balancing principles, equipment, shop balancing practices, and field balancing techniques, applied to both rigid and flexible rotors.

The published literature on balancing is contained in the transactions of professional societies, in technical journals, and in company publications. The books by Timoshenko [7] and by Den Hartog [8] provide a general introduction to rigid- and flexible-rotor balancing, with some comments on balancing machines. A more recent book by Wilcox [9] contains a comprehensive discussion of the principles and techniques of balancing, mostly applied to class 1 and class 2 rotors (i.e., rigid and quasi-rigid rotors). Wilcox does not discuss the wide range of literature available on balancing.

The balancing literature has been reviewed by Eubanks [10], who surveyed and evaluated several balancing methods; by Levit and Royzman [11], who discussed the balancing of gas-turbine engines; by Little [12], whose thesis on flexible-rotor balancing contains selected references on this subject; and by Kendig [13], whose thesis compares the modal and influence coefficient methods of flexible-rotor balancing, and discusses the literature of these two methods. Reviews by Kushul' and Shlyakhtin [14] (in English) and by Dimentberg [15] (in Russian) on flexible-rotor balancing techniques describe selected European works on modal balancing of shafts in rigid undamped bearings. Flexible-rotor balancing has recently been reviewed by Rieger [16].

The literature on rotor-bearing dynamics has been discussed in detail at various stages by Rieger [17], Gunter [18], Bishop and Parkinson [19], and, more recently, by Shapiro and Rumbarger [20] (bearing dynamics), Eshleman [21] (critical speeds), and Rieger [16] (unbalance response and balancing). An extensive bibliography, without annotation, on rotor dynamics has been presented by Loewy and Piarulli [22]. It contains many Czechoslovak and Soviet references not previously cited in an English-language review. The books by Dimentberg [23] on shaft dynamics and by Tondl [24] on rotor stability problems contain many additional references to the European literature on rotor-bearing dynamics.

The most useful sources of information on balancing machines and balancing equipment are the sales-related publications of firms manufacturing industrial balancing equipment. The reports by Eubanks [10] and by Laskin [25] appear to be the only independent critical

reviews on balancing machines. No reference work appears to exist on the many special-purpose balancing machines available (gyro balancers, universal balancer, etc.), nor on the many custom balancing facilities (turbine-generator spin pits, automated balancing facilities, satellite and space-vehicle mass-centering units, etc.) now in use, apart from these descriptive sales-related publications. The patent literature provides another source of information on balancing devices and innovations (see Section 3.7), but again no comprehensive discussion of this subject has been attempted.

1.8 Historical Notes on Balancing and Rotor Dynamics

Rotor dynamics and balancing are closely related to the development of power-generating and power-transmission equipment. Practical steam power began with the reciprocating engine (Watt, 1769) and with the steam turbine (DeLaval, 1883; Parsons, 1884). Steam screw propulsion of ships was proved feasible with the *Great Eastern* (Brunel, 1841). Steam turbine screw propulsion began with the yacht *Turbinia* (Parsons, 1897) and with submarine U.S.S. *Nautilus* (Rickover, 1955). Historical details are given in Refs. 26 and 27.

The first paper on rotor dynamics was published in 1869, by Rankine [28], who established the existence of a shaft critical speed, by analysis. Such critical speeds had been observed in practice at that time (though not explained), in association with factory overhead drive shafting, which often carried many massive pulleys. DeLaval [26] demonstrated in 1883 that with turbomachines of the type shown in Fig. 1.17 it was possible to pass through a critical speed while developing useful power. At that time critical speeds were thought to be due to unstable operating conditions, similar to the column-buckling phenomenon. This erroneous concept was inferred from the Rankine paper, and was indirectly endorsed by Greenhill [29] in 1883, in a paper on marine propulsion shaft buckling. Chree [30] in 1904 explicitly stated and endorsed this instability viewpoint. A comprehensive study of the shaft-pulley problem was made by Dunkerley [31] in 1894. This paper presented the results of experiments with many shaft system models and correlated them with the elegant critical speed analyses of Osborne Reynolds. These extensive results are still of value today. Föppl [32] in 1895 analyzed and explained the supercritical operation of the DeLaval turbine.

In 1916, an experiment by Kerr [33] caused a controversy in the literature about the fundamental mechanics of rotor response to unbalance, indicating that this topic was still widely misunderstood. A definitive paper by Jeffcott [34] in 1919 corrected this misunderstanding and established modern rotor-dynamics analysis—50 years after Rankine's paper.

CONICAL FRICTION DRIVE   HERO TURBINE

TURBINE AND GEAR
ARRANGEMENT

STEAM
FLOW

SUPERCRITICAL
NOZZLE

GEAR AND   IMPULSE
PINION   BLADES
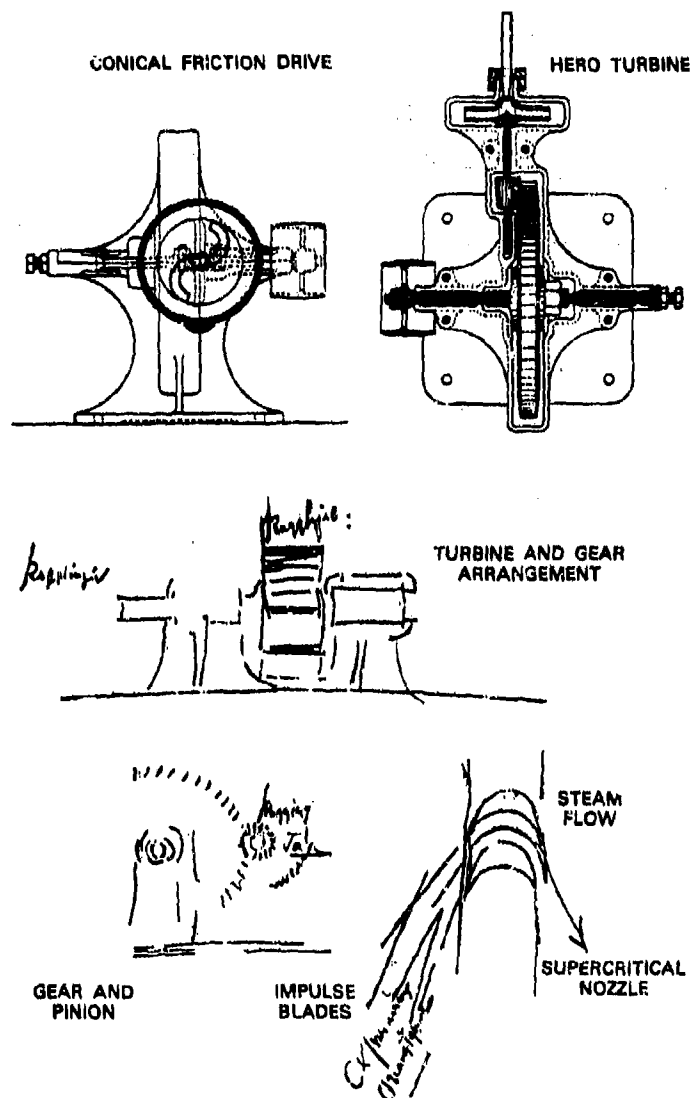
Fig. 1.17. High-speed reaction (Hero) turbine with conical friction
transmission (patented in 1883) and DeLaval's sketch of supercritical
nozzle and impulse blades (1888). (Illustration from the DeLaval
Memorial Lecture 1968, "Gustaf De Laval, the High Speeds and the
Gear," by Professor Ingvar Jung; reproduced by permission of Stal-
Laval Turbine AB, Finspong, Sweden.)

The first recorded balancing machine was devised and patented by Martinson in 1870, in Canada.* It allowed any machine component to be balanced as a rigid body. Components to be balanced were mounted in soft supports and end driven from a pulley. Dynamic subcritical magnification of the rotor amplitudes was used to obtain an improved balance indication. The location of the unbalance in this machine was determined by hand-held chalk marking the "heavy" spot, according to Dihrberg [35]. The number of such machines built and used is not known.

A balancing "stand" built by Marten (ca. 1900) is shown in Fig. 1.18. Known at the time as *Marten's balancing scale*, it incorporated a 10:1 mechanical lever arm magnification of rotor amplitudes to increase readout sensitivity. This principle, coupled with the dynamic magnification then available with Martinson's balancing machine, should have led to further improvements in the quality of balance attained.
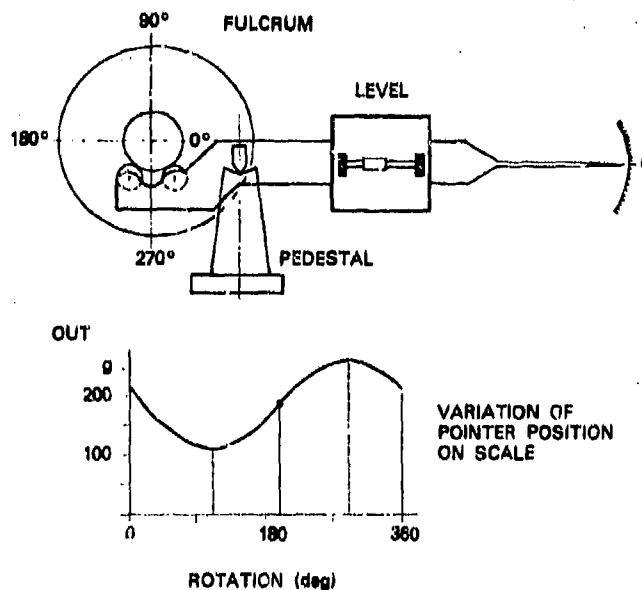
Fig. 1.18. Principles of Martin's balancing scale (ca. 1900). Slow rotation of the component being balanced gave rise to vibratory amplitudes in the vertical direction; these were magnified in the ratio 10:1 on the scale by the lever principle shown. (K. Dihrberg, "Schwingungstechnik bei Auswuchmaschinen," *Auswut-technik*, EED 0, Stand vom 1.1.65; ©Carl Schenck Maschinenfabrik GmbH, Darmstadt. Used by permission.)

*A detailed discussion of balancing machines and facilities is presented in Chapter 3, which also contains illustrations of several of the machines discussed here.

Lawaczeck (1907) wrote a short note on the theory and design of balancing machines, and in 1908 patented a new type of balancing machine (see Chapter 3). This machine operated in the vertical position and had a flexible lower bearing support, which allowed only horizontal motions of the lower bearing support. The lower support motion is then a large-amplitude, simple harmonic vibration at operating speed in which the maximum motion is in phase with the maximum amplitude. The angular position of the unbalance was again found by chalk marking, and the magnitude of unbalance could be found by a few trial-and-error tests with trial weights in the correction plane. One end of the rotor was balanced at a time. Lawaczeck (1912) also developed a horizontal version of this machine.

Both Lawaczeck machines suffered from the inconvenience of not being able to interchange the "free" and the "fixed" ends readily. This meant that the rotor had to be removed from the machine and then reinstalled with the ends reversed, to remove any unbalance remaining in the other plane with a second run. Heymann [36] overcame this limitation in 1916 with his "double-pendulum" machine, which allowed the horizontal restraint on both end bearing supports to be varied from rigid to flexible as needed. This allowed independent corrections to be made at either balance plane without removing the rotor, simply by clamping one end and measuring at the other end.

The ideas of Lawaczeck and Heymann were combined into a single machine around 1918; this was the forerunner of modern balancing machines. The first Lawaczeck—Heymann machines operated by running up to a speed above the support natural frequency and then coasting down in speed through resonance to obtain response-amplitude magnification. These machines allowed rotor residual unbalance to be determined and corrected to a satisfactory degree for the first time. The post World War I demand for rotating-machine components caused this idea to spread rapidly. Soderberg [37] describes a large similar machine built in Philadelphia in 1923.

Akimoff [38] in 1916 developed another type of balancing machine, which was based on the concept that the effects of unbalance could be nullified through the application of known centrifugal forces and moments, when these effects were applied at suitable locations. Thus the required unbalance details could be obtained directly from the vibration measured from the pedestal signals (i.e., zero pedestal motion indicated a null balance condition). The annulment was achieved by using a second (permanent) rotor attached beneath the rotor being balanced. The permanent rotor consisted of a drum of horizontal rods that could be adjusted radially and axially as required. The magnitude of the unbalance and its angular location were determined from the location of the horizontal rods when a null balance had been achieved.

Other null balancing machines that were patented during this period were the Newkirk machine [39], and the AEG—Lösenhausen machine, which used electromagnetic forces to excite a flexibly supported machine frame at such a frequency and phase angle that the original unbalance forces were canceled.

Most machines built during the period 1900 to 1940 measured rotor residual unbalance by some mechanical indicator. The first mention of electrical sensing and measurement is in an Allegemein Elektricität Gesellschaft (AEG) patent in 1932 on piezoelectric crystals, in which the wattmeter method is mentio....d as a meter and signal filter. The first mention of stroboscopic angle measurement occurs in a U.S. patent in 1935. In the same year, Thearle [40] mentioned the use of an electrodynamic pickup and stroboscopic angle indication, and Rose [41] discussed the use of the plane-separation principle and its application with electric analog circuits. Thearle further developed these ideas in 1938.

Federn [42] in 1942 developed an effective and sensitive phase-angle-measuring device using calibrated lines on an oscillograph. This device, used during World War II to balance ship gyros, made it possible to obtain a high degree of sensitivity by simple mechanical coupling, allowing displacement measurements down to 20 μin. Filtering remained a problem with such devices, and background noise was difficult to eliminate.

Following Jeffcott's clarification of the mechanics of rotor unbalance whirling, the most important problems of rotor dynamics have been mainly concerned with certain instabilities of the rotor (fluid-film whirl, hysteresis whirl, parametric instabilities, etc.). Recently, however, new questions of rotor balancing associated with the increased use of flexible rotating machinery (e.g., large turbine-generator sets) have reemerged. Groebel [43] in 1952 wrote a qualitative discussion of modal balancing applied to generator rotors, and Meldahl [44] indicated certain orthogonality relations on which modal balancing concepts are based. In a series of papers between 1959 and 1968, Bishop, Gladwell, Parkinson, and others [18,45,46] developed the theory of modal balancing and gave experimental verification to a high degree. Practical application of the modal balancing method to turbines, generators, and high-speed pumps was described by Moore [47,48] during this period. Development of the comprehensive modal balancing method was undertaken by Giers [49] and by Federn [42]. Both methods and the differences between them are discussed in Chapter 6.

The development of modal balancing was paralleled by a practical trial-and-error procedure which became known as the influence coefficient method. Thearle [40] described it in 1935, and Den Hartog [8] briefly outlined the theory of its application to rigid rotors.

Goodman [50] generalized the application of influence coefficient balancing for flexible rotors in 1962, and the first computer programs for influence-coefficient balancing became available around that time. Tessarzik, Badgley and Anderson [51] contributed to the continuing development of this procedure from 1964 on. The influence coefficient method is essentially computerized balancing performed in an efficiently organized sequence of operations, capable of mathematical optimization.

A wide variety of special devices are described in the patent literature of rotor balancing. Noteworthy are the original machine patents of Martinson (1870), Lawaczeck (1908) and Heymann (1916), the wattmeter concept (1932), Thearle's balancing head (1932), the plane-separation method (1935), electric plane separation (1938), and the electronic measuring technique of Federn (1942). Automatic balancing devices for supercritical operation have been proposed by LeBlanc (1904), Thearle (1932), and others; one such device has been used for domestic washing machines [52].

1.9 References

1. International Organization for Standardization, Draft Document ISO/TC 108/WG 6, "Balancing—Vocabulary," ISO 1925-1974 (E/F), 1974.

2. International Organization for Standarization, Document ISO 1940-1973(E), "Balance Quality of Rotating Rigid Bodies."

3. International Organization for Standardization, Draft Technical Report ISO/TC 108/SCI N16, "The Mechanical Balancing of Flexible Rotors," June 1976.

4. *Orbits*, Bently Nevada Corporation, Minden, Nev., 1970.

5. A. Parmakian, "Vibrations in Hydraulic Turbines," keynote address presented at the Conference on Vibrations in Hydraulic Pumps, Institution of Mechanical Engineers (London), September 1966.

6. B. Sternlicht and N. F. Rieger, "Rotor Bearing Stability," Institution of Mechanical Engineers (London), September 1968, paper presented at the Symposium on Lubrication and Wear, London, England.

7. S. Timoshenko, *Vibration Problems in Engineering*, 3rd ed., Van Nostrand Reinhold, New York, 1955.

8. J. P. Den Hartog, *Mechanical Vibrations*, 4th ed., McGraw-Hill Book Co., New York, 1956.

9. J. B. Wilcox, *Dynamic Balancing of Rotating Machinery*, Pitman & Sons, Ltd., London, 1967.

10. R. A. Eubanks, *Development of Methods and Equipment for Balancing Flexible Rotors*, Armour Research Foundation, IIT Final Report, NOBS contract 78753, March 1962.

11. M. Ye. Levit and V. P. Royzman, *Vibration and Oscillation of Aviation Engine Rotors* (translated from the Russian), Foreign Technology Division, Wright-Patterson Air Force Base, Ohio, 1970.

12. R. M. Little, *The Application of Linear Programming Techniques to Balancing Flexible Rotors*, University Microfilms Internatl., Ann Arbor, Mich.

13. J. R. Kendig, "Current Flexible Rotor-Bearing System Using Computer Simulation," M.S. thesis, Rochester Institute of Technology, Rochester, N.Y., 1975.

14. M. Ya. Kushul' and A. V. Shlyakhtin, "Modal Approach to Balancing with Additional Constraints," *Izvest. AN SSSR, Mekh. Mashinostr.*, No. 2, 1966.

15. F. M. Dimentberg, "Present Status of Flexible Rotor Balancing Theory," *Vestnik Mashinostr.* 11, 7—14 (1964).

16. N. F. Rieger, "Unbalance Response and Balancing of Flexible Rotors in Bearings," *Flexible Rotor-Bearing System Dynamics*, ASME Monograph, New York, 1973.

17. N. F. Rieger, *Rotor-Bearing Dynamics Design Technology, Part 1, State-of-the-Art*, Report AFAPL-TR-65-45, prepared for the Wright Patterson Air Force Base, Ohio, 1965.

18. E. J. Gunter, *Dynamic Stability of Rotor-Bearing System*, NASA SP-113, Office of Technical Utilization, Washington, D.C., 1965.

19. R. E. D. Bishop and A. G. Parkinson, "Vibration and Balancing of Flexible Shafts," *Appl. Mech. Rev.* 21(5), 439—451 (1968).

20. W. Shapiro and J. Rumbarger, "Dynamic Properties of Rolling Element and Fluid-Film Journal Bearings," *Flexible Rotor-Bearing System Dynamics*, ASME Monograph, New York, 1972.

21. R. L. Eshleman and R. A. Eubanks, "On the Critical Speeds of a Continuous Shaft-Disk System," paper presented at ASME Vibrations Conference, Boston, Mass., March 29—31, 1967 (Paper 67-Vibr-9). Also *Trans. ASME, J. Eng. Ind.* 89, 645-652 (1967).

22. R. G. Loewy and V. J. Piarulli, *Dynamics of Rotating Shafts*, SVM-4, DoD Shock and Vibration Information Center, Naval Research Laboratory, Washington, D.C., 1969.

23. F. M. Dimentberg, *Flexural Vibrations of Rotating Shafts*, Butterworth and Co., Ltd., London, England, 1961.

24. A. Tondl, *Some Problems of Rotor Dynamics*, Publishing House of the Czechoslovak Academy of Science, Prague, 1965.

25. I. Laskin, *Study of Industrial Balancing Machines*, Mechanical Technology Inc., Technical Report 66 TR 42, August 19. 1966.

26. I. Jung, "Gustaf DeLaval, The High Speeds and the Gear," DeLa-
    val Memorial Lecture, Stal-Laval Turbine AB., Stockholm, 1968.
27. *Encyclopedia Britannica*, 1967 ed., Vol. 20, "Turbine, Development
    of."
28. W. J. McQ. Rankine, "Centrifugal Whirling of Shafts," *Engineer*,
    26 (Apr. 1868).
29. G. Greenhill, "On the Strength of Shafting When Exposed Both to
    Torsion and To End Thrust," *Proc. Inst. Mech. Eng.*, 3 (No. 6),
    182—225 (1883).
30. C. Chree, "Whirling and Transverse Vibrations of Rotating
    Shafts," *Phil. Mag.*, Series 6, 37, 304 (1904).
31. S. Dunkerley, "Whirling and Vibration of Shafts," *Phil. Trans.
    Royal Soc. (London)*, 185A, 279—360 (1894).
32. O. Föppl, "Das Problem der Laval'schen Turbinewelle," *Der Civil-
    Ingenieur*, 41, 333—342 (1895).
33. W. Kerr, "On the Whirling Speed of Loaded Shafts," *Engineering*,
    51, 150, 296, 386, 410, 420 (Feb. 18, 1916).
34. H. H. Jeffcott, "Lateral Vibration of Loaded Shafts in the Neigh-
    borhood of a Whirling Speed—The Effect of Want of Balance,"
    Phil. Mag., 37, 304—314 (1919).
35. K. Dihrberg, "Schwingungstechnik bei Auswuchtmaschinen,"
    Auswuchttechnik, EED 0, Stand vom 1.1.65, Carl Schenck
    Maschinenfabrik GmbH, Darmstadt, Federal Republic of Ger-
    many, 1965.
36. H. Heymann, Ph.D. dissertation, Darmstadt University, 1916 (see
    Ref. 35 for details).
37. C. R. Soderberg, "Recent Developments in Balancing Machines,"
    Trans. ASME 45, 111 (1923).
38. B. Akimoff, "Balancing Apparatus," *Trans. ASME* 39, 779 (1917).
    Described in A. Stodola, *Steam and Gas Turbines*, Vol. 1,
    McGraw-Hill, New York, 1927, p. 423.
39. B. L. Newkirk, "Shaft Whipping," *General Electric Review*, 27, 169
    (1924).
40. E. L. Thearle, *Dynamic Balancing of Rotating Machinery in the
    Field*, APM-56-19, *Trans. ASME*, 56(10), 745—753 (1934).
41. F. C. Rose, "The Design of Balancing Machines," *Aircraft Eng.*, 17
    149 (1945).
42. K. Federn, *Auswuchttechnik*, EED 0, Carl Schenck Maschinenfa-
    brik GmbH, Darmstadt, Federal Republic of Germany, 1965.
43. L. P. Groebel, "Balancing Turbine-Generator Rotors," *General
    Electric Review*, 56(4), 22—25 (1953). See Also Vol. 59, 2—7
    (1956).
44. A. Meldahl, "Auswuchten Elastischer Rotoren," *A. angew. Math
    Mech.* 34, 8—9 (1954).

45. G. M. L. Gladwell and R. E. D. Bishop, "Vibration of Rotating Shafts Supported in Flexible Bearings," *J. Mech. Eng. Sci.,* 1(3), 195–206 (1959).
46. A. G. Parkinson, "The Vibration and Balancing of Rotating Shafts," Ph.D. dissertation, University of London, 1965.
47. L. S. Moore, "Balancing of Large Turbine Rotors," *Inst. Mar. Eng. Trans.* 81, 105–115 (Apr. 1969).
48. L. S. Moore, "Balancing of Large Turbine Rotors," *Shipping World and Shipbuilder*, p. 313 (Feb. 1969).
49. A. Giers, "Comparison of the Balancing of a Flexible Rotor Following the Methods of Federn-Kellenberger and Moore," *VDI Ber.* 161, 29–34 (1971).
50. T. P. Goodman, "A Least-Squares Method for Computer Balance Corrections," *Trans. ASME, J. Engr. Ind.* Ser. B, 86(3), 273–279 (1964).
51. J. M. Tessarzik, R. H. Badgley, and W. J. Anderson, "Flexible Rotor Balancing by the Exact Point-Speed Influence Coefficient Method," *J. Engr. Ind. Trans. ASME,* Series B, 94(1), 148–158 (1972).
52. A. Gerheardt, Thor Washing Machine, U.S. Pat. 2,420,592, May 13, 1947; see Ref. 8, p. 238.

CHAPTER 2
RIGID-ROTOR DYNAMICS

Nomenclature

a	distance from left bearing to rotor c.g.
$\bar{a}$	eccentricity of c.g.
a_i	eccentricity of disk c.g.
A	cross-sectional area
A_i	area of ith cross section
b	distance from right bearing to rotor c.g.
e	2.71828 ...
E	modulus of elasticity
f_C	critical whirl frequency, Hz
f_T	translatory critical whirl frequency, Hz
F	centrifugal force
g	gravitational acceleration
H	effective radius of gyrotron
i	$\sqrt{-1}$
I	second moment of area
K	stiffness of shaft end supports
L	rotor length
M	rotor mass
N_C	critical whirl speed
N_T	translatory critical whirl speed
$\mathbf{R}$	whirl radius vector
R	whirl radius at shaft centroid
$R_T^{\bullet}$	dimensionless translatory whirl radius
$_eR_{bb}^{\bullet}, \, _eR_{cb}^{\bullet}$	dimensionless whirl radius of shaft ends
$eR_C^{\bullet}$	dimensionless whirl radius of shaft ends in conical mode
$eR_T^{\bullet}$	dimensionless whirl radius of shaft ends in translatory mode
$_gR_{bb}^{\bullet}, \, _gR_{cb}^{\bullet}$	dimensionless conical whirl radius at bearings
$_gR_C^{\bullet}$	dimensionless whirl radius of shaft center in conical mode
$_gR_T^{\bullet}$	dimensionless whirl radius of shaft center in translatory mode

37

38

t	time
w	specific weight
W	weight of disk
x, y	coordinate directions
z	axial distance along shaft
γ	time-dependent complex whirl angle
Γ	complex whirl angle amplitude
θ	time-dependent whirl angle
ν	whirl frequency
π	3.14159 ...
ϕ	time-dependent whirl angle
ω	shaft speed, rad/s
ω_c	critical whirl frequency, rad/s
ω_T	translatory critical whirl frequency, rad/s

CHAPTER 2
RIGID-ROTOR DYNAMICS

2.1 Dynamic Properties of Rigid Rotors

The response of a rigid rotor to a dynamic forcing is most meaningfully expressed in terms of the natural modes of the rotor system. Rigid rotors in flexible supports have two such modes: translatory whirling and conical whirling. The rotor experiencing residual unbalance forces and moments responds with displacements involving combinations of these rigid-body modes. Consider the simple rigid-rotor system in Fig. 2.1. If the bearings have identical horizontal and vertical dynamic properties, this system will have only two whirl modes, translatory and conical; if however, the bearings have dissimilar horizontal and vertical stiffnesses, the rotor will have four whirl modes and four corresponding critical whirl frequencies. The rotor can become resonant with its unbalance force, in each of these four modes.

$$\text{Mass } M \sim \frac{W}{g}$$

$$\text{Translatory inertia } I_T = \frac{M}{12}\left(3R^2 + L^2\right)$$

$$\text{Polar inertia } I_P = \frac{M}{2}R^2$$

$$\text{Inertia } I = I_T - I_P \text{ (synchronous whirling)}$$
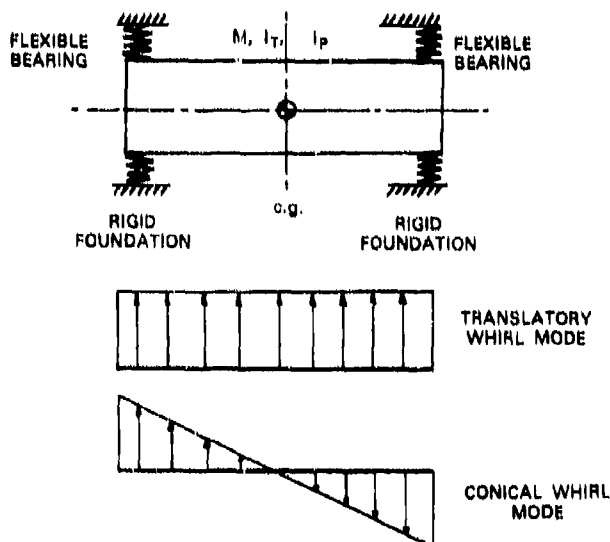
Fig. 2.1. Whirl modes for a rigid cylindrical rotor
in flexible bearings

A rotor is said to whirl when the c.g. of any cross section traces an orbit during rotation instead of remaining at a fixed point. Unbalance whirling occurs in synchronism with the rotational frequency of the shaft. Other types of whirling are also possible; these whirls may include unstable and asynchronous whirls [1-3].

The critical frequencies of any rotor system are the natural frequencies of the system. This means that under rotating conditions these frequencies are influenced by the rotatory inertia of the rotor and by the gyroscopic effect exerted on the polar inertia of the rotor by out-of-plane forces. When the rotational speed coincides with a critical frequency of the system, a condition of resonance develops between the rotating unbalance excitation and the critical frequency of the system. Residual unbalance then tends to excite the rotor into large-amplitude whirl motions. In practice, such motions are usually bounded by system damping effects. They may also be otherwise restrained by bearings or seals. It is well known that any resonant speed represents a potentially dangerous operating condition for rotating machinery. This danger can be removed by balancing the rotor and also by choosing suitable system parameters, such as supports with properties that allow the rotor to operate in speed ranges removed from its critical speeds.

2.2 Rotor Systems

The whirl amplitude of an unbalanced rotor depends on the dynamic properties of the rotor in its supporting structure (i.e., bearings, casing) and on the magnitude and distribution of the residual unbalance within the rotor. For any mechanical equipment, the dynamic response amplitude and the transmitted vibrations are strongly influenced by interaction between the rotor, its bearings, the casing, and the foundation. Together these components constitute a mechanical system. This chapter discusses the dynamic response of rigid rotors to unbalance forces imposed during operation.

The most significant rotor-system properties for studies of machinery response to unbalance forces are

1. Rotor mass, elastic, and damping properties
2. Bearing mass, elastic, and damping properties
3. Machine casing and foundation mass, elastic properties, and damping interaction with the environment
4. Rotor unbalance magnitude, orientation, and axial distribution
5. System critical speeds and their variation with bearing and support stiffness, operating speed, machine load, temperature, etc.

    6. Variation of rotor response amplitude with speed, particularly at bearing and seal locations

    7. Variation of bearing-transmitted force with speed and load

    8. Variation of foundation force with speed and load

    9. Instability threshold speed of the rotor system.

The first four items are basic mechanical properties that constitute any rotor system. The next five items are important dynamic properties of the rotor system; they are related to the system operating conditions, such as speed and load. Before the functions of these five system conditions are described, dynamic properties 1 through 4 will be discussed in greater detail.

2.3 Rotor System Properties

    This section discusses the factors affecting dynamic properties of the rotor system. Most of the important terms used are defined in ISO 1925 (1974), "Balancing Vocabulary." Any unbalanced rigid rotor can be described in terms of the properties listed in Table 2.1. Expressions for mass, inertia, and radius of gyration for several typical rotor sections are given in Table 2.2 [4].

Bearings

    Most rotors are supported in either rolling-element bearings or in fluid-film bearings. Both types of bearing possess static and dynamic properties. As used here, the term *static* properties means properties that depend on steady load conditions and constant speed, in a thermally stable environment, such as load capacity and operating oil temperature.

    The static properties of rolling-element bearings are governed by the tendency for the race to deform elastically at low speeds and by centrifugal force effects at high speeds. Most rolling-element bearings are limited to long-term operation below 77°C unless a special lubricant is used or unless provision is made for externally cooling the race. Load capacities and static design considerations have been discussed by Palmgren [5] and Harris [6]. Additional refr ences are given by Shapiro and Rumbarger [7].
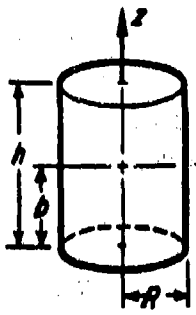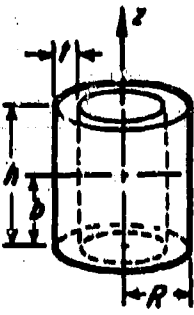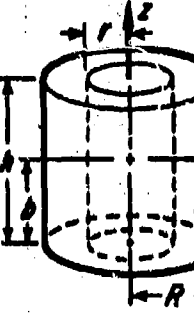
    The static properties of fluid-film bearings are determined by the bearing type (externally pressurized, self-acting; liquid- or gas-lubricated), by bearing geometry (plain cylindrical, tilting-pad, etc.), and by load, speed, structural and lubricant properties, and the operating environment (temperature, pressure, etc.). The governing dimensionless parameters are the Sommerfeld number of operation, the bearing length-to-diameter (L/D) ratio, and the operating Reynolds number

Table 2.1. Dynamic properties of unbalanced rigid rotors

Property	Symbol	Description
Mass	M	Acts at rotor c.g.
Inertia, polar	I_P	Acts at rotor c.g.; causes gyroscopic effect
Inertia, transverse	I_T	Acts at rotor c.g.; causes translatory inertia effect
Inertia, effective	I	Acts at rotor c.g.; $I = I_T - I_P$ for synchronous unbalance whirling*
Radius of gyration	H	Effective c.g. radius for rotor mass
Length	L	Rotor length between bearings
Location of c.g.	Z_g	Location of c.g. from reference origin, usually at the centerline of a bearing
Residual unbalance force	F	Acts of rotor c.g.
Residual unbalance moment	M	Acts about rotor c.g.
Location of unbalance planes	Z_1, Z_2	Distance from c.g. or other reference datum
Balance weight		
Plane 1	W_1	Acts radially in balance plane 1
Plane 2	W_2	Acts radially in balance plane 2
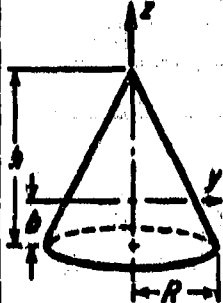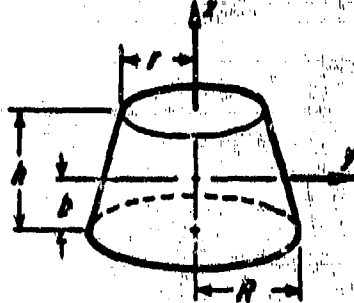
*$I = I_T - \frac{\omega}{\nu} I_P$ for non-synchronous whirling, where ω is the rotational speed and ν is the whirl frequency.

Table 2.2 Geometric Properties of Solids [4]*

		Cylinder	Cylindric Shell	Hollow Cylinder
Volume (cu in.)		$V = \pi R^2 h$	$V = 2\pi R h t$	$V = \pi (R^2 - r^2) h$
Distance to cg (in.)		$b = \frac{1}{2} h$	$b = \frac{1}{2} h$	$b = \frac{1}{2} h$
Moments of Inertia (in.-lb sec²)	Axial	$I_z = \frac{1}{2} m R^2$	$I_z = m R^2$	$I_z = \frac{1}{2} m (R^2 + r^2)$
	Transverse	$I_y = \frac{1}{2} I_z + \frac{1}{12} m h^2$	$I_y = \frac{1}{2} I_z + \frac{1}{12} m h^2$	$I_y = \frac{1}{2} I_z + \frac{1}{12} m h^2$
Radii of Gyration (in.)	Axial	$H_z = \frac{R}{\sqrt{2}}$	$H_z = R$	$H_z = \sqrt{\frac{R^2 + r^2}{2}}$
	Transverse	$H_y = \frac{1}{2} \sqrt{R^2 + \frac{1}{3} h^2}$	$H_y = \sqrt{\frac{1}{2} R^2 + \frac{1}{12} h^2}$	$H_y = \frac{1}{2} \sqrt{R^2 + r^2 + \frac{1}{3} h^2}$
Moment Ratio		$\frac{I_z}{I_y} = \frac{2}{1 + \frac{h^2}{3R^2}}$	$\frac{I_z}{I_y} = \frac{2}{1 + \frac{h^2}{6R^2}}$	$\frac{I_z}{I_y} = \frac{2}{1 + \frac{h^2}{3(R^2 + r^2)}}$
Critical Height (in.)		$h = R\sqrt{3}$	$h = R\sqrt{6}$	$h = \sqrt{3(R^2 + r^2)}$
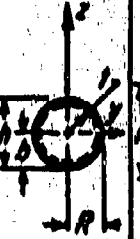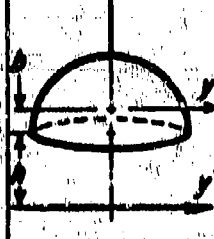
*Used by permission of Machine Design Magazine.

Table 2.2 (Cont'd) Geometric Properties of Solids [4]*

Right Cone	Frustrum of Cone
$V = \dfrac{1}{3}\pi R^2 h$	$V = \dfrac{1}{3}\pi (R^2 + Rr + r^2)h$
$b = \dfrac{1}{4}h$	$b = \dfrac{(R^2 + 2Rr + 3r^2)h}{4(R^2 + Rr + r^2)}$
$I_z = \dfrac{3}{10}mR^2$	$I_z = \dfrac{3}{10}m\dfrac{R^5 - r^5}{R^3 - r^3}$
$I_y = \dfrac{1}{2}I_z + \dfrac{3}{80}mh^2$	$I_y = \dfrac{1}{2}I_z + \dfrac{3}{80}m\dfrac{(R + r)^4 + 4R^2r^2}{(R^2 + Rr + r^2)^2}h^2$
$H_z = R\sqrt{\dfrac{3}{10}}$	$H_z = \sqrt{\dfrac{3(R^5 - r^5)}{10(R^3 - r^3)}}$
$H_y = \sqrt{\dfrac{3R^2}{20} + \dfrac{3h^2}{80}}$	$H_y = \sqrt{\dfrac{3(R^5 - r^5)}{20(R^3 - r^3)} + \dfrac{3(R + r)^4 + 4R^2r^2}{80(R^2 + Rr + r^2)^2}h^2}$
$\dfrac{I_z}{I_y} = \dfrac{3}{1 + \dfrac{h^2}{4R^2}}$	$\dfrac{I_z}{I_y} = \dfrac{2}{1 + \dfrac{(R - r)^5(R + r)^4 + 4R^2r^2}{4(R^3 - r^3)(R^5 - r^5)}h^2}$
$h = 2R$	$h = \dfrac{2}{R - r}\sqrt{\dfrac{(R^3 - r^3)(R^5 - r^5)}{(R + r)^4 + 4R^2r^2}}$
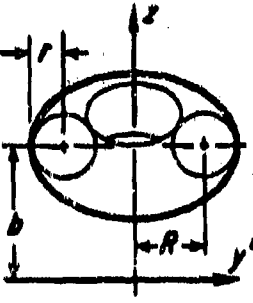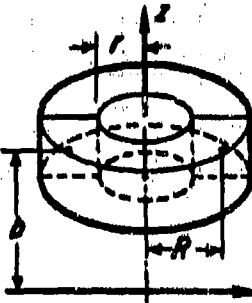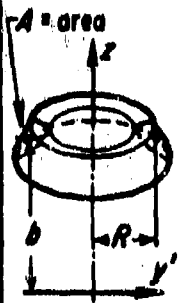
*Used by permission of Machine Design Magazine.

Table 2.2 (Cont'd) Geometric Properties of Solids [4]*

Sphere	Spheric Shell	Hollow Sphere	Ellipsoid	Hemisphere
$V = \frac{4}{3}\pi R^3$	$V = 4\pi R^2 t$	$V = \frac{4}{3}\pi(R^3 - r^3)$	$V = \frac{4}{3}\pi ABC$	$V = \frac{2}{3}\pi R^3$
$b = R$	$b = R$	$b = R$	$b = C$	$b = \frac{3}{8}R$
$I_z = \frac{2}{5}mR^2$	$I_z = \frac{2}{3}mR^2$	$I_z = \frac{2}{5}m\frac{R^5 - r^5}{R^3 - r^3}$	$I_z = \frac{1}{5}m(A^2 + B^2)$	$I_z = \frac{2}{5}mR^2$
$I_y = I_z$	$I_y = I_z$	$I_y = I_z$	$I_y = \frac{1}{5}m(A^2 + C^2)$	$I_y = \frac{1}{2}I_z + \frac{19}{320}mR^2$
$H_z = R\sqrt{\frac{2}{5}}$	$H_z = R\sqrt{\frac{2}{3}}$	$H_z = \sqrt{\frac{2(R^5 - r^5)}{5(R^3 - r^3)}}$	$H_z = \sqrt{\frac{A^2 + B^2}{5}}$	$H_z = R\sqrt{\frac{2}{5}}$
$H_y = H_z$	$H_y = H_z$	$H_y = H_z$	$H_y = \sqrt{\frac{A^2 + C^2}{5}}$	$H_y = \frac{R}{8}\sqrt{\frac{83}{5}}$
$\frac{I_z}{I_y} = 1$	$\frac{I_z}{I_y} = 1$	$\frac{I_z}{I_y} = 1$	$\frac{I_z}{I_y} = \frac{A^2 + B^2}{A^2 + C^2}$	$\frac{I_z}{I_y} = \frac{128}{83}$
$h \cong 2R$	$h \cong 2R$	$h \cong 2R$	$h = 2B = 2C = 2A$	$h = 0$

*Used by permission of Machine Design Magazine.

Table 2.2 (Cont'd) Geometric Properties of Solids [4]*

Offset Torus	Offset Hollow Cylinder	Offset Annulus
		A = area
$V = 2\pi^2 R r^2$	$V = \pi(R^2 - r^2)h$	$V = 2\pi R A$
$b \cong b$	$b \cong b$	$b \cong b$
$I_a = m\left(R^2 + \dfrac{3}{4}r^2\right)$	$I_a = \dfrac{1}{2}m(R^2 + r^2)$	$I_a = mR^2$
$I_{y'} = \dfrac{1}{2}I_a + m\left(b^2 + \dfrac{r^2}{4}\right)$	$I_{y'} = \dfrac{1}{2}I_a + m\left(b^2 + \dfrac{h^2}{12}\right)$	$I_{y'} = \dfrac{1}{2}I_a + mb^2$
$H_z = \dfrac{1}{2}\sqrt{4R^2 + 3r^2}$	$H_z = \sqrt{\dfrac{R^2 + r^2}{2}}$	$H_z = R$
$H_{y}' = \sqrt{\dfrac{R^2}{2} + \dfrac{3r^2}{8} + b^2}$	$H_{y}' = \dfrac{1}{2}\sqrt{R^2 + r^2 + \dfrac{1}{3}h^2 + 4b^2}$	$H_{y}' = \sqrt{\dfrac{R^2}{2} + b^2}$
$\dfrac{I_a}{I_{y'}} = \dfrac{2 + \dfrac{3r^2}{2R^2}}{1 + \dfrac{5r^2}{2R^2} + \dfrac{2b^2}{R^2}}$	$\dfrac{I_a}{I_{y'}} = \dfrac{2 + \dfrac{2r^2}{R^2}}{1 + \dfrac{r^2}{R^2} + \dfrac{h^2}{3R^2} + \dfrac{4b^2}{R^2}}$	$\dfrac{I_a}{I_{y'}} = \dfrac{2}{1 + \dfrac{2b^2}{R^2}}$
$b = \sqrt{\dfrac{R^2}{2} + \dfrac{r^2}{8}}$	$b = \dfrac{1}{2}\sqrt{R^2 + r^2 - \dfrac{1}{3}h^2}$	$b = \dfrac{R}{\sqrt{2}}$

*Used by permission of Machine Design Magazine.

if the lubricant flow is turbulent. The static design of externally pressurized bearings has been discussed by Rippel [8], Wilcock and Booser [9], and others. The design of self-acting bearings has also been discussed by these authors, and by Raimondi and Boyd [10], Warner [11], Lund [12], and others. Bearing technology has an extensive literature; the above references provide an introduction to this subject.

The dynamic properties of bearings are those characteristics that directly influence the response of the rotor system, with time. Bearing flexibility and damping both affect the response of rigid rotors to unbalance forces and to impulsive external loads. For small dynamic motions, these bearing properties are commonly expressed in terms of stiffness and damping coefficients. For rolling-element bearings,

$$F_x(t) = K_x X + B_x \dot{X}, \text{ where } \dot{X} = \frac{dx}{dt};$$

and

$$F_y(t) = K_y Y + B_y \dot{Y}, \text{ where } \dot{Y} = \frac{dy}{dt}.$$

For fluid-film bearings,

$$F_x(t) = K_{xx} X + K_{xy} Y + B_{xx} \dot{X} + B_{xy} \dot{Y}$$

and

$$F_y(t) = K_{yx} X + K_{yy} Y + B_{yx} \dot{X} + B_{yy} \dot{Y}.$$

The terms used in these equations are defined as follows:

$X, \dot{X}$ — time-dependent displacement and velocity in the X direction

$Y, \dot{Y}$ — time-dependent displacement and velocity in the Y direction

K_x, K_{xx} — stiffness coefficients relating force to displacement in the X direction

K_y, K_{yy} — stiffness coefficients relating force to displacement in the Y direction

K_{xy}, K_{yx} — stiffness coefficients relating force in one direction (X, Y) to displacement in the normal direction (Y, X)

B_x, B_{xx} — damping coefficients relating force to velocity in the X direction

B_y, B_{yy} = damping coefficients relating force to velocity in the X direction

B_{xy}, B_{yx} = damping coefficients relating force in one direction (X, Y) to velocity in the normal direction (Y, X).

The force-displacement properties of both rolling-element and fluid-film bearings are nonlinear, which indicates that the stiffness dF/de is variable with displacement (Fig. 2.2). Fortunately, large-amplitude journal motions in bearings typically occur only briefly (transition through critical speed with low damping), under conditions of machine distress (rotor instability, instantaneous unbalance, or excessive transient). In most instances, journal orbits about the static equilibrium position are small (Fig. 2.3). This allows the uncoupled bearing equations to be linearized, with use of the constant coefficients indicated above. The same is true of bearing damping, which is also frequently linearized to simplify discussion and analysis.

(a) Rolling-element bearing

(b) Fluid-film bearing
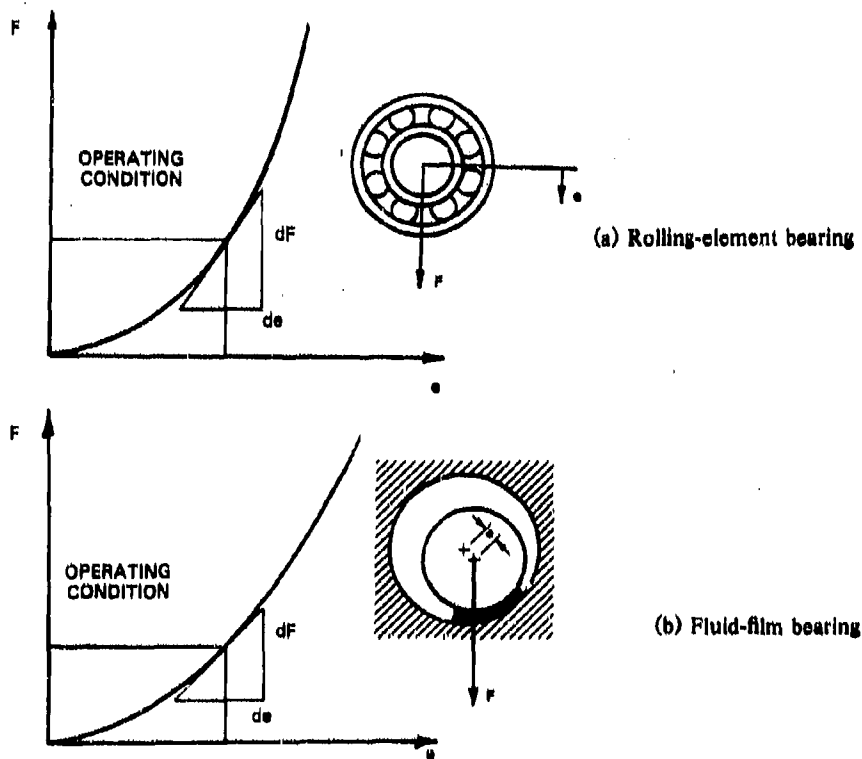
Fig. 2.2. Typical load-displacement curves for rolling-element and fluid-film bearings
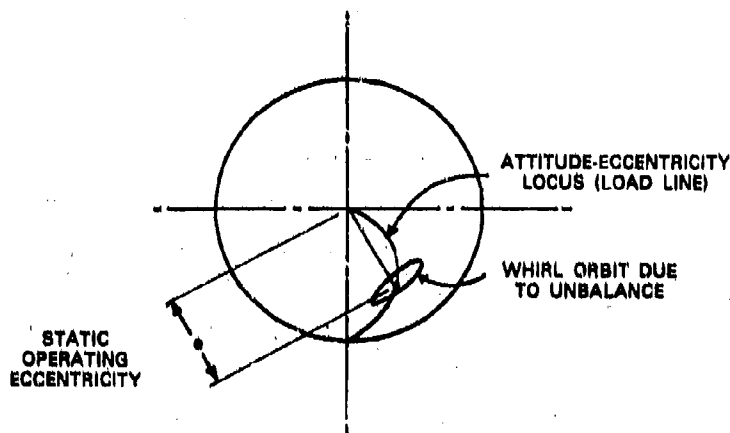
Fig. 2.3. Unbalance whirl orbit about static equilibrium position
for fluid-film journal bearings

Machine Casing and Foundation

Most rotors are supported in bearings mounted in a massive casing on some mass-elastic foundation. The effect of the casing and foundation on the dynamics of the rotor may be significant if the casing has natural frequencies that lie in the same region as those of the rotor and bearing system. In such cases the mass-elastic properties of the support system must also be considered in examining the dynamic properties of the machine. It is usual to linearize the stiffness and damping properties of the casing. However, foundation dynamics is often a complex, specialized area that should be approached with caution. For details of the dynamic interaction of soil and foundation, see Ref. 13. For present purposes, where foundation dynamic effects are referred to, they will be thought of as being made up of small-amplitude linear motions about a static mean position.

Rotor Unbalance

The two principal causes of rotor unbalance are local random mass eccentricities of the rotor c.g. along its length, and any distortion of the rotor elastic axis that may arise from differential thermal expansion, slippage of shrink fits, and so on. A comprehensive listing of sources of unbalance is given in Table 1.1.

In a rigid rotor, the cumulative effect of random c.g. eccentricities is felt as a single unbalance force that acts at the rotor c.g.; its magnitude is calculated as

$$F = \frac{W}{g} \Omega^2 a,$$

where

$$a = \frac{\int A_i a_i \, dz}{\int A_i \, dz}$$

is the effective unbalance radius acting about the rotor c.g. due to the sum of the moments of the elemental rotor sections, as shown in Fig. 2.4. In practical circumstances, the magnitudes and the orientation of the unbalance force and unbalance couple are seldom known in advance, though the effect they create is routinely determined at the balance planes by measurement in a balancing machine. The orientation of these effective unbalance forces to some arbitrarily chosen reference plane in the rotor is likewise determined as part of the balancing process. For the present discussion, the effect of unbalance is represented as an equivalent force and couple about the c.g. of the rigid rotor. This makes it possible to determine the effect of a prescribed nominal unbalance condition (e.g., 1.0 oz-in.) at the rotor c.g. on the rotor response. Such sensitivity analysis provides useful insight into the possible unbalance response of the rotor in its supports.

(a) Random distribution of unbalance in rigid rotor

(b) Equivalent unbalance force F and couple M acting at rotor c.g.
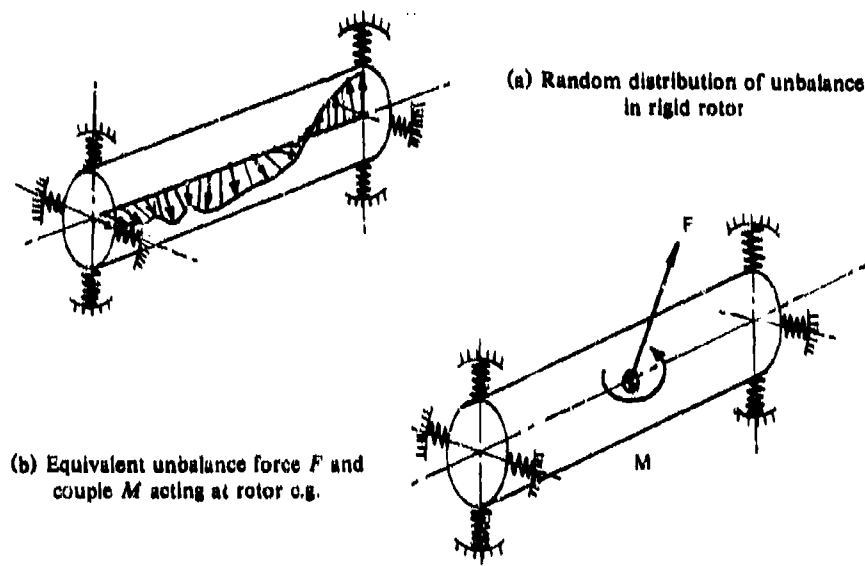
Fig. 2.4. General unbalance conditions induced by equivalent c.g. force and moment

2.4 Dynamic Modeling of Rotor Systems

Rotor properties, bearing properties, and casing and foundation properties may influence the response of the total machine system to unbalance. Figure 2.5 shows a typical high-speed grinding machine assembly. An understanding of the dynamic behavior of this or any other rotating mechanical system can be obtained by developing a representative model of the rotor system that includes numerical values of the critical parameters listed in the previous section. In practice, such dynamic models are now routinely developed during the design of most high-speed rotating equipment. The data come from rotor-system drawings, from bearing design charts (or computer programs), and from other system specifications, such as dynamic support properties (foundation impedance). The degree of refinement used in the model is arbitrary; it depends on the immediate need and on the extent of available data.
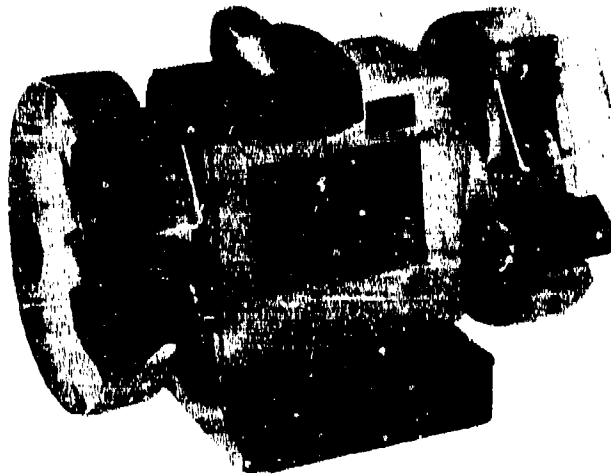
Fig. 2.5. High-speed motor-driven grinding machine (courtesy of Black and Decker Corp.)

Consider now the two rotor-system models shown in Fig. 2.6; both models represent the dynamic properties of the high-speed grinder in Fig. 2.5. Both models contain all of the parameters mentioned previously, but the amount of detail is obviously much different. The first model (Fig. 2.6) is a simple representation that could be used to estimate the two rigid-body critical speeds of the grinder and the response to unbalance. It assumes that the rotor is rigid, that the bearings are

flexible with low damping, and that the foundation is rigid (no dynamic interaction). The second model would be used for computer analysis of the high-speed grinder. It contains much more detail, a burden readily handled by the computer. This model does not assume that the rotor is rigid, though it may be. Both bearing stiffnesses and damping effects are considered in more detail (though still linear), and account is taken of bearing-support flexibility. Computer calculation of both critical speeds and unbalance response has been shown to be a reliable technique which provides valuable guidance to rotating machinery designers.

(a) Representation of high-speed grinder as a rigid rotor

(b) Flexible rotor-bearing system for high-speed grinder
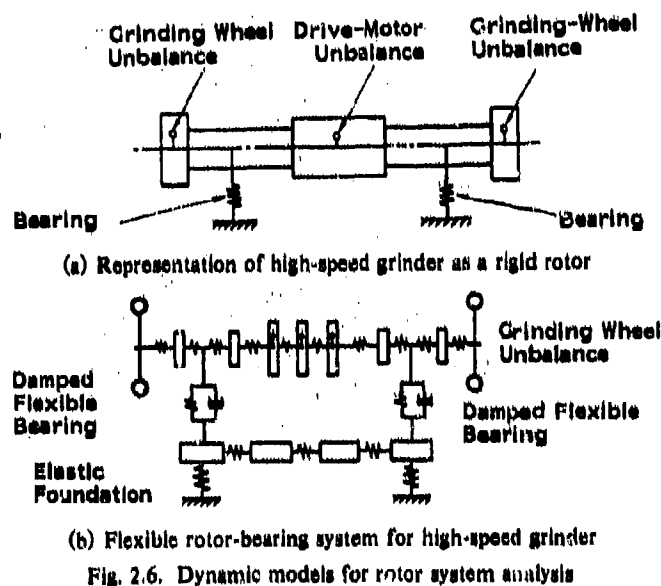
Fig. 2.6. Dynamic models for rotor system analysis

2.5 Critical Frequencies and Critical Speeds

When a natural mode of a rotor system is excited by some harmonic force applied at its natural frequency, a condition of resonance exists. This condition is often accompanied by large modal amplitudes of vibration. In general, the natural frequencies of a rotor system are dependent on speed because of gyroscopic coupling between the coordinate motions. For rotating machinery, the natural frequencies are often called critical frequencies, and each rotor system possesses several such frequencies. Any critical frequency can be excited into resonance, given a suitable source of excitation, although occasionally there may be other sources of asynchronous excitation (e.g., fan-guide vane excitation or reverse-whirl gear excitation) that will excite some less common form of whirling.

The calculation of critical frequencies for rigid-rotor systems is discussed in the remainder of this chapter. In certain instances, only the synchronous critical frequency is determined because of its practical importance. Simple cases using modal separation are discussed wherever possible. The following factors are examined.

Section	Rotor system investigated	Results observed
2.6	Midspan symmetry; identical bearings	Mass mode and inertial mode are independent and separable. Simple natural frequency expressions exist.
2.7	Offset rotor c.g.; identical bearings	Modes coupled
2.8	Midspan c.g.; different end bearing stiffnesses, identical coordinate stiffnesses	Modes coupled; biquadratic frequency equation
2.9	Combination of the two systems listed above; offset rotor c.g.; different end bearing stiffnesses	Modes coupled; biquadratic frequency equation
2.10	Midspan c.g.; identical bearings, dissimilar bearing coordinate stiffnesses	Modes separable; four natural frequencies, two for each coordinate stiffness direction
2.11	Midspan symmetry; dissimilar bearings dissimilar bearing coordinate stiffnesses	Modes coupled; four natural frequencies corresponding to coordinate stiffnesses; frequency determinant
2.12	Offset c.g.; dissimilar bearings, dissimilar coordinate bearing stiffnesses.	Modes coupled

A numerical example is given in each case studied to illustrate specific features. It should be noted that the effects of damping are not included in the rigid-rotor critical speed analyses that follow; they are, however, discussed in Sections 2.13 through 2.16. The results are more applicable to practical systems involving rigid rotors in rolling-element bearings or rigid rotors in fluid-film bearings with flexible, undamped bearing pedestals than to highly damped journal bearing systems. This has been done mainly to demonstrate the rotor-dynamics principles involved.

2.6 Critical Speeds

A critical speed of a rotor system is defined as any rotational speed of the rotor or rotating element at which resonance occurs in the system. Critical speeds are dynamic properties of the rotor system. They occur when some harmonic force becomes resonant (coincides in frequency) with a natural frequency of the system. Only radial whirl motions of the rotor in its supports caused by rotor unbalance are considered here.

Each natural frequency of a rotor system has a particular mode shape. At a critical speed, the harmonic force from centrifugal unbalance excites the corresponding mode of the system, causing the rotor to "whirl" in its supports in this mode shape, in synchronism with the rotor speed. Whirling often causes large rotor dynamic amplitudes, large transmitted vibrations, and possible component failure. It is customary practice to calculate the critical speeds and mode shapes of any new rotating equipment; such calculations are also the first step in the diagnosis of any vibration problems in rotation machinery.

The critical speeds of rotor-bearing systems are dependent on speed for the following reasons.

1. Gyroscopic stiffening of the rotor increases with speed. At zero speed, all gyroscopic effects are zero. The rotor translatory inertia affects the natural frequencies of the system. At operating speed, the inertial effect of any rigid component is $(I_P - I_T)\omega^2$ under synchronous excitation at frequency ω; here, I_P is polar inertia and I_T is translatory inertia.

2. Stiffness and damping properties of fluid-film bearings vary with speed, and squeeze-film vibration damping properties vary with forcing frequency. As most classes of rotating machinery incorporate either one or both of the above effects, it is evident that critical speed calculations for general rotor systems must include consideration of both effects to ensure accurate calculation of critical speeds. For rigid rotors this problem is simplified by the absence of rotor flexibility. Nonetheless, the above requirements still apply.

2.7 Simple Rigid Rotor in Flexible Supports

Figure 2.7a shows a rigid cylindrical rotor supported in flexible bearings with the rotor c.g. midway between the bearings. Both bearings have identical stiffness properties, and the stiffnesses of both bearings are identical in both the x- and the y-coordinate directions. The system has two natural whirl modes, translatory and conical, as shown in Figs. 2.7b and 2.7c. If damping effects are neglected, the critical frequencies of these two modes can be calculated by first recognizing that these modes are uncoupled because of the symmetry of the system.

SYMMETRICAL ROTOR
c.g. AT MIDSPAN
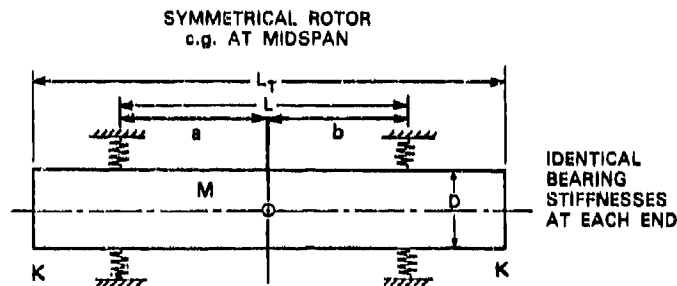
(a) Rigid rotor in symmetrical bearings
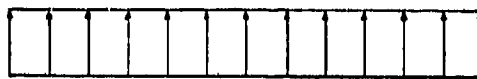
(b) Translatory whirl mode
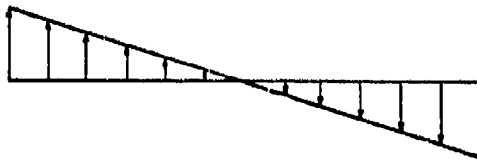
(c) Conical whirl mode

Fig. 2.7. Rotor with uncoupled rigid whirl modes

Translatory Critical Frequency

First consider the purely translatory motions of the rotor shown in Fig. 2.7b. The equations of small-displacement free motions are

$$M\ddot{X} + 2\,KX = 0$$

$$M\ddot{Y} + 2\,KY = 0$$

where

X, Y are time-dependent coordinate displacements
M is the rotor mass
K is bearing radial stiffness.

As the whirl orbit is circular in this case, the coordinate motions can be combined into a single whirl vector $\mathbf{R}$ of radius

$$\mathbf{R} = X + i\,Y$$

where

$$i = \sqrt{-1}$$

$$X = x\, e^{i\omega t}$$

$$Y = y\, e^{i\omega t}.$$

Substituting gives

$$M\ddot{R} + 2KR = 0.$$

A solution for harmonic motions at the frequency of rotation ω can be obtained by substituting $R = re^{i\omega t}$ in the above expression, r being the magnitude of the whirl radius. A nontrivial solution for ω does not permit $re^{i\omega t}$ to be zero, and therefore

$$2K - M\omega^2 = 0.$$

This requires that

$$\omega^2 = \frac{2K}{M} = \omega_c^2,$$

that is,

$$\omega_c = \omega_T = \sqrt{\frac{2K}{M}} \quad (\text{rad/s}),$$

where ω_T is the circular critical frequency of the free transverse vibrations for the simple symmetrical rotor in flexible supports. This can be expressed as

$$f_T = \frac{1}{2\pi} \sqrt{\frac{2K}{M}} \quad (\text{Hz})$$

$$N_T = \frac{60}{2\pi} \sqrt{\frac{2K}{M}} = 9.55 \sqrt{\frac{2K}{M}} \quad (\text{rpm}).$$

If the system is operated at this rotational speed with an unbalance force acting, the rotor whirl amplitude will grow toward an infinite value unless otherwise restrained, e.g., by system damping.

Conical Critical Frequency

The conical whirl motions shown in Fig. 2.7c are influenced by gyroscopic torques that arise from angular momentum changes. Such changes result from the small angular displacements θ and ϕ shown in

Fig. 2.8 for a typical cylindrical rotor element. In accordance with the right-hand rule, the direction of the torque vectors shown is determined by the θ, ϕ displacements, which cause the torque vector to move into the spin vector as shown.
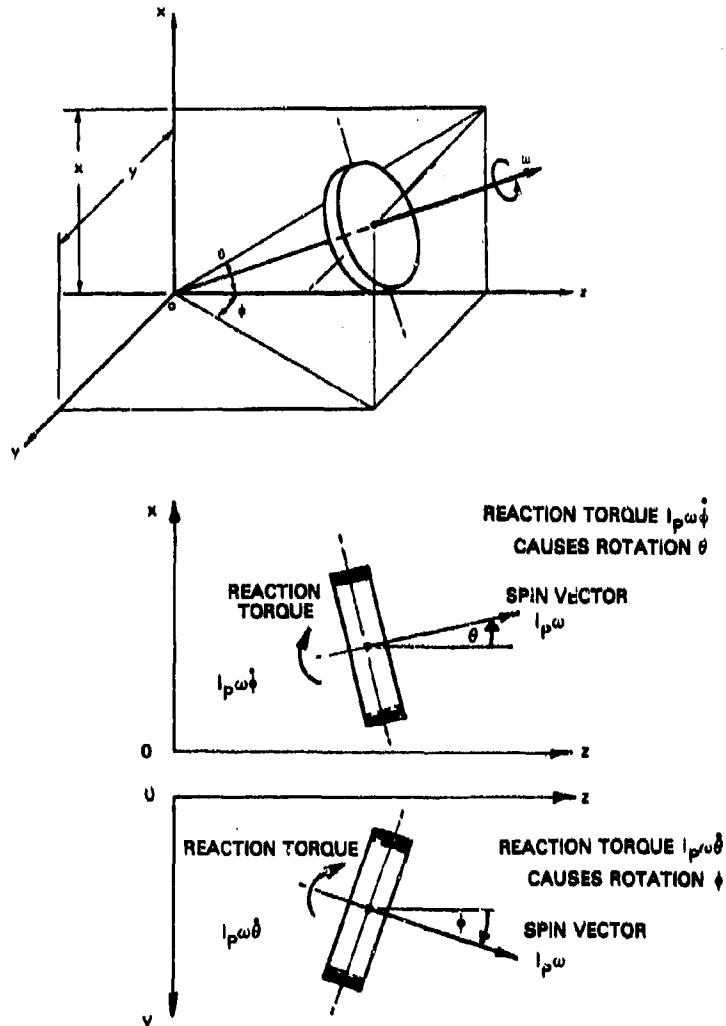
Fig. 2.8. Coordinate geometry and gyroscopic moments acting on a massive rotating disk

The cylindrical rotor section in Fig. 2.7c has both translatory iner-
tia I_T and polar inertia I_P. For small-amplitude harmonic motions, the
equations of free undamped conical whirling are

$$I_T\ddot{\theta} + \frac{1}{2}KL^2\theta + I_P\omega\dot{\phi} = 0$$

and

$$I_T\ddot{\phi} + \frac{1}{2}KL^2\phi - I_P\omega\dot{\theta} = 0,$$

where

K = bearing stiffness
L = rotor length
I_T = translatory inertia for the rotor about its c.g.
I_P = polar inertia of the rotor about its c.g.
θ = time-dependent whirl angle in the X, Z plane
ϕ = time-dependent whirl angle in the Y, Z plane.

To solve the above expressions, write

$$\gamma = \theta + i\phi.$$

Substituting in the equations of motion gives

$$I_T\ddot{\gamma} - iI_P\omega\dot{\gamma} + \frac{1}{2}KL^2\gamma = 0.$$

To solve for harmonic motions at rotational frequency ω, set

$$\gamma = \Gamma e^{i\omega t}.$$

where

γ = time dependent complex whirl angle

Γ = complex whirl angle amplitude

For synchronous whirling, $\dot{\gamma} = \omega$, and we may write

$$I = I_T - I_P.$$

Substituting gives

$$\left(\frac{1}{2}KL^2 - I\omega^2\right)\Gamma e^{i\omega t} = 0.$$

A nontrivial solution for the speed ω that satisfies this expression requires that

$$\frac{1}{2} KL^2 - I\omega^2 = 0.$$

Solving this expression gives the critical frequency for conical whirling,

$$\omega_C = \left[\frac{KL^2}{2I}\right]^{1/2} \quad \text{(rad/s)}$$

or

$$f_C = \frac{1}{2\pi}\left[\frac{KL^2}{2I}\right]^{1/2} \text{ Hz}; \quad N_C = 9.55\left[\frac{KL^2}{2I}\right]^{1/2} \text{ (rpm)}.$$

This expression allows the conical critical speed of the symmetrical rotor system shown in Fig. 2.7 to be calculated.

Sample Calculation 1

The steel cylindrical rotor shown in Fig. 2.7 is 3.0 in. in diameter and 8.0 in. long. The rotor is mounted on two bearings of radial stiffness $K_x = K_y = 10^5$ lb/in. with a span of 6 in., supported on a rigid foundation. Find the translatory critical speed and conical critical speed of the system. Specific weight w of steel is 0.283 lb/in.^{3}.

The rotor weight is

$$W = \frac{\pi}{4} D^2 L_T \, w = \frac{\pi}{4} (3)^2(8)(0.283) = 16.0 \text{ lb.}$$

The mass of the rotor is

$$M = \frac{W}{g} = \frac{16.0}{386.4} = 0.0414 \quad \text{lb-s}^2/\text{in.}$$

The translatory critical speed is

$$\omega_T = \left[\frac{2K}{M}\right]^{1/2} = \left[\frac{2 \times 10^5}{0.0414}\right]^{1/2} = 2198 \text{ rad/s}$$

$$f_T = 349.8 \text{ Hz} = 20,989 \text{ rpm.}$$

The translatory critical speed occurs at 20,989 rpm.
    The effective inertia for synchronous whirl is

$$I = I_T - I_P = \frac{1}{12} M\left[L_T^2 - 3\left(\frac{D}{2}\right)^2\right]$$

$$= \frac{0.0414}{12} [(8)^2 - 3(1.5)^2]$$

$$= 0.1975 \text{ lb-in.-s}^2$$

$$\omega_C = \left(\frac{KL^2}{2I}\right)^{1/2} = \left[\frac{(10^5)(6)^2}{(2)(0.1975)}\right]^{1/2} = 3019 \text{ rad/s}$$

and

$$f_C = 480.5 \text{ Hz} = 28,829 \text{ rpm.}$$

The conical critical speed occurs at 28,829 rpm. The simplicity of the above procedure results from the symmetry of the system, which allows the two modes to be considered independently. When such mode separation is not possible, the procedure described in the next section must be applied.

2.8 Coupled Modes of a Rigid Rotor in Flexible Supports

The c.g. of the system shown in Fig. 2.9 is displaced toward one end of the rotor. If the c.g. radial displacements are denoted by X and Y, their slopes by θ and ϕ, and the displacements at the bearings by $X_1 Y_1$ and $X_2 Y_2$, respectively, the equations of translatory motion are

$$M\ddot{X} = - KX_1 - KX_2$$

and

$$M\ddot{Y} = - KY_1 - KY_2.$$

The equations of angular motion are

$$I_T \ddot{\theta} = KaX_1 - KbX_2 - I_P \omega\dot{\phi}$$

and

$$I_T \ddot{\phi} = KaY_1 - KbY_2 + I_P \omega\dot{\theta}.$$
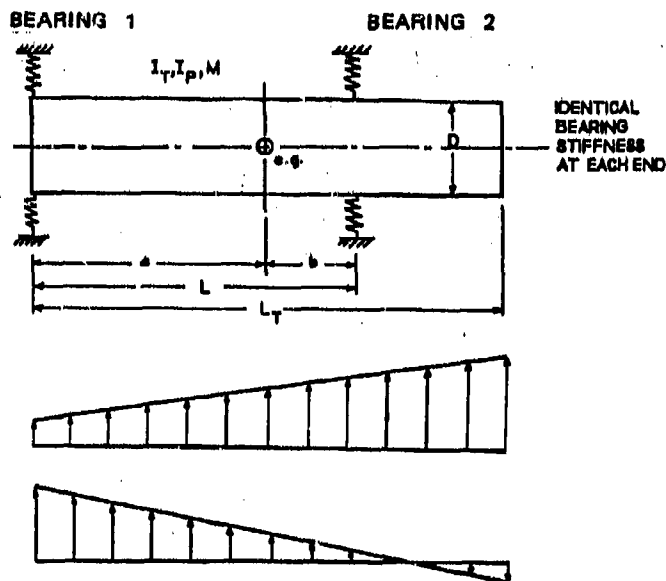
Fig. 2.9. Rotor with end bearings of dissimilar stiffnesses
and associated whirl modes

As both bearings are identical and have orthogonal radial stiffness properties, the whirl orbit of the rotor at any section will be circular. For a solution, set

$$R = X + iY$$

and introduce

$$\gamma = \theta + i\phi,$$

where $i = \sqrt{-1}$. For small whirl motions,

$$X_1 = X - a\theta, \qquad X_2 = X + b\theta,$$

$$Y_1 = Y - a\phi, \qquad Y_2 = Y + b\phi.$$

Writing

$$R_1 = R - a\gamma; \qquad R_2 = R + b\gamma$$

and substituting gives

$$M\ddot{R} + 2KR - K(a - b)\gamma = 0$$

and

$$I_T\ddot{\gamma} + K(a^2 + b^2)\gamma - K(a - b)R = i\,I_p\omega\dot{\gamma}.$$

For a synchronous whirl solution, we set

$$R = R_0 e^{i\omega t}$$

and

$$\gamma = \Gamma_0 e^{i\omega t},$$

and write

$$I = I_T - I_P.$$

This gives the matrix frequency equation

$$\begin{bmatrix} 2K - M\omega^2 & -K(a-b) \\ -K(a-b) & K(a^2+b^2) - I\omega^2 \end{bmatrix} \begin{Bmatrix} R_0 \\ \Gamma_0 \end{Bmatrix} = \begin{Bmatrix} 0 \\ 0 \end{Bmatrix}$$

Expanding the determinant of coefficients in this expression gives the system frequency equation,

$$\omega^4 - \omega^2 \left\{ \frac{K}{I}(a^2 + b^2) + \frac{2K}{M} \right\} + \frac{K^2(a+b)^2}{MI} = 0.$$

This system has two critical speeds, corresponding to the two roots of the above expression. The terms $K(a-b)$ in the determinant express the coupling between the two modes. Where $a = b$, the c.g. is equidistant between the bearings, and these terms are absent. For a uniform rotor this condition occurs when the overhung length is zero. The modes are then uncoupled, and the critical speeds are found directly from the uncoupled frequency equations as

$$\omega_1 = \omega_T = \left[\frac{2K}{M} \right]^{1/2} \text{ (rad/s)};$$

$$\omega_2 = \omega_C = \left[\frac{KL^2}{2I} \right]^{1/2} \text{ (rad/s)}.$$

These expressions agree with the equations obtained in the preceding discussion of uncoupled modes.

Sample Calculation 2

Consider the rigid cylindrical rotor 3.0 in. in diameter by 8.0 in. long with its c.g. displaced 1.0 in. to one side of the bearing span midpoint (Fig. 2.9) such that $a = 4.0$ in. and $b = 2.0$ in. Calculate the

critical speeds for this rotor mounted in identical bearings of stiffness $K_x = K_y = 10^5$ lb/in. with a span 6.0 in.

As before, the rotor mass is

$$M = 0.0414 \text{ lb-s}^2/\text{in.}$$

and the rotor inertia is

$$I = I_T = I_p = 0.1975 \text{ lb-in.-s}^2.$$

Substituting into the second equation gives

$$\omega^4 - \omega^2 \left[\frac{10^5}{0.1975} (4^2 + 2^2) + \frac{2(10^5)}{0.0414} \right] + \frac{(10^5)^2(4 + 2)^2}{(0.1975)(0.0414)} = 0,$$

$$\omega^4 - \omega^2(1.496 \times 10^7) + 4.403 \times 10^{13} = 0.$$

$\omega_1 = 2007$ rad/s, $\omega_2 = 3307$ rad/s,

$f_1 = 319.4$ Hz, $f_2 = 526.3$ Hz,

$N_1 = 19,165$ rpm, $N_2 = 31,580$ rpm.

These are the critical speeds of the rigid rotor in flexible bearings with its c.g. offset by 1.0 in. More generally, the influence of the c.g. offset is given below.

Mode	Critical speed (rpm)		
	No offset	With 0.5-in. offset	With 1-in. offset
First	20,989	20,427	19,165
Second	28,829	29,622	31,580

It can be concluded that offsetting the c.g. couples the modes, decreases the first-mode critical speed, and increases the second-mode critical speed.

The procedure for obtaining the mode shapes of rigid-rotor systems follows established lines (see, for example, Ref. 14). The mode shapes for the 1-in. offset c.g. case are not symmetrical about the midspan. Mode shapes can be obtained by inserting numerical values for the corresponding natural frequencies into the equations of motion:

$$\begin{bmatrix} (2 \times 10^5) - 0.0414\omega^2 & -10^5 \times (4-2) \\ -10^5 \times (4-2) & 10^5 \times (4^2 + 2^2) - 0.1975\,\omega^2 \end{bmatrix} \begin{Bmatrix} R \\ \Gamma \end{Bmatrix} = \begin{Bmatrix} 0 \\ 0 \end{Bmatrix}.$$

Without damping, modal amplitudes can be obtained only as relative values. To proceed, set the c.g. whirl radius R equal to unity and calculate Γ, R_1, and R_2. From the first equation, the relation between R and Γ is

$$\Gamma = \frac{1}{2 \times 10^5} \ (2 \times 10^5 - 0.0414\omega^2) = 1 - (0.207 \times 10^{-6})\omega^2$$

and the modal amplitudes are

$$R_1 = R - a\Gamma = 1 - 4 \ [1 - (0.207 \times 10^{-6}) \ \omega^2]$$

$$R_2 = R + b\Gamma = 1 + 2 \ [1 - (0.207 \times 10^{-6}) \ \omega^2].$$

For the first mode, substituting $\omega_1 = 2007$ rad/s gives

$$\Gamma_1 = 0.166$$

$$R_{11} = 0.336.$$

and

$$R_{21} = 1.332.$$

For the second mode, substituting $\omega_2 = 3307$ rad/s gives

$$\Gamma = -1.264$$

$$R_{12} = 6.056$$

and

$$R_{22} = -1.528.$$

R_1 and R_2 are bearing whirl amplitudes relative to c.g. amplitude $R = 1.0$. The corresponding mode shapes are plotted in Fig. 2.9.

Finally, the results can be validated by applying the principle of orthogonality. It is shown in standard vibration textbooks [14] that

$$\{Z_2\}^T \ [M] \ \{Z_1\} = \{0\},$$

where $\{Z_1\}$ and $\{Z_2\}$ are modal displacement vectors for modes 1 and 2; that is,

$$\{Z_1\} = \begin{Bmatrix} R \\ \Gamma \end{Bmatrix}_1 = \begin{Bmatrix} 1.0 \\ 0.166 \end{Bmatrix},$$

$$\{Z_2\} = \begin{Bmatrix} R \\ \Gamma \end{Bmatrix}_2 = \begin{Bmatrix} 1.0 \\ -1.264 \end{Bmatrix},$$

and $[M]$ is the mass matrix

$$[M] = \begin{bmatrix} M & 0 \\ 0 & I \end{bmatrix} = \begin{bmatrix} 0.0414 & 0 \\ 0 & 0.1975 \end{bmatrix}.$$

Thus,

$$\{Z_2\}^T [M]\{Z_1\} = \{1.0, -1.264\} \begin{bmatrix} 0.0414 & 0 \\ 0 & 0.1975 \end{bmatrix} \begin{Bmatrix} 1.0 \\ 0.166 \end{Bmatrix} = 0$$

These results verify the calculations and theory presented.

2.9 Rigid Rotor in Bearings of Dissimilar Stiffnesses

A rigid offset rotor in end bearings that have different radial stiffness properties is shown in Fig. 2.10. Since the coordinate stiffness properties of each bearing are identical, the rotor whirl orbits are again circular. The rotor c.g. is offset to one side of the midspan point. The equations of free motion for the rotor c.g. are

$$M\ddot{R} = -R_1 K_1 - R_2 K_2$$

and

$$I_T \ddot{\gamma} - iI_p \omega \dot{\gamma} = R_1 K_1 a - R_2 K_2 b,$$

with

$$R_1 = R - a\gamma \qquad R = X + iY$$

$$R_2 = R + b\gamma \qquad \gamma = \theta + i\phi.$$

The equations become

$$-M \omega^2 R + (K_1 + K_2) R + (K_2 b - K_1 a) \Gamma = 0$$

$$(K_2 b - K_1 a) R + (K_1 a^2 + K_2 b^2) \Gamma - I\omega^2 \Gamma = 0.$$

The matrix equation of motion is

$$\begin{bmatrix} K_1 + K_2 - M\omega^2 & K_2 b - K_1 a \\ K_2 b - K_1 a & (K_1 a^2 + K_2 b^2) - I\omega^2 \end{bmatrix} \begin{Bmatrix} R \\ \Gamma \end{Bmatrix} = \begin{Bmatrix} 0 \\ 0 \end{Bmatrix}.$$
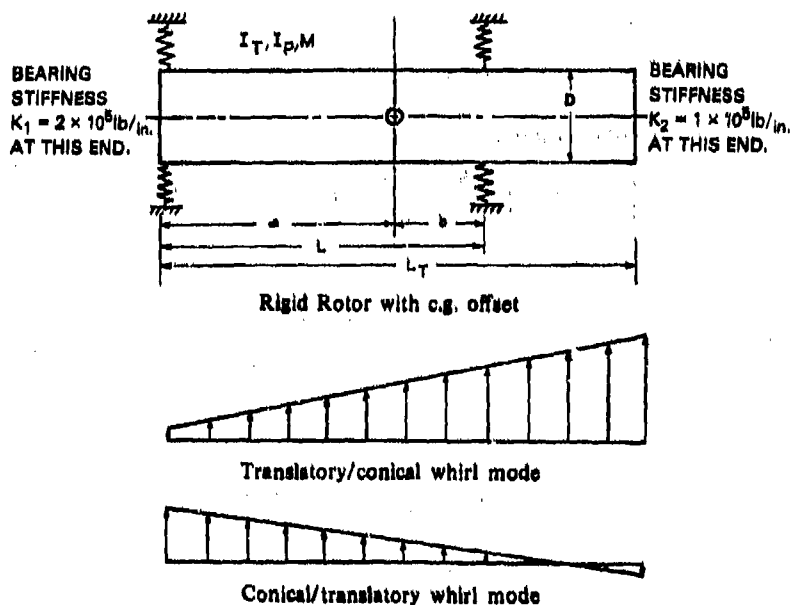
Fig. 2.10. Rotor with coupled rigid whirl modes

The frequency equation is

$$\omega^4 - \omega^2 \left[\frac{K_1 a^2 + K_2 b^2}{I} + \frac{K_1 + K_2}{M} \right] + \frac{K_1 K_2 (a + b)^2}{MI} = 0.$$

If $K_1 = K_2 = K$, this expression reduces to that given in sample calculation 2 for the rotor in identical bearings with an offset c.g. If, in addition, $(a - b) = \frac{L}{2}$, the above expression further reduces the expressions given in sample calculation 1 for the uncoupled modes ω_1 and ω_2 of the symmetrical rotor in symmetrical bearings.

Sample Calculation 3: Critical speeds of an offset c.g. rotor in bearings with dissimilar stiffness

Consider the same rotor as in sample calculation 2: $M = 0.0414$ lb-s.^{2}/in., $I = 0.1975$ lb-in.-s^2, $a = 4.0$ in., $b = 2.0$ in. but $K_1 = 2 \times 10^5$ lb/in., $K_2 = 1 \times 10^5$ lb/in. See Fig. 2.10.

Based on the preceding theory, the frequency equation for this system becomes

$$\omega^4 - \omega^2 \left[\frac{(2 \times 10^5)4^2 + (1 \times 10^5)\, 2^2}{0.1975} + \frac{3 \times 10^5}{0.0414} \right]$$

$$+ \left[\frac{(2 \times 10^5)\,(1 \times 10^5)\, 6^2}{(0.0414)\,(0.1975)} \right] = 0,$$

or

$$\omega^4 - \omega^2 (2.547 \times 10^7) + 8.806 \times 10^{13} = 0,$$

$$\omega_1^2 = 4.1257 \times 10^6, \qquad\qquad \omega_2^2 = 2.1344 \times 10^7,$$

$$\omega_1 = 2031 \text{ rad/s}, \qquad\qquad \omega_2 = 4620 \text{ rad/s},$$

$$f_1 = 323.3 \text{ Hz} = 19{,}396 \text{ rpm}, \qquad f_2 = 735.3 \text{ Hz} = 44{,}118 \text{ rpm};$$

that is, $N_1 = 19{,}396$ rpm and $N_2 = 44{,}118$ rpm. Stiffening one bearing has caused an increase in both critical speeds of this system.

Mode	Critical speed (rpm)		Percent change
	Identical bearings $K_1 = K_2$ $= 1 \times 10^5$ lb/in.	Dissimilar bearings $K_1 = 2 \times 10^5$, $K_2 = 1 \times 10^5$ lb/in.	
First	19,165	19,396	+ 1.2
Second	31,580	44,118	+ 39.7

Mode shapes can be calculated by the method described in sample calculation 2. The matrix frequency equation is

$$\begin{bmatrix} (3 \times 10^5) - 0.0414\,\omega^2 & (2 \times 10^5) - 4(2 \times 10^5) \\ (2 \times 10^5) - 4(2 \times 10^5) & 16(2 \times 10^5) + (4 \times 10^5) - 0.1975\,\omega^2 \end{bmatrix} \begin{Bmatrix} R \\ \Gamma \end{Bmatrix} = \begin{Bmatrix} 0 \\ 0 \end{Bmatrix}.$$

From the first equation,

$$\Gamma = \frac{1}{6 \times 10^5}\, [3 \times 10^5 - 0.0414\ \omega^2] = 0.5 - (6.9 \times 10^{-8})\ \omega^2,$$

$$R_1 = 1.0 - 4[0.5 - (6.9 \times 10^{-8})\ \omega^2],$$

and

$$R_2 = 1.0 + 2[0.5 - (6.9 \times 10^{-8})\ \omega^2].$$

For the first mode, $\omega_1 = 2031$ rad/s gives

$$\Gamma_1 = 0.2154, \qquad R_{11} = 0.1385, \qquad R_{12} = 1.431.$$

For the second mode, $\omega_2 = 4620$ rad/s gives

$$\Gamma_2 = -.9727, \qquad R_{11} = 4.891, \qquad R_{22} = -0.9454.$$

Mode shapes are shown in Fig. 2.10. When comparing Fig. 2.10 with Fig. 2.9, we can see that R_{11} and R_{12} of the former are smaller than those of the latter. Verifying these results by the principle of orthogonality gives

$$\{Z_1\} = \left\{ \begin{matrix} R \\ \Gamma \end{matrix} \right\}_1 = \left\{ \begin{matrix} 1.0 \\ 0.2154 \end{matrix} \right\}, \qquad \{Z_2\} = \left\{ \begin{matrix} R \\ \Gamma \end{matrix} \right\}_2 = \left\{ \begin{matrix} 1.0 \\ -0.9727 \end{matrix} \right\},$$

$$[M] = \begin{bmatrix} 0.0414 & 0 \\ 0 & 0.1975 \end{bmatrix}$$

$$\{Z_2\}^T [M] \{Z_1\} = \{1.0, \ -0.9727\} \begin{bmatrix} 0.0414 & 0 \\ 0 & 0.1975 \end{bmatrix} \left\{ \begin{matrix} 1.0 \\ 0.2154 \end{matrix} \right\} = 0.$$

2.10 Rigid Rotor in Identical Bearings with Dissimilar Coordinate Stiffness Properties

The rigid-rotor system shown in Fig. 2.11 has its c.g. at midspan and is mounted in identical bearings with different stiffnesses in the x- and y-directions, K_1 and K_2. Symmetry of the modes about midspan allows each mode to be analyzed separately, as in Section 2.7; however, the x- and y-coordinate motions cannot be combined directly because elliptical orbits occur in this case. For this system the equations of free motion for the first mode are

$$M\ddot{X} + 2K_1 X = 0$$

and

$$M\ddot{Y} + 2K_2 Y = 0.$$

To solve for these motions, set $X = x\,e^{i\omega t}$, $Y = y\,e^{i\omega t}$, and solve for ω. This gives the uncoupled equations

$$(2K_1 - M\omega^2)\,x\,e^{i\omega t} = 0$$

and

$$(2K_2 - M\omega^2)\,y\,e^{i\omega t} = 0.$$
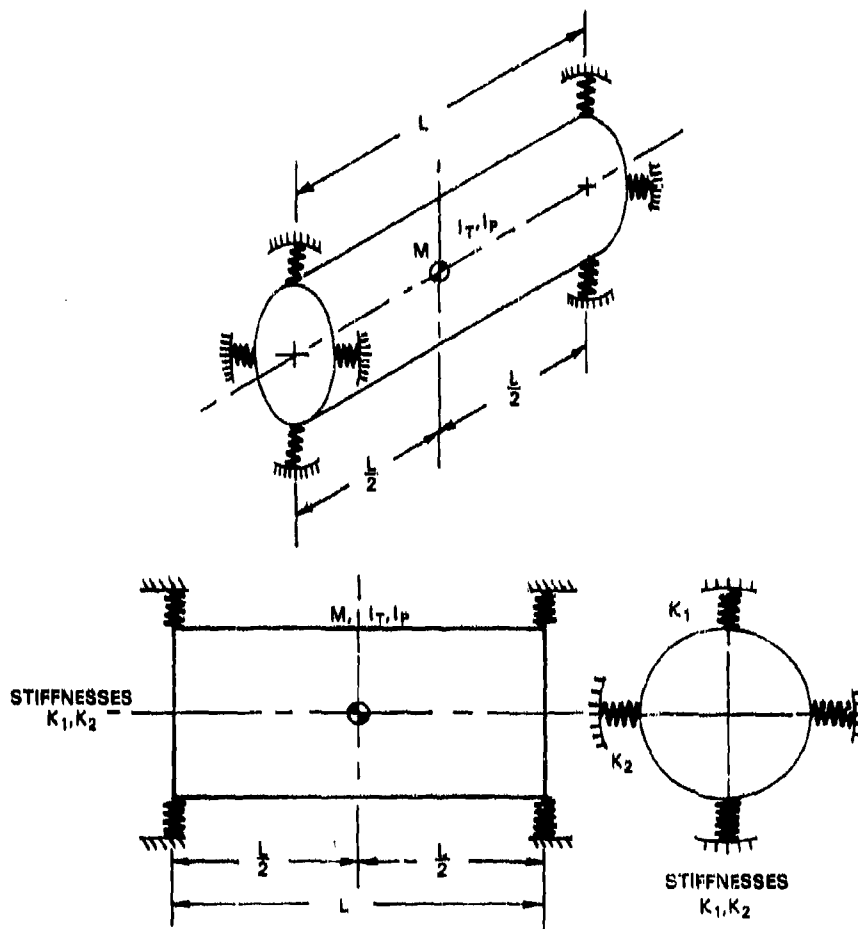
Fig. 2.11. Rigid rotor in identical bearings with dissimilar
coordinate stiffnesses

For nontrivial solutions, the critical frequencies in the principal stiffness
directions of the bearings are given by

$$\omega_1^2 = \frac{2K_1}{M}, \qquad \omega_2^2 = \frac{2K_2}{M}$$

$$\omega_1 = \left[\frac{2K_1}{M}\right]^{1/2} \text{(rad/s)}, \qquad \omega_2 = \left[\frac{2K_2}{M}\right]^{1/2} \text{(rad/s)}.$$

This system has two critical speeds at which the rotor can become
resonant and whirl. The location of each critical speed is governed by

the corresponding coordinate stiffness value of each bearing. If K_1 is the horizontal bearing stiffness and $K_1 < K_2$, the lower critical speed will occur at

$$\omega_1 = \left[\frac{2K_1}{M}\right]^{1/2} \ (\text{rad/s}), \qquad N_1 = 9.55 \left[\frac{2K_1}{M}\right]^{1/2} \ (\text{rpm}).$$

At speeds close to this speed, the rotor will whirl (under the influence of unbalance and damping) in an elongated ellipse whose major axis lies in the direction of bearing stiffness K_1. Similarly, the upper critical speed will occur at

$$\omega_2 = \left[\frac{2K_2}{M}\right]^{1/2} \ (\text{rad/s}), \qquad N_2 = 9.55 \left[\frac{2K_2}{M}\right]^{1/2} \ (\text{rpm}),$$

and the rotor will whirl in a second elongated ellipse with its major axis in the direction of K_2. Note that when $K_1 = K_2$, $\omega_1 = \omega_2$, and the two critical speeds occur at the same speed. For this condition, the whirl is no longer elliptical, but is circular. The latter result applies for the bearings discussed in the three preceding examples.

Conical whirling in this system is more complicated. To begin, consider a rotor—bearing system that is symmetrical about its midspan so that the modes can be separated. For identical bearings with dissimilar coordinate stiffnesses, the equations of free motion are

$$I_T \ddot{\theta} + 1/2 \, K_1 L^2 \theta + I_p \omega \dot{\phi} = 0$$

and

$$I_T \ddot{\phi} + 1/2 \, K_2 L^2 \phi - I_p \omega \dot{\theta} = 0.$$

The solution is obtained by setting

$$\theta = \Theta \, e^{i\nu t}$$

and

$$\phi = \Phi \, e^{i\nu t},$$

where ν is the whirl frequency at the rotational speed ω. This general approach allows any nonsynchronous critical frequencies to be found. Substitution gives

$$[(1/2) \, K_1 L^2 - \nu^2 I_T]\Theta + (i\nu\omega I_p)\Phi = 0$$

and

$$- (i\nu\omega I_p)\Theta + [(1/2)K_2 L^2 - \nu^2 I_T]\Phi = 0.$$

The frequency equation is

$$\nu^4 - \nu^2 \left[\frac{L^2}{2} \cdot \frac{(K_1 + K_2)}{I_T} + \left(\frac{\omega I_P}{I_T} \right)^2 \right] + \frac{K_1 K_2 L^4}{4 I_T^2} = 0.$$

Substituting

$$\nu_0^2 = \left(\frac{K_1 + K_2}{I_T} \right) \frac{L^2}{4}$$

and solving give

$$\left(\frac{\nu}{\nu_0} \right)^2 = \left[1 + \frac{1}{2} \cdot \left(\frac{\omega I_P}{\nu_0 I_T} \right)^2 \right] \pm \left[\left[\left(\frac{K_1 - K_2}{K_1 + K_2} \right)^2 + \left(\frac{\omega I_P}{\nu_0 I_T} \right)^2 + \frac{1}{4} \left(\frac{\omega I_P}{\nu_0 I_T} \right)^4 \right]^{1/2} \right].$$

This expression has four roots, corresponding to the forward and backward whirl modes, in both coordinate stiffness directions of the bearings. The frequencies are conjugates; that is, the backward whirl is the negative of the forward whirl, and therefore only the positive root need be considered. Critical whirling will occur wherever the rotational speed coincides with either frequency, but in this case the problem is more complicated because the gyroscopic effect of polar inertia causes the whirl frequencies to be dependent speed. The variation of the whirl frequency with speed must be found by plotting (ν/ν_0) vs (ω/ν_0). Resonant speeds can also be found from this plot by drawing lines representing the relationship between the exciting frequency and the rotational speed: For example, synchronous unbalance excitation occurs where ω equals the rotation speed Ω. Several examples to illustrate the gyroscopic effect on conical critical speeds are given below.

Sample Calculation 4a: Thin-disk rigid rotor with $I_T = (1/2) I_P$ in flexible bearings of dissimilar stiffnesses

Substituting $I_T = (1/2) I_P$ in the frequency expression gives

$$\left(\frac{\nu}{\nu_0} \right)^2 = \left[1 + 2 \left(\frac{\omega}{\nu_0} \right)^2 \right]$$

$$\pm \left[4 \left(\frac{\omega}{\nu_0} \right)^4 + 4 \left(\frac{\omega}{\nu_0} \right)^2 + \left(\frac{K_1 - K_2}{K_1 + K_2} \right)^2 \right]^{1/2}.$$

For $K_1 = 2K_2$, this expression gives values as listed below.

$\dfrac{\omega}{\nu_0}$	$\left[\dfrac{\nu}{\nu_0}\right]_1$	$\left[\dfrac{\nu}{\nu_0}\right]_2$
0	1.1547	0.8165
0.5	1.6330	0.5774
1.0	2.4183	0.3899
1.5	3.3043	0.2853
2.0	4.2368	0.2225
3.0	6.1625	0.1530
4.0	8.1232	0.1161

Sample Calculation 4b: Rotor with $I_T = I_P$ in bearings of dissimilar stiffnesses

Substituting $I_T = I_P$ into the frequency equation gives

$$\left[\frac{\nu}{\nu_0}\right]^2 = \left[1 + \frac{1}{2}\left[\frac{\omega}{\nu_0}\right]^2\right]$$

$$\pm \left[\frac{1}{4}\left[\frac{\omega}{\nu_0}\right]^4 + \left[\frac{\omega}{\nu_0}\right]^2 + \left[\frac{K_1 - K_2}{K_1 + K_2}\right]^2\right]^{1/2}.$$

For $K_1 = 2K_2$, this expression gives the following range of values.

$\dfrac{\omega}{\nu_0}$	$\left[\dfrac{\nu}{\nu_0}\right]_1$	$\left[\dfrac{\nu}{\nu_0}\right]_2$
0	1.1547	0.8165
0.5	1.3186	0.7150
1.0	1.6330	0.5774
1.5	2.0073	0.4697
2.0	2.4183	0.3899
3.0	3.3043	0.2833
4.0	4.2368	0.2225
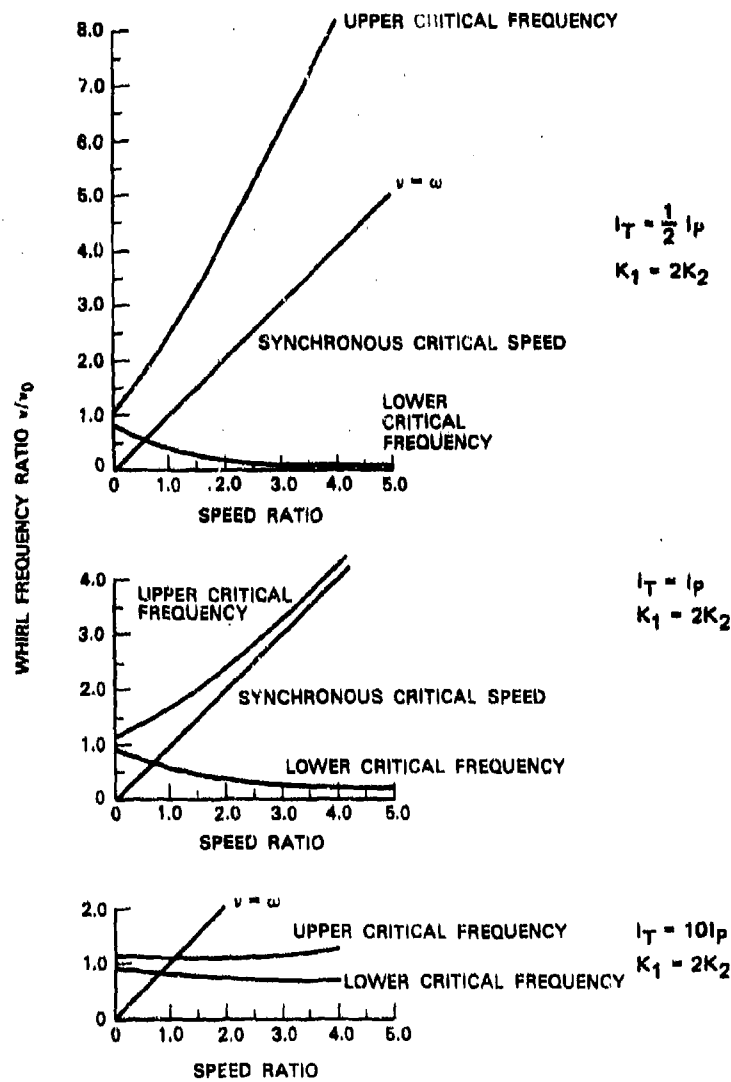
Fig. 2.12. Variation of critical frequencies with speed:
rigid rotor in flexible bearings

Sample Calculation 4c: Rotor with $I_T = 10 I_P$ in bearings of dissimilar stiffness

Substituting $I_T = 10 I_P$ into the frequency equation gives

$$\left[\frac{\nu}{\nu_0}\right]^2 = \left[1 + \frac{1}{200}\left[\frac{\omega}{\nu_0}\right]^2\right]$$

$$\pm \left[\frac{1}{4 \times 10^4}\left[\frac{\omega}{\nu_0}\right]^4 + \frac{1}{100}\left[\frac{\omega}{\nu_0}\right]^2 + \left[\frac{K_1 - K_2}{K_1 + K_2}\right]^2\right]^{1/2}.$$

For $K_1 = 2K_2$, this expression gives the following set of values.

$\dfrac{\omega}{\nu_0}$	$\left[\dfrac{\nu}{\nu_0}\right]_1$	$\left[\dfrac{\nu}{\nu_0}\right]_2$
0	1.1547	0.8165
0.5	1.1569	0.8150
1.0	1.1632	0.8105
1.5	1.1734	0.8035
2.0	1.1871	0.7942
3.0	1.2230	0.7709
4.0	1.2676	0.7438

Results for these three cases are shown in Fig. 2.12.

These results all show that bearings with different coordinate stiffnesses cause two forward whirl modes and two backward conjugate whirl modes (i.e., $\pm \nu_1$, $\pm \nu_2$). The frequencies of all these modes are influenced by gyroscopic effects. These modes may be excited by synchronous unbalance if the excitation frequency ω coincides with the natural frequency ν. The preceding figures show that in calculation 4b, where $I_T < I_P$, only one synchronous critical frequency will occur. In calculation 4b, where $I_T = I_P$, there is still one synchronous critical frequency, but the second frequency tends to become resonant at $\omega = \infty$. In calculation 4c, $I_T > I_P$, two resonant frequencies will occur, as indicated by the two intersections with the synchronous excitation line. Similar results were observed by Den Hartog [15] and Yamamoto [16] for flexible rotors. Asynchronous excitations ($\nu = 2\omega$, etc.) will lead to other resonance properties in rigid-rotor systems.

2.11 Rigid Rotor in Flexible Bearings: General Case

The general cylindrical rotor shown in Fig. 2.13 operates in bearings with dissimilar coordinate stiffnesses in the x- and y-directions.
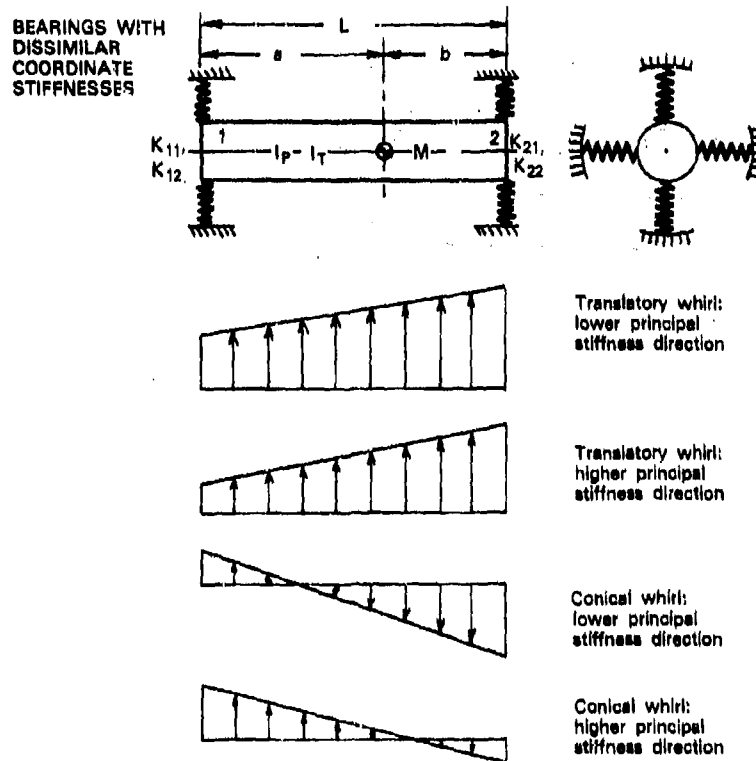
Fig. 2.13. General rigid rotor in bearings of dissimilar coordinate stiffnesses and with corresponding whirl modes

Its c.g. is at distances a and b from the left and right bearings. When mass, transverse inertia, and polar inertia effects are considered, the equations of transverse motion are

$$M\ddot{X} = - K_{11} X_1 - K_{12} X_2$$

and

$$M\ddot{Y} = - K_{21} Y_1 - K_{22} Y_2.$$

The equations for angular motions are

$$I_{\text{T}} \ddot{\theta} + I_{\text{P}} \omega \dot{\phi} = K_{11} a X_1 - K_{12} b X_2$$

and

$$I_{\text{T}} \ddot{\phi} - I_{\text{P}} \omega \dot{\theta} = K_{21} a Y_1 - K_{22} b Y_2.$$

Introducing the expressions

$$X_1 = X - a\theta, \qquad Y_1 = Y - a\phi$$

$$X_2 = X + b\theta, \qquad Y_2 = Y + b\phi$$

and substituting the solutions

$$X = x\, e^{i\nu t}, \qquad \theta = \Theta\, e^{i\nu t}$$

$$Y = y\, e^{i\nu t}, \qquad \phi = \Phi\, e^{i\nu t}$$

into the equation of motion yields the displacement solution

$$
\begin{bmatrix}
(K_{11}+K_{12}-M\nu^2) & 0 & -(K_{11}a-K_{12}b) & 0 \\[4pt]
0 & (K_{21}+K_{22}-M\nu^2) & 0 & -(K_{21}a-K_{22}b) \\[4pt]
-(K_{11}a-K_{12}b) & 0 & (K_{11}a^2+K_{12}b^2-I_T\nu^2) & +iI_P\omega\nu \\[4pt]
0 & -(K_{21}a-K_{22}b) & -iI_P\omega\nu & \begin{matrix}(K_{21}a^2+K_{22}b^2\\ -I_T\nu^2)\end{matrix}
\end{bmatrix}
$$

$$
\times
\begin{Bmatrix} x \\ y \\ \Theta \\ \Phi \end{Bmatrix}
=
\begin{Bmatrix} 0 \\ 0 \\ 0 \\ 0 \end{Bmatrix}.
$$

The above expressions cannot be simplified by combining because the whirl orbit is elliptical, not circular.

As usual, the determinant of the coefficients vanishes at any natural frequency. Although it is tedious to obtain, the frequency equation for the above biquartic system has the general form

$$a_0\nu^8 + a_1\nu^7 + a_2\nu^6 + a_3\nu^5 + a_4\nu^4 + a_5\nu^3 + a_6\nu^2 + a_7\nu + a_8 = 0,$$

where the coefficients a_i may be complex. For each real rotor system the roots $\pm\nu_r$ occur as four conjugate pairs, and so the system has four critical frequencies at any given speed ω, each corresponding to a pair of equal and opposite (i.e., forward and backward) rotor whirl motions.

Sample Calculation 5: General rigid-rotor system in dissimilar flexible bearings

The rotor system shown in Fig. 2.14 will be used to demonstrate the general critical frequency and resonant speed properties of a rotor in flexible bearings. The dynamic properties are determined by the rotor mass and inertia values, the location of the c.g. with respect to the bearings, and the bearing stiffness values, which are

$M = 0.0828$ lb-s^2/in.

$K_{11} = 2 \times 10^4$ lb/in.

$I_P = 0.0932$ lb-in.-s^2

$K_{12} = 4 \times 10^4$ lb/in.

$I_T = 1.813$ lb-in.-s^2

$K_{21} = 4 \times 10^4$ lb/in.

$I = I_T - I_P = 1.7198$ lb-in.-s^2 $K_{22} = 8 \times 10^4$ lb/in.

$a = 8.0$ in.

$b = 4.0$ in.

$c = 4.0$ in.

$L = 16.0$ in.

$D = 3.0$ in.

The frequency determinant for this system is

$$\begin{vmatrix} (6 \times 10^4 - 0.0828\nu^2) & 0 & 0 & 0 \\ 0 & (12 \times 10^4 - 0.0828\nu^2) & 0 & 0 \\ 0 & 0 & (192 \times 10^4 - 1.813\nu^2) & +i\omega(0.09319)\nu \\ 0 & 0 & -i\omega(0.09319)\nu & (384 \times 10^4 - 1.813\nu^2) \end{vmatrix} = 0$$
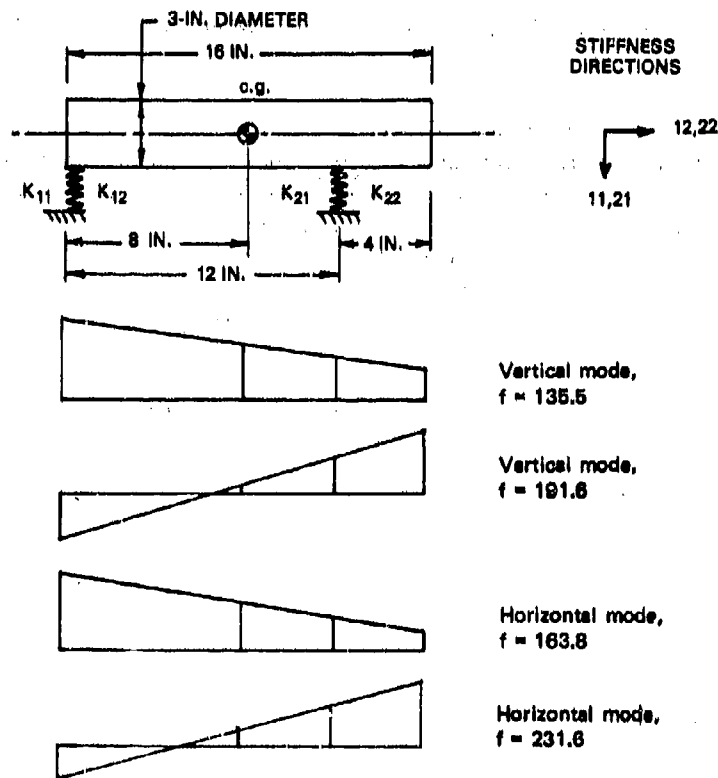
Fig. 2.14. Overhung rotor in flexible bearings; whirl
modes at $N = 4000$ rpm

for $N = 4000$ rpm; i.e., $\omega = 418.88$ rad/s. The roots of the above
expression for this speed are listed below.

ν (rad/s)	N (rpm)	f (Hz)
851.26	8,129.5	135.49
1,203.9	11,496.85	191.61
1,029.09	9,827.81	163.78
1,455.35	13,897.60	231.64

A computer solution for the above numerical example is shown in
Fig. 2.15, where values of the four natural frequencies ν_1, ν_2, ν_3, ν_4 are
plotted vs rotor speed ω. This chart shows the variation of the four
natural frequencies with speed. These frequencies correspond to trans-
latory whirl and conical whirl modes in both planes of principal stiffness
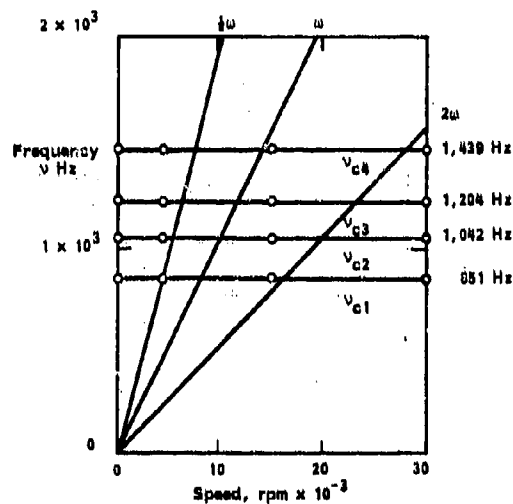
Fig. 2.15. Computer-calculated whirling
frequencies for rigid-rotor system shown
in Fig. 2.14

of the rotor end supports. Excitation-order harmonic lines are also shown, for 1×, 2×, and 3× rpm. The points of intersection between these lines and the natural frequency curves represent the corresponding critical speeds of the system. Other potential asynchronous critical speeds may also arise from such nonharmonic sources as ball-passing frequencies, for undamped rolling-element bearings, and from the vane-passing frequencies of rigid-rotor fan units.

2.12 Critical Speed Chart

The expressions developed in the preceding sections show how the critical speeds of a rotor system arise and how they are influenced by the radial stiffness of the rotor supports. This relationship between critical speed and support stiffness is the basis of a practical procedure for presenting information on the synchronous critical speeds of any rotor system. Figure 2.16 shows how the synchronous critical speeds of a typical rotor system will vary with support stiffness. Such a chart is called a *critical speed* chart; its vertical axis is the rotor speed and its horizontal axis is the rotor-support stiffness. The characteristics shown are the synchronous speed-dependent critical speed lines. The support stiffness may be the bearing stiffness, the pedestal stiffness, the foundation stiffness, or any combination of these stiffnesses. In practice, data for such a critical speed chart are obtained by calculating the critical
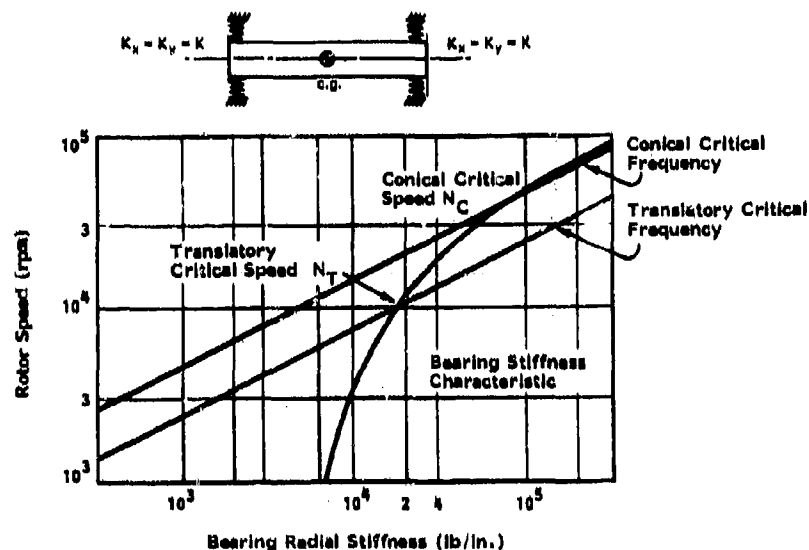
Fig. 2.16. Critical speed map for rigid rotor in externally pressurized gas bearings

speeds of the rotor system over a range of specified, or assumed, support stiffness values. The support stiffness is held constant in each calculation, and the several critical speeds of the rotor system corresponding to the given support stiffnesses are then found. Figure 2.16 shows typical critical speed curves for a sample calculation. The stiffness vs speed characteristic for an actual bearing support system is also plotted. The particular critical speeds of a rotor operating in such bearing supports will evidently occur at the speed points where the bearing characteristic intersects the natural frequency lines.

The following calculations demonstrate the properties of the critical speed chart.

Sample Calculation 6: Rigid rotor in undamped flexible bearings

A high-speed rotor operates in externally pressurized gas bearings at its ends. The rotor closely resembles a 3.0-in.-diameter solid-steel cylinder, 6.0 in. in length. The bearings have identical stiffnesses for which $K_{xx} = K_{yy} = K$ lb/in., with zero cross coupling and negligible damping. Develop the critical speed chart and determine critical speeds given the following stiffness properties for each hydrostatic bearing.

N (rpm)	K (lb/in.)
1000	6000
5000	10,000
13,000	40,000
60,000	100,000

The parameters of the system are as follows:

Rotor mass

$$M = \frac{\pi}{4} \frac{3^2(6) \; 0.283}{386.4} = 0.03106 \text{ lb s}^2/\text{in.}$$

Rotor inertia

$$I = I_T = I_P = \frac{M}{12}(L^2 - 3D^2/4) = 0.0758 \text{ lb-in.-s}^2$$

Translatory critical speed

$$N_T = 9.55 \left[\frac{2K}{M}\right]^{1/2} = 9.55 \left[\frac{2}{0.03106}\right]^{1/2}(K)^{1/2}$$

$$= 76.63 \; (K)^{1/2} \text{ rpm}$$

Conical critical speed

$$N_C = 9.55 \left[\frac{KL^2}{2I}\right]^{1/2} = 9.55 \left[\frac{36}{2(0.0758)}\right]^{1/2}(K)^{1/2}$$

$$= 147.2 \; (K)^{1/2} \text{ rpm.}$$

The critical speeds are as follows:

K (lb/in.)	N_T (rpm)	N_C (rpm)
1×10^3	2,423.3	4,654.8
3×10^3	4,197.2	8,062.5
1×10^4	7,663	14,720.
1×10^5	24,232	46,548.

In Fig. 2.16, the logarithmic plot shows a linear increase in rotor critical frequencies with speed, which is customary for rigid rotors. The critical speeds of the rotor system are found by plotting the bearing characteristic data on the same chart. The system critical speeds occur at the points of intersection shown, i.e., at speeds $N_T = 10,000$ rpm and $N_C = 55,000$ rpm.

Sample Calculation 7: Uniform rotor in flexible bearings

The solid uniform, steel rotor shown in Fig. 2.17 has a diameter of 3.0 in. and a length of 16.0 in. It is mounted in two flexible end bearings for which the variation of stiffness with speed is given in the following table.

K (lb/in.)	N (rpm)	N_0 (dimensionless)
1×10^4	11,000	0.20
4×10^3	19,425	0.35
2×10^3	55,000	1.0
1×10^3	6.1×10^5	11.0

Speed (rpm)	11,000	19,435	55,000	610,000
Stiffness (lb/in.)	10^4	4×10^3	2×10^3	10^3
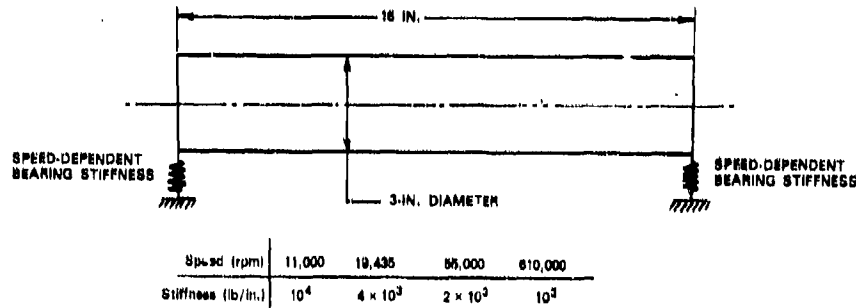
Fig. 2.17. Uniform rotor in end bearings with variable stiffnesses

Determine the first four critical speeds for this case, given that the modulus of elasticity $E = 29 \times 10^6$ lb/in.^{2} and the weight density $w = 0.283$ lb/in.^{3} for the rotor material.

These critical speeds may be obtained by first developing the rotor critical speed chart (Fig. 2.18), and then plotting the bearing characteristic on this chart. The rotor-system critical speeds are determined from the points of intersection. The speed coefficient is
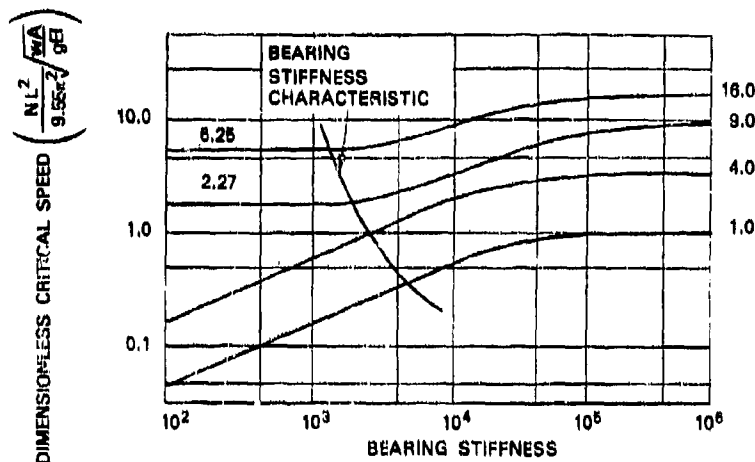
Fig. 2.18. Critical speed chart for uniform rotor in identical flexible supports

$$N = 9.55 \left[\frac{\pi}{L}\right]^2 \left[\frac{gEI}{wA}\right]^{1/2} = 9.55 \left[\frac{\pi}{16}\right]^2 \left[\frac{386.4 \ (29 \times 10^6) \ 3^2}{0.283 \times 16}\right]^{1/2}$$

$$= 55,000 \text{ rpm.}$$

The bearing stiffness characteristic intersects the critical speed lines at the following dimensionless critical speed values:

$$\left[\frac{NL^2}{9.55\pi^2}\right] \left[\frac{wA}{gEI}\right]^{1/2} = 0.42, \ 1.0, \ 2.28, \ 6.25.$$

The first four critical speeds are

$$N_1 = 0.42 \times 55,000 = 23,100 \text{ rpm}$$

$$N_2 = 1.0 \times 55,000 = 55,000 \text{ rpm}$$

$$N_3 = 2.28 \times 55,000 = 125,400 \text{ rpm}$$

$$N_4 = 6.25 \times 55,000 = 343,770 \text{ rpm.}$$

The first two critical speeds occur in the upper straight-line range of the two lowest critical frequency lines. This indicates that the rotor will bend very little in these rigid modes. The higher modes are flexural modes in which the rotor bending displacements would be as significant as the bearing displacements.

It is evident that a critical speed chart can be developed for any rotor—bearing system. In practice, this is done by means of a critical speed computer program to define the rotor critical speed lines, with data points calculated over a range of specified bearing stiffnesses. The critical speeds of a rotor in actual bearings with speed-dependent stiffness properties can then be determined by plotting the bearing stiffness characteristic on the chart as described above.

The main shortcoming of the critical speed chart is its exclusion of damping effects, which, for example, in fluid-film bearing systems, can exert significant effects on the locations of the critical speed lines. Recent developments in rotor dynamics have included such effects in the bearing properties [12].

2.13 Rigid-Rotor Unbalance Response

Residual unbalance causes rotors to whirl in their bearings at rotational frequency; this condition is called *synchronous* whirling. When the rotor approaches a critical speed of the rotor—bearing system, the rotor whirl radius will grow as resonance develops, and the maximum whirl amplitude will occur at the critical speed. Under such circumstances, the whirl amplitudes are restrained only by the system damping, whereas at speeds away from the critical, the system stiffness and mass act to restrain the rotor. Nonresonant whirl amplitudes are therefore usually smaller than whirl amplitudes at resonant speeds. The following sections discuss the synchronous unbalance response of rigid rotors in several types of flexible supports.

2.14 Symmetrical Rotor System with Midplane c.g. Unbalance Force

A symmetrical end-bearing rotor system with equal bearing stiffnesses in the x- and y-directions (Fig. 2.19) will be considered first. Initially, the unbalance force F is assumed to be acting alone (couple unbalance M = zero). For this system, the whirl modes are symmetrical about the midplane, and the equations of undamped forced whirling in the translatory mode under force F are

$$\ddot{M}X + 2KX = M\bar{a}\omega^2 \cos \omega t$$

and

$$\ddot{M}Y + 2KY = M\bar{a}\omega^2 \sin \omega t.$$

where

$$\bar{a} = \text{c.g. eccentricity}.$$
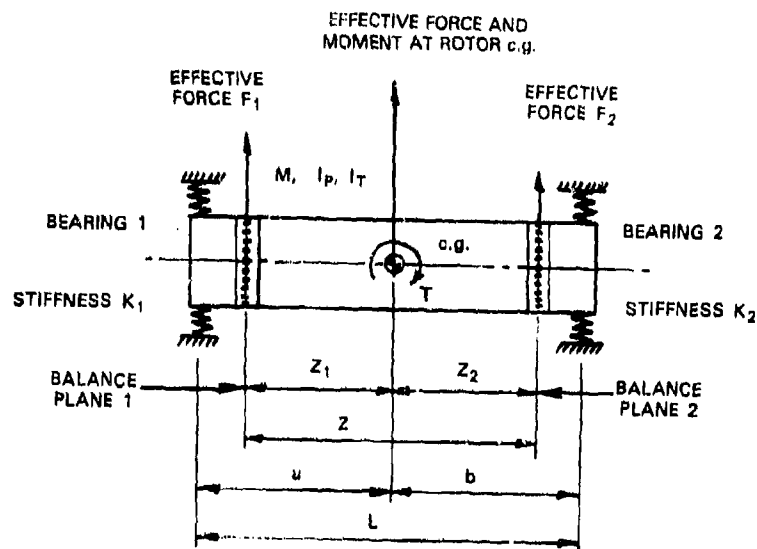
Fig. 2.19. Simple rotor system with force and couple unbalance

Again writing the whirl radius as $R = X + iY$ with $i = \sqrt{-1}$ and recalling that

$$\cos \omega t + i \sin \omega t = e^{i\omega t},$$

we find that the equations of motion reduce to

$$M\ddot{R} + 2KR = M\bar{a}\omega^2 e^{i\omega t}.$$

The solution is obtained by setting

$$R = R_0 e^{i\omega t}.$$

Substituting into the equation of motion gives

$$(2K - M\omega^2) R_0 e^{i\omega t} = M\bar{a}\omega^2 e^{i\omega t},$$

and thus

$$R_0 = \frac{M\bar{a}\omega^2}{2K - M\omega^2},$$

where R_0 is the magnitude of the steady-state whirl radius corresponding to speed ω. This can be written in dimensionless form as

$$R_T^\bullet = \left(\frac{R_0}{\bar{a}}\right) = \frac{M\omega^2}{2K - M\omega^2} = \frac{(\omega/\omega_T)^2}{1 - (\omega/\omega_T)^2},$$

that is,

$$R_T^\bullet = \frac{\Omega^2}{1 - \Omega^2},$$

where

$\Omega = \dfrac{\omega}{\omega_T}$, dimensionless speed

$R_T^\bullet =$ dimensionless translatory whirl radius

$\Omega =$ whirl frequency ratio $= \omega/\omega_T$

$\omega_T =$ undamped translatory natural frequency or critical speed of rotor bearing system $= \sqrt{2K/M}$ rad/s

$\omega =$ rotor speed, rad/s.

The well-known result for the undamped response vs speed of this symmetrical rotor system to midplane unbalance is plotted in Fig. 2.20. The amplitude is seen to increase greatly as the resonant condition is approached, and this result is commonly observed. In practice, the inclusion of damping in the rotor supports (i.e., bearings, pedestals) will serve to limit any build-up of large critical whirl amplitude to acceptable values. This verifies the results obtained for the frequencies and modes of the rotor system with dissimilar stiffnesses.

2.15 Symmetrical Rotor System with Midplane c.g. Unbalance Couple

Conical whirling may be induced in a rigid rotor by an unbalance couple M acting as shown in Fig. 2.19. For a simple uniform rotor with equal bearing stiffnesses, the equations of motion are

$$I_T\ddot{\theta} + (1/2)\,KL^2\,\theta + \omega I_P\,\dot{\phi} = (1/2)\,M\,\bar{a}\,\omega^2 L \cos \omega t$$

and

$$I_T\,\ddot{\phi} + (1/2)\,KL^2\,\phi - \omega\,I_P\,\dot{\theta} = (1/2)\,M\,\bar{a}\,\omega^2 L \sin \omega t.$$
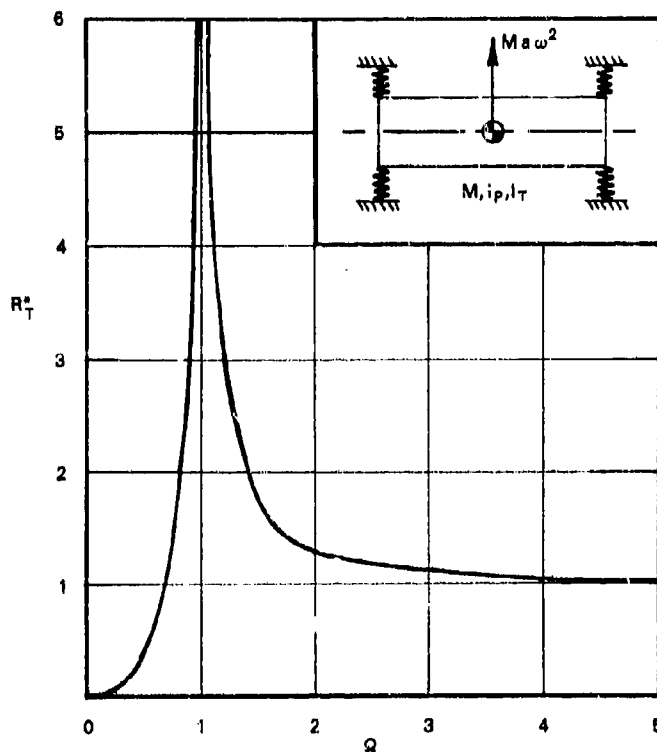
Dimensionless speed ratio: $\Omega = \dfrac{\omega}{\omega_T}$

Dimensionless response amplitude: $R_T^* = \dfrac{R_0}{a} = \dfrac{\Omega^2}{1-\Omega^2}$

Fig. 2.20. Dimensionless response of symmetrical rigid-rotor
system to c.g. balance

Because the bearings have equal coordinate stiffnesses $(K_x = K_y)$, the
whirl orbit will be circular and the whirl angles θ and ϕ will be equal
and related by a 90° phase difference. This may be represented by the
expressions

$$\vartheta = -i\,\phi, \qquad i = \sqrt{-1}.$$

Substitution of this and the complex angle expression

$$\gamma = \theta + i\,\phi$$

allows the equations of motion to be written as

$$I_T\,\ddot{\gamma} - i\,\omega\,I_p\dot{\gamma} + (1/2)\,KL^2\,\gamma = (1/2)\,M\,\bar{a}\,\omega^2\,L\,e^{i\omega t}.$$

The solution is obtained by setting

$$\gamma = \Gamma\, e^{i\omega t}$$

and writing, for synchronous whirling,

$$I = I_T - I_P$$

which gives

$$[(1/2)\, KL^2 - I\,\omega^2]\,\Gamma = (1/2)\,M\,\bar{a}\,\omega^2\,L;$$

that is,

$$\Gamma_0 = \frac{(1/2)\,M\,\bar{a}\,\omega^2\,L}{(1/2)\,KL^2 - I\omega^2}.$$

Recalling that the conical critical speed for this system is given by

$$\omega_C^2 = \frac{KL^2}{2I}$$

and writing

$$\Omega^2 = \left(\frac{\omega}{\omega_C}\right)^2, \qquad I = MH^2,$$

where M is the mass of the rotor and H is the equivalent radius of gyration for $I = I_T - I_P$, we obtain

$$\Gamma_0 = \frac{\dfrac{\bar{a}L}{2H^2}\left(\dfrac{\omega}{\omega_C}\right)^2}{1 - \left(\dfrac{\omega}{\omega_C}\right)^2} = \frac{\bar{a}L}{2H^2}\left(\frac{\Omega_C^2}{1 - \Omega_C^2}\right) = \frac{2R_b}{L},$$

where R_b is the complex conical whirl radius at either bearing. If we write the dimensionless conical whirl radius R_{cb}^* for the bearing amplitude as

$$R_{cb}^* = \frac{R_b}{\bar{a}} = \frac{L^2}{4H^2}\left(\frac{\Omega_I^2}{1 - \Omega_I^2}\right),$$

then R_{cb}^* has the same speed variation as R_T^*, given that $\omega_c^2 = (KL^2/2I)$ for conical whirling, in place of $(\omega_c^2 = (2K/M)$ for translatory whirling. With this notation, Fig. 2.20 may also be used to demonstrate the variation of rotor conical unbalance response with speed.

Sample Calculation 8

For the rotor described in sample calculation 1, see Fig. 2.7, c.g. at midspan, $D = 3.0$ in., $L = 6.0$ in., $L_T = 8.0$ in., $a = b = 3.0$ in., calculate the whirl radius at 10,250 and 20,500 rpm for (a) residual unbalance of 0.10 oz-in. applied at the c.g., and for (b) two equal and opposite unbalances of 0.05 oz-in. at the bearing locations of the rotor. Each bearing stiffness is 10^5 lb/in. in both coordinate directions, and the bearing radial clearance is 0.0045 in.

(a) For *c.g. unbalance*, the rotor parameters are as follows:

Rotor weight $\qquad W = 16.0$ lb $= 256$ oz

Rotor mass $\qquad M = 0.0414$ lb-s^2/in.

Unbalance force $\quad U = W\bar{a}$

For *c.g. eccentricity*,

$$\bar{a} = \frac{U}{W} = \frac{0.10}{256} = 0.391 \times 10^{-3} \text{ in.}$$

The translatory critical speed is

$$\omega_T = \left[\frac{2 \times 10^5}{0.0414}\right]^{1/2} = 2198 \text{ rad/s}$$

$$N_T = 20,989 \text{ rpm.}$$

Translatory critical speed ratio is

(i) $N = 10,250$ rpm $\quad \Omega_1 = \dfrac{10,250}{20,989} = 0.4884$

(ii) $N = 20,500$ rpm $\quad \Omega_1 = \dfrac{20,500}{20,989} = 0.9768.$

Translatory dynamic multiplier $[R_T^* = \Omega_1^2/(1 - \Omega_1^2)]$:

(i) $N = 10,250$ rpm, $R_T^* = \dfrac{(0.4884)^2}{1 - (0.4884)^2} = 0.3133$

$$\frac{R}{\bar{a}} = R_T, \quad R = 0.3133\,\bar{a} = 0.1225 \times 10^{-3} \text{ in.}$$

(ii) $N = 20,500$ rpm, $R_T^* = (0.9768)^2/[1 - (0.9768)^2] = 20.80$

$$R_T = 20.80 \, \bar{a} = 8.1348 \times 10^{-3} \text{ in.}$$

The conclusions to be drawn from this are as follows:

1. At about half the translatory critical speed, the whirl radius due to the stated unbalance is of acceptable size (0.00012 in.) for smooth operation within the bearing radial clearance.

2. At 97.68% of the translatory critical speed, the whirl radius due to the stated unbalance too is large (0.008 in.) for the bearing clearance.

3. This rotor must be balanced for operation at speeds approaching the translatory critical speed (unless adequate system damping can be provided).

(b) For *end-plane unbalance*, half the unbalance (0.05 oz-in.) is located in the rotor at the bearing locations. This is equivalent to half the rotor weight (128 oz) at a radius of 0.391×10^{-3} in. in each end plane, 180° apart. The parameters are as follows:

Conical critical speed

$$\omega_C = \left(\frac{KL^2}{2I}\right)^{1/2} = 3019 \text{ rad/s}$$

$N_C = 28,829$ rpm

Critical speed ratios

(i) 10,250 rpm, $\Omega_2 = \dfrac{10,250}{28,829} = 0.3555$

(ii) 20,500 rpm, $\Omega_2 = \dfrac{20,500}{28,829} = 0.7110.$

Dynamic multiplier $R_C^* = \Omega_2^2/(1 - \Omega_2^2)$:

(i) $N_1 = 10,250$ rpm $R_{C1}^* = \dfrac{(0.3555)^2}{1 - (0.3555)^2} = 0.1447$

(ii) $N_2 = 20,500$ rpm $R_{C2}^* (0.7110)^2/[1 - (0.7110)^2] = 1.0223.$

To determine the bearing whirl radius, recall that the radius of gyration H is given by

$$H^2 = \frac{I}{M} = \frac{0.1975}{0.0414} = 4.77$$

and

$$\Gamma_0 = \frac{\bar{a}L}{2H^2} \left[\frac{\Omega_2^2}{1 - \Omega_2^2} \right]$$

$$R_{cb}^* = \frac{L^2}{4H^2} \left[\frac{\Omega_2^2}{1 - \Omega_2^2} \right];$$

thus, at

(i) 10,250 rpm

$$\Gamma_0 = \left[\frac{\Omega_2^2}{1 - \Omega_2^2} \right] \frac{\bar{a}L}{2H^2} = 3.558 \times 10^{-5} \text{ rad}$$

$$R_{cb} = \left[\frac{\Omega_2^2}{1 - \Omega_2^2} \right] \frac{L^2}{4H^2}$$

$$= 0.1442 \times \frac{8^2}{4 \times 4.771^2}$$

$$= 0.1014$$

$$R_b = R_{cb}^* \bar{a} = 0.1014 \times 0.391 \times 10^{-3}$$

$$= 0.396 \times 10^{-4} \text{ in.}$$

(ii) 20,500 rpm

$$\Gamma_0 = 1.0223 \frac{0.391 \times 10^{-3} \times 6}{2 \times 4.771} = 2.5135 \times 10^{-4} \text{ rad}$$

$$R_{cb}^* = 1.0223 \frac{8^2}{4 \times 4.771^2} = 0.7185$$

$$R_b = R_{cb}^* \bar{a} = 0.7185 \times 0.391 \times 10^{-3} = 0.281 \times 10^{-3} \text{ in.}$$

We therefore conclude that the bearing whirl radii at both speeds due to end-plane out-of-phase unbalance are small. The magnitude of the residual conical unbalance does not indicate any dangerous unbalance condition at these speeds.

It should be noted that, as both the force unbalance and the couple unbalance results are based on linear bearing stiffness analyses, the results can be adjusted by proportioning. For example, if the unbalance force changes to $U = 0.84$ oz-in. and the moment unbalance changed to two equal and opposite forces of $F_1 = F_2 = 0.42$ oz-in., the above results would change linearly as follows:

Translatory mode:

10,250 rpm: $R = 0.1225 \times 10^{-3} \dfrac{0.84}{0.1} = 0.00103$ in.

20,500 rpm: $R = 0.0081 \times 10^{-3} \dfrac{0.84}{0.1} = 0.068$ in.

Conical mode:

10,250 rpm: $R = 0.396 \times 10^{-4} \times \dfrac{0.84}{0.1} = 3.326 \times 10^{-3}$ in.

20,500 rpm: $R = 2.81 \times 10^{-4} \times \dfrac{0.84}{0.1} = 2.360 \times 10^{-3}$ in.

Linear unbalance response analysis can be conveniently adapted in this manner to test the sensitivity of the system.

2.16 Rigid Rotor with Displaced c.g. in Symmetrical Bearings

If a rotor has its c.g. displaced toward one bearing, Fig. 2.9, with a single unbalance acting at its c.g., and it is operating in identical bearings with identical coordinate stiffnesses, the whirl modes are coupled as described previously. Considering first the case of unbalance at the c.g., the steady-state equations of motion are

$$M\ddot{X} + K\,X_1 + K\,X_2 = M\,\bar{a}\,\omega^2 \cos \omega t,$$

$$M\ddot{Y} + K\,Y_1 + K\,Y_2 = M\,\bar{a}\,\omega^2 \sin \omega t,$$

$$I_T\,\ddot{\theta} + \omega\,I_P\,\dot{\phi} + K\,a\,X_1 + K\,b\,X_2 = 0,$$

$$I_T\,\ddot{\phi} - \omega\,I_P\,\dot{\theta} - K\,a\,Y_1 + K\,b\,Y_2 = 0.$$

Introduce the geometric relations

$$X_1 = X - a\,\theta, \qquad Y_1 = Y - a\,\phi$$

$$X_2 = X + b\,\theta, \qquad Y_2 = Y + b\,\phi$$

and write the complex whirl radius and whirl slope as

$$R = X + i\,Y, \qquad R_1 = R - a\,\gamma$$

$$\gamma = \theta + i\,\phi, \qquad R_2 = R + b\,\gamma.$$

Substituting gives the equations of motion as

$$M\ddot{R} + 2\,KR - K(a - b)\gamma = M\,\bar{a}\,\omega^2 e^{i\omega t}$$

and

$$I_{\mathrm{T}}\,\ddot{\gamma} + K(a^2 + b^2)\gamma - K(a - b)R = i\,\omega\,I_{\mathrm{P}}\dot{\gamma}.$$

For a synchronous response solution, set

$$R = R_0\,e^{i\omega t}$$

$$\gamma = \Gamma_0\,e^{i\omega t}$$

and

$$I = I_{\mathrm{T}} - I_{\mathrm{P}}.$$

The matrix response equation then becomes

$$\begin{bmatrix} 2K - M\omega^2 & -K(a - b) \\ -K(a - b) & K(a^2 + b^2) - I\omega^2 \end{bmatrix} \begin{Bmatrix} R_0 \\ \Gamma_0 \end{Bmatrix} = M\,\bar{a}\,\omega^2 \begin{Bmatrix} 1 \\ 0 \end{Bmatrix}.$$

Solving for the whirl amplitudes at the rotor center in the c.g. plane gives

$$_\mathrm{s}R_{\mathrm{T}}^* = \frac{R_0}{\bar{a}} = \frac{\omega^2\,[(a^2 + b^2)(K/I) - \omega^2]}{\omega^4 - \omega^2[(a^2 + b^2)(K/I) + (2K/M)] + K^2(a + b)^2/MI}$$

$$_\mathrm{s}R_{\mathrm{C}}^* = \frac{\Gamma_0}{\bar{a}} = \frac{\omega^2\,(a - b)(K/I)}{\omega^4 - \omega^2[(a^2 + b^2)(K/I) + (2K/M)] + K^2(a + b)^2/MI}$$

$$_gR_{ba} = (_gR_c^* \, \bar{a})a = \Gamma_0 \, a$$

and

$$_gR_{bb} = (_gR_c^* \, \bar{a}) \, b = \Gamma_0 \, b,$$

where the g subscript denotes whirl caused by a single unbalance acting at the c.g., and $_gR_{ba}$ and $_gR_{bb}$ respectively denote the corresponding complex conical whirl radius of two bearings. The numerators of these expressions relate to the c.g. unbalance force, i.e., single-plane unbalance. Note that the denominator is the frequency equation obtained earlier for this displaced-c.g. case.

If $a = b$, that is, there is no c.g. offset, then

$$_gR_T^* = \frac{\Gamma_0}{\bar{a}} = \frac{\omega^2[(KL^2/2I) - \omega^2]}{[(KL^2/2I) - \omega^2][2K/M) - \omega^2]} = \frac{\omega^2}{[(2K/M) - \omega^2]}$$

$$= \frac{\omega^2}{[\omega_t^2 - \omega^2]}$$

$$= \frac{\Omega_t^2}{1 - \Omega_t^2}$$

and

$$_gR_c^* = 0.$$

These expressions coincide with those described previously in Section 2.14, for the zero c.g. offset condition. Couple unbalance in the same rotor system can be studied through the effect of two equal unbalances 180° apart at bearing locations, related back to the rotor c.g. as an unbalance couple of magnitude $0.5 \, Ma \, \omega^2 L$. As these unbalance forces are opposite and equal, no effective unbalance force acts at the rotor c.g. For this case, the coordinate equations of forced motion are

$$M\ddot{X} + KX_1 + KX_2 = 0$$

$$M\ddot{Y} + KY_1 + KY_2 = 0$$

$$I_T\ddot{\theta} + I_p\omega\dot{\phi} - KaX_1 + KbX_2 = 0.5 \, M \, \bar{a} \, \omega^2 \, L \, \cos \omega t$$

and

$$I_T\ddot{\phi} - I_p\omega\dot{\theta} - KaY_1 + KbY_2 = 0.5 \, M \, \bar{a} \, \omega^2 \, L \, \sin \omega t.$$

Introducing the expressions defined previously for R and γ allows these equations to be written as

$$M\ddot{R} + 2KR - K(a - b)\gamma = 0$$

and

$$I_T\ddot{\gamma} - i\omega I_P\dot{\gamma} + K(a^2 + b^2)\gamma - K(a - b)R = 0.5\,M\,\bar{a}\omega^2 Le^{i\omega t}.$$

The matrix equation of motion is

$$\begin{bmatrix} 2K - M\omega^2 & -K(a - b) \\ -K(a - b) & K(a^2 + b^2) - I\omega^2 \end{bmatrix} \begin{Bmatrix} R_0 \\ \Gamma_0 \end{Bmatrix} = 0.5M\,\bar{a}\omega^2 L \begin{Bmatrix} 0 \\ 1 \end{Bmatrix}.$$

Simplifying gives the c.g. whirl amplitudes

$$_eR_T^* = \frac{R_0}{\bar{a}} = \frac{\omega^2 L(a - b)K/2I}{\omega^4 - \omega^2[(a^2 + b^2)(K/I) + (2K/M)] + K^2(a + b)^2/MI}$$

$$_eR_C^* = \frac{\Gamma_0}{\bar{a}} = \frac{\omega^2 L(2K - \omega^2 M)/2I}{\omega^4 - \omega^2[(a^2 + b^2)(K/I) + (2K/M)] + K^2(a + b)^2/MI}$$

$$_eR_{ba} = (_eR_C^*\bar{a})a = \Gamma_0 a$$

and

$$_eR_{bb} = (_eR_C^*\bar{a})b - \Gamma_0 b,$$

where the e subscript denotes the whirl caused by two equal unbalances 180° apart at bearing locations, and $_eR_{ba}$ and $_eR_{bb}$ denote the corresponding complex conical whirl radius of two bearings, respectively.

If $a = b$, that is, there is no c.g. offset, then

$$_eR_T^* = 0$$

$$_eR_C^* = \frac{\Gamma_0}{\bar{a}} = \frac{M\omega^2 L}{2I} \cdot \frac{[(2K/M) - \omega^2]}{[(2K/M) - \omega^2][(KL^2/2I - \omega^2]}$$

$$= \frac{ML}{2I} \frac{\omega^2}{\omega_C^2 - \omega^2} \text{ where } \omega_C^2 = \frac{KL^2}{2I}$$

$$= \frac{ML}{2I} \left[\frac{\Omega_f^2}{1 - \Omega_f^2} \right] \text{ where } \Omega_f^2 = \frac{\omega^2}{\omega_C^2}$$

$$_rR_C^* = \left[\frac{\Omega_l^2}{1 - \Omega_l^2}\right]\frac{L}{2H^2}$$

and

$$\Gamma_0 = \frac{\bar{a}L}{2H^2}\left[\frac{\Omega_l^2}{1 - \Omega_l^2}\right].$$

These expressions coincide with those described previously in Section 2.15 for the case of no c.g. offset.

The combined case of force and moment unbalance acting at the rotor c.g. can be analyzed by linearly combining results obtained for force unbalance with those obtained for moment unbalance. Sensitivity to unbalance may also be studied by proportioning as described previously for the symmetrical rotor case.

Sample Calculation 9: Unbalance response of uniform rotor with offset c.g.

Consider the rotor discussed in the calculations of Sections 2.14 and 2.15, and in 2.9, but with its c.g. displaced axially from the midplane by 1.0 in. The rotor operates in identical end bearings. Determine the effect of this displacement on the rotor amplitudes at 10,250 and 20,500 rpm.

The rotor parameters are as follows:

$$M = 0.0414 \text{ lb s}^2/\text{in.}$$

$$I = I_T - I_P = 0.1975 \text{ lb-in.-s}^2$$

Unbalance

Translatory mode
$$U_T = 0.10 \text{ oz-in.}$$

Conical mode
$$U_C = 0.05 \text{ oz-in. (each bearing location)},$$

where the subscripts T and C stand for translatory and conical, respectively.

For the translatory whirl mode with eccentric c.g., at 10,250 rpm, $\omega = 1073.3$ rad/s, $\omega^2 = 1.152 \times 10^6$ rad/s; then,

$$_sR_T^* = \frac{R_0}{\bar{a}} = \frac{\omega^2[(a^2 + b^2)(K/I) - \omega^2]}{\omega^4 - \omega^2[(a^2 + b^2)(K/I) + (2K/M)] + K^2(a + b)^2/MI}$$

$$= \frac{(1.152 \times 10^6)\left[20\dfrac{10^5}{0.1975} - (1.152 \times 10^6)\right]}{(1.152 \times 10^6)^2 - (1.152 \times 10^6)\left[\dfrac{20 \times 10^5}{0.1925} + \dfrac{2 \times 10^5}{0.0414}\right] + \dfrac{10^{10} \times 36}{(0.0414)(0.1975)}}$$

$$= \frac{1.0339 \times 10^{13}}{2.8125 \times 10^{13}}$$

$$= 0.3676$$

and

$$_sR_0 = 0.3676 \times 0.391 \times 10^{-3}$$

$$= 1.4373 \times 10^{-4} \text{ in.}$$

For the conical whirl mode with eccentric c.g. at 10,250 rpm,

$$_sR_C^* = \frac{\Gamma_0}{\bar{a}} = \frac{\omega^2(K/I)(a - b)}{\Delta(\omega)}$$

$$= \frac{(1.152 \times 10^6)(10^5/0.1975)(4 - 2)}{2.8125 \times 10^{13}}$$

$$= \frac{1.1666 \times 10^{12}}{2.8125 \times 10^{13}}$$

$$= 0.04148$$

$$\Gamma_0 = {}_sR_C^* \, \bar{a} = 1.6218 \times 10^{-5} \text{ rad}$$

$$_sR_{ba} = R_0 - \Gamma_0 a = 0.1437 \times 10^{-3} - 0.0162 \times 10^{-3}(4)$$
$$= 0.0788 \times 10^{-3} \text{ in.}$$

$$_sR_{bb} = R_0 + \Gamma_0 b = 0.1437 \times 10^{-3} + 0.0162 \times 10^{-3}(2)$$
$$= 0.1761 \times 10^{-3} \text{ in.}$$

For a translatory mode with end couple unbalance, at 10,250 rpm, the expressions are:

$$_eR_T^* = \frac{R_0}{\bar{a}} = \frac{\omega^2 L(K/I)(a-b)/2}{\omega^4 - \omega^2[(a^2+b^2)(K/I) + (2K/M)] + K^2(a+b)^2/MI}$$

$$= \frac{(1.152 \times 10^6)6(10^5/0.1975)2/2}{2.8125 \times 10^{13}}$$

$$= \frac{3.4997 \times 10^{12}}{2.8125 \times 10^{13}} = 0.1244$$

$$_eR_0 = {_eR_T^*}\bar{a} = 0.1244 \times 0.391 \times 10^{-3} = 4.864 \times 10^{-5} \text{ in.}$$

For a conical whirl mode, with end couple unbalance, rotating at 10,250 rpm,

$$_eR_C^* = \frac{\Gamma_0}{\bar{a}} = \frac{\omega^2 L(2K - \omega^2 M)/2I}{\Delta(\omega)}$$

$$= \frac{(1.152 \times 10^6) 6\left[\frac{2 \times 10^5}{0.1975} - (1.152 \times 10^6)\frac{0.04}{0.1975}\right]}{2.8125 \times 10^{13}} \cdot \frac{1}{2}$$

$$= \frac{2.6656 \times 10^{12}}{2.8125 \times 10^{13}}$$

$$= 0.09478$$

$$\Gamma_0 = 0.9478\bar{a} = 0.3706 \times 10^{-4} \text{ rad}$$

$$_eR_{ba} = {_eR_0} - \Gamma_0 a = 0.1244 \times 10^{-3} - 0.371 \times 10^{-3}(4)$$
$$= -0.0238 \times 10^{-3} \text{ in.}$$

$$_eR_{bb} = {_eR_0} + \Gamma_0 b = 0.1244 \times 10^{-3} + 0.371 \times 10^{-3}(2)$$
$$= 0.1985 \times 10^{-3} \text{ in.}$$

For a translatory whirl mode with an eccentric c.g. operating at 20,500 rpm, i.e., $\omega = 2146.6$ rad/s and $\omega^2 = 4.608 \times 10^6$ rad/s,

$$_sR_T^* = \frac{R_0}{\bar{a}} = \frac{(4.608 \times 10^6)[(20)(10^5/0.1975) - (4.608 \times 10^6)]}{(4.608 \times 10^6)^2 - (4.608 \times 10^6)(1.4958 \times 10^7) + 4.4029 \times 10^{13}}$$

$$= \frac{2.543 \times 10^{13}}{-3.6619 \times 10^{12}}$$

$$= -6.941$$

and

$$_{\text{s}}R_0 = {}_{\text{s}}R_{\text{T}}^{+}\bar{a} = -6.941 \times 0.391 \times 10^{-3}$$

$$= -2.7139 \times 10^{-3} \text{ in.}$$

For a conical whirl mode with eccentric c.g. at 20,500 rpm,

$$_{\text{s}}R_{\text{C}}^{\ast} = \frac{\Gamma_0}{\bar{a}} = \frac{(4.608 \times 10^6)(10^5/0.1975)(4-2)}{-3.6638 \times 10^{12}}$$

$$= \frac{4.6663 \times 10^{12}}{-3.6619 \times 10^{12}}$$

$$= -1.2743$$

$$\Gamma_0 = (-1.2743)\bar{a} = -0.4983 \times 10^{-3} \text{ rad}$$

$$_{\text{s}}R_{ab} = -2.1739 \times 10^{-3} + 0.4983 \times 10^{-3}(4) = -0.7207 \times 10^{-3} \text{ in.}$$

$$_{\text{s}}R_{bb} = -2.7139 \times 10^{-3} - 0.4983 \times 10^{-3}(2) = -3.7106 \times 10^{-3} \text{ in.}$$

For the translatory mode with end couple unbalance at 20,500 rpm the expressions are:

$$_{\text{e}}R_{\text{T}}^{\ast} = \frac{R_0}{\bar{a}} = \frac{0.5\omega^2 L (a-b)(K/I)}{\Delta} = \frac{0.5(4.607 \times 10^6)6(2)(10^5/0.1975)}{-3.6614 \times 10^{12}}$$

$$= -3.8225$$

$$_{\text{e}}R_0 = (-3.8225)(0.391 \times 10^{-3}) = -1.495 \times 10^{-3} \text{ in.}$$

For the conical mode with end couple unbalance

$$_{\text{e}}R_{\text{C}}^{\ast} = \frac{\Gamma_0}{\bar{a}} = \frac{0.5\omega^2 L [2K - M\omega^2]}{\Delta \cdot I}$$

$$= \frac{0.5(4.607 \times 10^6)[2 \times 10^5 - 0.0414(4.607 \times 10^6)]}{(-3.6614 \times 10^{12})(0.1975)}$$

$$= 0.0295$$

$$_e\Gamma_0 = (0.0295)(0.391 \times 10^{-3}) = 0.0115 \times 10^{-3} \text{ rad.}$$

$$_eR_{ab} = -1.495 \times 10^{-3} - 0.0115 \times 10^{-3}(4) = -1.541 \times 10^{-3} \text{ in.}$$

$$_eR_{bb} = -1.495 \times 10^{-3} + 0.0115 \times 10^{-3}(2) = -1.4719 \times 10^{-3} \text{ in.}$$

The results of the above calculation are summarized in Table 2.3.

2.17 Rigid-Rotor Instability

Unstable whirling is a self-excited interaction between the rotor and its bearings in which potentially dangerous large-amplitude rotor motions may occur. The resulting rotor and pedestal oscillation: take place at some subharmonic frequency of the rotor speed. Such motions cannot be removed by balancing the rotor. This section describes the properties and the calculations of the threshold speed, beyond which unstable whirling is likely to commence. Unstable whirling of rotors in bearings has been discussed by Tondl [17], Sternlicht and Rieger [18], Lund [19], Badgley and Booker [20], and many others.

A rotor is said to be unstable when the journal orbit radius increases with time, without apparent limit, until prevented by some additional restraint. Unstable motions arising from the hydrodynamic action of the bearing fluid film on the rotor are possible with rigid-rotor systems. Any unstable condition can be distinguished from resonant vibrations by the fact that unstable whirls are initiated beyond a certain critical threshold condition, referred to as the threshold speed. This speed is an important operating variable for such systems. Once instability is established, continued operation beyond the threshold speed will cause the rotor orbit to increase in magnitude with time, usually quite rapidly, until a stable radius is found (bounded instability) or until some restraint surface such as a bearing (or seal) is struck. Many bounded instabilities may be tolerated, but once the journal contacts the bearing surface, a violent counterrotating whirl can occur that is capable of rapidly wearing both contacting surfaces. A typical bearing-whirl-instability orbit is shown in Fig. 2.21.

A distinguishing feature of bearing whirl instability is the frequency at which it occurs. Bearing whirls have been observed at frequencies within the following ranges.

Table 2.3. Unbalance response of a uniform rotor: influence of c.g. offset

Excitation	Rotating speed (rpm)	Transitory/Conical	Without c.g. offset				Whirl amplitude — With 1.0-in. c.g. offset			
			Translation of c.g. (in.)	Rotation about c.g. (rad.)	Translation at bearing location A (in.)	Translation at bearing location B (in.)	Translation of c.g. (in.)	Rotation about c.g. (rad.)	Translation at bearing location A (in.)	Translation at bearing location B (in.)
At c.g.	10,250	T	0.1225×10^{-3}		0.1225×10^{-3}	0.1225×10^{-3}	0.1437×10^{-3}		$.0788 \times 10^{-3}$	0.1761×10^{-3}
		C						1.6218×10^{-5}		
	20,500	T	8.134×10^{-3}		8.134×10^{-3}	8.134×10^{-3}	-2.7111×10^{-3}		-2.7139×10^{-3}	-2.7139×10^{-3}
		C						$-0.498 \times 3 \times 10^{-3}$	-0.721×10^{-3}	-3.711×10^{-3}
End couple	10,250	T					4.864×10^{-5}		-2.38×10^{-5}	19.85×10^{-5}
		C		3.558×10^{-5}	0.0396×10^{-3}	-0.0396×10^{-3}		3.745×10^{-5}		
	20,500	T					-1.6948×10^{-3}		-1.541×10^{-3}	-1.4719×10^{-3}
		C		2.5135×10^{-4}	0.283×10^{-3}	-0.283×10^{-3}	-0.115×10^{-4}		

Fig. 2.21. Typical bearing whirl instability orbit: half-frequency bearing whirl, $\nu < \omega/2$, superimposed on bearing unbalance whirl orbit

Bearing type	Frequency Ratio	
	Rigid rotor	Flexible rotor
Hydrodynamic	0.45—0.49	0.38—0.49
Externally pressurized	0.21—0.42	0.20—0.45

These whirls can be distinguished from certain other rotor-system whirl types that have been observed to occur at the following frequencies.

Shaft whirl	Frequency	Reference
Synchronous unbalance whirl	$\nu = \omega$, always	2,21,22
Dissimilar stiffness whirl	$\nu = 2\omega$	17,23,24
Subharmonic shaft whirls	$\nu = \omega/2, \omega/3, \omega/4$, etc.	15,25,26
Hysteresis whirl	$\nu = \omega_c$, independent of ω above ω_T	12,27,28

The above tables include flexible-rotor systems for completeness. Note that only unbalance whirling and bearing whirl occur in rigid-rotor systems. The major analytical interest in unstable bearing whirl lies in being able to predict accurately the whirl threshold speed for a given set of operating conditions. A method for doing this is described below.

Consider the rigid rotor in fluid-film bearings shown in Fig. 2.22. The rotor is taken as a cylinder (for convenience) and has mass M, translatory inertia I_T, and polar inertia I_P. Both bearings are identical
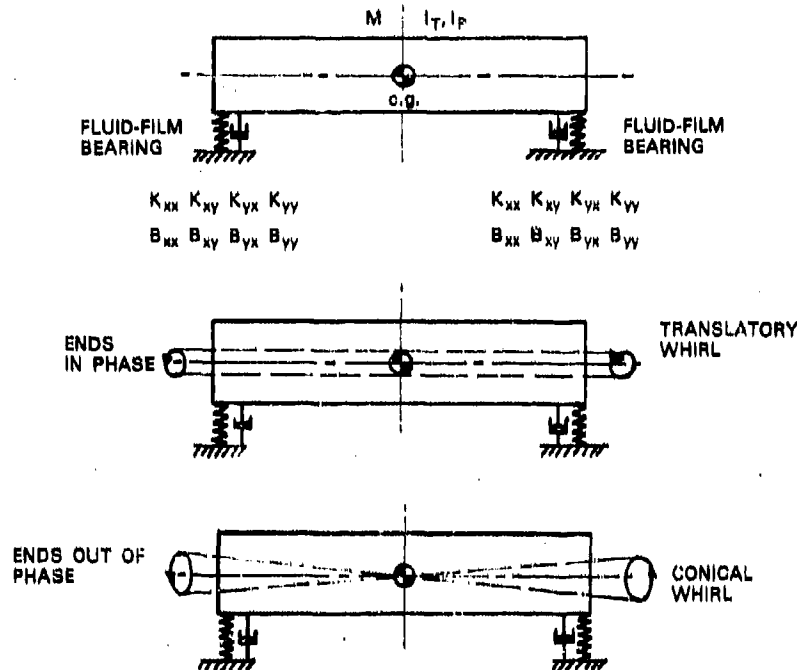
Fig. 2.22. Unstable whirl modes of rigid rotor in fluid-film bearings

and share the rotor load (gravity) equally, so that they both have the
same operating eccentricity and bearing dynamic coefficients. At the
instability threshold speed ω_t, the whirl frequency ν is usually some-
what less than 0.5ω, where ω is the rotor speed (rad/s). There are two
possible modes of whirling: (a) translatory whirl (ends in phase) and
(b) conical whirl (ends out of phase); see Fig. 2.22. The question of
which mode will occur first (i.e., at the lower operating speed ω, thus
constituting the system half-frequency whirl threshold) depends on the
ratio of the critical speeds, which, for synchronous whirling is given by

$$\left(\frac{\omega_{C1}}{\omega_{C2}}\right)^2 = \frac{4I}{ML^2} = \frac{4(I_T - I_P)}{ML^2} < 1.0$$

For the solid cylindrical rotor shown,

$$I_T = \frac{1}{12} M [3R^2 + L^2]$$

$$I_P = \frac{1}{2} MR^2.$$

Substituting shows that the resulting expression $(3R^2 - L^2)/3L^2$ is
always less than 1.0, and so the end-bearing cylindrical rotor shown in

Fig. 2.22 will always experience half-frequency whirl in its translatory mode. For a symmetric rotor with overhung ends, of length L_T and bearing span L, Fig. 2.7, the synchronous critical speed ratio is

$$\left(\frac{\omega_{C1}}{\omega_{C2}}\right)^2 = \frac{L_T^2 - 3R^2}{3L^2}.$$

When

$$L_T^2 > 3L^2 + 3R^2,$$

the conical mode occurs at a lower frequency than the translatory mode, and half frequency whirl instability will therefore be associated with the conical mode. Where $L_T^2 < 3L^2 + 3R^2$, any half frequency whirl instability will be associated with the translatory mode.

The above results show that the tendency for a rotor to whirl in its translatory mode occurs because I_T is usually much larger than I_P.

To obtain an expression for the half-frequency whirl threshold condition, consider the rigid rotor in damped flexible bearings shown in Fig. 2.23. The rotor is taken as being perfectly balanced and is symmetrical in all respects about the midplane. Assuming that the rotor will whirl first in its translatory mode, the threshold conditions can be obtained by considering the forces at either bearing as follows:

Writing Newton's law at either bearing gives

$$\frac{1}{2} M \ddot{X} = -K_{xx} X - K_{xy} Y - B_{xx} \dot{X} - B_{xy} \dot{Y}$$

and

$$\frac{1}{2} M \ddot{Y} = -K_{yx} X - K_{yy} Y - B_{yx} - \dot{X} - B_{yy} \dot{Y},$$

where the K terms K_{xx}, K_{xy}, K_{yx}, and K_{yy} are the bearing linear stiffness coefficients and the B terms B_{xx}, B_{xy}, B_{yx}, and B_{yy} are the bearing linear damping coefficients. The solution is obtained by setting

$$X = x\, e^{i\nu t}; \qquad Y = y\, e^{i\nu t}, \qquad i = \sqrt{-1}$$

where the instability threshold is to be determined from the condition that ν is the rotor whirl frequency at the onset of unstable whirling; that is, where the complex eigenvalue $p = \alpha + i\nu$ is at the boundary of the real axis and α is changing from $-\nu e$ to $+\nu e$ as shown in Fig. 2.24.

EQUILIBRIUM POSITION OF JOURNAL
IN BEARING

REPRESENTATION OF DYNAMIC
PROPERTIES OF FLUID-FILM
BEARING BY EIGHT LINEAR
SPRINGS AND DASHPOTS

RESULTANT FORCES FROM SPRINGS AND
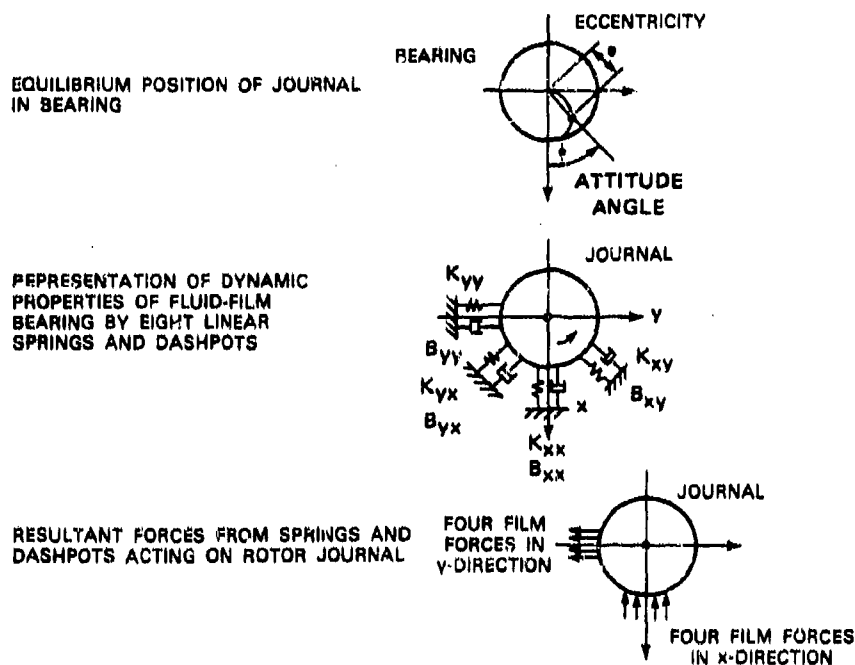DASHPOTS ACTING ON ROTOR JOURNAL

Fig. 2.23. Dynamic force effects for fluid-film bearings
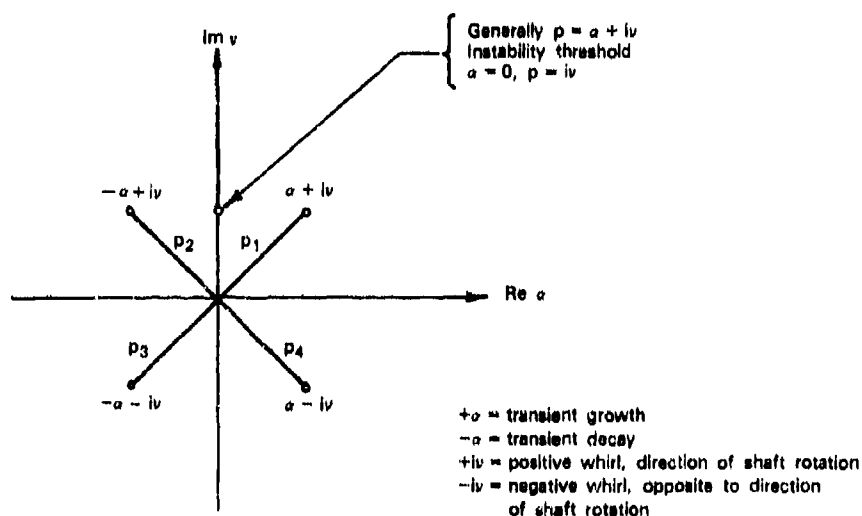
Fig. 2.24. Complex plan plot of eigenvalue: p conditions

Substituting this solution into the equations of motion gives

$$\begin{bmatrix} (2K_{xx} - Mv^2 + iv2B_{xx}) & (2K_{xy} + iv2B_{xy}) \\ (2K_{yx} + iv2B_{yx}) & (2K_{yy} - Mv^2 + iv2B_{yy}) \end{bmatrix} \begin{Bmatrix} x \\ y \end{Bmatrix} = \begin{Bmatrix} 0 \\ 0 \end{Bmatrix}$$

or

$$[2K_{xx} - Mv^2 + iv2B_{xx}][2K_{yy} - Mv^2 + iv2B_{yy}]$$

$$- [2K_{xy} + iv2B_{xy}][2K_{yx} + iv2B_{yx}] = 0.$$

Equating real and imaginary parts to zero gives

$$2K_{xx}2K_{yy} + (Mv^2)^2 - Mv^2(2K_{xx} + 2K_{yy}) - 2K_{xy}2K_{yx}$$

$$- v^2(2B_{xx}2B_{yy} - 2B_{xy}2B_{yx}) = 0$$

and

$$2B_{xx}2K_{yy} + 2B_{yy}2K_{xx} - Mv^2(2B_{xx} + 2B_{yy})$$

$$- (2K_{xy}2B_{yx} + 2K_{yx}2B_{xy}) = 0.$$

Writing $v = \gamma\omega$, where γ is the whirl frequency ratio $\left(\dfrac{v}{\omega}\right)$, gives

$$\frac{(K_{xx}\omega B_{yy} + K_{yy}\omega B_{xx}) - (K_{xy}\omega B_{yx} + K_{yx}\omega B_{xy})}{(\omega B_{xx} + \omega B_{yy})} \qquad (2.17.1)$$

$$= \frac{1}{2}M\omega^2\gamma^2 = \kappa$$

and

$$\frac{(K_{xx} - \kappa)(K_{yy} - \kappa) - K_{xy}K_{yx}}{\omega B_{xx}\omega B_{yy} - \omega B_{xy}\omega B_{yx}} = \left(\frac{v}{\omega}\right)^2 = \gamma^2. \qquad (2.17.2)$$

In these expressions the bearing stiffness and damping coefficients are expressed as usual in terms of the speed of rotation and so may be selected directly for any given operating condition. The procedure for determining the whirl threshold speed for a given case is as follows:

1. Select a trial threshold speed ω_{trial}.
2. Determine the corresponding bearing coefficients K_{xx}, ωB_{xx}, etc.

3. Substitute in Eq. (2.17.1); evaluate $\kappa = \frac{1}{2} M\omega^2\gamma^2$.

4. Substitute in Eq. (2.17.2); evaluate γ^2.

5. Calculate ω^2 from $2\kappa/M\gamma^2 = \omega_{calc}^2$. Hence obtain ω_{calc}.

6. Compare ω_{calc} with ω_{trial}. If they are equal, this is the threshold speed. If not, the required condition can be obtained by iterating the above procedure.

Several trial calculations may be needed before agreement is reached. A cross-plot facilitates convergence, as shown in Fig. 2.25. These equations can be easily programmed for direct solution. Values of the eight bearing coefficients must be supplied for each trial speed assumed.

Fig. 2.25. Plot of ω_{calc} vs $\omega_{assumed}$
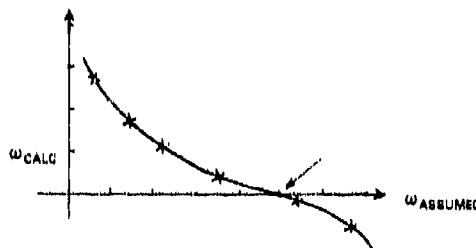
A sample calculation using the above procedure has been given by Rieger and Cundiff [29].

The threshold speed of rigid-rotor conical whirl stability can also be found by replacing the mass term in the above equations by the effective mass M_e acting at the bearing. This is given by

$$M_e \left(\frac{L}{2}\right)^2 = I_T - \frac{\omega}{\nu} I_P \approx I_T - 2.0 I_P \quad \text{(cylinder)},$$

$$M_e = \frac{4I}{L^2} = \frac{4(I_T - 2I_P)}{L^2}. \quad \text{(end)}$$

2.18 References

1. D. Robertson, "The Whirling of Shafts," *The Engineer* **158**, 216–217, 228–231 (1934).
2. H. H. Jeffcott, "The Lateral Vibration of Loaded Shafts in the Neighborhood of a Whirling Speed—The Effect of Want of Balance," *Phil. Mag.*, Ser. 6, **37**, 304–14 (1919).

3. R. E. D. Bishop and A. G. Parkinson, "Second Order Vibration of
    Flexible Shafts," *Phil. Trans. Roy. Soc. (London)*, Ser. A, **259**,
    619–649 (1965).
4. S. B. Rasmussen, "Practical Rotor Dynamics," *Machine Design*
    Feb. 6, 1969, pp. 142-145; Feb. 20, 1969, pp. 157-161; Mar. 6,
    1969, pp. 158–162.
5. A. Palmgren, *Ball and Roller Bearing Engineering*, 3rd ed., S. H.
    Burbank & Co., Philadelphia, Pa., 3, 1959.
6. T. A. Harris, *Rolling Bearing Analysis*, John Wiley & Sons, New
    York, 1966.
7. W. Shapiro and J. G. Rumbarger, "Bearing Influence and
    Representation in Rotor Dynamics Analysis," in *Flexible
    Rotor-Bearing System Analysis*, Part 2, ASME, 1973.
8. H. Rippel, *Hydrostatic Bearing Design Manual*, Cast Bronze Bearing
    Institute, Inc., Cleveland, Ohio, 1963.
9. D. F. Wilcock and E. Booser, *Bearing Design and Application*,
    McGraw-Hill, New York, 1957.
10. A. Raimondi and J. Boyd, "A Solution for the Finite Journal Bear-
    ing and Its Application to Analysis and Design," *Trans. ASLE*, **1**
    No. 1, (1958).
11. P. C. Warner, "Static and Dynamic Properties of Partial Journal
    Bearings," *Trans. ASME*, **85**, Ser. D, *J. Basic Eng.* **85**, 247–254
    (1963).
12. J. W. Lund, "Stability and Damped Critical Speeds of a Flexible
    Rotor in Fluid-Film Bearings," *Trans. ASME*, Ser. B, *J. Engr. Ind.*
    96, No. 2, 509–517 (1974).
13. N. M. Newmark, *Earthquake Engineering Design Handbook*,
    Prentice-Hall, Englewood Cliffs, N.J., 1973.
14. W. T. Thompson, *Theory of Vibration with Applications*, Prentice-
    Hall, Englewood Cliffs, N.J., 1972.
15. J. P. Den Hartog, *Mechanical Vibrations*, 4th ed., McGraw-Hill,
    New York, 4, 1956.
16. T. Yamamoto, "On the Critical Speeds of a Rotating Shaft," *Col-
    lected Works of Toshio Yamamoto*, AiResearch Manufacturing Co.,
    Phoenix, Ariz., 1961.
17. A. Tondl, *Some Problems of Rotor Dynamics*, Publishing House of
    the Czechoslovakian Academy of Sciences, Prague, 1965.
18. B. Sternlicht and N. F. Rieger, "Bearing-Rotor Instability," Paper
    No. 7, *Proc. Inst. of Mech. Engr.*, **182**, Part 3A, 82–99 (1968).
19. J. W. Lund, "Stability and Damped Critical Speeds of a Flexible
    Rotor in Fluid-Film Bearings," *Trans. ASME*, Ser. B, *J. Engr. Ind.*
    96, No. 2, 509–517 (1974).

20. R. H. Badgley and J. Booker, "Turborotor Instability: The Effect of Initial Transients on Plane Motion," *Trans. ASME*, Ser. F, *J. Lub. Technol.*, **91**, No. 4, (1969).

21. F. M. Dimentberg, *Flexural Vibrations of Rotating Shafts*, Butterworth and Co., Ltd., London, England, 1961.

22. N. F. Rieger, *Unbalance Response and Balancing of Flexible Rotors in Bearings* ASME, Flexible Rotor System Subcommittee Publication, Part 3, 1973.

23. W. Kellenberger, "Forced Double-Frequency Flexural Vibrations of a Rotating Horizontal Flexible Shaft," *Brown Boveri Rev.*, **42**, No. 3, 79-85 (1955).

24. H. D. Taylor, "Critical Speed Behavior of Unsymmetrical Shafts," *Trans. ASME, J. Appl. Mech.* **62** Paper 71-A-79, 1940.

25. C. R. Soderberg, "On the Sub-Critical Speeds of the Rotating Shaft," *Trans. ASME Appl. Mech.* **54**, 45-50 (1932).

26. W. D. McLaughlin, *Non-linear Oscillations*, Oxford University Press, 1945.

27. E. J. Gunter, *Dynamic Stability of Rotor-Bearing Systems*, NASA SP-113, 1966.

28. B. L. Newkirk, "Shaft Whipping," *General Electric Rev.*, **27**, 169-178 (1924).

29. N. F. Rieger and R. A. Cundiff, Discussion of paper by P. W. Morton, "Influence of Coupled Assymmetric Bearings on the Motion of a Massive Flexible Rotor," *Proc. Inst. Mech. Engr.*, **182**, No. 13, 271 (1967-1968).

CHAPTER 3
BALANCING MACHINES AND FACILITIES

3.1 Principles of Balancing

The objective of rotor balancing is to minimize the effects of rotor residual unbalance on the system during normal operation. The main effects of excessive rotor unbalance are

1. Undesirable vibratory forces applied at the rotor journals to the supporting structure and foundation
2. Undesirable rotor runout (i.e., nonconcentric rotor operation) and excessive whirl orbit size
3. Excessive noise level from transmitted vibratory forces.

A perfectly balanced rotor will transmit no unbalance vibratory force or vibratory motion to its bearings or supports at any operating speed. Acceptable levels of residual unbalance are described in ISO balancing documents [1,2]. The basic requirement for rotor balancing is that the c.g. of the rotor mass distribution in all normal modes of the rotor system shall lie on the axis of rotation. The objective of rotor balancing is to achieve this condition in an efficient manner. Typical rotor balancing involves the following steps:

1. Detection and measurement of the effect of unbalance at selected locations along the length of the rotor
2. Modification of the rotor mass distribution at the correction planes to minimize the effects of unbalance at the measurement locations
3. Repetition of the above steps until the residual unbalance effect is smaller than some specified balance criterion value.

The above balancing procedure can be undertaken in a general-purpose balancing machine, in a special balancing machine, in a balancing facility, or at the site. Small rigid rotors are usually balanced in a general purpose balancing facility, involving considerable ancillary equipment. Many rotors are also trim balanced at the site. In most cases the particular needs of the machine determine the type of balancing required.

111

This chapter describes the variety of balancing machines and facilities now in use. It discusses the basic components of various modern balancing machines and the balancing procedures involved in each instance. Field balancing is described in Chapter 4.

Single-Plane Balancing

The simple single-disk rotor shown in Fig. 3.1 consists of a thin, uniform, circular disk mounted eccentrically on a uniform shaft of circular cross section. This figure demonstrates how rotor unbalance may arise from disk eccentricity. The unbalance lies in the plane of the disk, and its effect can be removed by adding a suitable weight diametrically opposite the disk eccentricity. Usually, neither the magnitude of the unbalance nor its location are known at the start of the balancing process. It is common practice to determine the angular location of the unbalance in such a rotor by placing the shaft on two knife edges and allowing the rotor to roll until its c.g. finds its lowest position. A known trial weight is then added to the disk at some selected angular location, and the disk is again allowed to come to rest on the knife edges. The trial weight is then moved to another angular location, say 120° away from the first trial location, and the procedure is repeated. A third trial may be attempted with the weight another 120° from the previous two locations. The required balance weight can then be obtained by solving the resulting vector force problem. A construction for doing this has been described by Sommervaille [3]. A single-disk rotor can, of course, be balanced in any commercial balancing machine. The above construction is a simple alternative, to demonstrate the nature of single-plane unbalance and balancing.

Two-Plane Balancing

Any rigid rotor can be balanced by the addition of suitable correction weights in any two separate correction planes along the length of the rotor. In practice the selection of suitable correction planes is usually limited by convenience of access to the rotor in its casing. Increasing attention is now being given to effective positioning of balance
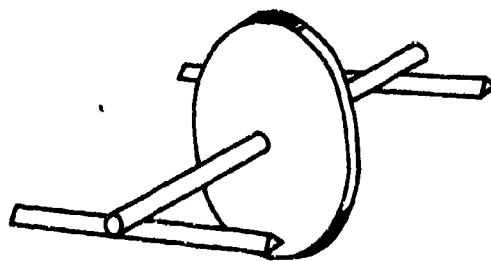

Fig. 3.1. Simple single-disk rotor on knife edges for single-plane balance correction

planes in many modern rotor designs. Two-plane balancing is required for stiff rotors of moderate length, of which the end-bearing drum-type rotor shown in Fig. 3.2 is typical. Two-plane balancing involves a series of measurements that are made with the rotor rotating at some low speed—commonly between 100 and 600 rpm. Simple two-plane balancing procedures require each end of the rotor to be balanced independently. This may involve considerable trial and error and some balance weight and angle calculations.* The most modern procedures allow balancing to be undertaken in three steps:

1. The rotor is rotated in a calibrated balancer that automatically defines the required correction weights needed for the specified balance planes.
2. The required correction weights are installed.
3. The new residual unbalance condition is measured.

In general, the operations required for a two-plane balance are as follows:

1. Spin the rotor at a suitable balancing speed.
2. Measure the transmitted unbalance force and phase angle at the left bearing.
3. Measure the transmitted unbalance force and phase angle at the right bearing.
4. Determine the correction weight and angular location required in either correction plane by a suitable calculation.
5. Insert the correction weights at the required locations in both correction planes.
6. Measure the new transmitted forces at the left and right bearings. Compare with the appropriate balance criterion.
7. Repeat the above sequence until the new balance condition matches the required criterion value.

Fig. 3.2. Rigid drum-type rotor with end correction planes

Multiplane Balancing

Flexible rotors usually require multiplane balancing, which can be done by a number of procedures. The best known of the multiplane balancing techniques are the following:

*These calculations can now be done with certain pocket calculators: see Section 4.3.

1. Modal balancing, in which the respective modal components of the unbalance are balanced out mode by mode

2. Influence coefficient balancing, in which rotor balance is achieved using a computer to process the trial weight test data, which are obtained in a prescribed manner.

Multiplane balancing can be accomplished in a balancing facility or in situ in the field. The particular technique used may range from trial-and-error balancing to a highly automated computer specification of balance weights. Multiplane balancing requires the following equipment:

1. Mechanical drive input for required balancing speeds

2. Vibration sensors for data acquisition (displacement probes, pedestal transducers, etc.)

3. Signal-processing and data-reduction equipment (e.g., tracking filters, wattmeter circuit, minicomputer, etc.)

4. Trial weights, and access to rotor correction planes.

Multiplane balancing differs from two-plane balancing in that it requires a high-speed balance. Two-plane balancing can be performed at any (low) speed at which a signal of adequate strength can be obtained. Several machines capable of balancing flexible rotors are described in this chapter. Several large, flexible, rotor balancing facilities for turbine-generators and for aircraft jet engines are also described.

3.2 Classification

The widespread need for balancing all types of rotating machinery has led to the development of efficient general purpose balancing machines and a variety of multipurpose balancing equipment. A variety of special semiautomated balancing facilities have also been developed to accommodate quantities of similar components on a production basis. For the purpose of discussion, balancing machines can be classified in several different ways, each of which provides insight into their functioning and special features. Three such classifications are described below.

Facility Classification

General purpose balancers. These units are designed to balance a range of rotor types and sizes. They are usually two-plane, slow-speed balancers, but larger units have been designed to function at higher speeds. There is a great diversity of such equipment. Modern general purpose balancers perform many operations of the balancing process automatically, using a minicomputer.

Custom balancers. Where the range of equipment to be balanced is more restricted in shape, size, and balancing speed, special purpose balancers are used for specific balancing tasks. Small fans, gyros, automotive wheels, satellite mass balancers, etc., are balanced on such equipment. Balancing units that accommodate and balance rotors of specific shapes and types with maximum convenience are commercially available as custom balancing units.

Complex automated facilities. Highly specialized custom balancing facilities have been designed to incorporate the related manufacturing functions; e.g., a crankshaft balancing facility with metal removal, automatic weighing, and inflow-outflow conveyor system; and a turbine-generator balance/spin-pit facility with resilient bearings and pedestals in a vacuum chamber for rotor overspeed tests. Varying degrees of automated operation are available, depending on requirements. Typical automated operations range from balance-weighing of connecting rods to fully automated operations such as small armature balancing and production wheel balancing.

Calibration and Readout Classification

McQueary [4] has commented that, from an operational viewpoint, the most important characteristics of a balancing machine are its calibration and readout capabilities. Calibration is the precision adjustment of the machine readout system; it may be permanent (built in) or temporary (requiring recalibration with a calibrating rotor). Readout is the manner in which residual unbalance magnitude and phase-angle data are acquired and displayed. This may range from trial-and-error observations of response on a voltmeter through digital displays of amplitude and phase data. McQueary gives the following classification of balancing machines:

Class 1. Trial-and-error balancing machines

Class 2. Calibratable balancing machines that require a balanced prototype rotor

Class 3. Calibratable balancing machines that do not require a balanced prototype rotor

Class 4. Permanently calibrated hard-bearing balancing machines.

Permanently calibrated machines are the most convenient and the most expensive. Such a machine is not always required, for instance, in field balancing, where an accelerometer and a readout device often suffice for the trial-and-error process involved. It is, however, evident that, besides basic considerations of machine size, operating principle (hard bearing, soft bearing), degree of automation, and so on, there are important questions to consider in planning the acquisition of balancing

equipment—namely, the nature and extent of calibration which a desired installation should possess.

Classification by Principle of Operation

Balancing machines are frequently classified as *soft-bearing*, *hard-bearing*, or *resonant*. These terms refer to the supports (bearings and pedestals) on which the rotor is mounted during the balancing process. The influence of the rotor supports on the performance of the balancing machine may be understood by considering the system shown in Fig. 3.3. The forced amplitude response for such a system, through the resonant speed excited by the rotor unbalance, is shown in Fig. 3.4a. This figure also indicates the regions of operation for soft-bearing, resonant, and hard-bearing machines in relation to the dynamic properties of the balancing machine. For a so-called hard-support machine, the natural frequency of the support system is high, and balancing operations are performed on this machine in the subcritical region, well below resonance; the unbalance force and support displacement are then always in phase, as shown in Fig. 3.4b. With a soft-support machine, the balancing is always performed well above the natural frequency of the support system, in the supercritical region. Unbalance force and response are then 180° out of phase (this causes no problem). Resonant balancing machines operate by passing down through the natural frequency of the rotor—support system as the rotor speed decreases. The associated large resonant amplitude build-up is used to amplify the unbalance readout signals. This avoids the cost of more elaborate electronics. These three principles of dynamic operation have resulted in the three different types of balancing machines identified above. Each machine type is discussed with examples later in this chapter. The supports of a soft-bearing machine are shown in Fig. 3.5.
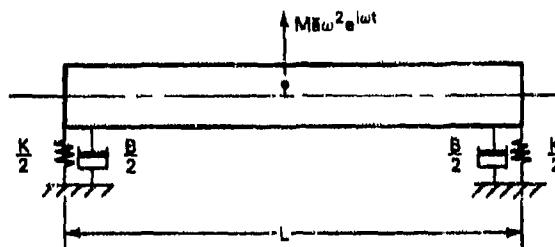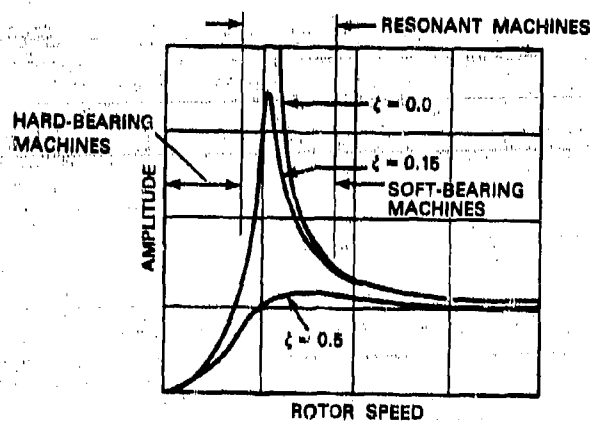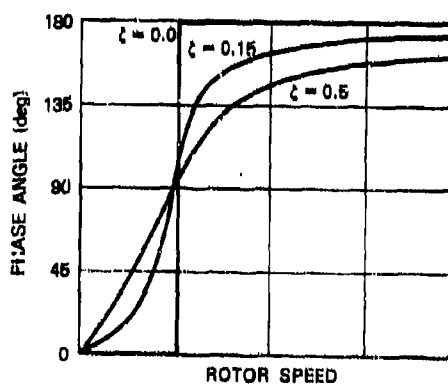
Fig. 3.3. Simple rigid rotor in damped flexible bearings with midspan unbalance

(a) Response amplitude vs rotor speed

(b) Phase angle vs rotor speed

Fig. 3.4. Response amplitude and phase angle as a function of rotor speed for several values of the damping ratio
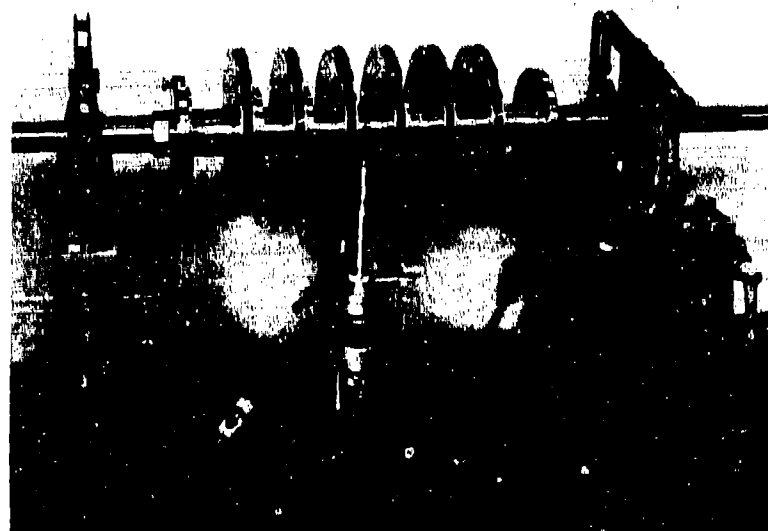
Fig. 3.5. Six-stage centrifugal compressor rotor supported on the soft-support pedestals of a balancing machine. The midplane probe shown measures any bending of the rotor. Balance adjustments are made in the two end-plane disks. (Courtesy of I.R.D. Mechanalysis.)

Rotor Classification

Balancing machines are sometimes described in general terms as being either *rigid-rotor* or *flexible-rotor* machines. This classification usually refers to whether the function of the machine is to balance a rotor in two planes at low speeds, or whether multiplane balancing must be used. This same type of classification is intended by the terms *low-speed* and *high-speed* balancers. None of these terms are precise, because they omit important understandings of the balancing process; for example, a two-bearing, low-speed balancer may also be capable of multiplane balancing using properly conditioned outputs from the two support pedestals. If this balancer were also capable of operating at higher speeds, a true flexible multiplane rotor balance might be possible. In such a case it is the operating speed of the balancer, not the readout, that limits the machine function. As the terms *low-speed* and *high-speed* balancer are imprecise, they are not used in this monograph.

3.3 Major Components of Balancing Machines

Rotor Supports

The rotor structure of a balancing machine may include (a) journal supports, which may range from hardened steel rollers to fluid-film

bearings with a lubricant supply system; (b) pedestals, which are commonly a rigid block of material to carry the bearings; (c) pedestal supports, which are essentially lateral-motion springs possessing a prescribed amount of flexibility while remaining rigid in the vertical direction; and (d) a foundation base, which rigidly supports the pedestals during operation and allows axial adjustment for rotors of different sizes.

The supports perform several functions: rotor support, low-friction rotation, calibrated motion for unbalance measurement, length adjustment for various rotor sizes, and provision for secure clamping during balancing. Two types of support in current use are the so-called soft supports and the hard supports. The soft-support principle is shown in Fig. 3.6. The system consists of a low-stiffness horizontal spring support with a free period of 1 to 2 seconds. The vertical stiffness is substantially higher and hence rigid by comparison. Soft-support machines operate above the natural frequency of the rotor-support system. They have an advantage in the increased strength of the output signal from the vibration sensors because of larger displacements for the same level of unbalance; strong signals at rotational frequency require less sophisticated electronic equipment for subsequent processing of the unbalance readout. Soft-support machines tend to be simpler and less expensive than hard-support machines and are well suited to most rigid-rotor balancing applications. They are used for a variety of small- to medium-size universal balancers and for the balancing of armatures, crankshafts, fan rotors, impellers, and drive shafts.
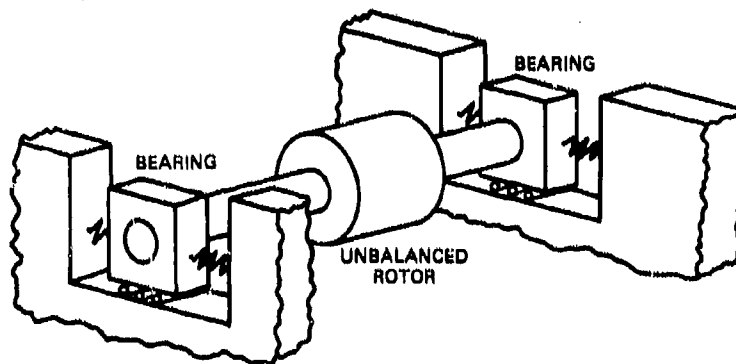
Fig. 3.6. Soft-bearing-support principle. The bearings are restrained so that only horizontal motion is possible.

A typical hard-support balancing machine is shown in Fig. 3.7. The hard support is moderately flexible in the horizontal direction and quite rigid in the vertical direction. The journal pedestal, hard springs,
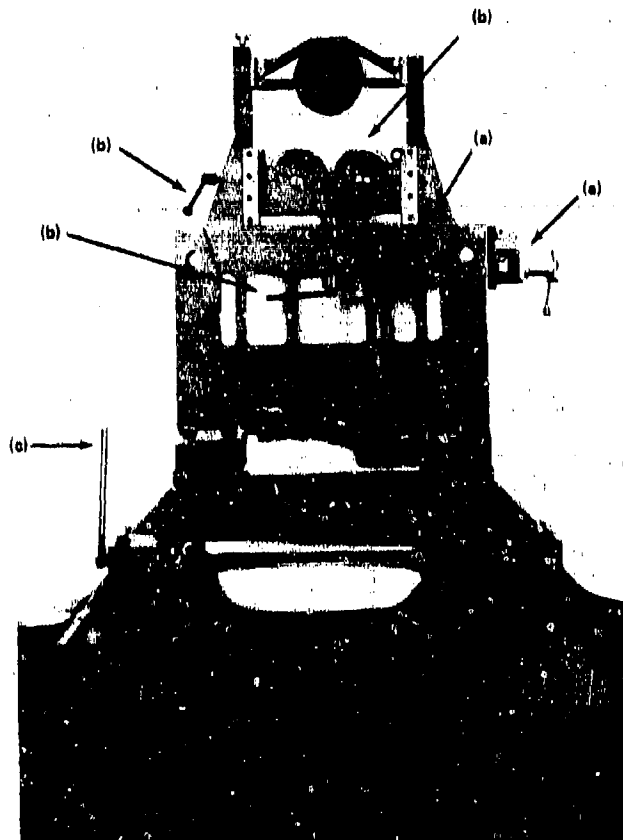
Fig. 3.7. Hard-support pedestal for universal balancing machine. Shown are patented aspects of a Schenck machine: hard-bearing pedestals with velocity-measuring transducer; rotor journal roller supports, with vertical adjustment and clamping; and pedestal quick adjustment and clamping device for machine frame. (Courtesy of Schenck Trebel Corporation.)

and the movable foundation block are now commonly made from a single piece of metal. Support motions may be sensed by displacement probes, strain gages, and by other means. A typical arrangement is shown in Fig. 3.8. Hard-support machines experience smaller displacements than soft-support machines for the same unbalance; the resulting displacement signals tend to be correspondingly smaller. The smaller unbalance signals are accommodated by the electronic equipment normally provided for this type of machine. This equipment may include

RIGID FOUNDATION
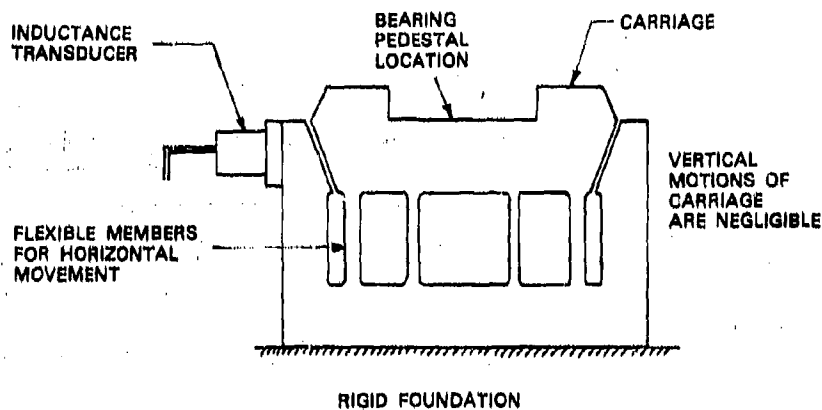
Fig. 3.8. Typical hard-support pedestal

amplifiers and a refined filter circuit. The amplifiers condition the
unbalance signals for amplitude and phase angle. Hard-support
machines are also more susceptible to extraneous vibrations (e.g., from
the shop floor) because these vibrations are less efficiently attenuated
by the stiffer support construction and the higher natural frequency of
the hard-support system.

Hard-support machines are used for both rigid- and flexible-rotor
balancing. Universal hard-support balancers are now available in a
range of sizes, and most large special purpose balancers and facilities
now use hard-support equipment. Rigidity of construction is a desirable
high-speed feature, and the electronic equipment now available is
attractive because of its versatility, permanent calibration, clean and
precise signal conditioning, and direct readout. If many other opera-
tions in a facility must also be considered (e.g., lubrication pumps,
vacuum pumps, Ward-Leonard drive), the incorporation of balancing
electronics is a lesser consideration.

Rotor Drive

A variety of techniques is used to impart rotary motion to the
component being balanced, with the belt drive and the end-drive shaft
being the most common. The choice of a drive system is based on the
requirements of the given application and is determined by rotor size,
power involved, influence of bearing eccentricity, and system dynamics.
Flat-belt drives are common in small bench-type balancers like the one
shown in Fig. 3.9a. Such belt drives are easy to set up, and allow
adjustment of drive tension and belt location on the rotor. There is
some question, however, as to how much additional vibratory motion is
imparted to the pedestal readout by the belt motion.

Another type of belt drive is shown in Fig. 3.9b. The cantilever belt drive spins the rotor up to speed when it is lowered to contact the upper surface of the rotor; the belt is moved away from the rotor when the desired speed is reached (somewhat above the critical speed of the rotor support). The rotor then drifts down in speed, passing through resonance. During measurement the belt is not in contact with the rotor, and this eliminates any unwanted belt excitation effects.

For installations with large rotor-inertia and drive-power requirements, it is often desirable to use an end drive. The end drive may consist of a suitably sized coupling shaft, with a universal joint at both ends, attached from the balancer drive unit to the rotor overhung end, as shown in Fig. 3.9c. Such drives are widely used in medium and large general purpose balancing machines and in many custom machines and facilities because of their higher power-transmission capability. This ability is of importance for acceleration and regenerative braking, where balance cycle time is potentially large (large-inertia rotor) and where windage requires a large power input (e.g., fan or bladed turbomachine rotors). In very large installations a specially designed drive-shaft coupling may be required to supply adequate drive power, which may exceed 1000 hp. A surrounding vacuum chamber is commonly used, especially with bladed turbomachines, to reduce windage power consumption.
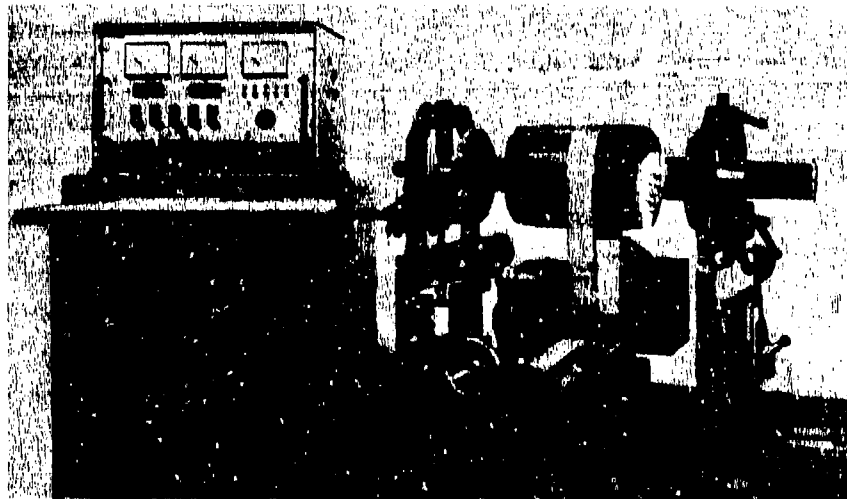
(a) Belt-drive, hard-pedestal, general-purpose machine: Belt tension is adjustable, and motor drive is between the hard-pedestal supports. (Courtesy of Schenck Trebel Corporation.)

Fig. 3.9. Various balancing-machine drives
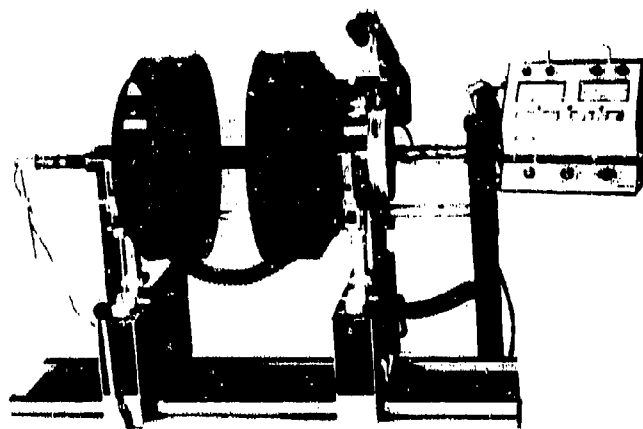
(b) Cantilever-drive, resonant-pedestal, general-purpose machine: Belt drive is pivoted into contact with rotor; after accelerating the rotor to speed, the arm swings back, allowing the rotor to coast down through resonance. (Courtesy of Stewart-Warner.)
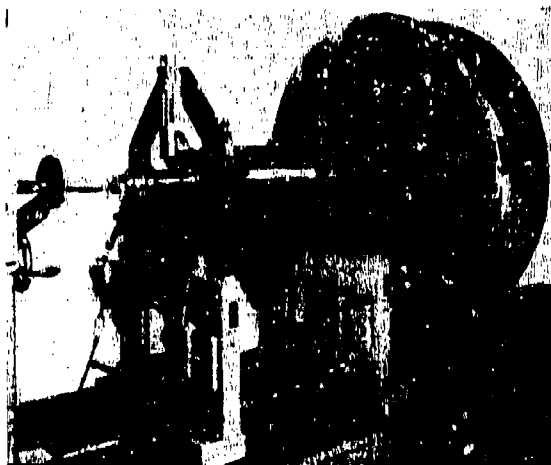
(c) End-drive, hard-pedestal, general-purpose machine: Motor end drive via a universal coupling rotates the motor-driven blower fan; pedestal supports are a variation of the rigid pedestals shown in (a) above. (Courtesy of Schenck Trebel Corporation.)

Fig. 3.9. (Continued) Various balancing-machine drives

The drive couplings for such drives must themselves be carefully balanced. They are attached at a sensitive location (i.e., at an overhung shaft end), which could introduce unwanted dynamic errors into the rotor. For large end-coupled drive shafts the associated problems can be very significant, not only for balancing the coupling but also for lubricating it against wear and seizure. A further need is for balanced quick-attach rotor flanges, to which the above drive couplings can be secured. Patented designs for such flanges have been developed.

A third method of driving a rotor for balancing is by its own internal drive system; an example is the motor-driven gyro unit shown in Fig. 3.10. For such applications it is frequently appropriate to balance the rotor in its own support system. This is possible where there is convenient access to the rotor correction planes through the casing. For example, the gyro unit shown has its own internal electric motor drive. It operates at 12,000 rpm and has a rotor weighing about 4 lb. The casing is mounted on soft supports for balancing. Examples of other self-drive units that can be balanced in this manner are aircraft

Fig. 3.10. Internal electric-motor-driven gyro in
balancing machine

cabin pressurizers (30,000 to 60,000 rpm, rotor weight 1 to 2 lb, internal air turbine drive), and complete internal combustion engine assemblies (for which special assembly balancing stands are available—Fig. 3.11). The wide range of industrial equipment that is customarily balanced in the field—turbines, generators, axial and centrifugal compressors, blowers, turbochargers, etc.—represents another group of self-drive balancing applications. In each instance there is some form of drive input to supply the motive power during field balancing, in contrast with shop balancer—driver applications where the components themselves possess no driver.
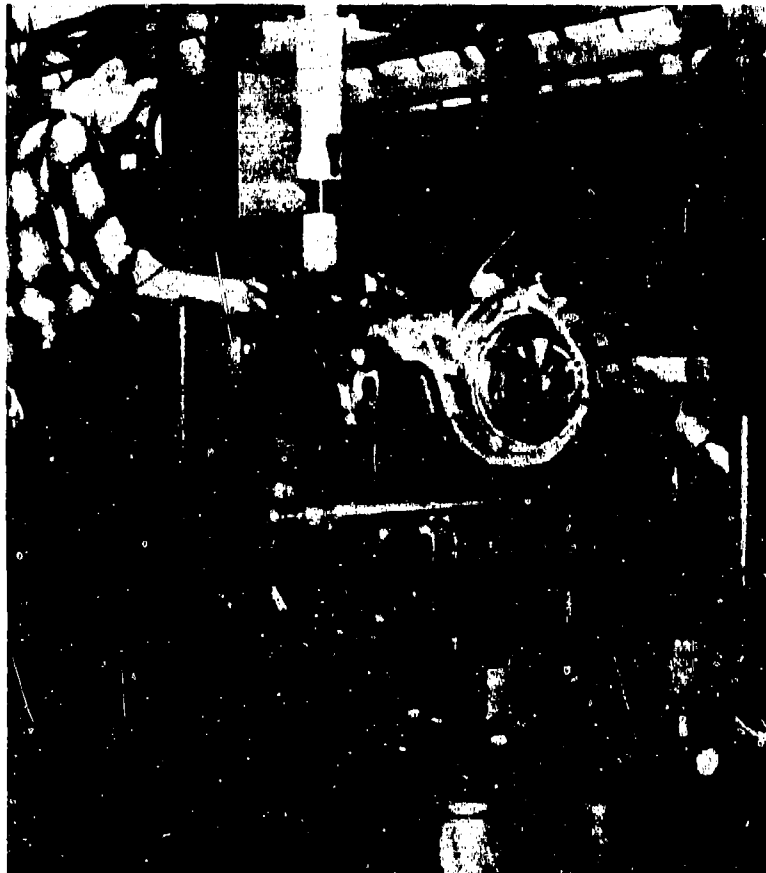
Fig. 3.11. Engine assembly balancing. Complete engines can be run and tested as assemblies in machines of this type. A two-plane trim balance is performed on the clutch housing and on the generator drive wheel. Note the velocity readout transducers on the frame beneath the engine. (Courtesy of Schenck Trebel Corporation.)

Foundation

Each balancing installation requires a foundation with strength and rigidity sufficient to support the rotor without introducing any structural resonances that may affect the accuracy of the readings. A massive foundation is also desirable to attenuate external vibration and impacts. The foundation must also permit axial adjustment of the balancer pedestals, either manually or mechanically. For small balancing machines (Fig. 3.12) the foundation may support only the pedestals, with the electronic equipment mounted elsewhere. Medium-size balancing installations (Fig. 3.13) are often built as a unit, with the electronic equipment mounted for convenience at one end, on the foundation. In large special purpose units, the foundation may merge with the protective equipment of the spin pit (Fig. 3.14). All foundations must be carefully designed to provide ease of accessibility during balancing. They must also exclude undesirable dynamic effects arising from inadequate rigidity and harmful structural resonances. In every instance, foundation resonances are a serious potential source of balancing errors.

Fig. 3.12. Wattmeter console and gyro balancing stand with movable supports.
(Courtesy of Schenck Trebel Corporation.)

Fig. 3.13. Medium-size balancer with electronic readout equipment on bedplate. (Courtesy of Schenck Trebel Corporation.)

Fig. 3.14. Rotor in burstproof spin pit. In the spin pit the pedestals are lowered and bolted to the tunnel floor. The oil hoses are attached to the bearings for lubrication and cooling. The spin pit is sealed and evacuated before operation.

Electronics

The heart of modern balancing machines lies in the electronic equipment used to acquire the vibration signals and to process the signals into unbalance information. The following electronic equipment is used:

1. Vibration sensors (inductance probes, accelerometers, strain gages)
2. Filtering circuits (wattmeter circuit, tracking filters)
3. Operational amplifiers
4. Plane-separation circuits.

Vibration sensors are usually routine components capable of sensing velocity, displacement, or acceleration, depending on the application. Though the output of the sensor may be weak or with high background noise, usually it can be filtered and amplified to provide a suitable balancing signal. Figures 3.15 and 3.16 show vibration sensors for soft- and hard-support machines, respectively.
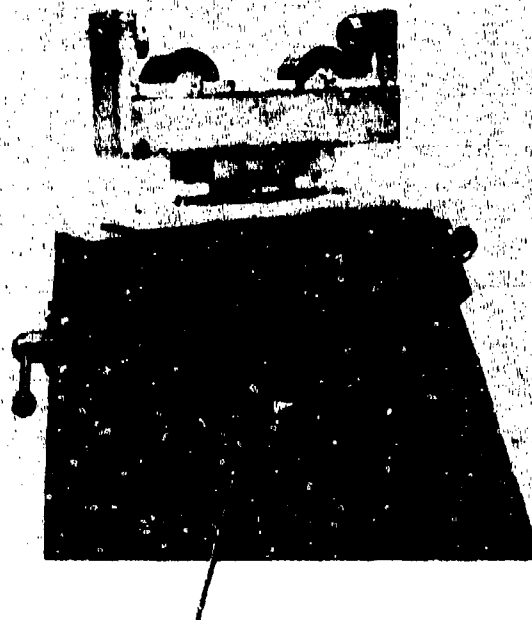
Pickup Installed in
Balancing Machine Pedestal

Fig. 3.15. Vibration sensors for soft-bearing machine.
(Courtesy of Schenck Trebel Corporation.)

Fig. 3.16. Vibration sensors for hard-bearing machine.
(Courtesy of Schenck Trebel Corporation.)

Signal filtering can be accomplished by a number of special circuits. The most widely used is the wattmeter circuit, discussed in the next section. The wattmeter circuit acts as a simple efficient filter to exclude all asynchronous ac components from the balance signal. The output signal is a clean harmonic waveform that can then be used to define the rotor unbalance. Other circuits use tracking filters with analog-to-digital converters coupled to a microprocessor, for example, in field balancing equipment.

Several amplifier circuits for balancing are mentioned in Section 3.7, *Review of Patents*. The amplifier principles involved are relatively straightforward, but this technology is changing rapidly as new solid state electronic concepts are incorporated.

Wattmeter Filtering Method

Moving-coil wattmeters are frequently used to filter the signal transmitted to the pedestals of a balancing machine by an unbalanced rotor. The wattmeter circuit acts as a frequency filter that excludes all asynchronous components of the vibration signal. This occurs because the wattmeter can function only when the alternating voltage supplied to its field coil and the alternating current supplied to its moving coil are identical in frequency.

A balancing-machine wattmeter circuit is shown in Fig. 3.17. Alternating current from an unbalance sensor attached to the flexible pedestal is supplied to the wattmeter field coil, and alternating voltage from an ac generator coupled to the drive shaft is supplied to the wattmeter moving coil. The deflection of the moving coil is then proportional to the wattmeter power $W = EI \cos \theta$, where E is the generator voltage, I is the unbalance sensor current, and θ is the phase angle between the voltage and current signals. Figure 3.18 shows how a wattmeter can combine waves of identical frequency and how waves of differing frequency fail to produce a reading. The wattmeter reading is the average of the product of voltage and current when these components are in phase. Where the unbalance current signal leads the ac voltage, the unbalance power signal is reduced by $\cos \theta$. The wattmeter also requires careful measurement of the sensor signal phase, to avoid incorrect balance readings. Because it functions as a frequency filter that excludes nonsynchronous frequency components from the wattmeter power signal, only voltages and currents with the same frequency can be combined in this instrument. Typical synchronous generator voltage and sensor current signals contain strong synchronous components, together with harmonics from structural resonances and background noise. The harmonics, resonances, and noise are removed when the wattmeter combines the synchronous component of the unbalance current with the generator voltage frequency. An accurate measure of the transmitted unbalance force can thereby be obtained.
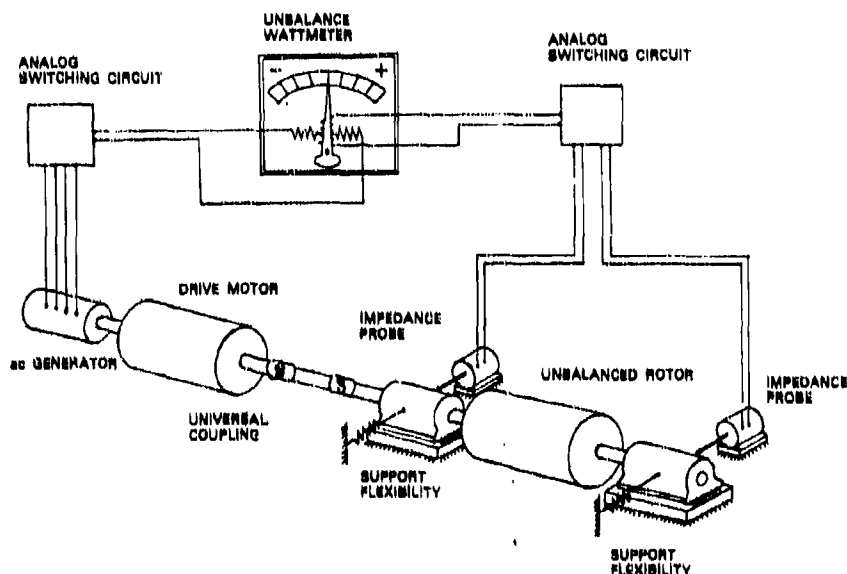
Fig. 3.17. Wattmeter unbalance-measuring system
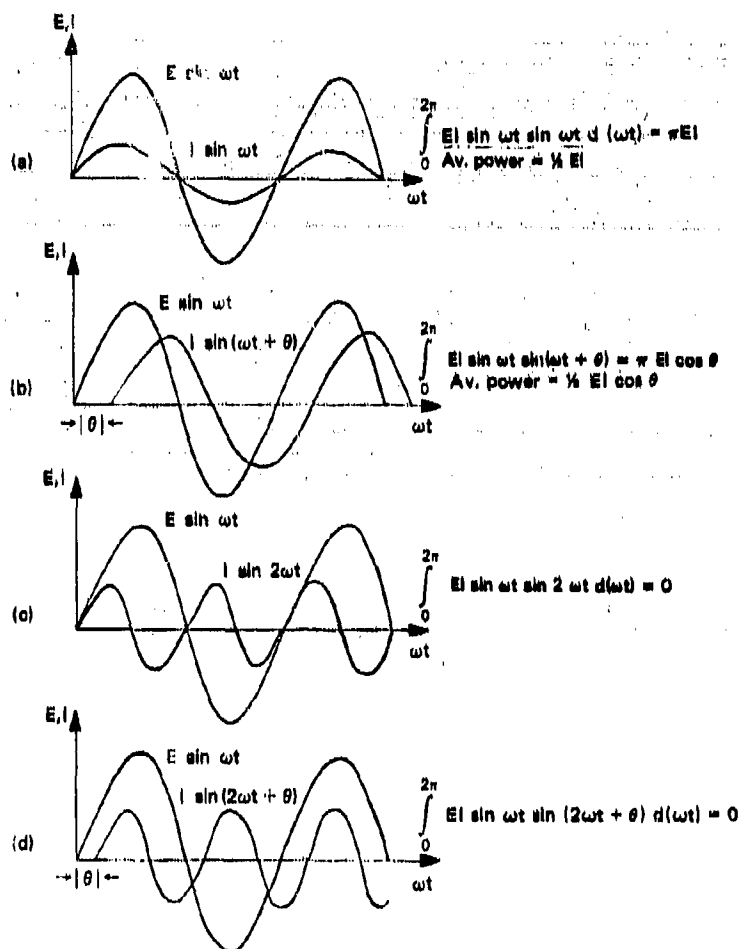
Fig. 3.18. Wattmeter measurement of power from product of current and voltage showing rejection of nonsynchronous signals

The feature by which the wattmeter is able to reject extraneous signals is shown in Fig. 3.18d where a nonsynchronous current component is multiplied by the synchronous voltage. The product within the integral is zero over each cycle of synchronous input. This results in zero net readout on the wattmeter. The periodic integral of the product of two sinusoids is

$$\int_0^{2\pi} \sin m\omega t \sin n\omega t \, d(\omega t) \begin{cases} = 0 & (m \neq n), \\ = \pi & (m = n). \end{cases}$$

For the case where the initial phase difference is nonzero, we obtain

$$\int_0^{2\pi} \sin \omega t \, \sin \, (a\omega t + \theta) \, d(\omega t) \begin{cases} = 0 & (a \neq 1), \\ = \pi\cos \theta & (a = 1), \end{cases}$$

where θ is the phase angle between the two sinusoids at $t = 0$ as shown in Fig. 3.18.

Accurate balancing depends on obtaining accurate signals that relate in a consistent, known manner to the unbalance force being imparted to the pedestal supports. The wattmeter method is a simple procedure for excluding unwanted signal components from the unbalance signal and also for excluding unwanted signals arising from rotation, such as noncircular journal harmonics, drive stick-slip effects, small impacts, misalignment, and excitation from the external environment.

Plane Separation. In-Plane Unbalance Distribution.

Figure 3.19a shows a rigid rotor that is to be corrected for unbalance in the two planes indicated. The rotor is supported in two end bearings. It has two correction planes inboard of the bearings, and the residual unbalance force is represented by the two applied forces shown. If the left bearing support is restrained so that no lateral motion is possible at that location and if the right bearing support is free to move, it is then possible to select a balance weight for the right correction plane such that the right end of the rotor would run in a smooth, balanced condition. The same rotor could also be corrected by restraining the right bearing and inserting a suitable correction weight in the left correction plane. The criterion of balance is that the rotor shall run smoothly without transmitting any dynamic force to the bearings. Having thus corrected the rotor in the left and right planes independently, we might think that the rotor would run smoothly if both bearing restraints were released. This is not the case: the rotor would again run roughly. The problem arises because the force balances have not been achieved independently of the support forces.

The reason for this failure to balance the rotor can be explained by considering the rigid rotor shown in Fig. 3.19b, which has a single unbalance force U acting as shown. If we restrain the rotor against transverse movement at bearing A while allowing end B to move freely, and balance it in correction plane 2, the required correction weight for this condition becomes:

$$C_2 = U \, \frac{b}{c}.$$
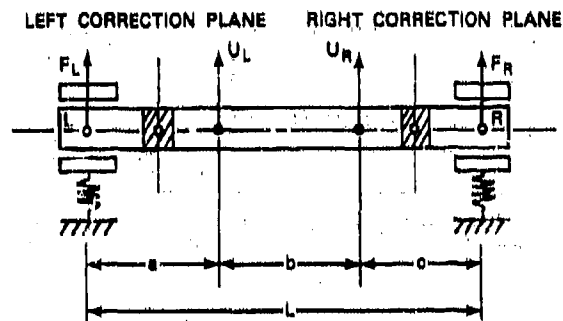
(a) Rigid rotor with two unbalance forces
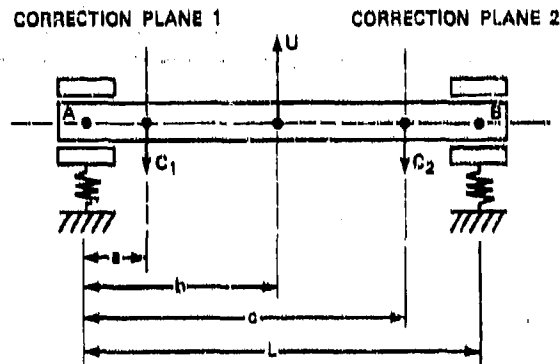
(b) Rigid rotor with single unbalance force

Fig. 3.19. Unbalanced rigid rotors in flexible bearings

The reaction force at A is given by

$$U - C_2 - F_A = 0, \quad \text{and so} \quad F_A = U\left(1 - \frac{b}{c}\right).$$

Next, attempt to remove the transmitted force F_A by restraining the rotor at bearing B and adding correction weights in plane 1. A moment balance about B gives

$$U(L - b) - C_2(L - c) - C_1(L - a) = 0,$$

$$C_1 = \frac{UL}{L-a}\left[1 - \frac{b}{c}\right]$$

When the rotor is freed in both bearings simultaneously, the resulting balance does not satisfy the force equilibrium condition.

$$U - C_1 - C_2 = 0;$$

that is,

$$U - U \frac{L-b}{L-a} + U \frac{b}{c} \frac{L-c}{L-a} - U \frac{b}{c} \neq 0.$$

This can only be satisfied for the condition

$$a \left(\frac{b}{c} - 1 \right) = 0,$$

which cannot exist unless $a = 0$, or if $b = c$.

This problem can be overcome using the principle of plane separation. For the system shown in Fig. 3.19b, instead of restraining the rotor motion at the left bearing, assume that lateral motion can be restrained at the *left balance plane*, that is,

$$\Sigma M_1 = 0: \quad U(b-a) - C_2(c-a) = 0, \quad C_2 = U \frac{b-a}{c-a};$$

$$\Sigma F = 0: \quad -F_1 + U - C_2 = 0, \quad F_1 = U \frac{c-b}{c-a}.$$

Correction weights are then added in the right balance plane until the rotor runs smoothly. The second step is to restrain the rotor at the right balance plane and then to balance it in the left balance plane until it again runs smoothly:

$$\Sigma M_2 = 0: \quad U(c-b) - C_1(c-a) = 0, \quad C_1 = U \frac{c-b}{c-a};$$

$$\Sigma F = 0: \quad -C_1 + U - F_2 = 0, \quad F_2 = U \frac{b-a}{c-a}.$$

Note from the above that $C_1 = F_1$ and $C_2 = F_2$. This indicates that, taken together, the balance corrections will automatically cancel the bearing forces, and both moment and force equilibrium for the rotor are thereby satisfied directly. If the rotor is then operated with corrections C_1 and C_2 installed, the transmitted forces at the bearings will be zero and the rotor will operate in a smooth, balanced manner. No further correction needs to be made to the balance in either plane.

For a numerical example, let the rotor shown in Fig. 3.20 have two unbalance forces $U_1 = -8.0$ lb and $U_2 = 5.0$. The correction planes are 6.0 in. and 30.0 in. from the left support, A. The first step is to restrain the rotor at the left correction plane, B. By taking moments
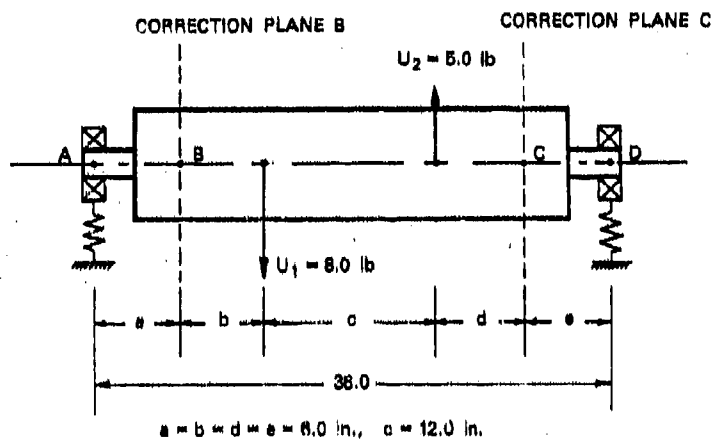
Fig. 3.20. Rigid rotor in flexible bearings
with two-plane unbalance

about this plane, the required correction weight in the right plane F_C is found to be

$$F_C = -\frac{U_2(b + c) + U_1 b}{(b + c + d)}$$

$$= -\frac{1}{24}(5 \times 18 - 8 \times 6) = -1.75 \text{ lb } (\downarrow).$$

The second step is to restrain the rotor in the right correction plane, C. The required balance weight in the left correction plane is

$$F_B = -\frac{U_1(c + d) + U_2 d}{(b + c + d)}$$

$$= -\frac{1}{24}(-8 \times 18 + 5 \times 6) = 4.75 \text{ lb } (\uparrow).$$

The rotor is now released, and the resultant radial force that acts on the rotor as a free body is found to be

$$\Sigma F = 0: \quad 4.75 - 8.0 + 5.0 - 1.75 = 0 \text{ (balanced)}.$$

The moments about either bearing are then taken in turn:

$$\Sigma M_A = 4.75(6) - 8(12) + 5(24) - 1.75(30) = 0 \text{ (balanced)}$$

and

$$\Sigma M_D = 4.75(30) - 8(24) + 5(12) + 1.75(6) = 0 \text{ (balanced)}.$$

Thus the resulting force is zero and the resulting moments are zero, as are the moments about B and C (checked previously). More generally, with the specified corrections installed, the moment about any location along the shaft will be found to be zero. It is evident that all resultant forces and moments are now in equilibrium. As all unbalance and correction forces relate to speed in the same manner, this rotor is now in a state of balance for all speeds. This demonstrates that an unbalanced rigid rotor can be corrected for all speeds by balancing the rotor about either correction plane in turn.

For balancing machines of the Lawaczeck-Heymann type, the rotor is supported in bearings mounted on flexible pedestals.[*] During balancing, it is convenient to measure the rotor unbalance from the movement of the pedestals. This movement is read as pedestal displacement with strain gages or capacitance probes, or as pedestal velocity with inductive-load cells. The required expression relating the magnitude of the balance weights in the correction planes to the measured pedestal motions is as follows.[*] Consider the rigid rotor in flexible pedestals with in-plane unbalance shown in Fig. 3.19a. The effect of the two unbalance forces U_L and U_R for this case is found by taking moments

$$U_L a + U_R(a + b) + F_R L = 0 \quad \text{about bearing L}$$

and

$$U_L(b + c) + U_R c + F_L L = 0 \quad \text{about bearing R.}$$

Solving these expressions for the transmitted forces F_L and F_R gives

$$\begin{bmatrix} -(b + c) & -c \\ -a & -(a + b) \end{bmatrix} \begin{Bmatrix} U_L \\ U_R \end{Bmatrix} = L \begin{Bmatrix} F_L \\ F_R \end{Bmatrix},$$

where the first set of braces represents residual unbalance forces and the second set of braces represents bearing transmitted forces.

Solving for U_L and U_R gives

$$\begin{Bmatrix} U_L \\ U_R \end{Bmatrix} = \begin{bmatrix} -\dfrac{a + b}{b} & \dfrac{c}{b} \\ \dfrac{a}{b} & -\dfrac{b + c}{b} \end{bmatrix} \begin{Bmatrix} F_L \\ F_R \end{Bmatrix},$$

where U_L and U_R represent the residual unbalance forces acting in the correction planes, computed from the forces measured at the bearing

---

[*]The term *flexible* means linear-elastic and deformable. This applies to both soft- and hard-support machines.

locations. The balancing weight required in each correction plane is given by the expressions

$$W_L = U_L \frac{g}{\omega^2 r_L} = \frac{4.237}{N^2 r_L} U_L$$

and

$$W_R = U_R \frac{g}{\omega^2 r_R} = \frac{4.237}{N^2 r_R} U_R,$$

r_L and r_R being the left and right correction radii, respectively, and N being the balancing speed in revolutions per minute.

The above example demonstrates the mechanics of rigid-rotor balancing for the simple case of in-plane unbalance.

Plane Separation. Spatial Unbalance Distribution

The general case for the prediction of correction weights for a spatial distribution of unbalance is shown in Fig. 3.21. First, the rotor unbalance distribution is represented as unbalance forces U_1 and U_2 in the correction planes (Fig. 3.21a). Next, these unbalance forces and the bearing forces F_1 and F_2 are resolved into rotating (ξ, η) coordinates, as shown in Figs. 3.21b and 3.21c. Force and moment equilibrium in the ξ, z plane then give

$$F_1^\xi + F_2^\xi + U_1^\xi + U_2^\xi = 0$$

and

$$U_1^\xi a + U_2^\xi (a + b) + F_2^\xi L = 0.$$

Force and moment equilibrium in the η, z plane give

$$F_1^\eta + F_2^\eta + U_1^\eta + U_2^\eta = 0$$

and

$$U_1^\eta a + U_2^\eta (a + b) + F_2^\eta L = 0.$$

Solving for the unbalance force components gives

$$U^\xi = \begin{Bmatrix} U_1^\xi \\ U_2^\xi \end{Bmatrix} = \begin{bmatrix} -\dfrac{a+b}{b} & \dfrac{c}{b} \\ \dfrac{a}{b} & -\dfrac{b+c}{b} \end{bmatrix} \begin{Bmatrix} F_1^\xi \\ F_2^\xi \end{Bmatrix} = [H]\{F^\xi\}$$
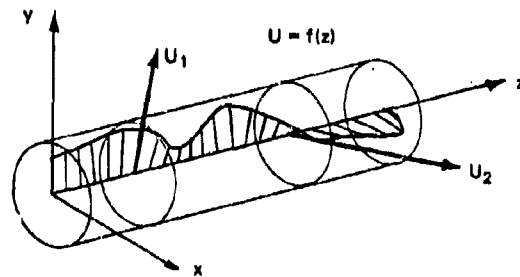
(a) General unbalance distribution represented by
unbalances in correction planes

$$F(x,y) = F(\xi,\eta) e^{i\omega t}$$
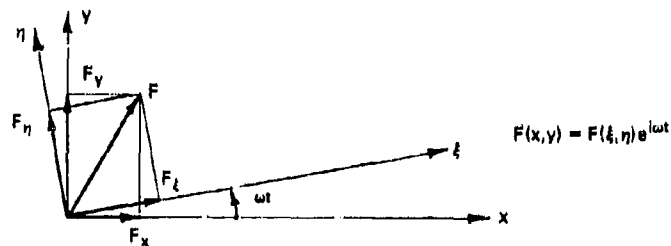
(b) Resolution of force into stationary and rotating components

$$a + b + c = L$$
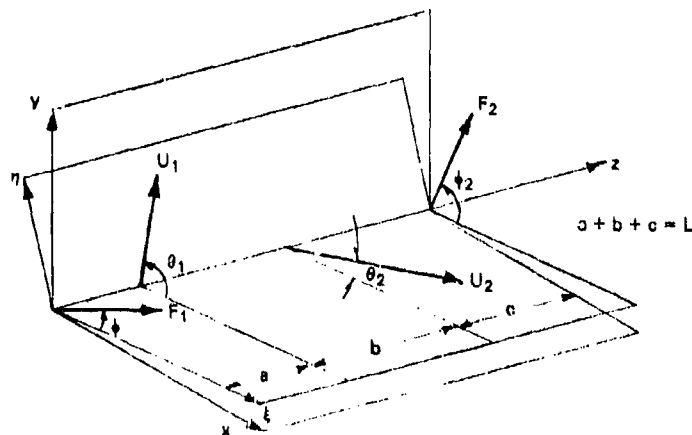
(c) Unbalance forces and pedestal forces for unbalanced rigid rotor

Fig. 3.21. Rigid rotor with spatial
unbalance distribution

and

$$U^\eta = \begin{Bmatrix} U_1^\eta \\ U_2^\eta \end{Bmatrix} = \begin{bmatrix} -\dfrac{a+b}{b} & \dfrac{c}{b} \\ \dfrac{a}{b} & -\dfrac{b+c}{b} \end{bmatrix} \begin{Bmatrix} F_1^\eta \\ F_2^\eta \end{Bmatrix} = [H]\{F^\eta\}.$$

Hence,

$$U_1 = U_1^\xi + iU_1^\eta, \qquad i = \sqrt{-1};$$

that is,

$$U_1 = \sqrt{(U_1^\xi)^2 + (U_1^\eta)^2}\, \exp(i\theta_1)$$

$$\theta_1 = \arctan\left(\frac{U_1^\eta}{U_1^\xi}\right)$$

$$U_2 = U_2^\xi + iU_2^\eta,$$

$$U_2 = \sqrt{(U_2^\xi)^2 + (U_2^\eta)^2}\, \exp(i\theta_2)$$

and

$$\theta_2 = \arctan\left(\frac{U_2^\eta}{U_2^\xi}\right).$$

Similarly,

$$F_1 = F_1^\xi + i\, F_1^\eta, \qquad i = \sqrt{-1},$$

$$F_1 = \sqrt{(F_1^\xi)^2 + (F_1^\eta)^2}\, \exp(i\phi_1)$$

$$\phi_1 = \arctan\left(\frac{F_1^\eta}{F_2^\xi}\right)$$

$$F_2 = F_2^\xi + i\, F_2^\eta$$

$$F_2 = \sqrt{(F_1^\xi)^2 + (F_2^\eta)^2}\, \exp(i\phi_2)$$

and

$$\phi_2 = \arctan\left[\frac{F_2^\eta}{F_2^\xi}\right].$$

These expressions are used for balancing as follows: the maximum values of the force signals $|F_1|$ and $|F_2|$ are read (detected) directly from the pedestal transducer output. The phase angles ϕ_1 and ϕ_2 of these maximum force signals are read with reference to some arbitrarily selected marker on the rotor. Having $|F_1|$, $|F_2|$, ϕ_1, and ϕ_2, we can obtain

$$F_1^\xi = |F_1|\cos\phi_1,$$

$$F_1^\eta = |F_1|\sin\phi_1,$$

$$F_2^\xi = |F_2|\cos\phi_2,$$

and

$$F_2^\eta = |F_2|\sin\phi_2.$$

The matrix expressions given above allow U_1^ξ, U_1^η, U_2^ξ, and U_2^η to be obtained from these force components, given the rotor dimensions a, b, and c. The unbalance components are then combined using the above expressions to give U_1, θ_1, U_2, and θ_2. The required correction weights are

$$W_1 = U_1\frac{4.732}{N^2 r_1} \text{ at } (\theta_1 + 180°) \text{ from } 0° \text{ phase}$$

and

$$W_2 = U_2\frac{4.732}{N^2 r_2} \text{ at } (\theta_2 + 180°) \text{ from } 0° \text{ phase}.$$

Modern field balancers and balancing computers perform the above operations automatically with internal analog circuits, usually with digital display of the required correction weights and phase angles. Equipment of this type is discussed in the next section. Field balancing with a balancing computer is described in Chapter 4.

3.4 Modern General Purpose Balancing Machines

A variety of general purpose balancing machines is available today from U.S. suppliers such as Hoffman, Schenck Trebel, International

Research and Development Corp., (IRD), Gilman-Gisholt, and Stewart-Warner, and other manufacturers. Types of machines available include soft-support, resonant, and hard-support. This section discusses the features of specific general purpose balancers.

Soft-Bearing Machines

The Gisholt Model 31 S (Fig. 3.22) is a typical soft-bearing general purpose balancing machine designed to operate well above the resonant speed of the supported test rotor. The balancer operates at drive speeds between 500 and 2000 rpm. It is able to accommodate rotors weighing between 1 lb and 500 lb. Drive power is supplied through a belt that wraps around the rotor, with a tension pulley arrangement. Unbalance

Fig. 3.22. Gisholt Model 31 S soft-bearing
balancing machine

data are obtained as velocity-transducer readouts from movements of the supporting pedestals. The electronic equipment includes plane-separation circuits and wattmeter filtering. The readout is calibrated in terms of the required balance correction units, in ounce-inches. The "heavy" spot can be located by either stroboscope phase measurement or by comparing surface photocell readings against numbered strips placed at the correction planes. The readout equipment is specified as being able to read down into the 10-μm range. The machine is not permanently calibrated, and precalibration against a rotor of known unbalance is required. The soft-pedestal construction is achieved with a pair of vertical flat springs. One end of each spring is attached to the machine frame, and the other end is secured to the adjacent pedestal support. A detailed comparison between this and the other two machines described in this section is given in Table 3.1.

The Schenck R 30B/8 unit shown in Fig. 3.23 is another example of a general purpose soft-bearing machine designed to operate above its support resonances. This machine accommodates rotors in the weight range from 6 to 660 lb, at balancing speeds between 770 and 1320 rpm. There is provision for overload and overspeed, and for unequal gravity loads of special nonsymmetrical rotors. Phase measurement is by the stroboscopic illumination of a numbered tape, as with the Gisholt 31 S machine. A plane-separation circuit supplies the required balance data

Fig. 3.23 Schenck R 30B/8 soft-bearing universal balancing machine with wattmeter readout, set up for balancing armatures with end drive

Table 3.1. Comparison of balancing-machine features*

Parameter	Soft-support machines	Resonant machines	Hard-support machines
Identification			
Manufacturer	Gisholt	Stewart-Warner	Schenck
Model	31 S	2380	H30U
Special attachments			Standard end drive
Classification			
Type of measurement	Displacement (soft-bearing)	Displacement (soft bearing)	Force (rigid bearing)
Dynamic region	Above resonance	At or near resonance	Well below resonance
Speed range	500—2000 rpm	Medium, usually 300—1000 rpm with 1800 max.	275—1500 rpm
Capacity			
Rotor weight	1—500 lb	1/2—1000 lb	880 lb max-sym.
Rotor length	40 in. max between shoulders	4 1/2—55 in. between journals	4—50 in.
Rotor diameter	24 in. max	1/2—44 in. between journals	40 in. max
Journal diameter	5 in. max	1/2—7 1/2 in.	5/8—3 1/8 on standard roller bearing
Drive diameter		1/2—24 in.	24 in. max (estimated) for optional belt drive
Accuracy			
Detection	20 μin.	0.004 oz in.	0.0035 oz-in.
Measurement			
General Construction			
Weight	2450 lb	1000 lb	2000 lb without foundation block
Size	Floor space 33 × 72 in.	Base 25 × 60 in. plus overhand and amplifier	Base 23 in. × 79 in.
Base design	Three steel tubes spacing end castings	Formed steel	Cast base on 16 in. foundation block
Installation			
Foundation	Any	Sound construction, preferably concrete	Requires heavy foundation
Fastening	Not required	Bolt, level, and grout	Bolt
Isolation from external vibration	Not required because of signal filter and horizontal motion	None	Not required because of filtering
Major design features			
	Special foundation or mounting not required	High sensitivity at resonance	Direct reading in unbalance or correction units
	Constant-speed drive—no waiting for speed change	Drive not in contact with rotor when unbalance readings are made	Complete indications in one run without calibration trial run
	Signal filter eliminates extraneous influences	Special bearing or drive adapters not required	Wattmeter system filters out extraneous influences
	Complete plane separation with guess variety of work	Ease of adjustment for work	Polar scale readouts for each correction plane with complete retention
	Calibration in terms of correction units		

*From Ref. 5.

Table 3.1. Comparison of balancing-machine features* (Cont'd)

Parameter	Soft-support machines	Resonant machines		Hard-support machines
		Force and couple system	left and right system	
Setup				
	Insert half-bearings to fit journal (unless roller type support is used)	Position and load	Position and load	Position supports
	Position supports, drive, idler pulleys, and strobe	Drive with vibrator	Place reference mark for phase angle	Load with unbalance rotor
	Load with calibrating rotors	Tune spring systems to decouple modes	Lock spring on one side	Adjust bearing support heights
	Drive and set filters, calibration, and plane-separation knobs	Note both resonant frequencies		Insert and fasten coupling
	Replace with unbalance rotor	Place reference mark for phase angle		Set knobs for rotor dimensions
	Place numbered angle reference strip			
Measurement				
	Drive	Adjust damping for anticipated unbalance	Adjust damping for anticipated unbalance	Drive
	Read unbalance in correction units and angle from strobe image on one side.	Drive to speed above upper resonance	Drive to speed above resonance	Read unbalance and location in correction units for both sides.
		Permit coastdown and read first peak amplitude	Permit coastdown and read peak amplitude	
		Note strobe image of reference mark, at peak	Note strobe image of reference mark at peak	
		(Alternate: note strobe image at above resonance speed)	(Alternate: note strobe image at above resonance speed)	
		Continue coastdown and read second peak	Repeat with other spring locked	
		Note strobe image at peak (or use alternate)		
Correction				
	Apply corrections as indicated	Apply force and couple corrections separately in estimated proportion to readings	Apply corrections in estimated proportion to readings and in estimated distribution between planes	Apply corrections as indicated
		Repeat as required, reducing damping as permitted	Repeat as required, reducing damping as permitted	

*From Ref. 5.

Table 3.1. Comparison of balancing-machine features* (Cont'd)

Parameter	Soft-support machine	Resonant machines	Hard-support machines
Work supports			
Position adjustment	Move and lock manually	Lever-operated column ratchet and lock	Move and lock manually
Location on rotor	Journals	Journals or other finished diameters	Journals or other finished diameters
Type of bearing	Half bearings (rollers optional)	Ball-bearing rollers in trunnion block	Ball-bearing rollers
Isolation from bearing runout	Not required	Change size of rollers	Change size of rollers
Diameter adjustment	Half bearing to suit (vertical on rollers)	Two spacings of bearing pockets	Vertical adjustment on roller support
Bearing friction control	Not required with continuous drive	Change size of ball-bearing rollers	Not required with continuous drive
Holddown of journal		Inverted trunnion may be added	Holddown bracket—no rollers
Use with unequal journal	Half bearings to suit (vertical adjustment on rollers)	Flat springs in trunnion flex to align rollers	Vertical adjustment on roller support
Prevention of journal damage	Suitable bearing material (provision for alignment?)	Extra care in bearing alignment	Crowning on roller OD
End restraint	Shoulders on rotor	Roller or flat, with 1/16 in. clearance	None—restraint from drive coupling
Isolation from end runout	None	Use ball in center hole	Not required
Drive system			
Use	Continuous drive	To drive rotor up to speed, then withdraw	Continuous drive
Type	Flat belt with 180° wrap around rotor	Flat belt contacting rotor	End drive through coupling (belt drive optional)
Location on rotor	Any diameter, preferably between journals	Any diameter, preferably large	Either end
Position adjustment	—	Lever-operated ratchet	Not required
Speed range	—	3800 and 1900 rpm	275, 500, 900, 1500 rpm
Speed adjustment	Motor pulley size	Two positions on drive handle switch	Lever-operated gear shift
Starting and Stopping	Foot switch	Drive handle switch	Manual switch
Tensioning at setup	Positioned idlers gravity loaded against belt	Hand pressure on drive handle	Not required
Clearance for loading	Lift work against idler weight (belt lifter optional)	Tilts up for clearance	Not required for end drive
Braking	Operated with start-stop foot switch	Drive handle controls belt brake	Dynamic braking with motor controls
Isolation from drive runout	Not required, extraneous signal filtered out	Drive not contacting during measurements is balanced	Not required if coupling
Spring system			
Type	Parallel flat springs, one end fixed, other clamped?	Flat spring with fixed end and intermediate fulcrum	Inherent in force transducer
Plane of Motion	Horizontal	Vertical	Horizontal
Adjustment	Not required	Screw-driven fulcrum	Not required
Prevention of axial motion	Relative stiffness of flat spring axially	Relative stiffness of flat spring in axial plane	—
Locking	Not required	External clamps on stabilizer link	Not required
Damping			
Type	Not required	Dashpot, viscous	Not required
Adjustment	—	Piston orifice, five alternative diameters	—
Calibration	—	None	—
Temperature stabilization	—	None	—
Plane-separation pivots	Not required	Special attachment only—not studied	Not required

*From Ref. 5.

Table 3 1. Comparison of balancing-machine features* (Cont'd)

Parameter	Soft-Support Machines	Resonant Machines	Hard-Support Machines
Measuring			
Vibration pickup	Velocity by magnetic induction.	Velocity by magnetic induction: integrated to give displacement	Force transducer
Speed	Not required	Frequency from pickup signal or from separate pickup driven by shaft-mounted magnet	Controller in drive
Phase	Timing from point of maximum positive displacement, i.e., when velocity changes from negative to positive polarity	Timing from zero displacement on down travel	Timing in relation to phase generator driven with rotor
Indicating			
Amplitude	Meter with numbered scale, no units	Meter with numbered scale, no units	Not required
Speed	Not required	Meter with 1800-rpm maximum scale	From drive speed setting
Phase	Strobe light directed horizontally gives position of heavy side by "stopping" circumferentially wound numbered strip	Strobe light gives position of reference chalk mark at or close to resonance	Wattmeter used with phase generator, signals displayed on vectormeter polar scale
Unbalance	From amplitude indication	From amplitude indication	Included in vectormeter polar scale
Other			
Vibrator	None required	Maintains vibration in force or couple mode to permit tuning of resonance	Not required
Signal filter	Two manually set to accept signal at same frequency as rotation	None	Wattmeter functions as filter of nonsynchronous signals
Computer for combining signals	None required	Sum and difference of left and right signals	None required
Calibration in correction units	Separate calibration knob for right and left	None (except with plane-separation attachment	Scale calibration setting with sensitivity multiplier
Phase angle adjustment	--	Circuit resistance adjustment to give 90° lag at resonance with lowest damping	Not required
Amplifier gain	Standard and high (5:1)	Low, high, and extra high	Variable-sensitivity multiplier
Computer for plane separation	Set by two knobs (from calibrated rotor)	None	Set by three knobs from rotor dimensions
Compensator	None	None	(Optional)
Memory circuit	Will hold, electronically or mechanically, both left and right unbalance and angle measurements. Angle measurement from photocell circuit triggered (in place of stroboscope) (optional)	Will store, hold, and read single unbalance reading (optional)	Will hold all unbalance and angle measurements
Synchronizer	Not required	None	Not required

*From Ref. 5.

by dialed-in values of the rotor proportions. The required correction details for each balance plane are read out on the two vectormeters shown in Fig. 3.24. The machine shown has an end drive, but belt-driven models are also available. The pedestal supports may be moved axially to accommodate different rotor sizes.
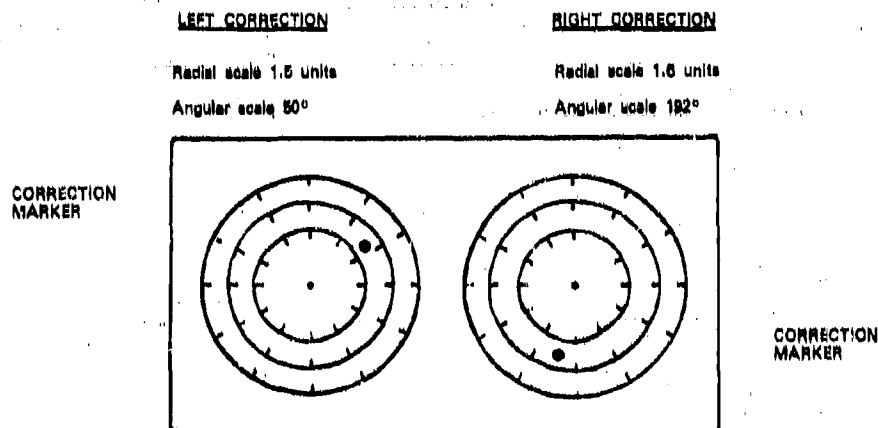
LEFT CORRECTION

Radial scale 1.5 units

Angular scale 50°

RIGHT CORRECTION

Radial scale 1.5 units

Angular scale 192°

CORRECTION
MARKER

CORRECTION
MARKER

Fig. 3.24. Vectormeters for machine shown
in Fig. 3.23

Resonant Machines

The Stewart-Warner 2380 S machine (Fig. 3.9b) has a unique pedestal support that permits it to be tuned so that the natural frequency of the rotor in its supports will occur at the desired balancing speed of the machine. In practice the rotor to be balanced is loaded into the pedestal supports, and the dashpot damping of the supports is manually set to zero. The rotor is then bumped gently, causing it to vibrate in its lowest mode on the supports. A vibration meter measures the frequency of this mode by observing the pedestal motions. A suitable value of damping is then obtained, for example, as follows: A suitable critical damping ratio is

$$\zeta = \frac{B}{B_C} = 0.5,$$

and the critical damping is

$$B = 2M\omega_n = \frac{4\pi}{g} Wf_n.$$

Thus the damping per support is

$$B_S = \frac{1}{2} B = \frac{\pi}{g} W f_n,$$

where W is the rotor weight and f_n is the lowest mode natural frequency of the rotor in its supports. Both dashpots are then adjusted to the selected damping value so that rotor vibration amplitudes will not become excessive when the rotor runs through this critical speed during balancing. An overhead cantilever belt drive is used to spin the rotor up to speed, with the required rotor speed preset on the handle of the cantilever drive arm. A common balancing speed for this machine is 450 rpm. The natural frequency of the rotor in its supports is adjusted to occur somewhat below this speed, so that a large mechanical amplitude magnification occurs as the rotor passes through resonance when the drive is removed. Rotor unbalance is read on a graduated scale (no units) for the left correction plane and for the right correction plane independently. Unbalance angular orientation is determined by triggered stroboflash, as with soft-bearing machines.

The Stewart-Warner 2380 S is a trial-and-error type of machine. Unbalance relative magnitude and angular location are detected in one plane while the other support is restrained against motion. Next a correction mass (usually putty) is added in one of the balancing planes. The rotor is then rerun to observe the effect on the rotor balance. After the rotor has been made to run smoothly with one support secured, the process is repeated with the other support secured. Plane-separation equipment is optional; it is not always needed in the applications for which the machine is used (e.g., motor-rebuilding shops, automotive single-plane balancing). Where the plane-separation calculation is included, it ensures that the first plane need not be rebalanced after the second plane has been corrected. Otherwise this is done by trial and error.

The advantages of this design are (a) easy setup and access, (b) simple mechanical magnification principle, (c) simple controls, and (d) simple operation. There are, however, disadvantages: (a) plane separation is not a built-in feature and requires a separate attachment; (b) the trial-and-error procedure may be time-consuming; (c) the unbalance scale is not calibrated in ounce-inches; and (d) the quality of balance depends on the operator's skill.

A study of this machine [5] has suggested that balancing accuracy down to 0.004 oz-in. (1×10^{-6} in. c.g. eccentricity for a 200-lb component) is attainable, but no basis is given for this figure. Further considerations are the operator experience and balancing time required to consistently achieve this balance quality, where needed. This type of machine has found widespread application in the automotive industry

for balancing crankshafts, crankshaft–flywheel assemblies, and other automotive components, especially in engine- and motor-rebuilding shops.

Hard-Support Machines

The Schenck Model H30V (Fig. 3.25) is a typical hard-bearing machine. It comes with either direct- or belt-drive options, plane-separation circuits, wattmeter filtering and measurement, and pushbutton setup of the balancing operations. Unbalance signals are detected at the pedestals with inductive force transducers. The balancing speed is usually within the range of 275 through 1500 rpm; this range is considerably below the resonant frequency of the rotor on its support system. A maximum rotor weight of 880 lb symmetrically disposed on the pedestals is permitted. Asymmetrical rotors (unequal pedestal loads) of smaller weight are also permitted.

Fig. 3.25. Schenck H30V hard-bearing machine.
(Courtesy of Schenck Trebel Corporation.)

This machine has the following advantages: easy setup and operation; permanent calibration—no trial weight runs; simple dial-in balance with vectormeters; precision balancing; and ability to handle a wide range of rotors. Among its disadvantages are a higher installation cost and the fact that it is a somewhat more delicate machine.

This Schenck machine is said to be capable of balancing down to 0.0035 oz-in. Such accuracy may be possible with light rotors (e.g., 30 lb), but even so this corresponds to a c.g. eccentricity of 3.5 μin.; for 880-lb rotors this would mean 0.25 μin., which may be difficult to achieve with such a machine under production circumstances, with long periods between overhauls. However, instances where such accuracy is essential are likely to be rare in practice.

McQueary [4] has made the following comments on hard supports for balancing machines:

1. The hard-bearing suspension system eliminates windage disturbances that can occur in soft-bearing machines when balancing blowers, fans, compressor rotors, and the like. The workpiece rotates as an assembly, with no swinging of the supports.

2. Erratic oscillations may build up on soft-bearing machines and mask unbalance signals. This is less likely with hard-bearing systems. Unbalance signals therefore come through without distortion.

3. Large unknown initial unbalances are unable to cause dangerous or damaging excursions of the suspension system, as may be possible with soft-bearing machines. Not only will such unbalances not damage the supports or pickups, but they can be directly measured with hard-bearing machines, without any necessity for prebalancing (by knife-edge or static means), which may often be required with soft-bearing balancing systems.

4. Hard-support machines measure unbalance forces rather than vibratory displacements. The parasitic mass of the suspension system does not limit sensitivity with smaller workpieces, and a wider capacity range is generally provided. Minimum rotor weight to maximum rotor weight ratios of 1:200, 1:250, or even more are possible.

5. The hard-suspension system is both sensitive and rugged. It is also difficult to damage with chips, grit, or dirt. The hard-suspension system has no moving parts to wear or loosen during extended operation.

6. Because of good sensitivity and accuracy in permanently calibrated hard-bearing machines, an inspector or supervisor may conveniently determine whether required balancing tolerances have been achieved.

7. Permanently calibrated hard-bearing machines are available for all required balancing speeds. Earlier machines were calibrated for one or more discrete balancing speeds, but the most modern machines are now equipped with integrator circuits so that calibration is valid for a wide range of balancing speeds.

General Purpose Hard-Support Machine

A typical industrial hard-support balancing machine is shown in use in Fig. 3.26. Hard-support machines of this type have been designed to balance a wide range of equipment: electrical armatures, fans, synchronous condensers, turbine rotors, jet-engine compressor rotors, cable-winding drums, and the like. These machines are available in a variety of sizes and speeds. Special purpose facilities of this type are also available for industrial turbine rotors, compressor impellers, and satellites.
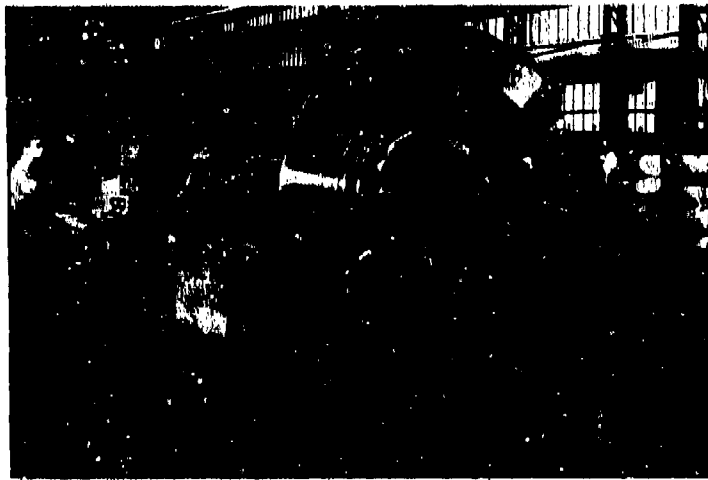

Fig. 3.26. General-purpose hard-support balancing machine with fan rotor installed. The Lawaczenk-Heymann principle is coupled with automatic plane separation and wattmeter dial readout to reduce the amount of trial and error involved in balancing a wide range of rotors. (Courtesy of Schenck Trebel Corporation.)

The general purpose hard-support machine is an efficient device for two-plane balancing. It operates on the Lawaczeck-Heymann principle. Strain gages or displacement sensors are attached to the hard-support frame, as shown in Fig. 3.27. These sensors transmit pedestal motions as electrical signals to the console. One special pedestal design for obtaining vertical rigidity and calibrated horizontal flexibility is shown in Fig. 3.8. Both pedestals are permanently calibrated before shipping, and no calibrating runs with special rotors are needed before balancing. A synchronous phase reference voltage signal is taken from the drive, which may be either a universal coupling or a quick-attach belt. Inductance-transducer signals are then processed by a wattmeter circuit in conjunction with a plane-separation circuit to give the

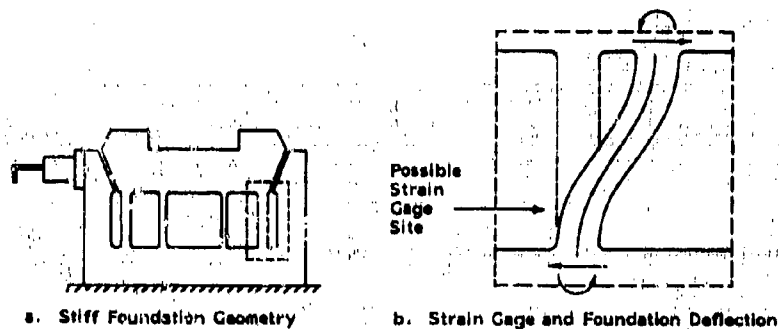a. Stiff Foundation Geometry   b. Strain Gage and Foundation Deflection

Fig. 3.27. Strain gage locations on hard-support frame

required balance correction magnitudes and orientation angles. Either the residual unbalance and phase angle in both balancing planes or the required balance weights and their orientation can be specified as output on the vectormeter screen used in the model of Fig. 3.25. A general purpose console face is shown in Fig. 3.28.

The permanent-calibration feature combined with the internal wattmeter and plane-separation electronics allows direct readout of the required balance weights and orientation angles on the console; an immediate two-plane balance is therefore possible for a wide variety of ISO class 1 and class 2 rotors. The basic dimensions of the rotor to be balanced (a, b, c, r_1, r_2 in Fig. 3.28) are first dialed into the balancer console. The rotor is then run at the desired balancing speed, and readings of the magnitude and location of the required balance weights and their phase angles are displayed directly on a circular calibrated scale, or vectormeter. The rotor is then stopped, the required correction weights are inserted in the two correction planes, and the rotor is rerun at the balancing speed to check the effectiveness of the balance. The simplicity of this process will permit a relatively unskilled operator to balance rotors rapidly and effectively without much training or special instruction. The amount of trial and error required is minimized by the sophistication of such machines. Specific advantages are the following:

1. Adaptable to a wide range of rotor sizes and configurations
2. Direct readout of correction details, requiring less skill and making production balancing efficient
3. Permanent calibration, allowing balancing to be done in one run (though a second check run is desirable)
4. Simultaneous two-plane balancing with plane separation, making direct readout possible with maximum convenience and simplicity of operation
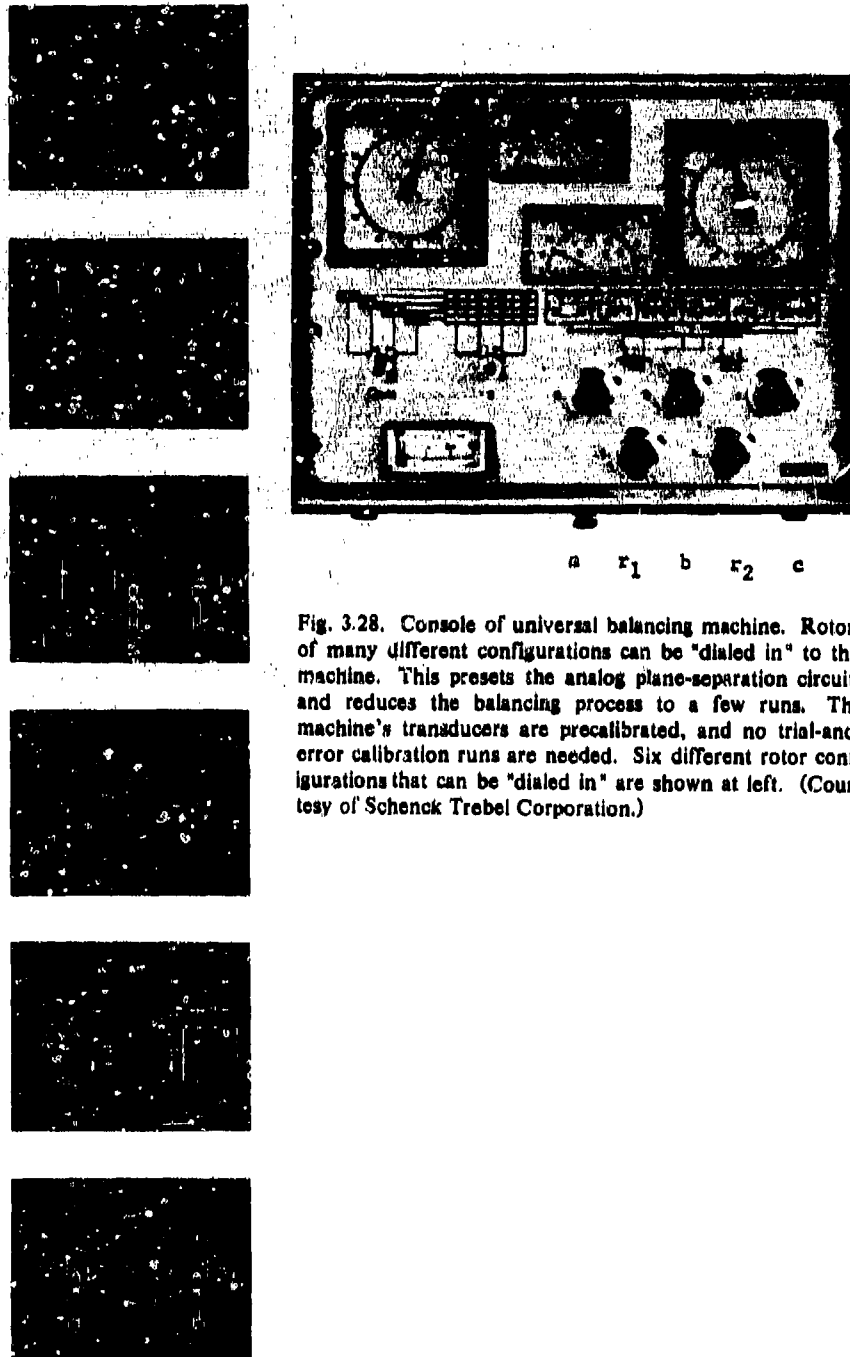
a r_1 b r_2 c

Fig. 3.28. Console of universal balancing machine. Rotors of many different configurations can be "dialed in" to this machine. This presets the analog plane-separation circuits and reduces the balancing process to a few runs. The machine's transducers are precalibrated, and no trial-and-error calibration runs are needed. Six different rotor configurations that can be "dialed in" are shown at left. (Courtesy of Schenck Trebel Corporation.)

5. The supports have great strength and stiffness and their parasitic mass is minimal, compared with soft-bearing-machine supports.

6. The influence of external forces (e.g., transmitted vibration, windage) is less than with soft-support machines.

There are, however, several disadvantages:

1. Only two-plane balancing is possible with standard arrangements. Multiplane balancing of ISO class 3 flexible rotors cannot be undertaken on such a machine without additional special features (e.g., midplane displacement sensor). General purpose balances are suitable for class 1 rigid and for class 2 flexible rotors.

2. Overhung disks cannot be accommodated without special provision (no negative distance provision is included on the standard dial panel). More recent machines include this provision.

3. Care must be taken to align the workpiece with the drive-motor axis if the direct-drive option is used. Such is not the case with the belt-drive option. Also a special adaptor coupling is required where a range of rotor sizes and ends is to be accommodated.

3.5 Balancing Facilities

Turbine and Generator Balancing

Turbine and generator balancing facilities are designed to permit both high-speed balancing operations and overspeed testing of assembled rotors once a given rotor is installed. Such facilities may incorporate the following features:

Concrete overspeed burstproof tunnel
Vacuum spin-test chamber
Variable-speed drive with 20 percent overspeed capability
Size provision for fully bladed rotor assemblies
Bearing pedestals designed to simulate machine-support properties
Transporter to move rotor assemblies and setup of rotor
Control room with full test instrumentation
Overhead crane
Rigid clamping of transporter to tunnel foundation.

Figures 3.29 and 3.14 show details of a transporter loaded with a rotor assembly, and certain internal details of the tunnels. Figure 3.30 is a section schematic of a turbine-generator balance facility. Figure 3.31 shows a modern U.S. facility with twin tunnels. Both tunnels are powered by dc-motor drive systems of 10,000 hp each. The lubrication systems are capable of supplying an oil flow of nearly 2000 gpm to each bunker. The generator bunker is suitable for balancing large generators

under full excitation. The bunker design incorporates antimagnetic bedways and more than a million insulated rebar joints, with special electrical grounding provisions. Both bunkers have interchangeable sets of pedestals, and two sets of specially designed steady bearings are available for handling extremely long rotor overhangs. Steel-reinforced concrete walls up to 9 ft thick provide burst protection. Hundreds of concrete piles form the foundation. The hard-vacuum liner contains over 800 tons of structural steel.

A variety of balancing machines is currently available for the balancing of turbine and generator rotors. The particular balancing equipment selected in a given case will depend on rotor size, equipment availability, and the extent of the need for high-speed balancing.* Both ISO class 1 and class 2 rotors will operate satisfactorily after being balanced in a low-speed balancing machine. Class 3 rotors require high-speed balancing. Such testing may require balance runs near one (or more) resonant speeds within the operating range. Sustained high-speed operating capabilities are required for such balancing. It is therefore convenient to have a common high-speed facility in which both balancing and overspeed testing can be undertaken. Class 3 rotors are usually large and long and may carry thousands of blades. This also influences the equipment associated with a high-speed facility.

The amount of drive power required for a high-speed facility is evidently a compromise between vacuum pump-down power and
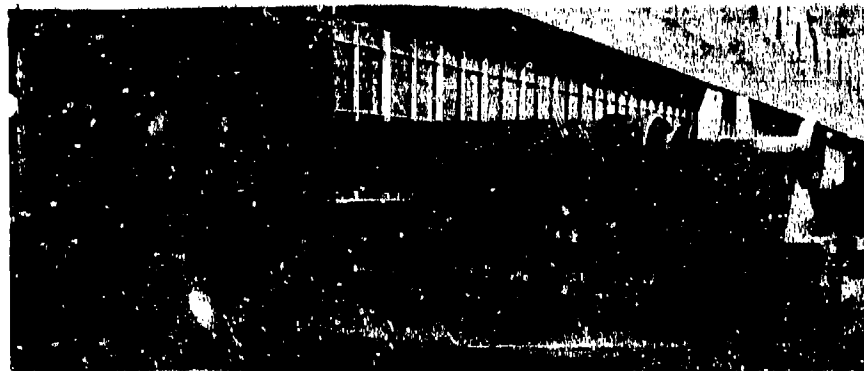

Fig. 3.29. Generator rotor supported in transporter in special bearings. The electric power unit is detachable and is removed when the rotor and supports are installed in the spin pit (Fig. 3.14). (Courtesy of Schenck Trebel Corporation.)

---

*The type of balance prescribed for a given rotor is usually based on previous satisfactory balancing experience with similar rotors. For new rotor designs, the rotor classification and balance requirements may also be guided by calculated data on machine critical speeds and unbalance response.
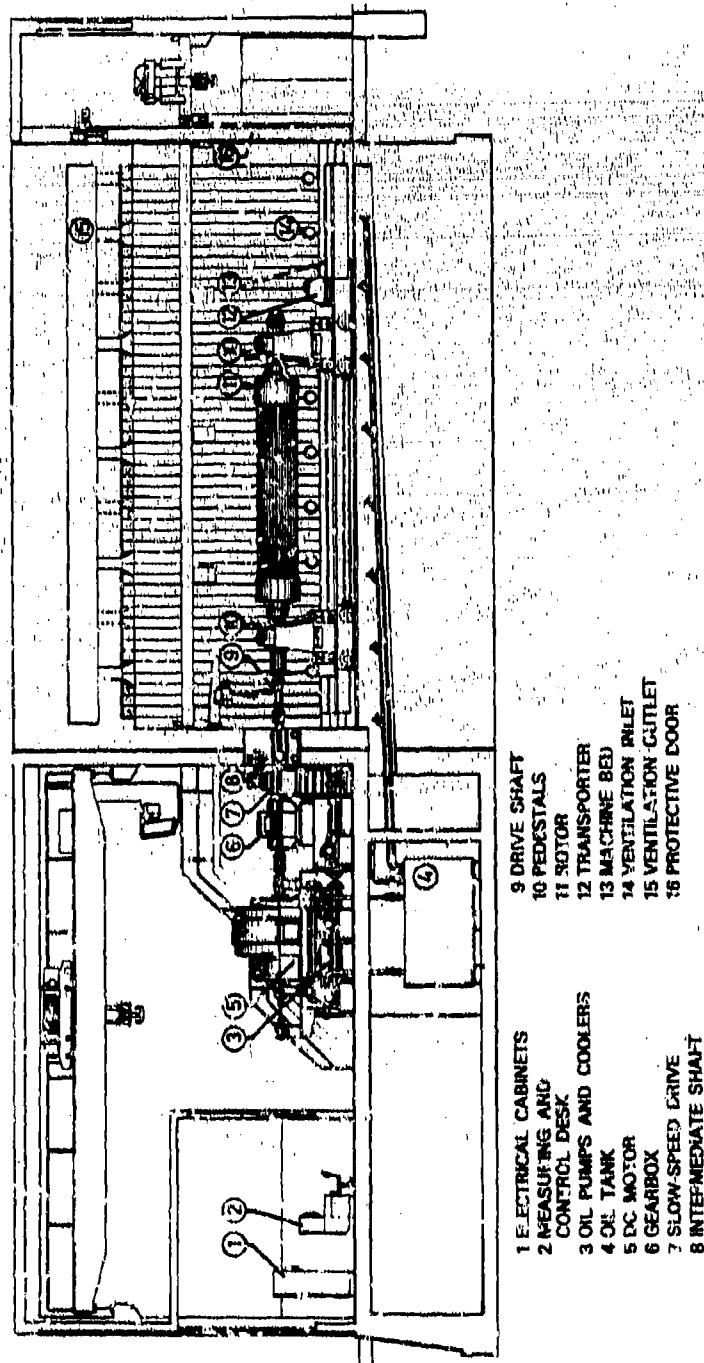
Fig. 3.30. Sectional view of spin-pit balancing facility showing main features: a dc motor with Ward-Leonard gear-driven speed-control system, lubrication system, reinforced-concrete burst pit for speeds of up to 4300 rpm, transporter in position, generator rotor, bearings, and hydraulic jacking system. Not shown are vacuum facilities for balancing steam-turbine low-pressure rotors and other large rotors. The rotor is precisely aligned with the drive shaft before startup. (Courtesy of Brown Boveri Corporation.)

1 ELECTRICAL CABINETS
2 MEASURING AND
  CONTROL DESK
3 OIL PUMPS AND COOLERS
4 OIL TANK
5 DC MOTOR
6 GEARBOX
7 SLOW-SPEED DRIVE
8 INTERMEDIATE SHAFT

9 DRIVE SHAFT
10 PEDESTALS
11 ROTOR
12 TRANSPORTER
13 MACHINE BED
14 VENTILATION INLET
15 VENTILATION OUTLET
16 PROTECTIVE DOOR

Fig. 3.31. Large twin–tunnel, high-speed balancing facility. This high-speed balancing and test facility at the General Electric plant in Schenectady, New York, is the largest of its type in the United States. This facility can handle rotors weighing 12 to 350 tons. The rectangular tunnel is for balancing generator rotors (maximum diameter 230 in.) under atmospheric conditions. The cylindrical tunnel is for balancing turbine rotors (maximum diameter 132 in.), in vacuum (down to 1 mm Hg). (Courtesy of General Electric Company.)

drive-power requirments. Typically, spin-pit drive power would be about 1 percent of the maximum rated power output of the rotor being tested; that is, a 500-MW generator would have a 5000-kW drive motor, and the spin pit would be evacuated down to about 0.03 to 0.07 atm. Without vacuum operation, testing of most large-bladed rotors would not be possible because of excessive fan-power requirements and the associated air heating and noise generation.

Modern spin-pit balance facilities are complex installations. Costs (1980) may range from $3 million to $20 million for a large completely installed facility. Table 3.2 indicates the location and details of some recent spin-pit installations. Figure 3.14 is a general view of a concrete balance spin-pit facility showing the rotor on its transporter, with special bearings and pedestals; details of the lubrication-system pipes are also shown. The bearings are bolted to the foundation during testing, as indicated. A 400-MW generator rotor on its transporter is shown leaving the assembly shop for balancing in Fig. 3.29. The transporter drive unit, shown attached to the transporter truck, is uncoupled and removed when the rotor is in the spin pit. A section through a balance facility is shown in Fig. 3.30 with a generator rotor installed. Details of the drive, drive coupling, lubrication system, and other features of such facilities are evident in this section drawing.

A section through a special bearing pedestal support for use in turbine-generator balance pits is shown in Fig. 3.32. Such units have been designed to provide a tuned pedestal support in which the specific bearings of the rotor being balanced are installed. This permits the rotor to be balanced while operating in its own bearings and simulated pedestals. It is shown in Chapter 5 that the rotor-support stiffness properties may exert a significant influence on the critical speeds and dynamic properties of a rotor—bearing system. If a rotor is balanced in hard bearings and then operated in softer bearing supports, the rotor-system modes will be different and the balance achieved in the balancing stand will not be fully realized during operation. The rotor may then run "rough" unless corrected by further in situ trim balancing.

The support design shown in Fig. 3.33 allows the rotor to be balanced in the bearings in which it will operate. Matched dynamic prop- erties are especially important for large class 3 rotors in which unbalance effects through the fourth flexural mode may influence the balance obtained. The stiffness properties of such supports can be adjusted within the range 30,000 lb/in. through 3.0×10^6 lb/in. according to whether soft- or hard-support balancing is required. This preserves the balance quality achieved for the required operating conditions, and leads to less field balancing. Figure 3.33 shows details of such bearings, including the lubrication inlet (foreground) and the tangential force transducers from which the transmitted unbalance force

Table 3.2. Details of recent high-speed balancing facilities

| Date	Firm/location	Speed (rpm)	Weight (tons)	Type
1970	Machinefabriek Stork Hengelo, Holland	20,000—40,000	5.0—0.5	Tunnel
	Ansaldo Genoa, Italy	2100—4320	180—60	Tunnel
	Stal-Laval Finspong, Sweden	3600—4500	160—150	Pit
	Kraftwerk-Union Muelheim, Germany	2250—4500	320—120	Tunnel
	Alsthom Belfort, France	200—4320	250	
1971	Stankoimport Moscow, USSR	8000—18,000	30—9	Tunnel
	Stankoimport Moscow, USSR	50,000	220 lb	Pit
	Westinghouse Electric Corp. Charlotte, NC	2200—4400	160—80	Heater box
	General Electric Co. Schenectady, NY	4000—12,000	22—0.4	Vacuum pit
	Westinghouse Electric Corp. Round Rock, Tex.	440	32	Vacuum pit
	Electric Machinery Mfg. Turbodyne St. Cloud, Minn.	2160—4320	50—32	Vacuum
1972	Allis Chalmers Milwaukee, Wisc.	2200—4400	250—160	Vacuum tunnel
	General Electric Co. Schenectady, N.Y.	2200—4400	300—190	Twin facility
	Brown Boveri Richmond, Va.	4320	270	Vacuum tunnel
	Stankoimport Moscow, USSR	1000—22,000	3300—1100 lb	Pit
1973	Mitsubishi Heavy Industries Nagasaki, Japan	180—15,000	20	Pit
	ACEC Ghent, Belgium	200—6,000	50	Tunnel
	Mitsubishi Heavy Industries Takasago, Japan		125	Vacuum pit
	Stankoimport Moscow, USSR	2250	320	Tunnel
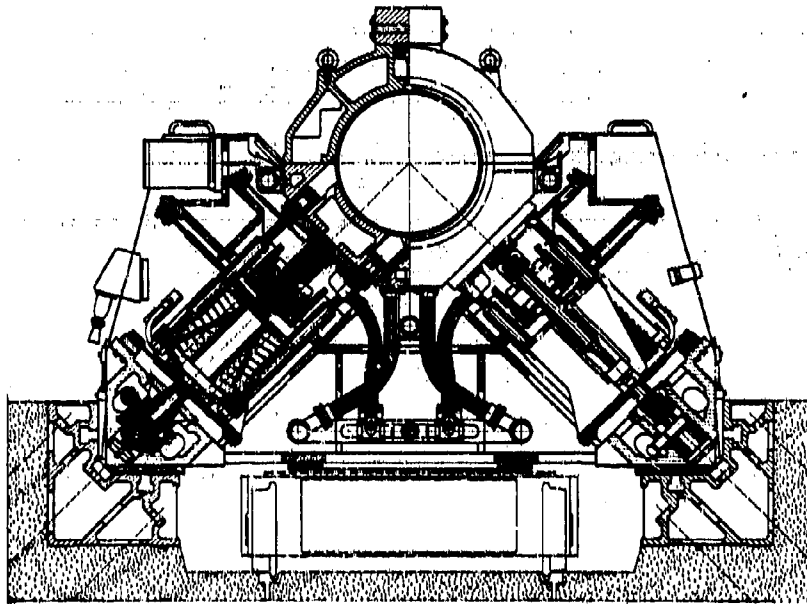
Fig. 3.32. Pedestal-bearing support for large flexible rotors. Many large rotors require fluid-film bearing supports for balancing. If allowed to remain on rolling-element bearings they may brinell the supports with their weight (up to 250,000 lb per support). Also, improved balancing is achieved with the rotor supported in bearings with dynamic properties resembling those occurring during operation. This is especially true for class 3 rotors, which can be influenced through the fourth flex-ural mode. The bearings shown provide nearly isotropic stiffness and mass distribu-tion for the pedestals. The bearings also conform more to the rotational axis of the rotor. The stiffness of the supports can be adjusted in the range 30,000 to 3×10^6 lb/in., according to whether soft- or hard-bearing balancing is required and accord-ing to the balance speed required. (Courtesy of Schenck Trebel Corporation.)

Fig. 3.33. Bearing pedestal for mounting rotor bearings during balancing. (Courtesy of Schenck Trebel Corporation.)

signals are read. Fluid-film supports also avoid the problem of "brineiling" that may be induced in rolling-element bearing supports by the rotor weight, which may range up to 250,000 lb per pedestal.

Automated Balancing Facilities

High-volume production industries depend on automated equipment to deal with large numbers of repeated operations. Automated and semiautomated balancing are widely used in the automotive industry for crankshafts, propeller shafts, tire-wheel assemblies, etc., and in the electric motor industry for vacuum-cleaner motors, blender motors, fan motors, and so on. These and other industries have incorporated automated balancing equipment into production lines to achieve high-volume balancing of the desired balance quality.

An example of an automated balance facility is the automated crankshaft balancing installation shown in Fig. 3.34. This facility incorporates a production line for

1. Initial measurement of residual unbalance in two planes
2. Correcting the unbalance by drilling at the required locations to correct for unbalance in these planes

Checking that the corrected crankshaft is within required balance specifications.

Some details of this crankshaft balancing stand are shown in Fig. 3.35. Incoming batches of crankshafts are loaded onto a conveyor with a gravity-feed roller conveyor in an ordered fashion. The process is automatic from this point. The foreground of Fig. 3.35a shows the residual unbalance measuring stand. Two displacement sensors record the unbalance as the crankshaft is rotated at low speed (400 rpm). The signals are stored and the crankshaft automatically conveyed to the drilling stand by the overhead conveyor unit. The crankshaft is automatically indexed to the required angular position for each plane in turn, based on the data obtained during the previous measuring operation. Two separate drills then remove the required depth of metal at the desired orientation. The drilled crankshafts are then transferred to a balance-checking unit for a second measurement. The jaws of the drilling unit open horizontally down the center, and once the crankshaft is correctly positioned, the two halves are moved together pneumatically to clamp the crankshaft for drilling. The linkage and pneumatic cylinder can be seen in Fig. 3.35b.

Cycle time for measuring, drilling, and checking each crankshaft is 40 s, including the transport time between stands; about the same

operation time is spent in each stand. Each stand has its own motive power, and while being measured the crankshafts are driven at balancing speed (400 rpm) by end rollers under the crankshaft journals. The measuring operation uses both plane separation and wattmeter filtering.

After being checked, crankshafts are classified "within tolerance" or "outside tolerance" automatically. Accepted crankshafts pass out on the conveyor; rejected crankshafts are removed by a swivel mechanism that places them on a separate conveyor for reprocessing. Residual unbalance in an uncorrected production crankshaft tends to be high because machining of the forged crankshaft blank is kept to a minimum to keep manufacturing costs low. When finished, the unmachined surface is still in the "as formed" condition, except for the machined journals, connecting-rod bearings, and balance areas.

Two types of crankshaft-balancing operations can be performed. First there is mass centering, in which the mass axis of the crankshaft is adjusted to coincide with the machining axis. Second, there is final balancing of the crankshaft. Machines for mass centering are used at the start of the crankshaft-machining operation. Initial mass-centering

Fig. 3.34. Automatic facility for balancing crankshaft—clutch housing assemblies. Automatic operation includes mechanical handling, unbalance readout, unbalance correction by drilling or milling, residual unbalance checkout, acceptability sorting, and dispatch conveyors. Design is highly customized and built to suit specific plant requirements. Cycle time is commonly 10 to 20 s, depending on size. (Courtesy of Schenck Trebel Corporation.)
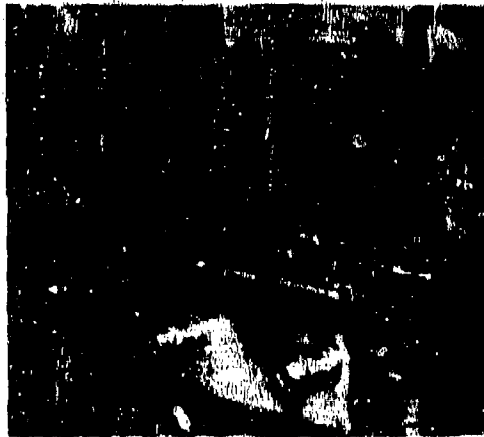
(a) Residual unbalance measuring stand. The rotor is spun up to speed on drive rollers. The transducers (foreground) measure the residual unbalance force. The transporter hooks are shown above the rotor.

(b) Unbalance correction by metal removal. The crankshaft is in a transporter, about to be lowered for clamping, indexing, and drilling, all automatically controlled. The two drill stems are shown in the foreground. Pneumatic clamping is used. (Courtesy of Schenck Trebel Corporation.)

Fig. 3.35. Details of automatic crankshaft-balancing facility

does not ensure a perfect final balance correction, but it greatly reduces the amount of metal removal necessary in the second step. Final machining is undertaken at the end of the production sequence. Although automated, it is really a trim-balancing operation, which is made necessary by the machining of journals.

Not all crankshaft-balancing machines are fully automatic. The degree of automation depends on many factors, including production volume requirements. Some machines are semiautomatic, with the operator setting the indicated amount of acceptable residual unbalance on the data input panel; the subsequent drilling operations are then carried out automatically by the machine. Other automatic and semiautomatic balancing machines are used for balancing clutch housings, brake drums, clutch–crankshaft assemblies, wheel–tire assemblies, universal drive shafts, fan assemblies, and so on.

When a number of balanced components are assembled, the assembly so formed frequently requires trim balancing to eliminate the effects of component-mounting eccentricity. An example of assembly balancing is the special machine shown in Fig. 3.11, which has been developed for the final balancing of complete engine assemblies. This machine provides a final trim balance for a total rotating assembly in its own bearings and casing. In the machine shown in Fig. 3.11, the final balance is achieved by correcting on the fan pulley and on the flywheel.

Another example of an automated balancing facility is a four-station fully automatic machine for dynamically balancing the rotors of drive motors for high-fidelity sound-reproduction machines. This balancing machine is stated to be capable of checking, correcting, and grading 180 rotors per hour to eccentricities of 0.00008 in. from the rotational axis, for displacements in two planes. It is a second-stage machine that accepts rotors that have been previously rough-balanced. There are four operations in the cycle: the first measures the initial unbalance, the second makes the required corrections in both planes, the third checks whether the rotor should be accepted or rejected, and the fourth directs the rotor to "accepted" or "rejected" conveyors. All operations are continuous and automatic.

During the preceding rough balancing operation, the rotors are balanced at one end only by cutting a slot in the periphery. In the fully automatic machine, this slot is used as the reference point. Rotors are loaded by the operator into the feed hopper, from which a transfer mechanism takes them to the balancer cradle. A field coil in the cradle is then energized, causing the rotor to revolve at its rated speed. A photocell uses the slot as the reference point and vibration pickups determine the position and magnitude of the existing unbalance in the usual manner.

Measuring takes about 20 s, and the rotor is then transferred to the unbalance correcting stand. Again the end slot is used as a reference. A dog key is then inserted to lock the rotor in position for drilling. There are two drillheads, one facing each end of the armature, and both are carried on faceplates. The control system rotates the faceplates to bring the drills into the correct position, and they are indexed in until a pressure switch starts the drilling. The depth drilled is regulated by the control system or by a safety stop that prevents the drills breaking through the rotor end plate. Drilling is carried out dry, with air jets used for debris extraction and cooling.

The check measuring station is similar to the original measuring station and uses the same instruments. After the check measurement, the rotor is accepted or rejected for reprocessing in a quality grading station, as in the crankshaft selection process described earlier. A similar series of operations is used with automatic electric motor armature balancing machines such as that shown in Fig. 3.36. Armature balancing cycle time may range from 1 to 8 s, depending on size, volume, and degree of automation.

Mass-Centering Machine for Communication Satellites

Most communication satellites rotate about their principal axis of inertia when in orbit. Although satellites have no bearings supports, they function as rotors while in orbit. The exterior surface of a communication satellite should rotate concentrically with its principal axis of inertia; this minimizes errors in signal transmission due to eccentric runout of the exterior surface.

A special balancing machine for mass centering of satellites is shown in Fig. 3.37. The rotor shown is to be balanced as a rigid body. The outer surface can be made concentric with the vertical (principal) axis of inertia by balancing the rotor in two planes. This adjusts the position of the mass center and the principal axis of inertia as follows: The rotor outer surface is first made concentric with the axis of rotation of the balancing machine. The balancer table rotates about its vertical axis. The rotating table is perfectly balanced, and it spins in high-pressure hydrostatic oil-film bearings for minimum friction and precise position control in the horizontal plane. Its support structure is flexibly mounted to permit small lateral motions U_1 and small tilt motions U_2, as shown in Fig. 3.38. Any centrifugal force arising from eccentricity of the c.g. of the satellite about the table's axis of rotation is then sensed by transducers at A and B. The unbalance forces F_1 and F_2 are then measured. The force readings at the transducers are related to the balance-plane corrections as follows:

$$U_1 = F_1 + F_2$$

$$U_2 = F_1 \frac{a+b}{c} + F_2 \frac{b}{c}.$$

Forces U_1 and U_2 are complex quantities, as are the unbalance forces F_1 and F_2. The signal of the horizontal transducer is proportional to the centrifugal force directly; the signal of the vertical transducer is proportional to the moment, or couple. The satellite rotor may therefore be balanced as a rigid body, using the customary equipment and principles for plane separation and wattmeter filtering as described previously.

Suitable analog circuits for processing the incoming signals and for defining the required correction weights are part of the satellite balancer unit shown in Fig. 3.38. Direct one-step balancing can also be performed with this equipment by specifying the dimensions a, b, c, r_1, r_2, as described previously for hard-bearing balancing machines.

Fig. 3.36. Automatic balancing machine for electric rotor armatures. (Courtesy of Schenck Trebel Corporation.)
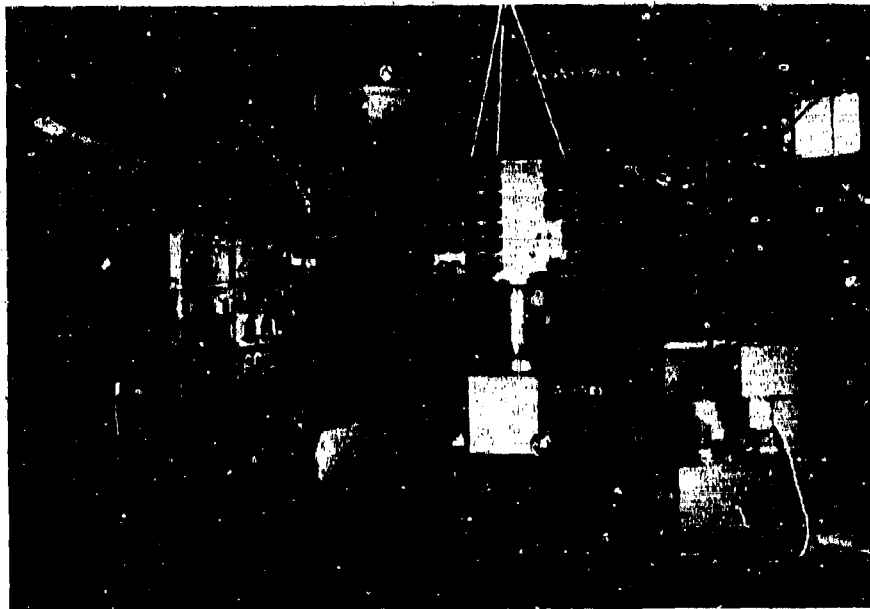
Fig. 3.37. Vertical satellite-balancing machine. The satellite is mounted on top of the balancer. Readout transducers are shown on the lower portion of the balancer. A wattmeter vector-scale console is shown to one side. In the foreground is the high-pressure lubrication system for the bearings. (Courtesy of Schenck Trebel Corporation.)
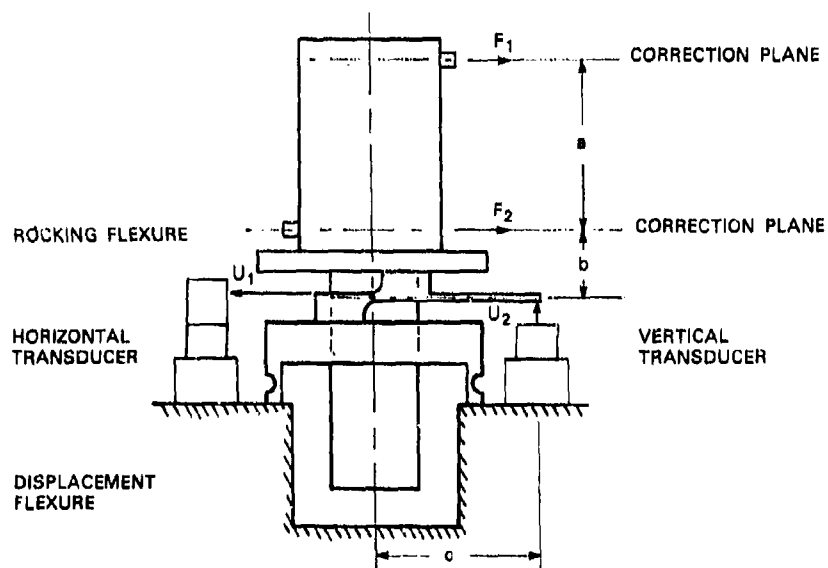

Fig. 3.38. Satellite balancer proportions for automated dial-in mass centering.
(Courtesy of Schenck Trebel Corporation.)

Rotor weights from less than 10 lb up to 3000 lb can be accommodated in existing satellite balancing machines. Balancing speeds of up to 500 rpm are available, usually in three speed ranges. Satellites are mounted on the spin-table surface plate either directly or with the aid of special lightweight clamps (which must be arranged very accurately to avoid introducing additional unbalance). Great care must be taken to mount the rotor square and concentric with the spin axis or to keep it from becoming tilted at some small angle. Care must also be paid to minimizing thermal distortions and to the effect of uneven tightening of bolts when setting up. This also induces unwanted tilting of the rotor.

Staedelbauer [6] attributes substantial improvements in the mass-centering capability of such units to the introduction of high-stiffness radial hydrostatic oil-film bearings. Early satellite balancers used rolling-element bearings, which proved to be the limiting factor in detecting and measuring very low levels of unbalance at low satellite spin rates. Noise signals from metal-to-metal rubbing and sliding contacts within the rolling-element bearings were sometimes three orders of magnitude greater than the unbalance signal itself. This produced significantly inaccurate unbalance readings and also erratic balance correction readings. Though much of the problem could be minimized by employing efficient filtering circuits, the introduction of hydrostatic bearings eliminated such contacts entirely. The higher radial stiffness properties of the pressurized bearings also provide improved table concentricity during operation. High amplification of a very clean unbalance signal is then possible. Superior satellite balance quality has been achieved in this manner.

A remote drive-control console is also shown in Fig. 3.37; it houses the drive-control hydraulic unit and the direct-readout balance equipment. Drive controls include variable accelerating and decelerating torque controls, a spin-rate preselector, and an analog or digital tachometer.

3.6 Development of Balancing Machines

Early balancing began with runout marking of rotors in low-speed machines. Resonant magnification of the unbalance runout during coastdown was also used to improve the sensitivity of rotor-unbalance measurements. No electronic readout capabilities existed before 1930, although devices for mechanically amplifying the dynamic response were available before then.

Electrical readout and measurement began to replace mechanical measurement between 1930 and 1950. Electronic procedures were also developed to replace plane separation, which initially had been developed as a mechanical procedure. The need for resonant

magnification became less important as better signal-detection and electrical amplification devices were developed and with the introduction of wattmeter filtering. Phase-angle measurement developed from a hand procedure, through the stroboscope method, to a direct signal-comparison procedure. The electronics of two-plane balancers now allows direct and automatic readout of the unbalance vector in the selected correction planes as an automated dial-in procedure. This section reviews the development of several important early balancing machines.

Martinson Machine

The first known balancing machine was patented by Martinson [7] in 1870 (Fig. 3.39). It was soft-support machine, suitable for balancing rigid rotors such as cast-iron pulleys, which were mounted on mandrels for the balance operation. The rotor journals were mounted in blocks containing bearing supports (possibly wooden). These bearing blocks were supported by a pair of horizontal and vertical springs at both ends. The rotor to be balanced was driven via a double-universal drive shaft, from a supported belt pulley, which presumably was driven from an overhead line shaft.

Initial rotor balancing appears to have been conducted in this balancer at a low speed to remove gross unbalance effects such as casting eccentricities. A double-pulley drive arrangement would have been employed to jog the rotor up to speed. For trim balancing, the rotor would have been run at a higher speed, probably above the rotor-support critical speed, for resonant amplification of the uncorrected unbalance.

Trial-and-error marking with chalk appears to have been used to identify high spots. The soft supports provided useful response magnification, but large response amplitudes in both directions (vertical and horizontal) would have been a disadvantage (one-directional movement is more convenient). This machine made rotor balancing a new aspect of machine operation. It is not known whether any Martinson machines are in existence today.

Lawaczeck Machine

The Lawaczeck balancer [8,9] shown in Fig. 3.40 was developed in 1908. It was a vertical belt-driven machine, in which the upper journal was firmly restrained against lateral movement. The lower journal was flexibly supported to allow observation of the effect of unbalance, as in the Martinson machine. Again, only one end of the rotor at a time could be balanced. The belt drive was adjacent to the flexible support.
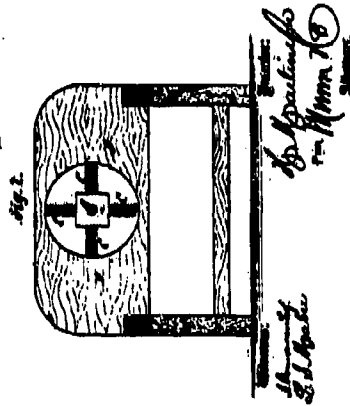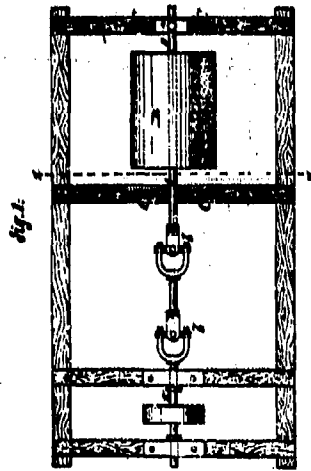
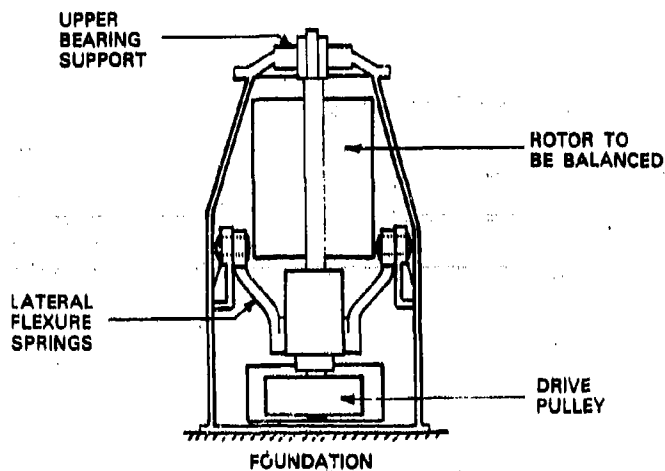Fig. 3.39. Patent for the Martinson balancing machine

Fig. 3.40. Lawaczeck balancing machine, vertical design built in 1908. The lower bearing is flexibly supported in the radial direction, with an overhung drive pulley (after Dihrberg [9]).

It is not evident from Fig. 3.40 how correction weights were attached to the rotor, though the correction planes are shown. Presumably the upper casing had access ports. The machine appears to have been operated much like Martinson's machine. The rotor was balanced first at one end and then the other, which required that the rotor be removed and replaced. The overhung pulley may have affected the dynamic response of the machine.

Heymann Machine

The need to reinstall the rotor after balancing one plane was overcome with the Heymann [10] "double-pendulum" machine (Fig. 3.41) developed in 1916. Only motions in the horizontal direction are permitted with this machine. The bearings of the rotor to be balanced are mounted in a pair of horizontal soft supports. This balancer was a refinement of the Martinson balancer in which the unnecessary vertical support motions were eliminated.

Lawaczeck-Heymann Machine

The ideas of Lawaczeck and Heymann were combined into a single machine around 1918. This machine allows only horizontal motions of the supports. During balancing, one end of the rotor is free to move in the horizontal direction, but the other end is restrained with a clamping

(a) Rotor in end bearing

(b) Bearing block free to rotate in horizontal direction; clamping bar inactive
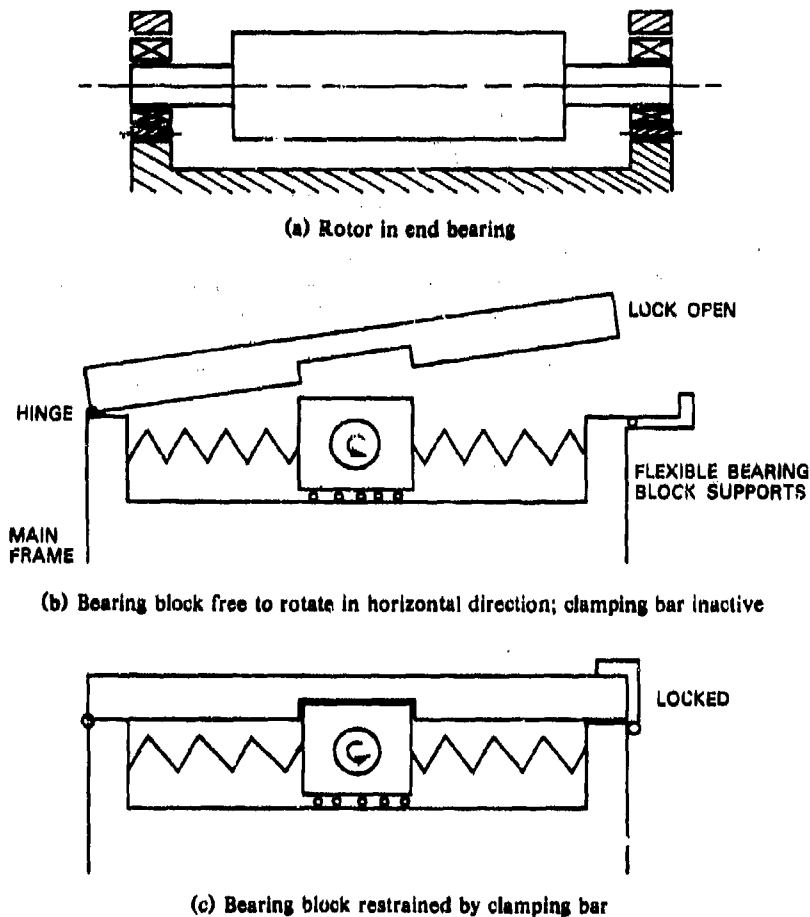

(c) Bearing block restrained by clamping bar

Fig. 3.41. Principle of the Heymann machine. This machine was the first device with the ability of independently lock and release either bearing block. This avoids the necessity of removing the rotor and changing the rotor ends in their supports.

bar as shown in Fig. 3.42. When the free end has been balanced, it is secured against movement with a clamping bar and the other end is released for balancing. Soft supports are used, and there is no mention of any special instrumentation to measure rotor runout. Trial-and-error balancing was presumably the method of operation.

Akimoff Machine

In 1916, Akimoff [11] described the novel null-balancing machine shown in Fig. 3.43. It consists of a rigid foundation member (similar to
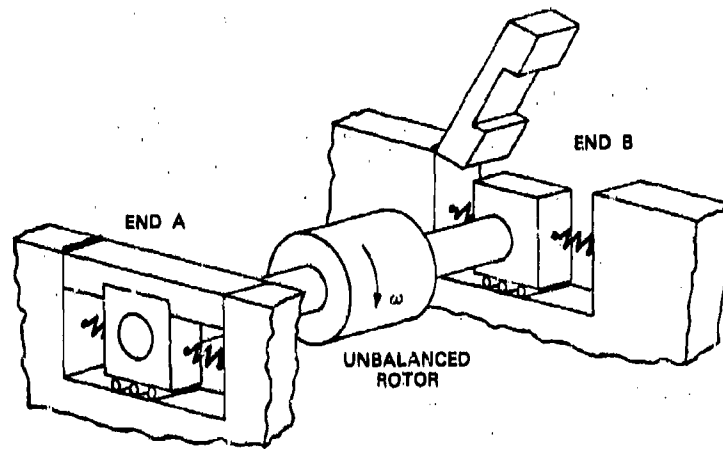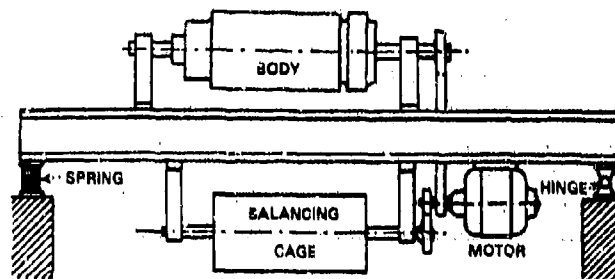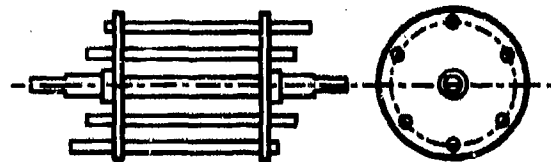
(a) End A clamped, end B free to translate horizontally
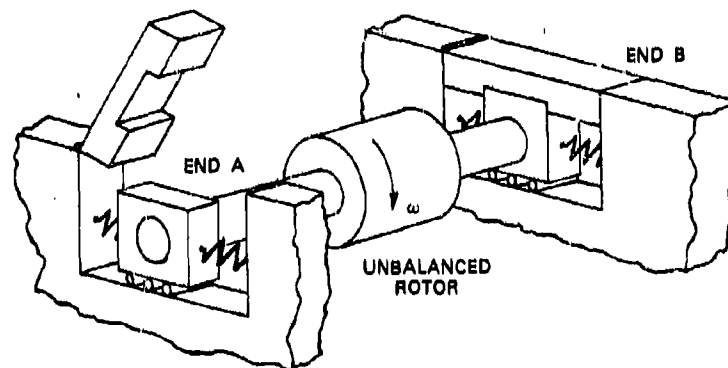
(b) End A free to translate horizontally, end B clamped

Fig. 3.42. Principle of Lawaczeck-Heymann balancing machine. The rotor is balanced first with end A clamped and end B free to move horizontally, and then end B clamped and end A free to move horizontally.

(a) Principle of Akimoff balancer

(b) Details of balancing rotor with rods displaced

Fig. 3.43. Details of Akimoff balancer (©ASME 1918; used
with permission [11])

a lathe bed), hinged at one end and spring-supported at the other end.
The rotor to be balanced is mounted in bearings or as a machine assembly to the upper surface of the bedplate. A second rotor, forming part
of the balancer, is attached beneath the foundation. The second rotor
consists of a set of sliding metal rods, each of known weight and size,
supported in two end plates. The drive for both rotors is supplied by a
common motor.

Initially, the balancing rotor has all its rods aligned in a uniform
position (no overhangs), and as such it is in a balanced condition for
both forces and moments. When both rotors are driven, any unbalance
transmitted to the foundation must then be coming from the rotor to
be balanced. The magnitude and location of this unbalance can be
found by adjusting the relative axial position of the rods in the cage to
generate a countermoment, so that the unbalance effect of the top rotor
is cancelled. This occurs when zero foundation motion is observed at
the spring support.

When a null condition has been achieved, the location (plane) of
the required balance correction is found from the relative movement of

the rods required to achieve the balance condition. The magnitude of
the balance couple is also obtained from the relative movement of the
rods. Akimoff recommended choosing the foundation spring stiffness
so that resonant magnification of the structure response could be
achieved by running close to the natural frequency of the system. The
maximum operating speed of the cage is 400 rpm.

The Akimoff machine is a low-speed dynamic balancer suited to
removing unbalance couples from rotors, armatures, and crankshafts
that have previously been statically balanced on knife edges. Akimoff
subsequently developed an addition that could accommodate static
balancing also.

Soderberg Balancing Machine

Soderberg [12] recognized the need for plane separation and incor-
porated this feature into his machine (Fig. 3.44) to reduce the end-by-
end iteration sequence. The Soderberg machine consists of an unbal-
anced rotor in bearing supports that are mounted on a bedplate. This
bedplate is mounted on a movable fulcrum and end spring supports.
Under unbalance excitation, the structure pivots about the fulcrum.
The spring is tuned to provide structurally resonant properties for signal
magnification. The fulcrum roller can be moved along the machine bed
as needed to any suitable location beneath a balancing plane of the
rotor. This sets the pivot point at the balancing plane rather than at the
bearing and thus eliminates any unwanted moment about the balance
plane due to support forces. A rigid rotor can be corrected in the
required balance plane, with the fulcrum beneath the other balance
plane. This achieves a complete force and moment balance in two
steps, without the need for further iteration. With its mechanical
plane-separation feature, the Soderberg machine thus had an advantage
over the Lawaczeck-Heymann machines until plane-separation features
were developed for these machines. This was done mechanically by E.
L. Thearle in 1934 and electronically by J. G. Baker and F. Rushing in
1937. For a discussion of these patents see the following section.

Earlier versions of the Soderberg machine were limited by having
the balancing planes high above the fulcrum. This impaired the accu-
racy of observation. Later versions overcame this problem, but still
there was no direct means for accurate measurement of unbalance
amplitude and phase. Soderberg [12] described several procedures for
making such measurements, the most successful using a thin steel reed
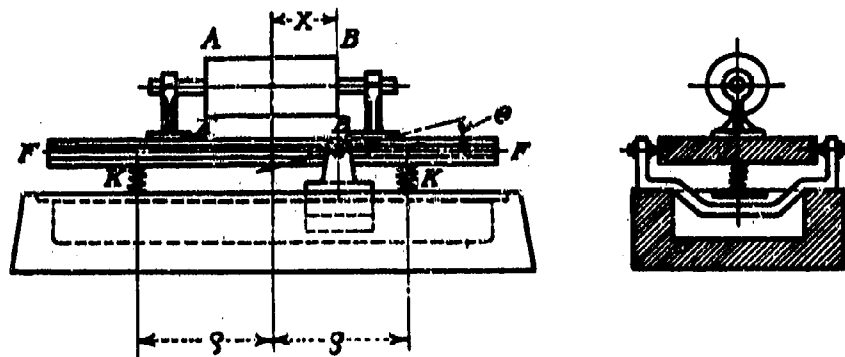that could be tuned to indicate vibratory amplitudes at operating speed.
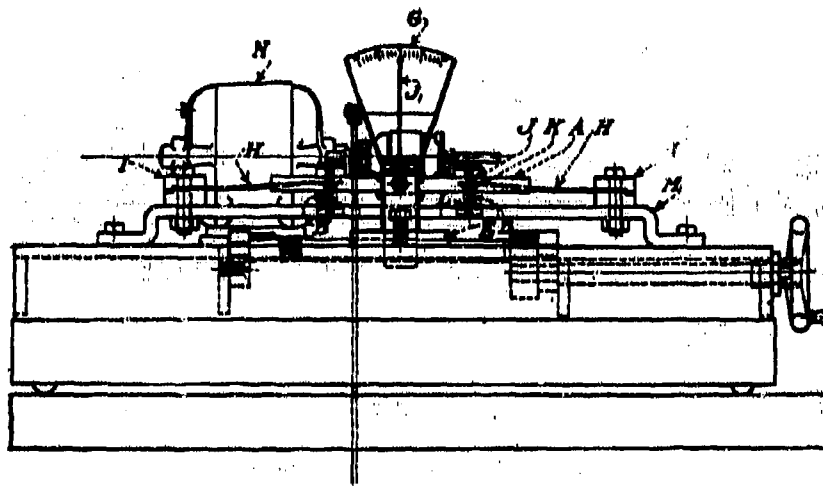
(a) Side view
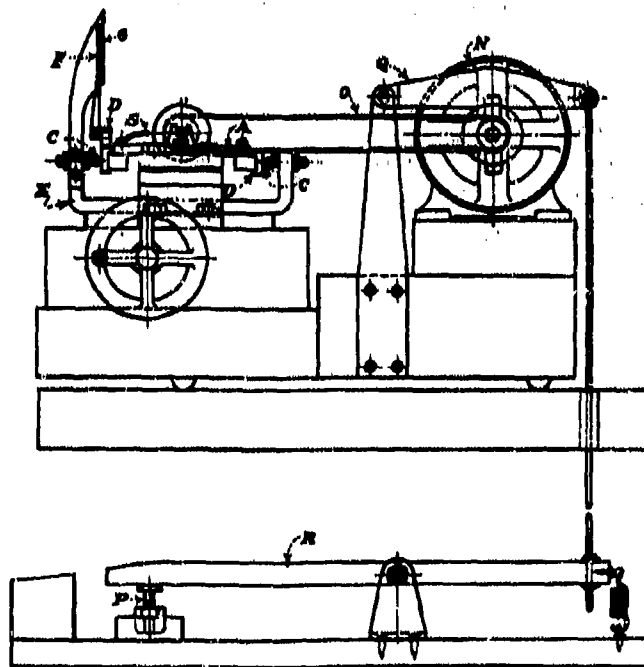
(b) End view

Fig. 3.44. Soderberg movable-fulcrum balancing machine
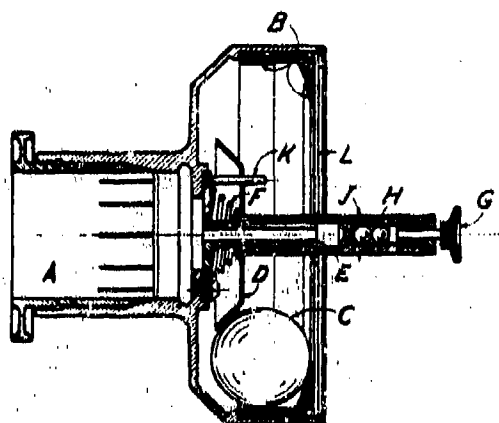(©ASME 1923; used with permission [12])

(c) Principle of Soderberg machine

Fig. 3.44. (Cont'd) Soderberg movable-fulcrum balancing machine
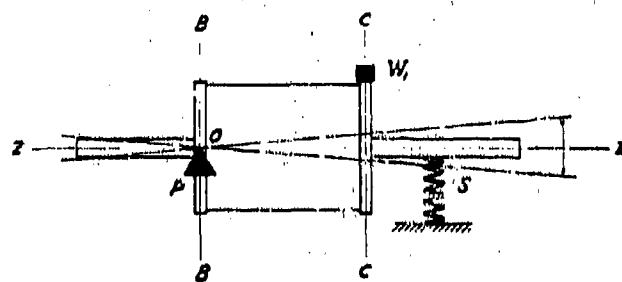(©ASME 1923; used with permission [12])

Thearle Three-Ball Balancer

Thearle [13] mathematically analyzed the motion of a rigid rotor in
two supports; one support restrains the motion laterally, and the other
is flexibly supported in both lateral directions (Fig. 3.45b). Observing
that the heavy side of the rotor would run out below the critical speed
and run in above the critical speed, Thearle proposed a mass-balancing
device that could be attached to the rotor during balancing and would
allow the amount of rotor balance required to be determined automati-
cally. Thearle's balancing head (Fig. 3.45a) is mounted rigidly on the
end of the rotor shaft. Pressed into the head is a hardened and ground
race groove in which two sizable steel balls of equal size are free to
move during operation. When not in use, the balls are clamped 180°
by a conical restraining clutch that is mounted on the center shaft and
held against the balls by a clamping spring. The clutch is released by
finger pressure on the end button. When freed, the balls assume a pre-
ferred position within the race during operation. At speeds above the
critical, the balls assume an angular position that tends to balance the
rotor.

The means by which balls balance a rotor automatically are as fol-
lows: Assume that the balancing head is mounted at the flexibly sup-
ported end of the unbalanced rotor shown in Fig. 3.45b. By freeing the
balls at any speed of rotation, an additional rotating force is introduced.
This force is located in the plane of the balancing head, and its magni-
tude varies from zero when the balls are diametrically opposed to the
full unbalance force of the head when the balls are in contact. When

(a) Thearle three-ball balancing head

(b) Balancing head on right end of rotor
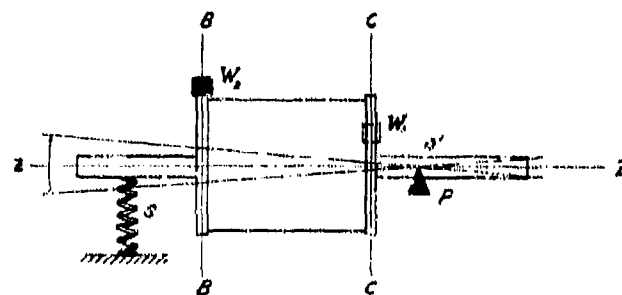
(c) Balancing head on left end of rotor

Fig. 3.45. Details of the Thearle balancing head
(©ASME 1932, used with permission [13])

the rotor is pivoted at the left support L, the effect of any unbalance (Fig. 3.45b) on the system will be proportional to the unbalance W_R and its moment arm L. When the rotor is running above the critical speed and the clutch is depressed, the balls thus freed will automatically assume positions that tend to suppress the unbalance whirling of the rotor in its supports. For this to occur, the moment of unbalance introduced by the balls must be equal and opposite to the unbalance moment of the rotor. Furthermore, the bisecting line between the angle of the balls indicates the angular location of the rotor unbalance.

The balancing head is to be used at either end of the rotor in turn, to balance out either end component of the rotor unbalance. Some iterations may be necessary, as the rotor is not supported in its correction planes. For this, Thearle balancers on both end of the rotor would be helpful. A further calculation is necessary to determine the magnitude of the balance weights required at each correction plane. The balancers are removed when rotor balance in the correction planes has been achieved.

The Thearle balancing method was a novel procedure in its day. Its disadvantages were the inconvenient end-by-end procedure, the additional unbalance calculation requirement, and the need for plane-separation calculations. Den Hartog [14] has discussed Thearle's apparatus and has also mentioned a similar apparatus used to balance automatic washing machines during their spin cycle. Ormondroyd [15] in discussing Thearle's paper draws attention to the LeBlanc (1913) automatic mercury balancer, which is also described by Stodola [16]. Olsen [17], in another discussion of Thearle's paper, describes a device by Sellars (1904) consisting of several balancing rings; it appears to be identical with the washing-machine patent described by Den Hartog (see also comments on page 182, on the centrifuge balancing patent by Adams).

3.7 Selected Patents on Balancing Machines and Equipment

This section contains details and illustrations from selected U.S. balancing patent documents. Important patents on balancing machines, balancing equipment, and special devices are reviewed. The list contains many important patents but does not attempt to be all-inclusive. No reference is made to foreign patent literature. The name of the inventor is followed by the year of patent application. Table 3.3 classifies a number of patents by specific area.

Table 3.3. Classification of balancing patents

Subject	Inventor	U.S. Patent No.
Turbine	LeBlanc	1,209,730
balancing	Rathbone	1,704,341
	Linn	1,776,125
	Greentree	2,078,796
	Meredith	2,442,308
	Frank	2,622,437
	Sjostrand	2,731,887
	McCoy	2,823,544
	Samsel	2,828,626
	Reud	2,842,966
	Wright	2,879,470
General rigid-	Huff	2,057,778
rotor balancing	Siversen	2,116,221
	Buckingham	2,140,398
	Exter	2,210,285
	Baker	2,235,393
	Saltz	2,327,608
	Kent	2,405,430
	Lindenberg	2,547,764
	Kolhagen	2,554,033
	Allen	2,737,813
	Swearingen	2,740,298
	Wright	2,861,455
	Donaldson	2,878,677
	Frank	2,899,827
Automobile	Morse	2,176,269
wheels	Hanson	2,177,252
	Hunter	2,341,444
	Martin	2,553,058
	Kiebert	2,718,781
	Ringerling	2,722,829
	Hemmeter	2,779,196
	Palmer	2,816,446
	Twiford	2,902,862
General	Hanson	1,603,076
rotating	Adams	1,952,574
machinery	Hem	2,186,574
	Bradbury	2,238,989
	Sharpe	2,377,045
	Kahn	2,534,268
	Rensselaer	2,772,465
	Phelps	2,915,901

BALANCING OF RIGID AND FLEXIBLE ROTORS

H. Martinson (1870), U.S. Patent 110,259, December 20, 1870

Soft-support balancing machine (Fig. 3.39) for rigid rotors. The rotor to be balanced is mounted in two end bearings supported by springs in the horizontal and vertical directions. The drive pulley is connected to the workpiece by a universal drive shaft. This allows the driven end of the workpiece to move laterally. The procedure involves trial-and-error balancing, using a marker (chalk) to locate the angular position of the maximum runout in each correction plane, in turn.

M. LeBlanc (1912), U.S. Patent 1,209,730, December 26, 1916

A balancing device by which the rotor is balanced semiautomatically. Tubes of mercury encased in resin are installed around the unbalanced rotor circumference. The rotor in its supports is brought to speed, and external heat is applied to melt the resin. The released mercury then flows automatically to a new position that balances the rotor. As the resin cools, the mercury is secured in the new position.*

A.H. Adams (1928), U.S. Patent 1,952,574, March 27, 1934

A self-balancing device for use with centrifuge equipment (Fig. 3.46). The centrifuge bowl is supported on a vertical spindle. An annular tube surrounds the bowl, containing a quantity of heavy flowable material (e.g., mercury, steel balls). When the centrifuge runs above its critical speed, the material causes the bowl to be self-balancing

T.C. Rathbone (1924), U.S. Patent 1,704,341, March 5, 1929

Field balancing machine. A pendulum device mounted on a bearing pedestal is caused to vibrate by unbalance forces transmitted from the rotor. The pendulum motion closes a contact once per period to trigger a flashing lamp. Two trial masses are placed on the rotor, and the location of the unbalance plane and its phase are measured in the usual manner. This allows the location of the original unbalance to be determined. The pendulum functions as a timing device for the lamp, and the timing indicates the angular location of maximum transmitted pedestal force. The rotor is balanced by trial and error.

D.D. Knowles (1930), U.S. Patent 1,979,692, November 6, 1934

Stroboscope testing apparatus, suitable for observing rapidly rotating objects. No direct application to balancing is mentioned in this

---

*Den Hartog [14] and Thearle [13] have both commented on the LeBlanc balancer, giving reasons why it will not work with mercury but will work with solid balls.

March 27, 1934.   A. H. ADAMS   1,952,574

CENTRIFUGAL TREATING MACHINE
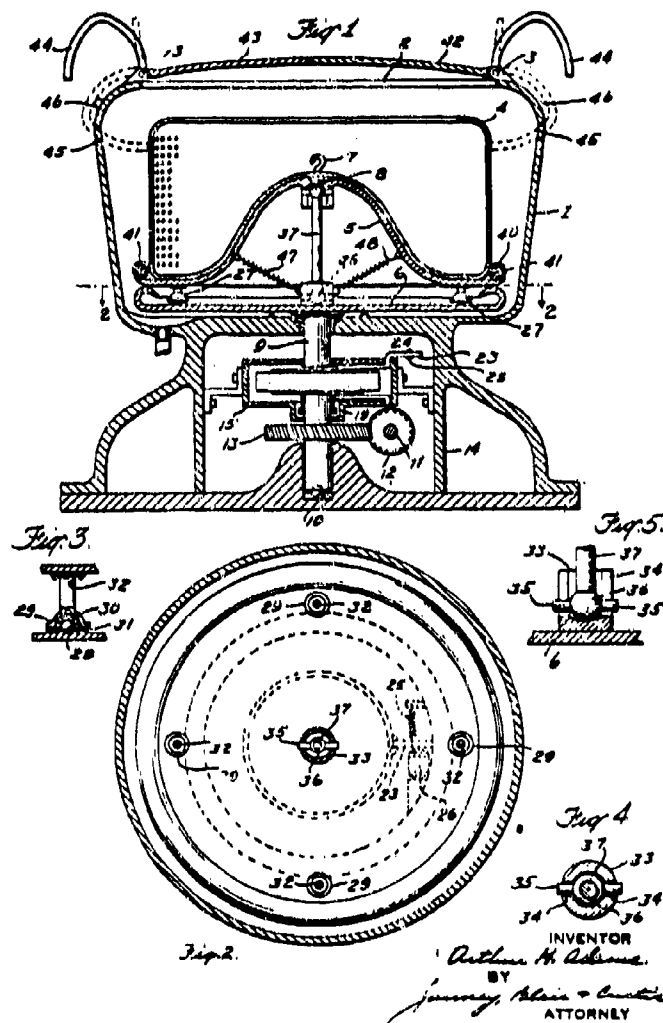
Original Filed April 13, 1928   2 Sheets-Sheet 1

Fig. 3.46. Centrifuge balancer patent by Adams (1934)

early stroboscope patent, and no reference is made to previous strobo-scope patents or concepts. A circuit diagram is given with full working explanation. "Grid-glow" discharge tubes are incorporated*.

S.S. Huff (1932), U.S. Patent 2,057,778, October 20, 1936

Crankshaft balancing machine. This is a mechanical device that determines the amount and angular location of material to be removed from the ends of the shaft to achieve balance. No direct measurement of unbalance magnitude is made. No electronic circuits or direct plane separation are specified.

L.E. Swedlund (1935), U.S. Patent 2,092,096, September 7, 1937

Strobe actuator circuit. Standard balancing practice is for pickups to generate an electric signal from transmitted rotor motions. How-ever, such a signal voltage is variable: it depends on the unbalance magnitude and its distribution and on the rotational speed. For improv-ing the strobe operation, a constant ac voltage is preferred. The patented circuit amplifies and conditions the pickup signal and gives improved strobe functioning by providing a strong, rapid-decay waveform.

J. Sivertsen (1938), U.S. Patent 2,116,221, May 3, 1938

A device for determining the angular location of unbalance. A rotating permanent magnet set in a stationary housing with alternating magnets gives the unbalance angle. The principle involved appears very similar to Thearle's (1936) patent, though the configuration is different.

E.L. Thearle (1936), U.S. Patent 2,131,602, September 27, 1938

Soft-support balancing machine (Fig. 3.45). A belt drive rotates a rigid rotor in end bearings mounted on flexible supports. The location and magnitude of the rotor unbalance are determined by an adjustable mechanical device that identifies the axial nodal points of the rotor whirl motion. The device requires calibration with a balanced rotor. Unbalance magnitudes are found by comparing the uncalibrated rotor response with the calibrated rotor response. Data are obtained with inductance probes. Synchronous voltage is fed into a null circuit with

---

*Rathbone's (1929) patent describes the principles needed for stroboscopic illumination but contains no significant circuit details for manufacturing such an illumination device. Knowles patent, applies for one year later, appears to describe a true stroboscopic device.

inductance current for phase-angle measurement. This invention contains early versions of several features that are now standard in modern balancing machines and circuitry: a plane-separation circuit, wattmeter filtering, and phase-angle circuitry.

J.G. Baker and F. Rushing (1935), U.S. Patent 2,165,034, July 4, 1939

High-speed balancing equipment (Fig. 3.47). The two-plane balancing procedure includes plane separation. The magnitude and phase of unbalance are determined electrically without additional mechanical devices. The end-by-end restraint sequence of earlier machines (Lawaczeck-Heymann, Soderberg, etc.) is not required. Electric circuit diagrams are given for plane separation and a stroboscopic means of phase-angle measurement. This is a comprehensive patent that discusses many important aspects of high- and low-speed balancing.

J. Lundgren (1937), U.S. Patent 2,228,011, January 7, 1941

Commutator and switch mechanism for phase-angle measurement. Amplifier circuitry for triggering strobes. The innovation is the reduction of the rise time associated with the current reversal that triggers the strobe.

J. Lundgren (1939), U.S. Patent 2,289,200, July 7, 1942

Soft-support balancing machine with mechanical means for establishing the balance clamping pivot location. The method employs the commutator switch circuitry of the previous patent. The balance point is locked electrically. A null circuit is used to determine the magnitude of unbalance.

F.C. Rushing and J.G. Baker (1937),
U.S. Patent 2,289,074, July 7, 1942

A carriage-type high-speed balancing machine. This device eliminates the need for a carriage pivot point, as used in a Soderberg-type machine. The pivot elimination is accomplished through the use of a mechanical linkage device. The patent desribes the machine and linkage construction. Little attention is paid to electronics.

J.G. Baker (1939), U.S. Patent 2,315,578, April 6, 1943

Concepts for balancing complicated shafts and other rotating members. The patent describes a two-plane crankshaft balancing machine, together with circuits with general applicability to shaft balancing. It also describes electrical circuits suitable for the determination of unbalance in two correction planes. Angular positions for two balance weights per balance plane are deduced by the circuits designed

BALANCING OF RIGID AND FLEXIBLE ROTORS
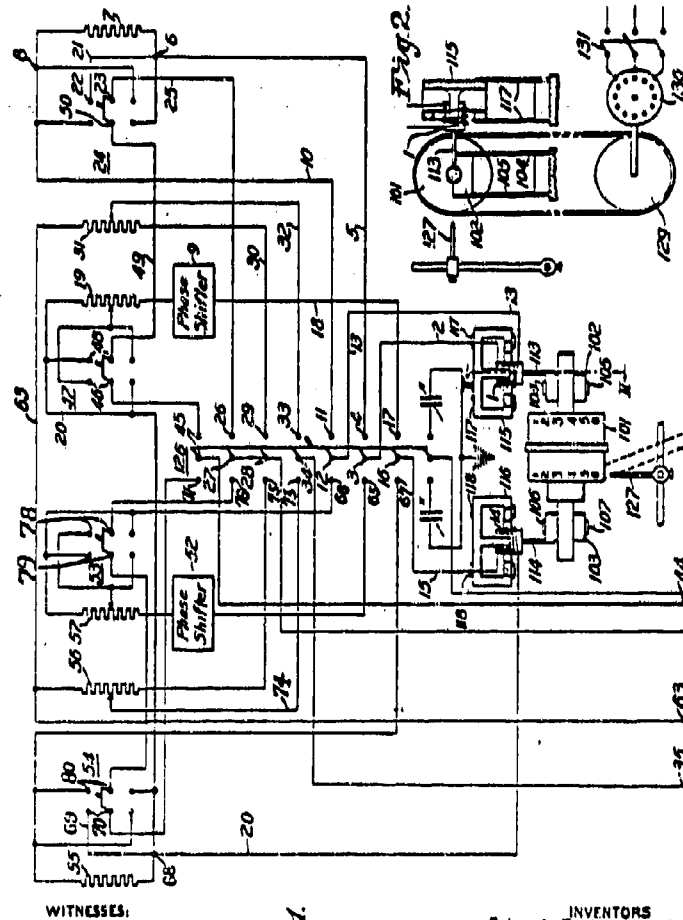
July 4, 1939.   J. G. BAKER ET AL   2,165,024

INDICATING BALANCING MACHINE

Filed Oct. 23, 1938   3 Sheets—Sheet 1

WITNESSES:

INVENTORS
John G. Baker, and
Frank C. Rushing.
BY
ATTORNEY

Fig. 3.47. Plane-separation circuits for balancing machine. Baker and
Rushing patent (1939).

to balance the rotating body. The method is suited for crankshaft balancing where access to the correction plane is limited. A null method is used to obtain unbalance readings. No analytical theory is given, but there is an extensive discussion of the complex circuitry.

S.G. Svensson and N.B. Langefors (1945),
    U.S. Patent 2,500,013, March 7, 1950
Apparatus for determining the magnitudes and angular dispositions of unbalances in a rotating body. A standard soft-support system, pick-ups, and voltage generator are used. Support amplitude pickups are connected in series with each other and with a current meter. The instrument is fed with the vector difference of the pickup currents. Improved circuit concepts for determining unbalance are claimed.

D.R. Whitney (1944), U.S. Patent 2,551,480, May 1, 1951
Balancing machine with electrical readout. A response signal from bearing transducers is projected onto a ground-glass screen for visual observation of unbalance response magnitude and phase angle, obtained with reference to an ac generator voltage signal. This appears to be the first patent for a screen readout device.

K. Federn (1952), U.S. Patent 2,731,592, January 17, 1956
Device for the photoelectric generation of an ac signal in syn-chronism with the rotation of a body. The innovation lies in the accu-rate generation of waveforms for use in determining unbalance phase angles.

W. Pischel (1951), U.S. Patent 2,815,666, December 10, 1957
Machine for measuring unbalance. It measures forces rather than displacements at the supports. Plane separation is incorporated through a potential divider mechanism that is part of the machine.

D.V. Wright (1953), U.S. Patent 2,861,455, November 25, 1958
Refinement for wattmeter balancing. The electrical network includes a ring demodulator wattmeter. The circuit is similar to that proposed in the Baker and Rushing patent (U.S. Patent No. 2,165,024). A noncontacting device is proposed for ac voltage generation with a wave-shaping circuit.

E.P. Larch (1957), U.S. Patent 2,937,613, May 24, 1960
Balancing machine that removes or adds material to balance rotor during rotation. A nozzle ejects weighting material that adheres to the rotor or sandblasts material off the rotor. Automatic operating controls are provided for the nozzles.

3.8 References

1. International Organization for Standardization, *Balance Quality of Rotating Rigid Bodies*, ISO/TC 108 DR 1940, 1967.
2. International Organization for Standardization, *The Mechanical Balancing of Flexible Rotors*, ISO/TC 108/SC1/WG2 (Secretariat-7), Document 12, 1976.
3. I. J. Sommervaille, "Balancing a Rotating Disc, Simple Graphical Construction," *Engineering*, Feb. 19, 1954.
4. D. E. McQueary, "Understanding Balancing Machines," American Machinist Special Report No. 656, June 11, 1973.
5. I. Laskin, "Study of Industrial Balancing Machines," Mechanical Technology Inc., Technical Report 66TR42, Aug. 19, 1966.
6. D. G. Staedelbauer, "A New Aerospace Balancing System for Mass Properties Determination," paper presented at the 28th Annual Conference of the Society Aeronautical Weight Engineers, San Francisco, Calif., May 1969.
7. H. Martinson, "An Improved Method for Balancing," U.S. Patent No. 110,259, 1870.
8. F. Lawaczeck, German patent (number unknown), 1907, for vertical balancer. Also patent (number unknown) 1912, for horizontal balancers (see Ref. 9).
9. K. Dihrberg, *Auswuchttechnik*, Carl Schenck Maschinenfabrik GmbH, Darmstadt, Federal Republic of Germany, 1965.
10. H. Heymann, "Double-Principle," Ph.D. dissertation, Darmstadt University, 1916 (see Ref. 9).
11. N. W. Akimoff, "Dynamic Balance," *Trans. ASME* 38, 367 (1916) (see also "Recent Developments in Balancing Apparatus," *Trans. ASME* 40 (1918)).
12. C. R. Soderberg, "Recent Developments in Balancing Machines," *Trans. ASME*, 45, 111 (1923).
13. E. L. Thearle, *A New Type of Dynamic-Balancing Machine*, APM-54-12, *Trans. ASME* 54, 131 (1932).
14. J. P. Den Hartog, *Mechanical Vibrations*, 4th ed., McGraw-Hill, New York, 1956.
15. J. Ormondroyd, discussion of paper by E. L. Thearle, Ref. 13, 1935.
16. A. Stodola, *Steam and Gas Turbines*, Vols. I and II, McGraw-Hill, New York, 1927, pp. 491, 1122, 1125.
17. E. A. Olsen, discussion of paper by E. L. Thearle, Ref. 13, 1935.

CHAPTER 4
LOW SPEED BALANCING

Nomenclature

a	eccentricity of unbalance from rotor axis
a, b, c	shaft distances to correction weights
F	centrifugal force due to unbalance
F_x, F_y	components of unbalance forces in rotating coordinates
P_x, P_y	
g	gravitational acceleration
L	distance between bearings
R_x, R_y	bearing force components due to unbalance
S_x, S_y	
u, v	unbalance components
U	unbalance, Wa
W	unbalance weight
α_{ij}	influence coefficients $i = 1 \ldots 4, j = 1 \ldots 4$
η, ζ	rotating coordinates
ω	operating frequency, rad/s

189

CHAPTER 4
LOW-SPEED BALANCING

4.1 Soft-Support Machine Procedures

Typical Soft-Support Machine System

Soft-support balancing machines are designed to operate above the critical speed of the rotor in the machine supports. Operation in this speed range eliminates resonant dynamic effects from the rotor response and makes accurate speed control a less important operating variable. A typical soft-support shop balancing machine (Fig. 3.5) consists of two support pedestals with an interconnecting frame structure, a dc motor drive with a lightweight belt, a stroboscopic flash lamp to identify the angular location of the shaft maximum runout, and a readout console with a means for determining the residual unbalance force at the readout location, e.g., rotor supports.

The purpose of any low-speed, two-plane balancing machine is to provide a means for removing the effects of static and dynamic unbalance from the rotor response. For such a procedure to be effective—that is, for the corrected rotor to run within acceptable vibration limits—the rotor must act as a rigid body during the balancing process. This means that lateral and torsional displacements of the rotor due to such effects as centrifugal forces, bending critical speeds, and torsional critical speeds must be absent or insignificant in the rotor displacements. Under such conditions the balancing machines and balancing techniques described in this chapter will allow a rotor to be balanced so that it will operate smoothly and without vibration in its machine supports.

ABC Method

The simplest commercial balancing procedure presently available is the Schenck ABC method, in which the rotor dimensions A, B, C, and R_1 and R_2 are dialed into the instrument console, or "vectormeter," as shown in Fig. 3.28. The rotor is then run at a selected balancing speed. The dials of the vectormeter will indicate the magnitude and location of the correction masses required in the two correction planes.

The functioning of this instrument depends on efficient filtering of all extraneous signals and on a plane-separation circuit that calculates the size of the required balance weights from transducer signals obtained from the rotor-support planes. The ABC method does not require the use of a strobe flash lamp to identify the phase location of the unbalance, and it overcomes the trial-and-error procedure of adding trial weights to the rotor to determine the required balance weight. The rotor thereby is balanced in a minimum number of test runs (nominally in two runs), which is of importance where high-volume balancing of rotors in involved. The cost of such sophisticated equipment is, of course, higher than that of simpler methods, such as the stroboscope method.

Stroboscope Method

For shop balancing, the stroboscope method requires a low-speed balancer and a small circumferential strip of indicating surface situated at some axial position along the rotor. A row of numbers 1 through 12 is commonly written around the indicating circumference, or a short flat black non-reflecting strip may be used as an angular marker. The photocell is positioned vertically above the rotor (see Fig. 4.1), and the readout circuitry is designed to operate with the photocell in this position unless otherwise adjusted. Stroboscopic balancing equipment is usually supplied with a single readout dial, which may or may not be directly calibrated in unbalance units. The procedure is as follows:
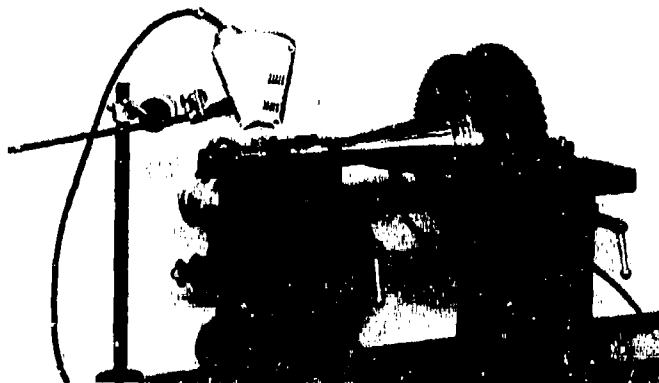

Fig. 4.1. Photocell in position for stroboscope measurement.
(Courtesy of Schenek Trebel Corporation)

1. Lock the left pedestal so that no lateral movement can occur. Let the right pedestal support be free to move horizontally.

2. Start the drive motor and run the rotor at the desired balancing speed (150 to 400 rpm as required).

3. Switch on the strobe flash lamp. Observe the rotor unbalance location marking (usually 1 through 12) indicated by the stroboscopic flash illumination of the angular location of the "eight" point on the rotor in the right measuring plane and the magnitude of the unbalance (or unbalance units) display on the console dial.

4. Add a suitably sized lump of clay in the right balance plane at the "light" angular position location determined in step 3.

5. Rerun the rotor and observe the corrected rotor amplitude and the angular location at which it occurs with the clay attached.

6. Repeat steps 3, 4, and 5 until rotor amplitude has been reduced to within acceptable limits.

7. Release the left support. Clamp the right support and proceed to balance the rotor in the left correction plane.

8. Repeat steps 2 through 6 until a satisfactory balance has been achieved at the left support by adding clay in the left correction plane.

9. Release the right support and reclamp the left support. Repeat steps 2 through 6 as required to verify that the balance in the right plane has not been affected by balancing in the left plane. If the balancer has a plane-separation circuit, this will have been done automatically; if not, some trial-and-error corrections may be needed.

10. If the amplitude at the right plane is unacceptable, modify the right-plane balance weight to achieve satisfactory balance and check the left-plane balance. Repeat this trim balancing procedure until both planes are within prescribed limits.

The stroboscope method clearly requires much less sophisticated equipment than does the ABC method because it relies more on the skill of the operator; for example, more judgement is required when there is no automatic plane-separation feature. As the trial balancing is done with lumps of clay, it is subsequently necessary to weigh the clay installed in the balance planes and then to add an equivalent balance weight to make the correction permanent.

The stroboscope method can be used with all rotors. It is most widely used for small shop balancing and also in field balancing. The essential aspects are the vertical pickup that triggers the stroboscope, the wattmeter filter used to detect the synchronous response component, and the trial weight procedure.

4.2 Hard-Support-Machine Procedures

Properties of Hard-Support Machines

With the development of sophisticated readout instrumentation (semiconductor load cells, strain gages, velocity transducers, accelerometers) and with back-up solid-state amplifiers, wattmetter filtering and/or on-line filtering, hard-support machines have become more popular in recent years. Their inherent ruggedness is attractive to equipment buyers, though it may be obtained at some sacrifice in accuracy (e.g., weaker displacement signals requiring more careful filtering and amplification). Hard-bearing balancing machines have recently become popular for the balancing of large rotors, such as generator rotors.

Mechanical magnification of the rotor response through resonant operation is no longer required with the sophisticated measurement equipment now available. Any balancing machine with pedestal resonances below the balancing speed has a built-in disadvantage in that smooth operation up to balancing speed (high or low) is desirable. Balancing speeds in modern hard-bearing equipment are inherently limited only by the sensitivity of the readout equipment on the one hand and by the flexibility of the rotor on the other hand. For typical rigid rotors, balancing speeds might range from 250 to 3000 rpm. The actual balance speed varies from case to case and is frequently determined by trial and error, guided by the signal strength obtained in a given case.

Hard-Support Balance Using ABC Method

The ABC console shown in Fig. 3.28 is commonly used with a hard-support balancer. In modern units the console would be an integral part of the balancing machine, which would consist of bearings and instrumented pedestal supports. It would be mounted on a massive foundation bedplate, with a variable-speed drive motor and universal drive coupling directly attached to the rotor to be balanced. The balancing system for the machine shown consists of a mechanical drive, readout instrumentation, signal processing and display circuitry, and safety equipment.

The procedure used to balance rotors with such equipment is as follows:

1. Place the rotor to be balanced on suitable pedestal supports (e.g., bearings, rollers).

2. Attach the drive unit (e.g., end coupling, midplane belt).

3. Set sensitivity S_1 to least sensitive position (depending on estimated balance conditions of rotor).

4. Set speed-range button.

5. Set add/remove mass button.

6. a. Set R_1, radius dial for radius of left correction plane.

b. Set R_2, radius dial for radius of right correction plane.

c. Set A, the distance from the left support to the left balance plane.

d. Set B, the distance from the right support to the right balance plane.

e. Set C, the distance between supports. (All dimensions $R1$, $R2$, A, B, and C must be in the same units.)

7. Run the rotor at the prescribed balancing speed.

8. Release reading-retention pushbutton.

9. Adjust sensitivity switch to give nearly full-scale readings.

10. Depress reading-retention pushbutton to store balance readings on vectormeters or console dials.

11. Stop machine. Insert/remove indicated balance correction weights corresponding to the magnitude of the vectors and the phase angles indicated on the console dials.

Periodically a series of routine tests is conducted on this type of balancing machine to determine whether the calibration is accurate. A test rotor with a precisely calibrated residual unbalance (or in a perfect state of balance) is used to check the calibration of such machines.

4.3 Field Balancing

Need for Field Balancing

It often happens that a machine operating in a plant begins to vibrate with increasing severity and must be rebalanced. It is usually desirable to perform such rebalancing in situ, rather than to "pull" the rotor and return it to the manufacturer. Such a balancing procedure is known as field balancing. The techniques used differ in certain respects from those used for initial rotor balancing in the manufacturer's plant (shop balancing).

Field balancing is undertaken with the unbalanced rotor in its own bearings and casing. This rotor must be provided with some source of rotational drive power, or, if the rotor is that of a prime mover (e.g., turbine rotor), it must be capable of developing sufficient rotational speed in situ to permit field-balancing measurements and corrections. Trim balancing is a common form of field balancing, in which a rotor that has been prebalanced in the manufacturer's shop is balanced again after installation, to ensure smooth operation.

Field-Balancing Instrumentation

To field balance a rotor it is desirable (though not essential) to use equipment that can measure rotor amplitude and phase angle at the desired balance speed. Such equipment may be portable or may be permanently installed in the machine frame. The essential requirements are reliable, accurate vibration measurements of the rotor response amplitudes (left and right supports) and similar measurement quality for the phase angle of each amplitude peak with respect to some rotating reference mark on the rotor.

There is a wide variety of equipment for obtaining such data. For example, rotor vibration amplitude can be measured (crudely) with a hand-held shaft-riding vibration meter, such as an IRD probe. As there are many sources of vibration, a filtering system is required to exclude all nonsynchronous inputs. Such a probe may contact the rotor surface directly via a low-friction shoe, or vibration measurements may be taken from the bearing caps adjacent to the shaft. Another method used to determine the shaft motions from changes in the air gap impedence is to install a noncontacting IRD or Bently Nevada inductance probe on a bracket attached to the bearing support. A third method is to use seismic accelerometer pickups mounted on the bearing caps. In each case, the observed vibration signals are passed through a filter to obtain the synchronous shaft amplitude at the readout location. This measurement gives the required shaft amplitude for balancing calculations.

The phase angle associated with the synchronous shaft amplitude, referred to some angular datum, can also be obtained by various methods. The simplest procedure is to use a pickup that briefly triggers a strobe lamp once during each cycle of shaft rotation. The same pickup can also be used to measure the shaft vibration amplitude. Such a system has been clearly described by Blake [1], who recommends it primarily because of its simplicity and proven effectiveness. Besides the pickup, no other connection to the machine is required. Blake further states that, although the wattmeter system described in Chapter 3 is the best of the simple phase-measuring systems because of its superior filtering ability, it requires an additional generator to provide the synchronous voltage.

The basic instrumentation can therefore be restricted to a single pickup and a strobe lamp. If more sophisticated instrumentation is needed to efficiently balance a rotor, the arrangement shown in Fig. 4.2 can be used. Signals are brought out from two probes located near each end of the machine. The two probes are oriented 90° of rotation apart. The signals are amplified, synchronously filtered, and then fed to an

(a) Two probe instrumentation for shaft orbits

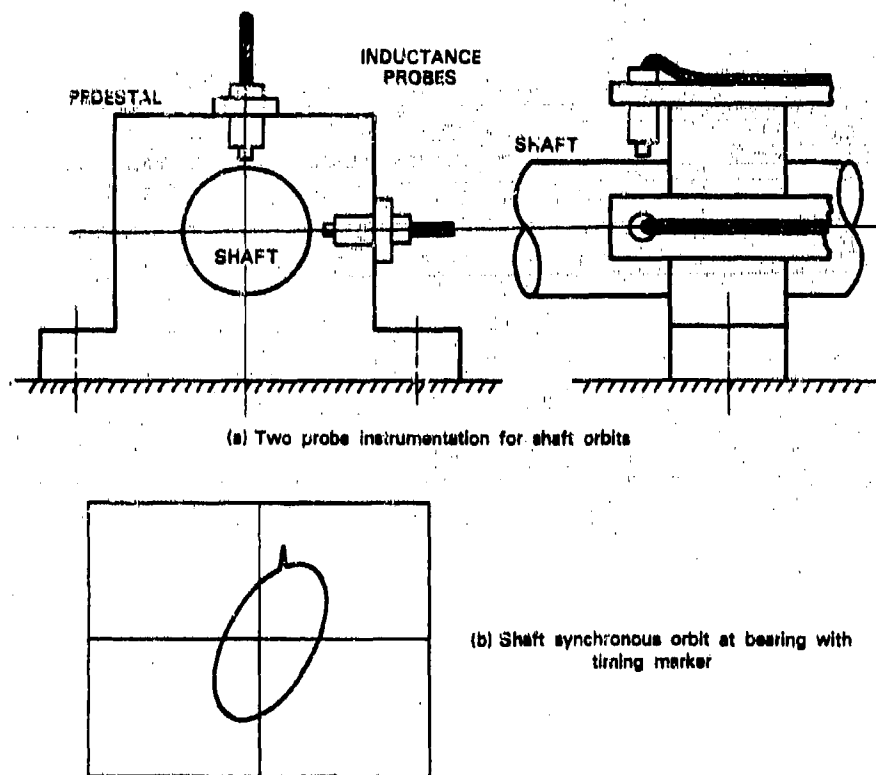(b) Shaft synchronous orbit at bearing with timing marker

Fig. 4.2. Instrumentation for measuring shaft orbits

oscilloscope, to display the shaft orbit in each case. A small mark (scratch or magnetic tape) is made on the shaft at the same angular location at either end, to serve as a phase-angle reference. Its angular position is arbitrary. This mark appears on the shaft orbit as shown in Fig. 4.2b. The angular distance between the maximum shaft amplitude and the shaft reference mark then becomes the phase angle.

Rotor balancing requires information on the rotor unbalance amplitude and on the phase angle, for the original unbalance condition and for several unbalance conditions with trial weights. This procedure is described in the sections that follow.

Stroboscope Balancing

A stroboscope is used in many balancing procedures to identify the angular location of the unbalance. It is used in conjunction with some motion-sensing device (e.g., velocity pickup, displacement probe). The

rotor unbalance transmits both force and displacement to the supports, either of which can be monitored by a sensor. The sensor output signal is filtered in a vibration analyzer to retain only the synchronous component of the motion. The filtered signal is a measure of the unbalance effect at the sensor location; it is displayed on a dial, a vectormeter, a digital display meter, or some other device. The signal is also used to trigger a strobe light that flashes at the instant the sensor output signal reaches a maximum value. The light pulse duration is in microseconds, and it is extremely bright.

Shop Balancing with a Strobe Light. A simple shop balancer that incorporates a strobe light is shown in Fig. 4.3. The rotor to be balanced rests in its supports. At some location, a row of numbers (usually 1 through 12) is taped or painted on the rotor. The strobe lamp is
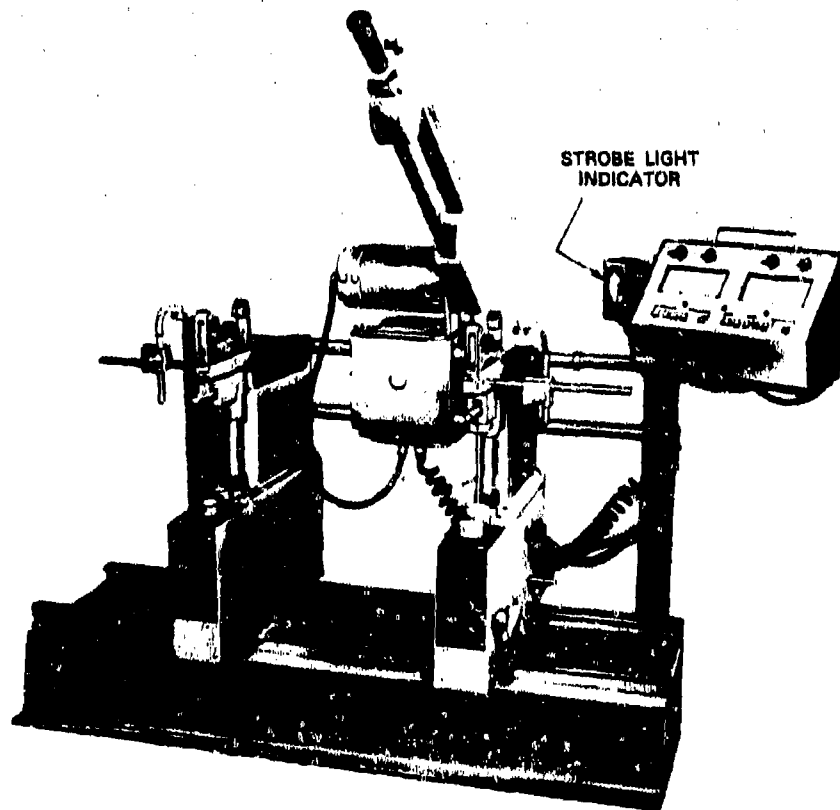
Fig. 4.3. Shop balancer with strobe light. (Courtesy of Stewart-Warner Balancing Machine Corporation.)

positioned to face this row of numbers, and the lamp circuit is so designed that, when the maximum force or displacement is sensed at the supports, the lamp fires and illuminates one number in particular. This number corresponds to the light spot at that rotor end. If the numbers are located around the rotor end, the circuit fires the lamp with a suitable built-up time delay so that the light side will be illuminated when it reaches the lamp. Some lamps illuminate the entire end of the rotor without reference to any number in particular. In this case, the heavy spot is usually at the number opposite the sensor (or pedestal). The required position of the lamp for locating the high spot in a given balancing procedure is stated in the operating manual for this equipment.

Velocity sensors are particularly good for triggering strobe lamps. They operate with a moving coil in a magnetic field, which produces an alternating voltage proportional to velocity. This voltage can easily be integrated electrically to give displacements corresponding to the vibration amplitude. The maximum amplitude corresponds to the point of zero velocity in the motion cycle. This point (i.e., the plus-to-minus voltage change) is much better for triggering the strobe lamp than the peak voltage, which is susceptible to considerable error in locating the exact value of the peak. For these reasons velocity sensors and a strobe lamp make an excellent combination.

Field Balancing with a Strobe Light. Essentially the same procedure as the above is used to balance a rotor in the field. The same equipment is required: vibration sensor, analyzer, and strobe light. However, the angular relation between the locations of the sensor and the strobe flash must be known in advance, or there is no way of determining the significance of the number being illuminated on the rotating shaft.

Assuming that the required angular relationship is known, balancing can be performed by any of the strobe techniques. If this angular relationship is not available, a procedure such as that described below [1] can be used.

Single-Disk-Rotor Balancing with a Strobe Light. This procedure [1] is suitable for balancing rigid rotors (e.g., fan rotors) in the field. Before balancing it is necessary either to install the rotor in a balancing machine or to use some device at or near the unbalanced disk to measure the motion of the rotor. This device can be a hand-held shaft-riding probe, a probe applied to a bearing or pedestal housing, an in-place displacement or velocity sensor, or an accelerometer. This sensor should be equipped with a filter to read only synchronous output and a strobe light whose angular relationship to the probe position is known (see page 196).

The balancing procedure is as follows:

1. Note the direction of rotor rotation and mark the rotor circumference at some suitable location with numbers 1 through 12.

2. Select a suitable balancing speed where the vibrations are discernible but not excessive. Run the unbalanced rotor at this speed.

3. Read the vibration sensor output and record the magnitude of the vibration in some consistent system of units (millimeters, volts, etc.). This is the magnitude of the vector OA in Fig. 4.4.

4. Using the strobe light, identify the circumferential location on the rotor corresponding to the maximum rotor amplitude.* This is the orientation of vector OA in Fig. 4.4.

5. Plot the magnitude and orientation of the original unbalance vector OA in Fig. 4.4.

6. Select a suitable balance weight of known magnitude (see pages 203 and 204) and add this to the rotor at a suitable radius about 90° from the original unbalance location.

7. Run the rotor at the same balancing speed. Measure the new vibration level and the new orientation of the maximum displacement.

8. Plot the new unbalance vector (original plus trial weight) as OB on Fig. 4.4.

9. Join points A and B. Find the magnitude of OA from the trial weight magnitude as follows:

$$\text{Original unbalance } OA = \frac{OB}{AB} \cdot (\text{trial weight, oz-in.}).$$

Check to see that the orientation of the trial weight lies at about 90° ahead of the original unbalance vector on the diagram.

10. Insert a correction weight in the balance plane at 180° to the original unbalance vector of magnitude equal to the original unbalance.

The following sample balance calculation will illustrate the above procedure: A single-disk overhung rotor gives an instrument reading of 5 units when run at 400 rpm. The orientation of the original unbalance is at 3 o'clock. A trial balance weight $T = 2.0$ oz is added to the disk at radius 10.0 in., at 6 o'clock, about 90° ahead of the original unbalance. The new rotor unbalance condition is then measured at the same speed as before. The new unbalance reading is 12.0 units, oriented at 5 o'clock. The vector diagram representing these conditions is shown in Fig. 4.4. The length of the trial weight vector is 5.56 in., or 11.2 units

---

*For a rotor system with low damping that operates away from the rotor critical speeds, the angular location of maximum amplitude corresponds to the unbalance location. Heavily damped rotor systems may be difficult to balance because of the phase lag that can develop between the maximum force and the maximum rotor amplitude.
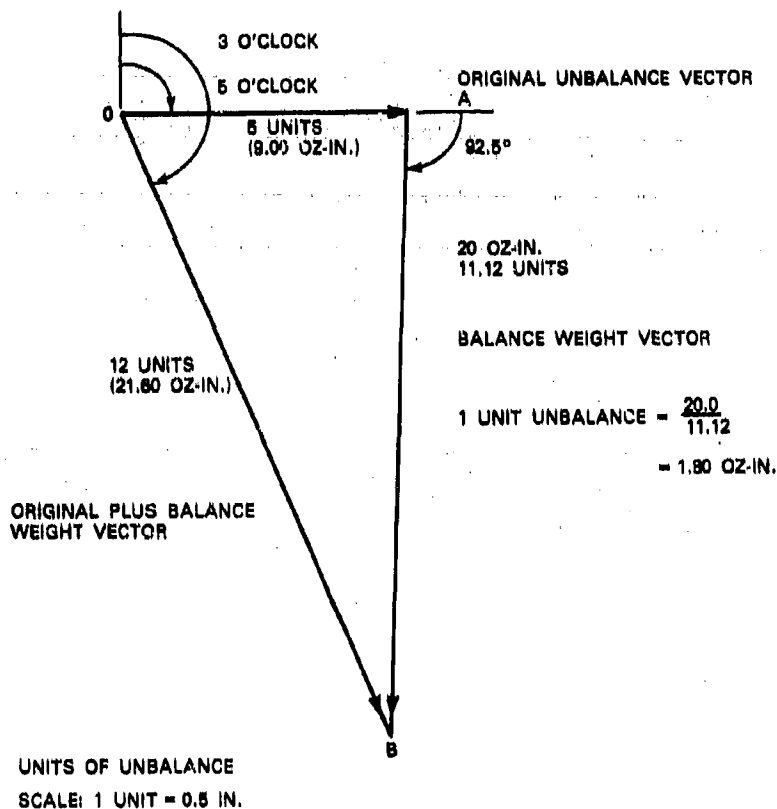
Fig. 4.4. Balance vector diagram for the stroboscopic method

of unbalance (1 unit = 0.5 in.). Therefore, this corresponds to 20.0 oz-in., that is,

$$1 \text{ unit of unbalance} = \frac{20.00}{11.12} = 1.80 \text{ oz-in.}$$

Thus

$$\text{Original unbalance} = 5 \times 1.80 = 9.00 \text{ oz-in.}$$

and

$$\text{Original plus trial unbalance} = 12 \times 1.80 = 21.60 \text{ oz-in.}$$

To balance this rotor requires installing a balance weight equal in magnitude and opposite in direction to the original unbalance OA. The required balance correction is 9.00 oz-in. oriented at 9 o'clock on the

strobe clock (i.e., 180° from OA, which is 87.5° further ahead of the trial-weight AB vector location). Using the same balance correction radius of 10.0 in. gives a correction weight of 0.9 oz at a radius of 10.0 in., at 9 o'clock.

Sources of Error. Errors in estimating correction weight details may occur in any of the following:

1. Original unbalance magnitude. This is read from a dial. The needle position fluctuates, and the instrument may be inaccurately calibrated.

2. Original unbalance angle. This is read from a clock face, the calibration of which is often quite rough. The location involved may also fluctuate because of imprecise drive speed control. This is a major source of error in most balancing operations.

3. Trial weight. Magnitude known imprecisely. Radius measured inaccurately. Angular location does not matter, as the vector diagram must close.

4. Original plus trial weight. Same problems as in items 1 and 2.

5. Correction weight installation. Same problems as in items 2 and 3.

Figure 4.5a shows the effect of cumulative plus and minus variations on the factors listed above. Assume that the above steps involved the following percent errors:

Original unbalance magnitude, %	+10.0 (9.9 oz-in., 5.5 units)
Original unbalance orientation, degrees	+10
Original plus trial weight magnitude, %	+10.0 (23.76 oz-in., 13.2 units)
Original plus trial weight orientation, degrees	−10

The original unbalance is read as 5.5 units at 100° (actually, it is 5.0 units at 90°). Installation errors plus misreading of the (trial weight and original unbalance) vector gives 13.2 units at 58° (actually, 12 units at 68°). Trial balance is deduced as 10.35 units at 81° (actually, 11.1 units at 92°). Hence the original unbalance is deduced as (5.5/10.35) × 20 = 10.628 oz in.

The correction weight of (10.628/10) = 1.063 oz is installed at 200° (additional 10° error). The new residual unbalance (Fig. 4.5b) is an unbalance vector of 2.20 units at 250°. This unbalance has resulted from errors both in measurement and in the installation of weights. Further small errors could result from the values used for the trial weight and trial radius.
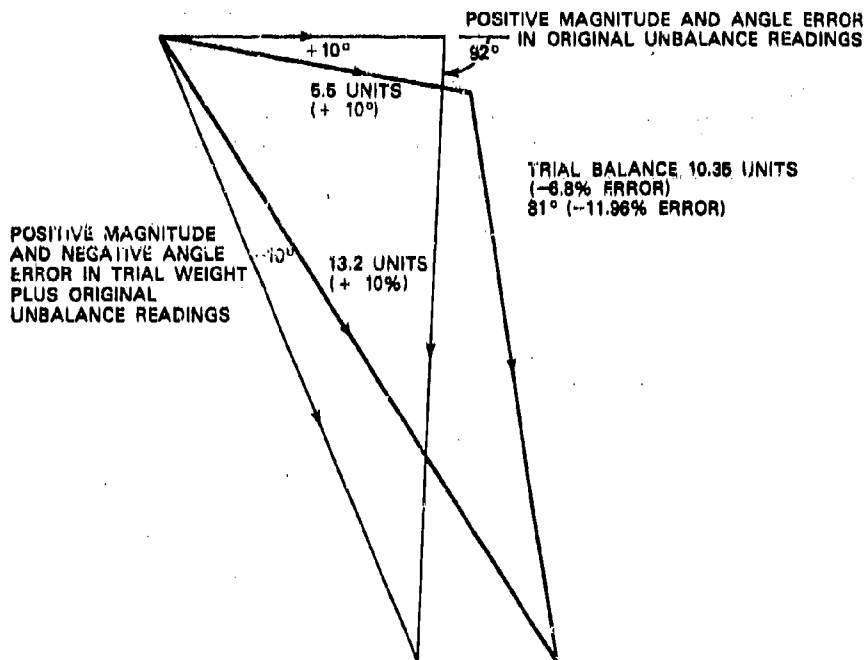
(a) Error effect on balance vector diagram
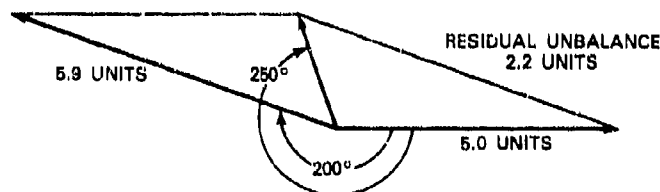
(b) Residual unbalance from error effect

Fig. 4.5. Effect of cumulative plus and minus errors on the balance vector diagram

The new residual unbalance could be corrected further by repeating the above procedure. The error percentages used are realistic values based on practical experience. Practical effects resulting from rotor assembly procedures and from various components have been discussed by Staedelbauer [2] with reference to fan and blower balancing.

The influence of errors on balancing procedures has been discussed by Tonneson [3], Iwatsubo et al. [4], and others. The residual unbalance found by the procedure described above shows why it is usually necessary to make several balance moves before arriving at a smooth operating condition.

Size of Trial Weights

Wilcox [5] has proposed that for a rotor of weight W lb with a disk unbalance vibration amplitude of r in., a suitable trial unbalance magnitude U_c can be obtained from the expression

$$\frac{W}{g} \omega^2 r = \frac{U_c \omega^2}{16g},$$

where ω is in radians per second. Thus

$$U_c = 16\,Wr \text{ oz-in.},$$

and the trial weight at balance radius r_T is therefore

$$W_T = \frac{U_c}{r_T} = 16W\,\frac{r}{r_T} \text{ oz.}$$

Jackson [6] has given a procedure based on the criterion of one-tenth of the rotating force transmitted to the adjacent bearing; that is,

$$U_c = \frac{1}{10}\,\frac{1}{2}\,\frac{W}{g}\,\omega^2\,(r + a).$$

Assuming a to be of the same order of magnitude as r gives

$$U_c = 1.6\,\frac{W}{g}\,\omega^2 r \text{ oz-in.}$$

The trial weight is

$$W_T = 1.6\,\frac{W}{g}\,\omega^2\,\frac{r}{r_T} \text{ oz.}$$

For a 20-lb rotor being balanced at 400 rpm with a disk whirl radius of 0.002 in., and a balance hole radius $r_T = 3.0$ in., the relative values of the trial weights are as follows:

Wilcox $\quad U_c = 16\ Wr = (16)(20)(0.002) = 0.64$ oz-in.

$\quad\quad\quad\quad W_c = 0.64/3 = 0.213$ oz

Jackson $\quad U_c = 1.6\,\dfrac{20}{386.4}\left(\dfrac{400}{9.55}\right)^2 (0.002) = 0.201$ oz-in.,

$\quad\quad\quad\quad W_c = 0.291/3 = 0.097$ oz.

The Wilcox method leads to larger trial weights than does the Jackson method, though both procedures lead to trial weights of similar magnitude.

Single-Plane Balancing: Circle Method. No Phase Measurement.

A rigid rotor whose unbalance is known to lie in a single plane can be balanced by the procedure given below. The graphical construction is shown in Fig. 4.6.

1. Run the rotor at a balancing speed (i.e., 200 to 400 rpm) sufficient to obtain a reasonable readout signal. Record the magnitude of the transmitted unbalance force at some adjacent location—for example, at a bearing cap near the unbalance plane.
2. To a suitable scale plot the unbalance force magnitude as a circle of radius OA (see Fig. 4.6).
3. Add a trial weight at position 1 on the disk. Run the rotor up to the same balancing speed and record the new transmitted force magnitude at the same readout location.
4. Using the same force scale, select any point on the circle OA as the center and draw a circle of radius A_1B_1 to represent the new unbalance force vector.
5. Move the trial weight 90° away from position 1 to position 2. Run the rotor up to the same balance speed. Record the new transmitted force at the same readout location.
6. Using the same force scale, select a point A_2 on the circle OA that is 90° from point A_1. Draw a circle of radius A_2B_2 to represent the new unbalance vector.
7. Move the trial weight 90° away from position 2 to position 3. Run the rotor at the same balance speed. Record the new transmitted force at the same readout location.
8. Using the same force scale, select a point A_3 on the circle OA that is 90° from A_2 and A_1. Draw a circle of radius A_3B_3 to represent the new unbalance vector.
9. Move the trial weight from position 3 to position 4, 90° from position 3. Repeat the procedure described above. Draw the radius A_4B_4 to the same scale, to represent the new unbalance vector.
10. It is seen that circles A_1B_1, A_2B_2, A_3B_3, and A_4B_4 intersect at a common point D. This point allows the correction-weight vector OD to be calibrated.

The original unbalance vector (OA_1, OA_2, OA_3, OA_4, equal) is defined in magnitude by its length in relation to OD. The required correction weight is therefore equal in magnitude to OA, and its orientation is
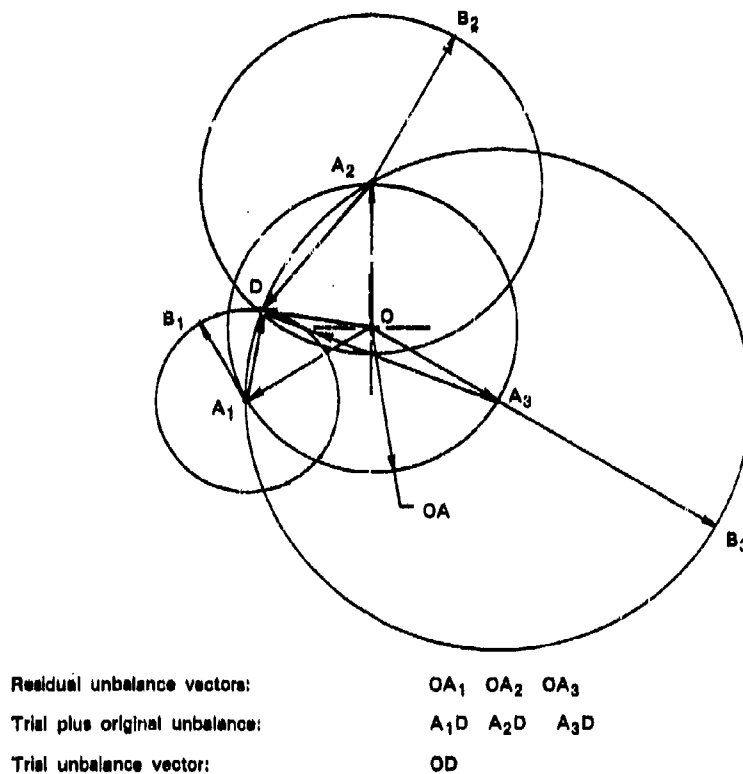
Residual unbalance vectors:	OA_1 OA_2 OA_3
Trial plus original unbalance:	A_1D A_2D A_3D
Trial unbalance vector:	OD

Fig. 4.6. Diagram of the circle method

defined by the angle between the trial weight vector **OD** and the selected unbalance vector **OA**. In relation on the trial weight in the first test, this is the angle DOA_1. This procedure can be used effectively when the rotor unbalance lies in a single plane and a rigid-body, low-speed balance is required (e.g., a single shaft carrying a disk-like rotor). This method can also be used to obtain a two-plane balance in an iterative manner, although if the interaction between the balance planes is strong, the process may not converge. Barrett et al. [7] have recently demonstrated the effective application of this method for modal balancing of a flexible rotor through two critical speeds.

The numerical example of Table 4.1 illustrates the above procedure. An accelerometer placed at the left bearing of an overhung disk rotor (Fig. 4.7) gave a reading of 1.13 units in the original unbalance condition. This is shown as circle OA in Fig. 4.8. A trial weight of 0.0312 oz is added to the rotor disk. The rotor is spun up to speed, and the accelerometer then reads 1.7 units. The trial weight is then

Table 4.1. Balancing of a rigid rotor with an overhung disk*

Test	Accelerometer reading	Trial weight (oz)	Angular location of trial weight
1	1.13	—	None
2	1.70	0.0312	330°
3	1.85	0.0312	60°
4	0.95	0.0312	150°
5	0.65	0.0312	240°

*After Wilcox [5] (©1967 Pitman & Sons Ltd., London; used by permission).
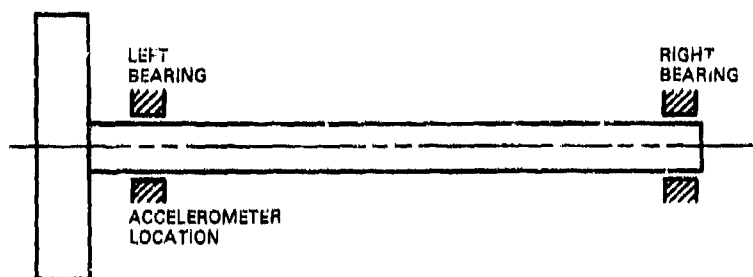All tests were conducted at 1250 rpm. The trial weight was inserted in the
overhung disk at 3.0-in. radius in each test.

LEFT
BEARING

RIGHT
BEARING

ACCELEROMETER
LOCATION

Fig. 4.7. Rigid rotor with overhung disk

Scale. 1 unit = 1 inch

B_2

1.85 in.

60°

A_2

FIGURE DATUM

150°

0.95 in.

B_3

A_3

+204°

D

1.03 in.

A_1 330°

330°

240°

A_4

170 in.

B_4

0.65 in.

B_1

OD ~ 0.80 in.
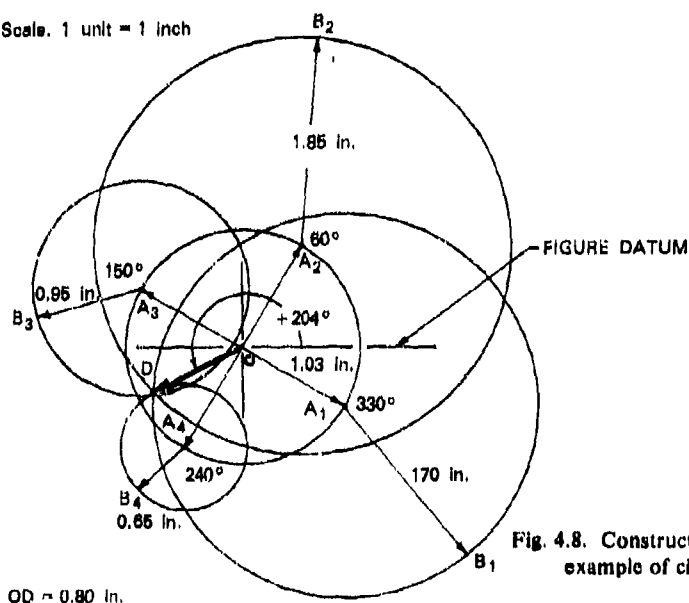
Fig. 4.8. Construction for numerical
example of circle method

moved 90°, and the procedure is repeated. The accelerometer reads 1.85 units. The weight is again moved 90°, and the reading is 0.95 units. A final reading of 0.65 units is obtained with the trial weight at the fourth 90° location.

The circle construction shows that the original unbalance of 1.13 units is located at 234° from the first trial weight position, or 204° from the figure datum shown.

In practice the balance correction sequence would be as follows:

1. Run the rotor at 1250 rpm. Measure the transmitted unbalance force of 1.13 units at the left pedestal.

2. Add 0.0312 oz at location 330° (arbitrarily selected from any chosen datum) at 3.0-in. radius on disk. Read the vibration level of 1.7 units.

3. Remove 0.0312 oz to location 60°. Read transmitted force of 1.85 units.

4. Remove 0.0312 oz to location 150°. Read transmitted force of 0.95 units.

5. Remove 0.0312 oz to location 240°. Read transmitted force of 0.65 units.

6. Draw circle OA representing original unbalance to scale (i.e., 1.13 units is drawn as circle of 1.13-in. radius).

7. Mark locations of 330°, 60°, 150°, and 240° on circle OA.

8. With center at each angular location point in turn, draw scale circles of radii 1.7 in. (330°), 1.85 in. (60°), 0.95 in. (150°), and 0.65 in. (240°). Note that all circles very nearly intersect at point D.

9. The measured length of vector OD is 0.80 in.

10. The magnitude of the original rotor unbalance U is given by

$$U = \frac{OA_1}{OD} \cdot (\text{trial weight, oz})$$

$$= \frac{1.13}{0.80} (0.0312) = 0.04407 \text{ oz.}$$

11. The angular location of the required correction weight is given by the direction of vector OD, which is $+204°$ from the figure datum.

12. The required correction weight is therefore 0.04407 oz at 3.0-in. radius, at an angle of $+204°$ from the datum.

It is shown later in this section that a similar test by Wilcox [5] gave a correction weight $C = 0.0442$ oz. at $\theta_c = 206°$ using a different construction than that described above.

This example demonstrates the effectiveness of the circle method using a bearing-mounted accelerometer for the single-plane balancing of rigid rotors.

Field Balancing Procedure: Simple Applications

Described below is an industrial procedure for balancing rotors in situ. The rotor discussed here is a rigid rigid rotor, but the method can be used for field balancing flexible rotors as well. The basic equipment includes a pickup (optical or magnetic), a strobe flash lamp, and a vibration-measuring device that contains some type of synchronous filter (e.g., a wattmeter circuit). A set of suitable balance correction weights is also needed.

The equipment installation procedure is as follows:

1. The pickup is installed so that the photocell is aligned normal to the rotating surface of the rotor. A special rigid mounting bracket is usually fabricated to clamp the pickup to the bearing pedestal or to the structural frame of the machine being balanced. It is desirable that the pickup should read in the direction of maximum vibration, which is frequently the horizontal direction.

2. The rotor circumference is calibrated into 12 equal divisions (hour markings) numbered in sequence on the surface.

3. The measurement circuit shown in Fig. 4.9 is set up. Signals from the strobe are received by the vibration analyzer, filtered, and displayed on the amplitude meter.
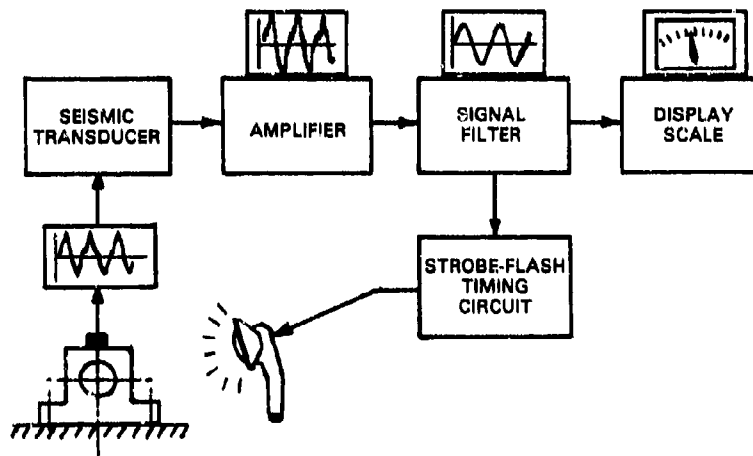
Fig. 4.9. Field-balancing equipment circuit

In the simplest kind of field balancing, there is no phase-angle-measuring equipment. Phase angles between the calibration zero mark on the rotor circumference and the angular location of the rotor maximum amplitude are determined by the strobe flash, which is arranged to fire when the "heavy" side of the rotor passes a certain angular location, as shown in Fig. 4.10. The flash illuminates the angular location corresponding to the unbalance location. A correction weight is then added to the rotor at 180° from the heavy side, in a plane close to the end being balanced.
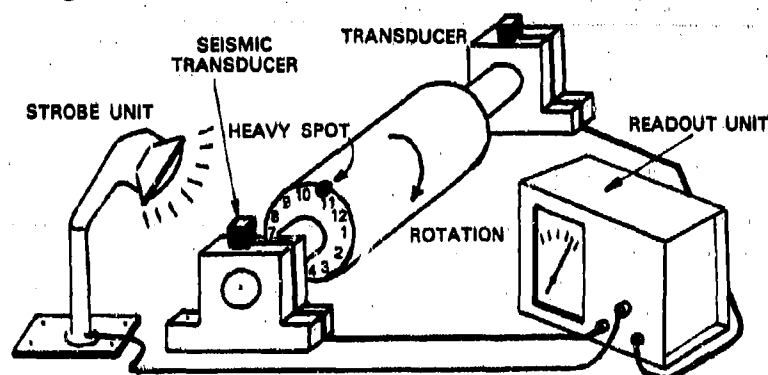
Fig. 4.10. Strobe-flash firing condition: rotor heavy spot triggers flash

The balancing sequence is as follows:

1. First trial run. Bring the rotor up to the balancing speed, which may be considerably below the operating speed (e.g., 400 rpm for an 1800-rpm rotor). With the equipment functioning as described above, observe either the amplitude of the rotor journal with a displacement sensor or the amplitude of a transducer voltage (e.g., accelerometer) on the bearing cap. Also observe the phase angle of the maximum vibration amplitude, as described earlier.

2. Stop the rotor and add a trial weight of known magnitude in the balance plane adjacent to the rotor end being observed, 90° from the heavy side of the rotor. For low-speed balancing, a lump of clay can be used as a trial balance weight if desired.

3. Second trial run. Run the rotor at the same balance speed and observe the new magnitude and location of the heavy side of the rotor.

4. Calculate the magnitude and orientation of the required correction weight using the construction shown in Fig. 4.4. Insert this correction weight.

5. Repeat the procedure until further balance runs make no discernible difference in the balance quality.

6. Repeat the procedure near the other end of the rotor until that end is also satisfactorily balanced.

7. Check the first balance. If this has been disturbed by the second balance, it should be trim balanced until the quality is again satisfactory.

8. Trim balance the second end of the rotor in a similar manner.

The balancing sequence should converge in relatively few balancing runs because in most instances adjustments at one end cause only secondary unbalance effects at the other end. The above procedure is usually effective for small rotors. It can also be used for large rotors at low balancing speeds (250 to 400 rpm). For large rotors, balancing weights are used instead of clay and the process requires more formal methods to achieve rapid convergence.

An interesting example of the above procedure is given by Blake [1], who describes in detail the balancing of an induced-draft boiler fan, shown diagrammatically in Fig. 4.11. With the pickup rigidly attached to the outer bearing B and reading in the horizontal direction, the fan was given a first trial run at 1175 rpm, and the shaft vibrations were measured near the bearing. A trial balance weight was then added at blade 24. When rotor was run again, it was observed that the strobe light flashed at the 3 o'clock position (blade 6). The rotor was then reoriented until the strobe index was brought into the same phase position as it was when the light flashed. After placing a trial weight at this same location, the rotor was run again. Under such circumstances, if the trial-weight placement is correct, the index illumination position
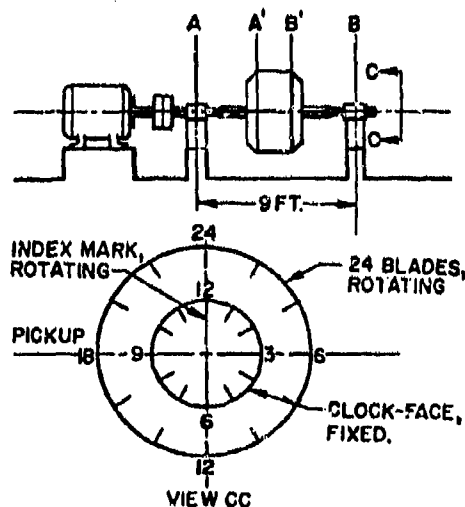
Fig. 4.11. Induced-draft boiler fan showing balance planes A' and B'. After Blake [1]. (©1967, Gulf Publishing Co.; used by permission)

will remain as before and the amplitude will change—or the index position will change by 180° regardless of any amplitude change. This indicates that the plane of unbalance has been identified. What remains then is amplitude reduction by the addition of suitable balance weights in this plane.

The history of this balance is shown in Table 4.2. In run 1 the bearing amplitudes were 17 mils at A and 17 mils at B. The addition of 2.0 oz. in plane A' and 2.0 oz in plane B' increased the bearing vibration amplitudes to 18 mils at A and 23 mils at B, with no change in phase angle. In the third run, the 4.0-oz balancing weights were all concentrated in plane B' at 12 o'clock (180° from the previous position because the unbalance plane was then known). This gave 13 mils at bearing A and 13 mils at bearing B, with a modest change in phase angle at both ends of the rotor. Vector representations of these changes are shown in Fig. 4.12.

The vector of 17 mils at 7:30 o'clock was changed into a vector of 13 mils at 6:30 o'clock; a vector of 9.5 mils at 3:00 o'clock was required to achieve this. If this argument is pursued, a vector of 17 mils at 1:30 o'clock would annul the rotor unbalance vector. The magnitude of the balance weight required is therefore $(17.0/9.5)(4.0)$ oz, and the required orientation is counterclockwise 45° from the 3:00 o'clock position where it was previously added.

The results of this change are shown as run 4. A trial weight of $(17.0/9.5)(4.0) \approx 8.0$ oz was added at 4:30 o'clock (blade 9). This resulted in 5.0 mils at bearing A and 5.0 mils at bearing B, both at 6:00 o'clock. The vector diagram for this suggests that the balance weight should be increased in the ratio $(17.0/14.0)$ to 11.0 oz and that the balance location be rotated counterclockwise by an additional blade (to blade 8, 4:00 o'clock). This adjustment was successful and resulted in small residual amplitudes. The weight was then *welded* into position before further trim balancing was performed with smaller balance weights.

Blake [1] mentions that after welding it frequently occurs that the residual unbalance vector changes in magnitude and orientation, that is, the unbalance is increased and its orientation is different from that in Table 4.2; compare run 5 (before welding) with run 6 (after welding). As shown in Fig. 4.12, the unbalance after welding becomes 7.0 mils at 3:00 o'clock. Based on prior experience, a weight of 4.0 oz is added at blade 17 (8:00 o'clock). This reduces the amplitude to 3.0 mils at 12:30 o'clock (run 7) which is subsequently reduced to 0.4 mil at bearing A and 0.7 mil at bearing B after run 8. This final adjustment was made by reorienting the 7-mil balancing vector ahead by two blades (to blade 19) to make the two 7-mil vectors in run 7 cancel each other.

Table 4.2 Details of balancing procedure for an induced-draft boiler fan*

Run No.	Trial weight amount and location				Vibration amplitude at bearings and phase clock			
	Angle Blade A'	A'	B'	Angle Blade B'	Mils PP A	Phase Clock A	Mils PP B	Phase Clock B
1	—		—		17	7:30	17	7:30
2	2	24	2	24	18	7:30	23	7:30
3	—		4	12	13	8:30	13	8:30

Now increase trial weight in the ratio 17/9.5 and, because angle S is about 45°, move trial weight counterclockwise 3 blades or 1.5 h.

4	—	—	8	9	5	6:00	5	6:00

Now increase trial weight in the ratio 17/14 and, because angle S is about 15°, move trial weight counterclockwise by one blade.

5	—	—	11	8	2.5	6:00	1.5	5:00

Now weld the 11-oz weight at B', blade 8, and start a new problem.

6	—	—	—	—	5	3:00	7	3:00

Note: From runs 1 and 5: if blade 8 is the proper correction position for index 7:30 and pickup at 9, then this position is 2.5 h clockwise from pickup, when strobe flashes, so now place 4 oz at blade 17.

7	—	—	4	17	1.2	12:30	3	12:30

Now use same trial weight and rotate through angle S, 30° clockwise.

6	—	—	4	19	0.4	12:00	0.7	7:00

Now weld on and make final check.

*From Blake [1] (©1967, *Hydrocarbon Processing*, used by permission). See Fig. 4.11 for a schematic of the balancing.

(a) After balancing run 3   (b) After balancing run 4   (c) After balancing run 7
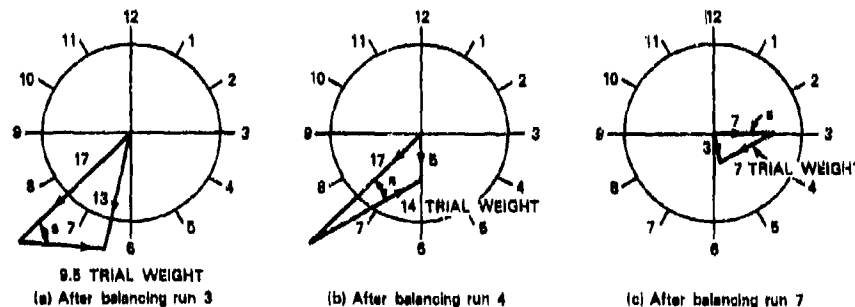
Fig. 4.12. Details of graphical solution to fan-balancing case history described by Blake [1] (©1967, Gulf Publishing Co.; used by permission)

The procedure described above is simple and relatively straightforward to apply. Its shortcomings are the difficulty of achieving a rapid and effective balance by operating on a single plane at a time and the tendency of the rotor to experience several vibration modes simultaneously. The latter is especially true in the case of overhung rotors. Other factors that may cause difficulties in achieving a satisfactory balance are rotor flexibility, any looseness of the impeller on the shaft, and occasional problems of looseness or excessive flexibility of the unit on its foundation. These effects can introduce other unexpected system modes with occasional nonlinear effects. Obvious safeguards are to design stiff rotors that operate as far below their bending critical speeds as possible, operating in a massive, solidly mounted foundation and casing.

The balancing of the stiff rotor in rolling-element bearings carrying an unbalanced overhung disk discussed previously and shown in Fig. 4.13 is also described in detail by Wilcox [5]. The measuring equipment consisted of two high-impedance coils, an integrating circuit (to convert velocity measurements into displacements), and a stroboscope to illuminate the angular location of the unbalance in the rotor. A procedure for estimating the size of the required correction weights has been described on pages 203 and 204. Details of the test sequence are listed in Table 4.3.

During the balancing process all amplitude measurements were made at the overhung disk, with the correction weights added in the plane of the overhung disk. The procedure is as follows:

1. The unbalanced rotor was run at 1250 rpm. An unbalance amplitude of 2.7 mils was observed at a phase angle of 240° at the disk.

2. The rotor was stopped, and a trial weight of 0.25 oz was added at an angle of 330°, in the end disk at a radius of 3.0 in.
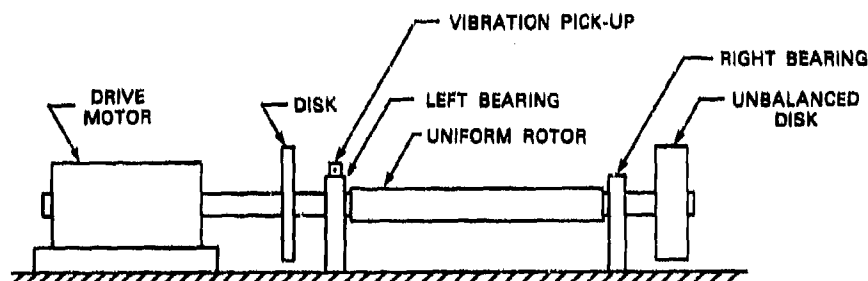
Fig. 4.13. Rigid rotor in rolling-element bearings with unbalanced overhung disk. After Wilcox [5]. (©1967, Pitman & Sons Ltd.; used by permission)

Table 4.3 — Balancing tests with stroboscopic phase measurement for a rigid rotor with unbalanced overhung disk*

Test number	Disk vibration		Details of test
	Amplitude (in.)	Phase position (deg)	
1	0.00270	240	Initial test
2	0.00426	195	0.25 oz added at 330°
3	0.00030	150	0.25 oz removed 0.218 oz added at 240°
4	0.00004		0.024 oz added at 150°

*After Wilcox [5] (© 1967 Pitman & Sons Ltd., London; used by permission). All tests were run at 1250 rpm.

3. The new unbalance condition resulted in a disk amplitude of 4.26 mils at 195°.

4. The initial unbalance condition and the calibration condition are shown in the vector diagram of Fig. 4.14. Initial unbalance $OA = 2.7$ in. Calibration unbalance $OB = 4.26$ in. The effect of the calibration weight alone is the vector $AB = 3.1$ in., which acts at 94° to the original unbalance vector OA.

5. The required balance correction weight can be determined as follows:

Magnitude $= (0.25)(2.7/3.1) = 0.218$ oz.

Orientation: 94° counterclockwise from the vector AB, i.e., at 330 $- 94 = 236°$.

6. A balance weight of 0.218 oz at 240°. This resulted in a rotor vibration of 0.3 mil at 150°.

Minor additional corrections reduced this amplitude to 0.040 mil at 1250 rpm. These balancing moves listed in Table 4.3 are shown vectorially in Fig. 4.14.

A second balancing procedure that requires only displacement amplitude measurements is also described by Wilcox [5]. No phase angles are measured. The same rotor with the same initial unbalance reading (2.7 mils at 240°) was balanced at 1250 rpm by use of this second procedure, as described in Table 4.4. The effect of a calibration weight placed in four angular locations equally spaced 90° apart around the circumference of the disk is determined. Using the four vibration readings with the original unbalance reading makes it possible to
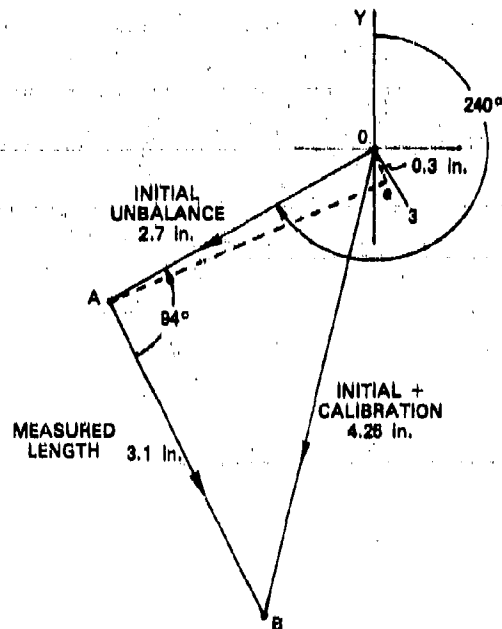
Fig. 4.14. Vector diagram for balancing a rigid
rotor, with subsequent trim balance. After
Wilcox [5]. (©1967, Pitman & Sons Ltd.; used
by permission)

Table 4.4 — Balancing of a rigid rotor with an overhung disk using only
amplitude measurements

Test No.	Vibrational amplitude (in.)	Details of test
1	0.00270	Initial test
2	0.00113	0.172 oz added at 240°
3	0.00170	0.0312 oz added at 330°
4	0.00185	0.0312 oz transferred from 330° to 60°
5	0.00095	0.0312 oz transferred from 60° to 150°
6	0.00065	0.0312 oz transferred from 150° to 240°
7	0.00005	0.0312 oz removed, 0.0442 oz added at 210°

*After Wilcox [5] (© 1967, Pitman & Sons Ltd., London; used by permission). All tests
were run at 1250 rpm, and all balance weights were added at a 3-in. radius.

construct an amplitude vector diagram (similar to the force vector diagram described previously) that will allow the original unbalance in the disk to be determined. The construction shown in Fig. 4.15 was readily achieved by trial and error. This procedure was applied after an initial balancing adjustment had been made (not a necessary part of the procedure), in which a correction weight of 0.172 oz was applied at 240°, as indicated by run 2 in Table 4.4. Improvement was substantial. The following trim adjustments were then made with a calibration weight of 0.0312 oz, applied at 330°, 60°, 150° and 240°. The magnitude of the required correction weight from Fig. 4.15 is

$$W_c = \text{(calibration weight)} \frac{\text{(length of 02)}}{\text{(length of 24)}}$$

$$= (0.0312) \frac{(1.13)}{(0.8)} = 0.0442 \text{ oz.}$$
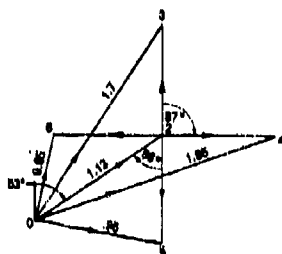
Fig. 4.15. Rigid-rotor balancing by the four-circle method. After Wilcox [5]. (©1967, Pitman & Sons Ltd.; used by permission)

The orientation of the required correction weight is found by observing that, when the calibration weight is added at 240° (test 6) the amplitude has its minimum value. When the trial weight is added at 60° (test 4) the amplitude is maximum. With the vector 24 as a reference, the above correction must be applied at (270-56) = 216° CCW from vector 24, as indicated in Fig. 4.16.

Wilcox [5] indicates that with the above vector solution a correction weight of 0.0442 oz was added at 210° (the next convenient hole). Test 7 showed a substantial improvement in the balance of the rotor. The results obtained with the above amplitude method and with the phase method described previously above are almost identical (see Fig. 4.17).

Two-Plane Field-Balancing Procedures

The procedures described previously are best suited to rigid rotors with thin simple disks. Longer rigid rotors require more complex two-

Fig. 4.16. Construction for determining the
angular location of correction weights

CORRECTION WEIGHT
VECTOR C

Ou = initial unbalance
01 = balance weights — first method
02 = balance weights — second method
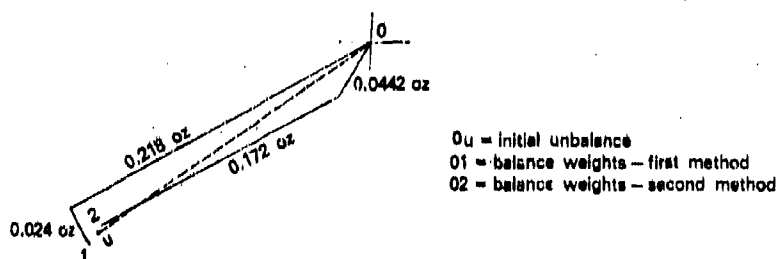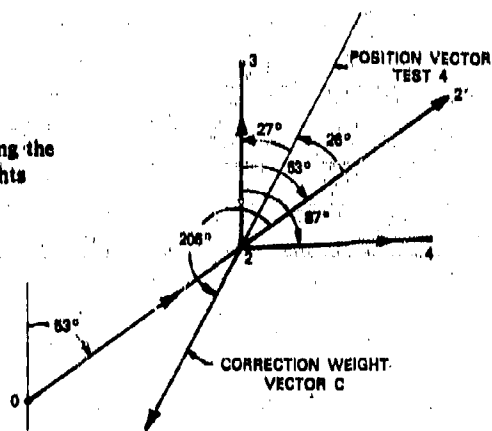
Fig. 4.17. Comparison of two rotor-balancing methods. After Wilcox [5].
(®1967, Pitman & Sons, Ltd.; used by permission)

plane balancing procedures. Two-plane rigid-rotor balancing procedures
must deal with the following problems:

1. *Plane separation*: Unbalance effects are usually measured near
the bearings. Correction weights are usually installed in planes located
away from the bearings, often about 10% of the rotor length inboard of
the bearings. The influence of the correction plane locations must be
considered when determining the required correction weights.

2. *Simultaneous two-plane balancing*: Unbalance corrections
applied in one plane will disturb the balance in the other balance plane.
A procedure that includes this interaction must be used to minimize
the trial and error involved.

Gross unbalance effects are usually removed during low-speed shop
balancing. Two-plane balancing of a rigid rotor in the field is com-
monly a trim-balancing operation, in which the remaining small unbal-
ance effects are removed. Built-up rotors often require trim balancing

after having been shipped to their destination. Large jet engines are trim balanced in engine test cells using two end planes (first compressor stage and last turbine stage).

The equipment needed for balancing a rigid rotor in two planes is shown in Fig. 4.18. This is the same as that used for the single-plane balance, except that an additional sensor and its circuitry are installed at the second bearing. The extended instrumentation network is shown in Fig. 4.19. The end of the rotor adjacent to the strobe lamp again has a "clockface" of numbers painted on it, and the strobe flash again occurs as the maximum force is transmitted to either pedestal during rotation.

The theory of two-plane balancing is given in the next section. An application of this procedure to the overhung rotor example discussed by Wilcox [5] is given on pages 223 through 228.
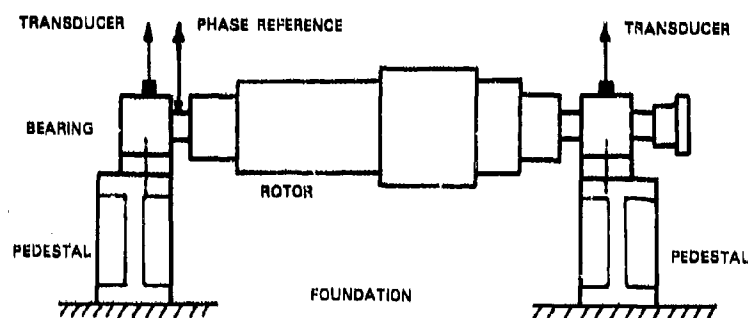
Fig. 4.18. Rigid rotor in foundations with instrumentation for balancing
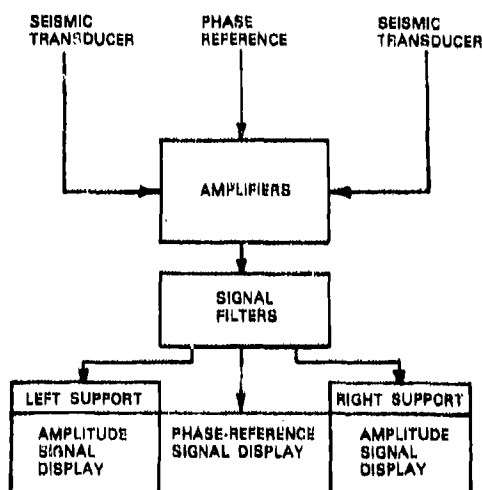
Fig. 4.19. Instrumentation for two-plane field balancing

Rigid-Rotor Influence Coefficient Balancing: Theory

Consider the overhung rigid rotor shown in Figs. 4.20 and 4.21 which operates with unbalance forces F, P acting at the two rotating disks. The rotor is supported in two inboard bearings which experience reaction forces R and S as a result of the rotating unbalance forces. The unbalance forces acting on the disks are defined by the relations:

$$\text{Unbalance force } F = \frac{W_1 a_1 \omega^2}{g} = \frac{\omega^2}{g} U_1; \quad U_1 = W_1 a_1$$

$$\text{Unbalance force } P = \frac{W_2 a_2 \omega^2}{g} = \frac{\omega^2}{g} U_2; \quad U_2 = W_2 a_2,$$

in which W_1, W_2 are the disk weight, and a_1, a_2 are the c.g. eccentricities, respectively.
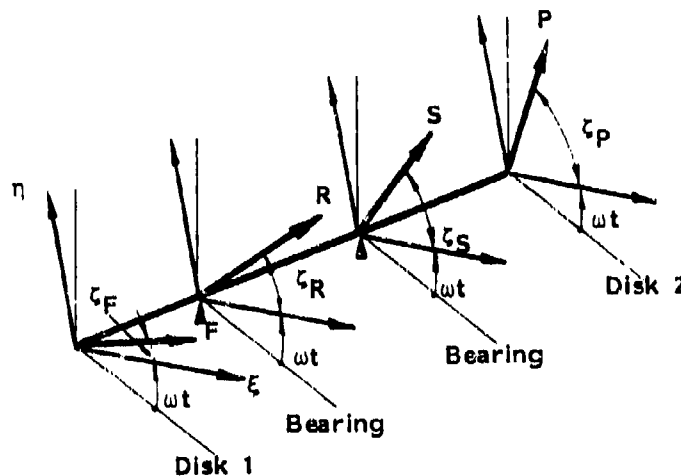
Fig. 4.20. Geometry of overhung two-disk rotor
in inboard bearings

The vector equilibrium equations for the bearing reactions R, S are:

$$\bar{\alpha}_{11} \cdot \bar{F} + \bar{\alpha}_{12} \cdot \bar{P} - \bar{R} = 0$$

$$\bar{\alpha}_{21} \cdot \bar{F} + \bar{\alpha}_{22} \cdot \bar{P} - \bar{S} = 0$$

where $\bar{\alpha}_{11}$, $\bar{\alpha}_{12}$, $\bar{\alpha}_{21}$, and $\bar{\alpha}_{22}$ are the vector influence coefficients relating the unbalance forces to the bearing reactions. Replacing each of these quantities by its complex form gives:

$$(\alpha_{11}^r + i\alpha_{11}^i)(F^r + iF^i) + (\alpha_{12}^r + i\alpha_{12}^i)(P^r + iP^i) = (R^r + iR^i)$$

$$(\alpha_{21}^r + i\alpha_{11}^i)(F^r + iF^i) + (\alpha_{22}^r + i\alpha_{22}^i)(P^r + iP^i) = (S^r + iS^i).$$

Expanding the equating real and imaginary parts separately gives:

$$\begin{bmatrix} \alpha_{11}^r & -\alpha_{11}^i & \alpha_{12}^r & -\alpha_{12}^i \\ \alpha_{11}^i & \alpha_{11}^r & \alpha_{12}^i & \alpha_{12}^r \\ \alpha_{21}^r & -\alpha_{21}^i & \alpha_{22}^r & -\alpha_{22}^i \\ \alpha_{21}^i & \alpha_{21}^r & \alpha_{22}^i & \alpha_{22}^r \end{bmatrix} \begin{Bmatrix} F^r \\ F^i \\ P^r \\ P^i \end{Bmatrix} = \begin{Bmatrix} R^r \\ R^i \\ S^r \\ S^i \end{Bmatrix}$$

or

$$[A]\{G\} = \{H\}.$$

The influence coefficients are each found by placing a trial balance weight B (oz in.) in each end disk (correction plane) in turn. This gives an unbalance force

$$\bar{T}_r = \frac{\omega^2}{g} \bar{B}_r, \quad r = 1,2.$$

Placing $\bar{T}_1$ in the first disk the vector equations for equilibrium at the bearings become:

$$\bar{\alpha}_{11} \cdot (\bar{F} + \bar{T}_1) + \bar{\alpha}_{12}\bar{P} - \bar{R}_1 = 0$$

$$\bar{\alpha}_{21} \cdot (\bar{F} + \bar{T}_1) + \bar{\alpha}_{22}\bar{P} - \bar{S}_1 = 0.$$

Subtracting the original unbalance from the first of these equations gives:

$$\bar{\alpha}_{11} \cdot \bar{T}_1 = \bar{R}_1 - \bar{R};$$

i.e.,

$$\bar{\alpha}_{11} = \frac{\bar{R}_1 - \bar{R}}{\bar{T}_1} = \frac{R_1}{T_1} e^{i(\zeta_{R_1} - \zeta_{T_1})} - \frac{R}{T_1} e^{i(\zeta_R - \zeta_{T_1})}$$

$$= \alpha_{11}^r + i\alpha_{11}^i.$$

Similarly

$$\bar{\alpha}_{21} = \frac{\bar{S}_1 - \bar{S}}{\bar{T}_1} = \frac{S_1}{T} e^{i(\zeta_{S_1} - \zeta_{T_1})} - \frac{S}{T} e^{i(\zeta_S - \zeta_{T_1})}$$

$$= \alpha_{21}^r + i\alpha_{21}^i.$$

If the trial unbalance is then placed in the second disk the vector equations are:

$$\bar{\alpha}_{11} \cdot \bar{F} + \bar{\alpha}_{12} \cdot (\bar{P} + T_2) = \bar{R}_2.$$

$$\alpha_{21} \cdot \bar{F} + \alpha_{22} \cdot (\bar{P} - \bar{T}_2) = \bar{S}_2.$$

The influence coefficients are:

$$\bar{\alpha}_{12} = \frac{\bar{R}_2 - \bar{R}}{\bar{T}_2} = \frac{R_2}{T_2} e^{i(\zeta_{R_2} - \zeta_{T_2})} - \frac{R}{T_2} e^{i(\zeta_R - \zeta_{T_2})}$$

$$= \alpha'_{12} + i\alpha''_{12}$$

$$\bar{\alpha}_{22} = \frac{\bar{S}_2 - \bar{S}}{\bar{T}_2} = \frac{S_2}{T_2} e^{i(\zeta_{S_2} - \zeta_{T_2})} - \frac{S}{T_2} e^{i(\zeta_S - \zeta_{T_2})}$$

$$= \alpha'_{22} + i\alpha''_{22}.$$

The real and imaginary terms in the influence coefficient matrix are therefore given by:

$$\alpha'_{11} = \alpha_{11} \cos \zeta_{11} = \frac{R_1}{T_1} \cos (\zeta_{R_1} - \zeta_{T_1}) - \frac{R}{T_1} \cos (\zeta_R - \zeta_{T_1}),$$

$$\alpha''_{11} = \alpha_{11} \sin \zeta_{11} = \frac{R_1}{T_1} \sin (\zeta_{R_1} - \zeta_{T_1}) - \frac{R}{T_1} \sin (\zeta_R - \zeta_{T_1});$$

$$\alpha'_{21} = \alpha_{21} \cos \zeta_{21} = \frac{S_1}{T_1} \cos (\zeta_{S_1} - \zeta_{T_1}) - \frac{S}{T_1} \cos (\zeta_S - \zeta_{T_1}),$$

$$\alpha''_{21} = \alpha_{21} \sin \zeta_{21} = \frac{S_1}{T_1} \sin (\zeta_{S_1} - \zeta_{T_1}) - \frac{S}{T_1} \sin (\zeta_S - \zeta_{T_1});$$

$$\alpha'_{12} = \alpha_{12} \cos \zeta_{12} = \frac{R_2}{T_2} \cos (\zeta_{R_2} - \zeta_{T_2}) - \frac{R}{T_2} \cos (\zeta_R - \zeta_{T_2}),$$

$$\alpha''_{12} = \alpha_{12} \sin \zeta_{12} = \frac{R_2}{T_2} \sin (\zeta_{R_2} - \zeta_{T_2}) - \frac{R}{T_2} \sin (\zeta_R - \zeta_{T_2});$$

$$\alpha'_{22} = \alpha_{22} \cos \zeta_{22} = \frac{S_2}{T_2} \cos (\zeta_{S_2} - \zeta_{T_2}) - \frac{S}{T_2} \cos (\zeta_S - \zeta_{T_2}),$$

$$\alpha''_{22} = \alpha_{22} \sin \zeta_{22} = \frac{S_2}{T_2} \sin (\zeta_{S_2} - \zeta_{T_2}) - \frac{S}{T_2} \sin (\zeta_S - \zeta_{T_2}).$$

Each of the above 8 terms appears twice in the influence coefficient matrix. When these expressions are evaluated from the trial weight test data, the influence coefficients are obtained. The influence coefficient matrix $[A]$ is formed from these results. Matrix $[A]$ is then inverted to evaluate the magnitude of the original unbalance vector $\{G\}$ from the operation:

$$\{G\} = [A]^{-1}\{H\},$$

where H is the vector of the bearing force components resulting from the rotor unbalance (without trial weight effects).

The required correction weights and angles are obtained from the real and imaginary parts of $\{F\}$ and $\{P\}$ from the $\{G\}$ vector as follows:

$$\{G\} = \begin{Bmatrix} F_1^r \\ F_1^i \\ P_1^r \\ P_1^i \end{Bmatrix}, \quad \{F\} = \begin{Bmatrix} F_1^r \\ F_1^i \end{Bmatrix}, \quad \{P\} = \begin{Bmatrix} P_1^r \\ P_1^i \end{Bmatrix}.$$

The required correction weights C_1 and C_2 are then found from the expressions

$$F_1 = \sqrt{(F_1^r)^2 + (F_1^i)^2},$$

$$P_1 = \sqrt{(P_1^r)^2 + (P_1^i)^2},$$

to be

$$C_1 = U_1 = (g/\omega^2)F_1 \text{ oz in.}, \quad W_{C1} = U_1/r_1$$

$$C_2 = U_2 = (g/\omega^2)P_1 \text{ oz in.}, \quad W_{C2} = U_2/r_2$$

where r_1 and r_2 are the radii of the correction planes in disk 1 and disk 2, respectively. The correction weight orientation angles ζ_1 and ζ_2 are found from the expressions

$$\zeta_F^{\mathscr{E}} = \arctan\ (F_1^{\prime}/F_1^{\prime}) + 180^{\circ}$$

$$\zeta_F^{\mathscr{E}} = \arctan\ (P_1^{\prime}/P_1^{\prime}) + 180^{\circ}.$$

Note that the magnitude of C_1 and U_1 are identical, likewise C_2 and U_2. The unbalance is corrected (cancelled) in each case by placing both correction weights at 180° from the determined angular location of the original unbalances.

Two-Plane Balance of Doubly-Overhung Rotor

Wilcox [5] has given details of the balancing of the doubly-overhung laboratory rotor shown in Fig. 4.21, which will now be used to demonstrate the theory of the preceding section. The two correction planes are located in the overhung end disks, and these planes are assumed to contain the rotor residual unbalance $\{G\}$. Vibration readings were taken on the bearing housings. The test results are summarized below, together with the unbalance corrections which Wilcox obtained using two methods, and which he found to be effective on trial.
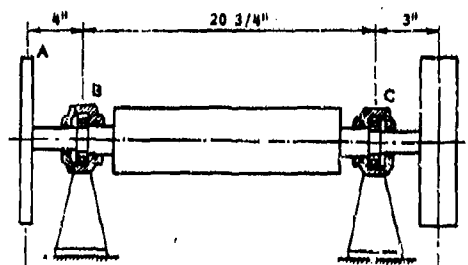
(a) Wilcox rotor

(b) unbalance forces and reactions

Fig. 4.21. Wilcox rotor and applied force distribution

Condition	Bearing	Magnitude, mils	Angle, deg.
Original unbalance	R	0.85	135
	S	1.00	0
Original plus	R	2.20	75
trial, plane 1	S	0.90	350
Original plus	R	0.90	150
trial, plane 2	S	1.70	30
Balance Corrections	Left disk C_1	0.09 oz	191
	Right disk C_2	0.235 oz	65

Writing Wilcox's data in terms of the notation from the previous section on theory of influence coefficient balancing, gives original unbalance:

$$R = 0.85, \quad \zeta_R = 135°$$

$$S = 1.00, \quad \zeta_S = 0°$$

$$T_1 = 0.25, \quad \zeta_{T_1} = 300°; \qquad R_1 = 2.20, \quad \zeta_{R_1} = 75°$$

$$S_1 = 0.90, \quad \zeta_{S_1} = 350°$$

$$T_2 = 0.25, \quad \zeta_{T_2} = 300°; \qquad R_2 = 0.90, \quad \zeta_{R_2} = 150°$$

$$S_2 = 1.70, \quad \zeta_{S_2} = 30°.$$

Substituting these values into the expressions given previously for the real and imaginary parts of the influence coefficients gives:

$$\alpha'_{11} = \alpha_{11} \cos \zeta_{R_1} = \frac{R_1}{T_1} \cos (\zeta_{R_1} - \zeta_{T_1}) - \frac{R}{T_1} \sin (\zeta_R - \zeta_{T_1})$$

$$= \frac{2.20}{0.25} \cos (75°\text{-}300°) - \frac{0.85}{0.25} \cos (135°\text{-}300°)$$

$$= -2.93839,$$

$$\alpha''_{11} = \alpha_{11} \sin \zeta_{R_1} = \frac{R_1}{T_1} \sin (\zeta_{R1} - \zeta_{T_1}) - \frac{R}{T_1} \sin (\zeta_R - \zeta_{T_1})$$

$$= \frac{2.20}{0.25} \sin (75°\text{-}300°) - \frac{0.85}{0.25} \sin (135°\text{-}300°)$$

$$= 7.10252.$$

In a similar manner,

$$\alpha f_2 = 0.16606, \quad \alpha f_2 = -0.92002$$

$$\alpha f_1 = 0.31404, \quad \alpha f_1 = -0.70634$$

$$\alpha f_2 = -2.00000, \quad \alpha f_2 = 3.33590.$$

The influence coefficient matrix may now be formed. This is done as shown below. The original unbalance vector is also formed, and the product of these two terms gives the real and imaginary components of the unbalance vectors $\{F\}$ and $\{P\}$, viz.,

$$
\begin{bmatrix}
-2.93839 & -7.10252 & 0.16646 & 0.92002 \\
7.10252 & -2.93839 & -0.92002 & 0.16646 \\
0.31404 & 0.70634 & -2.00000 & -3.33590 \\
-0.70634 & 0.31404 & 3.33590 & -2.00000
\end{bmatrix}^{-1}
\begin{Bmatrix}
-0.60104 \\
0.60104 \\
1.00000 \\
0.00000
\end{Bmatrix}
=
\begin{Bmatrix}
F'_1 \\
F''_1 \\
P'_1 \\
P''_1
\end{Bmatrix}
$$

$$
=
\begin{bmatrix}
-0.05196 & 0.12262 & -0.02199 & 0.02325 \\
-0.12262 & -0.05196 & -0.02325 & -0.02199 \\
-0.01337 & 0.02288 & -0.13690 & 0.22441 \\
-0.02288 & -0.01337 & -0.22441 & -0.13690
\end{bmatrix}
\begin{Bmatrix}
-0.60104 \\
0.60104 \\
1.00000 \\
0.00000
\end{Bmatrix}
=
\begin{Bmatrix}
0.0828 \\
0.0193 \\
-0.1150 \\
-0.2187
\end{Bmatrix}
$$

It now remains to obtain F and P in polar form, and the correction weights and angles. These are:

$$F = F_1 e^{i\zeta_F} = 0.08503\ e^{i(13.1°)}; \qquad F_1 = 0.08503\ oz = C_1$$

$$\zeta_F = 193.1°$$

$$P = P_1 e^{i\zeta_P} = 0.24727\ e^{i(242.3°)}; \qquad P_1 = 0.24727\ oz = C_2$$

$$\zeta_P = 62.3°.$$

These results agree with those reported by Wilcox in the preceeding table. Note that the results appear in the same units as the trial weights if the correction weights are to be inserted at the same locations (plane, radius) as the trial weights. Care is also needed in interpreting phase angle results, as the tangent values repeat every 180°.

Two-Plane Turbine Balancing with the Influence Coefficient Method

Jackson [6] has given details of how a turbine rotor (Fig. 4.22) was balanced in two planes using a programmed hand calculator. The
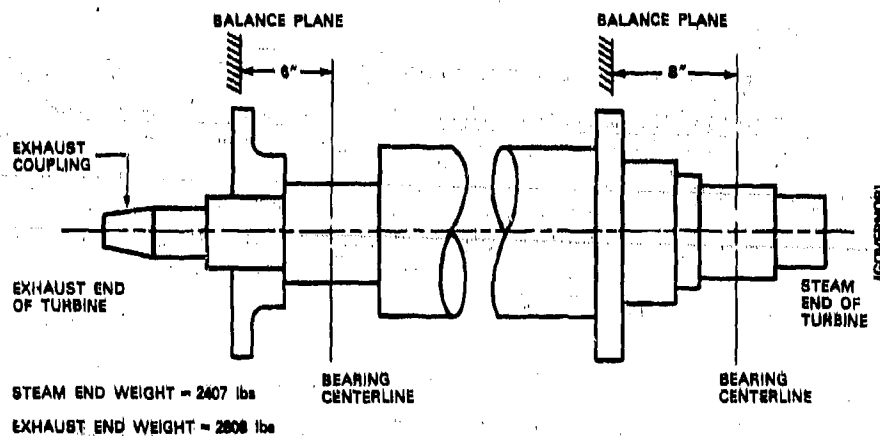
Fig. 4.22. Schematic of steam-turbine rotor for sample hand calculation of balance.
    After Jackson [6]. (©1972, The Vibration Institute; used by permission)

turbine rotor operated at 11,000 rpm, which was above its second criti-
cal speed. The bearing span was 98 in., and the rotor weight was 5200
lb. Details of the vibration readings obtained at either end of the rotor
during balancing are given in Table 4.5.

Table 4.5 Two-plane balancing of turbine rotor

Vibration measured	Amplitude (10^{-3} in.)	
	Governor end	Exhaust end
Initial peak bearing- cap relative vibration		
Vertical	2.6	1.5
Horizontal	2.6	1.0
Final peak bearing- cap relative vibration		
Vertical	1.1	0.6
Horizontal	0.8	0.6
Initial absolute bearing- cap vibration	0.36	0.4
Final absolute bearing- cap vibration	0.11	0.0035

Shaft-to-bearing relative displacements were measured with hor-
izontal and vertical proximity probes. Bearing-cap vibrations were

measured with a seismic velocity sensor. The governor-end phase reference was obtained by observing the orientation of the clockface for the governor-end balance plane with a stroboscope. The 20 balance-correction holes were numbered for angular reference in the counter-clockwise direction of rotation. The exhaust-end phase reference was taken from the 16-hole balance row.

The 12 o'clock position was the reference marker at both ends on the vector clockface. Displacement probes were mounted close to either bearing cap at +45° and at −45° to the vertical.

Calculation details are shown in Figs. 4.23 and 4.24. All results were calculated with a programmable hand calculator. A satisfactory rotor balance was achieved in the manner described.

```
THE RESIDUAL RUNOUT VECTORS ARE                      CONVENTION
ZR1    =        0.0        AT    0.0   DEGREES
ZR2    =        0.0        AT    0.0   DEGREES        Rotation—CCW
                                                     Phase Angles—CCW
                                                     Trial Weights—CW
                                                     Correction Weights—CW


THE ORIGINAL UNBALANCE VECTORS ARE
Z1    =        0.360       AT   270.0   DEGREES
Z2    =        0.400       AT   315.0   DEGREES
  THE ROTOR SPEED IS   11000.0  RPM


THE TRIAL UNBALANCES AND RESULTING VECTORS ARE
U11   =        0.240       AT    36.0   DEGREES
Z11   =        0.370       AT     0.0   DEGREES
Z21   =        1.200       AT   261.0   DEGREES
U22   =        0.240       AT    22.5   DEGREES
Z22   =        0.250       AT   261.0   DEGREES
Z12   =        0.200       AT   333.0   DEGREES




UNBALANCE MAGNITUDE AND LOCATIONS ARE
U1    =        0.101       AT    30.0   DEGREES
U2    =        0.389       AT  -143.0   DEGREES


THE CORRECTION WEIGHTS AND LOCATIONS ARE:
W1    =        0.101       AT.  210.0   DEGREES
W2    =        0.389       AT.   37.0   DEGREES
```
⟶ ILO Solution

```
AMPLITUDE AND PHASE ANGLE ARE MEASURED IN TWO ARBITRARY
PLANES, NOT NECESSARILY THE TWO BALANCE PLANES.
TRIAL WEIGHTS ARE PLACED IN EACH OF THE TWO BALANCE
PLANES SEPARATELY, AND THE RESULTING AMPLITUDE AND
PHASE ANGLES ARE MEASURED AT THE PROBE LOCATIONS.
THE ORIGINAL UNBALANCE VECTOR IS CORRECTED FOR
RESIDUAL LOW SPEED SHAFT RUNOUT.

THE BALANCE WEIGHTS AND AMPLITUDE CAN BE OF ANY
DIMENSIONS, BUT THE SAME DIMENSIONS MUST BE USED
CONSISTENTLY IN ALL THE INPUT DATA.
```

Fig. 4.23. Details of rigid-rotor balance by hand calculator. From Jackson [6]. (©1972, The Vibration Institute; used by permission)

VECTOR CALCULATIONS
FOR
TWO-PLANE BALANCING

ROTOR: 45620187 SPEED: 16000 TRIAL SHOT NO'S: _____

DATE: 9/10/72 CALCULATED BY: C.J. CHECKED BY: CHD.

OPERATION	ROTOR CONDITION & RUN NO. OR CALCULATION PROCEDURE		SYM	ITEM NO.	PHASE ANGLE	STEM NO.	VIBRATION READING SCALE MILS
I	Zero Rotor - TS #1		N	1	90	2	.36 mils P/P
			F	3	45	4	.40
II	Near End Trial Weight		W₁	5*	36	6*	.24 oz
III	Trial Shot - Near End TS #2		N₁	7	0	8	.37
			F₁	9	99	10	1.2
IV	Far End Trial Weight		W₂	11*	22½	12*	.24
V	Trial Shot - Far End TS #3		N₂	13	27	14	.20
			F₂	15	99	16	.25
VI	A=N₂-N (N+N₂)		A	17*	316	18*	.52
	B=F₂-F (F+F₂)		B	19*	187	20*	.33
VII	-A-F₂-F (F+F₂)		-A	21	118	22	1.02
	βB-N₂-N (N+N₂)		βB	23	304	24	.32
VIII	25=21-17	26=22-18	-	25*	162	26*	1.96
	27=23-19	28=24-20	β	27*	117	28*	.97
	29=25-1	30=26+2	-N	29	252	30	.7056
	31=27+3	32=28+4	βF	31	+162	32	.388
	C=-βF-N (N-βF)		C	33	214	34	.44
	D=-N-F (F=-N)		D	35	242	36	1.08
	37=25-27	38=26-28	-β	37	279	38	1.9622 UNITS
IX	Unity Vector - Plot		U	39	0	40	1 UNIT = 2 mils
	E=U--β (-β+U)		E	41*	70	42*	2.06 UNITS
X	43=33-41	44=34-42	-A	43	144	44	.213
	45=35-41	46=36-42	-B	45	172	46	.524
	47=43-17	48=44-18	-A	47	+158	48	.409
	49=45-19	50=46-20	-	49	+345	50	1.586
XI	51=5-47	52=6-48	W₁	51	+208	52	.09816 oz
	53=11-49	54=12-50	W₂	53	37½	54	.380 oz
XII	Graphic Check of Results						
XIII	Make Weight Corrections						
XIV	Additional Corrections						

CHECKS

X = .355 @ 269°
Y = .38 @ 255°

(1) Removed wt. at # 13 Gov. End.
    (Same as Add. Wt. # 3)

(2) Removed wt. at # 10 Exit End.
    (Same as Add. Wt. # 2)

Results on Wt. "Add"
2.78 gms. @ 208°
10.45 gms. @ 37½°

DETAILED CALCULATIONS

Fig. 4.24. Vector calculations for two-plane balancing. From Jackson [6].
(©1972, The Vibration Institute; used by permission)

4.4 Balancing Standards for Rigid Rotors

A number of documents outlining criteria for balancing rigid rotors have been developed to provide guidance on acceptable levels of residual unbalance. Examples of such documented criteria for various classes of machines are the following:

1. ISO Document 1940-1973(E) [8]. This is the basic balance criteria document for rigid-rotor balancing. It supersedes all previous requirements for rigid-rotor balancing. It contains comprehensive charts of residual unbalance levels for rotor acceptance and gives definitions of important balancing terms, based on wide industrial experience.

2. MIL-STD-167, 1954 [9]. An early balance criteria document for balancing. Contains charts and formulas for acceptance criteria for rigid rotors in terms of rotor weights and operating speeds.

3. National Electrical Manufacturers Association balance criteria, 1956 [10—12]. Specifies required quality for balancing of armatures. Also gives guidance on balancing technology and standards related to the electrical industry.

4. American Gear Manufacturers Association balance criteria [13]. Specifies quality criteria for balancing gears, shafts, and couplings. Gives guidance on balancing technology and standards related to the gear industry.

5. American Petroleum Institute balance criteria [14]. Statement of rigid-rotor balancing requirements and procedures. Simple formulas for balance criteria.

Other criteria are given by Rathbone [15] and Yates [16] in guidance papers with balance quality charts (see Figs. 4.25 and 4.26, respectively). Vibration tolerance criteria are given by Reiher and Meister [17]. Figure 4.27 is a vibration tolerance that developed by Feldman [18].

ISO Document 1940-1973(E)

Required quality of balance is defined as the amount of acceptable residual unbalance for smooth rotor operation. Balance quality is specified in ISO 1940 [8] in terms of a range of balance quality grades, G. Table 1 in ISO 1940 is used to specify a quality grade for any rigid-rotor application. It classifies similar equipment types into specific
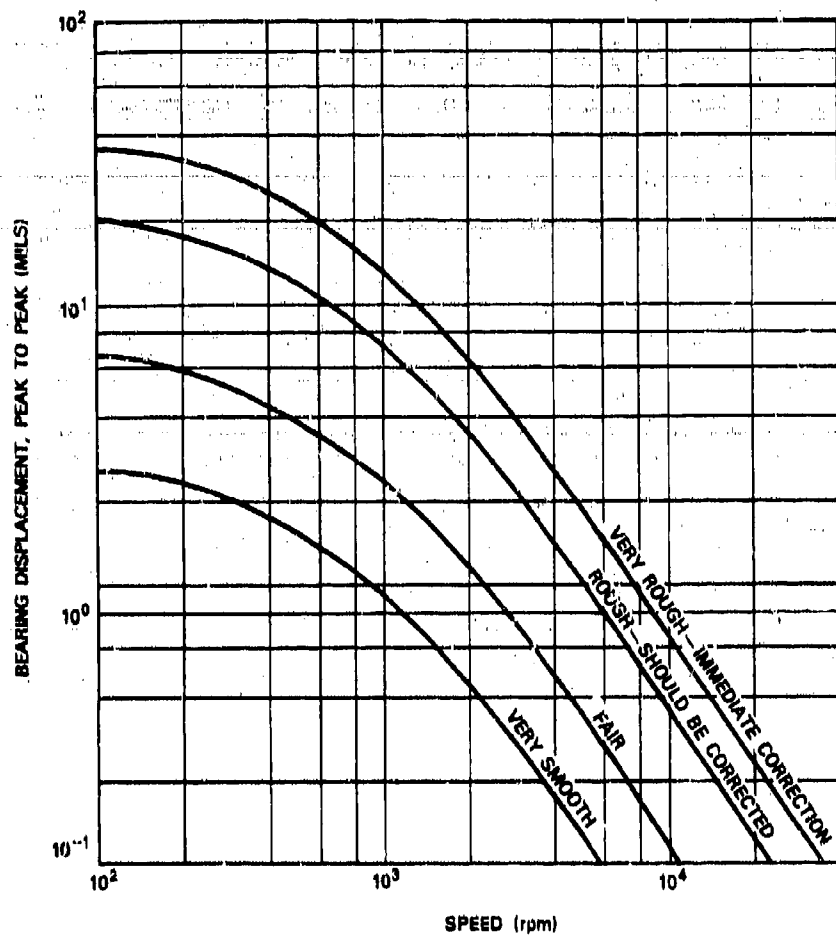
Fig. 4.25. Machinery vibration-tolerance chart constructed by
Rathbone [15]
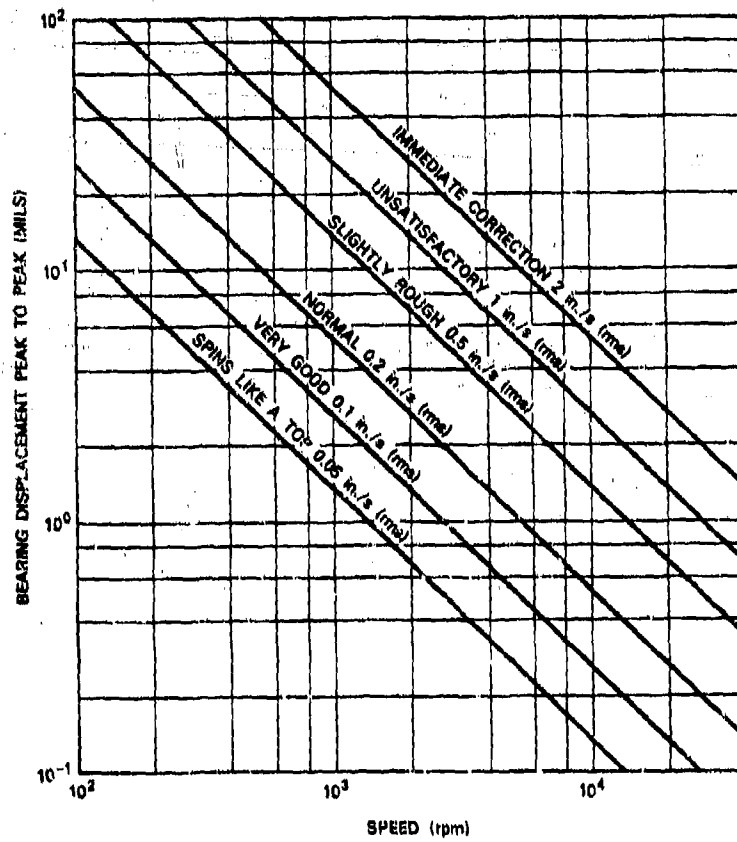
Fig. 4.26. Machinery vibration-tolerance chart constructed by Yates [16]
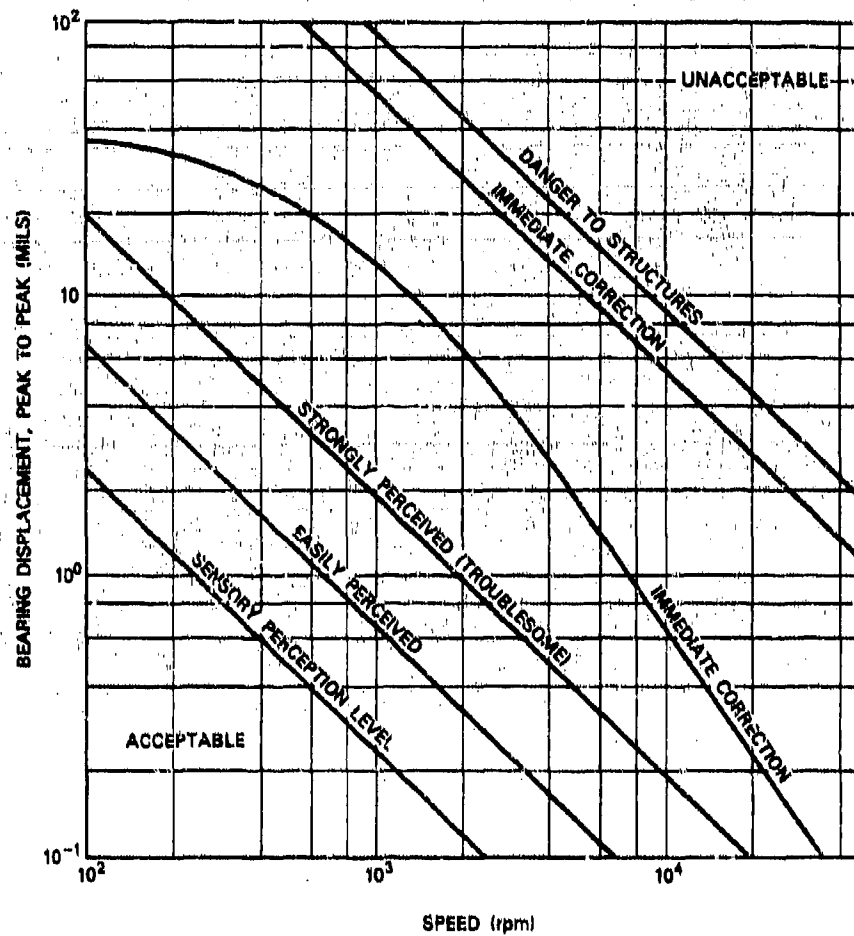
Fig. 4.27. Vibration-tolerance chart—physiological and mechanical.
After Feldman [18].

number grades; for instance, grade G 2.5 groups together the following machine types:

Gas turbines
Steam turbines
Antennas, rotating
Aircraft engines
Aircraft engine, compressor
Aircraft engine, turbine
Electric motor armatures
Centrifuges, rigid
Compressor, centrifugal
Compressor, turbine
Compressor, reciprocating
Compressor wheels
Couplings
Crankshafts, flexible
Crankshafts, rigid
Cutoff wheels
Cutters
Fans and blowers, two-plane
Fan wheels, single-plane
Gears
Grinders, general, precision
Gyro rotors
Magnetic memory drums
Missiles, space vehicles
Propellers, helicopters, aircraft
Paddle wheels
Pulleys, sheaves
Rolls, flexible
Rolls, rigid
Rotating optics
Satellites
Spindles, machine
Shafts, high speed > 10,000 rpm
Shafts, medium speed 1000–10,000 rpm
Shafts, low speed < 1000 rpm
Torque converters
Turbine wheels
Turbines (steam, gas, hydraulic), high speed > 10,000 rpm
Turbines (steam, gas, hydraulic), medium speed 1000–10,000 rpm

Turbines (steam, gas, hydraulic), low < 1000 rpm
Universal joint shafts
Wheels, automotive, aircraft landing
General machine and tool parts
    high speed, 10,000 rpm (bobbins, etc.)
    medium speed, 1000–10,000 rpm (rotary brushes, clutches,
        flywheels, textile flyers, cutters, size reduction equipment,
        air classifier, household motorized appliances, etc.)
    low speed, < 1000 rpm (brake drums, propeller (ship), pump
        refiner, pulverizer, telephoto machine, instrument
        components, recording drives, etc.)
Marine main turbines
Rigid generator rotors
Turbocompressor rotors
Machine tool drives
Medium-size electrical armature rotors
Small electrical armatures
Pump rotors.

The classification is broad, and it should be used with care, since there are exceptions and borderline rotors that do not fit this grouping. It should also be remembered that it is the dynamics of the rotor system (rotor, bearings, pedestal) that determine the overall response to unbalance. For all rigid rotors in any grade, the specific balance requirement for that grade should provide smooth operation. The grade number represents the product of

$$a\omega = (\text{rotor c.g. eccentricity, mm})(\text{speed, rad/s}), \text{mm/s}.$$

Thus a pump rotor that weighs 40 lb and operates at 2000 rpm should be balanced to 2.5 mm/s, or

$$a\omega = 2.5 = a\,\frac{2000}{2.55}\ \text{mm/s} = \frac{2.5}{25.4} = 0.1\ \text{in./s}.$$

The residual c.g. eccentricity is therefore $a = 0.0005$ in. From ISO 1940 Chart 2, at speed 2000 rpm quality grade 2.5 gives a c.g. eccentricity $a = 0.0005$ in., which agrees exactly with the above.

The source of the numerical data from which the criteria charts of ISO 1940 were constructed is a rotor balance survey made by Muster and Flores [19,20]. Responses were obtained from manufacturers representing a very wide variety of machinery, as listed below [19]. These rotor types were also divided into the following rotor weight classes.

less than 0.1 lb	100—300 lb
0.1—0.3 lb	300—1000 lb
0.3—1 lb	1000—3000 lb
1—3 lb	3000—10,000 lb
3—10 lb,	10,000—30,000 lb,

A statistical survey of the levels of acceptable unbalance reported by various manufacturers was made for each rotor class. The mean result for each instance became the level of acceptability for the specified operating speed. The chart shown in Fig. 4.28 was plotted from this data. This figure shows values of acceptable residual unbalance (in. lb/rotor lb) plotted against speed of rotation. For each class of machinery, at each speed level, the *mean* reported acceptable residual unbalance level was taken as the grade level, where $a\omega$ (in millimeters per second) was the grade number, as defined above.

The data obtained in the Muster and Flores survey, and the manner in which the results have been formalized, now constitute the basis of rigid-rotor balance criteria. These data can also be used, as specified in ISO Document 1940-1973(E) [8], as balance criteria for flexible-rotor balancing, where no other values are available. The need for overall, comprehensive, and validated rigid-rotor balancing criteria has been met with the development of ISO Document 1940-1973(E).

MIL-STD-167 (1954)

The military standard document, *Mechanical Vibrations of Shipboard Equipment* [9], is based on the following three formulas for maximum permissible residual unbalance:

Speed range, N (rpm)	Maximum residual unbalance
0 to 150	$U < 0.25\ W$
150 to 1000	$U \leqslant \dfrac{5630\ W}{N^2}$
Above 1000	$U \leqslant \dfrac{4W}{N}$

where N is the speed of rotation in rpm, U is the maximum permissible residual unbalance in the rotor in oz. in., and W is the rotor weight in pounds. Thus, for example, the maximum permissible unbalance for a shipboard generator weighing 220 lb and operating at 2400 rpm is found as follows:
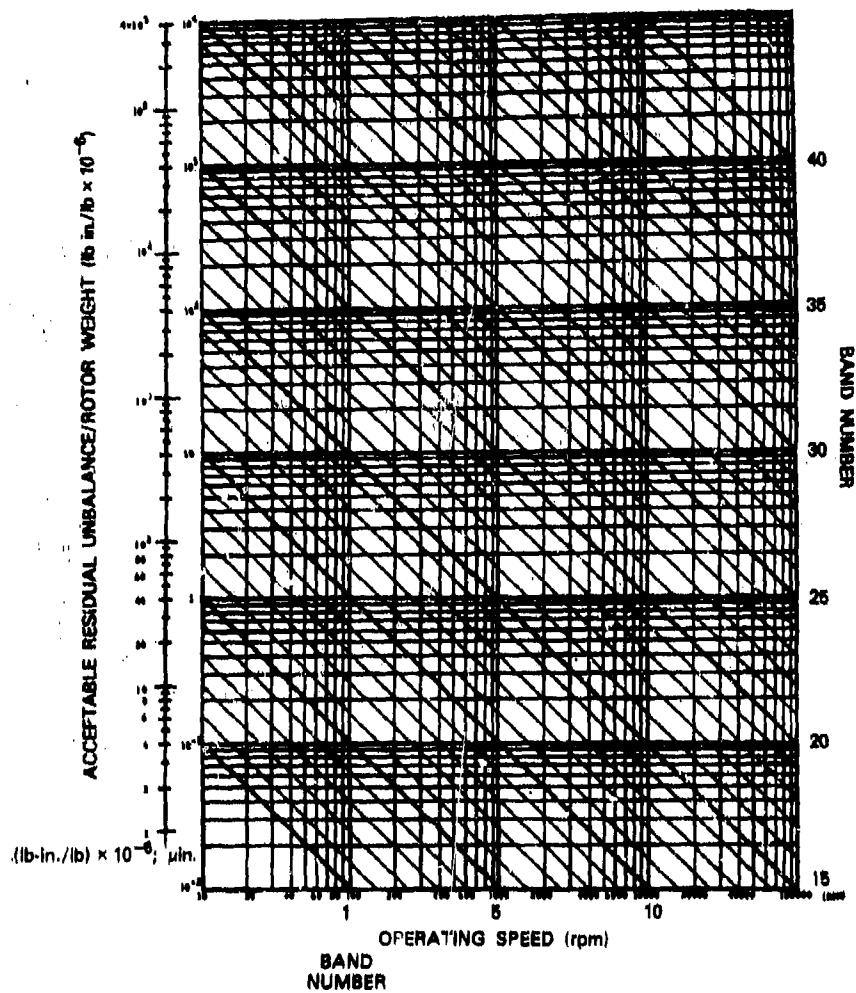
Fig. 4.28. Band classifications for rotor unbalance as a function of speed

$$U \leqslant \frac{4W}{N},$$

$$U = \frac{4 \times 220}{2400} = 0.367 \text{ oz-in.}$$

MIL-STD-167 is a vibration standards document. Besides residual unbalance formulas, it includes the standard for acceptable shipboard machinery vibration levels (Fig. 4.29). In shipboard (and other) machinery, residual unbalance is not the only source of vibration: there are many other potential sources. This fact is recognized by the vibration tolerance chart (Fig. 4.29), in which the maximum vibration criterion corresponds to a maximum peak-to-peak displacement level equal to 10 times ε, the rotor c.g. eccentricity.
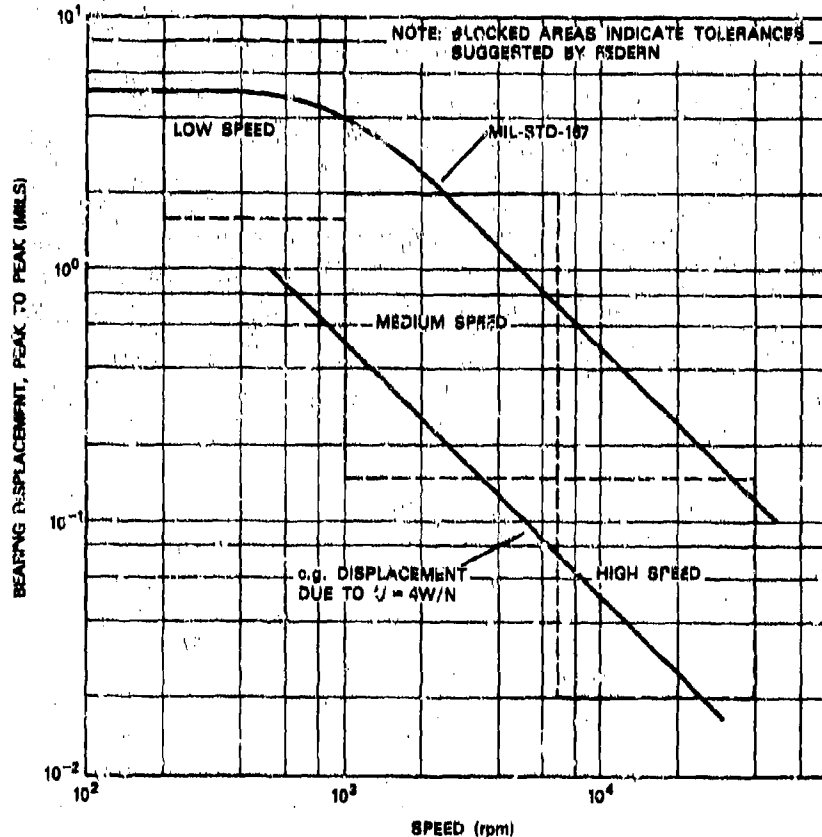
Fig. 4.29. Comparison of vibration criteria by Federn [21] and MIL-STD-167 [9]. After Feldman [18].

An informative review of MIL-STD-167 has been given by Feldman [18], who discussed the selection of unbalance tolerances for rigid rotors in terms of the overall vibration problem of shipboard equipment. Although balancing a rotor can do much to reduce the vibration of rotating machinery, other factors, such as structural resonances of the equipment support system, will also influence the transmitted force (and hence the transmitted noise level). Other sources of excitation occur from the windings of electrical machinery, from fluid-flow effects (e.g., cavitation flow vibration) in pumps, and in forced-draft fans. Each factor also influences the overall vibration level. Feldman [18] has used other published work by Rathbone [15], Yates [16], and Federn [21] to develop guidance charts for the overall vibration levels in shipboard machinery.

NEMA Vibration Criteria

Vibration criteria are available in National Electrical Manufacturers Association (NEMA) standards document [10—12]. These criteria do not apply to maximum residual unbalance values. They are specified in terms of maximum permissible vibration levels. The standards for ac and dc motors [10,11] give tables for recommended peak-to-peak vibration displacement amplitudes, measured at the bearing housing. Permissible vibration levels are specified in terms of unit frame diameter (see Table 4.6). The drive-turbine standards [12] give charts of recommended peak-to-peak amplitude criteria for shaft vibration amplitudes, measured close to the bearing housing. The acceptable level of vibration is related to the speed and weight of the turbine, as shown in Table 4.7.

Table 4.6. NEMA Acceptable limits of vibration for electric motors

Frame diameter series	Peak-to-peak displacement on bearing housing (in.)
180, 200, 210, and 220	0.001
250, 280, and 320	0.0015
360, 400, 440, and 500	0.002

Note: In general, larger frame sizes are associated with motors of higher power rating and/or lower operating speed.

Table 4.7. NEMA Acceptable limits of vibration
for turbines

Rated speed (rpm)	Peak-to-peak displacement on shaft at bearing support (in.)
<4000	0.0030
4001 to 6000	0.0025
>6000	0.0020

Note: Where it is not possible to measure the displacement of
the shaft directly, the peak-to-peak displacement shall not
exceed 50% of the above values.

Neither criteria were chosen for rigid-rotor balancing operations.
The criteria values provide some guidance for deciding whether a given
motor or turbine unit has an acceptable level of residual unbalance,
based on the observed vibration levels. A disadvantage of the support-
vibration test is that the structural dynamic properties of the rotor-
support system are involved in the given criteria values and also in the
measured vibration amplitudes. Measurements taken on the bearing
caps do not provide any measure of unbalance, per se. It appears desir-
able to incorporate the rotor balance criteria of ISO Document 1940-
1973(E) into the NEMA standards to guide electrical rotor balancing,
as unbalance is often a major source of observed vibrations. Electrical
equipment is specifically included in ISO 1940-1973(E) in several rotor
categories. Muster and Flores [19,20] mentioned in their review of the
NEMA standard for the balance of motors [10] that the displacement
measurements quoted were obtained with each unit soft-mounted on a
resilient suspension system. For such arrangements the ratio of operat-
ing speed to natural frequency lay in the range of approximately 5:1.

Other Vibration Criteria

Rathbone [15] and Yates [16] have also published charts of pro-
posed vibration criteria for machinery, based on observations of many
rotating machine systems. Charts given by these authors are shown in
Figs. 4.24 and 4.25. Other data for human perception of vibration were
developed by Reiher and Meister [17] and by Crandell [22]. These data
are shown, together with certain limits from the Rathbone and the
Yates curves, in Fig. 4.26. Further discussion of the above criteria and
charts can be found in Ref. 18.

Several other industrial criteria are used for vibration level assess-
ment, such as the American Petroleum Institute (API) criteria [14] and

the American Gear Manufacturers Association (AGMA) bal ince cri-
teria [13]. These criteria are relatively simple and are confined to lim-
ited types of rigid rotors. Both sets are covered by the rotor categories
included in ISO Document 1940-1973(E). In general, though specific
industry standards may accommodate the vibration requirements for the
rotating machinery of an industry, the guidance provided for rotor
balancing is often minimal and may not reflect the requirements of
modern rotating equipment. ISO Document 1940-1973 is preferred in
such instances because of its broad data base and comprehensive guide-
lines.

4.5 References

1.   M. P. Blake, "Use Phase Measuring to Balance Rotors in Place,"
     Hydrocarbon Proc., Aug. 1967.
2.   D. G. Stadelbauer, "Balance of Fans and Blowers," in *Vibration
     and Acoustic Measurement Handbook*, M. P. Blake, ed., Spartan
     Books, New York, 1973, pp. 337—350.
3.   J. Tonneson, "Further Experiments on Balancing of a High-Speed
     Flexible Rotor," ASME Paper 73-DET-99.
4.   T. Iwatsubo, Y. Murotsu, and F. Watanabe, "Analysis of Measure-
     ment Errors in Balancing of Rotors," in *Proc. Twentieth Japan
     National Congress for Applied Mechanics, Tokyo, Japan* (1970).
5.   J. B. Wilcox, *Dyanmic Balancing of Rotating Machinery*, Pitman &
     Sons Ltd., London, 1967.
6.   C. Jackson, *Two Plane Field Balance Hybrid System—Vectors and
     Orbits, Trim Balance*, Vibration Institute Technology Interchange
     Case History Series, The Vibration Institute, Clarendon Hills,
     1972.
7.   L. E. Barrett, D. F. Li, and E. J. Gunter, "Second Mode Balancing
     Without Phase Measurement Using the Three-Point Method,"
     Department of Mechanical Engineering, University of Virginia,
     Charlottesville, 1978.
8.   International Organization for Standardization, Document ISO
     1940-1973(E), "Balance Quality of Rotating Rigid Bodies."
9.   *Mechanical Vibrations of Shipboard Equipment*, MIL-STD-167-2
     (Ships), Naval Ship Engineering Center, U.S. Navy, May 1974.
10. National Electrical Manufacturer's Association, Standard Docu-
     ment MG 1, par 120.5, Dynamic Balance of Motor, 1978.
11. National Electrical Manufacturer's Association, Standard Docu-
     ment MG 1, par 12.06, Method of Measuring Dynamic Balance,
     1978.

12. National Electrical Manufacturer's Association, Standard Document SM 23, Steam Turbines for Mechanical Drive Service, 1979.

13. American Gear Manufacturers Association, Standard Document 151.01, "Balancing Classification for Flexible Couplings," Jan. 1974.

14. American Petroleum Institute, Turbine Balancing Standard 617; Turbocompressor Standard 813; Non-Contacting Monitoring Systems Standard 670, Oct. 1975; Fan Balancing Standard (proposed draft document).

15. T. C. Rathbone, "Vibration Tolerance," *Power Plant Eng.* 43 (Nov. 1939).

16. H. G. Yates, "Vibration Diagnosis in Marine Geared Turbines," *Trans. North East Coast Inst. Engineers and Shipbuilders* 65(4), 225 (1949).

17. H. Reiher and F. J. Meister, "Die Empfindlichkeit des Menschen gegen Erschutterungen," *Forschung. Geb. Ingenieurw.* 2 (11) (Nov. 1931).

18. S. Feldman, "Unbalance Tolerances and Criteria," in *Proc. Balancing Seminar* IV, Bureau of Ships, Washington D.C., April, 1958, Rpt. 58GL-122.

19. D. Muster and B. Flores, *Balancing Criteria and Their Relationship to Current American Practice*, Technical Report No. 3, NObs-88567, University of Houston, Tex., 1969.

20. D. Muster and B. Flores, "Balancing Criteria and Their Relationship to Current American Practice," *Trans. ASME*, Ser. B, *J. Eng. Ind* 91(4), 1035–1046 (1969).

21. K. Federn, "Unwuchttoleranzen rotierender Korper," *Werkstatt und Betrieb* 86(5) (May 1953).

22. F. J. Crandell, "Ground Vibrations Due to Blasting and Its Effect Upon Structures," *J. Boston Soc. Civil Engr.* (1949).

CHAPTER 5
FLEXIBLE-ROTOR DYNAMICS

Nomenclature

A	cross-sectional area
a	eccentricity of disk c.g. from shaft axis
a_n	major axis radius of whirl ellipse
$[B]$	damping matrix
B_x, B_y	components of bearing radial damping
b_n	minor axis radius of whirl ellipse
C	radial clearance of bearing
D	bearing diameter
E	modulus of elasticity
$\{F\}$	unbalance force vector
G	shear modulus
g	gravitational acceleration
I	second moment of area of shaft cross section
I_{Tn}	discrete translatory inertia at location n
i	$\sqrt{-1}$
J_P	polar inertia per unit length
J_T	transverse inertia per unit length
K	bearing radial stiffness
$[K]$	stiffness matrix
$\overline{K}$	$K/EI\lambda^3$
K_s	shaft radial stiffness
K_x, K_y	components of bearing radial stiffness
$\overline{K}_{xx--}$, $\overline{B}_{xx--}$	dimensionless stiffness and damping coefficients
L	bearing axial length
L	shaft length
M	local bending moment
M	mass of disk
$[M]$	mass matrix
M_n	discrete local mass
n	number of bearing location

243

R	whirl radius vector, $R = X + iY$
r	modal amplitude
U	unbalance, Wa
U_x, U_y	components of local unbalance
V	local shear force
w	specific weight
(X)	rotor displacement vector
x, y	rotor coordinate displacements
z	axial coordinate along rotor
α	cross section shape factor
α_{aa}, α_{ab}	flexibility coefficients
γ_n	angle between x-axis and major axis of ellipse
δ	$(EI/2\alpha GA)^{1/2}$
ζ	B/B_c, where $B_c = 2M\omega_n$, $\omega_n^2 = K/M$
θ, ψ	coordinate slopes corresponding to displacements x, y
λ	$\left\{ \dfrac{\rho A \omega^2}{EI} \right\}^{1/4}$
λ_1	$\lambda \{[(1 + (\delta\lambda))^4]^{1/2} - (\delta\lambda)^2\}^{1/2}$
λ_2	$\lambda \{[(1 + (\delta\lambda))^4]^{1/2} + (\delta\lambda)^2\}^{1/2}$
ν	whirl frequency
ξ	distance between disks on rotor
ξ, η	rotating coordinates in shaft
ρ	mass density (w/g)
(ϕ)	phase angle vector
ψ_n	angle between unbalance force and major axis
ω	rotational frequency
Z_{ij}	$K_{ij} + i\omega B_{ij}$

CHAPTER 5
FLEXIBLE-ROTOR DYNAMICS

5.1 Concepts and Classifications of Flexible Rotors

A flexible rotor is defined as being any rotor that cannot be effectively balanced throughout its speed range by placing suitable correction weights in two separate planes along its length. The operating speed range of such rotors includes or closely approaches at least one critical speed in which transverse bending is a significant cause of the corresponding rotor-system mode shape at that critical speed. The modern concept that distinguishes a flexible rotor from a rigid rotor lies in the nature of the balancing process required to make a given rotor operate satisfactorily throughout its speed range.

The classification of the International Organization for Standardization (ISO) is given in Table 1.2 for flexible-rotor types. Class 2 rotors are divided into a variety of subclasses to relate them more readily to specific industrial applications. All class 3 rotors are classified as flexible, meaning that they must be corrected in more than two planes by some flexible rotor balancing technique. Note that Table 1.2 is rotor-based rather than system-based, and should be used for guidance only. A good estimate of the dynamic properties of a machine can be obtained from a computer calculation of the system, but an absolute definition can be obtained only by testing under operating conditions.

Class 2 rotors are those that cannot be considered rigid but can be balanced for smooth operation with a low-speed balancing machine i.e., by rigid-rotor, two-plane techniques. There are two subcategories of class 2 rotors:

1.. Rotors whose axial distribution of unbalance is known, classes 2A through 2E.

2. Rotors whose axial distribution of unbalance is not known, classes 2F through 2H.

The axial distribution of unbalance is known in the sense that for balancing purposes the unbalance can be considered as concentrated in specific planes—for example, in the disk of the class 2A grinding-wheel rotor. By balancing in one (or preferably two) planes at the disk, the rotor can be balanced for practical operation. The same is true for the grinding wheel and pulley in the class 2B example. In formulating a balancing strategy, the axial unbalance distribution can be likewise surmised for the remaining machine categories 2C through 2E.

It is more difficult to surmise the axial distribution of unbalance for the 5-stage centrifugal pump rotor, class 2F. Even when the impellers appear identical, neither the magnitude of the unbalance nor its

spatial orientation is known. Similar remarks apply to class 2G and class 2H rotors. The class 2H steam-turbine rotor shown is an integral forging, which may carry several thousand attached blades whose weights are measured and are statistically distributed around each stage to minimize the overall unbalance. The blade-weight unbalance vector for each stage is therefore statistical and varies from case to case. The overall rotor unbalance comprises shaft unbalance and the unbalance contributions from each of the blade stages. Low-speed balancing is possible because of the geometry of the rotors shown; in general their mode shapes involve both substantial rigid-body motion (which can be removed by two-plane balancing) and a limited amount of flexure.

The effect of bearings on the dynamics of flexible rotors is shown in Fig. 5.1. Stiffening the bearings will raise the critical speeds; usually only the lowest critical speed is of interest in this class of rotors. Making the bearings more flexible lowers the critical speeds of the rotor system and increases the rigid-body component of the lowest modes. These effects can be seen in a critical speed chart, Fig. 5.2. Thus, where only the lowest mode of the rotor system is of practical interest, a two-plane balance will often be adequate. The dynamic properties of all rotor systems should be calculated before construction to ensure that the most suitable modes and critical speed location are selected to make the balancing operation most effective.

Class 3 rotors are fully flexible rotors requiring high-speed balancing; a large generator rotor is a typical example. During operation a large 3600-rpm generator rotor may encounter critical speeds in the region of 700 through 2300 rpm, and its operation may also be influenced by higher critical speed effects occurring around 4200 rpm. Operation between the second and third critical speeds requires more complex balancing procedures than the relatively simple two-plane technique discussed previously. The reasons for this complexity and methods for balancing class 3 rotors are discussed in Chapter 6.

Class 4 rotors carry flexible attachments such as blades. They can be prebalanced by a technique related to their basic rotor class and then trim balanced, if needed, by a suitable flexible-rotor technique. Class 5 rotors are essentially class 3 rotors that are balanced to provide smooth operation at a single speed only. This speed is commonly the operating speed, but to achieve smooth operation it may be be necessary to balance out a flexible critical speed within the operating range. An example of a class 5 rotor is a 400-Hz motor that has a critical speed of about 17,600 rpm (Table 1.3). Response amplitudes at the bearings before and after three-plane balancing are shown in Fig. 5.3. This rotor was balanced while operating near its first (bending) critical speed, to provide smooth operation at its design speed.

Mode 1 Mode 2 Mode 3

(a) Rigid rotor in flexible bearings

(b) Stiff rotor in flexible bearings (minor bending in first two modes)

(c) Flexible rotor in flexible bearings (substantial bending in first two modes)

(d) Flexible rotor in rigid bearings (no rigid-body modes)
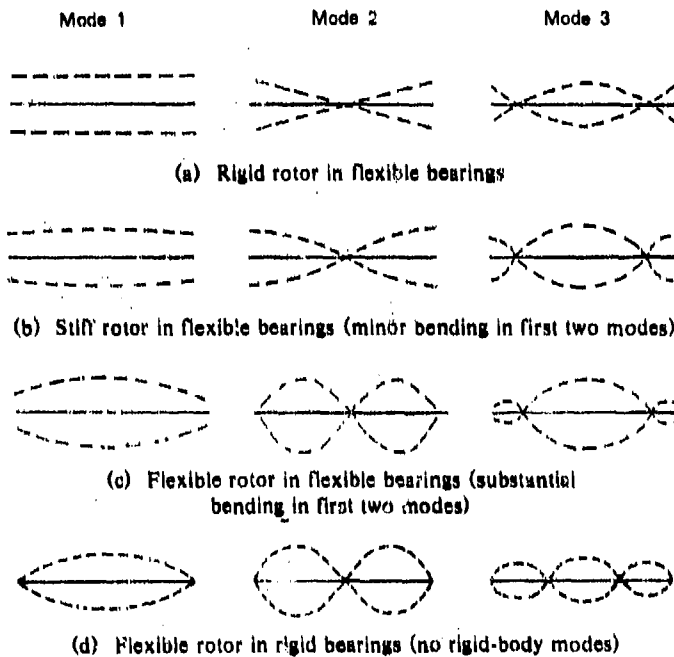
Fig. 5.1. Influence of bearing stiffness on flexible rotor modes
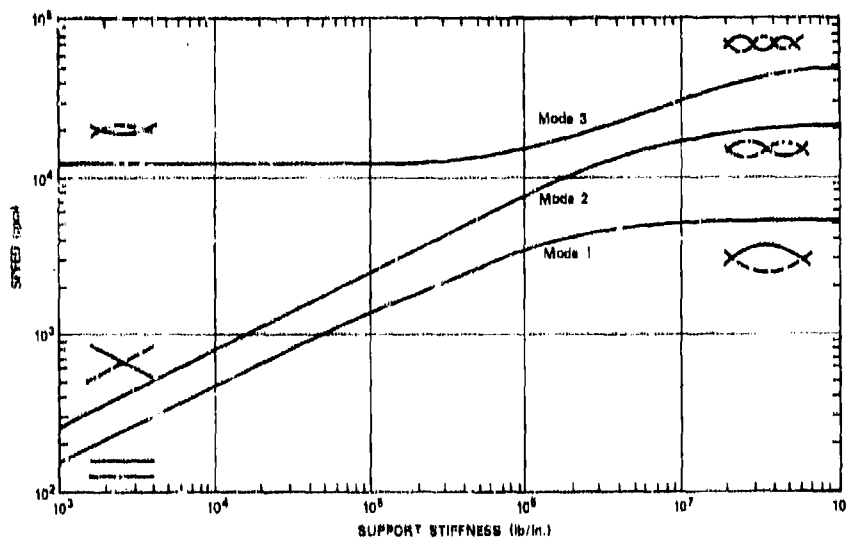
Fig. 5.2. Chart of critical speeds for uniform elastic rotor
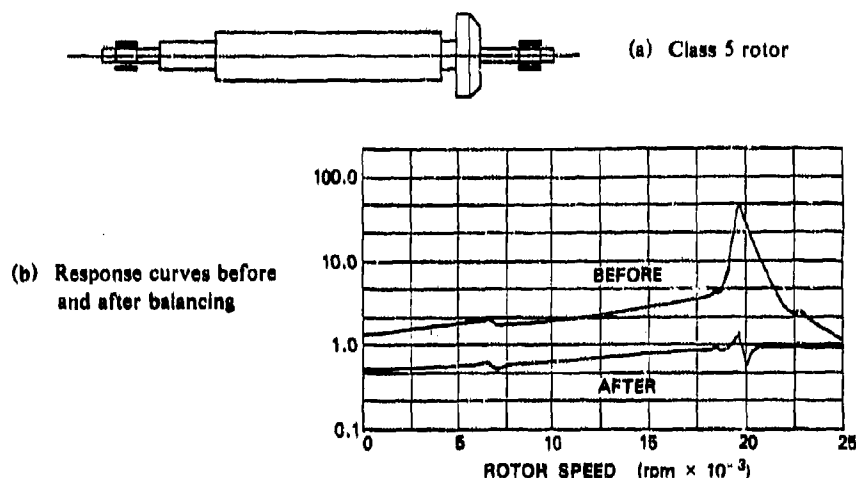
Fig. 5.3. Class 5, 400-Hz motor and response curves

The ISO rotor classification in Table 1.2 can be used to assign the type of balancing that will probably be required. A rotor-response study will usually be made during the rotor design process to define the dynamic characteristics of the machine system more exactly and to optimize these characteristics for low sensitivity to unbalance throughout the operating-speed range.

The following examples demonstrate the application of these principles:

Example 1

A 400-lb armature rotor is required to drive a shipboard fan unit at 2500 rpm. After balancing, the maximum whirl amplitude at either bearing is to be 0.002 in. peak-to-peak. The lowest critical speed of the rotor in its bearings is calculated to be 3500 rpm.

The rotor was two-plane balanced to 0.5 oz-in. in both correction planes in a low-speed balancing machine. When installed, it operated satisfactorily at all speeds within its range.

For a second application, the same fan unit was required to operate at speeds up to 3350 rpm. The armature was first low-speed balanced in its two end planes to 0.1 oz-in. On installation in the fan unit, it again met the required whirl amplitude criterion of 0.002 in. peak-to-peak at all speeds within the extended speed range. The armature mode shape consisted mainly of bearing displacements and some small flexing of the rotor at the higher operating speed (see Fig. 5.4).

(a) Rotor assembly
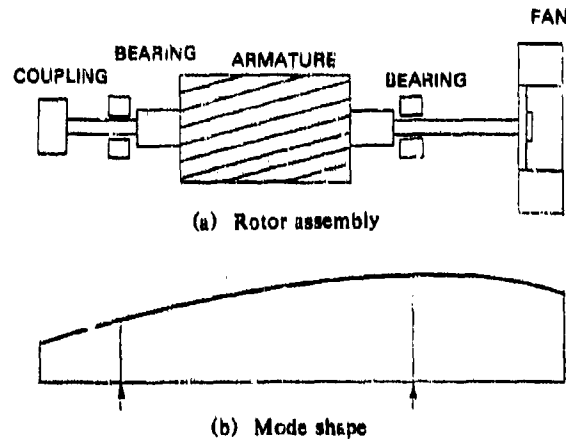
(b) Mode shape

Fig. 5.4. Armature and fan rotor with whirl-mode shape
in first mode

This armature is evidently a class 2 flexible rotor. As shown in
Fig. 5.5, ISO Document 1940-1973(E), the rotor quality class is G6.3,
and it can have a residual c.g. eccentricity of 10^{-3} in (6.4 oz-in.) at
2500 rpm, and 0.6×10^{-3} in (4.0 oz-in.) for operation at 3350 rpm.
Both balance criteria exceed the balance conditions indicated above.
Although the rotor exhibited some small flexural displacements at the
higher operating speed, it was still possible to achieve satisfactory
operation by balancing in two correction planes.

Example 2

An 800-lb centrifugal gas-compressor rotor operates at 10,500 rpm.
It was observed to pass through a first critical speed at 7720 rpm. The
maximum allowable journal whirl amplitude was 0.001-in. peak-to-peak
when passing through the critical speed and at the operating speed.

It was found that a satisfactory balance could be achieved in two
ways: (a) by balancing in three planes using data taken at 7500 and
10,000 rpm, (b) by rigid-body balancing all rotor components, and
finally trim balancing in two end planes at about 7000 rpm.

This rotor is actually a class 3 flexible rotor that requires flexible
or multiplane balancing for smooth operation. The first method pro-
vides the required balancing procedure directly, whereas the second
method removes all gross low-speed residual unbalance effects plane by
plane. The trim balance made near the critical speed in two planes,
when the amplitudes of the flexible whirl mode shape can be measured
and compensated for, directly confirms its class 3 classification. A class

Acceptable Residual Unbalance per Unit of Rotor Mass in $\frac{lb\text{-}in}{lb}$ or Center of Gravity Displacement e (in)

Maximum Service Speed of Rotation
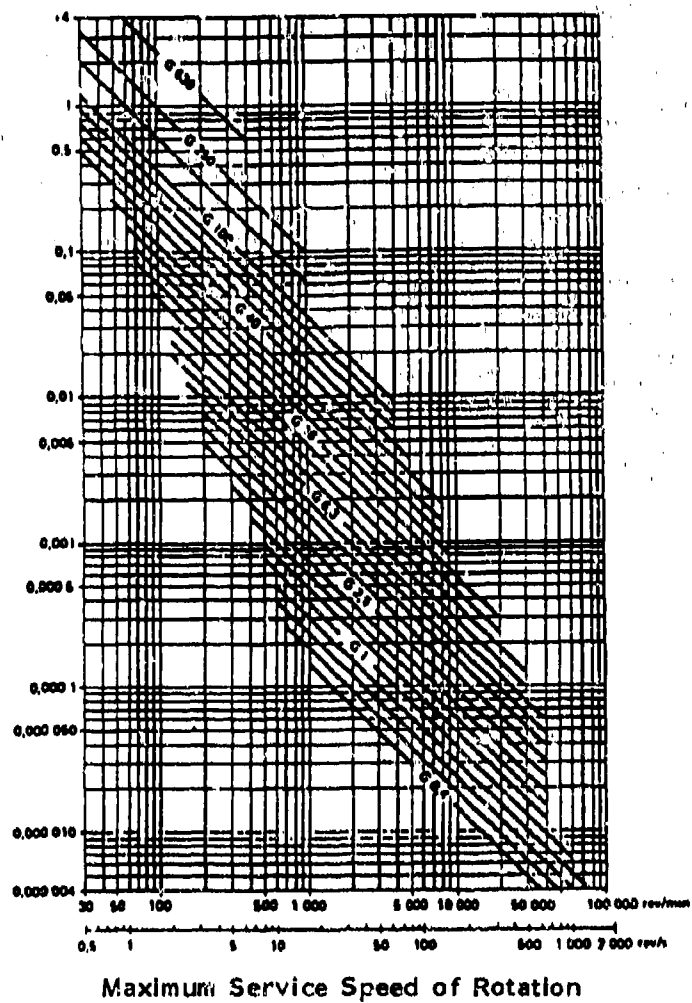
Fig. 5.5. Acceptable residual unbalance for various rotor grades. (From ISO Standard 1940-1973 (E) used by permission from ISO.)

2 rotor can be balanced in a rigid-rotor balancing machine, whereas a class 3 rotor requires more sophisticated balancing techniques (see Chapter 6). An effort should be made during design to make every rotor a class 2 rotor. This will simplify the initial balancing process by allowing a two-plane balance in a low-speed machine. It will also make subsequent field balancing easier by requiring corrections in two planes only. For rotors that clearly belong in class 3, this fact should be recognized early in the design process.

The modern tendency is to provide rotor midspan balance planes along with easy-access ports through the machine casing. Field balancing of such rotors is much simpler, and the need to remove the rotor from its casing for balancing is less likely to arise.

5.2 Dynamic Properties of Flexible-Rotor Systems

Flexible-rotor systems have critical speeds and characteristic mode shapes in the same manner as described for rigid-rotor systems. Flexible-rotor mode shapes tend to be more complex, though the underlying modal principles are identical in both cases. The important dynamic properties of flexible-rotor systems are given in Table 5.1. The interrelations among these factors are indicated in Fig. 5.6.

The matrix equation of motion for any rotor—bearing-foundation system acted on by any force vector can be written as

$$[M]\{\ddot{x}\} + [B]\{\dot{x}\} + [K]\{x\} = \{F\},$$

where

$$
\begin{array}{ll}
[M] & = \text{mass matrix for the system} \\
[B] & = \text{damping matrix} \\
[K] & = \text{stiffness matrix} \\
\{x\}, \{\dot{x}\}, \{\ddot{x}\} & = \text{harmonic displacement, velocity,} \\
& \quad\text{and acceleration vectors, respectively} \\
\{F\} & = \text{force vector.}
\end{array}
$$

The above interrelationship arises through the system dynamic equation as follows:

Undamped critical speed

$$[M]\{\ddot{x}\} + [K]\{x\} = 0.$$

The undamped critical speed equation arises from the omission of damping and forcing terms in the system equation. The roots ω_c of this
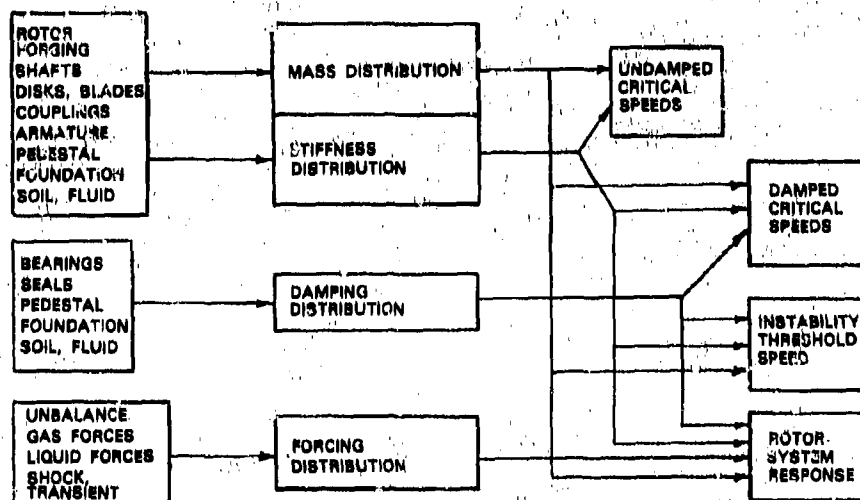
Fig. 5.6. Factors influencing rotor system properties and their
relation to rotor dynamics calculations

Table 5.1 Important dynamic properties of flexible-rotor systems

System property	Reason for importance
Critical speed	Defines speeds at which potentially large amplitudes may develop
Mode shape	Gives rotor amplitude distribution along length at a critical speed; indicates potentially large strain regions and rotor sensitivity in correction-plane locations
Unbalance response	Indicates effective system response at specified locations to given unbalance distribution, including the effect of bearing/support damping
Transmitted force	Defines the magnitude of the transmitted forces, incorporating the influence of system dynamics, damping (especially at bearings), and unbalance magnitude and direction
Stability threshold	Defines the speed at which the rotor may become unstable in its bearings and tend to whirl in an increasing orbit unless otherwise restrained

expression give the undamped natural frequencies $\omega_{o,i}$, $i = 1, 2, \ldots$ of the rotor system. The vector $\{x_i\}$ give the corresponding mode shape.

Damped critical speed

$$[M]\{\ddot{x}\} + [B]\{\dot{x}\} + [K]\{x\} = 0.$$

When the damping force terms are retained, the damped roots $\omega_{d,i} = \alpha_i \pm i\nu_i$ contain both damping (α_i) and frequency (ν_i) terms for each mode solution for the damped response $\{x\}$ to initial time boundary conditions may be obtained for a specific time interval.

Forced response amplitude

$$[M]\{\ddot{x}\} + [B]\{\dot{x}\} + [K]\{x\} = \{F(t)\}.$$

The damped system response to specified forcing inputs including synchronous forcing from unbalance is obtained by solving the complete system matrix equation. For unbalance forcing this solution is obtained at specified rotational speed values.

Transmitted force

$$\{F_n\} = [B_n]\{\dot{x}_n\} + [K_n]\{x_n\}, \qquad (n\text{th bearing}).$$

The force transmitted at any bearing location n can be determined using the force matrix equation. Both real (F_n^r in-phase) and imaginary (F_n^i quadrature) force components are obtained and combined to give the magnitude and phase of the transmitted-force responses,

$$F_n = F_n^r + iF_n^i, \qquad (i = \sqrt{-1}),$$

$$F_n = [(F_n^r)^2 + (F_n^i)^2]^{1/2},$$

and

$$\phi_n = \arctan \frac{F_n^i}{F_n^r}.$$

Stability threshold speed

$$[M]\{\ddot{x}(\omega)\} + [B(\nu)]\{\dot{x}(\omega)\} + [K(\nu)]\{x(\omega)\} = 0.$$

Solving the modified system equation for its lowest root, where both damping and stiffness are functions of the nonsynchronous whirl frequency ν, gives the stability threshold speed ω_s at which the rotor will begin unstable whirling with frequency ν.

The matrix equations presented above can be solved for constant coefficient values, though in practice the damping matrix and the

stiffness matrix may vary with frequency, amplitude of vibration, and other factors. In particular, the bearing coefficients may vary non-linearly with amplitude and frequency. The matrix equation can be solved point by point with constant coefficients over specified ranges of speed for amplitude or natural frequency values. Where the coefficients are nonlinear, special techniques involving time-step integration are required [1–3].

Several methods are available for the dynamic analysis of rotor systems. The Myklestad-Prohl iterative method has been extensively developed by Lund [4–6] and others for critical speeds, unbalance response, and stability analysis. Matrix analysis of rotor systems has been developed by Morton [7,8], Ruhl and Booker [9], and Thomas [10]. Matrix rotor-analysis techniques have not been widely used, probably because of the highly developed state of the iterative method and because of the inconvenience of the large coefficient matrices, which are commonly asymmetrical due to differing bearing coefficients in the coordinate directions.

5.3 Simple System Models Used for Rotor-System Analysis

Considerable insight into system response can be obtained with relatively simple analytical models. Such models are based on prior knowledge (or assumption) of the system response modes. For example, the lowest critical speed and unbalance response of a flexible rotor in rigid bearings (Fig. 5.7a) can easily be estimated by representing the rotor as a point mass on a massless beam, supported as shown in Fig. 5.7b. If the correct proportion of the rotor mass required at midspan for this case is not known in advance, a greater number (two or three) of masses can be used, as in Fig. 5.7c, and an influence coefficient matrix technique can be used (see below) to avoid matrix inversion problems when solving for the lowest root. Rotor–bearing systems may be analyzed in a similar manner. Several examples of rotor system analysis using simple models will now be given.

Symmetrical Single-Mass Rotor in Undamped Bearings

The system shown in Fig. 5.8 is symmetrical about midspan, and the bearings have identical properties in the x- and y-directions. Shaft stiffness K_1 is identical in all transverse directions. The equations of motion for the disk c.g. are:

$$\frac{1}{2} M \ddot{x}_1 + K_1(x_1 - x_2) = \frac{1}{2} M a \omega^2 \cos \omega t$$

$$\frac{1}{2} M \ddot{y}_1 + K_1(y_1 - y_2) = \frac{1}{2} M a \omega^2 \sin \omega t.$$
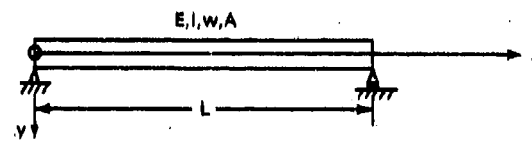
(a) Uniform rotor in rigid
bearings
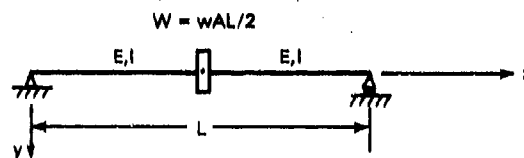
(b) Representation of rotor for
first mode analysis
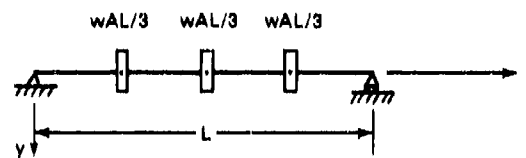
(c) Representation of rotor for
first three mode analysis

Fig. 5.7. Point-mass and massless-beam representations of rotor
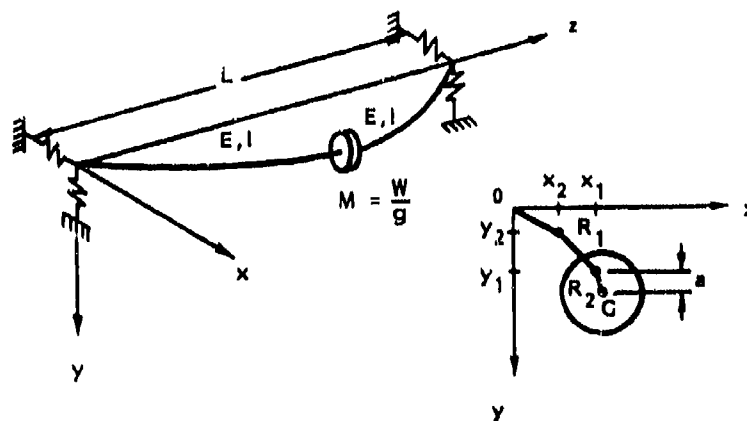
Fig. 5.8. Single-disk, flexible rotor in undamped flexible bearings:
E = Elastic axis of shaft at disk, G = c.g. of disk

Bearing force equilibrium gives:

$$F_x = K_2 x_2 = K_1(x_1 - x_2); \qquad x_2 = \frac{K_1}{K_1 + K_2} x_1$$

$$F_y = K_2 y_2 = K_1(y_1 - y_2); \qquad y_2 = \frac{K_1}{K_1 + K_2} y_1.$$

Combining the above expressions gives:

$$\frac{1}{2} M \ddot{R}_1 + K_0 R_1 = \frac{1}{2} M a \omega^2 e^{i\omega t},$$

where

$$R_1 = x_1 + i y_1$$

$$R_2 = x_2 + i y_2$$

$$K_0 = \frac{K_1 K_2}{K_1 + K_2}.$$

For harmonic motions,

$$R_1 = r_1 e^{i\omega t}, \qquad R_2 = r_2 e^{i\omega t}.$$

Substituting leads to the c.g. whirl radius response solutions,

$$r_1 = \frac{\frac{1}{2} M a \omega^2}{K_0 - \frac{1}{2} M \omega^2}, \qquad r_2 = \frac{K_1}{K_1 + K_2} \frac{\frac{1}{2} M a \omega^2}{K_0 - \frac{1}{2} M \omega^2}.$$

In dimensionless form,

$$r_1^* = \left(\frac{r_1}{a}\right) = \frac{\left(\frac{\omega}{\omega_c}\right)^2}{1 - \left(\frac{\omega}{\omega_c}\right)^2}, \qquad \omega_c^2 = \frac{2K_0}{M} \text{ at mass c.g.}$$

$$r_2^* = \left(\frac{r_2}{a}\right) = \frac{K_1}{K_1 + K_2} \frac{\left(\frac{\omega}{\omega_c}\right)^2}{1 - \left(\frac{\omega}{\omega_c}\right)^2}, \text{ at journal}$$

The transmitted force is

$$F_x = K_2 x_2, \quad F_y = K_2 y_2, \quad \text{i.e.,} \quad F = K_2 R_2$$

and

$$F = \frac{K_1 K_2}{K_1 + K_2} \cdot \frac{\frac{1}{2} M a \omega^2}{K_0 - \frac{1}{2} M \omega^2}$$

$$= K_0 \frac{\frac{1}{2} M a \omega^2}{K_0 - \frac{1}{2} M \omega^2}.$$

In dimensionless form,

$$F^* = \left(\frac{F}{\frac{1}{2} M a \omega^2} \right) = \frac{1}{1 - (\omega/\omega_c)^2} = \frac{1}{1 - r^2}, \quad r = (\omega/\omega_c).$$

Example: A 400-lb single-disk rotor has a bending stiffness of 10^5 lb/in. It is supported in identical end bearings, each having a stiffness of 3×10^5 lb/in. If the disk has a c.g. eccentricity of 0.005 in., find the journal response and the transmitted force (a) at 3000 rpm and (b) up to a speed of 10,000 rpm.

Solve the problem in dimensionless form. The stiffness K_0 is

$$K_0 = \frac{K_1 K_2}{K_1 + K_2} = \frac{(10^5)(6 \times 10^5)}{(7 \times 10^5)} = 0.857 \times 10^5 \text{ lb/in.}$$

The system critical speed is

$$\omega_c = \left(\frac{2K}{M} \right)^{1/2} = \left(\frac{2(0.857)(10^5)(386.4)}{400} \right)^{1/2} = 406.9 \text{ rad/s.}$$

$$N_c = 9.55 \omega_c = 3886.0 \text{ rpm.}$$

The c.g. whirl radius at 3000 rpm is

$$\frac{\omega}{\omega_c} = \frac{N}{3886} = \frac{3000}{3886} = 0.772$$

$$\left(\frac{\omega}{\omega_c} \right)^2 = 0.596$$

$$r_1^* = \frac{\left(\dfrac{\omega}{\omega_c}\right)^2}{1 - \left(\dfrac{\omega}{\omega_c}\right)^2} = \frac{0.596}{1 - 0.596} = 1.475$$

$$r_1 = ar_1^* = (0.005)\ (1.475) = 0.00738 \text{ in.}$$

$$r_2^* = \frac{K_1}{K_1 + K_2}\ \frac{\left(\dfrac{\omega}{\omega_c}\right)^2}{1 - \left(\dfrac{\omega}{\omega_c}\right)^2}$$

$$= \frac{K_1}{K_1 + K_2}\ r_1^* = \frac{1}{7}\ (1.475) = 0.2107$$

$$r_2 = r_2^* a = (0.2107)\ (0.005) = 0.00105 \text{ in.}$$

Bearing transmitted force is

$$F^* = \frac{F}{\frac{1}{2} M a \omega^2} = \frac{1}{1 - \left(\dfrac{\omega}{\omega_c}\right)^2} = 2.475$$

$$F = (\tfrac{1}{2} M a \omega^2) F^*$$

$$= \left(\frac{200}{386.4}\right) (0.005) \left(\frac{3000}{9.55}\right)^2 (2.475) = 632.2 \text{ lb.}$$

Transmitted force per bearing = 316.1 lb

The undamped response curve for c.g. whirl radius, journal whirl radius, and bearing transmitted force is shown in Fig. 5.9.

Symmetrical Two-Mass Rotor in Undamped Bearings

Warner and Thoman [11] gave the rotor c.g. equations for the case shown in Fig. 5.10 in the following form:

$$\frac{1}{2} M \ddot{x}_1 + \frac{1}{\alpha} (x_1 - \xi x_2) = \frac{1}{2} M a \omega^2 \cos \omega t$$
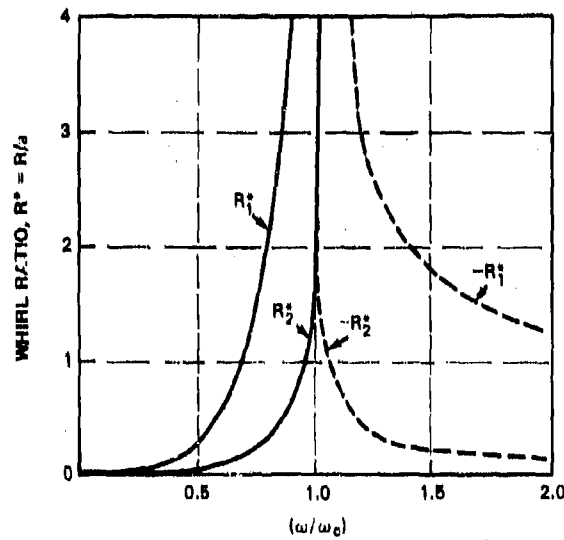
(a) C.g. and journal whirl radius vs frequency ratio
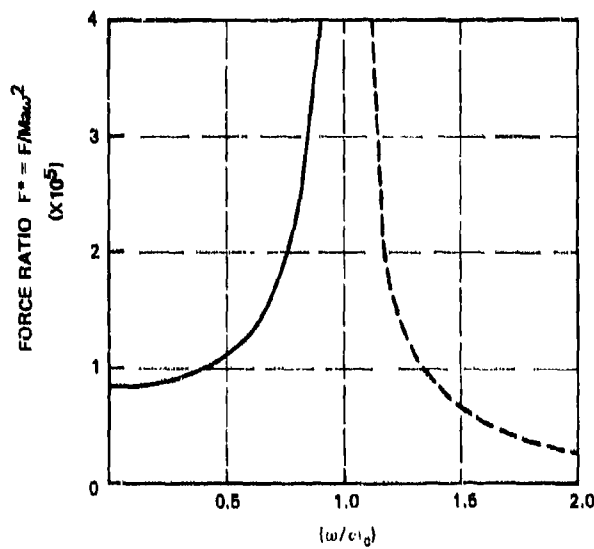
(b) Dimensionless transmitted force vs whirl frequency ratio

Fig. 5.9. Variation of amplitude and transmitted force with
rotor speed for single-mass rotor in undamped bearings

(a) Rotor system proportions

(b) First whirl-mode shape and unbalance excitation

(c) Second whirl-mode shape and unbalance excitation
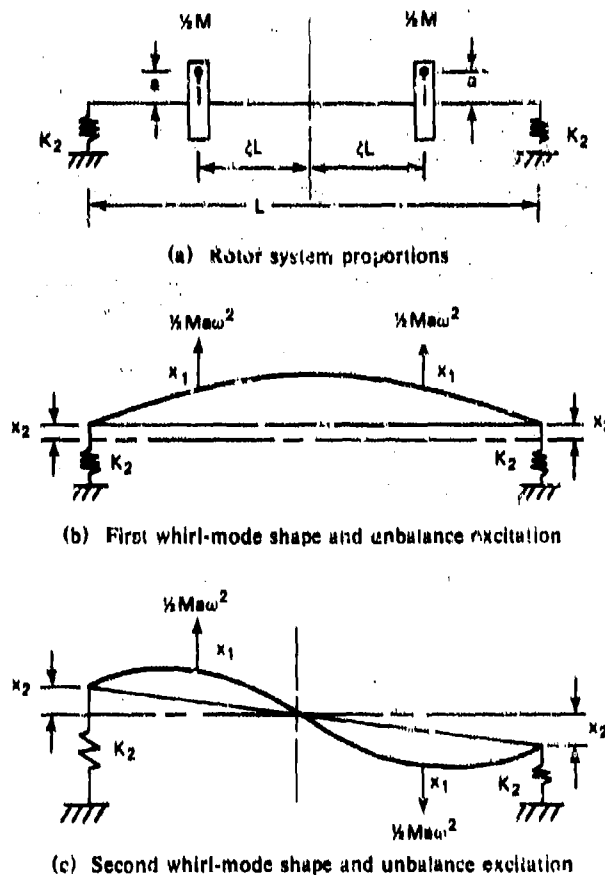
Fig. 5.10. Two-mass, flexible rotor in undamped flexible bearings

and

$$\frac{1}{2} M \ddot{y}_1 + \frac{1}{\alpha}(y_1 - \xi y_2) = \frac{1}{2} M a \omega^2 \sin \omega t,$$

in which M is the mass of each rotor disk, ξ is the distance between the disks, and α is the disk influence coefficient defined by:

First mode: $(x_1 - x_2) = F_{ax}\alpha_{aa} + F_{bx}\alpha_{ab}$

$(y_1 - y_2) = F_{ay}\alpha_{aa} + F_{by}\alpha_{ab}$

Second mode: $x_1 - \xi x_2 = F_{ax}\alpha_{aa} - F_{bx}\alpha_{ab}$

$$y_1 - \xi y_2 = F_{ay}\alpha_{aa} - F_{by}\alpha_{ab}.$$

Introducing the conventions

Mode	ξ	α
First	1	$\alpha_{aa} + \alpha_{ab}$
Second	ξ	$\alpha_{aa} - \alpha_{ab}$

allows the above expressions to be written as

$$x_1 - \xi x_2 = F_x\alpha$$

and

$$y_1 - \xi y_2 = F_y\alpha.$$

The bearing force balance is

$$\frac{1}{\alpha}(x_1 - \xi x_2) = K_2 x_2, \qquad x_1 = (\xi + \alpha K_2)x_2$$

and

$$\frac{1}{\alpha}(y_1 - \xi y_2) = K_2 y_2, \qquad y_1 = (\xi + \alpha K_2)y_2.$$

Solving gives the whirl radius at the journal as

$$r_2 = x_2 + i y_2 = \frac{(a/\alpha)(\omega/\omega_n)^2}{K_2[1 - (\omega/\omega_n)^2] - (\omega/\omega_n)^2\xi/\alpha},$$

and at the disk c.g.,

$$r_1 = x_1 + i y_1 = \frac{(\xi + \alpha K_2)(a/\alpha)(\omega/\omega_n)^2}{K_2[1 - (\omega/\omega_n)^2] - (\omega/\omega_n)^2(\xi/\alpha)}$$

where $\omega_n^2 = (2/M\alpha)$ and $i = \sqrt{-1}$. In dimensionless form these equations can be written as

$$r_2^* = \frac{r_2}{a} = \frac{(\omega/\omega_n)^2}{\alpha K_2[1 - (\omega/\omega_n)^2] - \xi(\omega/\omega_n)^2}$$

and

$$r_1^* = \frac{r_1}{a} = \frac{(\xi + \alpha K_2)(\omega/\omega_n)^2}{\alpha K_2[1 - (\omega/\omega_n)^2] - \xi(\omega/\omega_n)^2}.$$

The bearing transmitted force is

$$F = K_2 r_2 = \frac{K_2(a/\alpha)(\omega/\omega_n)^2}{K_2[1 - (\omega/\omega_n)^2] - (\omega/\omega_n)^2(\xi/\alpha)}$$

and the dimensionless transmitted force is

$$F^* = \frac{2F}{\frac{1}{2}Ma\omega^2} = \left\{\left[1 - \left(\frac{\omega}{\omega_n}\right)^2\right]^2 + \left(\frac{\omega}{\omega_n}\right)^2 \frac{\xi}{\alpha K_2}\right\}^{-1}.$$

Whirl Modes of Uniform Rotor in Undamped Flexible Bearings

The rotor modes for the system shown in Fig. 5.11 can be represented by the general modal equation

$$r = A \cos \lambda z + B \sin \lambda z + C \cosh \lambda z + D \sinh \lambda z,$$

where r is the whirl radius, A, B, C, and D are constants of integration, and λ is $(\rho A \omega^2/EI)^{1/4}$.

(a) Uniform cylindrical rotor in flexible end bearings

(b) Mode 1

(c) Mode 2
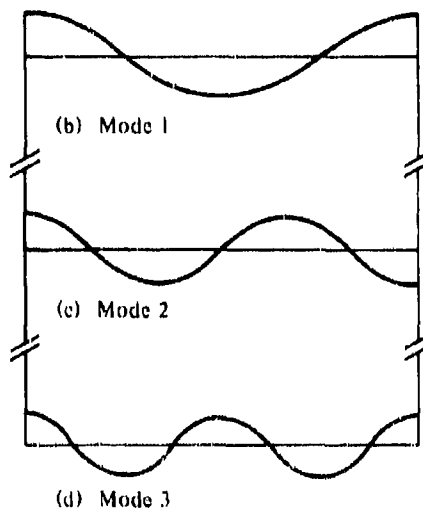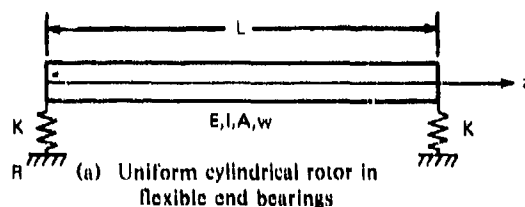
(d) Mode 3

Fig. 5.11. (a) Uniform rotor in undamped flexible bearings. (b) – (d) Mode shapes

The integration constants can be determined from the boundary conditions, which are:

For $z = 0$,

$$\frac{d^2 r}{dz^2} = 0 \quad \text{(zero end moment)}$$

and

$$Ky = EI \frac{d^3 r}{dz^3} \quad \text{(force equilibrium)};$$

For $z = L$,

$$\frac{d^2 r}{dz^2} = 0 \quad \text{(zero end moment)}$$

and

$$-Ky = EI \frac{d^3 r}{dz^3} \quad \text{(force equilibrium)}.$$

Substituting gives

$$-A + C = 0,$$

$$2\bar{K}A - B + D = 0,$$

$$-A(\cos \lambda L + \cosh \lambda L) - B \sin \lambda L + D \sinh \lambda L = 0,$$

$$B[\bar{K}(\cos \lambda L + \cosh \lambda L) - 2\bar{K}^2 \sin \lambda L + (\sin \lambda L - \sinh \lambda L)$$
$$+ 2\bar{K} \cos \lambda L]$$
$$-D[\bar{K}(\cos \lambda L + \cosh \lambda L) + 2\bar{K}^2 \sinh \lambda L + (\sin \lambda L - \sinh \lambda L)$$
$$+ 2\bar{K} \cosh \lambda L] = 0,$$

where

$$\bar{K} = \frac{K}{EI\lambda^3} = \frac{KL^3}{EI} \cdot \frac{1}{(\lambda L)^3}$$

is the dimensionless stiffness. Simplifying gives the frequency equation

$$(\cos \lambda L \cosh \lambda L - 1) - 2\bar{K}(\cos \lambda L \sinh \lambda L - \sin \lambda L \cosh \lambda L)$$

$$- 2\bar{K}^2 \sin \lambda L \sinh \lambda L = 0.$$

This expression reduces to the well-known frequency equations corresponding to the limiting cases $K = \infty$ (pinned-pinned) and $K = 0$ (free-free).

The mode shapes depend on the dimensionless stiffness $\overline{K}$, which is frequency dependent through the λ-term. The normalized modal displacements J_i for the i th mode are given by

$$J_i = \cos \lambda_i x_i + \cosh \lambda_i x_i - 2\overline{K} \sinh \lambda_i x_i + \alpha_i(\sin \lambda_i x_i + \sinh \lambda_i x_i),$$

where

$$\alpha_i = \frac{(\cos \lambda L - \cosh \lambda L + 2\overline{K} \sinh \lambda L)_i}{(\sin \lambda L - \sinh \lambda L)_i}, \quad i = 1, 2, \ldots.$$

Typical mode shapes are shown in Fig. 5.11.

Whirl Modes of a Rotor with Overhung Couplings in Undamped Flexible Bearings

Consider the rotor system shown in Fig. 5.12a, which consists of a flexible three-mass rotor, such as an auxiliary drive turbine in a compressor train with overhung couplings. The rotor operates in flexible undamped bearings with isotropic radial stiffness properties.

The system equivalent dynamical model is given an assumed displacement such that $R_1 > R_2 > \ldots > R_5$ and $\theta_1 > \theta_2 > \ldots > \theta_5$. The K_{i1} coefficients are the bending elastic coefficients; the K_{i2} coefficients are the slope elastic coefficients for the shaft sections. Neglecting the slope elasticity simplifies the model and the equations of motion. The equations of motion for this case are

$$M_1 \ddot{R}_1 + K_1 R_1 - K_1 R_2 = 0,$$

$$- K_1 R_1 + (K_1 + K_2 + K_3)R_2 - K_3 R_3 = 0,$$

$$M_3 \ddot{R}_3 - K_3 R_2 + (K_3 + K_4)R_3 - K_4 R_4 = 0,$$

$$- K_4 R_3 + (K_4 + K_5 + K_6)R_4 - K_6 R_5 = 0,$$

and

$$M_5 \ddot{R}_5 - K_6 R_4 + K_6 R_5 = 0.$$
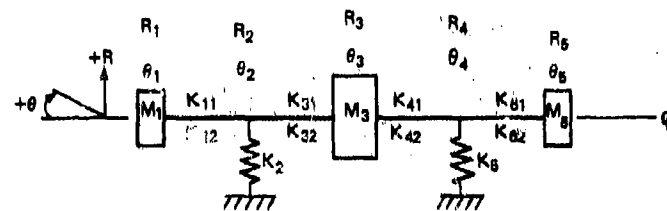
(a) Equivalent dynamical model
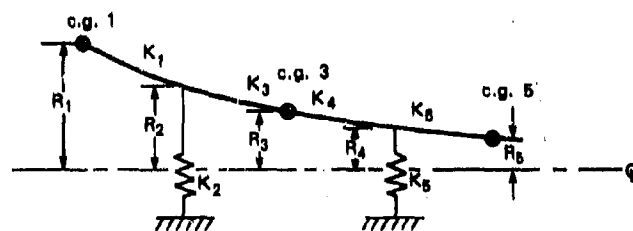
(b) Displaced system—slope effects neglected
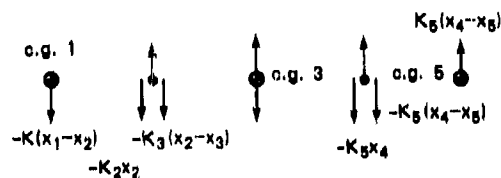
(c) Free body diagrams—slope effects neglected

Fig. 5.12. Equivalent dynamical model, displaced system, and free-body diagrams: rotor with overhung couplings and undamped flexible bearings

Assuming harmonic motions, substituting into the equations, and arranging in matrix form gives

$$\begin{bmatrix} (K_1-M_1\omega^2) & -K_1 & 0 & 0 & 0 \\ -K_1 & (K_1+K_2+K_3) & -K_3 & 0 & 0 \\ 0 & -K_3 & (K_3+K_4-M_3\omega^2) & -K_4 & 0 \\ 0 & 0 & -K_4 & (K_4+K_5+K_6) & -K_6 \\ 0 & 0 & 0 & -K_6 & (K_6-M_5\omega^2) \end{bmatrix} \begin{Bmatrix} r_1 \\ r_2 \\ r_3 \\ r_4 \\ r_5 \end{Bmatrix} = \begin{Bmatrix} 0 \\ 0 \\ 0 \\ 0 \\ 0 \end{Bmatrix}$$

where $R_i = r_i\, e^{i\omega t}$, the r_i are constants, and $i = 1$ through 5.

The resulting amplitude matrix expression is

$$[K - M\omega^2]\,\{r\} = \{0\}.$$

For the specific case in which

$$K_1 = K_3 = K_4 = K_6 = 1,$$

$$K_2 = K_5 = 2,$$

$$M_1 = M_5 = 1,$$

$$M_3 = 2,$$

substitution gives

$$\begin{bmatrix} (1-\omega^2) & -1 & 0 & 0 & 0 \\ -1 & 4 & -1 & 0 & 0 \\ 0 & -1 & (2-2\omega^2) & -1 & 0 \\ 0 & 0 & -1 & 4 & -1 \\ 0 & 0 & 0 & -1 & (1-\omega^2) \end{bmatrix} \begin{Bmatrix} r_1 \\ r_2 \\ r_3 \\ r_4 \\ r_5 \end{Bmatrix} = 0.$$

The matrix expression can be reduced by expanding rows 2 and 4 and solving for the amplitudes of r_2 and r_4:

$$-r_1 + 4r_2 - r_3 = 0,$$

$$-r_3 + 4r_4 - r_5 = 0,$$

$$r_2 = 0.25\,(r_1 + r_3),$$

$$r_4 = 0.25\,(r_3 + r_5).$$

Substituting these expressions into the matrix for r_2 and r_4 gives

$$\begin{bmatrix} (3 - 4\omega^2) & -1 & 0 \\ -1 & (6 - 8\omega^2) & -1 \\ 0 & -1 & (3 - 4\omega^2) \end{bmatrix} \begin{Bmatrix} r_1 \\ r_3 \\ r_5 \end{Bmatrix} = 0,$$

The nontrivial solution requires that the determinant of the coefficient matrix be equal to zero. Thus

$$(3 - 4\omega^2)(2\omega^4 - 3\omega^2 + 1) = 0.$$

The solutions for ω^2 are

$$\omega^2_{1,2,3} = 0.5, 0.75, 1.0.$$

Expanding the amplitude matrix gives

$$r_3 = (3 - 4\omega^2)r_1,$$

$$r_5 = [(6 - 8\omega^2)(3 - 5\omega^2) - 1]r_1.$$

If r_1 is unity, then corresponding values of r_3 and r_5 for the first three modes are found as follows:

	Mode 1	Mode 2	Mode 3
r_1	1	1	1
r_3	1	0	-1
r_5	1	-1	1

$$r_2 = (1/4)(r_1 + r_3),$$

$$r_4 = (1/4)(r_3 + r_5),$$

and

$$r_2^1 = 1/2, \qquad r_2^2 = 1/4, \qquad r_2^3 = 0,$$
$$r_4^1 = 1 \qquad r_4^2 = -1/4, \qquad r_4^3 = 0.$$

The three mode shapes are shown in Fig. 5.13.

(a) First mode $\omega_1^2 = 0.5$

(b) Second mode $\omega_2^2 = 0.75$

(c) Third mode $\omega_3^2 = 1.0$
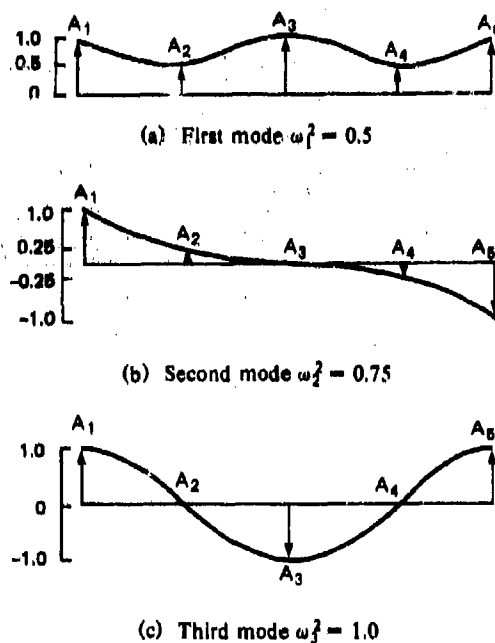
Fig. 5.13. Mode shapes for rotor with overhung couplings in
undamped flexible bearings

Uniform Shaft in Rigid Bearings with Overhang

The right-hand bearing in Fig. 5.14 represents a loading discontinuity that cannot be accommodated within a single equation of motion. There are thus two domains of integration for this system, for which the general modal equations are

$$r_1 = A \cos \lambda z_1 + B \sin \lambda z_1 + C \cosh \lambda z_1 + D \sinh \lambda z_1$$

for $0 < z_1 < L_1$ and

$$r_2 = E \cos \lambda z_2 + F \sin \lambda z_2 + G \cosh \lambda z_2 + H \sinh \lambda z_2$$

for $0 < z_2 < L_2$. In these equations $A, B, \ldots, G, H$ are constants of integration, to be determined according to the following boundary conditions:

For $z_1 = 0$,

$$r_1 = 0, \qquad \frac{d^2 r_1}{dz_1^2} = 0 \quad \text{(zero moment)};$$

(a) Rotor proportions

(b) Rotor deflection shape
in first mode
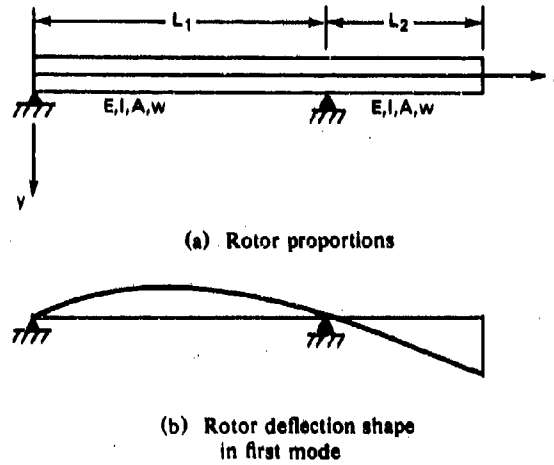
Fig. 5.14. Uniform shaft in rigid bearings with overhang

For $z_1 = L_1$,

$$r_1 = 0, \qquad \frac{dr_1}{dz_1} = \frac{dr_2}{dz_2} \quad \text{(equal slope)};$$

For $z_2 = 0$,

$$r_2 = 0, \qquad \frac{d^2 r_1}{dz_1^2} = \frac{d^2 r_2}{dz_2^2} \quad \text{(equal moment)};$$

For $z_2 = L_2$,

$$\frac{d^2 r_2}{dz_2^2} = 0 \quad \text{(zero moment)};$$

$$\frac{d^3 r_2}{dz_2^3} = 0 \quad \text{(zero shear force)}.$$

Substitution and elimination gives the frequency equation

$$(\cosh \lambda L_1 \sin \lambda L_1 - \sinh \lambda L_1 \cos \lambda L_1)(\cosh \lambda L_2 \sin \lambda L_2$$

$$- \sinh \lambda L_2 \cos \lambda L_2) - 2 \sinh \lambda L_1 \sin \lambda L_1$$

$$\times (1 + \cosh \lambda L_2 \cos \lambda L_2) = 0.$$

This expression was obtained and solved by Dunkerley [12], who gave
the following eigenvalue results for the lowest whirl mode.

Ratio L_1/L_2	λL_1
1.00	1.506
0.75	1.902
0.50	2.507
0.33	2.905
0.25	3.009
0.20	3.044
0.00	3.080

Dunkerley gave no results for the system normal mode shapes, but these are readily obtained by applying appropriate boundary conditions to the general solution, Eqs. (5.1). Writing $J_i^{(1)}$ and $J_i^{(2)}$ as the normalized modal forms across L_1 and L_2 for the ith mode, and $\alpha_i^{(1)}$ and $\alpha_i^{(2)}$ as the integration-constant ratios defined previously gives the following:

For $0 < x_1 < L_1$,

$$J_i^{(1)} = \sin \lambda x_i - \alpha_i^{(1)} \sinh \lambda x_i$$

and

$$\alpha_i^{(1)} = \frac{(\sin \lambda L_1)_i}{(\sinh \lambda L_1)_i}.$$

For $0 < x_2 < L_2$,

$$J_i^{(2)} = \cos \lambda x_i - \cosh \lambda x_i + \frac{\cos \lambda L_2 + \cosh \lambda L_2}{\sinh \lambda L_2} \sinh \lambda x_i$$

$$+ \alpha_i^{(2)} \sin \lambda x_i + \frac{\sin \lambda L_2}{\sinh \lambda L_2} \sinh \lambda x_i.$$

$$\alpha_i^{(2)} = \frac{[\sin \lambda L_2 + (\cos \lambda L_2 + \cosh \lambda\ L_2)(\cosh \lambda L_2/\sinh \lambda L_2)]_i}{[\cos \lambda L_2 - (\sin \lambda L_2/\sinh \lambda\ L_2)\cosh \lambda L_2]_i}.$$

5.4　Dynamic Properties of Rotors in Real Bearings

The practical deficiency in the analyses given in the previous section lies in the representation of the bearing dynamic properties. The rotor models, though they may appear simple, will often be adequate to represent the contribution of rotor flexure to the system modes. For instance, an analysis using a single-disk rotor system may provide use-

ful data on the lowest system mode; but it cannot provide data on the second system whirl mode, i.e., only one disk. Neither can the assumption of isotropic bearings provide information on elliptical orbit whirling. An important principle of practical rotor-dynamics analysis is to obtain the desired information with the simplest system model.

Several efforts have been made to correlate results obtained from the rotor models described in the preceding section with practical test results. This is desirable because to the extent that reliable calculations can be made, the need for prototype testing of actual rotors can be minimized or even eliminated. Such a capability also represents an important diagnostic tool for troubleshooting. System modeling may begin with the rotor configurations described previously,* but a more sophisticated bearing representation is usually needed to determine the performance of real systems. The concept of bearing dynamic properties dates back to Stodola [13], but the first significant contributions were made by Hagg [14], Hagg and Sankey [15], Raimondi and Boyd [16], and Sternlicht [17]. The Appendix gives a review of important aspects of the theory of bearing dynamic properties, with a selection of results from the open literature.

For the linear analysis of rotors in bearings, a major aspect is the representation of bearing dynamic forces in terms of stiffness and damping coefficients. For fluid-film bearings, the following linear representation is widely used:

$$F_x = K_{xx} X + K_{xy} Y + B_{xx} \dot{X} + B_{xy} \dot{Y}$$

and

$$F_y = K_{yx} X + K_{yy} Y + B_{yx} \dot{X} + B_{yy} \dot{Y}.$$

For rolling-element bearings, no cross-coupling exists and the bearing linear force relations become

$$F_x = F_x X + B_x \dot{X}$$

and

$$F_y = K_y X + B_y \dot{Y},$$

where F_x, F_y are the bearing dynamic force components occurring about the journal position of static equilibrium; $K_{xx} \ldots K_{yy}$, $B_{xx} \ldots B_{yy}$ are the bearing dynamic coefficients; X, Y are the journal dynamic displacements; and $\dot{X}$, $\dot{Y}$ are the journal dynamic velocities. The appendix

---

*More complex rotor models may be used in computer studies.

gives details of the derivation of such coefficients for fluid-film bearings. References [18] and [19] give data suitable for use with rolling-element bearings. Typical charts for several types of fluid-film bearings are given in the Appendix.

The study of rotor motions with the bearing dynamic coefficient approach has allowed the development of efficient computer programs for use in the analysis and design of rotor systems. Although this approach continues to be the basic analytical procedure used in industry today, there are certain instances where it is inadequate: rotor operation at a high bearing eccentricity ratio, prediction of post-threshold speed, and all strong nonlinear conditions. In such instances accurate analysis requires that the instantaneous forces (bearing, gas seal, blade, etc.) acting on the rotor be incorporated into a time-step integration procedure. A general purpose computer program for performing this type of nonlinear analysis has been developed by Giberson [2].

Details of several linear rotor-and-bearing unbalance-response analyses are given in the remainder of this chapter. These studies demonstrate the analysis technique and include typical results that can be achieved through the use of such calculations. Good comparison work between predicted and measured results is rare in the open literature, but that which exists demonstrates that computer rotor-dynamics analysis can be both valid and accurate when properly applied. Several studies of the damped response of rotors will now be discussed.

Unbalance Vibrations of a Single-Mass Rotor in Fluid-Film Bearings

The rotor-and-bearing system considered [14] is shown in Fig. 5.15. It consists of a flexible shaft of stiffness K_s (lb/in.) carrying a rigid mass section with a c.g. eccentricity a (in.) from the shaft elastic axis. Both bearings have a radial stiffness K (lb/in.) and radial damping B (lb s/in.). The bearing properties are assumed to be identical in both the x- and y-directions. The whirl orbits are therefore circular. Charts of the bearing stiffness and damping properties vs Sommerfeld number $S = [(\mu N/p)(R/C)^2]$ are included for bearing L/D ratios of 1.0 and 2.0. Stiffness coefficients in both horizontal and vertical directions are given. Only a single curve for damping coefficients is given. For this system the equations of motion are:

$$M\ddot{X}_1 + 2K_s(X_1 - X_2) = Ma\omega^2 \cos \omega t,$$

$$M\ddot{Y}_1 + 2K_s(Y_1 - Y_2) = Ma\omega^2 \sin \omega t,$$

$$K_s(X_1 - X_2) = K_x X_2 + B_x \dot{X}_2,$$

$$K_s(Y_1 - Y_2) = K_y Y_2 + B_y \dot{Y}_2.$$

With the stated assumptions $K_x = K_y = K$ and $B_x = B_y = B$, the whirl orbit is circular and the above expressions when combined give

$$M\ddot{R}_1 + 2K_s(R_1 - R_2) = Ma\omega^2 e^{i\omega t}$$

and

$$K_s(R_1 - R_2) = KR_2 + B\dot{R}_2,$$

where

$$R_n = X_n + iY_n, \qquad i = \sqrt{-1}, \qquad n = 1, 2.$$

For harmonic motions,

$$X_n = x_n e^{i\omega t}, \quad Y_n = y_n e^{i\omega t}.$$

and

$$R_n = r_n e^{i\omega t}.$$

Substituting gives

$$\left[\frac{2K_s K - (K + K_s)M\omega^2 + i\omega B(2K_s - M\omega^2)}{(K + K_s) + i\omega B} \right] r_1 = Ma\omega^2.$$

Writing

$$\bar{K} = \frac{K_s}{K}, \qquad \omega_n^2 = \frac{2K_s}{M},$$

$$r^2 = \left(\frac{\omega}{\omega_n}\right)^2, \qquad \zeta = \frac{B}{B_c} = \frac{B}{2M\omega_n}$$

gives

$$\frac{r_1}{a} = \frac{r^2}{1 - r^2} \frac{(1 + \bar{K}) + i2\zeta r}{[1 - \bar{K}(r^2/1 - r^2)] + i2\zeta r},$$

$$\frac{r_2}{a} = \frac{r^2}{1 - r^2} \frac{\bar{K}}{[1 - \bar{K}(r^2/1 - r^2)] + i2\zeta r}.$$

These are the normalized vector forms of r_1 and r_2. The respective modulus and phase angle for each are given by

$$\left|\frac{r_1}{a}\right| = r_0^2 \left[\frac{(1 + \bar{K})^2 + (2\zeta r)^2}{(1 - \bar{K}r_0^2)^2 + (2\zeta r)^2}\right]^{1/2},$$

$$\left|\frac{r_2}{a}\right| = r_0^2 \left[\frac{\bar{K}^2}{(1 - \bar{K}r_0^2)^2 + (2\zeta r)^2}\right]^{1/2},$$

$$\phi_1 = \arctan\left[\frac{(1 - \bar{K}r_0^2)^2 + (2\zeta r)^2}{(1 + \bar{K})^2 + (2\zeta r)^2}\right],$$

and

$$\phi_2 = \arctan\left[\frac{(1 - \bar{K}r_0^2)^2 + (2\zeta r)^2}{\bar{K}^2}\right].$$

where

$$r_0^2 = \frac{r^2}{1 - r^2}.$$

Hagg [14] gives

$$\left|\frac{r_1}{a}\right| = \left(\frac{\omega}{\omega_n}\right)^2 \left[\frac{\left(\frac{2K}{K_s}+1\right)^2 + \left(\frac{2B\omega}{K_s}\right)^2}{\left[\frac{2K}{K_s}\left(1-\frac{\omega^2}{\omega_n^2}\right)-\frac{\omega^2}{\omega_n^2}\right]^2 + \left(\frac{2B\omega}{K_s}\right)^2}\right]^{1/2},$$

which on substituting for the dimensionless quantities will be found to correspond with the first expression (for $|r_1/a|$) given above. In discrete form the expression for the journal whirl radius is

$$\left|\frac{r_2}{a}\right| = \left(\frac{\omega}{\omega_n}\right)^2 \left[\frac{\left(\frac{2K}{K_s}\right)^2}{\left[\frac{2K}{K_s}\left(1-\frac{\omega^2}{\omega_n^2}\right)-\frac{\omega^2}{\omega_n^2}\right]^2 + \left(\frac{2B\omega}{K_s}\right)^2}\right]^{1/2}.$$

The following numerical calculation for a turbine-rotor system is given by Hagg [14]:

Rotor weight $W = 20,000$ lb
Rotor mass $M = 621.118$ lb s²/ft.
Shaft stiffness $K_s = 2.07 \times 10^6$ lb/in.
Bearing type $= 120°$ partial arc
Bearing length $L = 10.0$ in.
Bearing diameter $D = 10.0$ in.
Bearing area $A = 100$ in.²
Bearing unit load $p = 100$ lb/in.²
Lubricant viscosity $\mu = 3.5 \times 10^6$ lb s/in.²
Sommerfeld number $S = \left[\frac{\mu N}{p}\right]\left[\frac{R}{C}\right]^2 = 6.5$
Bearing operation variable $(4S) = 26$
Horizontal bearing dimensionless stiffness $CK_H/W = 5.0$
Vertical bearing dimensionless stiffness $CK_V/W = 6.4$
Bearing dimensionless damping $C\omega B/W = 10.5$
System stiffness ratio $\bar{K} = K/K_s = 4.0$
System damping ratio $\zeta = B\omega/2K = 6.0$.

The dimensionless c.g. response amplitude $|r_2/a|$ of this system is compared in Fig. 5.16 with that of an undamped system and also with the undamped rigid-bearing case. It is evident that the peak amplitude response is less than that of either undamped system and that system
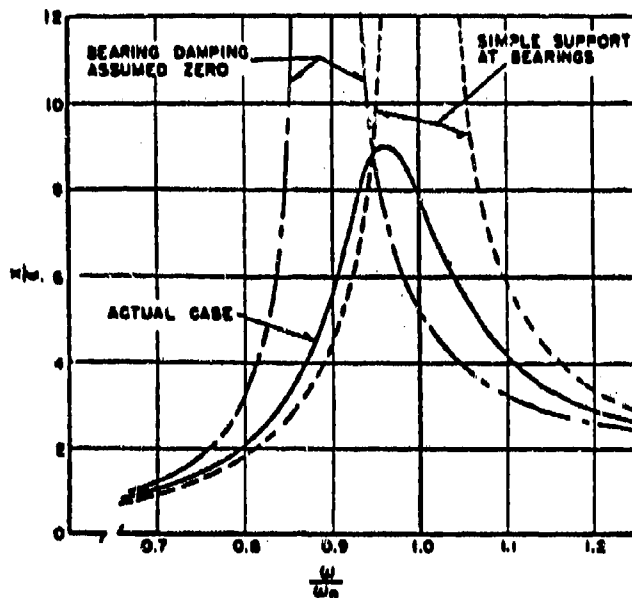
Fig. 5.16. Unbalance response of a simple massive rotor in
fluid-film bearings. (After Hagg [14].)

damping increases the critical response frequency toward the rigid-
bearing critical frequency.

This response could be converted into half-amplitude whirl data
$|r_2|$ if a value of the unbalance eccentricity a were given. The rotor of
this example would most likely be a class 2 rotor, and it would fit into
Quality Grade G 2.5. From Fig. 5.5 at 1950 rpm (200 r/s) a residual
balance of 0.16 oz-in./100 lb would be required for a satisfactory bal-
ance. This corresponds to a total unbalance of

$$U = 0.16 \times 200 = 32 \text{ oz-in.}$$

The c.g. eccentricity corresponding to this unbalance is

$$\frac{U}{W} = \frac{32.0}{20,000 \times 16} = 100 \times 10^{-6} \text{ in.} = 100 \,\mu\text{in.} = a.$$

The corresponding c.g. half-amplitude at the critical response peak is

$$\frac{r_1}{a} = 9.0,$$

and

$$\frac{\omega}{\omega_n} = 0.955.$$

Thus

$$|r_1| = (9.0)(100 \times 10^{-6}) = 0.9 \times 10^{-3} \text{ in.}$$

The c.g. peak-to-peak unbalance vibration amplitude for this case at resonance is therefore 1.8×10^{-3} in. under steady-state conditions.

It is of interest to extend Hagg's result to obtain the journal whirl amplitude, which is given by

$$\left|\frac{r_2}{c}\right| = \mathbf{r}_0^2 \left[\frac{\bar{K}^2}{(1 + \bar{K}\mathbf{r}_0^2) + (2\zeta\mathbf{r})^2}\right]^{1/2},$$

$$\mathbf{r}_0^2 = \frac{\mathbf{r}^2}{1 - \mathbf{r}^2} = \frac{0.912}{0.088} = 10.37,$$

$$\frac{r_2}{a} = 10.37 \left[\frac{(4)^2}{(1 + 4 \times 10.37)^2 + (2 \times 6)^2}\right]^{1/2} = 0.939,$$

and

$$r_2 = 0.939 \ (100 \times 10^{-6}) = 0.0939 \times 10^{-3} \text{ in.}$$

The journal peak-to-peak unbalance vibration amplitude is therefore 0.188×10^{-3} in. under steady-state conditions. For the bearings described (radial clearance 0.008 in.), this is well within acceptance requirements. As a rule of thumb, for eccentricity ratios less than 0.5, a whirl radius one-tenth of the radial clearance is *acceptable*. In the above case this corresponds to a whirl radius of 0.008 in., which would result from an unbalance of 1362 oz-in.

Single-Mass Flexible Rotor in Fluid-Film Bearings: The Influence of Different Bearing Types on Unbalance Response

A more extensive study of the influence of bearing properties on the response of a single-mass rotor was made by Lund and Sternlicht [20]. The bearings were represented by eight dynamic coefficients for which values had been obtained using (then) newly developed digital computer programs. Curves of the dimensionless transmitted force vs speed ratio are presented for various bearing operating eccentricity ratios, for the case of a plain cylindrical bearing with L/D ratios of 1.0 and 0.5. A typical result is shown in Fig. 5.17. These results show the influence of bearing operating eccentricity on the transmitted force. They show that transmitted force increases and then decreases as the

A = JOURNAL CENTER
E = ELASTIC AXIS OF
SHAFT AT DISK
G = c.g. OF DISK

ROTOR—BEARING SYSTEM

WHIRL RADIUS, DIMENSIONLESS

ϵ = Bearing
eccentricity
ratio
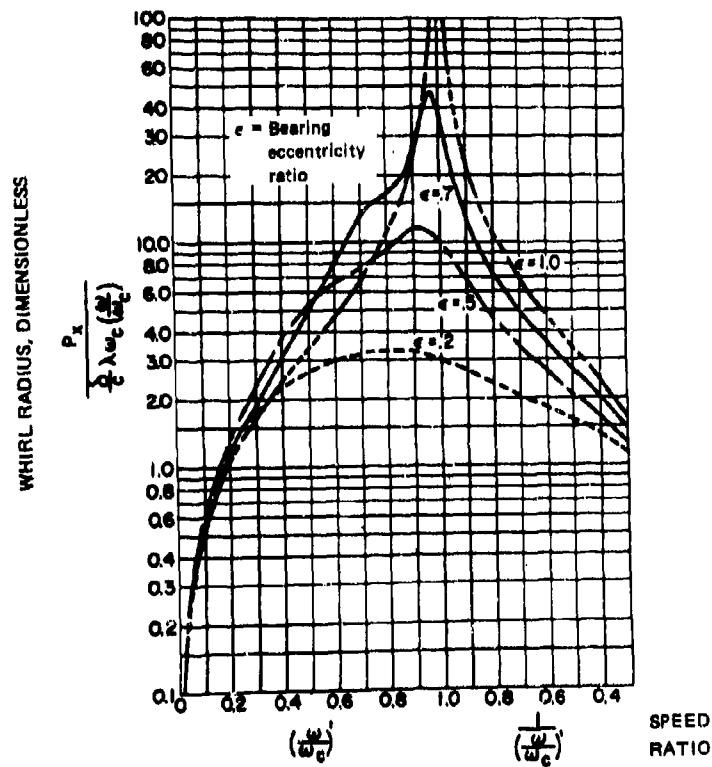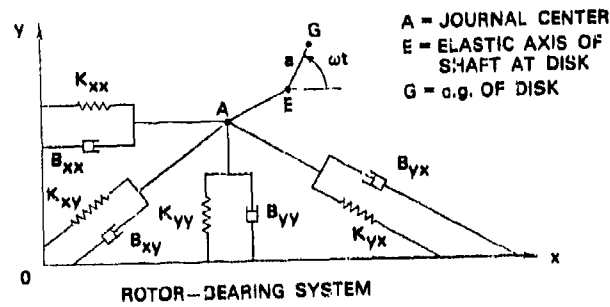
Fig. 5.17. Typical plot of dimensionless transmitted force
vs speed ratio for simple rotor in damped bearings

rotor passes through the system critical speed, and that this increase is less when the rotor operates at low eccentricity than when the operating eccentricity ratio is high. This occurs because the available stiffness effect is lower at lower eccentricity, and there is also more squeeze-film effect. More precisely, the parameter

$$\frac{B\omega}{K} = 2\zeta$$

is higher, and, as shown previously, this factor determines the rotor whirl amplitude and hence the bearing transmitted force throughout the critical speed range. The results are applicable to any rotor in plain cylindrical bearings with the given L/D ratio, in terms of the stated dimensionless parameters.

Data on the influence of two other bearing types—four-axial groove bearings and elliptical bearings—are given in a more comprehensive report by Lund and Sternlicht [21]. The same general force vs response pattern is again shown. Bearing geometry is prescribed, and the results are restricted to the bearing proportions given. Data on the dynamic properties of all bearing types used in this study are tabulated, and details are given of the theory from which these data were obtained.

Two-Mass Flexible Rotor in Fluid-Film Bearings: Design Charts for Response and Transmitted Force

Warner and Thoman [11] extended the work of Lund and Sternlicht to the case of a flexible rotor in 150° partial arc bearings. An eight-coefficient bearing model was again used. The rotor carries two disks, each with a mass of $(1/2)M$ a distance ξL apart, where L is the rotor span between bearings and ξ here is a coefficient < 1.0. The system has midspan symmetry; see Fig. 5.18.

Two disks are used in this example. By using the principle of mode separation, either the translatory whirl mode or the conical whirl mode can be obtained from the analytical formulation simply by selecting the appropriate value of the coefficient ξ. For a symmetrical first mode $\xi = 1$. For the second mode, the rotor inertia gives $\xi = \sqrt{I/M}$.

For the first mode, the shaft bending deflection between the disk and the bearing due to force F is given by

$$(X_1 - X) = F_{ax}\alpha_{aa} + F_{bx}\alpha_{ab},$$

and

$$(Y_1 - Y) = F_{ay}\alpha_{aa} + F_{by}\alpha_{ab},$$
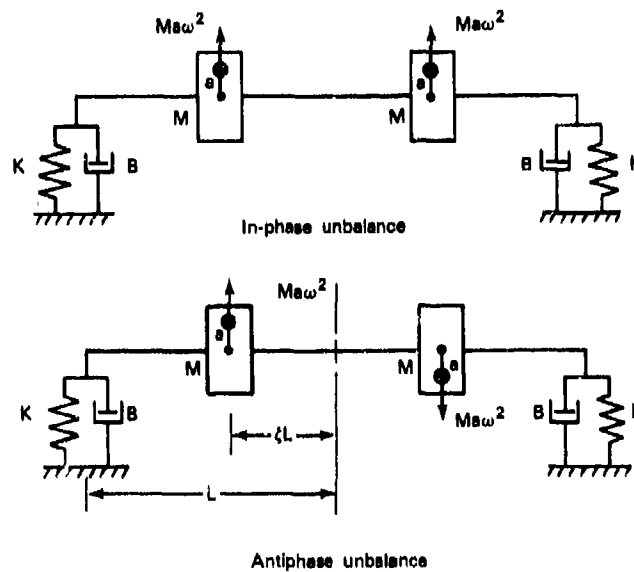
Fig. 5.18. Symmetrical, two-mass rotor in damped flexible bearings

as

$$F_{ax} = F_{bx} = F_x, \qquad (X_1 - X) = F_x(\alpha_{aa} + \alpha_{ab}),$$

$$F_{ay} = F_{by} = F_y, \qquad (Y_1 - Y) = F_y(\alpha_{aa} + \alpha_{ab}).$$

For the second mode the expressions are

$$X_1 - \xi X = F_{ax}\alpha_{aa} - F_{bx}\alpha_{ab},$$

$$Y_1 - \xi Y = F_{ay}\alpha_{aa} - F_{by}\alpha_{ab};$$

that is, as previously shown,

$$X_1 - \xi X = F_x(\alpha_{aa} - \alpha_{ab})$$

$$Y_1 - \xi Y = F_y(\alpha_{aa} - \alpha_{ab}).$$

With use of the conventions

Mode	ξ	α
First	1	$\alpha_{aa} + \alpha_{ab}$
Second	ξ	$\alpha_{aa} - \alpha_{ab}$

the following expressions are obtained for both modes:

$$X_1 - \xi X = F_x \alpha$$

and

$$Y_1 - \xi Y = F_y \alpha.$$

The equations of motion can now be formed by recognizing that

$$M \ddot{X}_1 = - F_x + Ma\omega^2 \cos \omega t$$

and

$$M \ddot{Y}_1 = - F_y + Ma\omega^2 \sin \omega t.$$

(5.1)

Hence,

$$\alpha M \ddot{X}_1 = (X_1 - \xi X) + Ma\omega^2 \cos \omega t,$$

$$\alpha M \ddot{Y}_1 = (Y_1 - \xi X) + Ma\omega^2 \sin \omega t.$$

(5.2)

The force balance at the bearings in the first mode is

$$\frac{1}{\alpha} (X_1 - \xi X) = K_{xx} X + K_{xy} Y + B_{xx} \dot{X} + B_{xy} \dot{Y}$$

and

$$\frac{1}{\alpha} (Y_1 - \xi Y) = K_{yx} X + K_{yy} Y + B_{yx} \dot{X} + B_{yy} \dot{Y}.$$

Similarly for the second mode moments,

$$F_x \xi L = (K_{xx} X + K_{xy} Y + B_{xx} \dot{X} + B_{xy} \dot{Y}) L = \frac{\xi L}{\alpha} (X_1 - \xi X)$$

and

$$F_y \xi L = (K_{yx} X + K_{yy} Y + B_{yx} \dot{X} + B_{yy} \dot{Y}) L = \frac{\xi L}{\alpha} (Y_1 - \xi Y).$$

With the convention given above, the equations for both modes can be written as

$$\frac{\xi}{\alpha} (X_1 - \xi X) = K_{xx} X + K_{xy} Y + B_{xx} \dot{X} + B_{xy} \dot{Y}$$

and

$$\frac{\xi}{\alpha} (Y_1 - \xi Y) = K_{yx} X + K_{yy} Y + B_{yx} \dot{X} + B_{yy} \dot{Y}.$$

(5.3)

It is now necessary to eliminate X_1, Y_1 from the above equations by substituting

$$X_1 = x_1 e^{i\omega t}, \quad X = xe^{i\omega t},$$

$$Y_1 = y_1 e^{i\omega t}, \quad Y = ye^{i\omega t}$$

into Eq. (5.2) and by solving for x_1, y_1. This gives

$$x_1 = \frac{\xi x + a}{1 - \alpha M\omega^2} = \frac{\xi x + a}{1 - (\omega/\omega_n)^2}$$

and   (5.4)

$$y_1 = \frac{\xi x - ia}{1 - \alpha M\omega^2} = \frac{\xi y - ia}{1 - (\omega/\omega_n)^2},$$

where $\omega_n^2 = 1/\alpha M$. Substituting Eqs. (5.4) into Eq. (5.3) gives

$$\frac{\xi}{\alpha}\left[\frac{\xi x + a}{1 - (\omega/\omega_n)^2} - \xi x\right] = K_{xx}x + K_{xy}y + i\omega B_{xx}x + i\omega B_{xy}y \quad (5.5)$$

and

$$\frac{\xi}{\alpha}\left[\frac{\xi y - ia}{1 - (\omega/\omega_n)^2} - \xi y\right] = K_{yx}x + K_{yy}y + i\omega B_{yx}x + i\omega B_{yy}y$$

on canceling the $e^{i\omega t}$. Multiplying through by C/W and writing

$$K = \frac{C\xi^2}{W\alpha}\frac{(\omega/\omega_n)^2}{1 - (\omega/\omega_n)^2}, \quad \bar{a} = \frac{C\xi}{W\alpha}\frac{a}{1 - (\omega/\omega_n)^2}$$

allows Eq. (5.5) to be written in terms of dimensionless stiffness and damping ratios, as follows:

$$\begin{bmatrix} \bar{K}_{xx} + K + i\omega\bar{B}_{xx} & \bar{K}_{xy} + i\omega\bar{B}_{xy} \\ \bar{K}_{yx} + i\omega\bar{B}_{yx} & \bar{K}_{yy} + K + i\omega\bar{B}_{yy} \end{bmatrix}\begin{Bmatrix} x \\ y \end{Bmatrix} = \bar{a}\begin{Bmatrix} 1 \\ -i \end{Bmatrix},$$

where

$$\bar{K}_{xx} = \frac{CK_{xx}}{W}, \quad \omega\bar{B}_{xx} = \frac{C\omega B_{xx}}{W},$$

$$\bar{K}_{xy} = \frac{CK_{xy}}{W}, \quad \omega\bar{B}_{xy} = \frac{C\omega B_{xy}}{W},$$

$$\overline{K}_{yx} = \frac{CK_{yx}}{W}, \qquad \omega\overline{B}_{xx} = \frac{C\omega B_{yx}}{W},$$

$$\overline{K}_{yy} = \frac{CK_{yy}}{W}, \qquad \omega\overline{B}_{yy} = \frac{C\omega B_{yy}}{W}.$$

Selected results by Warner and Thoman from this analysis for the dimensionless transmitted force and whirl radius are given in Fig. 5.19. The paper gives results for bearing eccentricity ratios between 0.01 and 0.95, and for a range of rotor-stiffness parameter α values. The bearings for which these results apply are 150° partial journal bearings.

The elegant formulation used by Warner and Thoman for this problem allows a great deal of valuable information to be presented in a relatively few charts. The charts apply for any value of L/D, and the only bearing parameters in the analysis are load W, radial clearance C, and operating eccentricity (η), which can be obtained from a table of Sommerfeld number vs eccentricity ratio given in the paper [11]. Furthermore, the entire range of rotor stiffness has been included with the rotor parameter α. The simple set of response curves describes the rotor response and transmitted force to both in-phase and out-of-phase unbalance. The main limitation is the symmetry of the system.

As the analysis model includes the complete set of eight dynamic coefficients, the rotor-whirl orbits are elliptical. The charts therefore contain data for the major ellipse amplitude radius and for the corresponding major force radius.

Validity of Results from Simple Rotor-System Models

The studies by Lund and Sternlicht [20] and Warner and Thoman [11] relate to discrete-mass rotors. The results obtained should be accurate where the shaft is relatively massless ($M_{shaft} < M_{disk}/10$) and where the rotor mass is concentrated in the disk, as in centrifugal compressor rotors and low-pressure turbine rotors. The results would also be accurate in cases where the rigid-bearing critical speed were known, so that an effective shaft stiffness and effective rotor inertia could be chosen, i.e., for a single-mass rotor,

$$K_s = M\omega_n^2,$$

where M is the total rotor mass (lb s²/in.) and ω_n is the rigid-bearing critical speed. For a two-mass rotor,

$$K_s = (1/2)M\omega_n^2,$$

and

$$I = M\xi^2 L^2,$$

where ξL is the effective distance between the rotor disks.
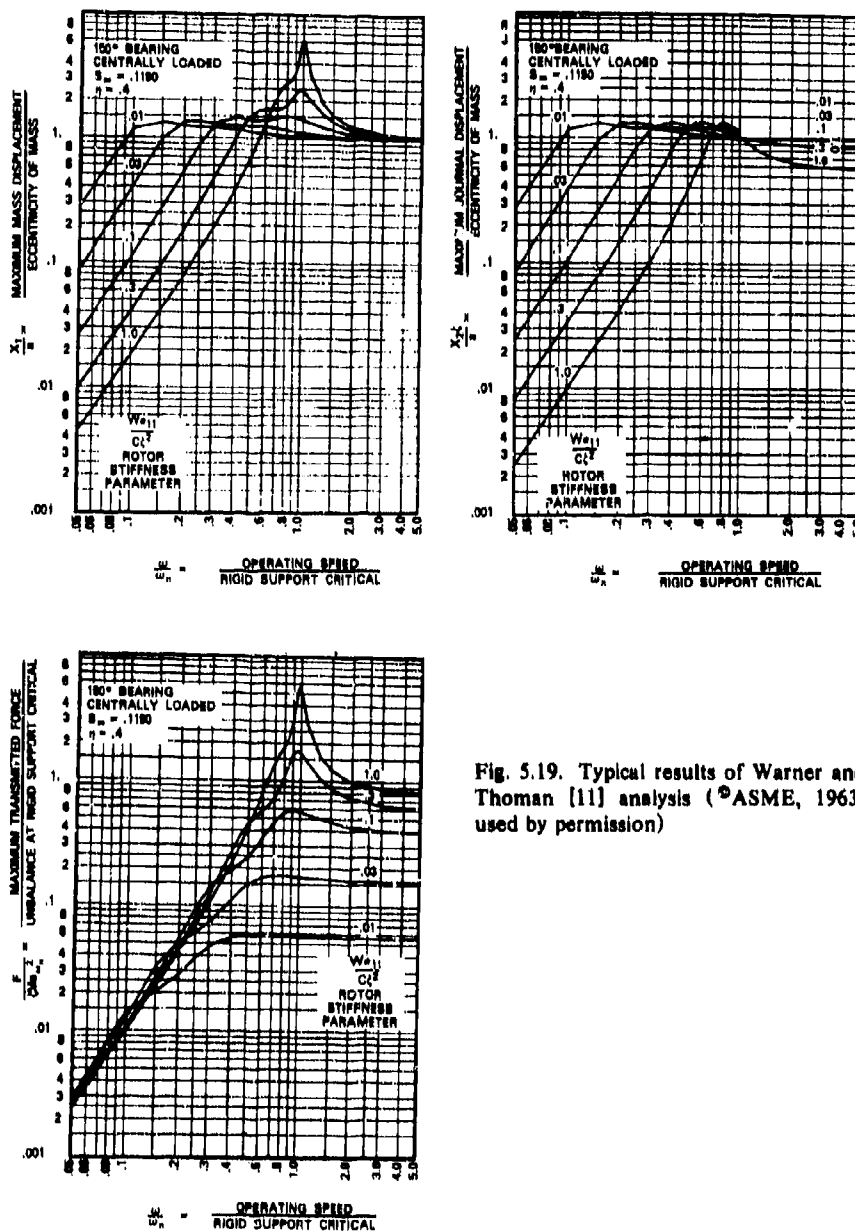
Fig. 5.19. Typical results of Warner and Thoman [11] analysis (©ASME, 1963; used by permission)

The above studies give useful design information on the influence of the bearings on rotor behavior in the first and second whirl modes. The influence of the bearings on rotor response in the higher modes cannot be determined because of the nature of the rotor models chosen. Such modes may exert an important influence on the effectiveness of the balancing process. Bishop and Parkinson [22] describe a procedure whereby the effects of higher modes can be considered during modal balancing. Moore and Dodd [23] discuss higher mode effects in relation to a pump rotor-balance problem. Rieger and Badgley [24] encountered troublesome effects from higher modes in computer balancing a gas-turbine rotor. These studies are discussed in Chapter 6, and the underlying modal theory is developed in Section 5.6.

Rieger [25] examined the influence of higher modes through use of the rotor model shown in Fig. 5.20. This rotor has a continuous distribution of mass and elastic properties along its length. The shaft is supported in identical fluid-film bearings at its ends. The bearings have direct and cross-coupled stiffness and damping properties in both the x- and y-directions (Fig. 5.21). The unbalance force rotates in synchronism with the shaft, causing it to whirl about its stationary equilibrium position. Shaft motions are opposed at the journals by the bearing forces. Any externally impressed journal motion gives rise to fluid-film
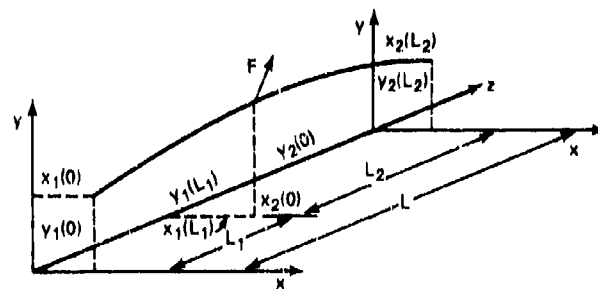
Fig. 5.20. Uniform rotor in damped flexible bearings

Fig. 5.21. Bearing stiffness and damping model
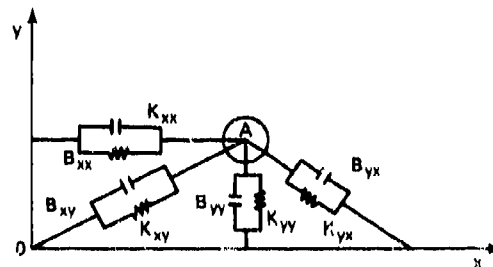
forces that oppose motion, both in the direction of the displacement and at right angles to it. The maximum and minimum values of the whirl amplitude and the transmitted force were calculated. Selected results for the maximum whirl amplitude and the maximum transmitted force obtained in this study are shown in Figs. 5.22 through 5.27.

(a) $\eta = 0.2$

(b) $\eta = 0.5$

(c) $\eta = 0.7$
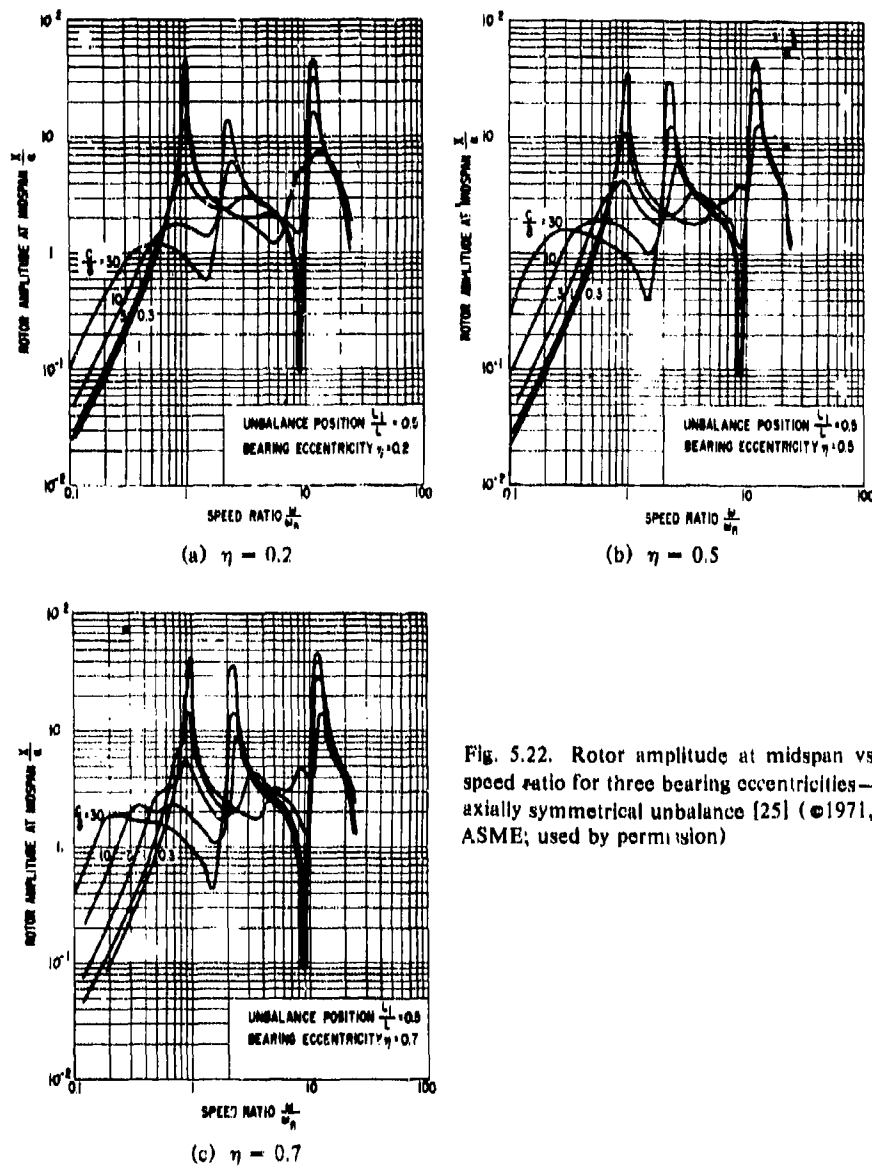
Fig. 5.22. Rotor amplitude at midspan vs speed ratio for three bearing eccentricities— axially symmetrical unbalance [25] (©1971, ASME; used by permission)

Fig. 5.24. Rotor amplitude at journal vs speed ratio—axially asymmetrical unbalance [25] (©1971, ASME; used by permission)
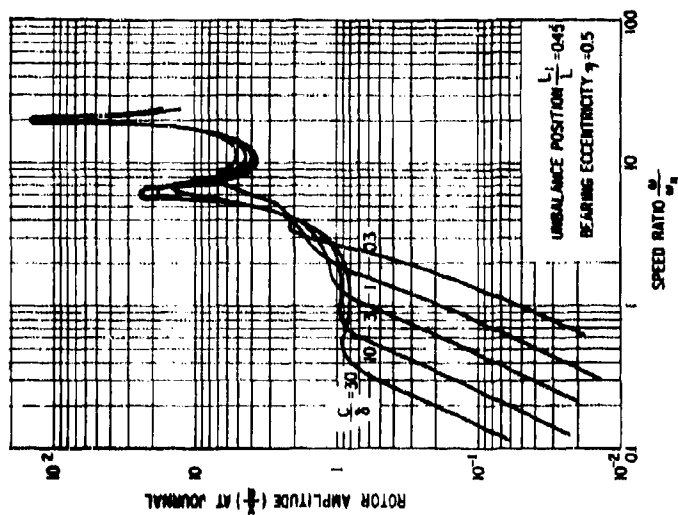
Fig. 5.23. Rotor amplitude at journal vs speed ratio—axially symmetrical unbalance [25] (©1971, ASME; used by permission)
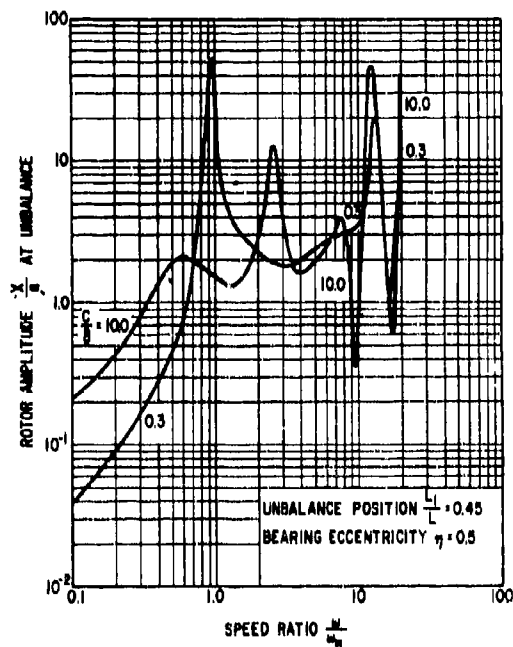
Fig. 5.25. Rotor amplitude at unbalance vs speed ratio — axially asymmetrical unbalance [25] (©1971, ASME, used by permission)

(a) $\eta = 0.2$

(b) $\eta = 0.5$

(c) $\eta = 0.7$
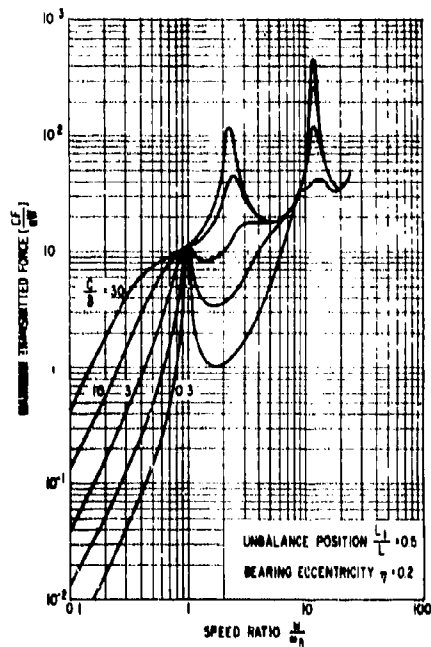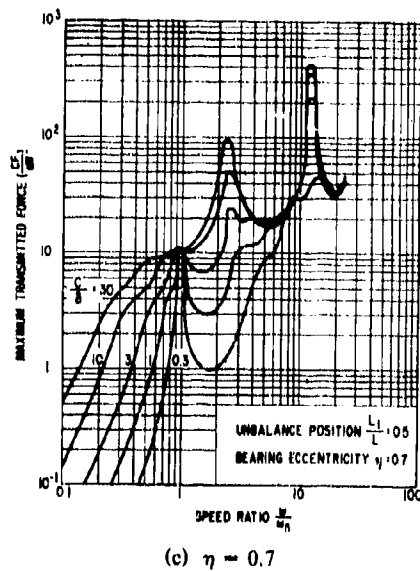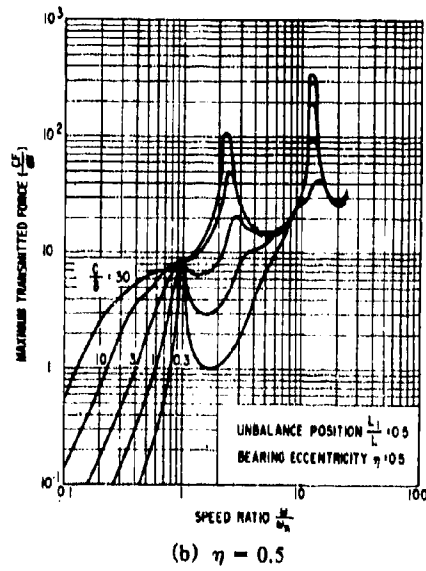
Fig. 5.26. Maximum transmitted force vs speed ratio for three bearing eccentricities—axially symmetrical unbalance [25] (©1971, ASME; used by permission)
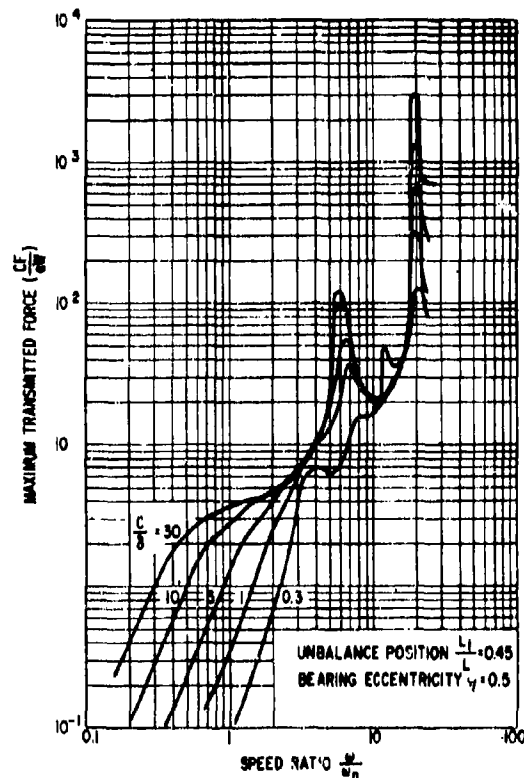
Fig. 5.27. Maximum transmitted force vs speed
ratio—axially   asymmetrical   unbalance   [25]
(©1971, ASME; used by permission)

5.5 Experimental Verification of Unbalance Response Theory

The analyses described in Sections 5.3 and 5.4 derive from the
Jeffcott [26] theory of whirling, which claims that a synchronous whirl
develops about the, axis of static equilibrium, as the shaft deflects to
reestablish equilibrium under the action of rotating centrifugal unbal-
ance. Downham [27] appears to have been the first to test this theory
in a comprehensive manner, although Jeffcott's paper describes an
experiment in support of his theory. Robertson [28,29] also describes
certain supporting experiments. While there appears to be no doubt
concerning the validity of the theory,* there is remarkably little pub-

---

*Development of the Jeffcott theory followed a discussion of certain experiments by Kerr
[30].

lished work in which practical rotor experiments have been compared with a predicted unbalance response. In such an experiment the rotor would first be carefully balanced to a high degree of precision; controlled unbalances would then be systematically inserted to test the system response. In a recent survey of industrial practice, Rieger [31] found that most users considered correlation between observed critical speeds (usually the lowest) and critical speed values predicted by their unbalance response program to be sufficient validation of an unbalance response program.

Several experiments that demonstrate the validity of the synchronous unbalance theory of rotor whirling will now be discussed.

Unbalance Response of a Three-Mass Rotor in Tilting-Pad Bearings

An extensive series of tests [32] was made on the rotor system shown in Fig. 5.28, covering both the unbalance response and the balancing of this rotor system.
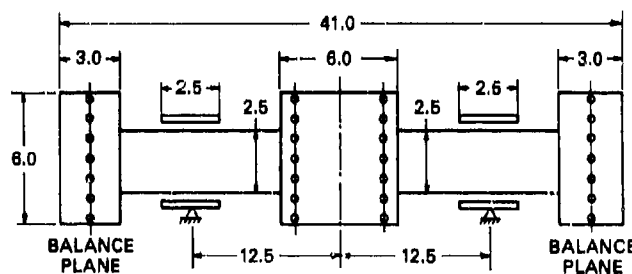
ROTOR WEIGHT: 88 LB	BEARINGS: FOUR-SHOE TILTING PAD
END DISKS: 18 LB EACH	L/D RATIO: 1.0
CENTER DISK: 36 LB	CLEARANCE RATIO: 3 × 10 IN./IN.
DRIVE: ELECTRIC MOTOR AT END	(MACHINED CLEARANCE)
SPEED RANGE: 24,000 RPM	PAD ARC LENGTH: 80°
FLUID VISCOSITY: 0.65 cSt (77°F)	PIVOT POSITION: 44°
0.51 cSt (130°F)	FROM LEADING EDGE
	GEOMETRIC PRELOAD: 0.5

Fig. 5.28. Three-mass rotor mounted in fluid-film, four-tilting-pad bearings [32] (©1965, ASME; used by permission)

The rotor was tested as a one-, two-, and three-mass body mounted in fluid-film, four-tilting-pad bearings. The system was clamped to a massive, rigid foundation. Controlled unbalance weights were inserted into a precision-balanced rotor during each test, as discussed previously. The rotor was driven by a high-frequency (400-Hz) motor, and the speed-control system was designed to allow precise operation anywhere within the range 0 to 24,000 rpm.

The system was so designed that with the three-mass rotor a strong bending critical speed would occur at about 12,000 rpm. This was the free-free bending mode of the rotor, which is to be anticipated from the disposition of the concentrated masses, and from the locations of the bearings, which are situated where the nodes of this free-free mode occur (Fig. 5.29). Thus at the bending critical speed the three-mass rotor will whirl in a mode where no motion occurs at the bearings, and hence no damping forces are generated.* The purpose of this design was to impose a severe test on the balancing theory. If the rotor could be balanced for smooth operation at its bending critical speed, with negligible external damping (i.e., theoretically infinite whirl amplitudes) and with overhangs, then the theory would have been fully tested.
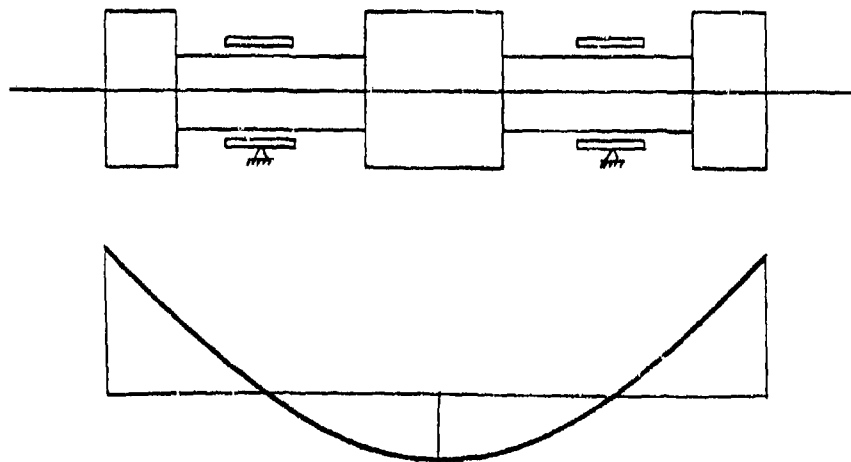
Fig. 5.29. Free-free bending mode of three-mass rotor

This balancing test, however, does not provide a complete test of unbalance response theory since fluid-film bearing effects are not included and there is no significant source of system damping with which predicted damped resonant response amplitudes might be verified. Tests were performed on one- and two-mass versions of this rotor to accommodate this requirement (see insets, Figs. 5.30 and 5.31). These figures show the extent of correlation achieved in the Lund—Orcutt study [32] and subsequently by Thomas and Rieger [10],

*Since the bearings have a finite length, some damping might result from the angular (slope) motions of the shaft. The tilting pads track the shaft and are mounted on spherical buttons of minimal angular resistance. With low pad inertia, both lateral and angular damping should be very small.

who used the Lund–Orcutt study as a test case for verification of their dynamic stiffness matrix unbalance response program.

When Figs. 5.30 and 5.31 are compared, the following conclusions can be drawn, at least for this study of unbalance response predictions vs experiment:

1. For small-to-moderate rotor amplitudes the linear theory is validated by the experimental results.

2. Correlation between results is generally very close, being closest where damping is smaller.

3. Discrepancies between response amplitude results are greatest above the critical speed and where the bearing forces strongly influence the motion.
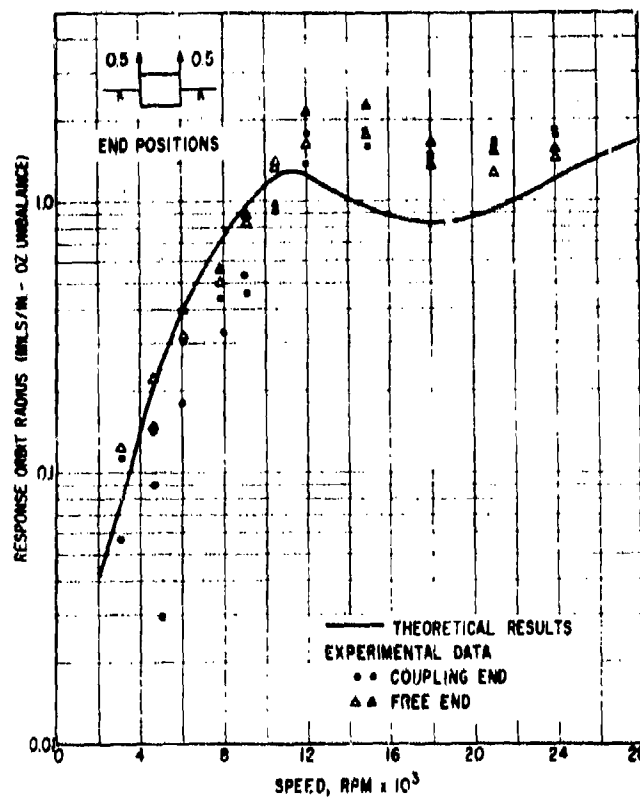
Fig. 5.30. Unbalance response of one-disk rotor, end positions [32] (©1965, ASME; used by permission)
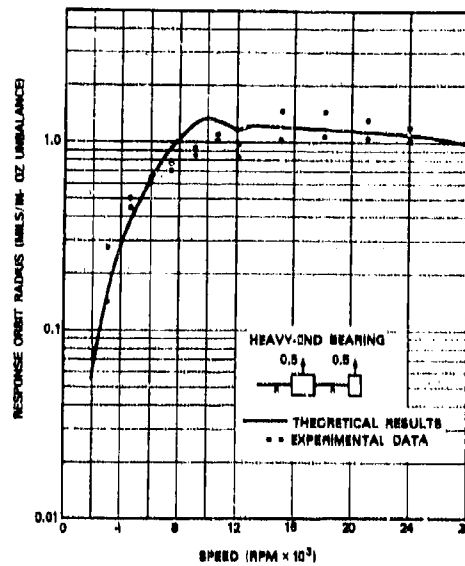
(a) Heavy-end-bearing position
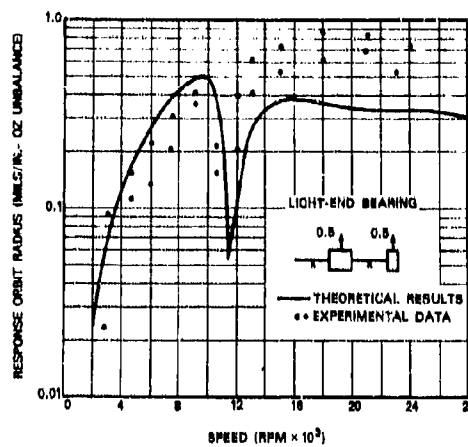
(b) Light-end-bearing position

Fig. 5.31. Unbalance response of two-disk
rotor, with weights in line [32] (©1965,
ASME; used by permission)

4. These discrepancies most probably indicate that further questions remain concerning the accuracy of the stiffness and damping coefficients used. The extent to which the observed amplitude differences could be resolved by the inclusion of nonlinear effects is not known.

5.6 Modal Theory of Rotor Motions

All linear structural motions can be described in terms of normal modes of vibration. The normal modes of a structure are the fundamental vibration forms which the structure will assume when disturbed from rest. Thorough discussions of the general theory of linear structural vibration have been presented by Rayleigh [33], Timoshenko [34], and Meirovitch [35]. The theory has been applied to shaft motions by Bishop and co-workers in a series of papers [36—39]. The purpose of this section is to describe the technique of modal analysis applied to rotor dynamics. Because a flexible rotor mounted in elastic bearings with damping constitutes a structural system, it follows that the dynamics of such a system can be examined by means of the normal mode theory. This powerful method is of fundamental importance in the analysis of rotating elastic systems. It also forms the basis of the modal balancing method, to be described in the next chapter.

Consider the prismatic elastic rotor shown in Fig. 5.32. In the absence of gravity deflections this shaft rotates at speed Ω and whirls about the axis OZ under the influence of residual unbalance. Both the rotor mass and the rotor elastic properties are distributed along the length of the rotor. An elemental slice taken from the rotor length is shown in Fig. 5.33. The displacement of this slice during the rotation can be resolved into two components at right angles projected on to the
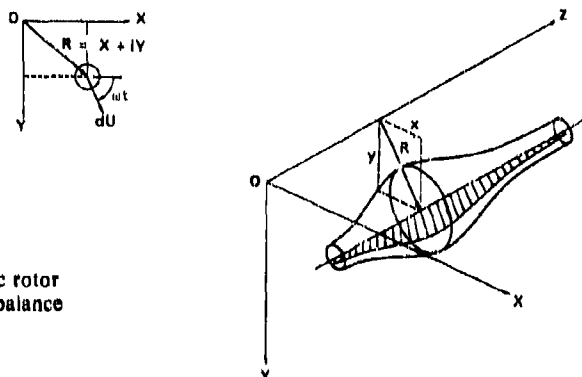
Fig. 5.32. Cylindrical elastic rotor
with general distributed unbalance
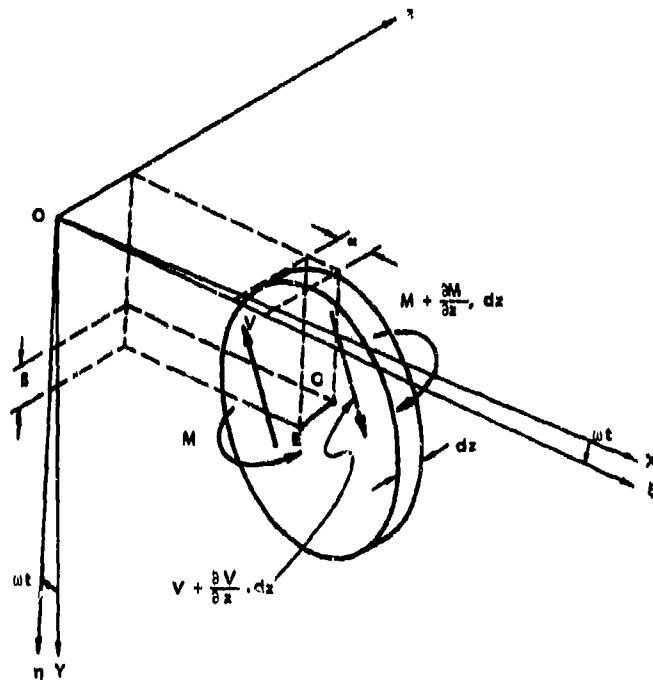
Fig. 5.33. Elemental slice of rotor length

planes XZ and YZ. As the shaft steadily rotates, the projected time-dependent components of the rotary motion will appear as vibrations on either plane, though the magnitude of the whirl radius itself does not vary—that is,

$$R = r e^{i\omega t} = X + iY,$$

$$X = x e^{i\omega t} \qquad (x = r \cos \omega t),$$

$$Y = y e^{i\omega t} \qquad (y = r \sin \omega t),$$

$$R^2 = X^2 + Y^2,$$

and

$$r^2 = x^2 + y^2 \qquad r = (x^2 + y^2)^{1/2}.$$

Now suppose that a second pair of axes OX' OY' is introduced to describe the harmonic motion of the shaft, and rotating in synchronism with it, about axis OZ at speed Ω; that is, the plane $OX'Y'$ rotates about OZ as shown in Fig. 5.33. In terms of these new axes the location of the elastic axis of the elemental slice can be expressed as

$$R = \zeta \, e^{i\omega t} = (\xi + i\eta) e^{i\omega t}, \qquad \xi = \zeta \cos \phi,$$

$$x = \xi \, e^{i\omega t} \qquad\qquad\qquad \eta = \zeta \sin \phi,$$

$$y = \eta \, e^{i\omega t} \qquad\qquad\qquad \zeta = (\xi^2 + \eta^2)^{1/2}$$

The projections of the whirl radius on to the rotating planes are constant in time since there is no relative rotation between the axes OX' and OY' and the shaft. With this concept it is now possible to study the shaft motions as two simultaneous vibrations with a phase difference of 90°, each of which can be considered as a component vibration of the overall steady rotation vector.

The equations of free motion for the cylindrical slice AA' in Fig. 5.33 can now be obtained. The slice is in equilibrium with the end moments and end forces shown. No axial force exists, and, for the present, no damping (external or internal) will be considered. The forces and moments can also be resolved into fluctuating components in the XZ and YZ planes, and the equations of motion are

$$\rho A \, dz \, \frac{\partial^2 X}{\partial t^2} = \left(V_x + \frac{\partial V_x}{\partial z} dz \right) - V_x$$

and

$$\rho A \, dz \, \frac{\partial^2 Y}{\partial t^2} = \left(V_y + \frac{\partial V_y}{\partial z} dz \right) - V_y.$$

From the Bernoulli–Euler beam theory, we have

$$V_x = \frac{\partial M_x}{\partial z} = - \frac{\partial}{\partial z} \left[EI \, \frac{\partial^2 X}{\partial z^2} \right],$$

$$V_y = \frac{\partial M_y}{\partial z} = - \frac{\partial}{\partial z} \left[EI \, \frac{\partial^2 Y}{\partial z^2} \right],$$

and hence

$$\frac{\partial^2}{\partial z^2} \left[EI \, \frac{\partial^2 X}{\partial z^2} \right] + \rho A \, \frac{\partial^2 x}{\partial t^2} = 0$$

and

$$\frac{\partial^2}{\partial z^2} \left[EI \, \frac{\partial^2 Y}{\partial z^2} \right] + \rho A \, \frac{\partial^2 y}{\partial t^2} = 0.$$

G

Writing the local whirl radius as $R = X + iY$ and combining these equations give

$$\frac{\partial^2}{\partial z^2}\left[EI\ \frac{\partial^2 R}{\partial z^2}\right] + \rho A\ \frac{\partial^2 R}{\partial t^2} = 0.$$

For harmonic motions of this shaft section, the solution is

$$R = r(z)\ e^{i\omega t},$$

where r is a function of coordinate z only. The equation of harmonic motion is then

$$\frac{d^2}{dz^2}\left[EI\ \frac{d^2 r}{dz^2}\right] - \rho A\omega^2 r = 0.$$

If the slice is uniform in cross section along its length, EI is constant. The equation of motion becomes

$$\frac{d^4 r}{dz^4} - \lambda^4 r = 0\ ; \qquad \lambda^4 = \frac{\rho A\omega^2}{EI}.$$

The solution to this equation is

$$r = A\ \cos \lambda z + B\ \sin \lambda z + C\ \cosh \lambda z + D\ \sinh \lambda z,$$

where A, B, C, D are constants of integration to be determined from the boundary conditions of a given case. The following examples demonstrate that, when these coefficients are known, the mode shape at any speed can be determined.

Uniform Cylindrical Rotor in Rigid End Bearings

Consider the system shown in Figs. 5.34a with the following boundary conditions:
For $z = 0$,

$$r = 0$$

$$M = -EI\ \frac{d^2 r}{dZ^2} = 0.$$

For $z = L$,

$$r = 0$$

$$M = -EI\ \frac{d^2 r}{dZ^2} = 0.$$

(a) Uniform cylindrical rotor in rigid bearings

(b) Mode 1

$$f_1 = \frac{1}{2\pi}\left(\frac{\pi}{L}\right)^2\left(\frac{EI}{\rho A}\right)^{1/2} \text{ Hz}$$

(c) Mode 2

$$f_2 = \frac{1}{2\pi}\left(\frac{2\pi}{L}\right)^2\left(\frac{EI}{\rho A}\right)^{1/2} \text{ Hz}$$

(d) Mode 3

$$f_3 = \frac{1}{2\pi}\left(\frac{3\pi}{L}\right)^2\left(\frac{EI}{\rho A}\right)^{1/2} \text{ Hz}$$
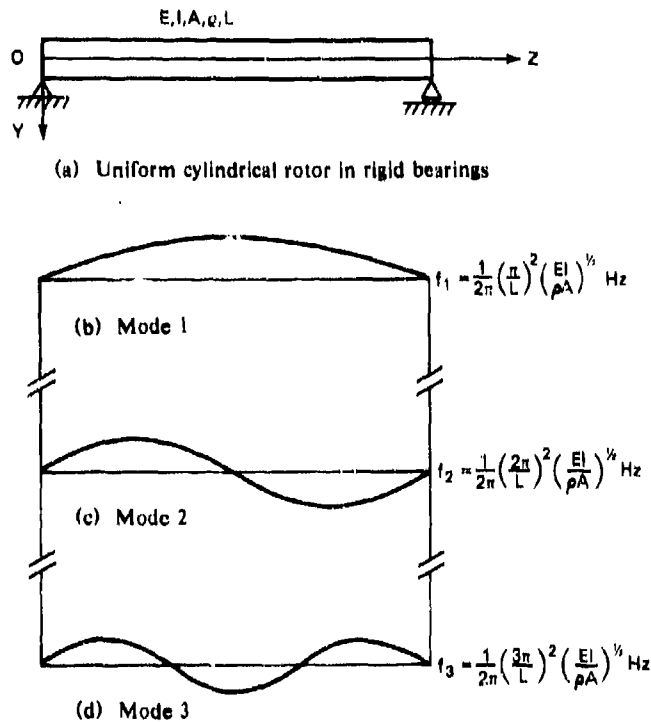
Fig. 5.34. Uniform cylindrical rotor in rigid end
bearings with mode shapes and critical speeds

Substituting gives

$$0 = A + C,$$

$$0 = -A + C,$$

$$0 = A\cos\lambda L + B\sin\lambda L + C\cosh\lambda L + D\sinh\lambda L,$$

$$0 = -A\cos\lambda L - B\sin\lambda L + C\cosh\lambda L + D\sinh\lambda L,$$

from which it follows that $A = C = 0$, and for nontrivial values of λL the characteristic equation for this system is

$$\sin\lambda L = 0.$$

This expression is satisfied when $\lambda L = n\pi$ ($n = 0, 1, 2 \ldots$). The critical speeds of this system can be found from

$$n\pi = \lambda L = \left(\frac{\rho A \omega^2}{EI}\right)^{1/4} L,$$

that is,

$$\omega = n^2 \left(\frac{\pi}{L}\right)^2 \left(\frac{EI}{\rho A}\right)^{1/2} \quad \text{rad/s)},$$

or

$$N_c = \frac{60}{2\pi} n^2 \left(\frac{\pi}{L}\right)^2 \left(\frac{EI}{\rho A}\right)^{1/2} \quad \text{(rpm)}.$$

At such speeds the mode shape is given by

$$r = B \sin \lambda z = B \sin \left(\frac{n\pi z}{L}\right) \qquad (n = 0, 1, 2 \dots).$$

Corresponding mode shapes and critical speeds are shown in Fig. 5.34 for this case. This example demonstrates that the normal modes for a rotor in rigid end bearings are composed of half sine waves, as expressed by the normal mode equation given above.

Uniform Cylindrical Rotor with Negligible Bearing Restraint

The boundary conditions for the system shown in Fig. 5.35 are as follows:

For $z = 0$,

$$M = -EI \frac{d^2 r}{dz^2} = 0$$

$$V = -EI \frac{d^3 r}{dz^3} = 0.$$

For $z = L$,

$$M = -EI \frac{d^2 r}{dz^2} = 0$$

$$V = -EI \frac{d^3 r}{dz^3} = 0.$$

(a) Uniform cylindrical rotor with negligible bearing restraint

(b) Mode 0 $f_0 = 0$ Hz

(c) Mode 1 $f_1 = \dfrac{1}{2\pi} \dfrac{(\lambda L)_1^2}{L^2} \left(\dfrac{EI}{\rho A}\right)^{\frac{1}{2}}$ Hz

(d) Mode 2 $f_2 = \dfrac{1}{2\pi} \dfrac{(\lambda L)_2^2}{L^2} \left(\dfrac{EI}{\rho A}\right)^{\frac{1}{2}}$ Hz

(e) Mode 3 $f_3 = \dfrac{1}{2\pi} \dfrac{(\lambda L)_3^2}{L^2} \left(\dfrac{EI}{\rho A}\right)^{\frac{1}{2}}$ Hz
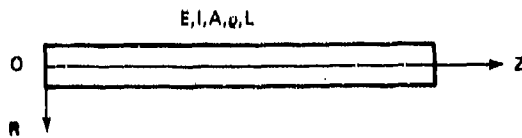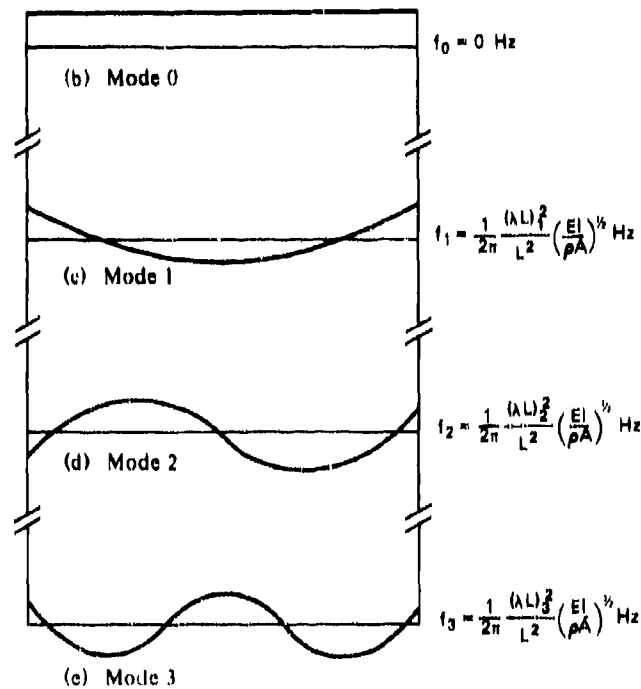
Fig. 5.35. Uniform cylindrical rotor with negligible bearing restraint,
and mode shapes and critical speeds for rotor

Substituting the first two conditions into the general modal expression
gives $B = D = 0$. The second two conditions give

$$A(-\cos \lambda L + \cosh \lambda L) + C(-\sin \lambda L + \sinh \lambda L) = 0$$

and

$$A(\sin \lambda L + \sinh \lambda L) + C(-\cos \lambda L + \cosh \lambda L) = 0.$$

The frequency equation is

$$\cos \lambda L \cosh \lambda L - 1 = 0,$$

which is satisfied when $\lambda L = 0.0, 4.730, 7.853, 10.996, \ldots$, or approximately when

$$\lambda L \approx \frac{2n + 1}{2} \pi \qquad (n \neq 0).$$

The normal modes for this case are given by

$$r = A (\cos \lambda z - \cosh \lambda z) + C (\sin \lambda z + \sinh \lambda z).$$

The mode shapes shown in Fig. 5.35 were determined by evaluating the ratio A/C from either of the two above expressions for a given value of λL and then substituting into the normal mode equation for this case. Finally, it is important to note that the lowest root $\lambda L = 0$ has a special significance in this case, that of a rigid-body whirl mode. The corresponding mode shape is found by observing that, on substituting this root into the equation of motion, we obtain

$$\frac{d^4 r}{dz} - \lambda^4 z = 0.$$

Integrating and substituting the above boundary conditions give

$$r = E + Fz,$$

which corresponds to a rigid-body whirl motion where E and F are integration constants. This feature has practical significance for rotors in very flexible bearings.

Uniform Cylindrical Rotor in Flexible End Bearings

This rotor operates in end bearings of identical stiffness K in all radial directions. As shown in Fig. 5.36a, the boundary conditions are as follows:
For $x = 0$,

$$M = - EI \frac{d^2 r_0}{dz^2} = 0,$$

$$S - Kr_0 = 0,$$

$$- EI \frac{d^3 r_0}{dz^3} - Kr_0 = 0 ;$$

(a) Uniform cylindrical rotor in flexible bearings

$$f_1 = \frac{1}{2\pi} \frac{(\lambda L)_1^2}{L^2} \left(\frac{EI}{\rho A}\right)^{1/2} Hz$$

(b) Mode 1

$$f_2 = \frac{1}{2\pi} \frac{(\lambda L)_2^2}{L^2} \left(\frac{EI}{\rho A}\right)^{1/2} Hz$$

(c) Mode 2

$$f_3 = \frac{1}{2\pi} \frac{(\lambda L)_3^2}{L^2} \left(\frac{EI}{\rho A}\right)^{1/2} Hz$$
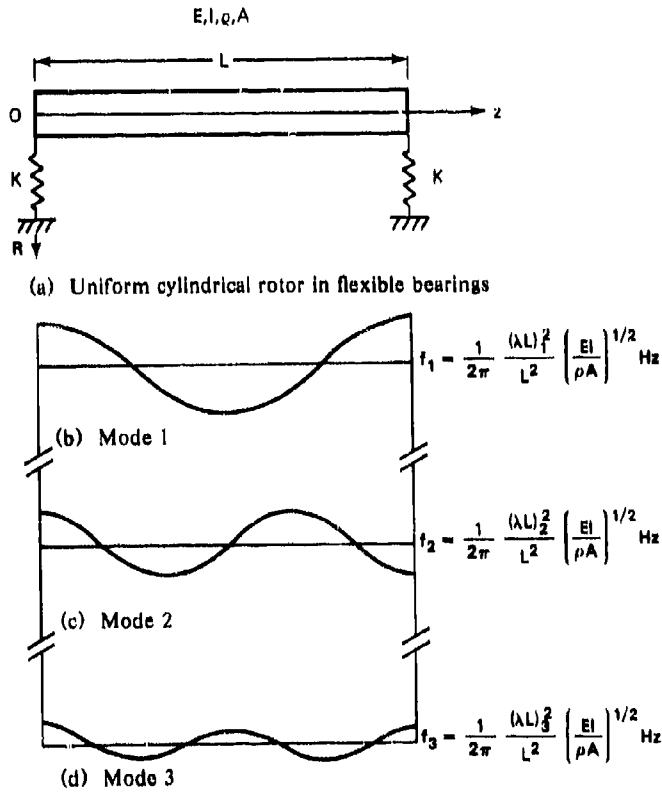
(d) Mode 3

Fig. 5.36. Uniform cylindrical rotor in flexible end bearings, and mode shapes and critical speeds for rotor

For $x = L$,

$$M = -EI \frac{dr_L^2}{dz^2} = 0,$$

$$-S - Kr_L = 0,$$

$$-EI \frac{d^3 r_L}{dz^3} + Kr_L = 0.$$

From the general solution

$$r = A \cos \lambda z + B \sin \lambda z + C \cosh \lambda z + D \sinh \lambda z,$$

and

$$\lambda^4 = \frac{\rho A \omega^2}{EI},$$

where A, B, C, and D are integration constants and other terms are as defined previously. Differentiating and substituting give the frequency determinant:

$$\begin{vmatrix} [\cos \lambda L - \cosh \lambda L + 2\bar{K} \sinh \lambda L] & [\sin \lambda L - \sinh \lambda L] \\[2ex] [-\sin \lambda L - \sinh \lambda L + \bar{K}(\cos \lambda L \\ + \cosh \lambda L) \\ + 2\bar{K} (\cosh \lambda L - \bar{K} \sinh \lambda L)] & [\cos \lambda L - \cosh \lambda L \\ \\ + \bar{K} (\sin \lambda L + \sinh \lambda L)] \end{vmatrix} = 0,$$

in which

$$\bar{K} = \frac{K}{EI\lambda^3}.$$

This expression reduces to

$$(\cos \lambda L \cosh \lambda L - 1) - 2\bar{K}(\cos \lambda L \sinh \lambda L - \sin \lambda L \cosh \lambda L)$$
$$- 2\bar{K}^2 \sin \lambda L \sinh \lambda L = 0.$$

The influence of the bearing-shaft stiffness ratio $\bar{K}$ on the first three eigenvalues of this expression is shown in Table 5.2.

Table 5.2. Variation of eigenvalues with stiffness ratio

$\bar{K}*$	Mode 1	Mode 2	Mode 3
0 (Free-free)	0	0	4.731
0.1	0.200	0.600	4.951
1.0	1.815	4.694	7.855
10	3.037	6.178	9.320
∞ (Pinned-pinned)	3.14159	6.28318	9.42477

$*\bar{K} = \dfrac{\text{bearing stiffness}}{\text{shaft stiffness}}$.

Mode shapes for the uniform rotor in flexible bearings are found by substituting the expressions for C and D in the general solution. This gives

$$r = A(\cos \lambda z + \cosh \lambda z - 2\bar{K} \sinh \lambda z) - B(\sin \lambda z + \sinh \lambda z)$$

and

$$J_i = \frac{r}{A} = \cos \lambda_i z + \cosh \lambda_i z - 2\bar{K} \sinh \lambda_i z - \frac{B}{A} (\sin \lambda_i z + \sinh \lambda z).$$

From Eq. (5.6),

$$\frac{B}{A} = \frac{\cos \lambda L - \cosh \lambda L + 2\bar{K} \sin \lambda L \sinh \lambda L}{\sin \lambda L - \sinh \lambda L}.$$

The normalized mode shapes J_i for any system with a specified value of $\bar{K}$ can be found by evaluating B/A for successive eigenvalues and then plotting values of the modal equation. For $\bar{K} = 1$, the following values apply.

Mode	(λL)	(B/A)
1	1.815	−1.192
2	4.694	+2.946
3	7.855	−1.001

The corresponding mode shapes are shown in Fig. 5.36.

5.7 Computer Analysis of Rotor-Bearing Systems

Nature of Analysis

In this section certain general results are developed through which the response of real rotors acting in real fluid-film bearings can be calculated. No new principle is involved, merely an efficient application of previous concepts using the Myklestad-Prohl recurrence formula. Very complex rotor systems are now routinely solved by this procedure, which forms the basis of most modern unbalance response computer programs.

The following types of rotor-response problem can be solved with existing programs:

1. General multimass, multibearing rotor, circular orbits, flexible damped pedestals, discrete foundation.

2. Same as item 1, except bearing properties in different coordinate directions are included. Elliptical orbits are obtained.

3. Same as item 2, with bearings set in a continuously flexible foundation. Known as a 'multi-level' problem.

The first type of analysis for a general rotor with circular whirl orbits will next be discussed.

Analysis Procedure

The following analysis is for the whirl amplitudes of a generalized unbalanced rotor in fluid-film bearings. The analysis takes into account the anisotropic stiffness and damping characteristics of the bearings causing the rotor whirl orbit to be elliptical. Furthermore, the gyroscopic moments of the rotor disks are included. The original analysis was given by Lund and Orcutt [32] in 1967, together with experimental verification as noted previously.

The rotor motion is defined in terms of the coordinate system shown in Fig. 5.37. The origin of the X and Y axes at any axial location coincides with the static deflection of the rotor, corrected at any given speed for the eccentricity of the journals in the bearings. Thus the rotor amplitudes are X and Y, the corresponding slope components are θ and ψ, and the bending moment and the shear force in the rotor are denoted by M and V, respectively. These have harmonically varying components M_x and M_y, and V_x and V_y, in the coordinate directions.
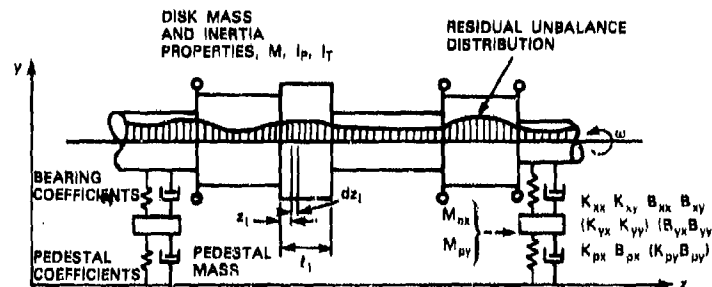
Fig. 5.37. Generalized rotor-bearing model

The rotor is represented as a series of mass-inertia stations, connected by cylindrical shafts of uniform cross section. Each station is assigned a mass m_n, a transverse mass moment of inertia I_{T_n}, a polar mass moment of inertia I_{p_n}, a bearing reaction, and an unbalance force. These unbalance forces are included by introducing two mutually perpendicular rotating axes in the rotor, denoted as the ξ-axis and the η-axis. The instantaneous angle between the ξ-axis and the x-axis is ωt, where ω is the angular speed of the rotor and t denotes time. The rotor unbalance can then be defined by its components U_ξ and U_η, and the corresponding forces, measured in the $X \cdot Y$ system, become

$$\omega^2 U_x = \omega^2 U_\xi \cos (\omega t) - \omega^2 U_\eta \sin (\omega t)$$

and

$$\omega^2 U_y = \omega^2 U_\xi \sin (\omega t) + \omega^2 U_\eta \cos (\omega t).$$

Considering the nth rotor station as shown in Fig. 5.37, a force balance and a moment balance yield

$$m_n \frac{d^2 X_n}{dt^2} = V_{xn} - V_{xn}' + \omega^2 U_{xn} - K_{xxn} X_n - B_{xxn} \frac{dX_n}{dt} - K_{xyn} Y_n - B_{xyn} \frac{dY_n}{dt},$$

$$m_n \frac{d^2 Y_n}{dt^2} = V_{yn} - V_{yn}' + \omega^2 U_{yn} - K_{yxn} X_n - B_{yxn} \frac{dX_n}{dt} - K_{yyn} Y_n - B_{yvn} \frac{dY_n}{dt},$$

$$I_{Tn} \frac{d^2 \theta_n}{dt^2} + \omega I_{Pn} \frac{d\phi_n}{dt} = M_{xn}' - M_{xn},$$

and (5.7)

$$I_{Tn} \frac{d^2 \phi_n}{dt} - \omega I_{Pn} \frac{d\theta_n}{dt} = M_{yn}' - M_{yn}.$$

The rotor is caused to vibrate by the unbalance forces at frequency ω. Since the vibration is harmonic, the amplitude, the slope, the bending moment, the shear force, and the unbalance can be expressed in complex notation:

$$X = \bar{x} e^{i\omega t}, \qquad M = \widehat{M} e^{i\omega t},$$

$$\theta = \bar{\theta} e^{i\omega t}, \qquad V = \bar{V} e^{i\omega t},$$

$$\omega^2 U_x = \omega^2 U e^{i\omega t}, \qquad \omega^2 U_y = - i\omega^2 U e^{i\omega t},$$

where $U = U_\xi + iU_\eta$, $\bar{x} = x_c + ix_s$, and so on, and only the real parts apply.

Similar definitions hold for the y-components. Further define

$$Z_{xx} = K_{xx} + i\omega B_{xx} \qquad (5.8)$$

and analogously for Z_{xy}, Z_{yx}, and Z_{yy}. With these definitions, and dropping the bar notation, Eqs. (5.7) become

$$V_{xn}' = V_{xn} + (\omega^2 m_n - Z_{xxn}) X_n - Z_{xyn} Y_n + \omega^2 U_n,$$

$$V_{yn}' = V_{yn} - Z_{yxn} X_n + (\omega^2 m_n - Z_{yyn}) Y_n - \omega^2 U_n, \qquad (5.9)$$

$$M_{xn}' = M_{xn} - \omega^2 I_{Tn} \theta_n + i\omega^2 I_{Pn} \phi_n,$$

and

$$M_{yn}' = M_{yn} - i\omega^2 I_{Pn} \theta_n - \omega^2 I_{Tn} \phi_n.$$

These equations express the change in shear force and bending moment across a rotor station.

The nth station is connected with the $(n + 1)$th station by a shaft section of length l_n with a cross-sectional area A_n, a cross-sectional moment of inertia I_n, and a cross-section shape factor α_n for shear deformation. The shaft material has a mass density ρ_n, Young's modulus E_n, and shear modulus G_n. Then, as shown in this section, it is possible to express x_{n+1}, θ_{n+1}, $M_{x,n+1}$, and $V_{x,n+1}$ as linear combinations of x_n, θ_n, M_{xn}', and V_{xn}' (the relationships for the y-components are analagous). The equations are given as Eqs. (5.19) in this section. The coefficients in the equations are functions of the shaft properties and the speed of the rotor. For simplicity, it is assumed that unbalance, rotatory inertia, and gyroscopic moments in the shaft can be ignored and that these effects instead are included at the rotor stations.

Equations (5.9) together with Eqs. (5.19) are a set of recurrence relationships from which the rotor amplitudes can be computed. If the rotor is assumed to have free ends, the bending moments and shear forces at the ends are zero:

$$M_{x1} = M_{y1} = V_{x1} = V_{y1} = 0$$

$$M_{xq}' = M_{yq}' = V_{xq}' = V_{yq}' = 0,$$

where station q is the last rotor station. If $x_1, y_1, \theta_1,$ and ψ_1 are selected as unknowns, repeated application of Eqs. (5.9) and (5.19) leads to:

$$\begin{Bmatrix} x_n \\ y_n \end{Bmatrix} = \{c_n\} \begin{Bmatrix} x_1 \\ y_1 \\ \theta_1 \\ \phi_1 \end{Bmatrix} + \begin{Bmatrix} c_{n15} \\ c_{n25} \end{Bmatrix}$$

and

$$
\begin{Bmatrix} M_{xq}{}' \\ M_{yq}{}' \\ V_{xq}{}' \\ V_{yq}{}' \end{Bmatrix} - (d) \begin{Bmatrix} x_1 \\ y_1 \\ \theta_1 \\ \phi_1 \end{Bmatrix} + \begin{Bmatrix} d_{15} \\ d_{25} \\ d_{35} \\ d_{45} \end{Bmatrix} = 0,
$$

where (c_n) is a 2×4 matrix and (d) is a 4×4 matrix. The matrix elements c_{nij} and d_{ij} are complex. They are found by performing a total of five rotor calculations. In the first calculation, set $x_1 = 1$ and $y_1 = \theta_1 = \phi_1 = U_n = 0$, whereby c_{n11}, c_{n21}, d_{11}, d_{21}, d_{31}, and d_{41} are obtained. Next, set $y_1 = 1$ and $x_1 = \theta_1 = \phi_1 = U_n = 0$ and determine the second columns of the matrices. In this way, all the coefficients are obtained. Solving Eqs. (5.9) for x_1, y_1, θ_1, and ϕ_1 allows computing x_n and y_n from Eq. (5.8) for all the rotor stations. Noting that, for x_n,

$$ x_n = x_{cn} + i x_{sn}, $$

$$ x_n = \bar{x}_n \, e^{i\omega t} = x_{cn} \cos (\omega t) - x_{sn} \sin (\omega t), $$

and similarly for y_n, the semiaxes and the orientation of the elliptical whirl orbit are calculated from

$$
a_n = \left\{ \frac{1}{2}(x_{cn}^2 + x_{sn}^2 + y_{cn}^2 + y_{sn}^2) \right.
$$

$$
\left. + \frac{1}{2}\left[(x_{cn}^2 + x_{sn}^2 - y_{cn}^2 - y_{sn}^2) + 4(x_{cn}y_{cn} + x_{sn}y_{sn})^2\right]^{1/2} \right\}^{1/2}
$$

$$
b_n = \frac{x_{sn}y_{cn} - x_{cn}y_{sn}}{a_n}
$$

$$
\gamma_n = \frac{1}{2}\tan^{-1}\left[\frac{2(x_{cn}y_{cn} + x_{sn}y_{sn})}{x_{cn}^2 + x_{sn}^2 - y_{cn}^2 - y_{sn}^2} \right],
$$

and

$$\psi_n = \frac{1}{2}\tan^{-1}\left[\frac{2(x_{cn}x_{sn} + y_{cn}y_{sn})}{x_{cn}^2 - x_{sn}^2 + y_{cn}^2 - y_{sn}^2}\right],$$

where a_n is the major semiaxis, b_n the minor semiaxis, γ_n the angle from the x-axis to the major semiaxis in the direction of rotor rotation, and ψ_n is the angle between the minor semiaxis and the y-axis in the direction of rotation. Thus γ_n and ψ_n represent the local phase angle. The definition of the phase angle is such that, if the x, y-coordinate system is rotated into the a_n, b_n system (i.e., x' is along the major semiaxis), then the rotor motion can be expressed as

$$x_n' = a_n \cos(\omega t + \psi_n)$$

and

$$y_n' = b_n \sin(\omega t + \psi_n).$$

If the value for the minor semiaxis is negative, the rotor precesses backward.

For those bearing types where $Z_{xx} = Z_{yy}$ and $Z_{xy} = -Z_{yx}$, it is seen from Eqs. (5.9) that

$$y = -ix, \qquad \phi = -i\theta.$$

In this instance, the whirl orbit is circular, and the outlined calculation procedure can be considerably simplified. This condition applies to the four-shoe tilting-pad bearings used by Lund and Orcutt in tests of this analysis.

Now consider a uniform shaft section. Relationships are established for the amplitude, slope, bending moment, and shear force at one end of the section in terms of the corresponding quantities at the other end.

Including shear deformation, the rotation θ of a shaft element becomes

$$\theta = \frac{V}{\alpha GA} + \frac{\partial x}{\partial z}$$

and similarly for the y-component, where G is the modulus of shear and α is a cross-sectional shape factor ($\alpha \simeq 0.75$ for a circular cross section). The bending equation is given by

$$M_x = EI \frac{\partial \theta}{\partial z}$$

and similarly for the y-component. When the shaft is subjected to unbalance forces per unit length of $\omega^2 u_x$ and $\omega^2 u_y$, a force balance yields

$$\rho A \frac{\partial^2 x}{\partial t^2} = - \frac{\partial V}{\partial z} + \omega^2 u_x,$$

and analogously for the y-direction. Finally, if the shaft has a transverse mass moment of inertia J_T per unit length and a polar mass moment of inertia J_P, a moment balance gives

$$J_T \frac{\partial^2 \theta}{\partial t^2} + \omega\, J_P \frac{\partial \phi}{\partial t} = \frac{\partial M_x}{\partial z} - V_x$$

and

$$J_T \frac{\partial^2 \phi}{\partial t^2} - \omega\, J_P \frac{\partial \theta}{\partial t} = \frac{\partial M_y}{\partial z} - V_y.$$

If the shaft section is assumed to have constant cross-sectional proper-ties, θ, ϕ, M, and V can be eliminated from the equations. In this way the equations governing the shaft motion become

$$EI\frac{\partial^4 x}{\partial z^4} - \rho I \left(\frac{E}{\alpha G} + \frac{J_T}{\rho I} \right) \frac{\partial^4 x}{\partial z^2 \partial t^2} + \rho A \frac{\partial^2 x}{\partial t^2} + \frac{\rho J_T}{\alpha G} \frac{\partial^4 x}{\partial t^4} - \omega J_P \frac{\partial^3 y}{\partial z^2 \partial t} + \frac{\omega \rho J_P}{\alpha G} \frac{\partial^3 y}{\partial t^3}$$

$$= \omega^2 \left[u_x + \frac{J_T}{\alpha GA} \frac{\partial^2 u_x}{\partial t^2} + \frac{\omega J_P}{\alpha GA} \frac{\partial u_y}{\partial t} - \frac{EI}{\alpha GA} \frac{\partial^2 u_x}{\partial z^2} \right]$$

and $\hspace{12cm}$ (5.14)

$$EI\frac{\partial^4 y}{\partial z^4} - \rho I \left(\frac{E}{\alpha G} + \frac{J_T}{\rho I} \right) \frac{\partial^4 y}{\partial z^2 \partial t^2} + \rho A \frac{\partial^2 y}{\partial t^2} + \frac{\rho J_T}{\alpha G} \frac{\partial^4 y}{\partial t^4} + \omega J_P \frac{\partial^3 x}{\partial z^2 \partial t} - \frac{\omega \rho J_P}{\alpha G} \frac{\partial^3 x}{\partial t^3}$$

$$= \omega^2 \left[u_y + \frac{J_T}{\alpha GA} \frac{\partial^2 u_y}{\partial t^2} - \frac{\omega J_P}{\alpha GA} \frac{\partial u_x}{\partial t} - \frac{EI}{\alpha GA} \frac{\partial^2 u_y}{\partial t^2} \right].$$

Since the analysis is restricted to forced vibrations with a frequency equal to the angular speed of the shaft ω, the following expressions

$$x = \bar{x}\, e^{i\omega t}$$

and

$$y = \bar{y}\, e^{i\omega t}$$

can be used for the coordinate displacements at any shaft cross-section, and similarly for the slope, the bending moment, and the shear force. Only the real part applies. Furthermore, setting

$$u_x = u\,e^{i\omega t}$$

results in $u_y = -\,i\,u\,e^{i\omega t}$. Thus Eqs. (5.14) can be written

$$EI\frac{d^4\bar{x}}{dz^4} + \omega^2\rho I\left[\frac{E}{\alpha G} + \frac{J_T}{\rho I}\right]\frac{d^2\bar{x}}{dz^2} - \omega^2\rho A\left[1 - \frac{\omega^2 J_T}{\alpha GA}\right]\bar{x}$$

$$\text{(5.15)}$$

$$- i\omega J_P\frac{d^2\bar{y}}{dz^2} - i\frac{\omega^4\rho J_P}{\alpha G}\bar{y} = \omega^2 u\left[1 + \frac{\omega^2(J_P - J_T)}{\alpha GA}\right] - \frac{\omega^2 EI}{\alpha GA}\frac{d^2 u}{dz^2},$$

$$EI\frac{d^4\bar{y}}{dz^4} + \omega^2\rho I\left[\frac{E}{\alpha G} + \frac{J_T}{\rho I}\right]\frac{d^2\bar{y}}{dz^2} - \omega^2\rho A\left[1 - \frac{\omega^2 J_T}{\alpha GA}\right]\bar{y}$$

$$\text{(5.16)}$$

$$+ i\omega^2 J_P\frac{d^2\bar{x}}{dz^2} + i\frac{\omega^4\rho J_P}{\alpha G}\bar{x} = - i\omega^2 u\left[1 + \frac{\omega^2(J_P - J_T)}{\alpha GA}\right] + i\frac{\omega^2 EI}{\alpha GA}\frac{d^2 u}{dz^2}.$$

Although these equations can be solved, the resulting solution is impractical. Instead, it will be assumed that the shaft section is free of unbalance forces ($u = 0$) and that the effect of rotatory inertia and gyroscopic moment can be neglected ($J_T = J_P = 0$). If these effects are significant, they can be accounted for with good accuracy by lumping them at the ends of the shaft section (i.e., at the rotor stations). It should be noted that, even though it is simple to keep the rotatory inertia terms in the foregoing equations, this is not permissible without also including the gyroscopic moments since they are of the same magnitude.

With these assumptions, Eqs. (5.15) and (5.16) become identical and it is necessary to consider only the first equation. The definitions

$$\lambda^4 = \left\{\frac{\rho A \omega^2}{EI}\right\}$$

$$\text{(5.17)}$$

as previously, and

$$\delta^2 = \frac{EI}{2\alpha GA}$$

are introduced. If we drop the bar notation and set $u = J_T = J_P = 0$, Eq. (5.15) becomes

$$\frac{d^4x}{dz^4} + 2\delta^2\lambda^4 \frac{d^2x}{dz^2} - \lambda^4 x = 0.$$

The characteristic equation has the roots $\pm\lambda_1$ and $\pm i\lambda_2$, where

$$\lambda_1 = \lambda\left\{[1 + (\delta\lambda)^4]^{1/2} - (\delta\lambda)^2\right\}^{1/2}$$

and

$$\lambda_2 = \lambda\left\{[1 + (\delta\lambda)^4]^{1/2} + (\delta\lambda)^2\right\}^{1/2}.$$

Hence the general solution can be written

$$x = C_1 \cosh(\lambda_1 z) + C_2 \sinh(\lambda_1 z) + C_3 \cos(\lambda_2 z) + C_4 \sin(\lambda_2 z), \quad (5.18)$$

where C_1 to C_4 are constants to be determined from the boundary conditions. Combining Eqs. (5.10) through (5.13) and setting $u = J_T = J_P = 0$ gives

$$\frac{l}{EI} M_x = (\lambda_2^2 - \lambda_1^2)x + \frac{d^2x}{dz^2},$$

$$V_x = \frac{dM_x}{dz},$$

$$\theta = \frac{(\lambda_2^2 - \lambda_1^2)}{\lambda^4} \frac{V_x}{EI} + \frac{dx}{dz}.$$

Substitution from Eq. (5.18) allows M_x, V_x, and θ to be found. Next, the four constants can be evaluated by setting, at $z = 0$,

$$x = x_n, \qquad \theta = \theta_n, \qquad M_x = M_{xn}', \qquad V_x = V_{xn}'.$$

At the other end of the shaft section, we set, at $z = l_n$,

$$x = x_{n+1}, \qquad \theta = \theta_{n+1}, \qquad M_x = M_{x,n+1}, \qquad V_x = V_{x,n+1}.$$

Thus the desired relationships become

$$x_{n+1} = a_{1n}x_n + l_n a_{3n}\theta_n + k_{2n}a_{4n}M_{xn}' + k_{3n}a_{7n}V_{xn}',$$

$$\theta_{n+1} = \frac{1}{3}\mu_n k_{2n}a_{5n}x_n + a_{2n}\theta_n + k_{1n}a_{6n}M_{xn}' + k_{2n}a_{4n}V_{xn}',$$

$$\tag{5.19}$$

$$M_{x,n+1} = \frac{1}{2}\mu_n l_n a_{4n}x_n + \frac{1}{6}\mu_n l_n^2 a_{5n}\theta_n + a_{2n}M_{xn}' + l_n a_{3n}V_{xn}',$$

and $\tag{5.19}$

$$V_{x,n+1} = \mu_n a_{3n}x_n + \frac{1}{2}\mu_n l_n a_{4n}\theta_n + \frac{1}{3}\mu_n k_{2n}a_{5n}M_{xn}' + a_{1n}V_{xn}',$$

where

$$a_{1n} = (\lambda_1^2 \cosh\beta_1 + \lambda_2^2\cos\beta_2)/(\lambda_1^2 + \lambda_2^2),$$

$$a_{2n} = (\lambda_2^2 \cosh\beta_1 + \lambda_1^2 \cos\beta_2)/(\lambda_1^2 + \lambda_2^2),$$

$$a_{3n} = (\lambda_1 \sinh\beta_1 + \lambda_2 \sin\beta_2)/(\lambda_1^2 + \lambda_2^2)l_n,$$

$$a_{4n} = 2(\cosh\beta_1 - \cos\beta_2)/(\lambda_1^2 + \lambda_2^2)l_n^2,$$

$$a_{5n} = 6(\lambda_2 \sinh\beta_1 - \lambda_1 \sin\beta_2)/(\lambda_1^2 + \lambda_2^2)\lambda^2 l_n^3,$$

$$a_{6n} = (\lambda_2^3 \sinh\beta_1 + \lambda_1^3 \sin\beta_2)/(\lambda_1^2 + \lambda_2^2)\lambda^2 l_n,$$

$$a_{7n} = 6(\lambda_1^3 \sinh\beta_1 - \lambda_2^3 \sin\beta_2)/(\lambda_1^2 + \lambda_2^2)\lambda^4 l_n^3,$$

$$k_{1n} = \frac{l_n}{EI},$$

$$k_{2n} = \frac{l_n^2}{2EI},$$

$$k_{3n} = \frac{l_n^3}{6EI},$$

$$\beta_1 = \lambda_1 l_n, \qquad \beta_2 = \lambda_2 l_n,$$

$$\mu_n = \omega^2 \rho A l_n.$$

It should be noted that k_{1n}, k_{2n}, and k_{3n} are the static influence coefficients, neglecting shear deformation. Furthermore, for sufficiently low speeds and a sufficient number of mass stations, the shear effect can be ignored and $\lambda \simeq 0$. Then, the coefficients a_{1n} to a_{7n} become equal to 1 and the shaft mass can be lumped with good approximation at the ends of the shaft section, setting $\mu_n = 0$ in the foregoing equations. In many practical cases, this will be sufficiently accurate.

5.8 References

1. V. Castelli and H. G. Elrod, "Solution of the Stability Problem for 360 Degree Self-Acting, Gas-Lubricated Bearings," *Trans. ASME, J. Basic Eng.,* Paper No. 64-LUB-10 (1964).
2. M. F. Giberson, General Electric Company Report, Generator Department, Schenectady, N.Y., May 1969.
3. E. J. Gunter, *Dynamic Stability of Rotor-Bearing System,* NASA SP-113, Office of Technical Utilization, U.S. Government Printing Office, Washington, D.C., 1966.
4. J. W. Lund, "Modal Response of a Flexible Rotor in Fluid-Film Bearings," ASME Paper No. 73-DET-98.
5. J. W. Lund, *Rotor-Bearing Dynamics Design Technology,* Part V: *Computer Program Manual for Rotor Response and Stability,* Technical Report AFAPL-TR-65-45, Air Force Aero Propulsion Laboratory, Wright-Patterson AFB, Ohio, May 1965.
6. J. W. Lund, "Stability and Damped Critical Speeds of a Flexible Rotor in Fluid-Film Bearings," *Trans. ASME,* Ser. B, *J. Eng. Ind.* 96, No. 2, 509–517 (1974).
7. P. G. Morton, "Analysis of Rotors Supported Upon Many Bearings," *J. Mech. Eng. Sci.* 14, No (1), 25–33 (1972).
8. P. G. Morton, "Measurement of the Dynamic Characteristics of a Large Sleeve Bearing," *Trans. ASME,* Paper No. 70-LUB-14, 1970.
9. J. F. Booker and R. L. Ruhl, "A Finite Element Model for Distributed Parameter Turborotor Systems," *Trans. ASME,* Ser. B, *J. Eng. Ind.* 94, 126–132 (1972).
10. C. B. Thomas and N. F. Rieger, "Dynamic Stiffness Matrix Approach for Rotor Bearing System Analysis," in *Proc. Inst. Mech. Eng. Conf. on Vibrations in Rotating Machinery,* Churchill College, Cambridge University, Sept. 1976.
11. P. C. Warner and R. J. Thoman, "Effect of the 150-Degree Partial Bearing on Rotor-Unbalance Vibration," ASME Paper 63-LUB-36, 1963.

12. S. Dunkerley, "Whirling and Vibration of Shafts," *Phil. Trans. Royal Soc. (London)*, **185A**, 279 (1894).

13. A. Stodola, *Steam and Gas Turbines*, McGraw-Hill, New York, 1927, Vols. I and II, pp. 491, 1122, 1125.

14. A. C. Hagg, "Some Vibration Aspects of Lubrication," *Lub. Engrg.*, 4 (4), 166—169 (Aug. 1948).

15. A. C. Hagg and S. O. Sankey, "Some Dynamic Properties of Oil-Film Journal Bearings wth Reference to the Unbalance Vibration of Rotors," *Trans. ASME, J. Appl. Mech.* 78, 302—306; AMR Vol. 9, *Review* 1665 (1956).

16. A. A. Raimondi and J. Boyd, "An Analysis of the Pivoted-Pad Journal Bearing," *Trans. ASME* 75, 380 (1953).

17. B. Sternlicht, "Stability and Dynamics of Rotors Supported on Fluid Film Bearings," ASME Paper No. 62-WA-190, 1963.

18. P. Lewis and S. B. Malanowski, *Rotor-Bearing Dynamics Design Technology Part IV; Ball Bearing Design Data*, Wright-Patterson AFB, Dayton, Ohio, Technical Report AFAPL-TR-65-45, 1965.

19. M. Elsermans, "Study and Contributions—Tapered Roller Bearing Stiffness and Load Distribution Under Combined Loading Misalignment," Ph.D. dissertation, Catholic University of Leuven, Leuven, Belgium, 1975.

20. J. W. Lund and B. Sternlicht, "Rotor-Bearing Dynamics with Emphasis on Attenuation," *Trans. ASME, J. Basic Engr.* 84 Ser. D (1962).

21. J. W. Lund and B. Sternlicht, *Bearing Attenuation*, General Electric Co., Technical Report Nobs 78930, Task 3679, Area F131105, General Engineering Laboratory, Schenectady, N.Y., 1961.

22. R. E. D. Bishop and A. G. Parkinson, "On the Isolation of Modes in the Balancing of Flexible Shafts," *Proc. Inst. Mech. Engr.* 177(16), 407 (1963).

23. L. S. Moore and E. G. Dodd, "Mass Balancing of Large Flexible Rotors," *G.E.C. J.* 31(2) (1964).

24. N. F. Rieger and R. H. Badgley, "Flexible Rotor Balancing of a High-Speed Gas Turbine Engine," SAE Paper No. 720-741, 1972.

25. N. F. Rieger, "Unbalance Response of an Elastic Rotor in Damped Flexible Bearings at Supercritical Speeds," *J. Engr. Power* 93, Ser. A, 265-278 (1971).

26. H. H. Jeffcott, "Lateral Vibration of Loaded Shafts in the Neighborhood of a Whirling Speed—The Effect of Want of Balance," *Phil. Mag.* **XLII**, 635 (1921).

27. E. Downham, *Some Preliminary Model Experiments on the Whirling of Shafts*, A.R.C. R and M No. 2768, 1953.

28. D. Robertson, "Hysteretic Influences on the Whirling of Rotors," *Proc. Inst., Mech. Engr.*, **131**, 513–537 (1935).

29. D. Robertson, "Transient Whirling of a Rotor," *Phil. Mag.*, Series 7, **20**, 793 (1935).

30. W. Kerr, "On the Whirling Speed of Loaded Shafts," *Engineering* (February 18, 1916).

31. N. F. Rieger, "Rotor-Bearing Systems," *Structural Mechanics Computer Programs*, University of Virginia Press, Charlottesville, Va., 1974, pp. 473–498.

32. J. W. Lund and F. K. Orcutt, "Calculations and Experiments on the Unbalance Response of a Flexible Rotor," *ASME Trans.*, **89**, Ser. B, 785–796 (1967).

33. J. W. S. Rayleigh, *Theory of Sound*, Dover, New York, 1945.

34. S. Timoshenko, *Vibration Problems in Engineering*, Van Nostrand Reinhold, New York, 1955.

35. L. Meirovitch, *Analytical Methods in Vibrations*, Macmillan, New York, 1967.

36. R. E. D. Bishop, "The Vibration of Rotating Shafts," *J. Mech. Engr. Sci.*, **1** (1) (1959).

37. G. M. L. Gladwell and R. E. D. Bishop, "The Vibration of Rotating Shafts Supported in Flexible Bearings," *J. Mech. Engr. Sci.*, **1** (3) (1959).

38. R. E. D. Bishop and G. M. L. Gladwell, "The Vibration and Balancing of the Unbalanced Flexible Rotor," *J. Mech. Engr. Sci.*, **1** (1) (1959).

39. R. E. D. Bishop and S. Mahalingham, "Some Experiments in the Vibration of a Rotating Shaft," *Proc. Roy. Soc. (London)*, **292**, Series A, 1 (1965).

CHAPTER 6
FLEXIBLE-ROTOR BALANCING

Nomenclature

a	mass eccentricity of local shaft c.g.
a	modal coefficient
a_{rs}	influence coefficient
a,b,c	sections of shaft span
A	cross section area
A	matrix of influence coefficients
B	number of bearings along the length of a rotor
B_i, B_e	internal, external damping coefficients
D	unbalance mass vector
E	modulus of elasticity
F	concentrated force
g	state vector for transfer matrix
i	$\sqrt{-1}$
I	second moment of area of shaft cross-section
j	modal equation
K	correction plane number
K_a, K_b	stiffness of end bearings
L	length between bearings
$m(z)$	axial distribution of mass along shaft
M_p	discrete unbalance mass
N	number of critical speeds within the operating speed range
N	rotor speed, rpm
P	bearing force
q	load per unit length
r	whirl radius at given shaft location, $= x + iy$
r	correction weight radius
r_p	unbalance eccentricity from local shaft centerline
T	trial unbalance weight
$u(z)$	distributed unbalance $= \rho A(z)a(z)$
U	residual unbalance in rotor
U_p	local unbalance at pth location

V vibration amplitude (peak-to-peak)

$\mathbf{V}$ vector of forced response measured at rotor supports

w lateral deflection of shaft

w rotor radial displacement

$\mathbf{w}$ unbalance vector

W balance weight

$\mathbf{W}$ calibration weight

x, y coordinate amplitudes of shaft deflection

$y_i(z)$ modal displacement coefficients

z axial coordinate along shaft

$\alpha(z)$ complex correction mass distribution

$\delta(z-z_p)$ Dirac delta function

Δ_j modal determinant

ζ shaft transverse displacement in rotating coordinates

η axial location factor for correction plane locations of class 2 rotor

ν, μ velocity damping ratios corresponding to B_1, B_e

ξ, η rotating coordinates of shaft center displacement during whirl

Ξ frequency function $= \omega/\omega_t$

ρ mass density of shaft $= w/g$

ϕ phase angle

$\phi_j(z)$ modal functions representing shaft transverse displacements

ω speed of rotation (influence coefficient method)

ω_j frequency of j th mode

Ω speed of rotation (modal method)

CHAPTER 6
FLEXIBLE-ROTOR BALANCING

6.1 Preliminary Considerations

Flexible rotors represent a special topic in balancing practice because of additional considerations raised by rotor flexure. Many flexible rotors are large and may rotate at high speeds; therefore, they can experience significant bending deformations along their length caused by interactions between the rotor residual unbalance and the rotor whirl modes. Bending deformations are usually largest in the vicinity of some flexural critical speed of the rotor system. Rotor deformations are speed-dependent in both magnitude and shape, and maximum modal amplitudes occur at resonant speeds. A given rotor may have several critical speeds within its operating range, and significant vibrations may occur at any of these speeds unless the rotor is adequately balanced.

To balance a flexible rotor requires cancelling the effects of its residual unbalance on all modes likely to cause rotor vibrations. Procedures that can be used to achieve multiplane corrections are described in this chapter. To select a suitable balancing procedure it is first necessary to know whether the rotor can be balanced adequately by the addition of correction weights in two correction planes, i.e., as a class 1 rigid rotor. For an unproven rotor type, a two-plane balance should first be attempted, in a low-speed balancer. If the rotor remains unacceptably out of balance at its operating speed after two-plane correction at low speed, the rotor is classified as a class 3 flexible rotor. If the residual unbalance is acceptable for operation, the rotor needs no further correction and is classified as a class 2 quasi-flexible rotor. This category includes rotors that experience some bending but remain in satisfactory balance after being corrected as rigid rotors. Other special types of flexible rotors—for example, impellers with long flexible blades and high-constant-speed armatures—can also be balanced in two correction planes for satisfactory operation with low transmitted-force levels. These rotors are respectively class 4 and class 5 flexible rotors.

Class 3 flexible rotors require multiplane balancing to operate smoothly. They commonly have one or more critical speeds within their operating range, with uncorrected mode shapes that may involve substantial bending of the rotor. Excitation of these modes by the rotor

residual unbalance may lead to noticeable (or even dangerous) transmitted vibrations, unless the rotor is balanced by some effective multiplane balancing procedure. The rotor must be balanced in such a manner that correction weights added in the balance will effectively cancel all rotor unbalance effects within the operating range.

Commonly used methods for multiplane balancing of flexible rotors are

1. Various iterative modal methods (Lindsay, others)
2. Modal averaging method (Moore, Bishop)
3. Comprehensive modal method (Kellenberger, Federn)
4. Influence coefficient method (Goodman, others).

Each method is described in this chapter. Also included is a discussion of experiences, from the published literature, associated with the use of each method. Each method has the following qualifications:

1. It is a general balancing procedure, i.e., capable of balancing any flexible rotor.
2. It has been verified in practice on real rotors.
3. It is supported by significant published literature.

There is at present some controversy concerning the various methods used in multiplane balancing. It centers around the need to remove the rigid-body modes before multiplane balancing. This leads to the larger question as to the "best" balancing method. Present information suggests that there is no simple answer to this question. The practical answer must always consider the availability of the requisite operator skills, the availability of suitable instrumentation, and the number of repetitions needed to balance the rotor to a degree that is suited to the application involved, in addition to considering which multiplane algorithm should be used.

Factors Affecting Flexible-Rotor Balance

This section discusses various questions that must be decided before attempting to balance a flexible rotor. Many of these questions can be answered from previous experience with related equipment or with similar types of equipment. Some are related to facility scheduling demands.

Type of rotor. Rotor size, speed, and previous operational characteristics determine the type of balance facility required. A small rotor may be shop-balanced in its casing; a large rotor will require special supports to simulate field conditions in the spin pit. Rotor type also determines the planes available for balancing.

Class of rotor. All rotors are now readily classified for balancing, according to ISO procedures [1]. The prescribed rotor classes in [1] give guidance based on experience and indicate the type of balance generally needed. This helps to decide on the facilities required, the number of planes, the number of balance speeds, and so on.

Balancing facility. Small flexible rotors are balanced either in their casings or in a balancing machine. Medium or large flexible rotors are prebalanced in a balance facility (machine or spin pit) and/or at the site. Low-speed balancing may also be prescribed as part of the prebalancing preparation.

Onsite balancing. Onsite balancing is usually a final trim-balance operation. If there are severe unbalance problems, such as after initial construction or repair, shop balancing in a machine or in a facility may be required.

Correction method. A variety of proven flexible-rotor balancing methods are in use. The method used depends on rotor size, speed, number of planes, plane accessibility, field requirements (such as easy trim balancing and rotor handling facilities), access to a computer and personal preferences.

Low-speed balancing. Comprehensive modal balancing requires a low-speed balance; pure modal balancing does not, nor does the modal averaging method or the influence coefficient method. The decision whether or not to balance at low speed depends on the dynamics of the rotor system. The closer the system resembles a flexible rotor in rigid bearings at its operating speed, the less significant is the low-speed balance requirement for smooth operation.

Correction planes. The number of correction planes required depends on the balancing method selected. Pure modal balancing and influence coefficient balancing usually require $N + 1$ planes, where N is the number of critical speeds in the operating range. The extra plane is for residual unbalance effects from critical speeds outside the operating range. The comprehensive modal method requires at least $N + 2$ planes for N flexural critical speeds and two additional planes for low-speed balancing. Additional planes may be required for any significant critical speeds beyond the operating range.

Correction speeds. Balance corrections are usually defined near each critical speed and also at the operating speed. This helps in deciding how many measurements must be taken in relation to the balancing method being used.

Measurement locations. Measurement locations are primarily determined by rotor accessibility. Certain generator rotors can be balanced using only pedestal-mounted accelerometers. Centrifugal compressors may require shaft-displacement sensors (rigid casing) plus one or more

midspan probes, depending on the number of critical speeds influencing the rotor operating range.

Instrumentation. Many types of instruments may be used in balancing: accelerometers, proximity sensors, velocity probes, tracking filters, spectrum plotters, tape recorders, etc. Good diagnostic instruments such as accurate signal filters and phase meters assist the balancing procedure. It is also necessary to know whether the shaft will be stable in its bearings. Tape-stored balance data from similar machines or from previous balance runs provide helpful guidance.

Trial runs. The number of trial runs must be minimized consistent with balance accuracy and production demands. Ultimately, flexible-rotor methods will seek an optimum balance quality with a minimum of efficient data-taking and data-processing effort.

Preliminary analysis. For new rotors, calculated estimates of damped critical speeds, damped mode shapes (with plots), and stability threshold speed should be regarded as mandatory basic information before balancing. Unbalance response data give additional guidance, and any likely instability problems should be anticipated in advance, rather than being discovered on the test stand. For repaired or rebalanced rotors, these data, together with a log of previous balancing experiences on present and similar rotors, should be available for reference, preferably in computer files.

Balance quality. Guidelines for setting acceptable balance quality criteria are now available for all rotor classes from ISO documents 1940 and 5343 [1,2]. Balance quality and acceptable operating vibration levels should conform to these standards and should be agreed to before rotor balancing, as a basis for machine acceptance.

6.2 Modal Balancing

Modal Properties of Rotors

Modal balancing is a process by which the principal modal responses of a rotor in bearings are corrected in succession, to remove any undesirably large rotor whirl amplitudes. As the rotor modes are orthogonal, any mode that is removed by balancing cannot cause vibrations at any other speed, provided it is not reintroduced (reexcited) by the balance-correction weights of some other mode. This general procedure is demonstrated in the examples that follow.

Consider a uniform cylindrical rotor in rigid end bearings, with the normal modes shown in Fig. 6.1. For convenience assume that these modes occur in the same radial plane. Only the mode shapes and the

(a) Rotor and first modal
component of unbalance

(b) Normal modes

(c) Amplitude buildup in region
of first critical speed

(d) Decreased amplitudes after
addition of correction weight
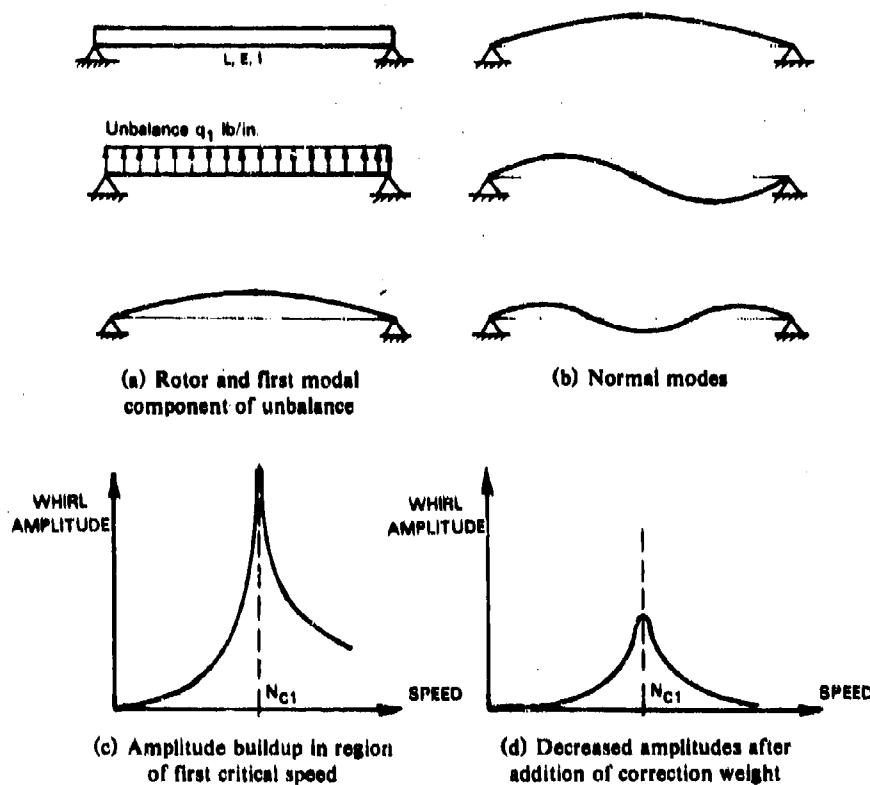
Fig. 6.1. Unbalance effects on first mode of rotor

location of the correction planes are important. Let the modal distribution of unbalance in the first mode be as shown in Fig. 6.1a. This distribution will cause rotor whirl amplitudes to build up in the first mode as the first critical speed is approached, as shown in Fig. 6.1c.

It is evident that the addition of a balance weight of suitable magnitude at rotor midspan, oriented 180° from the direction of the unbalance force, is capable of eliminating the rotor midspan whirl amplitude. It should also cause near-zero amplitudes to develop elsewhere on the rotor, as shown in Fig. 6.1d.

If the rotor midspan deflection in mode 1 under the uniform unbalance q_1 oz in./in. shown is w_1, the required balance load is found by setting

$$w_1 = \frac{5q_1L^4}{384EI}$$

for the unbalance deflection at rotor midspan, and

$$w_1' = -\frac{F_1 L^3}{48EI}$$

for the correction-weight effect on the deflection at midspan. Then for zero midspan deflection,

$$w_1 - w_1' = 0,$$

and thus

$$F_1 = \frac{5}{8} q_1 L.$$

Next, let the modal distribution of unbalance in the second mode be as shown in Fig. 6.2. This distribution will excite the second mode, and the required correction force for zero deflection at the quarter-span points can be found by setting

$$w_2 = \frac{5q_2(L/2)^4}{384EI}$$

for the original unbalance deflection and

$$w_2' = -\frac{F_2(L/2)^3}{48EI}$$

for the balance-force deflection. Thus, for zero quarter-span deflection under this load,

$$F_2 = \frac{5}{16} q_2 L.$$
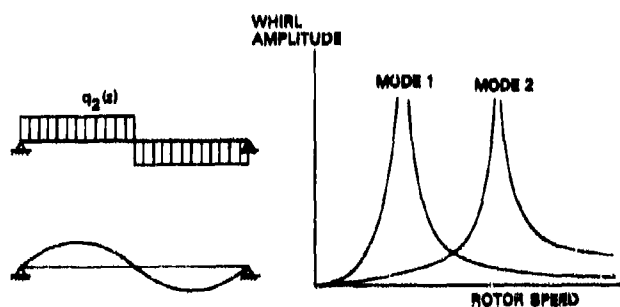
Fig. 6.2. Modal unbalance and its effects on the second mode of rotor

Similar conditions apply for the third mode: for the unbalance distribution shown in Fig. 6.3, the third-mode shape will be excited and
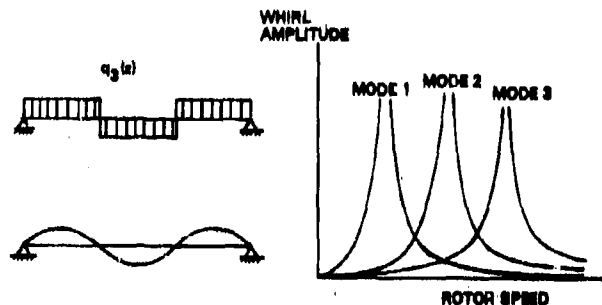
Fig. 6.3. Modal unbalance effects on the third mode of rotor

the required balance force for zero deflection at the one-sixth-span points is

$$F_3 = \frac{5}{24} \, q_3 L.$$

The modal method of balancing is to select a distribution of the required correction weights such that individual modes will be suppressed by these corrections and not be reintroduced by similar effects from other modes. For the example this can be accomplished as shown in Fig. 6.4.* First, mode 1 is removed by applying the F_1 correction at midspan. This leaves only small residual first-mode displacements along the rotor, as noted above. Next, mode 2 is removed by applying F_2 as a couple at the two quarter-span points to oppose the unbalance distribution of the second mode. This does not reintroduce mode 1 since there is no resultant force; the two F_2 values, being equal and opposite, cancel each other out. Only minor residual deflections then remain from the difference between the uniform residual unbalance and the point loads that balance the shaft in these modes.

Mode 3 must be balanced in a slightly different manner. If F_3 is set to counteract the residual unbalance shown over each one-third of the total span, the third mode will be suppressed in the manner described for modes 1 and 2. However, mode 1 would be reintroduced with a $+F_3$, $-F_3$, $+F_3$ arrangement, due to resultant of $+F_3$. Mode 2 would not be reintroduced because of the symmetry of the balance couple. The force summation for mode 3 is

$$q_3 \frac{L}{3} - q_3 \frac{L}{3} + q_3 \frac{L}{3} + F_3 - F_3 + F_3 = 0,$$

---

*The influence of the axial location of the correction planes on the correction mass values is discussed later in this section.

(a) First mode correction
at $z = L/2$

(b) Second mode corrections
at $z = L/4$, $z = 3L/4$

(c) Third mode corrections
at $z = L/6$, $z = L/2$, $z = 5L/6$
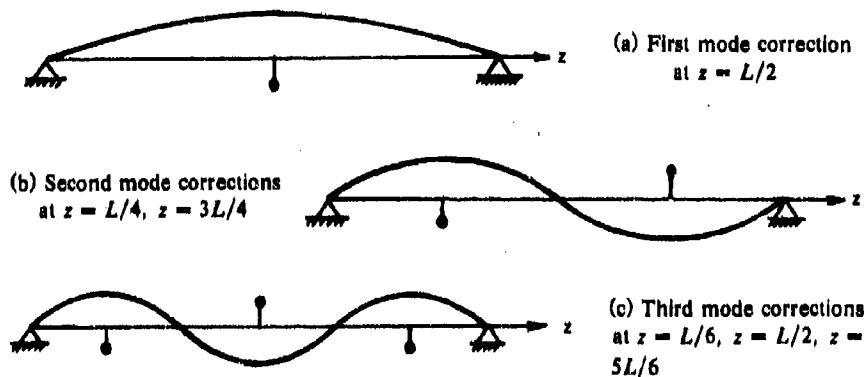
Fig. 6.4. Modal balancing theory of balance-weight distribution

but, considering the radial force balance,

$$F_3 - F_3 + F_3 = + F_3.$$

Thus there is a residual radial force that could excite mode 1. This force can be removed by making $F_3 = q_3 L/4$ and by placing two balancing forces F_3 at the midspan and two at the one-sixth-span points. Then we have

$$q_3 \frac{L}{3} - q_3 \frac{L}{3} + q_3 \frac{L}{3} + F_3 - 2F_3 + F_3 = 0$$

$$F_3 - 2F_3 + F_3 = 0.$$

As shown in Fig. 6.5, the balance thus obtained for mode 3 is effective, but not perfect.

In practice it is desirable to minimize the number of balance planes used. Thus, for the example presented, it would be preferable to use only three correction planes (excluding for the present any other factors, such as lack of suitable access to the rotor, that may preclude the use of a specific location) to correct the first three modes of the rotor. Furthermore, it is usually preferable to locate certain correction planes fairly close to the ends of the rotor—but usually not at a bearing location since the least effect is achieved where modal amplitudes are small.

Many end-bearing rotors are of the "generator" type shown in Fig. 6.5, with correction planes at the ends of the large-diameter section. It is informative to reconsider the above discussion of modal balancing in terms of such a rotor. The objective is to obtain a modal balance of the generator rotor with a minimum number of correction planes. Consider first a rotor with rigid bearings and principal modes as shown in Fig. 6.5.

(a) Generator rotor in rigid bearings with three
    correction planes
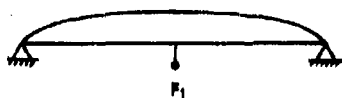
(b) Balance weight in midspan plane balances
    the lowest mode

(c) Balance weights in end planes balance second
    mode without disturbing first mode

F_2

F_2 $\Sigma F_2 = 0$

$2F_3$

F_3 F_3

$\Sigma F_3 = 0$, $\Sigma M_3 = 0$
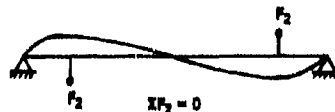
(d) Balance weights in end and mid-planes
    balance third mode without disturbing first
    and second modes

Fig. 6.5. Modal balance of the first three mdoes of generator rotor

The procedure is the same as that described previously. The
second mode has the condition that the sum of the radial forces must
equal zero, $\Sigma F_2 = 0$, so that the first mode will not be reexcited. The
third mode has the conditions $\Sigma F_3 = 0$ and $\Sigma M_3 = 0$, so that neither
the first nor the second mode is reexcited. The magnitude of the bal-
ance weights must be chosen to achieve the above conditions. In prac-
tice it is necessary to know the magnitude and the form of the mode
shapes. This is best done by directly measuring the rotor amplitudes,
where possible. Another procedure is to make a computer calculation
of the mode shapes, with spot checks on the machine to verify the rela-
tive proportions.

To demonstrate how the correction weights must be adjusted in
accordance with the plane location, assume that the modal loops are
half-sine waves and that the end balance planes coincide with the one-
sixth-span points along the rotor length (Fig. 6.6). The balance weights
will have their maximum effect at the crests of the loops and zero effect
at the nodes. Thus, moving the F_2 weight from $L/4$ to $L/6$ reduces its
effectiveness from 1.0 to 0.866, that is, from $\sin(\pi/2)$ to $\sin(\pi/3)$.
Thus, as the weight is moved from $L/4$ to $L/6$, its size must be
increased by the inverse of this proportion to achieve the same effect as
F_2 at $L/4$.

The influence of bearing flexibility is shown in Fig. 6.7. For
demonstration purposes, sine-wave modes have been assumed, together

(a) General location of balance planes for
first three modes

(b) Most effective location of balance
weights for second-mode correction

(c) Most effective location of balance
weights for third-mode correction

$w_{23} = \dfrac{\sqrt{3}}{2} w_2$ in second mode

$F_{23} = \dfrac{2}{\sqrt{3}} F_2$ for same effect at reduced
amplitude, w_{23}. Larger balance
weight needed at location A than
location B.
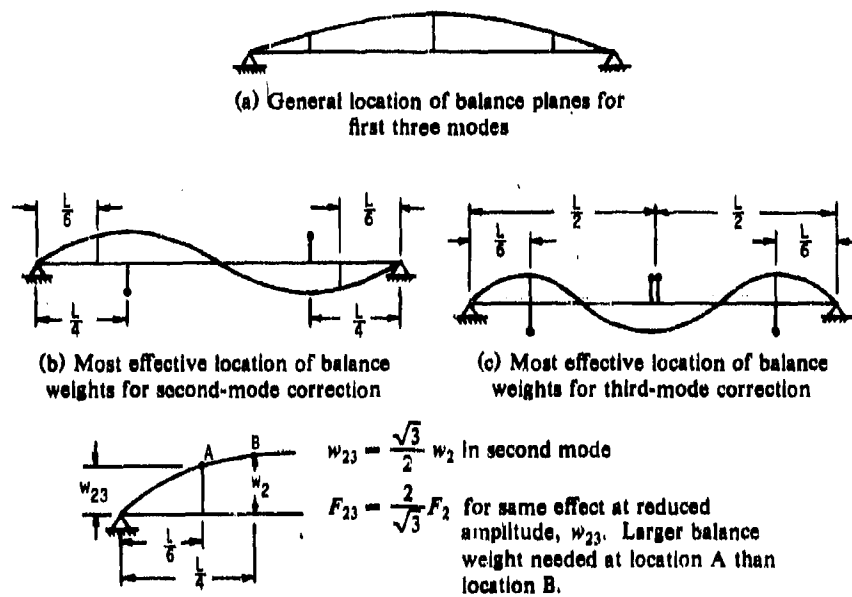
Fig. 6.6. Balance weight adjustment to compensate for reduced effectiveness.

(a) First mode with midplane
balance weight

(b) Second mode with endplane
balance weights

(c) Third mode with endplane and
midplane balance weights
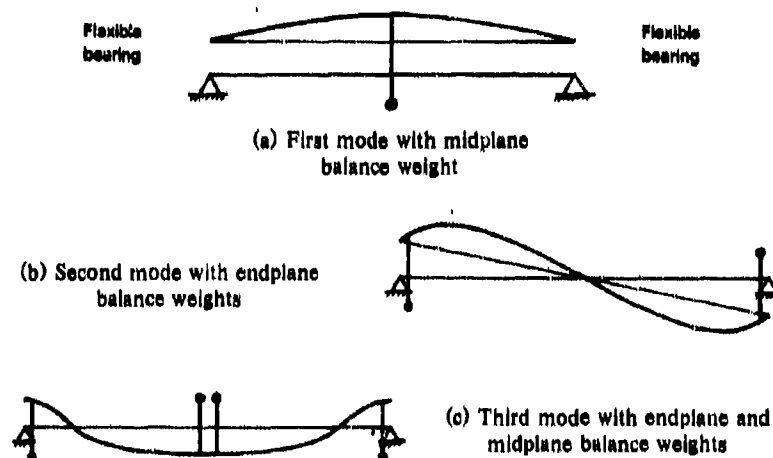
Fig. 6.7. Flexible rotor in flexible bearings: balance at first, second, and third
modes at ends and at midplane

with bearing flexibilities equal to rotor flexibility at maximum deflection. The mode shapes will then be as shown. Note that the third mode has nodes close ($0.21L$ and $0.79L$) to the crests of the second-mode loops ($0.25L$ and $0.75L$). Unless a five-plane balance is required, it is necessary to define end balance planes close to the bearings, where both the second and third modes show significant modal amplitudes, simultaneously (in space). The first mode remains unaffected.

The adjusted magnitudes of the balance weights are then as follows:

Mode 1: Unaffected; F_1 as found originally.

Mode 2: At modal crests, amplitudes $= 0.5 + 1.0 = 1.5$. At $0.05L$, modal amplitude $= 0.95 + 0.3 = 1.2$ and

$$F_2^1 = \frac{1.5}{1.2}F_2 = 1.25\ F_2,$$

that is, F_2^1 must be 25% greater than the corresponding F_2 for a rigid-bearing rotor that is balanced at the quarter-span points. The F_2 weights must again conform to the conditions $\Sigma F_2 = 0$ to avoid reexciting the first mode.

Mode 3: Balance weights near ends, $0.05L$ and $0.95L$, and at midspan. Proportions $+F_3$, $-2F_3$, $+F_3$. The F_3 weights must again conform to the force condition $\Sigma F_3 = 0$ and to the moment condition $\Sigma M_3 = 0$ about the node of mode 2.

As a final example, consider a two-bearing generator with a heavy overhung coupling shaft (Fig. 6.8). The modes are found (by measurement in a spin pit or by calculation) to be those shown. A three-plane balance is desired.

The first step is to select the balance-plane locations. To facilitate field balancing, these planes will be located in the generator end planes and in the coupling (no generator midplane correction). It will first be shown how a rough first mode may result from an inappropriate distribution of correction weights between the modes; how this condition can be improved will next be shown.

First, mode 1 is balanced with weights in planes 1 and 2. These can have any desired relative proportioning, but usually equal in-phase weights would be chosen, as shown. Next, mode 2 is balanced with equal and opposite weights in the generator end planes. Finally, an attempt is made to balance mode 3 in the generator end planes and at the coupling, so that $\Sigma F_3 = 0$ and $\Sigma M_3 = 0$. The latter conditions determine the magnitude of the correction weights (see Fig. 6.8). The weight distribution shown will balance mode 3, but it will also *reexcite* mode 1. This is because a resultant force
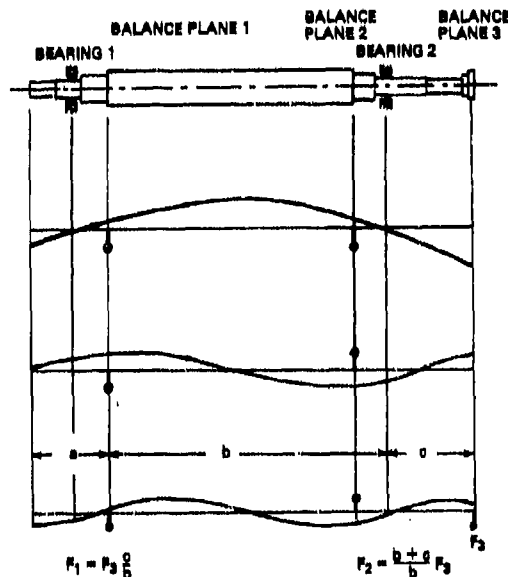
Fig. 6.8. Modal balance leaving a rough first mode
in generator rotor

$$F_3 \frac{c}{b} - F_3 \frac{b+c}{b} = -F_3$$

acts on the first loop of mode 1 (Fig. 6.8a) and a force $+F_3$ acts at the coupling on the second loop of mode 1. *These forces tend to develop mode 1 amplitudes even though they are equal and opposite.*

To avoid such a situation, an alternative balancing procedure can be used. Mode 1 is balanced as shown in Fig. 6.9, using plane 1 and plane 3. Next, mode 2 is balanced in planes 1 and 2, so that $\Sigma F_2 = 0$, that is $F_{21} = F_{22}$.

Mode 3 is next balanced in planes 1 and 3 only, with both corrections acting in the same direction. For the modal amplitudes shown, of approximately equal magnitude, this is sufficient to balance mode 3. The effect on mode 2 is to introduce additional correction forces to counteract the mode 2 amplitudes. This additional balance effect should be considered in establishing the mode 2 correction weights. The effect on mode 1 is to introduce two opposing forces that will cancel each other if the condition

$$w_{11} F_{31} = w_{13} F_{33}$$

is satisfied, w_{11} being the amplitude in mode 1 at plane 1 and w_{13} the amplitude at plane 3 in mode 1.
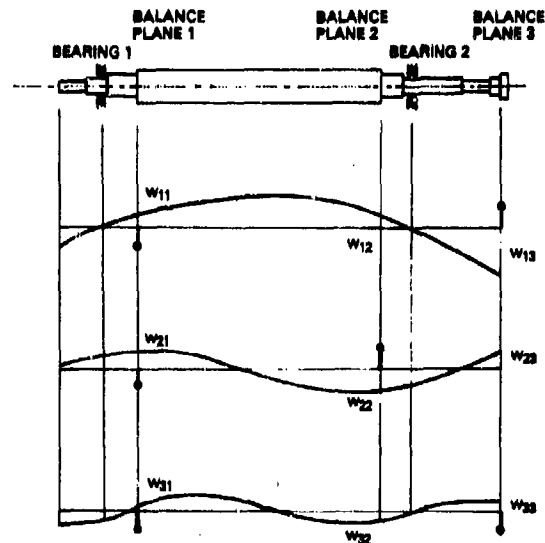
Fig. 6.9. Modal balance to minimize re-excitation of the
first mode by effective distribution of weights in the third
mode

This example shows that any procedure for balancing flexible
rotors becomes more difficult to use when the balancing planes are re-
stricted to practical locations and also when the rotor has flexible bear-
ings and adjacent rotor spans or shaft overhangs. Some knowledge of
the rotor modes is always required in advance; it can be acquired in
practice either by direct measurement (though this is inconvenient and
time consuming and requires good speed control and tracking filters),
by computer calculation with adequate knowledge of the relevant bear-
ing dynamic properties, from previous experience with similar rotor
systems, or, ideally, by all of these methods.

Theory of Modal Balancing

The theory of modal balancing has been discussed by Bishop and
co-workers [3—5] Federn [6], Miwa [7], and others. The discussion
that follows is based on the works of Bishop, Gladwell, and Parkinson.
The objective of the theory presented in this section is to provide a
theoretical basis for the normal mode analysis of shaft dynamics as a
preparation for the various modal balancing methods described later.

It is shown in Chapter 5 that the synchronous whirling induced in
a section of a uniform circular shaft by mass unbalance can be
described in rotating coordinates by the equations

$$\ddot{\xi} - (\xi + a_r)\Omega^2 - 2\Omega\dot{\eta} = - \frac{EI}{A\rho} \frac{\partial^4\xi}{\partial z^4} - \frac{B_i\dot{\xi}}{A\rho} - \frac{B_e}{A\rho} (\dot{\xi} - \Omega\eta)$$

and

$$\ddot{\eta} - (\eta + a_s)\Omega^2 + 2\Omega\dot{\xi} = - \frac{EI}{A\rho} \frac{\partial^4\eta}{\partial z^4} - \frac{B_i\dot{\eta}}{A\rho} - \frac{B_e}{A\rho} (\dot{\eta} + \Omega\xi),$$

where

ξ, η = rotating coordinates shown in Fig. 5.33

a_r, a_s = coordinates of mass unbalance from shaft axis

Ω = speed of rotation

EI = flexural stiffness

$A\rho$ = mass per unit length

B_i, B_e = internal and external damping coefficients

z = shaft axial coordinate.

These expressions can be reduced to a single equation in terms of the complex whirl radius ζ by writing

$$\zeta = \xi + i\eta \qquad i = \sqrt{-1},$$

$$a = a_r + ia_s$$

$$B_i = 2\nu\omega A\rho,$$

and

$$B_e = 2\mu\omega A\rho,$$

where ν and μ are velocity damping ratios and ω is the frequency of shaft vibration. Substitution gives

$$\ddot{\zeta} + 2[(\nu + \mu)\omega + i\Omega]\dot{\zeta} + \frac{EI}{A\rho} \zeta^{IV} - (\Omega^2 - 2i\mu\omega\Omega)\zeta = \Omega^2 a.$$

To solve this equation, introduce the substitutions

$$r = \zeta e^{i\Omega t}, \quad \zeta = re^{-i\Omega t}$$

and $r = x + iy$. The motion of the shaft referred to nonrotating axes is thus found to be

$$\ddot{r} + 2(\nu + \mu)\omega\dot{r} + \frac{EI}{A\rho} r^{IV} - 2i\nu\omega\Omega r = \Omega^2 a e^{i\Omega t}.$$

This equation may be solved by the normal mode method. This method is well suited to shaft balancing analysis, as the shaft critical speeds are discrete modes of the rotor and may be corrected in

sequence. To proceed, we first express the mass eccentricity a in the form of a modal series:

$$a = a(z) = a_1 \phi_1(z) + a_2 \phi_2(z) + \ldots = \sum_{j=1}^{\infty} a_j \phi_j(z),$$

where the $a_j = a_j^R + i a_j^I$ are complex coefficients and the $\phi_j(z)$ terms are characteristic functions of the shaft. Next write the complex displacement ζ as the series

$$\zeta = \zeta(z,t) = \zeta_1(t) \phi_1(z) + \zeta_2(t) \phi_2(z) + \ldots = \sum_{j=1}^{\infty} \zeta_j(t) \phi_j(z),$$

where the $\zeta_j = \zeta_j^R + i\zeta_j^I$ are complex coefficients and the $\phi_j(z)$ are again the characteristic functions of the shaft. Recalling the property of characteristic functions that

$$\frac{EI}{A\rho} \phi_j^{IV}(z) = \omega_j^2 \phi_j(z)$$

and substituting this property and the above series into the ζ-equation of motion gives the set of independent modal equations

$$\ddot{\zeta}_j + 2[(\nu_j + \mu_j)\omega_j + i\Omega]\dot{\zeta}_j + (\omega_j^2 - \Omega^2 + 2i\mu_j\omega_j\Omega)\zeta_j = \Omega^2 a_j,$$

where ν_j and μ_j are the modal damping ratios and ω_j is the jth natural frequency of free undamped flexural vibration. Bishop and Gladwell [3] have commented that, because the coordinates ζ_j remain independent both with and without damping, the mode shapes with shaft damping are the same as those for the undamped modes. It should be noted, however, that different conditions may apply when damping is imposed by the boundary conditions. The equations may then be decoupled only under certain circumstances: see Meirovitch [8] for a discussion of this topic.

The solution of each separate modal equation consists of a complementary function plus a particular integral. If only the forced-response case is considered, the solution for the jth mode is

$$\zeta_j = \frac{a_j\Omega^2}{(\omega_j^2 - \Omega^2) + 2i\mu_j\omega_j\Omega} = \frac{a_j\Omega^2 e^{-i\theta_j}}{[(\omega_j^2 - \Omega^2)^2 + 4(\mu_j\omega_j\Omega)^2]^{1/2}}$$

and

$$\theta_j = \arctan\left[\frac{2\mu_j\omega_j\Omega}{\omega_j^2 - \Omega^2}\right].$$

In nonrotating coordinates, the above transforms to

$$r_j = \frac{a_j \Omega^2 e^{i\Omega t}}{(\omega_j^2 - \Omega^2) + 2i\mu_j\omega_j\Omega} = \frac{a_j \Omega^2 e^{i(\Omega t - \epsilon_j)}}{[(\omega_j^2 - \Omega^2)^2 + 4(\mu_j\omega_j\Omega)^2]^{1/2}}$$

and

$$r_j = x_j + iy_j$$

with the appropriate components.

It remains to evaluate the a_j modal unbalance terms in the above result. To do this multiply the $a(z)$ series by the kth characteristic function:

$$a(z)\,\phi_k(z) = \sum_{j=1}^{\infty} a_j\,\phi_j(z)\,\phi_k(z).$$

Integrating over the shaft section gives

$$\int_0^L a(z)\,\phi_k(z)\;dz = \sum_{j=1}^{\infty} a_j \int_0^L \phi_j(z)\,\phi_k(z)\;dz.$$

For $j \neq k$, the orthogonality principle gives

$$\int_0^L \phi_j(z)\,\phi_k(z)\;dz = 0$$

and for $j = k$,

$$\int_0^L \phi_j(z)\,\phi_k(z)\;dz = \int_0^L [\phi_j(z)]^2\;dz = Z.$$

Thus

$$a_j = \frac{\int_0^L a(z)\,\phi_j(z)\;dz}{\int_0^L [\phi_j(z)]^2\;dz} = \frac{1}{Z}\int_0^L a(z)\,\phi_j(z)\;dz.$$

Tables of results for a_j for several unbalance distributions are given by Miwa [7].

The unbalance effects of any concentrated load (e.g., disk unbalance, correction weights) can also be resolved as a modal series. First, we write the pth discrete unbalance as

$$U_p = M_p a_p$$

and then

$$U_p = U_p \delta(z - z_p),$$

where $\delta(z - z_p)$ is the Dirac delta function, defined as follows:

$$\delta(z - z_p) = \begin{cases} 0, & (z \neq z_p) \\ \infty, & (z = z_p) \end{cases}$$

and

$$\int_0^L \delta(z - z_p) \, dz = \begin{cases} 1, & z_p \in [0,L] \\ 0, & z_p \notin [0,L] \end{cases}.$$

The modal components of such discrete forces are found by writing

$$M_p a_{p,j} = M_p \sum a_j \phi_j(z) = U_p \delta(z - z_p).$$

Multiplying through by the qth modal function $\phi_q(z)$ and integrating over the length of the shaft section gives

$$a_{p,j} = \frac{U_p}{M_p} \frac{\int_0^L \phi_p(z) \delta(z - z_p) \, dz}{\int_0^L [\phi_p(z)]^2 \, dz} = \frac{U_p \phi_j(z_p)}{M_p Z}.$$

The $a_{p,j}$ value is the jth component of the pth discrete unbalance. Similar relations will apply for any other discrete force applied to the shaft.

Bishop and Gladwell [3] state that the two objectives of rigid-rotor low-speed balancing are, first, "to ensure that the center of mass of the rotor lies on the centerline of the bearings so that no net force is applied to the shaft due to centrifugal action." This condition requires that

$$\int_0^L A\rho \, a(z) \Omega^2 \, dz = 0,$$

where $a(z)$ is the vector distribution of unbalance along the rotor. If this condition is to be met, correction masses can be added, and the first balance condition becomes

$$\int_0^L A\rho \, a(z) \Omega^2 \, dz + \sum_{p=1}^2 M_p r_p \Omega^2 = 0,$$

where M_p is the mass and r_p is the radius of the pth balance correction. For two-plane balancing, $p = 2$.

The second purpose of low-speed balancing is to ensure "that the rotating shaft does not transmit to its bearings a rotating couple—due to centrifugal action." For a balanced rotor this requires that

$$\int_0^L A\rho \, a(z) \Omega^2 z \, dz = 0.$$

If balance corrections are required, the couple balance condition is

$$\int_0^L A\rho \, a(z) \Omega^2 z \, dz + \sum_{p=1}^{2} M_p r_p(z_k) \Omega^2 z_k = 0.$$

It should be noted that the unbalance distribution $a(z)$ along the rotor will be changed to $\alpha(z)$ when unbalances U_p act on the rotor. Likewise, each modal component will then have an unbalance acting on that mode:

$$\alpha_j(z) = a_j(z) + \frac{U_p}{M_p Z} \phi_j(z).$$

Bishop and Gladwell [3] have shown that, if the balanced mass distribution is written as the complex vector $\alpha(z)$, the new modal series for the rotor unbalance is

$$\alpha(z) = \sum_{j=1}^{\infty} \left[a_j + \frac{M_1 r_1}{A\rho Z} \phi_j(z_1) + \frac{M_2 r_2}{A\rho Z} \phi_j(z_2) \right] \phi_j(z),$$

where a_j and r_1, r_2 are complex quantities as mentioned previously. This modification of the unbalance distribution will affect the rotor response in all modes because of the addition of low-speed corrections. The previous balance conditions can now be written as

$$\sum_{j=1}^{\infty} A_j \alpha_j(z) = 0,$$

where

$$A_j = \int_0^L \phi_j(z) \, dz,$$

and

$$\sum_{j=1}^{\infty} B_j \alpha_j(z) = 0,$$

where

$$B_j = \int_0^L z \phi_j(z) \, dz.$$

The quantities A_j and B_j can be evaluated for each rotor system. For a pinned-pinned shaft, the characteristic equation is

$$\phi_j(z) = \sin \frac{j\pi z}{L}$$

and thus

$$A_j = \begin{Bmatrix} 0 \\ \dfrac{2L}{\pi j} \end{Bmatrix} \qquad B_j = \begin{Bmatrix} -\dfrac{L^2}{\pi j} \\ +\dfrac{L^2}{\pi j} \end{Bmatrix}.$$

Substituting gives the balance conditions

$$\sum_{j=1}^{\infty} A_j \alpha_j(z) = \alpha_1 - \frac{1}{3}\alpha_3 + \frac{1}{5}\alpha_5 + \dots \quad \text{(odd modes)}$$

and

$$\sum_{j=1}^{\infty} B_j \alpha_j(z) = \frac{1}{2}\alpha_2 + \frac{1}{4}\alpha_4 + \frac{1}{6}\alpha_6 + \dots \quad \text{(even modes)}.$$

Bishop and Gladwell [3] have commented that, where a rotor is balanced as a rigid body though it is experiencing flexure, the above result shows that some residual modal unbalance may still exist, even in the rigid-body modes. This unbalance may also be felt in the higher flexural modes where its effect may be quite substantial, unless some appropriate form of flexible-rotor balancing is subsequently applied to these modes. This point is illustrated in Fig. 6.10.

The conditions for modal balancing of flexible rotors can now be discussed using the above developments as an introduction.

Method of Bishop, Gladwell, and Parkinson

The following modal procedure was first developed by Bishop and Gladwell [3]. Additional aspects have since been developed by Bishop, Gladwell, and Parkinson [4, 5, 9—11]. The literature on modal balancing has been discussed by Bishop and Parkinson [12], Parkinson [13], and Rieger [14]. The modal procedure specified by these authors is as follows:

1. Locate the plane of the shaft radial deflection in the first whirl mode, slightly below the first critical speed. This can be done either by using x, y displacment sensors to measure shaft motions, by pedestal transducers, or by any suitable method of identifying the angular position of the shaft runout.

(a) Rotor in rigid end bearings

(b) Mass axis and flexural axis of given uncorrected rotor

(c) Mass axis after low-speed balancing

(d) Deformation at speed approaching first flexural critic

(e) Deformation at speed approaching third flexural critical speed
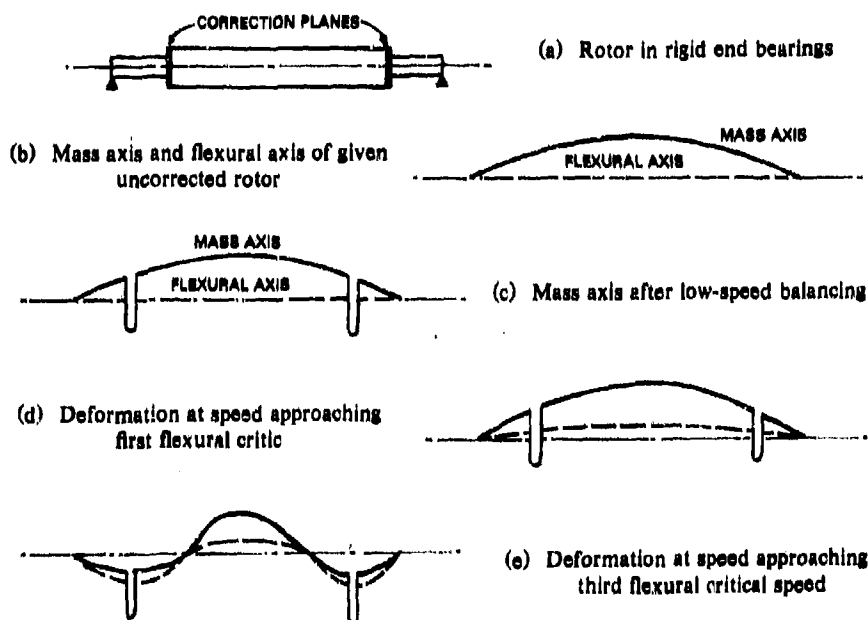
Fig. 6.10. Influence of rigid-rotor corrections on flexural modes. After Bishop and Gladwell [3]. Used by permission.

2. Add calibrating weights to the shaft in the plane of maximum shaft runout to determine the magnitude of the first-mode unbalance. These weights should be so located that they cancel the effect of the original first-mode unbalance. They should be placed close to the maximum modal amplitude location to minimize the size of the calibration weight required.

3. Add correction masses that cancel the first-mode unbalance. The conditions for achieving this are given later in this section. Since the correction masses should not excite other modes, they should be inserted at shaft axial locations where the amplitudes of other modes are small or zero (e.g., at the nodes of other modes). The first mode has been completely balanced when the unbalance distribution lies on the shaft flexural centerline for this mode and no forces are transmitted to the supports.

4. The second mode is next balanced by the same procedure. The angular position of the plane of maximum runout in the second mode is determined by running the rotor close to (but below) the second critical speed. Second-mode correction plane locations are selected so that the required balance conditions may be satisfied with minimal excitation of other shaft modes.

5. Second-mode calibration is then undertaken with a pair of calibration masses, subject to certain modal conditions mentioned below. The calibration masses are installed 180° apart around the circumference of the shaft, in two correction planes a specified distance apart. Both calibration weights are positioned so that their effect is to reduce the modal unbalance and shaft runout. The size of each calibration mass is again influenced by the amount of modal participation occurring at the prescribed calibration location.

6. Second-mode correction masses are added to cancel the second-mode unbalance. These corrections are added in two planes, at axial positions that are most effective in canceling the second mode. The second mode has been completely balanced when its modal unbalance component lies on the shaft flexural centerline, when no forces are transmitted to the bearings, and when no adjacent mode has been excited by the second-mode corrections.

7. The third mode is then balanced in the same manner. The plane of maximum runout is determined for the third mode. Correction planes are selected into which balance masses can be inserted effectively for the third mode, and which are least likely to excite shaft response in the other modes.

8. The third mode is calibrated with three masses inserted in the selected correction planes. The relative proportions of these masses are given later in this section. Each mass is inserted in the correction planes at 180° to its neighbors and at 180° to the angular position of maximum runout.

9. Balance corrections are added to cancel the effects of third-mode unbalance in the selected correction planes. The third mode has been completely balanced when its unbalance lies on the shaft flexural axis for this mode, when no forces are transmitted to the bearings, and when no adjacent mode has been excited by the chosen disposition of correction masses.

10. The fourth and higher modes now remain to be balanced by the same procedure.

Analytically, the conditions for balancing a rotor in the above modal sequence are outlined below.

First mode

Force equilibrium is given by

$$a_1 + \frac{m_1 r}{A \rho Z} \phi_1(z_1) = 0,$$

where a_1 is the first-mode unbalance, m_1 is the first-mode correction mass, and $\phi_1(z)$ is the first-mode participation factor. For the first mode of the simply supported shaft shown in Fig. 6.11, $\phi_1(z) = 1$ at $z = L/2$. In practice a_1 is unknown and is found by trial and error using the calibration-weight procedure. The quantity $\phi_1(z)$ is also unknown; it can be estimated from experience or calculated. To minimize m_1, it is desirable to maximize $\phi_1(z)$.

The first-mode balance correction is therefore

$$m_1 r_1 = a_1 \frac{A \rho Z}{\phi_1(z_1)}$$

at 180° from the maximum runout amplitude.
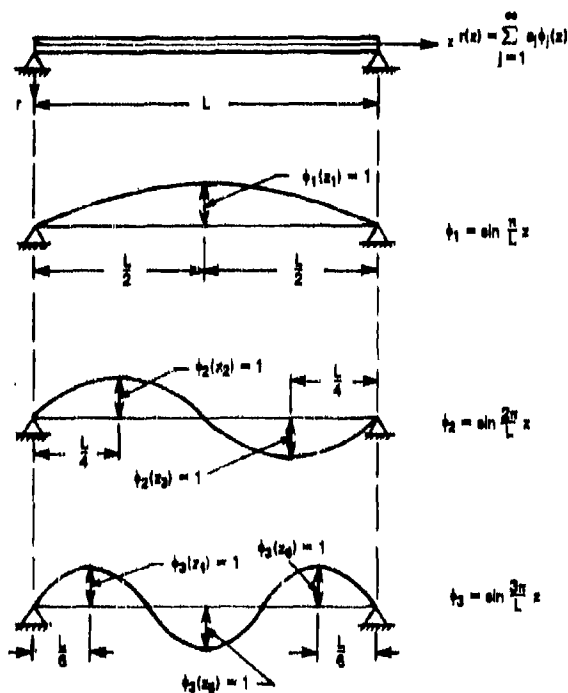
Fig. 6.11. Values of characteristic functions in the first three modes

Now $m_1 r_1$ is placed at the node of the second mode, where $a_2 \phi_2(z) = 0$. The second mode will then be unaffected by this first-mode correction.

Second mode

The force equilibrium condition is

$$a_2 + \frac{m_2 r}{A\rho Z} \phi_2(z_2) + \frac{m_3 r}{A\rho Z} \phi_2(z_3) = 0,$$

where a_2 is the second-mode unbalance, m_2 and m_3 are the second-mode correction masses, and $\phi_2(z_2)$ and $\phi_2(z_3)$ are the second-mode participation factors. The condition for the first mode not to be affected by second-mode balance is

$$m_2\phi_1(z_2) + m_3\phi_1(z_3) = 0,$$

and the second-mode corrections are found from

$$\begin{bmatrix} \phi_1(z_2) & \phi_1(z_3) \\ \phi_2(z_2) & \phi_2(z_3) \end{bmatrix} \begin{Bmatrix} m_1 r \\ m_2 r \end{Bmatrix} = A\rho Z \begin{Bmatrix} 0 \\ -a \end{Bmatrix},$$

which gives

$$\begin{Bmatrix} m_1 r \\ m_2 r \end{Bmatrix} = a_2 \frac{A\rho Z}{\Delta_2} \begin{Bmatrix} \phi_1(z_3) \\ \phi_2(z_3) \end{Bmatrix},$$

Δ_2 being the determinant of the $\phi(z)$ matrix.

The condition for no singularities to exist in the correction mass values is

$$\Delta_2 = \begin{vmatrix} \phi_1(z_2) & \phi_1(z_3) \\ \phi_2(z_2) & \phi_2(z_3) \end{vmatrix} \neq 0.$$

Third mode

The force equilibrium condition is

$$a_3 + \frac{m_4 r}{A\rho Z}\phi_3(z_4) + \frac{m_5 r}{A\rho Z}\phi_3(z_5) + \frac{m_6 r}{A\rho Z}\phi_3(z_6) = 0,$$

where the symbols correspond to those given previously.

The condition for the first mode not to be affected by third-mode balance is

$$m_4\phi_1(z_4) + m_5\phi_1(z_5) + m_6\phi_1(z_6) = 0,$$

the condition for the second mode not to be affected by third-mode balance is

$$m_4\phi_2(z_4) + m_5\phi_2(z_5) + m_6\phi_2(z_6) = 0,$$

and the condition for no singularities to exist in the balance details selected is

$$\Delta_3 = \begin{vmatrix} \phi_1(z_4) & \phi_1(z_5) & \phi_1(z_6) \\ \phi_2(z_4) & \phi_2(z_5) & \phi_2(z_6) \\ \phi_3(z_4) & \phi_3(z_5) & \phi_3(z_6) \end{vmatrix} \neq 0.$$

The third-mode corrections are found in the manner described:

$$\begin{Bmatrix} m_4 r \\ m_5 r \\ m_6 r \end{Bmatrix} = a_3 \frac{A\rho Z}{\Delta_3} \begin{Bmatrix} -\phi_1(z_5)\,\phi_2(z_6) + \phi_2(z_5)\,\phi_1(z_6) \\ \phi_1(z_4)\,\phi_2(z_6) - \phi_2(z_4)\,\phi_1(z_6) \\ -\phi_1(z_4)\,\phi_2(z_5) + \phi_2(z_4)\,\phi_1(z_5) \end{Bmatrix}$$

Fourth and higher modes can be balanced by applying the procedures demonstrated above.

Bishop and co-workers, notably Parkinson, have extended this procedure to deal with many additional aspects of flexible-rotor balancing (see, for example, Refs. 10, 11, 15, and 16). The modal balancing procedure has been applied to industrial practice by L. S. Moore and E. G. Dodd [18]. At present, the *analytical* procedures described above do not form the basis of any balancing algorithm or technique in use, though with a dedicated minicomputer it should be possible to use the analytical procedures of Bishop et al. to balance industrial rotors.* The steps given therefore serve mainly to validate the mechanics of the proposed modal balancing process and to provide a set of basic guidelines for practical rotor balancing (which Moore has utilized). As Bishop et al. have indicated, certain practical questions still remain concerning definition of the precise location of each modal unbalance, since measurement errors always exert a strong influence on the quality of the balance obtained.† Knowledge of the shaft modes, and of the influence of

---

*Kendig [17] has programmed these procedures and has investigated their use on typical industrial rotors via computer studies.
†Identification of maximum runout locations is now a minor problem when modern instrumentation (sensors, tracking filters, digital readout) is used.

damping on these modes, is usually needed for selecting the correction planes, for selecting the $\phi(z)$ values, and for evaluating the Z integral. Time-efficient trial-weight procedures and modal data acquisition procedures are also needed for any production balancing method. Weight-traversing methods and multiprobe observations of modes are now too inefficient for modern flexible-rotor balancing.

The section that follows describes the practical procedures for modal balancing developed by L. S. Moore.

Practical Modal Balancing

The application of modal balancing to large industrial rotors has been described by Moore and Dodd [18,19] and by Moore [20,21]. The procedures developed by these authors depend on modal principles and are quite simple in application. The methods described here have been applied to rotors with overhangs and couplings, supported near their ends in bearings with both stiffness and damping properties. Such rotors may be class 2 or class 3 flexible rotors. The modes encountered during operation with such rotors will be similar to those shown in Fig. 6.12.
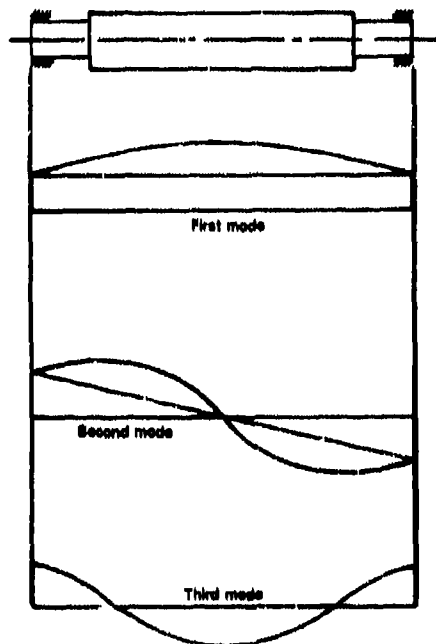
Fig. 6.12. Class 2 or class 3 rotors in bearings: typical mode shapes consisting of both rigid-body and flexural effects

It is important to recognize that the modes shown in Fig. 6.12 apply with minor variations to all two-bearing rotors. The effectiveness of the modal methods described by Moore and Dodd depends on an understanding of these modes and on the positioning of correction weights for maximum effectiveness at locations where other modes have nodes, or may be counterbalanced out.

Simple Procedure for Flexible-Rotor Balancing. Consider first the modal balancing of the single-disk flexible-shaft rotor shown in Fig. 6.13. For simplicity, let the bearings be radially rigid. This rotor can be balanced in its lowest flexural mode, Fig. 6.13b, using either accelerometers mounted on the bearing pedestals or proximity sensors that observe shaft motions (e.g., near the disk). The balancing procedure is as follows:

1. Run the rotor up to some speed below but close to the first critical speed at which safe, measurable vibration amplitudes occur. Record the vibration amplitude w_0 and its phase angle ϕ_0.

(a) Flexible single disk rotor

(b) First flexural mode

(c) Phase reference
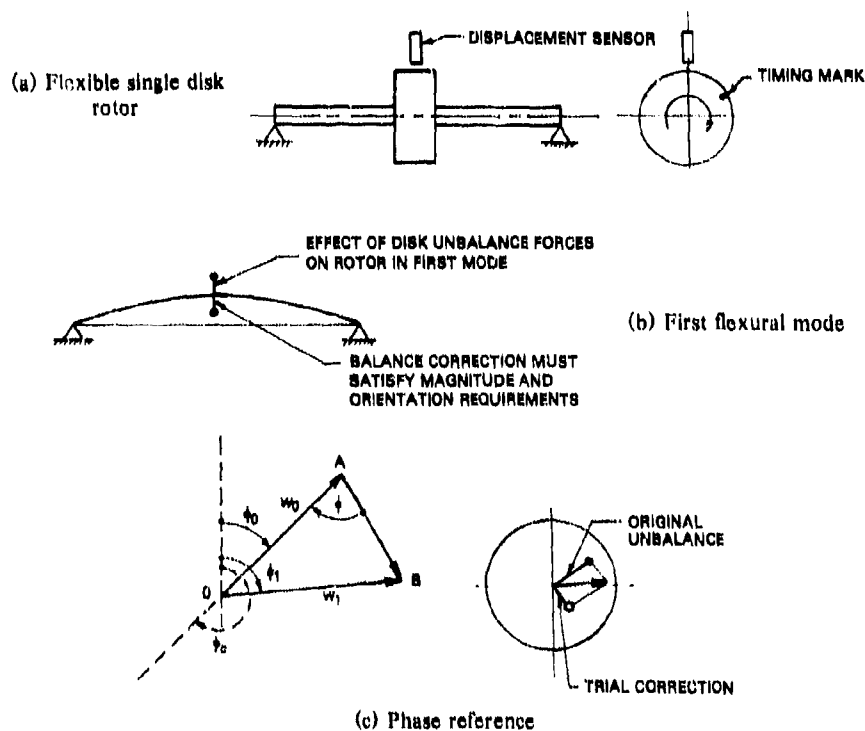
Fig. 6.13. Practical modal balancing procedure for flexible single-disk rotor

2. Stop the rotor and insert a small known weight W (oz) in the disk at a given radius r (in.) such that $Wr = T$ (oz-in.). This will provide a known calibrating unbalance.

3. Rerun the rotor with its calibrating unbalance at the same speed, and measure the vibration amplitude w_1 and phase angle ϕ_1 relative to the same datum.

4. Plot both unbalance vectors to some convenient scale as shown in Fig. 6.13c. Here **OA** represents the original unbalance and **OB** represents the original unbalance plus the correction weight. The vector **AB** then represents the effect of the calibrating unbalance in amplitude and phase at the chosen scale.

5. Calibrate the original unbalance vector by the ratio

$$U = OA = \frac{OA}{AB} T \quad \text{oz-in.}$$

6. The orientation of the trial weight AB to the original unbalance OA is angle OAB.

7. The magnitude of the required balance-correction weight is therefore

$$C = U = \frac{OA}{AB} T \quad \text{oz-in.}$$

8. The angular position of the required correction weight is at

$$\phi_C = 180 + \phi_0 \quad \text{(deg)}$$

to the phase reference datum i.e., at $\phi = 180 - $ angle OAB degrees ahead of its present location, as shown in Fig. 6.13.

The rotor in this example could therefore be balanced by the installation of a correction weight of C oz-in. at an angle OAB degrees ahead of the calibration weight location.

Industrial Rotor Without Modal Coupling. Next consider the balancing of the symmetrical rotor shown in Fig. 6.14 in its lowest flexural mode. For shop balancing the rotor should be mounted in bearings and pedestals that simulate onsite conditions as much as possible. Where balancing is performed at the site, no support problem arises, but if the balance is performed in a shop facility, the type of bearing supports described in Section 3.5 should be provided. The required steps are as follows.

1. Run the rotor at some convenient speed near its first critical speed to magnify the vibrations in this mode. Record the synchronous vibration amplitude w_0 and relative phase angle ϕ_0, as described previously. Assume for now that identical readings are obtained at either pedestal.

(a) Correction of first flexural mode

(b) Correction of second flexural mode
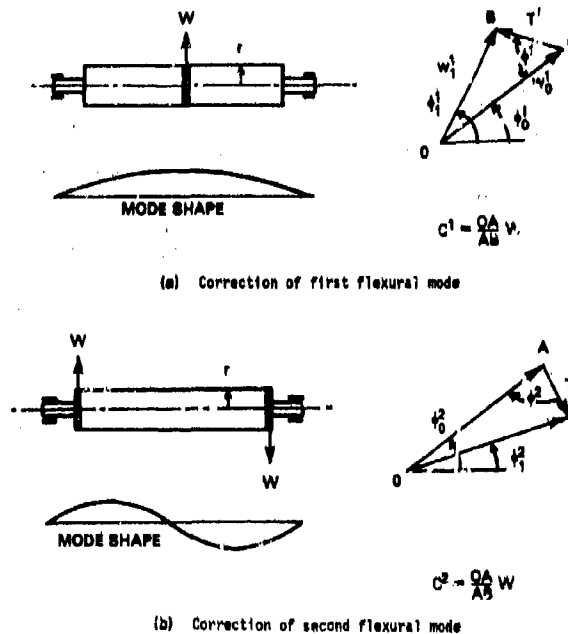
Fig. 6.14. Correction of flexural modes for symmetrical roto.

2. Add a single calibrating weight W oz at a radius r in a correction plane near the rotor midspan. Again record the rotor synchronous vibration amplitude w_1 and phase angle ϕ_1.

3. Plot the original unbalance vector w_1^1 = **OA** and the original-plus-calibration unbalance vector w_2^1 = **OB** to a convenient scale as shown in Fig. 6.14. The effect of the calibration weight is the vector **AB** = T^1.

4. Determine the first-mode balance correction weight,

$$C^1 = \frac{\mathbf{OA}}{\mathbf{AB}}\ W\ \text{oz.}$$

5. Determine the required angular adjustment of the first-mode correction: ϕ^1 = angle OAB degrees circumferentially forward from the location of the calibration weight.

On inserting the required correction weight C at the calibration radius r at midspan, the rotor will be balanced in its first flexural mode. Approximately the same correction would be determined from transducer measurements at either pedestal. Some small residual vibration

would remain after balancing, primarily from the second mode and possibly from higher modes also. The second mode is now balanced by running the rotor sufficiently close to its second flexural critical speed. Vibration and phase readings are taken at both pedestals. Again, if these readings are assumed to be symmetrical, the second-mode correction is obtained as follows:

1. Measure the vibration amplitude w_0^2 and phase ϕ_0^2 on a bearing cap.

2. Insert a pair of calibration weights W in planes located near the ends of the rotor but on opposite sides to form an unbalance calibration couple.

3. Rerun the rotor near its second critical speed and again measure the vibration amplitude w_1^2 and phase ϕ_1^2.

4. Plot the original unbalance as vector **OA** and the original-plus-calibration unbalance as vector **OB** in Fig. 6.14 to a convenient scale. The calibration couple effect is then the vector $\mathbf{AB} = T^2$.

5. The required correction weights are then

$$C^2 = \frac{\mathbf{OA}}{\mathbf{AB}} \ W \ oz.$$

6. The required orientation for this second mode is $\phi^2 =$ angle OAB degrees circumferentially forward from each calibration-weight location.

On inserting these correction weights at the required radius r and angle ϕ, the rotor will be balanced in its second flexural mode.

The third mode for this symmetrical rotor can be balanced in a similar manner, with a combination of three correction weights in three planes. To avoid reintroducing the first mode may require use of the following relative third-mode correction-weight proportions: C^3 (plane 1, 0°); $2C^3$ (plane 2, 180°); C^3 (plane 3, 0°) (see Fig. 6.13).

The example demonstrates the balance procedure for a symmetrical rotor in which the unbalance modal interactions are negligible. Procedures for cases where the modes are coupled are discussed in the following section.

Industrial Rotor with Modal Coupling Near the First Critical Speed. Moore [20] has observed that "it invariably becomes apparent that the rotor is distorting in two modes simultaneously" during any flexible-rotor balancing operation. Moore and Dodd [18] have proposed a series of operations for dealing with such conditions. Vibration readings must now be taken at both bearings as follows:

1. Run the rotor close to the first critical speed. Record the vibration amplitude and phase reference at both bearings.*

2. Insert a calibration weight in the rotor midplane.

3. Rerun the rotor at the same speed and again record the vibration amplitude and phase at both bearings.

4. Draw the original unbalance vibration vectors **OA** and **OB** to some convenient scale, as in Fig. 6.15.

5. Draw the original-plus-calibration unbalance vectors **OA₁** and **OB₁** to the same scale. The effects of the calibration weight are the vectors **AA₁** and **BB₁**.

6. Join *AB* and *A₁B₁*. Bisect *AA₁* in *T* and *BB₁* in *T₁*. Join *TT₁*. Join *OT*.

7. It is now presumed that **OT** is the unbalance vector in the first mode. The required correction is

$$C_1 = \frac{OT}{TT_1} \cdot W \ oz.$$

at

$$\phi_1 = angle \ OTT_1 \ degrees.$$

C_1 lags the vector **OT** in the configuration shown. The first mode is then corrected by installing a weight C_1 in the rotor midplane at angle ϕ_1.

8. The second mode is corrected by installing a pair of weights, each with a magnitude of

$$C_2 = \frac{OA}{AA_2} W = \frac{OB}{AA_2} = \frac{OB}{BB_2} W$$
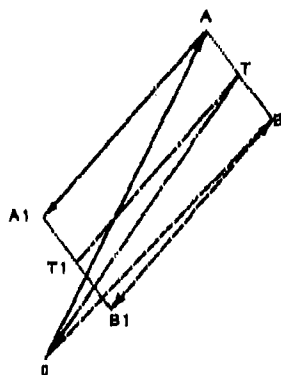
Fig. 6.15. Balancing construction for a mixed-mode condition near the first critical speed [19] (© C. A. Parsons Co., 1970; used with permission)

---

*If the orbits are elliptical, record the major-axis amplitude and orientation using an oscilloscope.

at angle

$$\phi_2 = \text{angle } OAA_2 = \text{angle } OBB_2$$

to the plane of the calibrating unbalance (see Fig. 6.15).

Step 8 is not included in the procedure given by Moore [20]. It can, however, be used to suppress strong effects from the second mode which occasionally arise at the first-mode balancing speed, to enable the rotor to safely approach the second mode after first-mode effects have been corrected. With the rotor at a speed close to the second critical speed, the second mode can be corrected as described below. The given construction allows the second-mode correction to be determined when there is a mixed-mode condition between the second and third modes at the balancing speed.

    1. Record the original unbalance magnitude and phase at both bearings.

    2. Insert a pair of known calibrating weights near the ends of the rotor, 180° apart circumferentially.

    3. Run the rotor at the same balance speed and again measure the original-plus-calibration unbalances and phase angles.

    4. Plot the original unbalance vectors as **OA** and **OB** in Fig. 6.16. Plot the original-plus-calibration unbalance vectors as **OA$_2$** and **OB$_2$** and identify the calibration unbalance vectors as **AA$_2$** and **BB$_2$**.

    5. Divide **AB** at T so that $TA/TB = AA_2/BB_2$.

    6. The required second-mode correction weights are each

$$C = \frac{TA}{AA_2} W \text{ oz.}$$
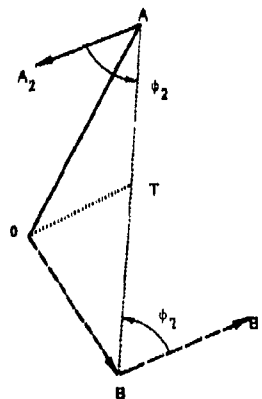
Fig. 6.16. Balancing construction for a mixed-mode condtion near the second critical sppod [19] (© C. A. Parsons Co., 1970; used by permission)

7. The required circumferential angle through which the correction weights must be moved is

$$\phi_2 = \text{angle } TAA_2 = \text{angle } TBB_2.$$

With these correction weights in the rotor end planes, the rotor will be balanced in its second mode.

Balancing for a Mixed-Mode Condition Remote from Either Critical Speed. Consider the case of a rotor that is balanced in its first mode but remains unbalanced in the second and third modes. Further, assume that at full speed the rotor is running well below either its second or third critical speed. Under this condition there might well be a significant contribution from both higher modes. The measured vectors of vibration must first be split into modal components where the asymmetry of the modes is not known. Each component is then corrected independently.

For balancing purposes it can be assumed that the effect of calibrating weights added mostly for the second mode represents the asymmetry of the second mode and that the effect of such weights added mostly for the third mode represents mainly third-mode asymmetry. Thus it is necessary to split the observed original vibration vectors into second- and third-mode (or out-of-phase and in-phase) components of the same proportions as those deduced from the calibrating weights. The way this is done is shown in Fig. 6.17, taken from Ref. [19].
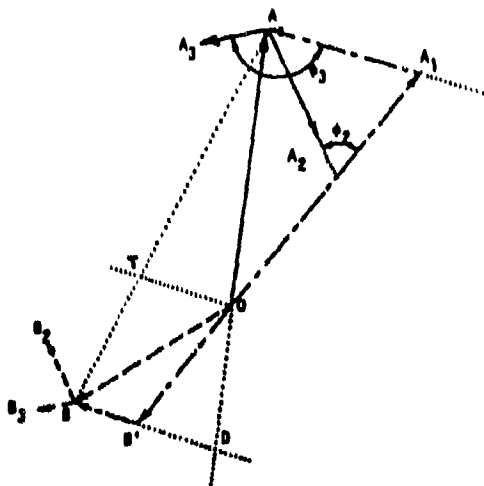
Fig. 6.17. Balancing consturction for a mixed-mode condtion remote from either critical speed [19] (© C. A. Parsons Co., 1970; used by permission)

1. Let the vectors **OA** and **OB** represent the original unbalance.

2. Let the vectors **OA$_2$** and **OB$_2$** represent the vibration measured when a calibration pair of weights is added to the rotor, mostly to affect the second mode.

3. Then the vectors **AA$_2$** and **BB$_2$** represent the effect of the calibrating weights for the second mode.

4. Let the vectors **OA$_3$** and **OB$_3$** represent the vibration when the calibrating weights for the second mode are removed and replaced by a three-weight calibrating configuration that will have the greatest effect on the third mode.

5. Then the vectors **AA$_3$** and **BB$_3$** represent the effect of the calibrating weights for the third mode.

6. Divide **AB** at T so that $TA/TB = AA_2/BB_2$ and call this m. Let $AA_3/BB_3 = n$.

7. Construction: Draw **TO** and lines parallel to it through A and B. Produce AO to meet the parallel line through B in D. Divide **DB** in B' so that $B'D/BB' = n/m$. Join $B'O$ and produce it to meet the parallel line through A in A'. Then the original vectors **OA**, **OB** are equivalent to an out-of-phase component **OA'**, **OB'** plus an in-phase component **A'A**, **B'B**. It can further be shown that $OA'/OB' = m$ and $A'A/B'B = n$. Therefore the out-of-phase component can be corrected by adjusting the calibrating weights for the third mode.

8. Second-mode correction: Increase the calibrating weights for the second mode in the ratio OA'/AA_2 and move them circumferentially through the angle labeled ϕ_2.

9. Third-mode correction: Increase the calibrating weights for the third mode in the ratio of $A'A/AA_3$ and move them circumferentially through the angle labeled ϕ_3.

Note that in both cases the proportions among the individual weights in each configuration must be maintained. As it happens, in the example illustrated, the correction for the second mode would have to be placed clockwise from the calibrating position, and the correction for the third mode would have to be placed counterclockwise from the calibrating position, always regarding the rotor from one end throughout.

Example of Rotor Balance Corrected in the Second and Third Modes. Moore and Dodd [18] describe an application of the procedures discussed above to an actual boiler-feed pump rotor that had coupled (mixed-mode) unbalance in its second and third modes. This unbalance distribution was preventing smooth operation of the pump between its first and second critical speeds: see Fig. 6.18. The shapes of the first three modes are shown in Fig. 6.19. The best available balancing planes for the second mode are at 25 in. and 70 in. from
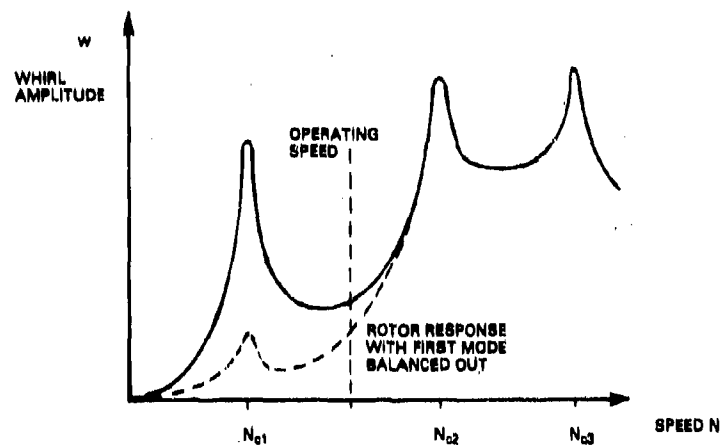
Fig. 6.18. Unbalance-response representation for rotor balanced in the first mode with residual unbalance in the second and third modes
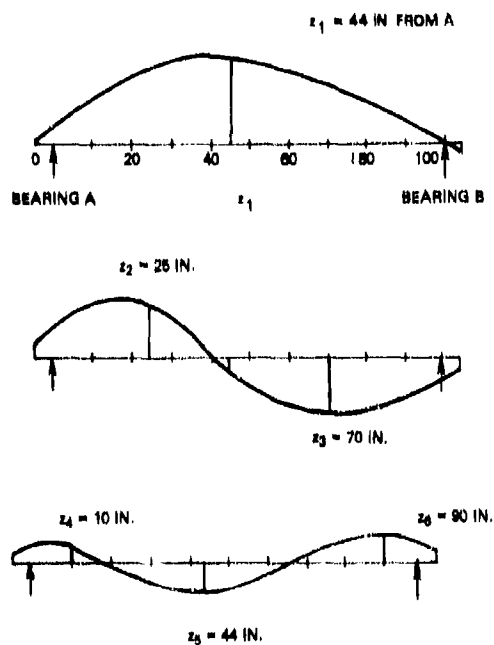
Fig. 6.19. Modes and correction planes for feed pump turbine rotor

bearing A, respectively, and for the third mode at 10 in., 44 in., and 90 in. from bearing A. All weights were added at the same radius in each balance plane.

A construction for determining balance weights for the second and third modes is given in Fig. 6.17 as follows:

1. Let **OA** be the original unbalance vector at pedestal A, and **OB** the original unbalance vector at pedestal B.

2. Add a set of calibrating weights for the second mode. Let the ratio of effects at the pedestals be

$$\frac{\text{effect on reading } A}{\text{effect on reading } B} = m.$$

3. Add a set of calibrating weights for the third mode. Let the ratio of effects at the pedestals be

$$\frac{\text{effect on reading at } A}{\text{effect on reading at } B} = n.$$

4. Find the components of **OA** and **OB** in the second and third modes as follows:

a. Join **AB**. Divide in T so that $AT/TB = m$.

b. Join OT. Draw lines parallel to OT through A and through B. Produce AO to meet parallel line through B in O.

c. Divide **DB** in B' so that $DB'/B'B = n/m$.

d. Join $B'O$ and produce it to meet the parallel line through A in A'.

e. Let $B'B = Y$. Then $DB' = ny/m$, $OA' = MOB'$, and $A'A = MB'D = ny$. Hence $A'A/B'B = ny/y = n$.

f. As $OA + A'A = OA$ and $OB' + B'B = OB$, the vibration readings OA, OB consist of the out-of-phase components OA', OB', where $OA' = MOB'$, plus the in-phase components $A'A$, $B'B$, where $A'A = nB'B$.

The above construction can now be applied to the boiler-feed rotor as follows:

1. Let **OA** and **OB** be the original unbalance vectors at bearings A and B, respectively.

2. Let OA_2, OB_2 be the original-plus-calibrating weight effect for the second mode. Then AA_2, BB_2 are the effects of the second-mode calibrating weights.

3. Let OA_2, OB_2 be the original-plus-calibrating weight effect for the third mode. Then AA_3, BB_3 are the effects of the third-mode calibrating weights.

4. Calibration for the second mode

$$\frac{\text{effect on end } A}{\text{effect on end } B} = m = \frac{2.30}{1.175} = 1.96.$$

5. Calibration for the third mode

$$\frac{\text{effect on end } A}{\text{effect on end } B} = n = \frac{1.175}{0.525} = 2.24.$$

6. Join AB. Divide at T so that $AT/TB = m$.
7. Join OT. Draw lines parallel to it through A and B.
8. Produce AO to meet parallel lines through B to D.
9. Divide BD in B' so that $B'D/BB = n/m = 1.145$.
10. Join $B'D$ and produce this to meet he parallel line drawn through A at A'.
11. The required correction weights can now be obtained as

$$OA, \ OB = OA', \ OB' + A'A, \ B'B,$$

where OA, OB are the original readings, OA', OB' are the out-of-phase components, and $A'A$, $B'B$ are the in-phase componnts. Thus, for the second mode,

$$\frac{OA'}{AA_2} = \frac{OB'}{BB_3} = 2.38 \quad (\theta_2 = 63\,^\circ)$$

and for the third mode,

$$\frac{AA'}{AA_3} = \frac{BB'}{BB_3} = 2.50 \quad (\theta_3 = 150\,^\circ).$$

12. To make the second-mode correction add $(5 \times 2.38) = 11.9$ oz-in. in correction plane B, both 63° clockwise from the position of the second-mode calibrating weights.
13. To make the third-mode correction add $4 \times 2.5 = 10$ oz-in. in correction plane C, $5 \times 2.5 = 12.5$ oz-in. in correction plane D, and $6 \times 2.5 = 15$ oz-in. in correction plane E, all 150° counterclockwise from the positions of the third-mode calibrating weights.

Moore [21] gives no details about the final balance state achieved with the above construction. He has, however, given a mathematical procedure [21] for the determination of the ratios m and n. It is stated that the advantage of this modal technique lies in the time saved in balancing large rotors. However, any time spent calibrating the rotor for the influence of the traverse weight and in defining the mode shapes must also be included in the assessment of balancing efficiency. Runup and rundown time in such cases can be substantial. The taking of trial weight readings can be a costly aspect of any balance procedure.

Comprehensive Modal Balancing. Federn [6] began the development of modal balancing procedures for flexible rotors in which the rigid-body modes were corrected first in a low-speed balancing machine, followed by balancing of the higher modes in a systematic modal manner. Kellenberger [22] described the application of this procedure to generator rotors and subsequently [23] compared the modal N-plane balancing procedure with the comprehensive $(N + 2)$-plane balancing method. Miwa [24—27] developed refined theories for comprehensive modal balancing and demonstrated the effectiveness of this method with a six-disk rotor mounted on supports with transverse flexibility. Giers [28] compared comprehensive modal balancing with modal balancing.

Consider a cylindrical rotor that operates in linear elastic bearings located near its ends. The rotor bending stiffness is linear and isotropic. The influences of viscous and hysteretic damping are considered to be negligible, and the rotor gyroscopic effect is negligible. Rotor stiffness $EI(z)$ and mass distribution $\rho A(z)$ may vary along the rotor length.

The rotor distributed unbalance is represented by the expression

$$u_0(z) = \rho A(z)\, a(z),$$

where $\rho A(z)$ is the distribution of rotor mass per unit length and $a(z)$ is the mass axis eccentricity. The discrete unbalances acting on the rotor are written as

$$U_p = U_p \delta(z - z_p),$$

where U_p is the vector unbalance at location z_p and δ is the Dirac delta function. The total axial unbalance distribution is therefore

$$u(z) = u_0(z) + U_p \delta(z - z_p).$$

The balance conditions for a rigid rotor require that force equilibrium and moment equilibrium must each equal zero. In terms of the above equations this gives

$$\int_0^L u(z)\, dz = \int_0^L u_0(z)\, dz + \sum_p U_p \delta(z - z_p) = 0$$

and

$$\int_0^L u(z)z\, dz = \int_0^L u_0(z)z\, dz + \sum_p U_p \delta(z - z_p)z_p = 0.$$

For a flexible rotor it is also necessary to ensure that the rotor deflections under the influence of the unbalance distribution are zero in

addition to satisfying the above rigid-rotor conditions. To develop the required conditions, first express the unbalance distribution as

$$u(z) = u_0(z) + \sum_{j=1}^{\infty} u_j \, \phi_j(z)$$

and

$$u_0(z) = \sum_{p} U_p(z - z_p).$$

Also express the mass axis eccentricity as the series

$$a(z) = a_0(z) + \sum_{j=1}^{\infty} a_j \, \phi_j(z),$$

and the rotor elastic axis deflection vector as the series

$$r(z) = \sum_{j=1}^{\infty} r_j(t) \, \phi_j(z).$$

If these forms for $a(z)$ and $r(z)$ are used the modal unbalance components a_j and the shaft modal response components r_j can be evaluated. As already shown, the complex rotor response

$$r(z) = x(z) + iy(z)$$

is governed by the equation of motion in nonrotating coordinates,

$$\ddot{r} + 2(\nu + \mu)\omega\dot{r} + \frac{EI}{A\rho} r^{IV} - i2\nu\omega\Omega r = \Omega^2 a \, e^{i\Omega t}.$$

For present purposes the damping terms ν and μ can be omitted. To obtain a modal solution to this equation, the rotor deflection $r(z)$ and the unbalance distribution $a(z)$ are expressed in series form:

$$r(z,t) = r_1(t) \, \phi_1(z) + r_2(t) \, \phi_2(z) + \ldots = \sum_{j=1}^{\infty} r_j(t) \, \phi_j(z)$$

and

$$a(z) = a_1 \, \phi_1(z) + a_2 \, \phi_2(z) + \ldots = \sum_{j=1}^{\infty} a_j \, \phi_j(z),$$

where the coefficients $r_j(t)$ and a_j are complex quantities and the $\phi_j(z)$ are characteristic functions of the rotor. We again recall that, for shafts with distributed mass and stiffness,

$$\frac{EI}{A\rho} \phi_j^{IV}(z) = \omega_j^2 \, \phi_j(z).$$

Substituting the above series and the characteristic function condition into the equation of motion gives the infinite set of modal equations:

$$\ddot{r}_j + \omega_j^2 r_j = \Omega^2 a_j\, e^{i\omega t}.$$

In each case the solution for the forced motion is

$$r_j = \frac{\Omega^2 a_j\, e^{i\Omega t}}{\omega_j^2 - \Omega^2},$$

where

$$a_j = \frac{1}{Z} \int_0^L u(z)\, \phi_j(z)\, dz$$

$$Z = \int_0^L [\phi_j(z)]^2\, dz.$$

It is evident that the shaft displacements $r(z)$ depend on $a(z)$, and hence we may write

$$r(z) = \sum_{q=1}^{\infty} A_j(\omega)\, a_j\, \phi_j(z), \quad \text{with } A_j(\omega) = \frac{\Omega^2}{\omega_j^2 - \Omega^2}.$$

Consider now the equations of force equilibrium and moment equilibrium for a flexible rotor in two bearings:

$$P_A + P_B = \Omega^2\, e^{i\Omega t} \int_0^L [\rho A(z)\, r(z) + u(z)]\, dz$$

and

$$P_B L = \Omega^2\, e^{i\Omega t} \int_0^L [\rho A(z)\, r(z) + u(z)]z\, dz.$$

If the unbalance distribution is written as

$$u(z) = \rho A(z)\, a(z) = \rho A(z) \left[a_0(z) + \sum_{j=1}^{\infty} a_j\, \phi_j(z) \right]$$

$$= \rho A(z)\, a_0(z) + \sum_{j=1}^{\infty} \rho A(z)\, a_j\, \phi_j(z),$$

the shaft centrifugal force may now be written as

$$\rho A(z)\, r(z) = \rho A(z) \sum_{j=1}^{\infty} A_j(\omega)\, a_j\, \phi_j(z)$$

$$= \sum_{j=1}^{\infty} A_j(\omega)\, \rho A(z)\, a_j\, \phi_j(z)$$

$$= \sum_{j=1}^{\infty} A_j(\omega) \ u_j \ \phi_j(z),$$

where

$$u_j(z) = \rho A(z) \ a_j(z).$$

Substituting into the equations of equilibrium gives

$$P_A + P_B = \Omega^2 \ e^{i\Omega t} \int_0^L \left[\sum_{j=1}^{\infty} A_j(\omega) \ u_j \phi_j(z) + u(z) \right] dz$$

$$= \Omega^2 \ e^{i\Omega t} \int_0^L \left\{ \sum_{j=1}^{\infty} [A_j(\omega) + 1] u_j \ \phi_j(z) + u_0(z) \right\} dz,$$

as

$$u(z) = u_0(z) + \sum_{j=1}^{\infty} u_j \ \phi_j(z).$$

Hence

$$P_A + P_B = \Omega^2 \ e^{i\Omega t} \left[\sum_{j=1}^{\infty} B_j(\omega) \ u_j \int_0^L \phi_j(z) \ dz + \sum_p U_p \right]$$

and

$$P_B L = \Omega^2 \ e^{i\Omega t} \left[\sum_{j=1}^{\infty} B_j(\omega) \ u_j \int_0^L \phi_j(z) z \ dz + \sum_p U_p z_p \right],$$

where

$$B_j(\omega) = A_j(\omega) + 1 = \frac{\omega_j^2}{\omega_j^2 - \Omega^2}$$

The conditions for flexible-rotor balance can be deduced from these equations. It is required to make

$$P_A + P_B = 0 \quad \text{and} \quad P_B L = 0.$$

These conditions will evidently be achieved when

$$\int_0^L u(z) \ dz = 0$$

$$\int_0^L u(z) z \ dz = 0$$

and

$$\int_0^L u(z)\,\phi_j(z)\,dz = 0 \quad \text{for} \quad j = 1,\, 2,\, \ldots,\, \infty.$$

In terms of the distributed unbalance and the discrete unbalances

$$u(z) = u_0(z) + \sum_k U_k,$$

the balance conditions become

$$\int_0^L u_0(z)\,dz + \sum_k U_k = 0,$$

$$\int_0^L u_0(z)z\,dz + \sum_k U_k z_k = 0,$$

and

$$\int_0^L u_0(z)\,\phi_j(z)\,dz + \sum_k U_k\,\phi_j(z_k) = 0, \qquad k = 1,\, 2,\, \ldots.$$

It can now be seen that if p modes are balanced using $(p + 2)$ correction planes, the above expressions will form $(p + 2)$ equations in $(p + 2)$ unknowns; that is, the balance conditions become

$$\int_0^L u_0(z)\,dz + \sum_{k=1}^{p+2} U_k = 0,$$

$$\int_0^L u_0(z)z\,dz + \sum_{k=1}^{p+2} U_k z_k = 0,$$

and

$$\int_0^L u_0(z)\,\phi_j(z)\,dz + \sum_{k=1}^{p+2} U_k\,\phi_j(z_k) = 0,$$

or

$$
\begin{bmatrix}
1 & 1 & \cdots & 1 \\
z_1 & z_2 & \cdots & z_{p+2} \\
\phi_1(z_1) & \phi_1(z_2) & \cdots & \phi_1(z_{p+2}) \\
\phi_2(z_1) & \phi_2(z_2) & \cdots & \phi_2(z_{p+2}) \\
- & - & - & \\
- & - & - & \\
- & - & - & \\
\phi_p(z_1) & \phi_p(z_2) & \cdots & \phi_p(z_{p+2})
\end{bmatrix}
\begin{Bmatrix}
U_1 \\
U_2 \\
U_3 \\
U_4 \\
- \\
- \\
- \\
U_{p+2}
\end{Bmatrix}
=
\begin{bmatrix}
\int_0^L u_0(z)\,dz \\
\int_0^L u_0(z)z\,dz \\
\int_0^L u_0(z)\,\phi_1(z)\,dz \\
\int_0^L u_0(z)\,\phi_2(z)\,dz \\
- \\
- \\
\int_0^L u_0(z)\,\phi_p(z)\,dz
\end{bmatrix}
$$

These expressions were given by Miwa [24]. Similar relations have been presented by Kellenberger [22]. Sample calculations developed to demonstrate the above procedure now follow.

Example 1: Uniform flexible rotor in simply supported end bearings.

For the rotor shown in Fig. 6.20, uniform unbalance distribution $u(z) = U/L$ = constant, uniform flexible rotor $EI(z) = EI$, $\rho A(z) = \rho A$ = constant, and

$$\phi_j(z) = \sin \frac{j\pi z}{L}.$$
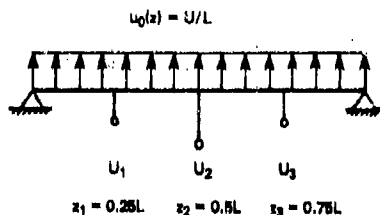
Fig. 6.20. Uniform rotor in rigid end bearings with distributed unbalance. After Miwa [7]. Used by permission.

The requirement is to balance the first mode $(j = 1)$, and this requires $k = p + 2$ correction planes. The integrals of the forcing vector become

$$\int_0^L u_0(z)\, dz = \int_0^L \frac{U}{L} dz = U,$$

$$\int_0^L u_0(z) z\, dz = \int_0^L \frac{U}{L} z\, dz = \frac{UL}{2},$$

$$\int_0^L u_0(z)\, \phi_1(z)\, dz = \int_0^L \frac{U}{L}\sin\frac{\pi z}{L}\, dz = U(\frac{2}{\pi}).$$

For correction planes $k = 1$, 2, 3 at $z_1 = 0.25L$, $z_2 = 0.5L$, and $z_3 = 0.75L$, $\sin(\pi z_k/L) = 0.707$, 1.000, 0.707, and the balance equations become

$$\begin{bmatrix} 1 & 1 & 1 \\ 0.25 & 0.5 & 0.75 \\ 0.707 & 1.0 & 0.707 \end{bmatrix} \begin{Bmatrix} U_1 \\ U_2 \\ U_3 \end{Bmatrix} = -U \begin{Bmatrix} 1 \\ 0.5 \\ 2/\pi \end{Bmatrix},$$

which gives $U_1 = -0.6203 U$, $U_2 = 0.2406 U$, and $U_3 = -0.6203 U$. This agrees with the result for the balance corrections given by Miwa [24], who has also plotted the corrections as functions of axial location.

Example 2: Uniform rotor in flexible end bearings

The rotor shown in Fig. 6.21 is to be balanced in its first mode. Correction planes are located at $z_1 = 0$, $z_3 = 0.5L$, and $z_2 = L$. The end bearings have identical stiffness properties k, and the flexural stiffness of the rotor is $K = 48EI/L^3$ (first mode). This indicates that only symmetrical modes need to be considered in balancing this rotor. The characteristic equation is therefore

$$\phi_j(z) = a_j + b_j \sin\left(\frac{j\pi z}{L}\right).$$
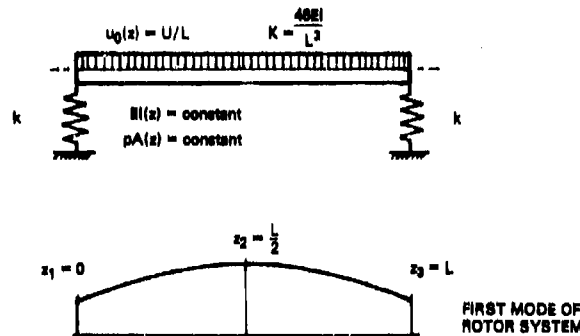
Fig. 6.21. Uniform rotor in flexible bearings with distributed unbalance. Example from Miwa et al. [26]. Used by permission.

To balance the first mode, $J = 1$, and the mode shape can be obtained from the deflection diagram, i.e., $a_1 = k$, $b_1 = 48EI/L^3$, and $\alpha = b_1/a_1$. Normalizing this expression gives

$$\Phi_1(z) = 1 + \frac{48EI}{kL^3} \sin\left(\frac{\pi z}{L}\right).$$

The balance conditions can now be formed. For a uniform radial distribution of unbalance along the rotor, $u_0(z) = U/L = $ constant, and

$$\int_0^L u_0(z)\, dz = U,$$

$$\int_0^L u_0(z) z\, dz = 0.5 UL,$$

and

$$\int_0^L u_0(z)\,\phi_1(z)\,dz = \frac{U}{L}\int_0^L \left[1 + \alpha\,\sin\left(\frac{\pi z}{L}\right)\right]dz = U\left(1 + \frac{2}{\pi}\,\alpha\right).$$

The balance equations are therefore

$$\begin{bmatrix} 1 & 1 & 1 \\ 0 & 0.5 & 1.0 \\ 1 & 1+\alpha & 1 \end{bmatrix} \begin{Bmatrix} U_1 \\ U_2 \\ U_3 \end{Bmatrix} = -U \begin{Bmatrix} 1 \\ 0.5 \\ 1 + 2\alpha/\pi \end{Bmatrix}.$$

The required balance corrections are $U_1/U = -0.18$, $U_2/U = -0.64$, and $U_3/U = -0.18$. It is noted that the balance corrections are independent of the shaft-bearing stiffness ratio α. Thus the above corrections are valid irrespective of the stiffness ratio. In an actual case it now remains to determine the unbalance U by a trial-weight procedure. The required corrections can then be determined and applied.

Example 3: Uniform rotor in flexible end bearings with nonuniform unbalance distribution

Figure 6.22 shows a rotor of uniform stiffness $K = 48EI/L$ and mass distribution $A\rho$; it is supported in end bearings of stiffness k_a and k_b. The rotor is to be balanced for smooth operation at its first critical speed, using three correction planes symmetrically situated about the midspan.

The number of correction planes $k = p + 2 = 3$ meets the stated requirements for comprehensive modal balancing. The unbalance distribution varies linearly along the rotor length, that is,

$$u(z) = u_1 + u_2\,\frac{z}{L}.$$

Let the shape of the first mode be described by the characteristic equation

$$\phi_j(z) = A + B\frac{z}{L} + C\,\sin\frac{\pi z}{L}.$$

Let U_1, U_2, U_3 be unbalance corrections applied in the three correction planes at $z_1 = \zeta L$, $z_2 = \frac{L}{2}$, and $z_3 = (1 - \zeta)L$, respectively, ζ being a chosen fraction of the rotor length. Miwa [27] has given a general

solution for this problem in terms of measured forces U_L and U_R at the rotor supports. If U_L and U_R are measured close to the first critical speed, the required balance corrections will be

$$U_1 = U_L \left(1 - \frac{\beta}{2} \right) - U_R \frac{\beta}{2},$$

$$U_2 = U_L \beta + U_R \beta,$$

and

$$U_3 = - \left(\frac{\beta}{2} \right) U_L + U_R \left(1 - \frac{\beta}{2} \right),$$

where

$$\beta = \frac{(2/\pi) - \sin \pi \zeta}{1 - \sin \pi \zeta}.$$

It is again noted that the required balance corrections are independent of the relative stiffness α of the rotor and the bearings. Furthermore, the balance corrections are independent of the relative bearing stiffnesses. The corrections are dependent on the location of the correction planes along the rotor.

Miwa [27] has commented that, where $\zeta = 0$ (i.e. for correction planes at the ends of the rotor), the ratio $\beta = 0.64$. He also notes that, when $\zeta = 0.22$, the central correction U_2 becomes zero. Two-plane balancing with $\zeta = 0.22$ and $\zeta = 0.78$ is therefore optimal for this balancing case. Figure 6.23 shows a chart developed by Miwa [27] for determining the correction ratio as a function of balance-plane location ζ.

$$\beta = \frac{\text{Central Correction}}{\text{Initial Static Unbalance}}$$

$$\zeta = \frac{z_1}{L}, \quad \text{Balance Plane Location}$$
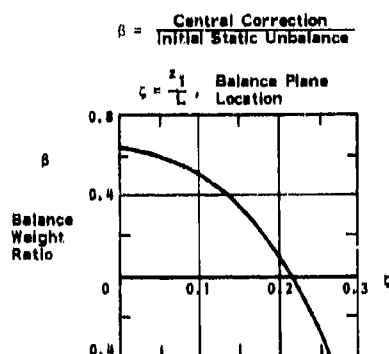
Fig. 6.23. Variation of balance weight ratio with location of correction planes along rotor. After Miwa [27]. Used by permission.

Example 4: Alternator rotor in undamped flexible bearings

Kellenberger [22] has described the balancing of an alternator rotor supported in flexible bearings (with zero damping). This machine runs above its second critical speed, and there are therefore at least two modes requiring balance corrections. The minimum number of correction planes by the comprehensive modal method is therefore $p = k + 2 = 4$. It is further assumed that this rotor has previously been balanced as a rigid body in two planes. If the origin of the coordinates is set at the left bearing, the chosen correction planes are at $z_1 = 0$, $z_2 = 2535$ mm, $z_3 = 4935$ mm, and $z_4 = 7440$ mm $= L$, as shown in Fig. 6.24a.

The mode shapes for this rotor were calculated with a computer and are shown in Fig. 6.24(b) and (c). Calculated modal amplitudes at the correction planes for both modes were used for the characteristic function values $\phi_j(z_k)$ in the third and fourth balance equations. Terms in the forcing vector were obtained by setting

$$\int_0^L u_0(z) \, dz = \int_0^L u_0(z) z \, dz = 0$$

for the first and second terms because the rotor had been previously balanced as a rigid body. The third term is arbitrarily set equal to
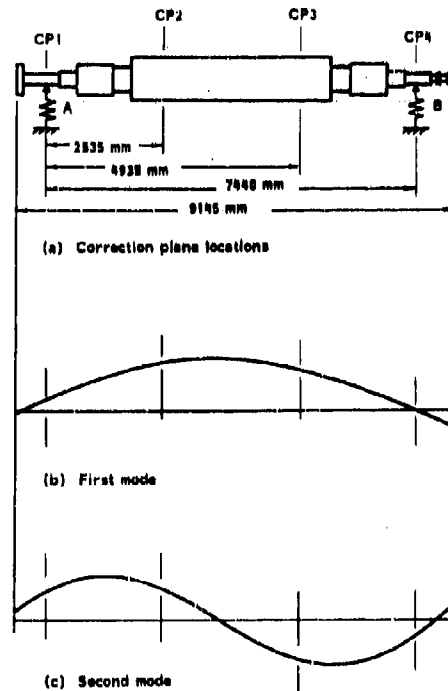
Fig. 6.24. Alternator rotor in flexible bearings:
first and second mode shapes

$100\,\phi_1$, where ϕ_1 remains to be calibrated from first-mode measurements (presumably by trial-weight runs). The fourth term is also set equal to zero, as the first-mode balance correction must not influence the second mode. The balance equations for both modes are given in Table 6.1.

Table 6.1. Balance equation terms*

U_1	U_2	U_3	U_4	Mode 1 balance	Mode 2 balance
1	1	1	1	0	0
0	0.341	0.663	1	0	0
3.426	18.734	18.569	3.418	$-100\,\phi_1$	0
11.225	12.241	−12.457	−11.453	0	$-100\,\phi_2$

*From Ref. 22; used by permission.

The solutions for the unbalance corrections are as shown in Table 6.2.

Table 6.2. Unbalance corrections for Alternator Rotor

Unbalance correction	Mode 1		Mode 2	
	Absolute	Normalized	Absolute	Normalized
U_1	$+3.264\,\phi_1$	$+1.000$	$+1.821\,\phi_2$	$+1.000$
U_2	$-3.264\,\phi_1$	-1.000	$-5.718\,\phi_2$	-3.140
U_3	$-3.303\,\phi_1$	-1.012	$+5.779\,\phi_2$	$+3.174$
U_4	$+3.303\,\phi_1$	$+0.012$	$-1.882\,\phi_2$	-1.034

*From Ref. 22; used by permission.

The balancing procedure requires the first measurements near but below the first critical speed. The actual magnitudes of the first-mode corrections are found by a procedure similar to the trial-weight methods previously described. The remaining unbalance corrections are then obtained from the ratios given in Table 6.2. When the first mode has been corrected, the procedure is repeated to balance the second, third, and fourth modes.

Discussion of Modal Methods

The three modal methods described on the preceding pages are the most widely used modal balancing procedures in current practice, and they merit some further comment. Two questions are consistently raised about these methods: What are the differences between them, and which method gives the best results?

The modal balancing method of Bishop, Gladwell, and Parkinson is basically a set of instructions given together with a matrix equation that can be solved or satisfied for the modal correction weight values as desired. As far as is known, the balance matrix equation given by these authors has never been implemented as an analytical procedure for determining balance weights and locations, though it appears possible to do this if desired. Publications on the modal method have been mainly concerned with the definition of procedures based on rigorous principles for the balancing of flexible rotors. These publications have examined a wide range of balancing problems (flexible supports, anisotropic supports, dissimilar shaft stiffnesses, etc.) with this in mind and have been less concerned with the practical details of flexible-rotor balancing.

The modal balancing principles defined by Bishop et al. have been applied in practice by Moore, specifically for the correction of medium to large, two-bearing, electrical equipment rotors. Moore has had good

success for more than 20 years, using the modal guidelines described by Bishop and the practical vector techniques for unbalance determination that he devised and perfected over several decades. Moore does not mention having made any use of the matrix equations of Bishop and Gladwell, though he appears to have satisfied these criteria mode by mode with his diagram approach.

The methods of Bishop and of Moore both nominally use N planes,* where N is the number of modes to be balanced. Bishop and Parkinson [5] have discussed methods for reducing effects from modes that lie beyond the operating speed, and Moore [20] has described practical techniques for dealing with such modes. Although Parkinson [15] has analyzed the influence of massive flexible supports on modal balancing, the influence of bearing damping appears not to have been included in any modal analysis. Shaft damping has been included, and this does not invalidate the modal approach. The possible effects of modes coupled by damping in the bearings on the attainable balance should be examined because the quality of balance may indeed be affected by such damping.

In contrast to the other balancing procedures described in this chapter, it appears that there have been few experimental investigations of the modal method. While there is ample evidence that the method is consistently successful in practice, questions concerning its effectiveness are inevitable, especially in comparison with such methods as the comprehensive modal method and the influence coefficient method, both of which have been extensively tested. There seems to be little doubt that claims advanced for the modal method are weakened by the lack of a series of experimental studies that could test the effectiveness and the efficiency of the method. Such tests appear to be particularly needed, since studies by Giers [28] have pronounced the comprehensive modal method to be superior: see Chapter 7.

The comprehensive modal method has been studied by Federn, Kellenberger, Miwa, and Giers. The most notable difference between this method and the modal method of Bishop and Moore is the requirement that the rigid-body modes be balanced before proceeding to the flexible modes. Claims that this leads to a balance of superior quality have been made by Miwa et al. [26] because of the removal of an Ω^2 term in the dynamic magnifier equation; by Kellenberger [23] because of the satisfaction of the three balance equations; and by Giers [28] based on comparisons of comprehensive modal test results with modal

---

*Moore [20] describes how the correction weights are typically distributed along the length of a generator in practice. The principle, however, is valid and is used widely in field balancing.

results obtained by Moore's method. These tests are discussed in Chapter 7.

On examining the shaft equations of motion written in the most general terms, it appears that one must work with the true modes, and not with pseudomodes such as the rigid-body components of class 2 rotor rigid/flexible modes. If this is so, it could be expected that a single-plane balance of a class 2 rotor would give at least equivalent balance quality as a low-speed plus a high-speed balance of such a rotor (see Fig. 6.25). It also appears that all significant "rigid-body" effects are taken into account in the modal method because it deals with real modes at all times. Bishop argues convincingly that it is meaningless to balance rigid modes in a rotor that experiences only highly flexible modes. Kellenberger and Federn reply that it is frequently necessary to balance at low speed in order to be able to run up to higher speeds. This appears to be a clear case for the removal of gross unbalance rather than a need to remove modes. Therefore the rigid-mode argument does not appear to support the comprehensive modal method.

(a) First mode showing correction mass.

(b) Residual rotor deflection near first critical speed.

Modal method: N-plane corrections
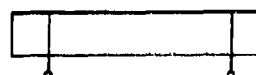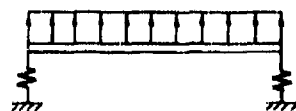
(c) 'Mode' and corrections in low speed balancing machine.

(d) First mode with distribution of low speed correction and first mode correction.

(e) Corrected first mode near critical speed.

Comprehensive Modal Method. (N+2)-plane corrections.

Fig. 6.25. Rotor in flexible bearings with uniform unbalance: effectiveness of corrections by the modal method (left) and the comprehensive modal method (right)

Miwa's elegant series of papers with their experimental confirmation clearly demonstrate the effectiveness of the comprehensive modal method. Kellenberger's paper, [22] is also interesting in the sense that he selects four planes to balance the first two flexible modes, *after* having balanced the rigid modes (i.e., gross unbalance has first been effectively removed). Even if shop procedures do frequently result in rotors that are slightly bowed or have slightly eccentric disks requiring two-plane removal of gross unbalance, it is still not clear why four planes are needed to achieve what the modal method could presumably achieve with two planes, and without gross unbalance correction. Moore does not discuss this situation. The fact that modal practice commonly distributes the correction weights along the length of the rotor is irrelevant. Adherance to the principles of the method should ensure balance even if only two planes were used.

Another point that should be mentioned is the plane of unbalance Kellenberger refers to; in practice it must be found and calibrated. This in turn appears to require a trial-weight procedure, and, as the generator rotor used in the example is similar to Moore's rotors, it must possess the same transmitted-force vector properties. Therefore constructions similar to those developed by Moore are needed to balance such rotors, or else some type of influence coefficient method must be used. This brings the entire procedure into question: could not the same result be achieved with gross unbalance correction, followed by Moore's procedure or by a simple influence coefficient calculation? It would be useful to have the authors of comprehensive modal balancing explain how these aspects are dealt with in practice.

There appears to be no meaningful answer to the question as to which method is "best." Best balance commonly means three things: convenience in operation, high quality throughout the speed range, and minimum time and minimum operations. A summary of experience with the N modal method and with the N+2 modal method is given below:

Modal method

Sound in principle
Entensively tested in practice
Simple to apply (vector constructions)
Rated inferior in tests by competitor
Efficiency not known
Lacking in independent experimental verification
Not yet adapted to computers
Experience restricted to turbine-generator industry

Comprehensive modal method

    Less rigorous theoretical foundation
    Extensively tested in practice
    Found competent in tests by several investigators
    Calculations more complex
    More operating steps
    Efficiency not known
    Rated superior in tests by proponents
    Well adapted to computers
    Experience extends to all high-speed-machine industries

Further comments on modal balancing methods are given in Section 6.5.

6.3 Influence Coefficient Methods

The influence coefficient method is a formalized correction procedure whereby

1. Trial weights are inserted at selected locations along a rotor in a specified sequence of locations and speeds.
2. Rotor amplitudes and phase angles are read at convenient locations along the rotor at selected speeds where large amplitude vibrations may occur.
3. Required balance corrections are determined from the amplitude and phase data, using a computer program.
4. Balance weights are installed in the rotor correction planes. The process may be repeated until the rotor runs smoothly.

This method requires no advance knowledge of the system dynamic response characteristics, though such information may be helpful in selecting the most effective balance-plane and readout locations for a given system. The influence coefficient method has been applied with equal effectiveness to class 1, 2, and 3 rotors with the properties listed below.

Unbalance

    Distributed
    Concentrated
    Bent rotor (geometric or thermal)

Bearings

Rigid

Flexible undamped (support springs, roiling element)

Flexible, damped (fluid film, rolling element with
backup squeeze film damper)

No bearing effects (free-free modes)

Aligned bearings, poorly aligned bearings, and catenary-string
rotor sets (e.g., turbine-generator)

Symmetrical and nonsymmetrical bearing properties

Foundation

Rigid

Discrete flexible, with and without mass effects

Continuously flexible (rotor in flexible outer casing—e.g.,
jet engine)

Damped flexible foundation

Axisymmetrical and asymmetrical foundation

The influence coefficient method is not a modal balancing procedure per se, but in view of the modal nature of rotor unbalance response, it is evident that a similar overall effect is being achieved to balance the rotor. The emphasis here is on procedure and formalized convenience rather than on physical understanding of the mode shapes. Because of the size of the matrix calculations in most instances, it is desirable to use a computer program or a dedicated minicomputer when applying the influence coefficient method. The use of a computer program is now essential for balancing all but the simplest rotors, because of the complexity of the mode shapes which arise due to bearing stiffness and damping, support asymmetry, and multiple and concentric shaft and foundation effects.

The earliest theoretical studies on the influence coefficient method appear to have been made by Goodman [29] and Lund [30]. Brief comments on this method have also been made by Thearle [31], Groebel [32], Den Hartog [33], and others.

Basic Steps of the Influence Coefficient Method

Let the flexible rotor in undamped bearings shown in Fig. 6.26 have p planes along the axial length of the rotor where measurements of whirl radius and phase angle (referred to some angular datum on the
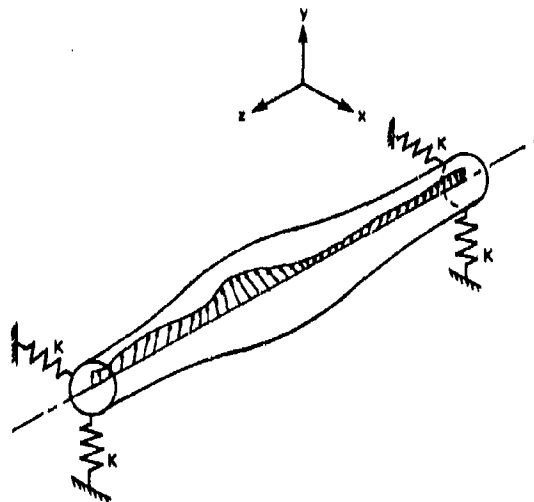
Fig. 6.26. Flexible rotor in undamped bearings with
identical stiffnesses in coordinate directions

rotor) may be taken. Also assume that there are q prescribed correction planes in which balance weights can be added and oriented as required. The influence coefficient balancing sequence is as follows:

1. Run the rotor up to some suitable initial balancing speed ω_1. Measure rotor whirl amplitudes and phase angles at each of the p measuring planes for this speed. Record the acquired data for subsequent processing.

2. Place a trial weight of known magnitude and radius in correction plane 1 at a phase angle equal to zero.

3. Again run the rotor at speed ω_1 and take measurements of whirl amplitude and phase angle in the p measuring planes. Record the data.

4. Remove the trial weight from plane 1 and place it in correction plane 2 at phase angle zero.

5. Run the rotor at speed ω_1, measure the whirl amplitude and phase angle, and record the data.

6. Repeat steps 4 and 5 for the remaining correction planes.

7. Compute the coefficients:

$$a_{rs} = \frac{\left(\begin{array}{c}\text{whirl amplitude}\\ \text{with unbalance}\end{array}\right) - \left(\begin{array}{c}\text{whirl amplitude}\\ \text{without unbalance}\end{array}\right)}{\text{trial unbalance weight}}$$

$$= \frac{w_{rs}^r - w_{rs}^0}{T'}.$$

Note that both the w_{rs} (and w_{rs}^0) and the a_{rs} are complex:

$$w_{rs}^r = (w_{rs}^r)_R + i(w_{rs}^r)_I; \quad a_{rs} = (a_{rs})_R + i(a_{rs})_I \quad (i = \sqrt{-1}).$$

8. Form the influence coefficient matrix [A] that relates the original rotor whirl amplitudes $\{w^0\}$ (a p-row vector) to the original "discretized" unbalance $\{U^0\}$ (a q-column vector), which unbalance is assumed to be concentrated in q correction planes, as follows:

$$\{w^0\} = [A]\{U^0\}.$$

9. Determine the original discretized rotor unbalance $\{U^0\}$ by premultiplying the original whirl-amplitude vector by the inverse of the [A] matrix:

$$\{U^0\} = [A^{-1}]\{w^0\}.$$

10. Determine the required correction weights and phase angles from the negative of the original discretized unbalance;

$$\{U_c^0\} = -\{U^0\}.$$

The U terms are also complex,

$$U_r^0 = (U_r^0)_R + i(U_r^0)_I, \qquad i = \sqrt{-1},$$

and hence

$$|U_r^0| = \sqrt{(U_r^0)_R^2 + (U_r^0)_I^2}; \quad \tan \phi_r = \frac{(U_r^0)_I}{(U_r^0)_R}.$$

Theory of the Influence Coefficient Method

Consider the elastic rotor in damped flexible bearings shown in Fig. 6.27. The rotor system is axisymmetrical and may include any practical variation of its axial geometry. At speed, it experiences circular synchronous whirling under the influence of residual unbalance and mode distortion. The influence coefficient procedure requires only that the whirl amplitude and phase angles be accessible to measurement at the specified locations. In essence, the method is a formalized procedure for determining the influence coefficients $a_{ij}(\omega)$, which are speed dependent and relate the rotor whirl amplitudes w_i to the unknown rotor unbalances U_i by the matrix expression
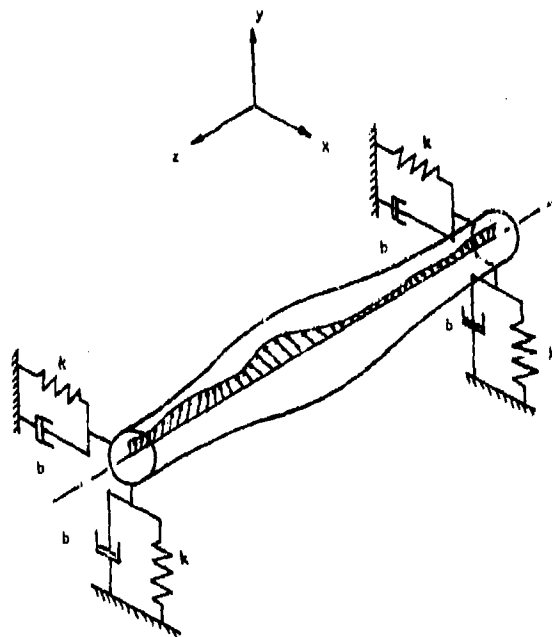
Fig. 6.27. Elastic rotor in bearings with identical damping
and stiffnesses in coordinate directions

$$
\begin{Bmatrix} w_{A0}^1 \\ w_{B0}^1 \\ \cdot \\ \cdot \\ \cdot \\ w_{p0}^1 \end{Bmatrix} = \begin{bmatrix} a_{A1}^1 & a_{A2}^1 & \ldots & a_{An}^1 \\ a_{B1}^1 & a_{B2}^1 & \ldots & a_{Bn}^1 \\ \cdot & \cdot & & \cdot \\ \cdot & \cdot & & \cdot \\ \cdot & \cdot & & \cdot \\ a_{p1}^1 & a_{p2}^1 & \ldots & a_{pn}^1 \end{bmatrix} \begin{Bmatrix} U_1 \\ U_2 \\ \cdot \\ \cdot \\ \cdot \\ U_n \end{Bmatrix}.
$$

This expression is equivalent to modeling the unknown rotor unbalance
distribution by a set of equivalent unbalance forces in the q correction
planes. If the rotor unbalance is concentrated in the correction planes,
the balancing procedure is to first run the unbalanced rotor at speed ω_1,
and at this speed to measure the maximum rotor whirl amplitudes w_0
and phase angles ϕ_0 at p locations along the rotor due to this original
unbalance. This gives

where

$$
\{w_0^1\} = [A(\omega_1)]\{U_0\} = [a_{ji}]\{U_0\},
$$

$$
w = w(\cos\phi + i\sin\phi) = w_c + iw_s,
$$

as shown in Fig. 6.28.

Fig. 6.28. System of fixed (x,y) and rotating (ξ, η) coordinates
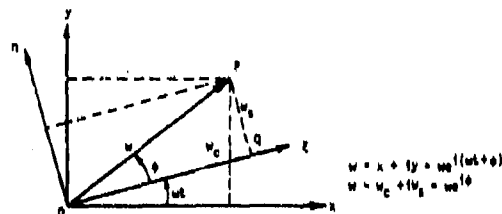
Next insert a trial weight T in correction plane 1 and rerun the rotor at speed ω_1. Again read w and ϕ, which correspond to

$$
\begin{Bmatrix} w_{A1}^1 \\ w_{B1}^1 \\ \cdot \\ \cdot \\ \cdot \\ w_{p1}^1 \end{Bmatrix} = \begin{bmatrix} a_{A1}^1 & a_{A2}^1 & \cdots & a_{An}^1 \\ a_{B1}^1 & a_{B2}^1 & \cdots & a_{Bn}^1 \\ \cdot & \cdot & & \cdot \\ \cdot & \cdot & & \cdot \\ \cdot & \cdot & & \cdot \\ a_{p1}^1 & a_{p2}^1 & \cdots & a_{pn}^1 \end{bmatrix} \begin{Bmatrix} U_1 + T \\ U_2 \\ \cdot \\ \cdot \\ \cdot \\ U_n \end{Bmatrix} .
$$

(measured)   (unknowns)   (unknown) (known)

Subtracting the trial weight response $\{w^1\}$ from the original response $\{w^0\}$ gives

$$
\begin{Bmatrix} w_{A1}^1 - w_{A0}^1 \\ w_{B1}^1 - w_{B0}^1 \\ \cdot \\ \cdot \\ \cdot \\ w_{p1}^1 - w_{p0}^1 \end{Bmatrix} = \begin{bmatrix} a_{A1}^1 & a_{A2}^1 & \ldots & a_{An}^1 \\ a_{B1}^1 & a_{B2}^1 & \ldots & a_{Bn}^1 \\ \cdot & \cdot & & \cdot \\ \cdot & \cdot & & \cdot \\ \cdot & \cdot & & \cdot \\ a_{p1}^1 & a_{p2}^1 & \ldots & a_{pn}^1 \end{bmatrix} \begin{Bmatrix} U_1 + T - U_1 \\ U_2 & -U_2 \\ \cdot & \cdot \\ \cdot & \cdot \\ \cdot & \cdot \\ U_n & -U_n \end{Bmatrix} ,
$$

from which we obtain

$$
a_{A1}^1 = \frac{w_{A1}^1 - w_{A0}^1}{T},
$$

$$
a_{B1}^1 = \frac{w_{B1}^1 - w_{B0}^1}{T},
$$

$$
a_{p1}^1 = \frac{w_{p1}^1 - w_{p0}^1}{T}.
$$

The trial weight T is then removed from correction plane 1 and is inserted into the remaining $(q - 1)$ correction planes as required, to acquire additional data. Successively rerunning the rotor at ω_1 and measuring w and ϕ for each trial gives, in general,

$$a_{kq}^1 = \frac{w_{kq}^1 - w_{kq}^0}{T}.$$

This procedure must be repeated $q = (n/2)$ times (n-even), and $q = (n+1)/2$ times (n-odd), where n is the number of modes to be balanced. This results in the following set of simultaneous equations which are then solved to obtain the rotor residual unbalance, referred to the correction planes:

$$
\left\{
\begin{array}{c}
w_{A1} \\
w_{B1} \\
\vdots \\
\vdots \\
w_{p1} \\
w_{A2} \\
w_{B2} \\
\vdots \\
\vdots \\
w_{p2} \\
w_{A3} \\
w_{B3} \\
\vdots \\
\vdots \\
w_{pn}
\end{array}
\right\}
=
\left[
\begin{array}{cccccc}
a_{A1}^1 & a_{A2}^1 & a_{A3}^1 & \cdots\cdots & a_{An}^1 \\
a_{B1}^1 & a_{B2}^1 & a_{B3}^1 & \cdots\cdots & a_{Bn}^1 \\
\vdots & \vdots & \vdots & & \\
\vdots & \vdots & \vdots & & \\
a_{p1}^1 & a_{p2}^1 & a_{p3}^1 & \cdots\cdots & a_{pn}^1 \\
a_{A1}^2 & a_{A2}^2 & a_{A3}^2 & \cdots\cdots & a_{An}^2 \\
a_{B1}^2 & a_{B2}^2 & a_{B3}^2 & \cdots\cdots & a_{Bn}^2 \\
\vdots & \vdots & \vdots & & \\
\vdots & \vdots & \vdots & & \\
a_{p1}^2 & a_{p2}^2 & a_{p3}^2 & \cdots\cdots & a_{pn}^2 \\
a_{A1}^3 & a_{A2}^3 & a_{A3}^3 & \cdots\cdots & a_{An}^3 \\
a_{B1}^3 & a_{B2}^3 & a_{B3}^3 & \cdots\cdots & a_{Bn}^3 \\
\vdots & \vdots & \vdots & & \\
\vdots & \vdots & \vdots & & \\
a_{p1}^q & a_{p2}^q & a_{p3}^q & \cdots\cdots & a_{pn}^q
\end{array}
\right]
\left\{
\begin{array}{c}
U_1 \\
U_2 \\
\vdots \\
\vdots \\
U_p \\
\vdots \\
\vdots \\
\vdots \\
\vdots \\
\vdots \\
\vdots \\
\vdots \\
\vdots \\
U_n
\end{array}
\right\}
$$

i.e.

$$\{w\} = [A]\{U\},$$

where $[A]$ is a square matrix of coefficients as defined above. Inverting $[A]$ gives

$$\{U\} = [A]^{-1}\{w\}.$$

Once the effective unbalance vector U has been determined, the placement in the correction planes of n weights equal in magnitude but opposite in sense to (U) has the effect of canceling the original unbalance of the rotor.

Verification of the Influence Coefficient Method

In 1934, the application of an influence coefficient method was described by Thearle [31] with reference to the balancing of a two-rotor, three-bearing turbine generator. Between 1940 and 1955, Groebel [32] used practical influence coefficient methods to balance large generator rotors mode by mode. Den Hartog [33] has commented on the influence coefficient principle (for two-plane correction) in his book. It appears that influence coefficient methods were used effectively for several decades before development of the computer.

An analytical study of the effectiveness of influence coefficient balancing was made by Rieger [34], who examined three practical rotor-bearing systems: (a) rigid rotor in gas bearings, (b) a supercritical, flexible, three-disk overhung rotor in fluid-film bearings, and (c) a supercritical, flexible rotor with one disk overhung in three fluid-film bearings. Rieger studied the effect of measurement errors and of correction-weight installation errors on the resulting balance, as well as the relative balance improvement obtained with two, three, and four correction planes. The number of bearing supports involved was shown to exert no direct influence on the quality of balance attainable. Bearing misalignment may affect the critical speed location and shaft bending stresses, but it has no effect on the quality of balance attained unless the whirl ellipses are excessively elongated or the ellipse axes are oriented at different angles by the misalignment.

The effectiveness of the influence coefficient method was evaluated by Tessarzik et al. [35] with a flexible three-disk rotor operating through its lowest bending critical speed. Tessarzik calculated the balance weights by a computerized influence coefficient procedure. The flexible rotor-bearing system used was designed to contribute negligible damping to the rotor whirl mode at the bending critical speed. Under such circumstances, large resonant amplitudes could be expected unless the balancing procedure was effective. After the balance corrections were made, maximum peak-to-peak critical whirl amplitudes of 1.6×10^{-3} in. were measured. Tessarzik and Badgley [36] also developed a least-squares influence coefficient procedure along the lines proposed by Goodman [37] to obtain a best-fit balance for a rotor operating over a speed range containing several critical speeds.

Other experimental studies using a least-squares approach, described by Lund and Tonnesen [38], further verified the effectiveness of this method. Another interesting least-squares development has been reported by Little [39], who used a linear programming technique to optimize the balance of rotors operating through several bending critical speeds. Baier and Mack [40] describe the balancing of long helicopter drive shafts through six critical speeds, to speeds beyond 7000 rpm. They report having achieved smooth shaft operation by developing their own influence coefficient balancing, after having tried modal methods and other flexible-rotor balancing techniques.

The influence coefficient method has the advantage of simplicity in application and is readily adapted to computer-aided balancing. These features make it suitable for balancing a wide range of complex turbomachinery (helicopter shafts, multispool aircraft engines, ultracentrifuges, etc.) and for computerized unbalance weight calculations. Its effectiveness is not influenced by the presence of damping in the system, or by vibratory motions of the locations at which readings are taken. Initially bent rotors can be balanced as readily as straight rotors, and no assumptions concerning perfect balancing conditions are involved to detract from the quality of balance attained. It shares certain disadvantages with the other balancing methods: the number of readings required to acquire the input data can become large, and must be minimized. The accuracy with which these amplitude and phase readings must be made requires care in the data-taking. This has been simplified by recent equipment developments. Existing computer programs for this method assume circular whirl orbits. Where elliptical orbits occur (e.g., from certain fluid-film bearing conditions or from some dissimilar pedestal stiffness condition), the dissimilar amplitudes can be averaged to achieve an average balance, or a technique similar to that proposed by Parkinson [11] can be used. Changes in bearing operating eccentricity induced by load changes will not affect the balance of the rotor or its operation unless the mode shape is substantially changed. Such effects are independent of the method, as are the effects of drive torque fluctuations, bearing stiffness changes, system nonlinear influences, and parametric resonances.

The major experiments that have been conducted on the influence coefficient method are described in Chapter 7.

Least-Squares Optimization of Correction Weights

Goodman [37] developed a theoretical balancing procedure that uses a least-squares technique to minimize the rms residual whirl amplitudes at selected locations along the rotor. This procedure allows

optimum balance corrections to be obtained. The least-squares procedure can also be used as a data-conditioning tool where large numbers of readings are utilized (time-monitoring) or a rectangular matrix array must be adapted before being inverted in the influence-coefficient program.

Consider a rotor that has q correction planes and on which m vibration readings $(m > q)$ have been obtained for K different speed conditions, at l different locations; then $m = Kl$. The least-squares balancing procedure finds the optimum size and angular orientation of the required q balance weights by minimizing the sum of the squares of the m vibration readings. The initial unbalance data w_0 and the trial weight unbalance data w_l at the m measuring locations are first obtained. Influence coefficients a_{ij} are then calculated by the procedure described previously. However, the previous case is for $m = q$, in which the required values of the correction weights were computed directly by matrix inversion. This reduces the whirl amplitudes to zero at q locations at the selected speeds and generally reduces the amplitude whirl rotor throughout the speed range (see Fig. 6.29). At speeds other than the balancing speeds, a small residual unbalance e_l remains such that at the r th location and speed

$$w_{er} = w_{er}^r + iw_{er}^i = w_{r0} + a_{r1}U_1 + \cdots + a_{rs}U_s = w_{r0} + \sum_{s=1}^{\infty} a_{rs}U_s.$$
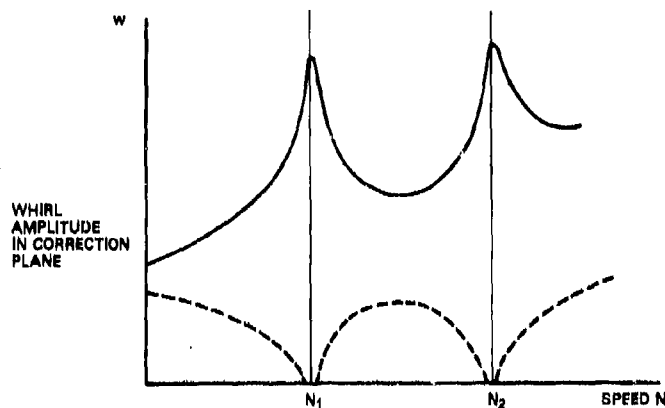
Fig. 6.29. Typical result of influence coefficient balance at correction plane: correction of the first and second modes and overall decrease in rotor whirl amplitude

The response amplitudes w_{er} and w_{m0}, the influence coefficients a_{rs}, and the unbalances U_s are complex quantities. Dividing this expression into its real and imaginary components gives

$$w_{er}^r = w_{r0}^r + a_{r1}^r U_1^r - a_{r1}^i U_1^i + \cdots = w_{r0}^r + \sum_{n=1}^{\infty} (a_{rs}^r U_s^r - a_{rs}^i U_s^i)$$

$$w_{er}^i = w_{r0}^i + a_{r1}^i U_1^i + a_{r1}^r U_1^r + \cdots = w_{r0}^i + \sum_{n=1}^{\infty} (a_{rs}^i U_s^i + a_{rs}^r U_s^r).$$

Let

$$S = \sum_{r=s}^{m} (w_{er})^2 = \sum_{i=s}^{m} [(w_{er}^r)^2 + (w_{es}^i)^2].$$

The objective is now to select the balance weights $W_r = W_r^r + iW_r^i$ so that S is a minimum. This requires that

$$\frac{\partial S}{\partial W_1^r} = \frac{\partial S}{\partial W_1^i} = \cdots = \frac{\partial S}{\partial W_m^r} = \frac{\partial S}{\partial W_m^i} = 0.$$

This leads to $2N$ linear equations of the form

$$\sum_r \left\{ a_{rs}^r \left[w_{0s}^r + \sum_s (a_{rs}^r U_s^r - a_{rs}^i U_s^i) \right] \right.$$

$$\left. + a_{rs}^i \left[w_{0s}^i + \sum_s (a_{rs}^i U_s^r + a_{rs}^r U_s^i) \right] \right\} = 0$$

and

$$\sum_r \left\{ -a_{rs}^i \left[w_{0s}^r + \sum_s (a_{rs}^r U_s^r - a_{rs}^i U_s^i) \right] \right.$$

$$\left. + a_{rs}^r \left[w_{0s}^i + \sum_s (a_{rs}^i U_s^r + a_{rs}^r U_s^i) \right] \right\} = 0.$$

The unknowns in these equations are the components of the balance weights U_s^r and U_s^i required to minimize the rotor response. These terms can be found using standard equation-solving routines when the above procedure is programmed.

Goodman [37] has described the first iteration that is performed with this procedure, followed by a weighted least-squares procedure to be applied in several successive iterations. This will minimize the residual unbalance remaining after each iteration until a satisfactory final balance is achieved. The final set of balance weights and orientations can be obtained automatically by continuing the iterations until a

prespecified balance criterion is achieved. See Refs. 41 through 44 for more on computerized balancing.

Linear Programming Optimization of Influence Coefficient Method

The influence coefficient method involves the solution of the matrix equation

$$\{w\} = [A]\{U\}, \tag{6.1}$$

where $\{w\}$ is a column vector of observed displacements, $[A]$ is the matrix of influence coefficients and $\{U\}$ is an unknown column vector of the effective rotor unbalance related to the corrections planes, to be determined from trial-weight tests. Little and Pilkey [45] have sought an optimum solution to this problem through the use of linear programming techniques, as follows. Let it be required to minimize the above matrix expression, and to determine values for the unbalance column vector $\{U\} = \{U_1, U_2, \ldots, U_n\}^T$ (T = transpose) subject to this minimum condition. Suppose the number of observations is less than the number of unbalances wa sought (i.e., $m < q$); then Eq. (6.1) becomes a system constraint, which is expressed as

$$w_S = [C]\{U\}. \tag{6.2}$$

Equation 6.2 is called the system constraint equation. It represents the response of the rotor at a particular speed and axial location, where C is a row vector representing suitable combinations of influence coefficients. Equation (6.2) can be taken to represent what in linear terminology is known as the *objective function*. If w_S is chosen at a particular axial location—such as at a bearing, where large deflections would produce large forces—or at a particular speed—for example, at a high speed that cannot be successfully negotiated with the unbalance rotor—then maximization of w_S leads to the identification and subsequent removal of a potentially troublesome unbalance distribution related to that particular mode.

The size of the unbalance moments in this procedure is controlled through constraints of the type

$$U_p^L \leqslant U_p \leqslant U_p^U, \qquad p = 1, 2, \ldots, n, \tag{6.3}$$

where U_p^L, U_p^U are lower and upper bounds chosen for the parameter U_p. In terms of linear programming, this inequality constraint is converted to the equality form of Eq. (6.2), which is thereby increased in its permissible size. In practice, with most major linear programming

software systems this conversion is fully automatic and is simple to apply in practice with standard routines.

In applying a linear programming formulation to a rotor, the vectors {U}, {w} are considered to contain the components of the unbalance moments and observed deflections. If there are q correction planes, and m observations, {U} and {w} are $2q$- and $2m$-dimensional column vectors and [A] is $2q \times 2n$. Since the unbalance moment components may be negative, a change in variables is required to satisfy Eq. (6.2). This adjustment is accommodated automatically in most major linear programming systems.

For a given rotor in supports, the influence coefficients a_{ij} can be obtained either experimentally or theoretically. If the objective function is taken at a speed or location that cannot be dealt with experimentally, then it is necessary to compute the influence coefficients for the objective function theoretically. This is normally done with a rotor-response computer program. Where possible it is also desirable to verify the accuracy of the rotor-system model at speeds that can be observed experimentally.

The linear programming formulation requires the maximization of the objective function, Eq. (6.2). It is also desirable to maximize the response amplitude w_S at a given speed and location, given by

$$|w_S| = (w_{Sx}^2 + w_{Sy}^2)^{1/2}. \tag{6.3}$$

In this form $|w_S|$ is a linear but inconvenient function of the response components and therefore of the unbalance components. The use of Eq. (6.3) as an objective function requires that the problem be undertaken in a quadratic programming form. This is not as desirable as linear programming from the standpoint of available computer software. However, it is also possible to maximize the linear combination $|w_{Sx} + w_{Sy}|$ of the x and y components of the objective-function response. It should be noted that the set of unbalance components thus identified might not, in all cases, correspond to the set that produces the maximum objective-function response, although the corresponding response should be large. Thus, instead of identifying the unbalance that satisfies all observations and is potentially most harmful to objective-function response, one obtains an unbalance distribution that is simply potentially large. This formulation, which maximizes the linear combination of the objective-function response components instead of the actual magnitude of the response, produces excellent results while allowing for a linear programming solution. Using linear and quadratic programming, Little and Pilkey [45] have computed several sets of unbalance moments with virtually identical results.

As an example, consider the rotor system shown in Fig. 6.30. The rotor consists of an aluminum shaft 180 in. long, 3.0 in. in diameter, and with a maximum speed of 6000 rpm. It operates in damped flexible bearings both with identical isotropic stiffnesses $K = 5000$ lb/in., and with damping $B = 3.0$ lb s/in. The mode shapes at the three critical speeds within the operating range are shown in Fig. 6.31. Details of the assumed initial unbalance distribution are given in Table 6.3.

k = 5000 lb/in. (875 kN/m)
c = 3.0 lb-s/in. (0.526 kN-s/m)
E = 10.4 × 10⁶ psi (72.8 GN/m²)
I = 0.96 in.⁴ (39.96 cm⁴)

I_p = 0.726 lb in.² (212.41 kg mm²) for 1 and 25
   1.453 lb in.² (425.11 kg mm²) for 2 through 24

DISK MASS = 0.345 lb (0.156 kg) for 1 and 25
   0.090 lb (0.313 kg) for 2 through 24
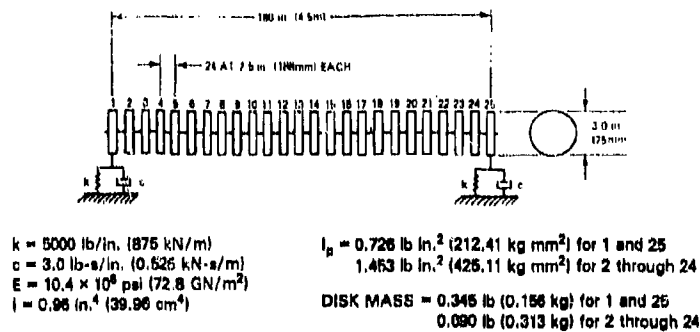
Fig. 6.30. Model of uniform shaft on two end supports.
From Little and Pilkey [45]. Used by permission.

591 RPM

2312 RPM

5010 RPM

1 3 5 7 9 11 13 15 17 19 21 23 25
ROTOR STATION
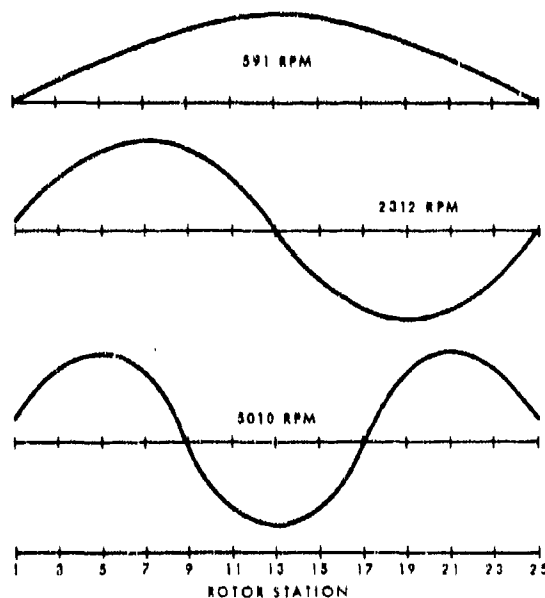
Fig. 6.31. Critical speeds and mode shapes for Little and
Pilkey rotor [45]. Used by permission.

Table 6.3. Arbitrary initial unbalance
distribution for rotor in Fig. 6.30*

Rotor station	x-Component		y-Component	
	oz-in.	mN m	oz-in.	mN m
1	0.56	4.0	0.74	5.2
2	0.84	5.9	0.37	2.6
3	0.47	3.3	0.74	5.2
4	0.74	5.2	0.46	3.3
5	−0.20	−1.4	0.28	2.0
6	0.46	3.3	−0.59	−4.2
7	0.37	2.6	−0.44	−3.1
8	−0.58	−4.1	−0.25	−1.8
9	−0.14	−0.99	0.50	3.5
10	0.58	4.1	0.26	1.8
11	0.24	1.7	0.46	3.3
12	−0.42	−3.0	−0.29	−2.1
13	0.46	3.3	−0.44	−3.1
14	0.10	0.8	−0.29	−2.1
15	0.68	4.8	0.27	1.9
16	0.27	1.9	0.41	2.9
17	0.66	4.7	−0.52	−3.7
18	−0.23	−1.6	0.36	2.5
19	−0.52	−3.7	0.09	0.6
20	0.49	3.5	0.31	2.2
21	0.42	3.0	−0.77	−5.4
22	−0.18	−1.3	0.69	4.9
23	−0.36	−2.5	−0.96	−6.8
24	0.18	1.3	0.25	1.8
25	−0.30	−2.1	−0.50	−3.5

*After Little and Pilkey [45]

Modal response curves corresponding to the initial unbalance condition are shown in Fig. 6.32; examples of rotor amplitude response curves are given in Fig. 6.33. Eight balance planes were chosen along the length of the rotor. Data from seven sets of observations at selected rotor stations and speeds were used in conjunction with the selected balance planes. A standard linear programming code was used to satisfy this optimization problem. The results are shown in Tables 6.4 and 6.5. In each instance the original response amplitudes were potentially high and an amplitude reduction of about 99 percent was achieved by linear programming optimization of the balance correction vector. Thus the optimization method has been shown to work satisfactorily, and the required number of steps and balance planes required
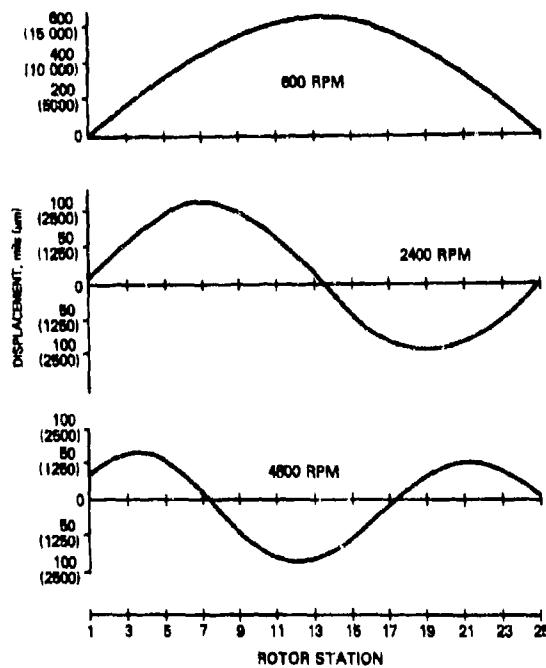
Fig. 6.32. Response of Little and Pilkey rotor to
original unbalance [45]. Used by permission.
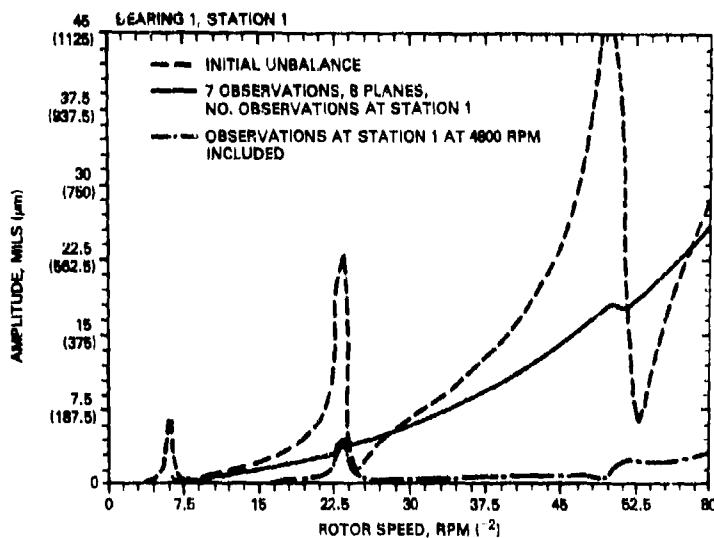
Fig. 6.33. Response of rotor to unbalance, before and after
correction [45]. Used by permission.

Table 6.4. Comparison of balance weight distributions used*

Rotor station	Linear programming[†] x-Component		y-Component		Direct inversion[‡] x-Component		y-Component	
	oz-in.	mN m	oz-in.	mN m	oz-in.	mN m	oz-in.	mN m
5	−2.11	−14.90	−1.33	−9.39	−2.03	−14.3	−1.49	−10.5
7	0.24	1.70	0.81	5.7	0.22	1.6	1.04	7.35
11	−1.20	−8.48	−1.50	−10.6	−2.45	−17.3	−3.44	−24.3
12	3.00	21.2	2.14	15.1	7.23	51.1	6.71	47.4
13	−1.93	−13.6	−0.87	−4.7	−6.32	−44.6	−3.79	−26.8
16	−2.89	−20.4	−0.31	−2.2	—	—	—	—
19	3.00	21.2	−0.03	−0.2	−0.17	−1.2	0.46	3.3
21	−2.04	−14.4	0.41	2.9	−0.19	−1.3	−0.04	−0.3

*After Little and Pilkey [45] (© 1976, ASME; used by permission).
[†]Seven observations, eight planes.
[‡]Seven observations, seven planes.

Table 6.5. Comparison of unbalanced and balanced response of rotor shown in Fig. 6.30*

Rotor station	Speed (rpm)	Initial unbalanced response		Balanced response		Percent reduction
		(mils)	(mm)	(mils)	(μm)	
13	600	654	16.4	5.37	134	99.2
7	2400	109	2.73	2.52	63.0	97.6
19	2400	91.6	2.29	2.28	57.0	97.4
5	4800	56.1	1.40	1.14	28.5	98.0
11	4800	75.5	1.89	0.33	8.3	99.5
12	4800	82.4	2.06	0.56	14	99.1
21	4800	52.0	1.30	1.08	27.0	98.1
16	6000	23.9	0.598	0.29	7.3[†]	98.8

*From Little and Pilkey [45]. Seven observations, eight planes.
[†]Objective function, no observation.

to achieve this amplitude reduction has been demonstrated. A comparison between the linear programming approach and the influence coefficient method is shown in Table 6.6. The results obtained with both methods are comparable through three critical speeds. At the end of the speed range (i.e., 6000 rpm) the linear programming amplitude is significantly smaller than the influence coefficient result for the example and procedures applied.

Table 6.6. Comparison of rotor response obtained by different balancing techniques*

| Rotor station | Speed (rpm) | Initial Unbalanced Response | | Balanced response | | | |
| | | | | Linear programming[†] | | Direct inversion[‡] | |
		mils	mm	mils	mm	mils	μm
13	600	654	16.4	5.37	134	5.37	134
7	2400	109	2.73	2.52	63.0	0.45	11
19	2400	91.6	2.29	2.28	57.0	0.16	4.0
5	4800	56.1	1.40	1.14	28.5	0.87	22
11	4800	75.5	1.89	0.33	8.3	0.72	18
12	4800	82.4	2.06	0.56	14	0.58	14
21	4800	52.0	1.30	1.08	27.0	0.63	16
16	6000	23.9	0.598	0.29[‖]	7.3	5.90[§]	148

*After Little and Pilkey [45] (© 1976, ASME; used by permission). Rotor from Fig. 6.30.

[†]Eight observations, seven planes.

[‡]Seven observations, seven planes.

[‖]No observation, objective function.

[§]No observation, no balance plane.

Difficulties experienced by Little and Pilkey [45] in applying this method are described in their paper. A relatively large number of balance planes has been used in the example, and from a practical standpoint the volume of data reduction and time involved might not be justified, except in special applications. However, in emerging versions of the influence coefficient method such data-taking is performed automatically. A comparison calculation using, say, three or four balance planes to remove the effects of two bending critical speeds (e.g., of the rotors analyzed by Kendig [17]) would provide an indication of the accuracy of the method under more usual circumstances.

Discussion of the Influence Coefficient Method

Successful applications of the influence coefficient technique appear to include a wider range of rotating machinery types than those

reported for other flexible-rotor balancing methods, although there are substantially fewer publications on influence coefficient balancing than on the other methods. Known applications include a high-speed (24,000 rpm) pump simulator; a long helicopter drive shaft (28 ft, six critical speeds); certain ultracentrifuge applications; and several small steam turbines and small aircraft gas-turbine applications. Notable features reported in these applications are summarized below.

Convenience of Application. The method is simple to apply but usually requires the acquisition of a large amount of data: $2N$ sets of amplitude and phase-angle data are required for the exact-point-speed version of this method and preferably several more than $2N$ sets for the least-squares version. The data acquisition is fairly straightforward, but the amount of data required may become very large in cases where the operating speed range involves many critical speeds (e.g., helicopter drive shafts). Some automated form of data taking and recording on tape or minicomputer is needed, preferably arranged in a form suitable for direct use as input for the balance weight and angle calculations that follow. Such equipment is available, and with such an arrangement, this method provides a rapid and efficient balancing procedure.

Accuracy of Balance Attainable. The factors that limit the present form of the influence coefficient method are (a) the precision to which measurements of amplitude and phase can be taken, (b) the repeatability of the readings taken during a balance operation, and (c) the assumption of a circular rotor whirl orbit.

To remove the first two shortcomings involves the use of a precision electronic data-sampling system capable of reading and storing amplitude and phase data at all readout locations simultaneously, coupled with a programmed statistical technique for evaluating the sampled amplitude, phase, and speed data. Experience shows that these input data may vary substantially, even over a short time period. The variation comes mainly from speed fluctuations, and is especially serious in the vicinity of a critical speed. With precise speed control each reading can be electronically sampled many times over a fairly short time period (1000 revolutions, 1000 readings). The statistically analyzed results may then be used to compute the required balance weights and angles to give a refined statistical balance. An indication of the accuracies attainable in practice with present methods is shown in the results of Bishop et al., Hundal and Harker [46], and Church and Plunkett [47]. The effect of errors in measurement and in balance-weight installation on the quality of balance obtained has been studied by Rieger [34].

The third shortcoming mentioned occurs when the whirl orbit is elliptical because of the asymmetrical stiffness properties of the bearings or their supports. To date, no analytical balancing techniques that

account for such elliptical whirling have been published. Anisotropic rotor stiffness effects on the rotor orbit can be accounted for by splitting the rotor unbalance U^0, deflections w_j, and influence coefficients a_{ij} into components corresponding to the principal stiffness directions of the rotor:

$$U_j^0 = H_j^0 + iV_j^0; \qquad w_j = S_j + iT_j$$

$$a_{jkx} = \alpha_{jk} + i\beta_{jk}; \qquad a_{jky} = \delta_{jk} + i\epsilon_{jk}.$$

The resulting influence coefficient matrix is then

$$
\begin{bmatrix}
S_1 \\
T_1 \\
\cdot \\
\cdot \\
\cdot \\
S_i \\
T_i \\
\cdot \\
\cdot \\
\cdot \\
S_p \\
T_p
\end{bmatrix}
=
\begin{bmatrix}
\alpha_{11} & \epsilon_{11} & \cdots & \alpha_{1j} & \epsilon_{1j} & \cdots & \alpha_{1q} & \epsilon_{1q} \\
\beta_{11} & \delta_{11} & \cdots & \beta_{1j} & \delta_{1j} & \cdots & \beta_{1q} & \delta_{1q} \\
\cdot & \cdot & & \cdot & \cdot & & \cdot & \cdot \\
\cdot & \cdot & & \cdot & \cdot & & \cdot & \cdot \\
\cdot & \cdot & & \cdot & \cdot & & \cdot & \cdot \\
\alpha_{i1} & \epsilon_{i1} & \cdots & \delta_{ij} & \epsilon_{ij} & \cdots & \alpha_{iq} & \epsilon_{iq} \\
\beta_{i1} & \delta_{i1} & \cdots & \beta_{ij} & \delta_{ij} & \cdots & \beta_{iq} & \delta_{iq} \\
\cdot & \cdot & & \cdot & \cdot & & \cdot & \cdot \\
\cdot & \cdot & & \cdot & \cdot & & \cdot & \cdot \\
\cdot & \cdot & & \cdot & \cdot & & \cdot & \cdot \\
\alpha_{p1} & \epsilon_{p1} & \cdots & \alpha_{pj} & \epsilon_{pj} & \cdots & \alpha_{pq} & \epsilon_{pq} \\
\beta_{p1} & \delta_{p1} & \cdots & \beta_{pj} & \delta_{pj} & \cdots & \beta_{pq} & \delta_{pq}
\end{bmatrix}
\begin{bmatrix}
H_1^0 \\
V_1^0 \\
\cdot \\
\cdot \\
\cdot \\
H_j^0 \\
V_j^0 \\
\cdot \\
\cdot \\
\cdot \\
H_q^0 \\
V_q^0
\end{bmatrix}
$$

To obtain the above expression requires that trial weights be added in both principal directions in each of the n balancing planes. In general, two correction weights must be added in each balancing plane, corresponding to the H_j^0 and V_j^0 unbalances. It may be possible in some correction planes to insert a single correction weight whose magnitude and angular orientation are determined by the vector addition of the H^0 and V^0 unbalance vectors.

6.4 Other Flexible-Rotor Balancing Procedures and Experiences

Many other methods for balancing flexible rotors have been proposed, and several are discussed in this section. In general, the methods described have not received the widespread acceptance accorded the methods of Sections 6.2 and 6.3, usually due to some lack of generality in the proposed approach.

Church and Plunkett [47] applied the mobility method to the balancing of a simple, uniform, flexible rotor. This method depends on the known relationship between a point force F applied at location k on a uniform shaft in rigid supports, and the transverse deflection of the shaft at location j:

$$r_j = \frac{2L^3}{A\rho} \sum_{n=1}^{\infty} \frac{\sin\,(n\pi c/L)\,\sin\,(n\pi z/L)}{n^4\pi^4\lambda^2 - w^2L^2}\,F_k,$$

where L is shaft length, $A\rho$ is the mass per unit length, n is the mode number, c is the location of F_k, and z is the location of r_j. Evidently, r_j depends on the location of F_k as well as its value. Also, for several forces applied simultaneously,

$$r_j = \alpha_{1j}F_1 + \alpha_{2j}F_2 + \alpha_{3j}F_3,\ \text{etc.}$$

Letting each force correspond to an unknown rotating unbalance gives a specific relation at each speed between the whirl radius r_j and the effective distribution of unbalance at the measurement locations.

The method was tested experimentally with a long, uniform, flexible shaft in end ball bearings with critical speeds at 500, 2000, and 4500 rpm. Maximum shaft speed was 2000 rpm. Measurement locations were at $0.4L$ and $0.7L$. Correction planes were at $0.2L$, $0.5L$, and $0.9L$, to balance first-, second-, and third-mode effects. "Mobility" values $\alpha = r/F$ were calculated for the test rotor using the above expression. Simultaneous equations relating measured displacement to unknown unbalance were then formed:

$$\frac{1}{2}\,A\gamma L \begin{Bmatrix} r_1 \\ r_2 \\ r_3 \end{Bmatrix} = \begin{bmatrix} \alpha_{11} & \alpha_{12} & \alpha_{13} \\ \alpha_{21} & \alpha_{22} & \alpha_{23} \\ \alpha_{31} & \alpha_{32} & \alpha_{33} \end{bmatrix} \begin{Bmatrix} U_1 \\ U_2 \\ U_3 \end{Bmatrix}.$$

These expressions relate whirl amplitude at locations $j = 1, 2, 3$ to unbalance at locations $k = 1, 2, 3$. The shaft balancing procedure was as follows:

1. Shaft runout was measured at each location j by hand rotation in 30° steps. Runout size and orientation were measured.

2. The shaft was then rotated at three selected speeds, in turn. The whirl maximum amplitude and its orientation were determined at each capacitance displacement sensor location.

Since considerable difficulty was experienced in confirming the α-mobility values, the shaft was shaken with a vibrator. The critical speeds were measured at 550, 2000, and 4180 rpm. Resonant frequencies were about 15 percent below calculated values. Nodes did not occur precisely at the ideal locations (e.g., second mode $0.49L$, third mode $0.353L$, and $0.676L$). The effective unbalance at each measurement location was calculated, and correction masses were added to balance the shaft. The shaft was tested through the speed range after balancing. It continued to show amplitudes on the order of 60×10^{-3} in. at the first and second critical speeds. Church and Plunkett concluded that the method represented a practical procedure for flexible rotors and that it is not feasible to balance a shaft for operation at high speeds when the data taking must be performed near the required operating speeds. Recent practice has now overcome this restriction, using other methods.

The procedure described is an influence coefficient method that is without the trial-weight steps, which has been optimized using modal concepts. Such a procedure should be very efficient, but the test results showed that excessive amplitudes remained. Since other studies have shown that the influence coefficient method is workable, the problem appears to reside in the influence (mobility) coefficients themselves. With small very flexible rotors, high-precision measurement is essential and very precise speed control is needed. The control over those factors may have been insufficient in the test described [47]. Similar problems were reported by Voorhees et al. [48] in model tests on long, flexible, helicopter drive shafts. The substitution of calculation procedures for tests to determine the influence coefficients is potentially a time-saving alternative, but it remains to be seen whether calculation can give sufficiently accurate influence coefficients in practice.

Hundal and Harker [46] developed a modal procedure for balancing flexible rotors having an arbitrary distribution of mass and stiffness along their length, with or without lumped masses, and without rotor damping or gyroscopic effects. The unbalance distribution is not known initially and is also assumed to be arbitrary. The unbalance "function" is determined by calculating a limited number of natural frequencies and normal modes, which are subsequently calibrated using measured dynamic amplitudes at selected axial locations, at suitable speeds. Much of the work described is similar to the analysis of Gladwell and Bishop [4], of which these authors appear to have been unaware. Hundal and Harker begin with the basic dynamic equation of shaft dynamics:

$$\frac{d^2}{dz^2}\left[EI(z)\ \frac{d^2r}{dz^2}\right] = \omega^2 m(z)r,$$

where the symbols have their previous meaning. Rigid bearings are next assumed, and a solution is sought for the boundary conditions

$$r(0) = r''(0) = r(L) = r''(L) = 0.$$

The expression for the complex unbalance whirl radius $r(z) = x(z) + iy(z)$ is again used to specify the shaft whirl radius in terms of modal coefficients $Y_i(z)$ and shaft characteristic functions $\phi_j(z)$:

$$r(z) = \sum_{j=1}^{\infty} Y_i(z)\phi_j(z).$$

The transfer matrix approach is next introduced as a procedure for coupling the critical frequencies and characteristic functions (modal equations) of the rotor:

$$\{g_q\} = [T_{qp}]\{g_p\},$$

where

$$\{g_p\}^T = \{r_p, r_p', r_p'', r_p'''\}$$

and $\{g_p\}$, $\{g_q\}$ are state vectors of the transfer matrix $[T_{qp}]$, which can be solved for critical frequencies ω and mode shapes $\phi(z)$ of the rotor in the usual manner (see Ref. 49).

To define the rotor balance conditions, the rotor eccentricity is expressed as a modal series:

$$a(z) = \sum_{j=1}^{\infty} a_j \, \phi_j(z),$$

and the orthogonality relations

$$\int_0^L m(z) \, \phi_j(z) \, \phi_k(z) \, dz = \begin{cases} 0 & (j \neq k) \\ M_j & (j = k) \end{cases}$$

and

$$\int_0^L EI(z) \, \phi_j(z) \, \phi_k(z) \, dz = \begin{cases} 0 & (j \neq k) \\ K_j & (j = k) \end{cases}$$

are used to define the generalized mass M_j and the generalized stiffness K_j.

The coefficients in the rotor amplitude equation are then obtained by writing

$$\int_0^L m(z)\, r(z)\, \phi_j(z)\, dz = \phi_j \int_0^L m(z)\, \phi_j^2(z)\, dz = \phi_j M_j$$

or

$$\phi_j(z) = \frac{1}{M_j} \int_0^L m(z)\, r(z)\, \phi_j(z)\, dz,$$

where M_j corresponds to Z_j in the modal analysis of Bishop and Gladwell [4]. The principle of virtual work is then used to find that the jth modal amplitude is given by

$$r_j(z) = -\frac{\omega^2}{\omega_j^2 - \omega^2}\, a_j(z).$$

Consideration is then given to expressing the modal components of any concentrated unbalance (eccentric disk, correction mass) as a modal series. A concentrated correction P at $z = c$ is thereby expressed as

$$P_c = \sum_{j=1}^{\infty} \frac{P\, m(c)\, \phi_j(c)}{M_j}.$$

Hundal and Harker [46] state that, in order for the rotor to be balanced in the jth mode, the jth component of the unbalance must vanish. Writing the unbalance as

$$m(z)\, r(z) = m(z) \sum_{j=1}^{\infty} a_j\, \phi_j(z)$$

means that, for a rotor with inherent unbalance, a correction P must be located at a point $z = c$ such that

$$a_j\, \phi_j(z) + b_j\, \phi_j(z) = 0;$$

that is, $a_j = -b_j$. Substituting allows the balance equation for the jth mode to be written as

$$P\, m(c)\, \phi_j(c) = -\int_0^L m^2(z)\, a(z)\, \phi_j(z)\, dz = -a_j.$$

This determines that a single correction P applied at any point along the rotor other than at a node will cancel the component of distributed unbalance associated with any selected normal mode. The optimum location of the correction plane is such that the least amount of correction is required. This requires that $m(c)\, \phi_j(c)$ be maximum in the above expression (that is, at a local maximum in the characteristic function for the mode).

Balancing may be undertaken in several modes simultaneously. The component of unbalance in the j th mode is

$$\frac{1}{M_j} a_j \phi_j(z),$$

and therefore, for the rotor to be balanced in the jth mode as a result of the combined effect of corrections P_k $(k = 1, 2, \ldots, l)$, the sum of the balance equations should vanish, or

$$\frac{\phi_j(z)}{M_j} \sum_{k=1}^{l} P_k \, m(c_k) \, \phi_j(c_k) + \frac{1}{M_j} a_j \phi_j(z) = 0$$

and

$$\sum_{k=1}^{l} P_k \, m(c_k) \, \phi_j(c_k) = -a_j.$$

Therefore, selecting the number of modes k to be balanced and assigning values results in a set of simultaneous equations of the form

$$[m\phi]\{P\} = -\{a_j\},$$

which can be developed and solved for the required values of the P_j.

Hundal and Harker specify the following rotor-balancing procedure:

1. Determine the required critical speeds and modes of the rotor.
2. Measure dynamic deflections at speed close to each critical speed.
3. Determine each modal unbalance $a_j(z)$.
4. Evaluate the integrals for M_j and $\phi_j(z)$.
5. Select the most suitable correction planes z_k.
6. Calculate the required modal coefficients at the correction planes.
7. Formulate the simultaneous equations required to balance the rotor and solve for the required corrections P_j.

Note that the determinant $|m\phi|$ must not vanish. Also, the number of correction planes must equal the number of modes to be balanced. Numerically, a well-defined solution for P will exist when the elements on the main diagonal of the matrix are the dominant elements of the matrix. This emphasizes that the balancing planes should be located (a) at the maxima of the successive mode shapes, and (b) at the maxima of the mass-distribution curve of the rotor.

Hundal and Harker [46] conducted experiments on a model rotor of general shape to verify the above analysis. The first three natural

frequencies were computed by the matrix method and confirmed by a vibration test. The dynamic response of the rotor was measured by sweeping the length of the rotor at given speeds with a special amplitude transducer head. Balancing was carried out in the first and second modes, and a 4:1 reduction in amplitude was obtained. An important observation made by the authors is that no trial weights are required. Their subsequent comment that successive approximations are needed does not appear valid (as far as the balance obtained is concerned), though it may be correct in the sense that a closed-form exact solution can be achieved without iteration.

This method closely resembles the Bishop and Gladwell method in its analytical approach and in the final balance equations. The balancing experiment, though simple, demonstrates the effectiveness of the modal balancing method using a computer approach.

Findlay [50] made a useful review of the modal balancing method with special reference to the analysis and experiments of Hundal and Harker [46]. Findlay first reviewed the modal approach and its assumptions, and then discussed the practical limitations of modal methods. It is noted that the rotor must be run close to each normal mode when obtaining modal data in order to achieve the accuracy required for effective balancing calculations. Also, in practice, residual unbalance makes mode-by-mode balancing essential in almost every case. Several questions are left unanswered by Hundal and Harker: How should the balance planes be selected? Which combination of correction weights and angles will optimize the balance? How to deal with the problem of two critical speeds close together? Details of the number of balance runs and measurements required to obtain suitable balance data were omitted. Findlay has not commented on questions of satisfying the orthogonality conditions for a rotor in flexible damped (real) bearings, though this is covered by implication in the Hundal-Harker analysis. He commented in general terms on several other balancing procedures, such as the influence coefficient method, and briefly compared these with the modal balancing method. Findlay's conclusion was that pure modal balancing is not a generally applicable balancing technique because of serious practical difficulties involved in acquiring useful rotor response data and because the method described relies on calculated normal modes and frequencies. Subsequent experience has demonstrated that, while these comments may perhaps apply to "pure" modal balancing, such methods as modal averaging have indeed proved effective in practice.

Den Hartog [33] discussed the requirements for shaft balancing and reduced his results to the following theorem:

A rotor consisting of a straight weightless shaft with N *concentrated masses along its length, supported in* B *bearings along its length, and having an arbitrary unbalance distribution along the shaft but not restricted to the locations of the concentrated masses can be perfectly balanced at all speeds by placing appropriate small correction masses in* (N — B) *different planes along the length of the shaft.*

By perfect balance Den Hartog means that, "The bearings have no motion at rotational frequency, and feel no force at rotational frequency." He claims that nearly perfect balances can be obtained at all speeds by balancing in $N - B$ planes, where N now means the number of rigid-bearing rotor critical speeds in the range from zero to four times the maximum service speed of the machine. The objective of the balancing process is to achieve the following conditions:

1. Cause the shaft deflection to be zero at all concentrated masses and at all intermediate bearings; these conditions can be expressed as $(N - B - 2)$ equations.

2. Cause the sum of all centrifugal forces acting on the shaft to be zero (one equation).

3. Cause the sum of all the moments of the centrifugal forces to be zero about some fixed point (one equation).

When this is achieved, the deflection at the disks is zero and their centrifugal forces are zero, and the only remaining forces are due to small unbalances and the correction masses themselves. Since the rotor then has no significant centrifugal force, no force is transmitted to any bearing. Whether the bearings are rigid or flexible then becomes irrelevant because no force is transmitted. The basic requirement is to force nodes to occur at the disks and at the bearings. The above is expressed by the balance equations

$$\Sigma \, m_k a_k = 0 \quad \text{(one equation)},$$

$$\Sigma \, z_k m_k a_k = 0 \quad \text{(one equation)},$$

$$\Sigma \, \alpha_k m_k a_k = 0 \quad ((N - B - 2) \text{ equations}).$$

Den Hartog next demonstrates this procedure with four numerical examples: (a) uniform shaft in two rigid end bearings, (b) three-span shaft in rigid bearings, (c) two-span rotor in rigid bearings, and (d) two-span rotor with midspan hinge. These examples are all for uniform beam rotors for which the influence coefficients are easily obtained; the rotors are mounted in rigid bearings. The requirement that all rigid-bearing whirl modes should lie within the range of four times the operating speed is based on practical considerations.

For practical purposes the procedure for Den Hartog's method is as follows:

1. Determine the required number of correction planes based on the rules given above.
2. Select suitable locations for the correction planes.
3. Determine the influence functions for the proposed correction planes. The rotor is to be tested for these functions throughout the operating speed range, using the trial-weight method. At each balance speed, an influence function is required for each correction plane with a trial weight in the other correction planes.
4. Set up the required $(N - B)$ balance equations.
5. Solve the balance equations for the required correction masses.

Theory and examples are given to demonstrate this method, which is quite general in application. The balance conditions are vector equations in the general case. The method appears to prescribe reasonable balance conditions and gives clear guidelines for required correction planes and balance speeds. In general, the requirement to run through the speed range to determine the influence functions would seldom be possible initially: a mode-by-mode procedure would be required until an approximate balance was achieved. Then the full-speed-range balance could be undertaken, checked, and repeated where necessary. This procedure should give excellent results.

Tang and Trumpler [51] described a balancing procedure for rotors with shrunk-on disks in which the angular orientation of the disks on the shaft would be arranged to reduce or eliminate the rotor residual unbalance effect. A "disk sensitivity" criterion is described for determining which disk locations would exert the greatest balancing effect on rotor performance. The bearing transmitted force is used to assess the quality of balance attained, and, as described previously, this involves rigid-rotor equilibrium and modal equilibrium considerations. A numerical example of the proposed procedure is presented. Calibrated rotor mode shapes, obtained both before and after balancing by the disk reorientation theory, are shown. The calculated transmitted force at the overhung bearing is reduced from 3024.6 lb (unbalanced) to 24.6 lb (balanced). It is the authors' recommendation that built-up rotors should be assembled *after* the optimum orientation of disk unbalances has been determined by calculation, as opposed to the current procedure of assembling the disks in a random sequence, followed by assembly balancing. However, assembly eccentricity, warping misorientation, misalignment, high-temperature operation, etc., would still require trim balancing after rotor assembly. It appears that this procedure remains to be tested on an actual rotor. Also, overspeed testing of all high-speed rotors is now accepted practice, and with a rotor set up in a

spin pit, the balance operations are readily undertaken. A possible compromise is to assemble blade-carrying rotors in the usual manner and to distribute the blade masses around the circumference so that any differences in blade masses are used to optimize the rotor balance. It appears that the Tang—Trumpler procedure will satisfy the condition

$$\sum m(z)\, r(z) = 0.$$

It may also be possible to satisfy the second rigid-body condition

$$\sum m(z)\, r(z) z_k = 0,$$

but with evidently greater inconvenience. This condition could require require axial disk movement, which clearly is less possible for most turbomachines. Further, this condition must be satisfied with (at least) the first modal condition

$$\sum m(z)\, a(z)\, \phi_1(z) = 0$$

if the Tang—Trumpler procedure is to apply to a flexible rotor. Thus the proposed procedure becomes more difficult to implement in practical flexible rotors.

Lindsay [52] has described certain practical balancing procedures used in the turbine-generator industry. A vibration reduction of up to 75 percent in one balance "move" is claimed. The method relies on reasonably circular journal whirl orbits and assumes that vibration responses are independent from span to span in a unit. These procedures rely on extensive previous experience with similar size units in similar bearings. Also, the size ranges of the various influence coefficients that relate rotor response to correction weights must be well understood. The steps involved are

    1. Vibration vectors at both ends of the rotor are separated into modal components.

    2. Location of the "high spot" for each mode is determined.

    3. Location of the phase angle of the high spot is determined for each mode. This is done by observing a high-spot traverse of 180° through the speed range for each mode.

    4. Calculation by computer of the amount of the required correction for each mode.

The shaft vibration vectors can be divided into modal components by a graphical method, related to the construction given by Moore [20] but without any trial-weight procedure. Lindsay [52] indicates that if the three-loop mode is to be corrected, its components are separated from

the single-loop components by an analysis of relative journal displacements at the respective critical speeds. Details are given of how the dynamic high-spot phase angle can be found for each mode. A reference bolt in the turbine coupling is used as a phase datum. This method requires no trial-weight runs, and accurate placement of the correction weight in the first trial requires an understanding of the high-spot traverse mechanics associated with the relevant critical speed. Details of a sample balance for a 200-MW unit are given, including the use of the "balance shot calculator" used by Lindsay. It is stated that more than one hundred rotors have been balanced in this manner, with good (50 to 75 percent) vibration reductions achieved in most instances in one balance move.

LeGrow [53] has discussed multiplane balancing of flexible rotors and has described a matrix method for the direct solution of the equations of motion, in which the disk unbalance is the unknown. Reliable solutions by this procedure depend on accurate measurement of the whirl amplitude and especially the phase angle. The direct method has the practical advantage of not requiring many costly trial runs to establish a matrix of influence coefficients. In this procedure the rotor influence coefficients are obtained by calculation, not by trial-weight tests. The resulting coefficients were verified by a critical speed test on a model rotor. The observed critical and calculated critical speeds were 3200 and 3125 rpm, respectively (2.4 percent accuracy based on frequency or 5.8 percent accuracy in the coefficients themselves). Unbalance-response data were taken at 2800 rpm, and the balance weights were calculated. The balance corrections obtained were found to be insufficiently precise to balance the rotor, and a trial-weight procedure was used to obtain an average amplitude reduction of 8:1. Subsequent experience with medium-size generator rotors appears to have been more encouraging: amplitude reductions of between 9:1 and 43:1 have been observed at various locations using the direct method.

Kushul' and Shlyakhtin [54] have given a detailed review of modal balancing theory, together with descriptions of certain modal balancing techniques used in the Soviet Union. The theory and procedures apply to complex multidisk rotors with both concentrated and distributed mass-elastic properties. Two or more radially rigid bearings are included. The authors give a number of theorems for balancing flexible rotors and discuss the determination of balancing planes for the most effective suppression of certain modes for four given rotor configurations. Three numerical examples are given to demonstrate practical applications. Although complicated, the mathematical procedures are described in sufficient detail to make this a valuable paper.

The influence of gyroscopic and rotatory inertia on the balancing process is recognized as a defect in the theory that affects the critical frequency and the associated mode shapes on which the balancing theorems depend. The methods presented are further restricted to rigid-bearing concepts. The authors comment on the procedure given by Den Hartog in this regard—perfect balance requires zero journal motion—and they express reservations about the degree to which this condition can be met with a continuous mass-electric rotor for which only the lower modes are corrected. Furthermore, they have observed slow convergence of the modal series, which again suggests to them that the higher modes will in general require some degree of correction. They again concur with Den Hartog's recommendation that rotors should be corrected for all modes below four (or five) times their lowest rigid-bearing critical speed. The influence of damping is omitted, and the modal forms are plane curves. These assumptions are necessary to make the analysis tractable. No correlation with experimental or test results is mentioned.

The modal theory developed by Kushul' and Shlyakhtin results in the following theorem for flexible-rotor balancing:

In order to remove vibrations to the k-order under any angular rate of rotation with the use of n balance weights distributed in the given rotor sections, without causing vibrations of order 1, 2, ... , (k−1), (k+1), ... , n, the balance weights must first of all be placed in axial plane k and inclined at a specified angle. Secondly, n static moments U_{kj} of mass M_{kj} (j=1, 2, ... , n) for the balance weights must be determined from the system of equations:

$$\sum_{j=1} M_{kj} \, \phi_k(z_j) + a_k = 0$$

and

$$\sum_{j=1} M_{kj} \, \phi_s(z_j) = 0,$$

where $s = 1, 2, ... , (k − 1), (k + 1), ... , n$. The first equation is identical with the modal balance condition expressed by Bishop and Gladwell [4]. The second equation is the condition for suppressing the higher modes. Kushul' and Shlyakhtin [54] comment on this procedure as follows:

> In this manner, for each order of vibrations a strictly determined relationship of static moments M_{kj} is established; they do not depend on the distribution of inbalance [sic] of the rotor, but are determined by its calculated diagram (mode shape) and the selection of places of

distribution of the balance weights alone. Tne proportion of M_{k1}, $M_{k2}, \ldots, M_{kn}$ can be calculated in advance for each mode. Their knowledge simplifies the process of rotor balancing. By keeping these ratios fixed it is sufficient to vary only one parameter, independent of the number of balance weights, to completely eliminate the k harmonic, as long as its plane of action is known.

The requisite theory for these operations is included in the paper. Higher orders than n remain unbalanced.

Kushul' and Shlyakhtin discuss several other topics, using the theoretical developments as a basis for the explanations, in a general attempt to formulate guidelines. For example, they consider the most effective location of the correction planes, together with certain practical factors that influence plane selection (e.g. maximum error tolerance).

The authors next present a theoretical treatment for the balancing of multibearing rotors, stating that, irrespective of the number of bearings, k balance planes are able to correct the k lowest modes of a rotor. Again, k is to be selected so that the kth mode is four to five times greater than the lowest critical frequency of the system. A "combined" method of balancing is described in which $(n - k)$ additional corrections planes are used $(n > k)$ to correct through the nth mode.

In this manner, the lower modes are to be completely suppressed and the higher mode effects are reduced. Mathematically, convergence of the modal series to zero is hastened. A sample application for a rotor in b bearings with a single concentrated mass per span is given. The authors also give a procedure for estimating the unbalance force at the sth bearing from unbalance in a given plane for unbalance. The reaction at the bearing distance z_l from the origin is

$$P_l(\omega) = \frac{\omega^2}{\omega_0^2} P_l(\omega_0) + \sum_s a_s \nu_s \{\phi_R \ \phi_L\},$$

where

ω = circular frequency for which force $P_l(\omega)$ is required

ω_0 = circular frequency for which bearing force $P_l(\omega_0)$ is known

a_s = modal unbalance for the sth mode

ϕ_L = characteristic equation value to left of the sth bearing

ϕ_R = characteristic equation value to right of the sth bearing.

The quantity ν_s is defined as

$$\nu_s = \frac{EI}{\rho A \omega^2} \ \frac{1}{4} \ (\omega^2 \omega_0^2) \ \Xi \left(\frac{\omega}{\omega_s}\right) \phi(\lambda_s z),$$

with

$$\Xi\left(\frac{\omega}{\omega_s}\right) = \left(\frac{\omega}{\omega_s}\right)^{3/2} + \left(1 + \frac{\omega_0}{\omega}\right)\left(\frac{\omega}{\omega_s}\right)^{3/2} + \ldots,$$

$$\lambda_s \quad = \frac{\rho\omega_s^2}{EI},$$

$\omega_s \quad =$ critical frequency for the sth mode,

$\phi(\lambda_s, z) \quad =$ value of the modal function for argument $\lambda_s z$,

and $\rho(= w/g)$. The terms E and I have their usual meaning for a uniform rotor. The authors recommend the above formula for evaluating the quality of balance.

Dimentberg [55] has discussed the theory of flexible-rotor balancing, a topic which is not covered in his book [56] on rotor dynamics. This paper is a review of balancing papers that includes selected results. The stated intention is to describe most of the recent developments. The basic criterion for balance is that the bearing reaction forces shall be reduced to negligible proportions. This question resolves itself into (a) determining the axial locations where the correction weights are to be placed, (b) how many axial planes are required, and (c) measuring the effect of the rotor residual unbalance on response magnitude and phase with the rotor revolving.

Several charts are presented for the effect of balance weights at various locations on a two-bearing rotor. Brief discussions of several methods with applications from Soviet authors are given. The paper by Den Hartog [33] is briefly discussed.

In addition to the balancing of deformed shafts and other rotating components that have not yet been fully studied, Dimentberg indicates several important problems:

1. The balancing of rotors carrying large disks subjected to angular precession of a velocity different from the velocity of the rotor.

2. Methods for correcting unbalances induced by differences in the elastic properties of both the rotor and the bearings in two mutually perpendicular directions and induced by the torsion of a long shaft subjected to constant torque (turbogenerator rotors).

3. Temperature effects and complex conditions in bearings.

4. Methods for balancing rotors of varying masses in process machinery.

5. Developments in automatic balancing of flexible rotors.

Dimentberg discusses the work of Hubner [57] in some detail. He makes no reference to the influence coefficient method as an important recent development. (Both papers may have been in press at the same

time.) He makes no reference to any application of computers to balancing.

Several other interesting papers by Czechoslovakian and Russian authors are discussed below. In general, the Russian papers appear to be oriented more toward theoretical procedures, whereas the Czechoslovakian papers deal more with the practical aspects of the problem.

Simek [58] proposed an early balancing method that uses two sets of balancing masses in several (four to six) balancing planes. Three trial runs are needed to determine balancing masses. The first run is made with the first set of three balancing masses chosen in such a way that the balance of the rigid rotor would not be influenced. The third run is made with the second set of three balancing masses. The test results are used in the following equations:

$$\begin{Bmatrix} V_a \\ V_b \end{Bmatrix} = \begin{bmatrix} \beta_{a2} & \beta_{a3} \\ \beta_{b2} & \beta_{b3} \end{bmatrix} \begin{Bmatrix} D_2 \\ D_3 \end{Bmatrix},$$

where {V} is the forced-response vector measured at the rotor supports, [β] is a matrix of influence coefficients to be determined, and {D} is the unbalance mass vector. The method has been used in practice and is suitable for rotors whose operating speed does not exceed the first critical speed by too great a margin. This paper was one of the first publications to deal with flexible-rotor balancing and is a condensed research report written in 1953 at the National Research Institute for Machine Design, Prague, Czechoslovakia.

Fryml and Boruvka [59] have proposed a method for balancing rigid and flexible rotors that have unequal shaft stiffnesses. This method is suitable for an operating speed approaching the first critical speed. In the case of a rotor with equal stiffnesses, at least three balancing runs are necessary; in the case of unequal shaft stiffnesses, at least five runs are necessary. This paper and that by Parkinson [16] appear to contain the only methods specifically proposed for such shafts. A paper by Julis and Boruvka [60] describes a procedure for the optimal placement of balancing planes (two planes are considered in the example). The influence of the balance plane locations on the response curves is shown for different cases. In each case the rotor was balanced for its operating speed. The second part of the paper discusses the effect of unbalance distribution on response curves.

Julis [61] has discussed the problems of balancing a rotor that operates in several bearings. The paper covers both rigid and flexible

rotors. First, a theoretical discussion of a rotor mounted in three supports suggests that the balancing of such rotors may be very difficult; and then a balancing method for these rotors is described. After low-speed balancing, a set of three balancing masses is used to eliminate the deflection due to the internal moment. The balancing masses should be chosen in such a way that the resulting static and dynamic effect of the set of balancing masses equals zero. The location of the necessary three balancing planes should be based on the mode shape of the shaft at speeds close to the critical speed.

Gusarov and Dimentberg [62] studied the dynamic effect of distributed and concentrated unbalance forces on the balancing of rotors, including the problem of balancing flexible rotors with a limited number of correction planes. The absence of dynamic reactions at the supports and optimal reduction of bending stress is required, and the influence of damping is considered.

Mikunis [63] has investigated the forced vibrations of a flexible shaft mounted in two rigid supports. A constant cross-section and a uniform mass distribution of the shaft are considered. The effect of external damping is incorporated into the solution for forced vibrations of the shaft.

Gusarov [64] has investigated the problem of eliminating the first and second unbalance modes for speeds below the second critical speed. The balancing is provided in two balancing planes by two correction masses. It is assumed that the influence of higher modes on the low-speed balance can be neglected. The question of the optimum locations of the balancing masses is also discussed. A shaft of constant cross section without disks is considered. The paper indicates that, unless the rigid-rotor modes have been previously removed, there may be insufficient balancing planes available to significantly improve the rotor balance condition.

Yanabe and Tomara [65] have presented an analytical study of multiplane balancing for a general two-disk rotor with end bearings. Their method makes the usual assumptions: bearing amplitudes are to be reduced to zero by correct balancing; damping is negligible; gyroscopic and rotatory inertia are negligible; and pedestal—foundation resonances do not affect rotor operation. The method is a matrix solution for the amplitudes at both bearings and at the correction plane locations: that is,

$$[a_{ij}] \{x\} - \omega^2[m] \{x\} = \omega^2\{U\},$$

where

$[a_{ij}]$ — matrix of influence coefficients (6×6)

$[m]$ — system mass matrix (6×6)

ω — rotor circular frequency

$\{U\}$ — unbalance vector (6×1)

$\{x\}$ — displacement amplitude vector. (6×1)

This expression is then inverted, and a solution for $\{x\}$ is obtained:

$$\{x\} = [[a_{ij}] - \omega^2[m_i]]^{-1} \{U\}; \quad \{U\}^T = \{U_c, U_d\}^T.$$

Next $\{x\}$ is set equal to zero, and the above expression is partitioned to solve for the four unknown balance corrections $\{U_c\}$ by substituting measured values of the disk amplitudes, from which the disk unbalances $\{U_d\}$ are determined. The required solution is

$$\begin{bmatrix} a_{ij}^{(1)} - \omega^2 m_i & a_{ij}^{(2)} \\ a_{ij}^{(3)} & a_{ij}^{(4)} \end{bmatrix} \begin{Bmatrix} U_d \\ U_c \end{Bmatrix} = \begin{Bmatrix} 0 \\ 0 \end{Bmatrix};$$

that is,

$$\{U_c\} = [a_{ij}^{(2)}]^{-1} [(a_{ij}^{(1)} - \omega^2 m_i)] \{U_d\}.$$

The method should be generally applicable for an N-disk rotor with $(N + 2)$ arbitrarily selected balancing planes. As presented, the method requires that a matrix of influence coefficients be calculated from the rotor geometry to establish the balance conditions. The use of a computer is required, and while the method works quite well for the simple examples given, the analytical approach could lead to numerical difficulty and error with rotors of complex geometry or with multibearing rotors. The calculated rotor stiffness may be significantly in error where disk shrink-fit construction contributes any stiffening to a built-up shaft assembly.

The procedure is a discrete mass version of the $(N + 2)$ modal method in which the balance corrections are to be developed directly from the whirl amplitudes, similar to the procedure described by Hundal and Harker [46]. Two shaft measurement locations adjacent to the bearings were used. Amplitude reductions of about 4:1 were observed from the test results, and the resonant amplitudes appear to have been eliminated in each instance. It remains to be seen whether repeated application of such "direct" methods will lead to improved balance.

Present indications are that residual amplitudes are high. Experiments with modern instrumentation are needed to resolve this important question. Lindsay's [52] successes should provide strong encouragement for additional work with direct methods.

6.5 Comparison of Flexible-Rotor Balancing Methods

The basic requirements for all rotor balancing methods are

1. *Functionality.* The method must work in a reliable, consistent, and predictable manner.

2. *Efficiency and economy.* All aspects of the balancing process must be undertaken in an efficient, cost-effective manner, with a minimum number of intermediate steps.

3. *Quality of final balance.* The method must be capable of bringing the rotor to a prescribed balance quality consistent with its function.

These basic requirements can be used as criteria to evaluate the various methods and procedures described in this chapter. In making this comparison, information on each method was obtained primarily from the available literature, though personal experience and discussions with various authors have also contributed. It should also be recognized that not all methods need be general techniques. The eventual criterion is the extent to which a given method meets the above requirements in a particular circumstance, which clearly may involve the facilities available to the balancing engineer as well as his skill and experience. The comments presented here therefore attempt to compare the various balancing methods on the basis of the above criteria.

N-Modal Method: Bishop, Gladwell, and Others

This method is a set of guidelines and criteria for N-modal balancing. No specific hardware or algorithm is associated with this method, though Kendig [17] has programmed the results and computer-balanced two rotors by the procedures described.

Functionality. The method works in that a capable engineer can balance a given rotor by adhering to the guidelines provided. Parkinson et al. [66] have verified this method in the laboratory. Lindley and Bishop [67] and Morton [68] have applied it to turbine-generator rotors.

Efficiency and economy. The required steps are concise and efficient. The time needed to balance any rotor depends on operator skill and the equipment available.

Quality of final balance. Not documented. Kendig found balance quality comparable with that obtained by other methods in most

instances. This method was generally superior to the $(N + 2)$ modal method and inferior to the influence coefficient method. Miwa [25] found the N-modal method to be inferior to the $(N + 2)$ modal method in a theoretical comparison.

Comments. The Bishop—Gladwell method will continue to be a valid set of guidelines, which are now well accepted. The method is generally applicable to high-speed rotating machinery. Baier and Mack [40] found difficulty in applying these principles to long slender shafts. Published work suggests that the method becomes increasingly difficult to apply as the number of modes involved becomes more than three.

Practical N-Modal Method: Moore and Dodd

This method is a set of empirical procedures based on N-modal principles. The techniques involved are simple and well documented. Several vector constructions are available for specific balancing problems encountered in practice. The method has been proved on high-speed electrical equipment and turbine rotors.

Functionality. Moore has applied this method for 20 years to medium and large flexible rotors. Giers has tested the method against the $(N + 2)$ comprehensive modal method. Kendig has tested the method for two rotors. There is ample evidence that the method works well.

Efficiency and economy. No documented information is available on how long this method typically requires to give a balance of the prescribed quality. Few trial runs seem necessary, but this could result in less quality improvement per operation. In practice the hand operations can easily be performed on a programmable calculator. The balance moves are time consuming, and a moderate level of operator skill appears to be necessary.

Quality of final balance. Acceptable balance quality may be inferred from the number of rotors (hundreds) that Moore has successfully balanced for shipment. No additional documentation appears to be available on quality for this method, though Bishop (private communication, 1971) has commented that superior results were being achieved with this method compared to other flexible rotor balancing procedures then in use.

Comments. Data published by Moore and Dodd, Giers, and Kendig establish this method as a primary one for flexible-rotor balancing. It requires a well-trained operator and apparently has not yet been computerized in general usage.

(N + 2) Comprehensive Modal Balancing: Federn and Others

This method is a set of procedures widely used under a variety of names. Rotors are first low-speed balanced and then modal balanced. The low-speed balance step is controversial but is practiced extensively. Certain users have recently computerized this method.

Functionality. The method has been widely applied, and its abilities have been well documented by Federn, Giers, Kellenberger, Miwa Kendig, and others. Widespread use demonstrates that it works well. Effectiveness may depend on the class of rotor involved, and on the quality of rotor manufacture.

Efficiency and economy. No information appears to be available on the efficiency of this method. The low-speed step requires additional time.

Quality of final balance. Acceptable quality may again be inferred from the number of rotors that have been balanced by this method. This method also requires a trained operator.

Comments. Most applications appear to proceed with a trial-weight technique. Commonly, this is done in a balancing machine or balance facility where low-speed balancing can be undertaken. Kellenberger has computerized the $(N + 2)$ procedure, and he does not specify the use of trial weights [22]. If $(N + 2)$ balancing were to be computerized and effectively converted to a *direct* procedure (no trial weights, just mode shapes and rotor measurements), it would be far more time-efficient than the other modal methods.

Influence Coefficient Method: Goodman and Many Others

A specified sequence of measurements is made involving the original unbalance condition and for trial-weight runs. Neither modal knowledge nor precalculation is necessary, but such information is useful for guidance.

Functionality. A wide variety of different rotors has now been documented as having been successfully balanced by this method. The method has been extensively documented in the literature.

Efficiency and economy. Even though the method has been computerized, the trial-weight procedure is time-consuming; this reduces efficiency. In use, the method may be comparatively costly because of the equipment now available for data acquisition, signal conditioning, and data reduction. Conversely, machine operating costs should be lower because the resulting balance can easily be made superior by repeated application: see Chapter 7.

Quality of final balance. The high quality of the resulting balance is well documented (see Badgley, Tonnesen, and others). The influence

of errors on balance quality has been thoroughly studied (see Chapter 7). This method probably has the most comprehensive documentation of any balance procedure in use. The literature indicates that the highest quality balances have been achieved by this method. No decrease in effectiveness appears to occur as the higher modes are balanced (more planes are used).

Comments. The method is computerized and very effective. It may be time consuming and is best used with instrumentation which at present is somewhat costly. The method contains many features (e.g., computerization) that should make it well adapted to the balancing requirements of the future—for example, in jet engines, generators, and production balancing.

Direct Methods: Hundal, LeGrow, Yanabe

Direct methods bypass the time-consuming trial-weight procedure and solve the balance equations directly. Apart from the authors mentioned above, there do not appear to have been many attempts to develop the direct method into a workable technique. Hundal and Harker balanced their rotor using this method, but substantial amplitudes remained at both critical speeds. Yanabe et al. balanced their two-disk rotor in four planes (the $(N + 2)$ concept) and achieved small, constant residual amplitudes throughout the speed range (no resonant buildup was apparent). LeGrow has reported encouragingly on the direct balancing of generators, but no recent develoments have been published.

Functionality. The method appears to work, but further development is needed. Problems may arise from poor speed control causing amplitude fluctuations. Signal filtering should no longer be a problem with modern electronics. There is no known information on whether the direct method is viable with bearing probes or bearing accelerometers. No direct field balancing has been reported as yet.

Efficiency and economy. If a workable direct method in which the trial-weight operations can be bypassed is developed, an important step forward in efficient balancing and in economy in operation will be achieved. Equipment costs should not be significantly reduced over those of existing methods. The same facility and operator costs will apply.

Quality of final balance. This must be rated fair to good at present, judging from the few reports available.

Comments. Computer programs for calculating the rotor deflection coefficient matrices are fully developed, and the accuracy reported by LeGrow (to within 5.8 percent) could be much improved with more

development and experience. The possibility of direct balancing using inputs from the bearing pedestals merits further investigation.

Empirical Methods: Lindsey, Howard, and Others

The "one-shot" method developed by Lindsey [52] is apparently reliable and very efficient in most applications. The quality of final balance appears to be acceptable within the utilities industry. Similar methods have been described by Howard [69] and by others. These methods have been developed through years of experience with similar rotors. A large backlog of related data now exists in certain industries and is available in computer memory for easy reference.

Functionality. The method worked well for Lindsey. LeGrow also reported good success. Howard [69] reported a similar successful method.

Economy and efficiency. Simple equipment and a minimum of trial run effort makes such methods very time-efficient. However, the related empirical technology may involve years of slow development.

Quality of final balance. This is apparently sufficiently acceptable for the methods reported to be used as official practice with reputable companies.

Comments: Little data or reporting exist on such methods. They are simple and efficient, and thus are highly desirable techniques. Skilled personnel are usually needed to use the methods in a reliable manner.

6.6 Criteria for Flexible-Rotor Balancing

Sources of Balance Criteria Values

Flexible-rotor balancing criteria are in a formative stage. A variety of criteria are used to evaluate the balance quality of flexible rot ...s. These criteria are mostly industry-related standards based on accu nu-lated experience. However, it remains common practice to specify the balancing of flexible rotors using rigid-rotor criteria values, as until recently there was no criteria document devoted to flexible rotors. Recently, the International Organization for Standardization published Draft Technical Document ISO/TC 108/SCI N16 (1976), "The Mechanical Balancing of Flexible Rotors." Numerical criteria given in this document are based on Standard Document ISO 2372 [70] for tolerable limits of balance criteria for flexible rotors in any mode. Several numerical examples given in the text of this document describe the application of these criteria to flexible rotors. An International Standard Document on balance quality criteria for flexible rotors is being developed.

Section 4.4 of this monograph discusses the various categories and balance quality grades for rigid rotors and describes how numerical balance quality criteria can be selected for specific rotors of a given rotor class. Rigid-rotor balance criteria are now fully developed and have been accepted internationally as the formal basis for rigid-rotor balancing. These criteria values have been shown to be reasonable and are well within normal balancing practice. These criteria were obtained from a broad statistical survey of balancing practice for a variety of rigid-rotor types, conducted by Muster and Flores [71]. This survey, along with other related data, formed the basis for the rigid-rotor balancing document ISO 1940-1973(E), which was discussed in Chapter 4.

No similar survey appears to have been made on the balance quality of industrial flexible rotors, probably because the need for generally applicable balance criteria for flexible rotors has not been sufficiently widespread until recently, except for certain key industries (e.g., turbine generators and centrifugal compressors). Furthermore, it was only in the past decade or so that efficient techniques for general flexible-rotor balancing developed from an art into a science.

The problem of establishing flexible-rotor balance criteria for use by industry is complicated by such factors as the following:

1. Attention must be given to the class of flexible rotor which is involved, when specifying the quality of balance required.

2. It may be a requirement to apply criteria for several flexible modes of the rotor simultaneously.

3. Unresolved questions still exist concerning the need to balance the rigid-body modes of class 3 flexible rotors.

4. Development of criteria is still under consideration for cases where several modes must be balanced.

To be acceptable for use in industry, the flexible-rotor criteria must be simple to use and of a reasonable standard such that a good rotor balance is obtained in all modes within the operating range. Moreover, the criteria should be simply related to the measured unbalance readout results, irrespective of the measuring technique (proximity probe, accelerometer, etc.) and of readout location (pedestal, midplane on casing, etc.). Flexible-rotor balance quality criteria that incorporate these considerations are given in the above-mentioned ISO draft technical report ISO/TC 108/SCI N16.

Interim ISO Procedure for the Selection of Acceptance Criteria

The following procedure has been developed by the ISO Balancing Committee as an interim measure to guide the selection of acceptance

criteria for the residual unbalance level after the balancing of flexible rotors (Class 2—5) in bearing supports:[*]

Step 1. Determine the class of the rotor in question (see Table 1.2 for guidance). Using the table from ISO 1940-1973(E) in Chapter 4, establish the required machine balance quality grade.

Step 2. Determine the recommended residual unbalance from Fig. 4 of ISO DR 1940. Find the applicable rigid-body unbalance criterion U_R lb-in./lb for the maximum speed of operation (rpm) and machine balance quality grade.

Step 3. Determine the balance quality criteria values. If low-speed balancing is intended, select the maximum recommended unbalance U (oz-in.) for low-speed balancing in two planes plus the residual equivalent of the first-mode unbalance from

$$U_R \left[\frac{\text{lb-in.}}{\text{lb}}\right] \times \text{rotor weight (lb)} \times 16\left[\frac{\text{oz}}{\text{lb}}\right] = U \text{ oz-in.}$$

If low-speed balancing is not intended, determine the recommended residual unbalance from the following formulas:

First mode: $U_1 = 0.50 \times$ recommended residual unbalance,

Second mode: $U_2 = 1.00 \times$ recommended residual unbalance,

Third mode: $U_3 = 1.50 \times$ recommended residual unbalance,

where the recommended residual unbalance is from ISO 1940-1973(E).

The following example illustrates the above procedure.

Determine the appropriate balance criteria for a medium steam-turbine rotor weighing 22,000 lb and operating at 4400 rpm. From design calculations the first three critical speeds occur at 2750, 5600, and 11,700 rpm.

Step 1. According to Table 1, in ISO 1940-1973(E), the required balance quality grade is 2.5.

Step 2. From Fig. 4a of ISO 1940-1973(E), the rigid-body balance quality criterion is

$$U_R = 0.16 \times 10^{-3} \frac{\text{lb-in.}}{\text{lb}},$$

Step 3. The balance quality criterion is found to be

$$U = (0.16 \times 10^{-3})(22,000) = 3.52 \text{ lb-in.} = 56.32 \text{ oz-in.}$$

---

[*]Class 1 rotor acceptance criteria are discussed in ISO 1940-1973(E). See Chapter 4.

This criterion will be adequate if the rotor is to be balanced at low speed. The criterion then represents the total permissible residual unbalance at any speed.

For high-speed balancing, the recommended residual unbalance for the first, second, and third modes is respectively

$$U_1 = 0.50(3.52) = 1.76 \text{ lb-in. } (28.16 \text{ oz-in.}),$$

$$U_2 = 1.00(3.52) = 3.52 \text{ lb-in. } (56.32 \text{ oz-in.}),$$

and

$$U_3 = 1.50(3.52) = 5.28 \text{ lb-in. } (84.48 \text{ oz-in.}).$$

These criteria apply in the case where no rigid-rotor balance is to be undertaken. At the first critical speed a residual unbalance of 28.16 oz in. is the maximum acceptable value. As the turbine operating speed of 4400 rpm is 78.6 percent of its second critical speed, the full second-mode unbalance limit of 56.32 oz in. is applicable. Since the rotor operating speed is only 37.6 percent of its third critical speed, no restrictions relating to the third-mode amplitudes apply in this case.

Balance Quality Criteria Based on Acceptable Vibration Limits

Guidelines are provided in ISO document ISO/TC 108/SCI N16 for evaluating the balance quality of rotating machinery based on the rms value of the synchronous pedestal vibration velocity. Table 2 in Appendix A of the document gives balance quality bands for various rotor categories. A draft version of this table is given in Table 6.7. The quality bands A, B, C, and D are related to the machine balance condition as follows:

A: acceptable when the machine is new
B: commercially acceptable
C: in need of attention at the next overhaul
D: in need of immediate attention.

Three correction factors C_1, C_2, and C_3 are also listed in Table 6.7, to permit correlation of vibration measurements made in situ with those obtained during shop balancing. The meaning of these factors are:

C_1: measurement in a high-speed balancing machine where bearing conditions differ from service conditions

C_2: shaft vibrations measured in or adjacent to the bearings of the machine

C_3: shaft vibrations measured at the location of maximum shaft lateral deflection.

Table 6.3. Balance criteria for flexible rotors

Rotor Category	Ranges of effective pedestal vibration velocity at once-per-rev frequency V_1 (mm/sec) rms			Correction Factor		
			Quality Bands	C_1	C_2	C_3
I	A B C D Small electric motors up to 20 HP. Superchargers.			0.63 0.63	2	
II	A B C D Paper making machines Medium size electric motors & generators, 20-100 HP on normal foundations. Electric motors and generators up to 400 HP on special foundations. Pumps and compressors. Small turbines.			0.63 0.63 0.63 0.63 0.63	4 4 8 4	20 15 8
III	A B C D Large electric motors. Turbines and generators on rigid and heavy foundations.			0.63 0.63	5 5	20
IV	A B C D Large electric motors, turbines, and generators on lightweight foundations. Small jet engines.			0.63 0.63	3	10
V	A B C D Jet engines larger than category IV.			0.63	2	10

The acceptable residual synchronous vibration for a given machine is the product of the rms vibration velocity V_1 and the appropriate correction factor as determined from Table 6.7. The quantity V_1 can be obtained from the measured peak-to-peak vibration amplitude a_1 as follows:

$$V_1 = 0.707 \frac{a_1}{2} N \frac{\pi}{30},$$

where N is the rotational speed of the rotor in rpm.

The following example demonstrates the use of this data for determination of vibration acceptability criteria.

Consider the steam-turbine unit described in the preceding example. The measured peak-to-peak vibration level of the rotor in a hard-pedestal balancing machine is 0.5×10^{-3} in. at 2400 rpm and 0.25×10^{-3} in. at 4400 rpm. Comment on the balance quality of the rotor.

The steam-turbine unit under consideration is a class 3 machine. A correction factor of $C_1 = 0.63$ should be used for the balancing machine test measurements.

The hard-support balancing machine test gives the following values of V_1:

At 2400 rpm,

$$V_1 = 0.707 \frac{a_1}{2} N \frac{\pi}{30}$$

$$= 0.074 (0.25 \times 10^{-3})(2400) = 0.0444 \text{ in./s}$$

$$= 1.128 \text{ mm/s.}$$

At 4400 rpm,

$$V_1 = 0.074(0.125 \times 10^{-3})(4400) = 0.0407 \text{ in./s}$$

$$= 1.034 \text{ mm/s.}$$

The maximum acceptable vibration velocities by quality band are

$$V_{max} = 1.12 C_1 = (1.12)0.63 = 0.706 \text{ mm/s}$$

$$V_{max} = 2.8 C_1 = (2.8)0.63 = 1.764 \text{ mm/s.}$$

From the balancing machine measurements it is evident that the rotor falls in quality band B. The balance quality must be improved for a new machine application; that is, the synchronous vibration velocity must be reduced by 37 percent for the rotor to be acceptable as a quality grade A rotor (see listing on page 415).

As a further example, consider the same turbine after installation. The measured peak-to-peak vibration amplitude at the bearing caps is 5.6×10^{-3} in. at the operating speed of 4400 rpm. A correction factor of $C_2 = 5.0$ should be used for measurements taken in or adjacent to bearings. The machine vibration velocity at 4400 rpm is

$$V_1 = 0.074(2.8 \times 10^{-3})(4400) = 0.912 \text{ in./s}$$

$$= 23.2 \text{ mm/s,}$$

and the maximum acceptable vibration velocities by quality band are

Band A: $V_{max} = 1.12 C_2 = (1.12)5.0 = 5.6 \text{ mm/s.}$
Band B: $V_{max} = 2.8 C_2 = (2.8)5.0 = 14.0 \text{ mm/s.}$
Band C: $V_{max} = 7.1 C_2 = (7.1)5.0 = 35.5 \text{ mm/s.}$

The rotor is functioning in quality grade C based on the field measurements; it therefore requires attention at the next overhaul.

Influence of Flexible-Rotor Type on Balance Quality

Much of the inherent difficulty in the selection of flexible-rotor balancing criteria arises from the breadth of the problem itself. Such criteria must be general enough to account for machine operation over broad ranges of rotor speed and flexibility. Many rotors of classes 2 through 5 behave as rigid rotors in their lower modes; that is, the system mode shape involves more bearing amplitudes than rotor bending amplitudes because of the dynamic flexibility of the bearing and support system. For these lower modes rigid-rotor balancing criteria are adequate. When such a rotor system experiences higher modes, the rotor bending amplitude will be larger than in the lower modes and rigid-rotor criteria will no longer suffice.

Class 3 rotors are characterized by modes in which significant bending deflections predominate. Flexible-rotor balancing criteria are required in order to provide a range of numerical values that will constitute a realistic, effective criterion for all the modes a given rotor will experience during its operation. Until comprehensive criteria are developed for such rotors, effective criteria can be developed (a) by specifying rigid-rotor standards where the lower modes are known by calculation or previous tests to be "rigid" modes, and by using the flexible rotor balancing guidelines presented in ISO/TC 108/SCI N16 (1976); and (b) by using the proposed criteria and procedures in the same reference to check the rotor vibration levels for acceptability.

6.7 References

1. International Organization for Standardization, "Balance Quality of Rotating Rigid Bodies," ISO 1940-1973 (E).
2. International Organization for Standardization, ISO DP 5343.
3. R. E. D. Bishop and G. M. L. Gladwell, "The Vibration and Balancing of an Unbalanced Flexible Rotor," *J. Mech. Eng. Sci.*, 1, No. 1, 66—77 (1959).
4. G. M. L. Gladwell and R. E. D. Bishop, "The Vibration of Rotating Shafts Supported in Flexible Bearings," *J. Mech. Eng. Sci.*, 1, No. 3, 195 (1959).
5. R. E. D. Bishop and A. G. Parkinson, "On the Isolation of Modes in the Balancing of Flexible Shafts," *Proc. Inst. Mech. Eng.*, 177, No. 16 (1963).
6. K. Federn, "Fundamentals of Systematic Vibration Elimination from Rotors with Elastic Shafts," *VDI Ber.*, 24 (1957).
7. S. Miwa, "Balancing of a Flexible Rotor: First Report," *Trans. Jap. Soc. Mech. Eng.* 37, No. 297 (1971) (in Japanese).

8. L. Meirovitch, *Analytical Methods in Vibrations,* Collier-Macmillan Canada, Ltd., Toronto, Ontario, 1969.

9. A. G. Parkinson and R. E. D. Bishop, "Residual Vibration in Modal Balancing," *J. Mech. Eng. Sci.,* 7, No. 1 (1965).

10. A. G. Parkinson, "On the Balancing of Shafts with Axial Asymmetry," *Proc. Roy. Soc. (London),* 292, Ser. A (1966).

11. A. G. Parkinson, "The Vibration and Balancing of Shafts Rotating in Asymmetric Bearings," *J. Sound Vibration,* 2, No. 4, 477—501 (1965).

12. R. E. D. Bishop and A. G. Parkinson, "Vibration and Balancing of Flexible Shafts," *Appl. Mech. Rev.,* 21, No. 5 (1968).

13. A. G. Parkinson, "An Introduction to the Vibration of Rotating Flexible Shafts," *Bull. Mech. Eng. Educ.,* 6, No. 47 (1967).

14. N. F. Rieger, *Flexible Rotor-Bearing System Dynamics,* Part III, "Unbalance Response and Balancing of Flexible Rotors in Bearings," ASME Design Engineering Division Publication, 1973.

15. A. G. Parkinson, "Balancing of Flexible Shafts Rotating in Massive Flexible Bearings," *J. Mech. Eng. Sci.,* 15, No. 6 (1973).

16. A. G. Parkinson, "The Balancing of Flexible Rotors," *Proc. Dynamics of Rotors Symposium,* International Union of Theoretical and Applied Mechanics, Lyngby, Denmark, 1974.

17. J. R. Kendig, "Current Flexible Rotor-Bearing System Balancing Techniques using Computer Simulation," M.S. thesis, Rochester Institute of Technology, Rochester, N.Y., 1975. (Advisor: N.F. Rieger)

18. L. S. Moore and E. G. Dodd, "Mass Balancing of Large Flexible Rotors," *GEC J. Sci. Technol.,* 31, No. 2, (1964).

19. L. S. Moore and E. G. Dodd, "Mechanical Balancing of Large Rotors," *Parsons Journal,* C.A. Parson Company, Heaton Works, Newcastle-upon-Tyne, England (June 1970).

20. L. S. Moore, "Balancing of Large Turbine Rotors," *Trans. Inst. Marine Eng.* (London) 81 (1969).

21. L. S. Moore, "The Significance of Anisotropy of Support Conditions When Balancing Very Large Flexible Rotors," *Proc. Inst. Mech. Eng. Conf. on Vibrations in Rotating Systems, London, February 14—15, 1972.*

22. W. Kellenberger, "Balancing Flexible Rotors on Two Generally Flexible Bearings," *Brown Boveri Rev.* 54, No. 9, 603 (1967).

23. W. Kellenberger, "Should a Flexible Rotor be Balanced in N or $(N + 2)$ Planes?" *Trans. ASME, J. Eng. for Ind.,* 94, No. 2 (1972).

24. S. Miwa and T. Nakai, "Balancing of a Flexible Rotor: Second Report," *Trans. Jap. Soc. Mech. Eng.,* 38, No. 305 (1972) (in Japanese).

25. S. Miwa, "Balancing of a Flexible Rotor: Third Report," *Bull. Jap. Soc. Mech. Eng.,* 16, No. 100 (1973).

26. S. Miwa, T. Nakai, I. Mimura and Y. Minami, "Balancing of a Flexible Rotor: Fourth Report," *Bull. Jap. Soc. Mech. Eng.*, **16**, No. 114 (1974).

27. S. Miwa, "Low Speed Three-Plane Balancing of Class 2D Rotors," Annex E, International Standard Document DP 5406, Sept. 1976.

28. A. Giers, "Comparison of the Balancing of a Flexible Rotor Following the Methods of Federn-Kellenberger and Moore," *VDI Ber.* **161**, (1971).

29. T. P. Goodman, *Least-Squares Program for Computing Balance Corrections,* General Electric Co. Rpt. No. 61GL46, Feb. 15, 1961.

30. J. W. Lund, *Rotor-Bearing Design Technology:* Part I; "State-of-the-Art," Rpt. AFAPL-TR-54-45, May 1965.

31. E. L. Thearle, "Dynamic Balancing of Rotating Machinery in the Field," *Trans. ASME,* **56** (1934).

32. L. P. Groebel, "Balancing Turbine-Generator Rotors," *General Electric Rev.* **56**, No. 4, (1953).

33. J. P. Den Hartog, "The Balancing of Flexible Rotors," *Air Space and Instruments,* Stark Draper Commemoration Volume, McGraw-Hill, 1963.

34. N. F. Rieger, *Computer Program for Balancing of Flexible Rotors,* Mechanical Technology Inc., Report 67TR68, Sept. 1967.

35. J. Tessarzik, R. H. Badgley, and W. J. Anderson, "Flexible Rotor Balancing by the Exact Point-Speed Influence Coefficient Method," Third ASME Vibrations Conference, Toronto, Canada, 1971, Paper 71-Vibr-91.

36. J. M. Tessarzik and R. H. Badgley, "Experimental Evaluation of the Exact Point-Speed and Least Squares Procedures for Flexible Rotor Balancing by the Influence Coefficient Method," ASME Paper 73-DET-115 1973.

37. T. P. Goodman, "A Least-Squares Method for Computing Balance Corrections," ASME Paper 63-WA-295, 1964.

38. J. W. Lund and J. Tonnesen, "Analysis and Experiments on Multi-Plane Balancing of a Flexible Rotor," ASME Third Vibrations Conference, Toronto, Canada, 1971, Paper 71-Vibr-89, 1971.

39. R. M. Little, "Critique of the Application of Linear Programming Techniques to Balancing Flexible Rotors with Particular Emphasis on Current State-of-the-Art of Flexible Rotor Balancing," Ph.D. thesis, University of Virginia, Charlottesville, 1971. (Advisor: W. Pilkey)

40. R. Baier and J. Mack, "Design and Test Evaluation of a Supercritical Speed Shaft," The Boeing Company, Vertol Division, Morton, Pa., USAAVLABS Technical Rpt. 66-49/R 458 (1966).

41. J. Tonnesen, "Further Experiment on Balancing of a High-Speed Flexible Rotor," Trans. ASME, J. Eng. Ind., **96**, No. 2 (1974).

42. J. M. Tessarzik and R. H. Badgley, "Balancing of High-Speed
     Interconnect Shafting for Operation Above Multiple Bending Crit-
     ical Speeds," American Helicopter Association, 30th Annual
     National Forum, AHS Paper No. 61GL46, Feb. 15, 1961.

43. J. M. Tessarzik, R. H. Badgley and D. P. Fleming, "Experimental
     Evaluation of Multiplane Multispeed Rotor Balancing Through
     Multiplane Critical Speeds," ASME Paper No. 75-DET-73, Design
     Engineering Technical Conference, Washington, D.C., 1975.

44. A. Palazzolo and E. J. Gunter, "Multimass Flexible Rotor Balanc-
     ing by the Least Squares Error Method," Proc. Vibration Institute,
     Machinery Vibration Seminar, Cherry Hill, N.J., Nov. 8-10, 1977.

45. R. M. Little and W. D. Pilkey, "A Linear Programming Approach
     for Balancing Flexible Rotors," *Trans. ASME J. Eng. Ind.* 98(3),
     1030—1035 (1976).

46. M. S. Hundal and R. J. Harker, "Balancing of Flexible Rotors
     Having Arbitrary Mass and Stiffness Distribution," *Trans. ASME,
     J. Basic Eng.* 87, No. 2 (1955).

47. A. H. Church and R. Plunkett, "Balancing Flexible Rotors," *Trans.
     ASME, J. Eng. Ind.,* 83, No. 4 (1961).

48. J. E. Voorhees, H. S. Meacham, J. B. Day and D. E. Close, *Design
     Criteria for High-Speed Power-Transmission Shafts,* Part II,
     "Development of Design Criteria for Supercritical Shaft Systems,"
     Battelle Memorial Institute, Tech. Documentary Rpt. ASD-
     TDR-62-728, Dec. 1964.

49. W. T. Thompson, "Matrix Solution for the Vibration of Non-
     Uniform Beams," *Trans. ASME, J. Appl. Mech.* 17 (1950).

50. J. A. Findlay, Review of "Balancing of Flexible Rotors," by Hun-
     dal and Harker, Ref. 46 (unpublished).

51. T. M. Tang and P. Trumpler, "Dynamics of Synchronous-
     Precessing Turborotors with Particular Reference to Balancing,
     Part II, Application," *Trans. ASME, J. Appl. Mech.* 90 (1968).

52. J. R. Lindsey, "Significant Developments in Methods for Balanc-
     ing High-Speed Rotors," Paper presented at ASME Vibration
     Conference, Philadelphia, Pa., 1969, Paper No. 69-Vibr-53.

53. J. V. LeGrow, "Multiplane Balancing of Flexible Rotors—A
     Method of Calculating Correction Weights," paper presented at
     3rd ASME Vibration Conference, Toronto, Canada, 1971, Paper
     71-Vibr-52.

54. M. Y. Kushul' and A. V. Shlyakhtin, "Modal Approach to Balanc-
     ing with Additional Constraints," *Izv. AN SSSR Mekh. mashinostr.*
     4, No. 2 (1966).

55. F. M. Dimentberg, "Certain Problems of High-Speed Shaft Bend-
     ing Vibrations," Ph.D. thesis, Institute of Machine Science of the
     Soviet Academy of Science, 1955.

56. F. M. Dimentberg, *Flexural Vibrations of Rotating Shafts,* Butter-
     worth and Sons, Ltd., London, 1961.

57. E. Hubner, "Balancing of Flexible Rotors, A Problem of Structural Analysis," *Ing. Archiv.*, **30**, No. 3 (1961).
58. J. Simek, "Balancing of Rotors with Flexible Shafts," *Strojirenstvi* (Machinery), **4**, No. 9 (1954).
59. B. Fryml and V. Boruvka, "Balancing of Rotors with Unequal Shaft Stiffness," *Strojirenstvi* **9**, No. 3 (1959).
60. K. Julis and V. Boruvka, "Results of Balancing Method Research of Flexible Rotors with Free Mass," Parts I and II, *Dynamics of Machines*, Publ. House of the Slovakian Academy of Science, Bratislava, 1963.
61. K. Julis, "Balancing of Rotors with Statically Indeterminant Supports," *Strojirenstvi*, **14**, No. 1 (1964).
62. A. A. Gusarov and F. M. Dimentberg, "Balancing of Flexible Rotors with Distributed and Concentrated Mass," *Problem procnosti v machinostroenii* (Problem of Elasticity in Machinery), Publ. House of the Academy of Science, Moscow, No. 6, 1960.
63. S. I. Mikunis, "Balancing Flexible Rotors in Turbine Generators," *Russian Eng. J.* **41**, No. 9 (1961).
64. A. A. Gusarov, "Balancing Flexible Rotors with Two Weights," *Dynamika strojov. sbornik prac z konferencie SAV*, Vydav. Slov. Akad. Vied, Bratislava, 1963.
65. S. Yanabe and A. Tomara, "Multi-Plane Balancing of Flexible Rotor Consisting of Two Disks," *Bull. Jap. Soc. Mech. Eng.* **12**, No. 54 (1969).
66. A. G. Parkinson, K. L. Jackson, and R. E. D. Bishop, "Some Experiments on the Balancing of Small Flexible Rotors," Part I, "Theory," *J. Mech. Eng. Sci.* **5**, No. 1 (1963); Part II, "Experiments," *J. Mech. Eng. Sci.*, **5**, No. 2 (1963).
67. A. G. Lindley, and R. E. D. Bishop, "Some Recent Research of the Balancing of Large Flexible Rotors," *Proc. Inst. Mech. Eng.* **177**, No. 30 (1963).
68. P. G. Morton, "On the Dynamics of Large Turbo-Generator Rotors," *Proc. Inst. Mech. Eng.*, **180** (12) (1965).
69. W. E. Howard, Westinghouse Large Steam Turbine Division, unpublished presentation at ASME Flexible Rotor Technology Panel Discussion, Philadelphia, Pa., April, 1974.
70. International Organization for Standardization, Standard Document ISO 2372 (1974), *Mechanical Vibration of Machines with Operating Speeds from 10 to 200 rev/s—Basis for Specifying Evaluation Standards*.
71. D. Muster and B. Flores, *Balancing Criteria and their Relationship to Current American Practice*, University of Houston, Technical Rpt. No. 3, 1967. Also available as ASME Paper 69-Vibr-60 (1969).

CHAPTER 7
PRACTICAL EXPERIMENTS WITH
FLEXIBLE-ROTOR BALANCING

Nomenclature

$\phi_r(z_i)$	normalized amplitude of r th mode at z_i location
ϕ_i	modal function
$u'(z_i)$	radial component of shaft displacement on r th mode
$u'(z_0)$	maximum radial displacement in r th mode
m_i	unbalance mass
r_i	eccentricity of unbalance mass from shaft axis
L	bearing axial length
D	bearing diameter
C	bearing radial clearance
μ in.	microinch
N	number of modes to be balanced within range of operating speeds
B	number of additional modes to be balanced; also used as a weighting factor
$W^R(z,\omega)$	unbalance vector, function of z and ω
z	axial position coordinate
Ω	angular velocity, rad/s
P	number of correction planes
a	balancing coefficient
ζ	phase angle
γ	balancing coefficient, (actual/ideal) correction
ω_r	critical speed, rad/sec

CHAPTER 7
PRACTICAL EXPERIMENTS WITH
FLEXIBLE-ROTOR BALANCING

7.1 Information Sources on Rotor Balancing
Tests and Experiments

Practical rotor balancing is changing in response to new technology and procedures developed in the past twenty years: minicomputers, solid-state electronics, influence coefficient balancing procedures, modal balancing procedures and the rapid evolution of highly flexible rotors. New methods of balancing have been evolved in response to developments in rotating machinery: speed, size, weight, flexible supports, and so on. New developments in instrumentation have made possible the application of these new methods.

This chapter describes several important practical investigations which were undertaken to evaluate the effectiveness of certain balancing procedures. Listed below are the primary methods now used for flexible-rotor balancing; all but modal averaging require the use of a computer.

Method	Originators	Country	Firm
Modal	Bishop, Parkinson, Gladwell, et al.	England	University College
Modal averaging	Moore, Dodd (Bishop)	England	G.E.C. (England)
Comprehensive modal	Federn, Giers	Federal Republic of Germany	Schenck Trebel
	Kellenberger	Switzerland	Brown Boveri et Cie.
Influence coefficient	Goodman, Lund, Rieger, Badgley	United States United States	General Electric, Mechanical Technology Inc.

In addition, there are several specialized influence coefficient methods used for rotors whose balancing properties are well known and which can often be balanced by applying data from experience with similar machines (size, rotor weight, speed, etc.). Several turbine manufacturers balance their rotors in this way, employing data stored in the computer for easy access and guidance.

The published information on rotor balancing and rotor test experience deals with

- Verification of specific methods
- Investigation of aspects of methods for efficient balancing
- Investigation of method effectiveness under nonroutine circumstances.

Few publications concerned with rotor balancing have discussed the very significant developments in electronics that have been introduced, especially recently. Few publications aside from patent documents describe the range of mechanical and electrical innovations that have been introduced over the past thirty years to make modern balancing machines and equipment the sophisticated and efficient devices they now are.

The sources of information on the rotor-balancing tests and experiments reported in this chapter are summarized below.

Modal balancing. This method was developed by Bishop and associates at University College, London, England. Comprehensive listings of published work on this method have been given by Bishop and Parkinson [1], by Parkinson [2], and by Rieger [3]. The work itself is published mainly in the *Journal of Mechanical Engineering Science*, the *Proceedings of the Institution of Mechanical Engineers*, and the *Proceedings of the Royal Society of London.* Publications date from 1959.

Modal averaging method. This method is based on the modal method of Bishop, et al. It was formalized by Moore. The early work is referenced by Bishop and Parkinson [1] and by Rieger [3]. The journals in which it has been reported are the *Transactions of the Institution of Marine Engineers, Parsons' Turbine Works Journal,* and the *Proceedings of the Institution of Mechanical Engineers.* Publications date from 1964.

Influence coefficient method. Initial work is attributed to Goodman, with Lund, Rieger, and Badgley, et al. following later. Experimental verification has been reported by Tessarzik, Badgley, Anderson and Fleming, and Tonnesen. A literature listing has been compiled by Rieger [3]. The work itself has been published mainly in the *Transactions of the American Society of Mechanical Engineers* from 1971 onward.

Comprehensive modal method. Initial work was done in 1956 by Federn, who was followed by Giers [4] and Kellenberger [5]. Little published information appears to be available beyond that reported by Giers, Kellenberger, and Drechsler, as discussed in this chapter.
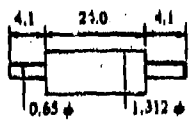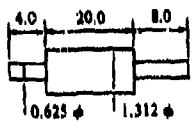
7.2 Laboratory Verification of Modal Balancing: Parkinson, Jackson, and Bishop

Parkinson, Jackson, and Bishop [6,7] conducted several laboratory experiments to validate the modal balancing method in the laboratory before attempting large-scale verification and application in practice. For the small-diameter shafts studied, the initial bend of the shaft was observed to exert an important effect on the balancing process, and therefore a preliminary study was made to evaluate the relative significance of initial bend and residual unbalance. This work is

reported in Ref. 6. The experimental investigation of the validity and some characteristics of the modal balancing method are discussed in Ref. 7.

The rotors used in this study (Table 7.1) consisted of a number of steel shafts, 0.625 in. and larger in diameter and ranging in length from 25 to 50 in.; two stepped shafts were also used. Each shaft was mounted in single-row self-aligning bearings. The shaft was driven by a double Hooke's joint coupling from a 2.5-hp dc motor in the speed range 1200 through 2000 rpm.

Table 7.1. Details of shafts used in modal balancing verification tests*

Shaft identification letter	Uniform or nonuniform shaft section	Critical speeds (c/s)		Shaft dimensions (in.)		Approximate support conditions	Theoretical[†] critical speeds (c/s)	
		ω_1	ω_2	Diameter	Length		ω_1	ω_2
A	Uniform	26	156	0.625	25.0	Clamped-free	28.2	177
B	Uniform	28.8	94	0.625	50.0	Clamped-pinned	30.9	100
C	Uniform	39	112	0.625	49.8	Clamped-clamped	45.2	125
D	Uniform	20	80	0.625	50.0	Pinned-pinned	19.7	79
E (as D, but additional ε_1)	Uniform	20	80	0.625	50.0	Pinned-pinned	19.7	79
F	Uniform	26	104	0.625	44.0	Pinned-pinned	25.5	102
G	Nonuniform (symmetrical)	69	—			Pinned-pinned	—	—
H	Nonuniform (unsymmetrical)	66.5	—			Pinned-pinned	—	—

*Ref. 7. ©1963, Institution of Mechanical Engineers; used by permission.

†Based on the assumption of ideal supports.

The test shafts carried small aluminum collars attached by grub screws. Balancing masses were added by inserting these into holes in the collar. Typically, these correction masses were between 0.125 and 0.50 oz in weight, 0.25 or 0.50 in. in diameter, and up to 0.50 in. long.

Inductive pickups were used to measure the vertical component of shaft displacement. Signals were transmitted to a radio-frequency oscillator operating at 2 MHz. The frequency-modulated signals were then preamplified and displayed on a two-channel oscilloscope. Displacement calibration was achieved with a 0.0001-in. dial indicator.

As the modal balancing method depends on a knowledge of the characteristic functions (mode shapes) of the rotor to be balanced, some prior knowledge of the characteristic functions of the shafts in their bearings was obtained by exciting the nonrotating shafts. Excitation was provided by an electromagnet and a variable-frequency oscillator. The form of each characteristic function was defined using nine inductive pickups stationed along the shaft, with their traces displayed on the oscilloscope. In this manner the r th modal shape of vibration was determined in the normalized form

$$\phi_r(z_i) \propto \frac{u'(z_i)}{u'(z_0)},$$

where u' is the radial component of shaft displacement. Tests were carried out for the first and second modes of vibration for shafts B, C, and D. Figure 7.1 shows typical correlation achieved between these tests and the corresponding theoretical predictions of the modal shapes.

With a shaft in the test rig, the lowest natural frequency was first obtained in the nonrotating condition. The orientation of the plane containing the first component of unbalance was then found by running the shaft slightly above (or below) its first critical speed and identifying the "heavy" (or "light") side. A correction mass was then placed in the aluminum balance weight ring, directly opposite the unbalance. The shaft waveform was displayed and monitored to observe any changes, and the shaft was rotated at about the same speed as before. Observation of the waveform determined whether the correction weight was too small or too large. The correction mass was adjusted so that a low-amplitude passage through the critical speed was possible, after a number of sensitive adjustments. In addition, the variation of the balancing mass $m_i r_i$ with distance along the shaft z_i was also investigated. The resulting values of

$$\frac{m_0 r_0}{m_i r_i} = \frac{\phi_1(z_i)}{\phi_1(z_0)}$$

where obtained and compared with the stationary mode shapes. The results are in agreement with the modal balancing theory. The second mode was balanced in a similar manner.

Elastic unbalance (i.e., bent shaft) was also investigated in a series of tests. Variation of distortion with speed and variation of angle with speed were observed for the lowest two shaft modes. As both elastic unbalance and residual unbalance exist in the shaft concurrently, the shaft was first balanced as accurately as possible. Phase-vs-speed curves were obtained from which the variation of the phase angle with the speed of elastic unbalance was determined for a variety of conditions. Typical phase-vs-speed curves are shown in Fig. 7.2.

(a) First-mode shapes for shaft B

(b) Second-mode shapes for shaft B

(c) First-mode shapes for shaft C

(d) Second-mode shapes for shaft C

(e) First-mode shapes for shaft D

(f) Second-mode shapes for shaft D
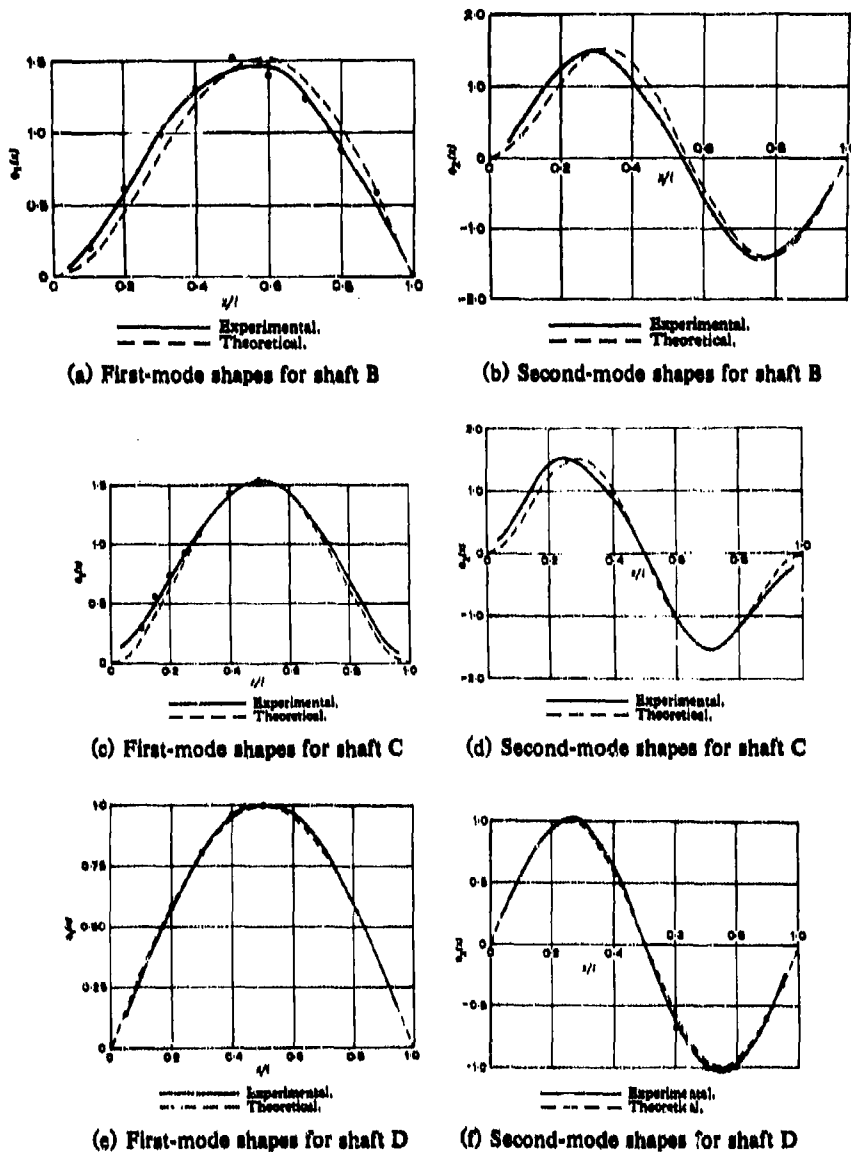
Fig. 7.1. Experimental mode shapes (solid curves) observed in tests by Parkinson, Jackson, and Bishop [6] and shapes predicted from theory (broken curves). The points in plots a, c, e, and f refer to a second series of tests and represent $m_0 r_0 / m_1 r_1$ (suitably normalized). (©1963, Mechanical Engineering Publications, Ltd; used by permission)

(a) Shaft E, vicinity of second
critical speed

SHAFT UNDERBALANCED 78 PERCENT (γ_2 = 0.34).
SHAFT UNDERBALANCED 46 PERCENT (γ_2 = 0.54).
SHAFT OVERBALANCED 13 PERCENT (γ_2 = 1.13).
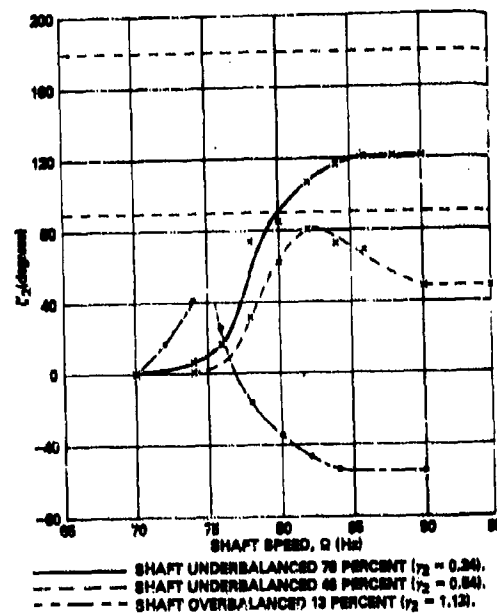
(b) Shaft H, vicinity of first
critical speed

x————— SHAFT OVERBALANCED 23 PERCENT (γ_1 = 1.23).
•————— SHAFT UNDERBALANCED 17 PERCENT (γ_1 = 0.83).
— — — PART OF CURVE SHOWN IN FIG. 30.
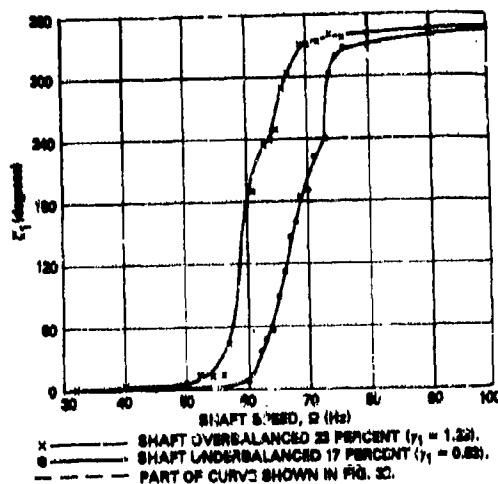
Fig. 7.2. Typical phase-vs-speed curves for shafts E and H (see Table 7.1) plotted by Parkinson et al. [7] (©1963, Mechanical Engineering Publications, Ltd; used by permission)

Additional tests were carried out to determine the effects of inaccurate balancing (i.e., overbalancing and underbalancing). Curves of variation in phase angle and distortion as a function of speed were obtained for these conditions with elastic unbalance and residual unbalance. A comparison of these results with those predicted by the modal theory is shown in Fig. 7.3.
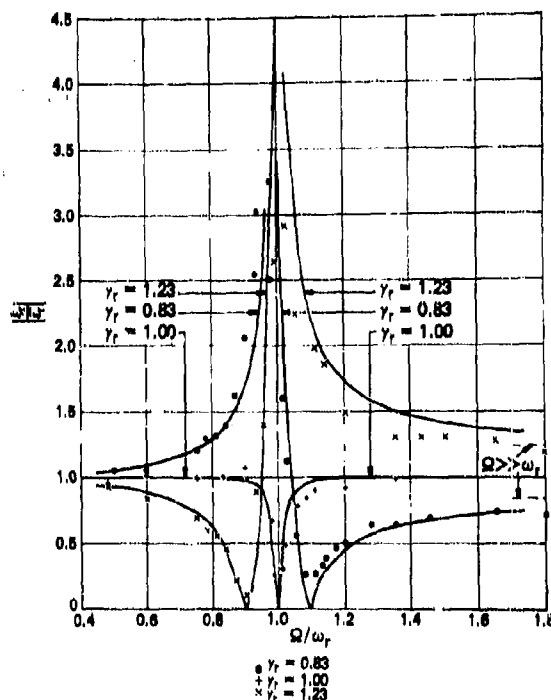
Fig. 7.3. Experimentally observed amplitude near the antinode shaft H in the vicinity of the first critical speed and amplitude predicted from theory (curves). From Parkinson et al. [7] (©1963, Mechanical Engineering Publications, Ltd; used by permission).

The following general comments are made by Parkinson et al. [7] on their results.

1. Experimental results indicate a need for a theory for balancing shafts with an initial bend. This theory is given in Ref. 6.

2. There appears to be little doubt as to the validity of the modal balancing process. The practical value of this process remains to be determined. Such tests have subsequently been conducted by Lindley and Bishop [8] and are discussed in Section 7.4.

3. Preliminary industrial tests indicate that the use of fluid-film bearings and measurements made on bearing pedestals do not materially affect the usefulness of the modal balancing method.

The tests were conducted with simple undamped two-bearing rotors. They offer encouraging results, but more exhaustive testing is required to define the limitations, if any, of this technique. It should be added that the degree of complexity involved in carrying out the balancing operations has not been discussed, and many additional factors remain to be investigated, e.g. the number of balancing planes required for full effectiveness; effect of errors in positioning the correction weights, etc.

7.3 Experiences in Balancing Rotors with Mixed Modes:
Moore and Dodd

The modal averaging method of rotor balancing is described with details of practical examples in a paper by Moore and Dodd [10] and in subsequent papers by Moore [11,12]. The several techniques of this method are described in Chapter 6. The method utilizes a knowledge of the rotor modes obtained from experience, or calculation, or intuition to guide the balancing process. The paper by Moore and Dodd [10] describes the basic steps of the balancing process with application to a typical two-bearing flexible rotor operating under the influence of its first three flexible modes. Moore and Dodd describe how they have applied the modal balancing procedure proposed by Bishop, Gladwell, and Parkinson in which the rotor modes are balanced out in turn as they are encountered in such a manner as to not reintroduce (re-excite) the lower modes by unsuitable positioning of the correction weights.

The main purpose of the paper by Moore and Dodd is to discuss the application of the modal method when mixed modes are present. It mentions an initial application to an unslotted rotor forging that gave "very promising results." It was possible to run the rotor near the first critical speed, balance this mode out, then run near the second critical speed and balance the second mode without reintroducing the first mode.

The limitations of this procedure became apparent when balancing of the complete rotor was attempted. After the first mode was balanced, the rotor experienced strong vibrations when operated at full speed. The second mode was beyond the operating speed, and it was not possible to run at a suitable higher speed to balance it out. Balancing was attempted at the operating speed, assuming that the rotor mode shape was predominantly that of the second mode, though not

resonant. Correction weights were added on opposite sides of the rotor, near the estimated points of maximum deflection.

Moore and Dodd describe the balancing as follows:

> If the corrections for the second mode were adjusted to nullify the vibration of one bearing, the vibration at the other bearing increased. The best compromise left equal in-phase vibrations on the two pedestals. It was first thought that as the vibrations were in phase at the two ends, they might have been caused by an error in the first mode, which could have been introduced by a misproportioning of the weights added for second mode. The problem turned out to be much more complex. In fact, no progress was made *until it was appreciated that the rotor was responding to second and third modes [unbalances] simultaneously, even though it was running well below second critical speed.*

The remaining problem is one of mode separation. Under the effect of unbalance forces from the second and third modes, the bearing pedestals will receive simultaneously an out-of-phase component from the second mode and an in-phase component from the third mode. These two components can occur at any angle to one another. It is necessary to resolve the resultant vectors back into their modal components. Moore and Dodd have devised the vector diagram shown in Fig. 7.4 to accomplish this modal separation. Their procedure is as follows:

Step 1. Let the vibration readings at pedestals A and B be represented by the vectors OA and OB in Fig. 7.4.

Step 2. Add calibrating weights in the correction planes for the second mode. Let their relationship be

$$\frac{\text{effect on end A amplitudes}}{\text{effect on end B amplitudes}} = m \text{ (ratio)}$$

Step 3. Add calibrating weights in the correction planes for the third mode. Let their relationship be

$$\frac{\text{effect on end A amplitudes}}{\text{effect on end B amplitudes}} = n \text{ (ratio)}$$

Step 4. Join A and B. Divide AB so that AC/CB $= m$.

Step 5. Join O and C. Draw lines parallel to OC through A and B.

Step 6. Produce AO to meet the line parallel to OC through B at point D.

Step 7. Divide DB so that DB′/B′B $= n/m$.

Step 8. Join B′O. Produce this line to meet the line parallel to OC through A at point A'.

Step 9. Any line through O will meet the parallel lines through A and B in A' and B' so that OA′/OB′ $= m$.

READINGS TAKEN.

SPEED IN REV/MIN.	D.E. UNBALANCE MAGNITUDE	D.E. UNBALANCE ANGLE	O.D.E. UNBALANCE MAGNITUDE	O.D.E. UNBALANCE ANGLE
2300	3.30	72°	3.45	199°
2300	3.35	52.5°	3.35	180°
2300	3.05	85°	3.95	197°

CONDITIONS.

"Original";
"Original" + 3 oz on D.E. bell and 3 oz on O.D.E. ring.
"Original" + 4 oz on fan hub, 5 oz in core and 6 oz on sliprings.
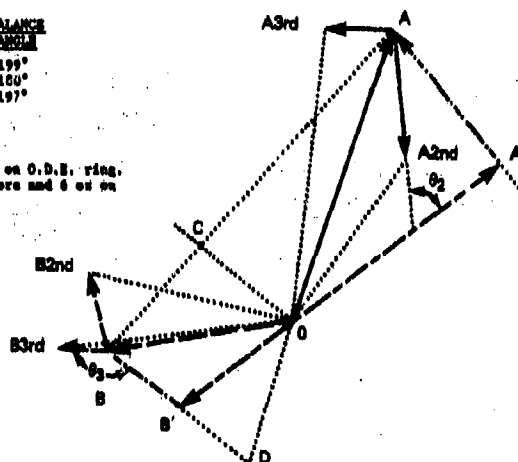
INTERPRETATION OF READINGS:

Let
OA, OB represent the "original" readings at the D.E. and O.D.E. respectively.
OA2nd, OB2nd represent the "original" + calibrating weights for second mode.
OA3rd, OB3rd represent the "original" + calibrating weights for third mode.

Then
AA2nd, BB2nd represent the effect of the calibrating weights for the second mode.
AA3rd, BB3rd represent the effect of the calibrating weights for the third mode.

Resolution of "original" readings into "in phase" and "out of phase" components.

Calibrating for Second Mode

$$\frac{\text{Effect on nA}}{\text{Effect on nB}} = m = \frac{2.3}{1.175} = 196$$

Calibrating for Third Mode

$$\frac{\text{Effect on nA}}{\text{Effect on nB}} = n = \frac{1.175}{0.525} = 224$$

Join A3 and divide in C so that $\frac{AC}{CB} = m$.

Join OC and draw lines parallel to it through A and B.
Produce AO to meet parallel line drawn through B in D.

Divide BD in B' so that $\frac{B'D}{DB} = \frac{n}{m} = 1.145$.

Join B'O and produce to meet parallel line drawn through A in A'.

Then

"Original" readings OA, OB = "out of phase" components OA', OB' + "in phase" components A'A, B'B.

Considering Second Mode

$$\frac{OA'}{AA2nd} = \frac{OB'}{BB2nd} = 2.38 \qquad \theta_2 = 63°.$$
∴ to correct the second modal defect, add (3 x 2.38) = 11.9 oz on the D.E. bell and (3 x 2.38) = 7.14 oz on the O.D.E. ring, both 63° clockwise from the positions of the calibrating weights.

Considering Third Mode

$$\frac{A'A}{AA3rd} = \frac{B'B}{BB3rd} = 2.50 \qquad \theta_3 = 150°.$$
∴ to correct the third modal defect, add (4 x 2.5) = 10 oz on the fan hub, (5 x 2.5) = 12.5 oz in the core, and (6 x 2.5) = 15 oz on the sliprings, all 150° anticlockwise from the positions of the calibrating weights.

Fig. 7.4. Simultaneous correction of second and third modes: example given by Moore and Dodd [10] for a boiler-feedpump rotor (©1964, General Electric Company Ltd; used by permission)

Step 10. If

$$OA = OA' + A'A$$

and

$$OB = OB' + B'B$$

then the vectors OA' and OB' are the out-of-phase components of the vibration readings OA and OB, in which OA' = m(OB'), and the vectors A'A and B'B are the in-phase components of the vibration readings OA and OB in which A'A = n(B'B).

Note that the out-of-phase components apply to the second-mode unbalance, in which the pedestal forces are in the ratio m, and that the in-phase components apply to the third-mode unbalance, in which the pedestal forces are in the ratio n.

A detailed example that describes the application of the above construction to a 7900-hp boiler-feed pump rotor is reproduced in Fig. 7.4. Moore and Dodd [10] gave a further construction for the case where mixed-mode effects are present near the critical speed of one of the modes involved. Under such conditions the phase angle of the vibration is subject to rapid changes with respect to the angular location of the rotor in space, for the critical mode. A graphical procedure for mode separation in such balancing is also given. In this instance, as with the previous case of modal separation, no finite solution to the problem may be possible if the balancing planes are situated in unsuitable positions along the length of the rotor.

Moore and Dodd commented that the best drive connection is through a double Hooke's joint and that when balancing near a critical speed, fine speed control is required for accurate determination of amplitude and phase angle, which may vary significantly with small speed increments under such conditions. Seismic transducers should be mounted to operate at frequencies away from their own resonances. The authors comment in conclusion that the quality of balance achieved both when running up and when at full speed is far higher than had been previously considered possible. That good balance can be achieved by the modal averaging method is supported by the balance figures quoted by Moore and Dodd. It should be noted that the balance quality obtained in this case was achieved without correcting the rigid rotor modes.

7.4 Industrial Rotor Balancing by Modal Methods

Certain points raised by Moore and Dodd [10] are discussed in greater detail by Moore [12]. This second paper begins with a discussion of the modal behavior of flexible rotors in flexible supports and

the significance of rigid-rotor modes in comparison with flexible-rotor modes. Transducer signals are presented as vectors, and the properties of the rotor modes are then discussed in terms of the related vector diagrams from the pedestal signals. The problems of "mixed" modes (two close modes, or two strong modal responses in the same signal) are then reexamined, first using the vector-diagram approach and then with the use of complex algebra. Application of these techniques to flexible rotors with various unbalance conditions is discussed, for example, with regard to the need for the low-speed balancing of a high-speed flexible rotor. It is the position of Moore, Bishop, and Parkinson that low-speed balancing is unnecessary for class 3 flexible rotors that have rigid (or quasi-rigid) modes only in a soft-pedestal balancing machine. The opposite position is held by Federn, Kellenberger, and Giers, who maintain that both the quality of the balance achieved and the efficiency of the balancing process are improved by an initial low-speed balance operation. As discussed in Sections 7.7 and 7.8, attempts to resolve this question have been made by Giers [4] and by Kendig [25].

Moore [12] addresses the need for low-speed balancing by first mentioning that any unbalance-correction weight added to the rotor will produce balancing and unbalancing effects, in relation to the rigid modes and the flexible modes. He contends that

> It is likely therefore that an unbalanced rotor will have defects in several modes, and the relationship between these defects will depend not only on the modal shapes but on the axial disposition of the unbalances. As a balancing machine considers rigid modes only, some residual unbalance will remain in the flexural modes. This will result in vibration when the rotor is run to speed in its own bearings.

Moore shows how different distributions of unbalance may affect modes above the first mode. It is concluded that "a low speed balancing machine can have only limited use in the balancing of large flexible rotors." This use appears to be restricted to rotors that operate well below the first critical speed or well above the first and well below the second critical speed. The success of this procedure would depend on a variety of factors, such as degree of rotor axial symmetry, uniformity of unbalance distribution, and magnitude of unbalance.

The degree to which a high-speed balancing machine can be used to balance a flexible rotor was also reviewed by Moore [12],* who suggests that, despite the high-speed, variable-support flexibility (capabilities then available), no further balance computation capability is provided in commercially available high-speed balancing machines, and

---

*See also Ref. 11 for a more detailed explanation of this procedure.

practical modal techniques must be employed in the final stages of balancing. Moore therefore concludes that a skilled operator is still required to balance flexible rotors efficiently.

The remainder of Ref. 12 is a discussion of various techniques for balancing flexible rotors. These techniques are presented in terms of vector diagrams for dealing with the following additional cases:

1. Balancing when there is a mixed-mode condition near the first critical speed. Typical application: generator rotor at low speed.

2. Balancing when there is a mixed-mode condition near the second critical speed. Typical application: turbine-generator rotor above the first critical speed.

3. Balancing for a mixed-mode condition remote from either critical speed. Typical application: gas-compressor rotor or large slip-ring induction motor rotor near full speed.

4. Balancing for a mixed-mode condition with a limited choice of balancing planes. Typical application: large turbine-generator rotor or the semirigid rotor of large motor near full speed.

The situations in which these constructions are of use will be readily apparent to the balancing engineer. A brief discussion of each case is given by Moore [12], who concludes that a flexible rotor that is prebalanced in a low-speed balancing machine may still be unbalanced in its flexural modes, possibly to a higher degree than before. The importance of employing some modal balancing techniques is emphasized, to eliminate all relevant modes within the operating-speed range.

The techniques described in this section have been applied by Moore to a wide range of rotors, ranging from turbine-generator rotors (i.e., class 3 rotors), whose response can be influenced by several modes simultaneously, to induction motor and salient-pole alternator rotors, which have previously been considered as rigid (i.e., class 1 or 2 rotors). Smooth operation without prebalancing at low speed is claimed in all cases. This endorses the efficiency of the modal averaging method and demonstrates its validation in practice.

Alternator Rotor Balancing Evaluation of Modal Averaging Method: Lindley and Bishop

In a comprehensive paper on recent developments in the balancing of large flexible rotors, Lindley and Bishop [8] describe the application of modal methods during the balancing of a 200-MW generator rotor, with extensive supportive discussion on the dynamic properties of such rotors. The paper also contains discussions contributed by many

balancing experts. The principles of modal balancing are first reviewed, i.e., procedures for successive mode suppression without re-excitation. The authors recognize the value of having mode shapes available, from computer results or from previous practical experience, for the modes to be eliminated. In general, however, the plane in which the response occurs for each mode will be different because of the predominantly random distribution of residual unbalance in a rotor. The total rotor response at any given speed is the sum of the individual modal responses in the various directions. This is the basis of modal balancing. As noted previously, preliminary tests on laboratory models by Parkinson, Jackson, and Bishop [6] had indicated that the modal balancing concepts would work in practice (see also Ref. 1).

Balancing tests were conducted on the 200-MW alternator rotor shown in Fig. 7.5. The rotor was first balanced by customary procedures in an overspeed test pit, but without any low-speed balancing. The drive was from a dc motor through a double Hooke's joint coupling, at speeds from 0 through 3000 rpm as required. A signal generator and a frequency counter were used for precision speed measurement to within 1.0 rpm. Seismic vibration transducers were attached to the bearing pedestals to monitor vibrations in the horizontal direction. A small phase-reference alternator was driven directly from the rotor in conjunction with the transducers to measure the phase angle between any required circumferential location on the rotor and the pedestal vibration signal.

Two tests were made to determine whether the dynamic (modal) behavior of a large rotor was consistent with the predictions of elementary theory. The balanced 200-MW alternator rotor was first deliberately unbalanced by the addition of a 17.5-oz weight at 22.0-in. radius, midspan between the main bearings, to introduce rotor amplitudes associated primarily with the first mode. When the rotor was running through the speed range at 1020 rpm, this 385-oz-in. unbalance caused a 1.82×10^{-3}-in. amplitude peak at the left-hand bearing and a 0.8×10^{-3}-in. amplitude peak at the right-hand bearing. The Kennedy–Pancu polar response plots show that rotor response amplitudes at the two bearings are in phase at the critical speed; this suggests that the first mode is of the customary half-sine-wave shape, as would be expected. Another test was conducted to determine whether the rotor response was axisymmetric, by moving the unbalance mass circumferentially around the rotor and measuring at 898 rpm (90 percent of the critical speed). Affirmative results were again reported for this test, consistent with rotor dynamic theory.

For balancing, the 200-MW alternator rotor was run close enough to the first critical speed for stable phase measurements to be taken

(a)

(b)
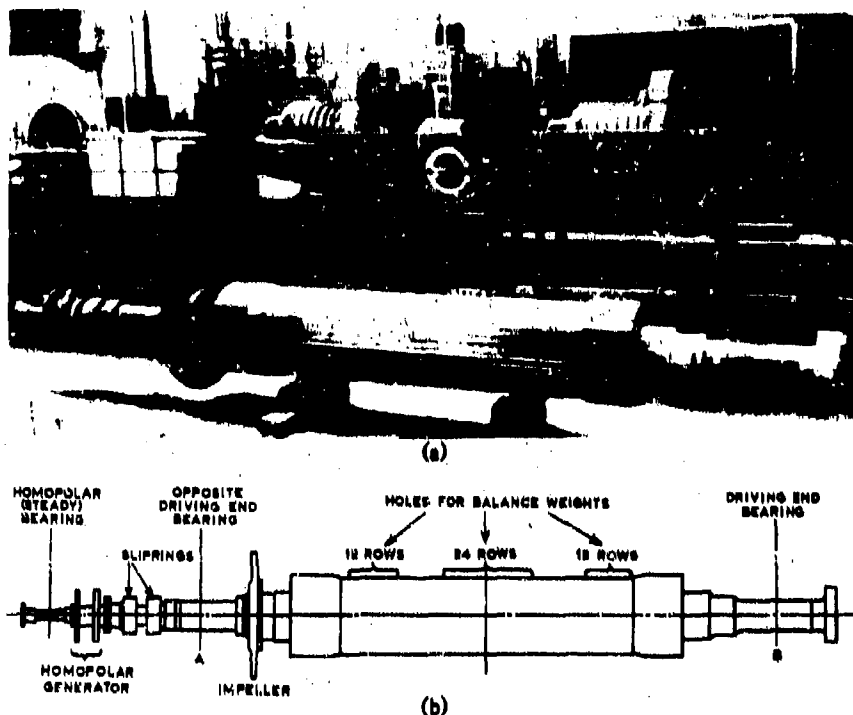
Fig. 7.5. Alternator rotor of 200-MW generating set used in tests by Lindley and Bishop [8] (©1963, Institution of Mechanical Engineers; used by permission)

where the first mode was strongly magnified. The rotor was then shut down, and a calibrating weight was added near the midspan. Measurements were repeated at the same speed as before. The readings taken at the pedestals in both trials could then be plotted as vectors to determine the magnitude and location of the correction weight needed to balance the rotor. Usually the two resulting correction vectors are not in identical phase, and a compromise or average location is therefore selected for the addition of a single correction mass.* The corrected rotor was then run through the first critical speed without observing undue vibration of the pedestals. Details of results obtained in this and other balancing runs are given in Table 7.2.

For second-mode balancing, Lindley and Bishop [8] discuss the selection of a suitable balancing speed based on the size of the pedestal vibrations. The second mode of this rotor system lies beyond the

---

*This is the reason for the term *modal averaging*, to distinguish it from the pure modal method, which requires a computer for the selection of correction masses for several modes simultaneously.

Table 7.2. Initial unbalance state of amplitudes*

Bearing pedestal		Unbalance vibration amplitude, peak-to-peak (in. × 10⁻³)	
		Running through first critical speed	At 3000 rpm
Initial unbalanced state	Driving end	15.0	2.2
	Opposite driving end	7.5	1.9
	Homopolar	14.0	5.0
After balancing	Driving end	1.0	0.3
	Opposite driving end	0.7	0.75
	Homopolar	0.8	0.2

*Ref. 8. Used by permission.

operating speed (3000 rpm) but, unless balanced, it is of sufficient strength to cause strong vibrations at the operating speed. The operating speed was selected as the second-mode balancing speed, and pedestal vibration readings were taken with related phase angle data. A pair of calibrating weights were then added to the rotor at the estimated axial locations of the maximum second-mode amplitudes (but not necessarily in phase circumferentially with this amplitude). The calibrating couple was proportioned so as to leave the first mode undisturbed. A vector diagram for this condition is shown in Fig. 7.6a. Assuming at this stage that the second mode has an equal out-of-phase effect at the two axial calibration locations, the required magnitude of the second-mode correction couple is found from the construction shown in Fig. 7.6b. Like the first-mode correction, this construction is approximate. A more precise correction might have been obtained at this stage by using the corrections proposed by Moore and Dodd [11].

The final balancing process follows the hot overspeed test for such a rotor. Ideally this will consist of a repeat of the first- and second-mode correction procedures. If problems are to be encountered with a rotor, they will usually occur with the basic correction. Trim balancing is usually a straightforward repeat, especially if Moore's mixed-mode, separation-compensation procedures have been applied after initial diagnosis of the vector diagrams. In the given case Moore's procedure would compensate the first mode and a portion of the second mode at the first critical speed; it would also completely compensate the second
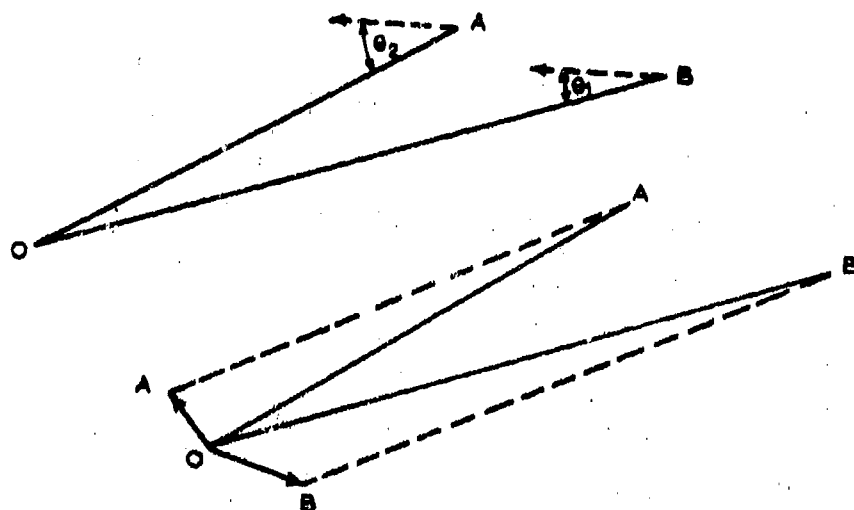
(a) Vector diagrams for the first chosen speed
(near but below first critical)
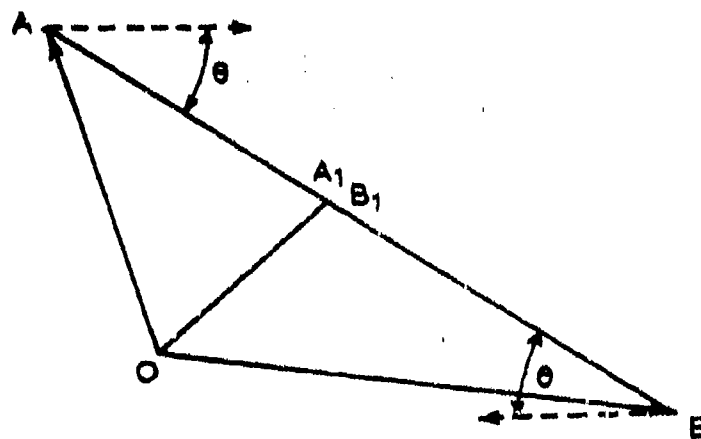
(b) Vector diagram for the second chosen speed (near running
speed and below second critical)

Fig. 7.6. Vector diagrams for vibration at the first and second speeds chosen by
Lindley and Bishop [8] to balance an alternator rotor (©1963, Institution of
Mechanical Engineers; used by permission)

mode and a significant portion of the third mode at running speed, without disturbing the first mode.

Details of a second balancing test on the 200-MW alternator are also given. For balancing the first mode at a speed just below the first critical, a correction weight of 9.5 lb was added at midspan at 12.0-in. radius (3344 oz-in.). Critical speed amplitudes at both bearings were reduced to less than 1.5×10^{-3} in. peak to peak. The second mode was balanced at 3000 rpm by placing two out-of-phase correction weights of 11.0 oz at 21.0-in. radius (231 oz-in.) on opposite sides of the rotor near the quarter-points. This left a residual in-phase unbalance component of about 1.0×10^{-3} in. at either bearing. After the hot overspeed test, the following additional corrections were required:

First mode: one weight (-13.0 oz) at 21.0 in. (-273.0 oz-in.).
Second mode: two weights (-3.0 oz) at 21.0 in. (-63.0 oz-in.) at the quarter-points.

The remaining in-phase component was corrected by adding weights to the main half coupling.

These experiments led Lindley and Bishop to conclude that the method can be used quite generally to balance flexible rotors. They draw attention to the need for adequate provision of balancing planes during the design of any flexible shaft. The same sentiment has been echoed by Badgley and Rieger [13] on several occasions.

Several important comments were published with this paper. Morton [14] questioned the use of pedestals as transducer locations on account of their own dynamic response. In one instance he had observed a pedestal to resonate in one instance at 52 Hz. He recommended monitoring shaft motions relative to ground. Morton further suggested an influence coefficient procedure to replace the trial-and-error modal technique. In response, Lindley and Bishop stated that they had concluded on consideration that an algebraic technique was not as good as one involving physical reasoning but that they had not followed up seriously on this procedure. Consterdine [15] gave a brief and interesting review of flexible-rotor balancing techniques and their development, and commented on the field balancing of large generator rotors in which access to only a few correction planes is possible. Attention is drawn to the work of Mikunis [16,17], who describes both single-plane and two-end-plane correction procedures that are able to reduce vibrations in the first three modes.

Generator-Rotor Balancing by the Modal Averaging Method: Moore

Moore [9] has studied the effects of differing rotor-support conditions (anisotropy) on the balancing of large flexible rotors. A large

generator rotor was examined during production balancing. It was found to possess a large unbalance near one end, which caused a large response in the second mode of the system. The rotor was mounted in its own bearings in an overspeed pit on pedestals and foundations that closely resembled those to be used on site. Transducers were attached to the bearing pedestals to measure vibrations in both horizontal and vertical directions.

Typical experimentally-determined mode shapes for the rotor in flexible bearings are shown in Fig. 7.7. Horizontal and vertical vibrations of the rotor in its first mode were balanced out at unstated speeds by the "normal" modal balancing process, (i.e., no low-speed balancing was undertaken). The growth of rotor amplitudes in the second mode between 1400 and 2100 rpm is shown in Fig. 7.8. The second horizontal critical speed occurs at about 1550 rpm, whereas the second vertical critical speed occurs at about 1950 rpm. The small loops at 1950 rpm horizontally and 1550 rpm vertically indicate the degree of coupling between motions in these two directions.

The two second mode shapes of the rotor are shown in Fig. 7.7. By inference, the rotor modal shape is a plane curve. This is in agreement with other results (see, for example, Ref. 25) for such rotor-support configurations. The rotor deflected shapes were determined by a method of mass traversing, which permits measurement of the response to a known mass acting at each of several different locations along its length. When such measurements are taken close to the second critical speeds, the second-mode components are dominant.
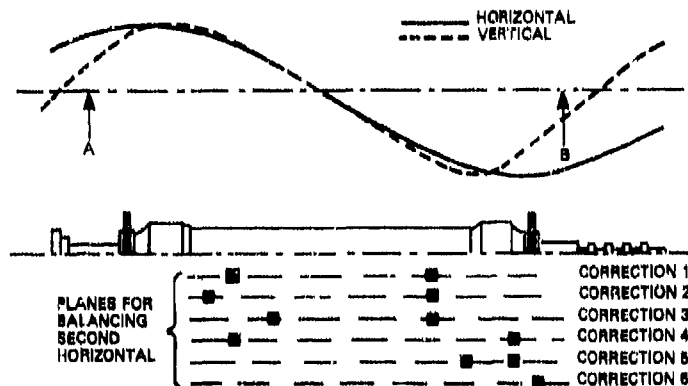
Fig. 7.7. Experimentally determined second-mode shapes for generator rotor studied by Moore [9], showing relation to rotor body and the choice of balancing planes for correcting second-mode horizontal vibrations. (©1972, Institution of Mechanical Engineers; used by permission)
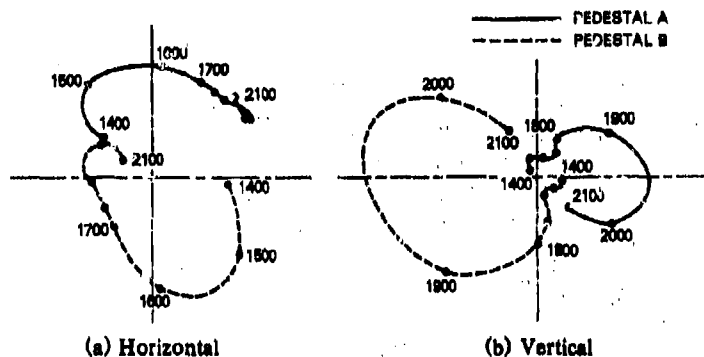
Fig. 7.8. Experimental determination of second horizontal and vertical critical speeds: Moore's [9] study of generator rotor. (©1972, Institution of Mechanical Engineers; used by permission.)

Moore [12] refers to the process of modal separation by which the influence of other modes is eliminated to obtain the second-mode forms shown.

With the effects of the first horizontal and vertical modes removed, the rotor was then operated at 1300 rpm to begin balancing the second horizontal mode. A pair of masses 180° out of phase were added in the correction planes normally used for production balancing. These planes are shown in Fig. 7.7 as "correction 1." Subsequent corrections were made at the other locations indicated. With these masses added, the vibration of the bearing pedestals at the second horizontal critical speed was about 0.3×10^{-3} in., well within normal vibration limits for this class of rotor.

Rotor speed was then increased to 1800 rpm, and vibrations from the second vertical mode were observed. The corresponding vectors measured at the left and right pedstals are shown in Fig. 7.9 as OA and OB. At the second vertical critical speed the vibration responses were 1.2×10^{-3} in. (pedestal A) and 1.8×10^{-3} in. (pedestal B). Although not explicitly stated by Moore [9], the vectors OA and OB most likely represent the pedestal vibrations resulting from the first balance correction at 1300 rpm. The additional vectors in Fig. 7.9 represent pedestal motions observed at 1950 rpm after corrections 2 through 6 (see Fig. 7.7). Scaling the vectors indicates that the final balance gave amplitudes of 0.28×10^{-3} in. at pedestal B and 0.46×10^{-3} in. at pedestal A, are both acceptable for a class 3 rotor.

Moore [9] discusses the effect of dissimilar pedestal stiffnesses in the horizontal and vertical directions and mentions that, because of differences in the corresponding mode shapes, the balance condition for the second horizontal mode may not hold for the second vertical mode.
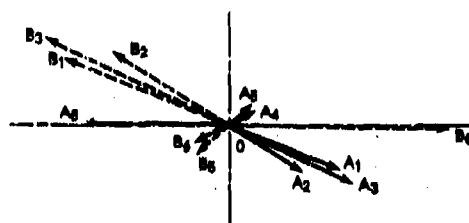
Differences in the mode shapes require somewhat different balance weight distributions to eliminate both modes. The test results indicate that rotor unbalance effects in the two modes were not exactly in phase. This is shown in Fig. 7.9 by the change in the orientation of the response vectors that occurred when corrections 4 and 5 were made. Moore attributes this variation to the differences in the two second-mode shapes and also to other unbalances in the rotor. This last comment is supported by Moore's polar response charts, which show that responses are not exactly 90° apart, even though the pedestal transducers were exactly 90° apart.

The findings of this experiment can be compared with tests by Badgley, Tessarzik, and Fleming [18] in which support anisotropy was also considered. Theoretical works by Parkinson [2] and by Badgley and Rieger [13] also discuss changes in mode shapes with support flexibility and their effect on the quality and efficiency of the balance obtained. The experiment demonstrated the effectiveness of the modal balancing method with relatively few balance corrections applied in a few balancing planes. It also demonstrated that, if balancing is carried out by considering the modes occurring in one principal stiffness plane, it is still possible, because of differences in the support stiffnesses of the two principal planes, for the rotor to be significantly out of balance in the other principal stiffness plane, even though the modes are nominally related. Moore comments that bearings and supports used for balancing should closely resemble those used on site. and the use of special isotropic bearings for balancing is not recommended because different unbalance responses may result from subsequent operation of the rotor in real (i.e., anisotropic) bearings.

7.5 Laboratory Verification of the Influence Coefficient Method

Badgley and co-workers have conducted a comprehensive series of experiments to examine the validity and effectiveness of the influence coefficient method for balancing flexible rotors. The scope of these experiments was as follows:

    1. Demonstration of the capability of the influence coefficient method for balancing a flexible rotor with various unbalance combinations through a strong bending critical speed without the aid of bearing damping [19].

    2. Demonstration of the least-squares influence coefficient procedure and comparison with the standard "exact-point-speed" influence coefficient procedure [20].

    3. Application of the influence coefficient method to the balancing of rotors whose operating-speed range contains several critical speeds; and other advanced considerations [18].

These investigations are described in detail in this section. The overall result is a thorough verification of the influence coefficient method in a wide variety of circumstances.

Flexible-Rotor System and Apparatus Used

    The test rotor used in the investigation of the exact-point-speed influence coefficient balancing method is shown in Fig. 7.10. This rotor was designed in conjunction with studies reported by Lund and Orcutt [21]. It was basically a solid, cylindrical steel shaft with an
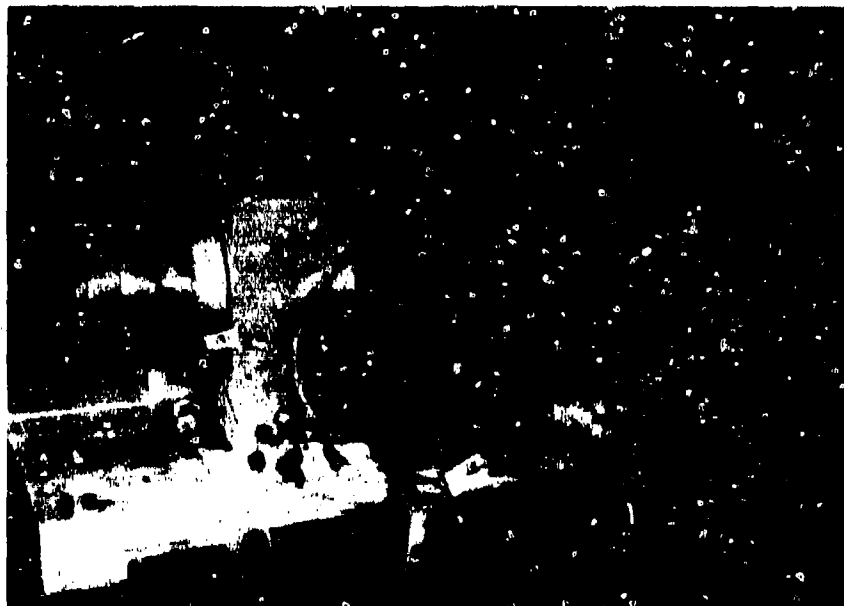
Fig. 7.10. Aluminum end disk for a two-mass rotor [20]

overall length of 41 in. and a diameter of 2.5 in. An integral disk 6 in. in diameter and 6 in. long was located at the center of the shaft. Detachable steel disks 6 in. in diameter and 3 in. long were mounted on the ends of the rotor by means of heavy interference fits and lock nuts that clamped them against shoulders on the shaft. The total weight of the rotor, exclusive of the detachable end masses, was 83 lb. The center disk, not counting the inner 2.5-in. diameter section, weighed approximately 36 lb, and the end disks each weighed 18 lb.

The rotor was supported by two four-tilting-pad journal bearings whose centerlines were 12.5 in. on either side of the rotor center plane. Bearing design characteristics included

Slenderness ratio (L/D), in.	1.0
Diameter, in.	2.5
Clearance ratio (C/R), in./in.	0.003 (based on machined clearance)
Pad arc length, degrees	80
Pivot position	0.55 of arc length $(44°)$ measured from the leading edge
Geometrical preload coefficient	0.5.

The journal bearings were lubricated by a low-viscosity silicone fluid (0.65 cSt at 77°F and 0.51 cSt at 130°F). Lubricant at a controlled temperature was pumped into the bearing housing to keep the bearings submerged in the lubricant. Bearing temperature rise was held at 10°F or less, as measured by thermocouples set in the two lower bearing pads in each bearing. On either side of the bearing housing there were clearance seals and scavenging rings to facilitate the recirculation of lubricant.

Geometrical preloading was used to give improved bearing film stiffness at high speeds with low steady-state loads. It was achieved by moving the pads radially inward so that the actual clearance at the pivot was less than the machined clearance (based on pad and shaft radii of curvature). In this case, the clearance at the pivots was half the machined clearance. The pivot configuration was a sphere seated in an internal cylindrical surface machined into the back surface of the pad. The bearings were so oriented in the housing that the steady-state gravity load line bisected the pivot positions; that is, the pivots were at 45° from a vertical line drawn through the bearing center.

The shaft was positioned axially by means of externally pressurized, gas-lubricated thrust bearings on either side of the center disk. These bearings were rigidly mounted in housings machined from single blocks of aluminum. The housings were keyed and bolted to a massive structural steel base.

The rotor was driven by an electric motor through a crowned spline coupling. The coupling was designed to accommodate misalignments between the motor and rotor axes up to 0.030 in. without restraint to the shaft. The motor was bolted and keyed to the same base surface that supported the bearing housing. A variable-frequency motor-generator set supplied power to the motor and provided for variable-speed operation within the range of 3000 to 24,000 rpm. The rotor system critical speed map is shown in Fig. 7.11. Rotor mode shapes corresponding to actual bearing stiffness are shown in Fig. 7.12.

During balancing, vertical rotor motions were measured in four planes along the length of the rotor. The selection of the vertical plane instead of the horizontal plane for displacement measurements was arbitrary. At the time of this study, no rule was available for specifying a priori the required number of measuring stations along the axis of the rotor for balancing by the exact point-speed influence coefficient method. In fact, this topic was one of the items under study. The computer program allows the substitution of data obtained at different speeds for data obtained at different rotor locations, provided that the product of the number of measuring stations and the rotational speeds at which trial-weight data are taken is equal to the number of balancing
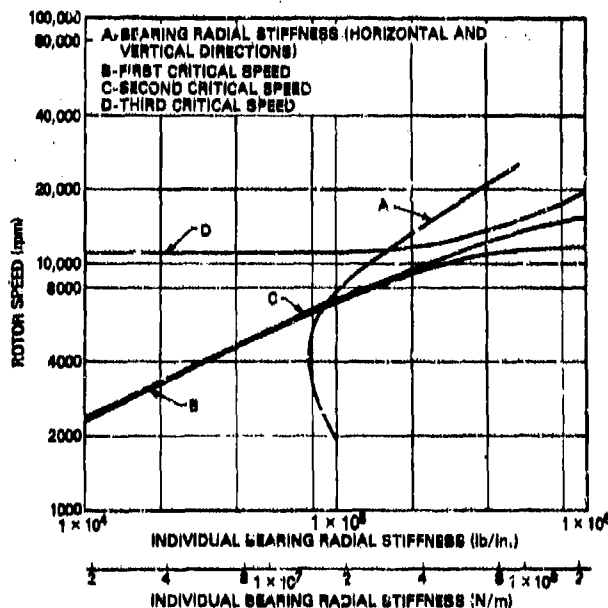
Fig. 7.11. Critical speed map for flexible-rotor test
rig used by Badgley et al. [20]
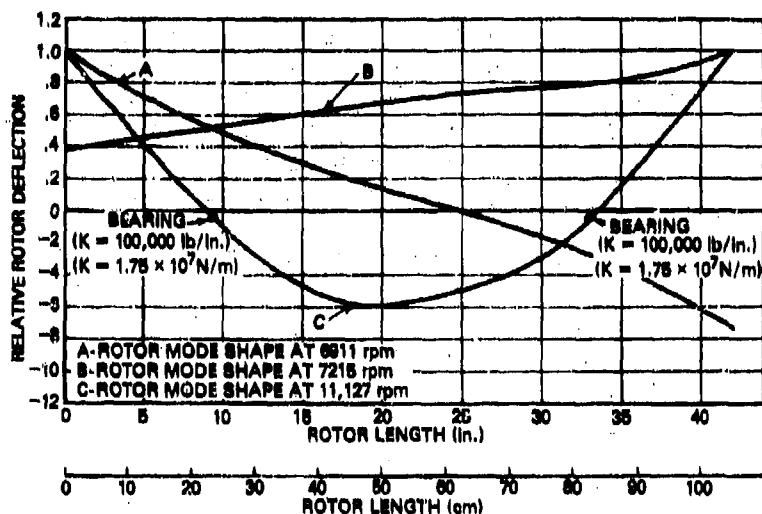
Fig. 7.12. Undamped critical speed mode shapes for flexible-rotor test rig used by Badgley et al. [20]

planes in which correction weights are to be added. For this test, four measurement stations were used. The data from each station were always recorded so that different combinations of speeds and measuring stations could be selected, as desired, for computing the correction weights.

Rotor displacements were measured with capacitance-type proximity sensors. Readout of rotor vibration amplitudes was obtained by means of an analog meter in a tracking analyzer. The tracking analyzer automatically filtered the incoming displacement signal to remove all frequency components other than the first harmonic corresponding to the rotational speed of the shaft. The tracking (frequency) signal for the tracking analyzer was provided by a square-wave reference signal, which was produced by an optical proximity sensor together with a narrow strip of reflective foil located on one-half the circumference of one of the end masses of the rotor. The square-wave reference signal was also used to relate a fixed angular position on the rotor to the angular position at which maximum dynamic displacement occurred at each of the four measurement stations. This angular relationship, (phase angle) was measured using a phase meter. The probe and reference-signal sensor locations are shown in Fig. 7.13.

The data acquisition system described above is satisfactory for flexible-rotor balancing. However, depending on the mechanical characteristics of the rotor system, it may be important, and at the same time difficult, to obtain amplitude data for all four probes at exactly the
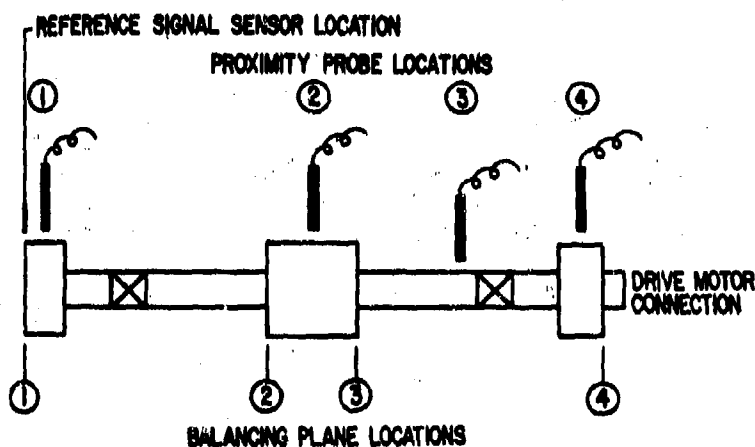
Fig. 7.13. Locations of probe and reference-signal sensor
used by Badgley et al. [20]

same speed if either the amplitude or the phase angle is highly sensitive
to small changes in the nominal value of the data-taking speed, as, for
example, near an undamped shaft critical speed. On the other hand,
particular rotor-drive controls, temperature effects, and damping may
make it difficult to hold the rotor speed constant long enough to take all
required readings. The requirement of nearly simultaneous readings
was met through the use of a seven-channel tape recorder. Five
phase-tied channels were used for the four displacement signals and the
reference signal, and two direct-reading channels were used for data
identification (voice and rotational speed). By playing back the mag-
netic tape four times and switching from one displacement signal to the
next, data were obtained at nearly identical rotational speeds.

Fundamental Verification of Method

The rotor was initially balanced in a low-speed balancing machine
so that a high-quality rigid-rotor balance was obtained. The disposition
of the rotor residual unbalance was not known. The rotor was then
assembled in its bearings, and on attempting to pass through the third
critical speed at about 10,960 rpm in an exploratory run, journal orbits
of 0.010-in. diameter developed. In subsequent measuring runs, rotor
orbit amplitudes were deliberately restricted to diameters of less than
0.006 in.
The rotor was then balanced to annul the effects of the original
unbalance. Amplitudes and phase angles were measured at probe sta-
tions 1, 2, 3, and 4, located as shown in Figs. 7.14 through 7.17. The
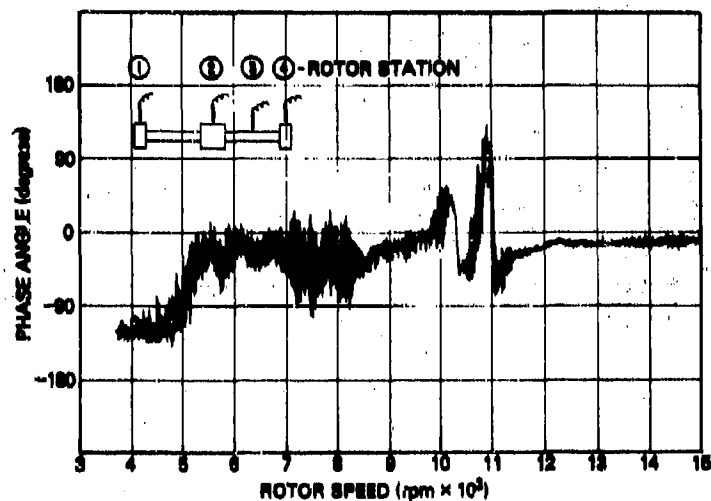
Fig. 7.14. Phase angle between reference signal and maximum dynamic displacement at station 1 after balancing rotor with residual unbalance at 5000, 6000, and 10,960 rpm [19]
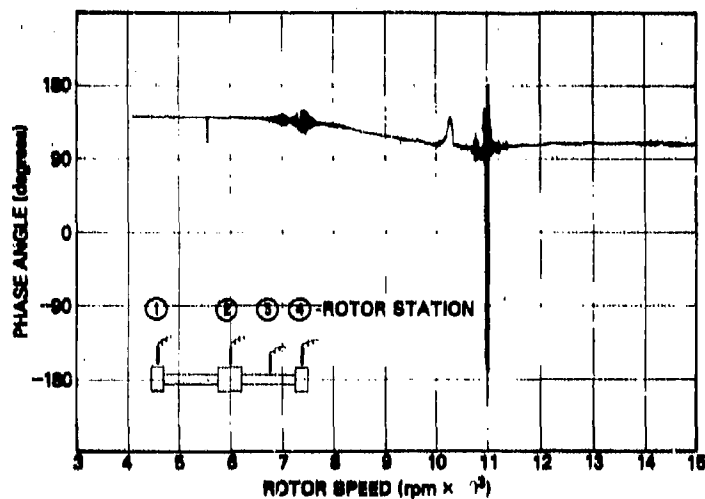
Fig. 7.15. Phase angle between reference signal and maximum dynamic displacement at station 2 after balancing rotor with residual unbalance at 5000, 6000, and 10,960 rpm [19]
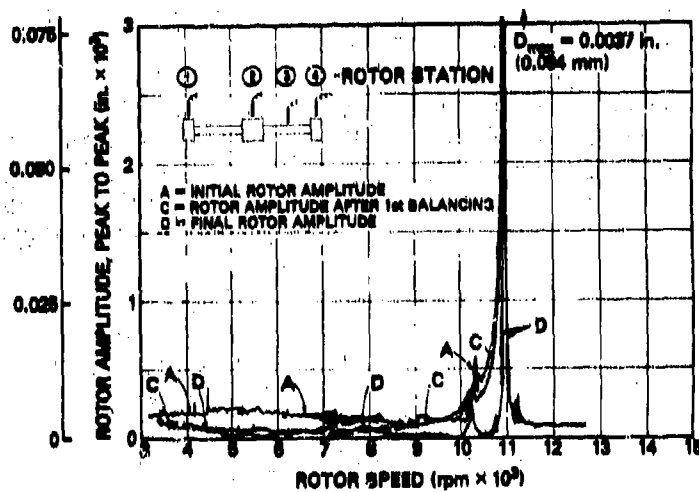
Fig. 7.16. Rotor amplitudes at station 1 before and after two consecutive balancing runs: rotor with residual unbalance [19]
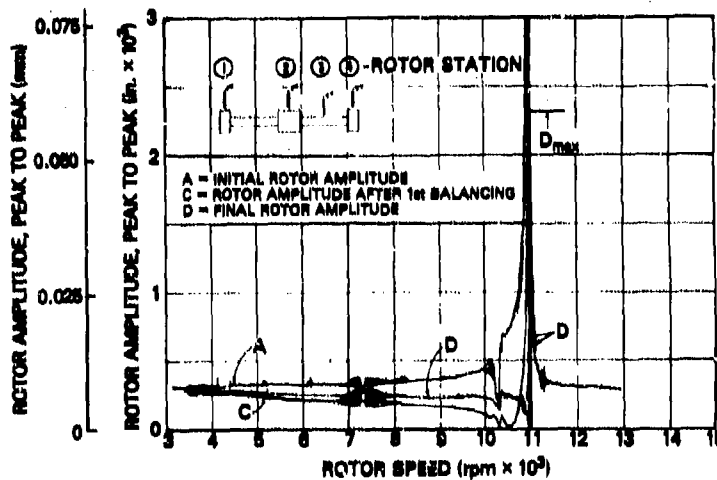
Fig. 7.17. Rotor amplitudes at station 2 before and after two consecutive balancing runs: rotor with residual unbalance [19]

balancing speeds were 5000, 6000, and 10,960 rpm, the latter speed coincides with the rotor bending critical speed in its bearings. Balancing at this speed was not attempted until after the second balancing run because of the large rotor amplitudes.

The changes in rotor amplitudes that resulted from the insertion of correction weights in the balancing planes are given in Table 7.3. The changes in phase angle between the reference signal and the maximum dynamic displacement of the rotor at given measurement locations are shown in Figs. 7.14 and 7.15; rotor amplitudes at probe stations 1 and 2 after two consecutive balancing runs are shown in Figs. 7.16 and 7.17. The curves are representative of the data curves that were plotted directly from each probe during testing. An acceptable balance existed to about 10,000 rpm—that is, to within 10 percent of the bending critical speed, as a result of low-speed balancing. The corresponding rigid-body critical speeds occurred at approximately 7000 and 7200 rpm.

Table 7.3. Balance improvement for rotor with residual unbalance [19]

Rotor speed (rpm)	Probe station	Peak-to-peak rotor amplitudes							
		Rotor amplitude before balancing*		After balancing Run 1*		Reduction (%) after balancing Run 1	After balancing Run 2*		Reduction (%) after balancing Run 2	Total reduction (%)
		μin.	μm	μin.	μm		μin.	μm		
6,000	1	200	5.04	50	1.27	73.0	35	0.89	30.0	82.5
	2	325	8.26	210	5.33	35.4	250	6.35	(19.0)†	23.1
	3	75	1.91	180	4.57	(140.0)†	180	.57	0.	(140.0)†
	4	185	4.70	235	5.97	(27.0)	180	4.57	23.4	2.7
9,000	1	110	2.79	85	2.16	22.7	20	0.51	76.5	82.0
	2	365	9.27	175	4.45	52.0	235	5.97	(35.6)†	35.6
	3	100	2.54	225	5.72	(125.0)†	175	4.45	22.2	(75.0)†
	4	180	4.57	180	4.57	0.	125	3.18	30.6	30.5
10,960‡	1					—	3700	93.98	—	—
	2					—	2900	73.66	—	—
	3					—	1800	45.72	—	—
	4					—	3300	83.82	—	—

*Because 5000 μin. was the maximum amplitude permitted in the test rig, the rotor was not actually operated to 10,960 rpm until after the second balancing run.

†Increase in amplitude.

‡Third critical speed of rotor (first flexural critical).

Once the effects of the actual initial unbalance in the rotor had been eliminated, further experiments were carried out to study the effectiveness of the influence coefficient method under conditions of specific unbalance distributions:

1. Unbalances in line and in phase
2. Unbalances in line and out of phase.

In these tests the rotor was intentionally unbalanced with unbalances of 0.343 oz-in., attached to the rotor at equal radii in four separate planes.

Unbalances in line and in phase. The unbalance configuration was such that it would tend to strongly excite the first critical speed. The resulting changes in rotor amplitudes through three balancing trials are shown in Table 7.4. Rotor-response details at probe stations 1 and 2 are shown in Figs. 7.18 and 7.19, respectively. The applied unbalance condition was substantially greater than that existing in the rotor after the original low-speed balance mentioned above, and the rotor whirl mode was essentially cylindrical in the speed range 5000 to 10,000 rpm. Balancing was conducted at 6000 and 9000 rpm, and three correction planes were used: on both end disks and on one side of the center disk. Substantial amplitude reductions (up to 88 percent) were achieved in the first two balancing runs. After the third balancing run, rotor amplitudes were of a similar order to those of the rotor in its original unbalance condition. Further balancing was not pursued, and it was concluded that at least three or four more balancing runs would have been required to attain the level of balance necessary to pass through the third critical speed with this particular rotor.

Unbalances in plane and out of phase. The unbalances in both end disks were rotated 180°. The overall unbalance configuration was then such that it would tend to excite the third rotor mode very strongly while canceling the unbalance effect on the first and second modes. Rotor-response details for this balance test are given in Table 7.5 and in Figs. 7.20 and 7.21 for probe stations 1 and 2, respectively. The rapid increase in rotor whirl amplitudes with speed for the initial unbalance condition is clearly evident in both figures. Initial balancing speeds were restricted to below 5000 rpm. The first balancing run reduced rotor amplitudes by 94 percent, at 9000 rpm. The second and third balancing runs resulted in only minor additional improvement. The rotor was again balanced until it operated in a manner comparable to the original balanced condition.

These tests validate the influence coefficient method and demonstrate its effectiveness in producing, for a specific rotor under laboratory conditions, whirl orbits of less than 0.002-in. diameter through and including the critical speeds. The circumstances chosen were unfavorable for smooth operation in each case, i.e., heavy test unbalances, no inherent amplitude suppression by bearing damping, and a very strong bending mode to be balanced before smooth operation could be achieved. It is noteworthy that influence coefficient balancing achieved smooth operation at precisely the bending critical speed in each test. Few tests of other flexible-rotor balancing methods have been conducted with such rigor.

Table 7.4. Balance improvement for rotor with in-plane, in-phase unbalance [19]

Rotor speed (rpm)	Probe station	Rotor amplitude before balancing		After balancing Run 1*		Reduction (%) after balancing Run 1	After balancing Run 2*		Reduction (%) after balancing Run 2	After balancing Run 3		Reduction (%) after balancing Run 3	Total reduction (%)
		µin	µm	µin	µm		µin	µm		µin	µm		
6000	1	1450	36.83	260	6.60	82.1	230	5.84	11.5	75	1.91	67.4	94.8
	2	1450	36.83	200	5.08	86.3	280	7.11	(40.0)*	280	7.11	0	80.7
	3	1800	45.72	210	5.33	88.3	335	8.51	(59.5)*	335	8.51	0	81.4
	4	2000	52.83	325	8.26	84.4	250	6.35	23.1	225	5.72	10.6	89.2
9000	1	1700	43.18	190	4.83	88.8	350	8.89	(84.2)*	100	2.54	71.4	94.1
	2	1700	43.18	200	5.08	88.2	350	8.89	(75.0)*	300	7.62	14.3	82.4
	3	2300	58.80	375	9.53	81.3	430	10.92	(14.7)*	405	10.29	5.8	79.8
	4	2060	52.32	250	6.35	87.9	110	2.79	56.0	110	2.79	0	94.7

*Increase in amplitude.
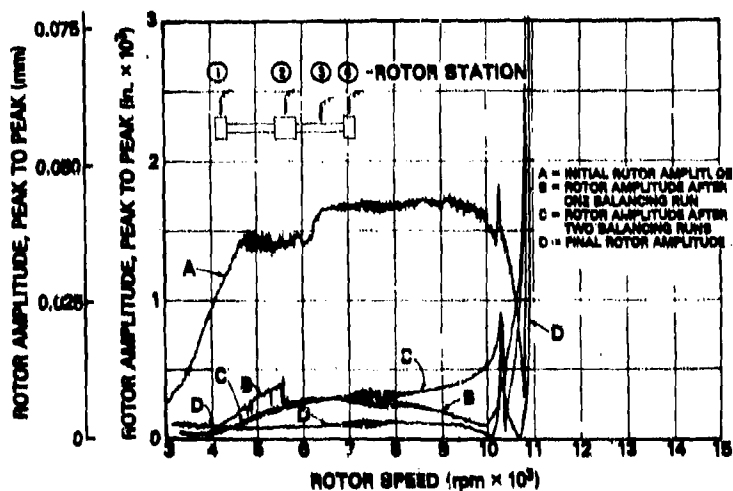
Fig. 7.18. Rotor amplitudes at station 1 before and after three consecutive balancing runs: rotor with in-line, in-phase unbalance [19]
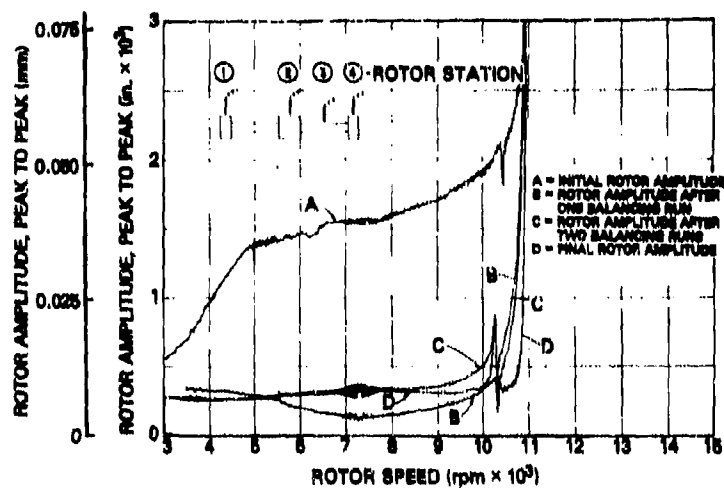
Fig. 7.19. Rotor amplitudes at station 2 before and after three consecutive balancing runs: rotor with in-line, in-phase unbalance [19]

Table 7.5. Balance improvement for rotor with in-plane, out-phase unbalance [19]

Rotor speed (rpm)	Probe stations	Peak-to-peak rotor amplitudes												
		Rotor amplitude before balancing[*]		After balancing Run 1[*]		Reduction (%) after balancing Run 1	After balancing Run 2'		Reduction (%) after balancing Run 2	After balancing Run 3		Reduction (%) after balancing Run 3	Total reduction (%)
		μin.	μm	μin.	μm		μin.	μm		μin.	μm		
6000	1	810	20.57	250	6.35	69.1	100	2.54	80.0	185	4.70	(85.0)†	77.2
	2	425	10.90	75	1.91	82.4	75	1.91	0.	100	2.54	33.3	76.5
	3	625	15.88	220	3.55	64.8	175	4.45	20.5	110	2.79	37.1	82.4
	4	420	10.67	190	4.83	54.8	250	6.35	(31.6)†	85	2.16	66.0	79.8
9000	1	2730	69.34	125	3.18	95.4	75	1.91	40.0	230	5.84	(206.7)†	91.6
	2	2510	63.75	150	3.81	94.0	40	1.02	73.3	100	2.54	(150.0)†	96.0
	3	2530	64.26	250	6.35	90.1	180	4.57	28.0	85	2.16	52.8	96.6
	4	2810	71.37	125	3.18	95.6	185	4.70	48.0	70	1.78	62.2	97.5
10,960‡	1									2125	53.98	—	—
	2									2075	52.71	—	—
	3									1400	35.56	—	—
	4									3100	78.74	—	—

*Because 5000 μin. was the maximum amplitude permitted in the test rig, the test rig was not actually run up to 10,960 rpm until after the second balancing run.

†Increase in amplitude.

‡Third critical speed of test rig (first flexural critical).
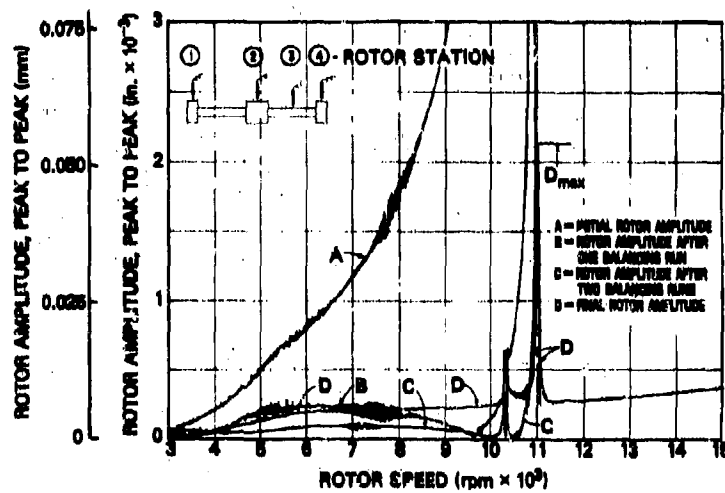
Fig. 7.20. Rotor amplitudes at station 1 before and after three consecutive balancing runs: rotor with in-line, out-of-phase unbalance [19]
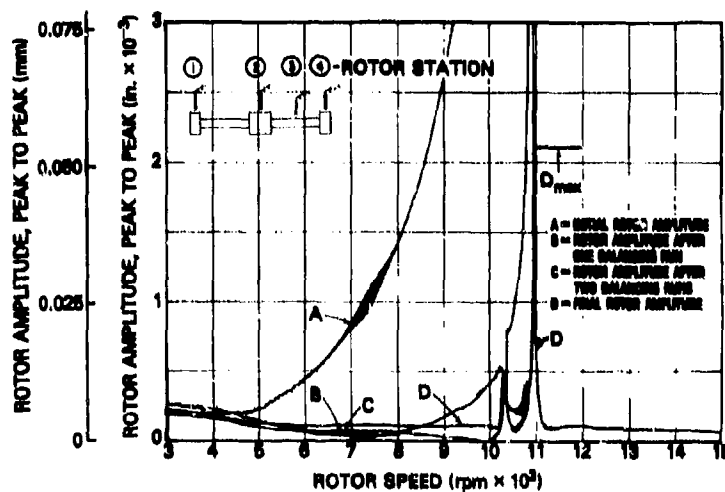
Fig. 7.21. Rotor amplitudes at station 2 before and after three consecutive balancing runs: rotor with in-line, out-of-phase unbalance [19]

Comparison of Exact-Point-Speed and Least-Squares Influence Coefficient Balancing

The least-squares procedure differs from the exact-point-speed procedure in that it minimizes the sum of the squares of the rotor residual amplitudes for a nonsquare matrix of influence coefficients, whereas the exact-point-speed method results directly in a square influence coefficient matrix. In both procedures a square matrix of influence coefficients is required before the balance corrections can be calculated and the required correction weights are prescribed.

The test conditions under which these two balancing methods were compared are as follows:

1. Rotor with "corkscrew" distribution of unbalances imposed
2. Rotor with in-plane, in-phase unbalances
3. Rotor with in-plane, out-of-phase unbalances.

The first test represents a severe test of the influence coefficient procedure, in which the exact-point-speed and the least-squares techniques were evaluated and compared. Tests (2) and (3) are similar to the tests reported on the preceding pages.

Rotor with "Corkscrew" Unbalance. Four different unbalance masses were placed on the rotor, one in each disk end and one in either face of the center disk; placed 90° apart, they progressed in corkscrew fashion down the shaft. Initial rotor amplitudes for the speed range 3000 to 10,000 rpm are shown as curves A in Figs. 7.22 and 7.23 for
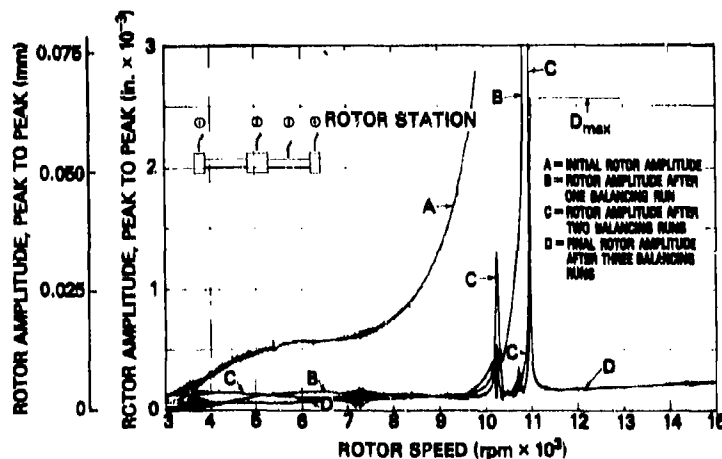
Fig. 7.22. Vertical amplitudes at station 1 before and after three consecutive balancing runs by the exact-point-speed influence coefficient method: rotor with corkscrew unbalance [20]
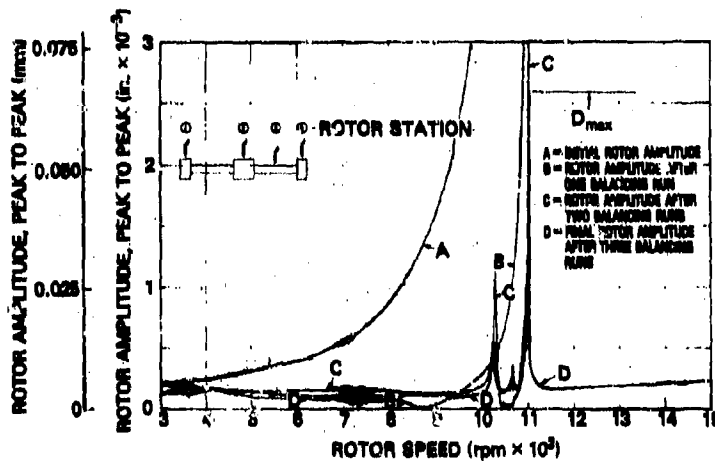
Fig. 7.23. Vertical amplitudes at station 2 before and after three consecutive balancing runs by the exact-point-speed influence coefficient method: rotor with corkscrew unbalance [20]

probe locations 1 and 2. The rotor was then balanced by the exact-point-speed method, with results similar to those observed in the original rotor-balancing tests described earlier in this section. A very substantial decrease in amplitudes occurred after the first balancing run, followed by more gradual improvements during successive runs (Table 7.6). Trial data were taken at 9970, 10,670, and 10,830 rpm in order to pass through the third critical speed. The total combined improvement at 6000 and 9000 rpm (for comparison purposes) was 77.4 percent, i.e., somewhat less than in the tests described earlier.

Least-squares balancing was tried next for the same corkscrew-unbalance configuration. The results (see Figs. 7.24 and 7.25 and Table 7.7) differed from those obtained with the exact-point-speed procedure. Amplitude reductions near the third critical speed were not as great as those obtained with exact-point-speed balancing, but the overall reduction of amplitudes throughout the rotor speed range at most locations was greater. As might be expected, the least-squares method is an efficient compromise for overall balance improvements.

Rotor with in-plane, in-phase unbalance—least-squares balancing. Use of the least squares method (Figs. 7.26 and 7.27; Table 7.8) led to a very rapid decrease in rotor amplitude. After two balancing runs, rotor amplitudes had decreased by 94 percent and passage through the third critical speed was possible, with maximum rotor orbit values of 0.003 in. (0.0076 cm) at the critical speed. Successive trials with the exact-point-speed method gave only slow improvements.

Table 7.6. Rotor with corkscrew unbalance: results of exact-point-speed-procedure [20]

Rotor speed (rpm)	Probe station	Peak-to-peak rotor amplitudes											
		Rotor amplitude before balancing*		After balancing Run 1*		Reduction (%) after balancing Run 1	After balancing Run 2*		Reduction (%) after balancing Run 2	After balancing Run 3		Reduction (%) after balancing Run 3	Total reduction (%)
		µin.	µm	µin.	µm		µin.	µm		µin.	µm		
6,000	1	575	14.6	150	3.81	74	100	2.54	33.3	75	1.9	25	86.7
	2	375	9.52	75	1.9	80	100	2.54	86.7	150	3.81	(50)†	60.5
	3	325	8.25	280	7.11	13.9	258	6.35	10.8	210	5.33	16	44
	4	1025	26.03	250	6.35	75.7	175	4.44	30	175	4.44	0	83
9,000	1	1175	29.84	110	2.79	90.7	110	2.79	0	110	2.79	0	91.7
	2	1650	41.91	30	0.76	98.2	125	3.17	(318)†	100	2.54	20	93.9
	3	650	16.51	310	7.87	52.4	250	6.35	19.4	225	5.71	10	65.4
	4	2100	53.34	325	8.25	84.6	160	4.06	50.8	125	3.17	21.8	94.2
10,670	1			1125	28.57		200	5.08	82.2	200	5.08	5†	
	2			1000	25.4		30	0.76	97	200	5.08	(566)†	
	3			800	20.32		310	7.87	61.3	230	5.84	-25.8	
	4			1800	45.72		275	6.98	84.7	160	4.06	41.8	

*Because 3000 µin. was the maximum amplitude permitted in the test rig, the rotor was not actually run up to 10,670 rpm until after the second balancing run.

†Increase in amplitude.

Fig. 7.24. Vertical amplitudes at station 1 before and after four consecutive balancing runs by the least squares method: rotor with corkscrew unbalance [20]
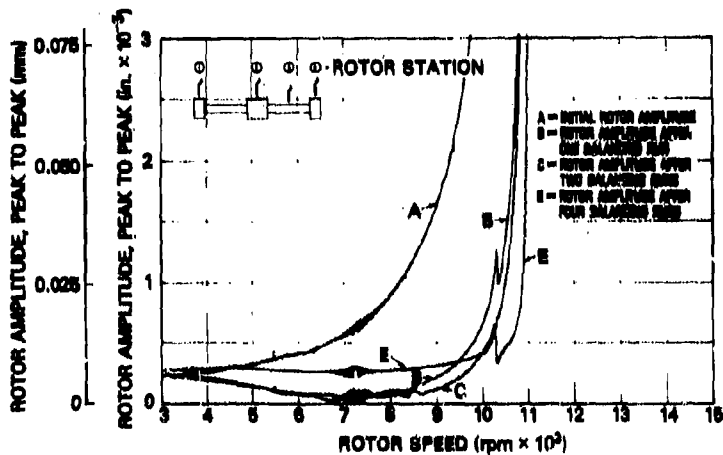
Fig. 7.25. Vertical amplitudes at station 2 before and after four consecutive balancing runs by the least squares method: rotor with corkscrew unbalance [20]

Table 7.7. Rotor with corkscrew unbalance: results of least squares procedure [20]

Peak-to-peak rotor amplitudes

Rotor speed (rpm)	Probe station	Rotor amplitude before balancing		After balancing Run 1*		Reduction (%) after balancing Run 1	After balancing Run 2*		Reduction (%) after balancing Run 2	After balancing Run 3		Reduction (%) after balancing Run 3	Total reduction (%)
		μin.	μm	μin.	μm		μin.	μm		μin.	μm		
6,000	1	575	14.6	125	3.17	78.3	30	0.76	76.0	30	0.76	0	25
	2	375	9.52	230	5.84	38.7	50	1.27	78.3	75	1.90	(50)†	50
	3	325	8.25	280	7.11	13.9	255	6.47	9.0	250	6.35	2.0	25
	4	1025	26.03	300	7.62	70.7	325	8.25	(8.3)†	350	8.89	(7.6)†	200
9,000	1	1175	29.84	375	9.52	68.1	200	5.08	46.7	150	3.81	25.0	75
	2	1650	41.91	200	5.08	87.9	100	2.54	50.0	30	0.76	70.0	285
	3	650	16.51	500	12.7	23.1	400	10.16	20.0	375	9.52	6.3	100
	4	2100	53.34	250	6.35	88.1	300	7.62	(20)†	300	7.62	0	175
10,670	1			2375	60.32		1750	44.45	26.3	1375	34.92	21.5	375
	2			2250	57.15		1625	41.27	27.8	1500	38.1	7.7	525
	3			2000	50.80		1325	33.65	33.8	1150	29.21	13.3	250
	4			2500	63.5		1875	47.62	25.0	1625	41.27	13.4	1000

*Because 3000 μin. was the maximum amplitude permitted in the test rig, the rotor was not actually run up to 10,670 rpm until after the second balancing run.

†Increase in amplitude.
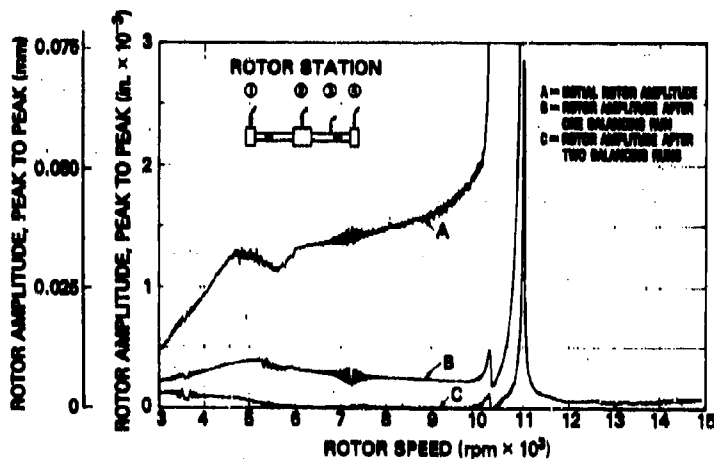
Fig. 7.26. Vertical amplitudes at station 1 before and after two consecutive balancing runs by the least squares method: rotor with in-plane, in-phase unbalance [20]
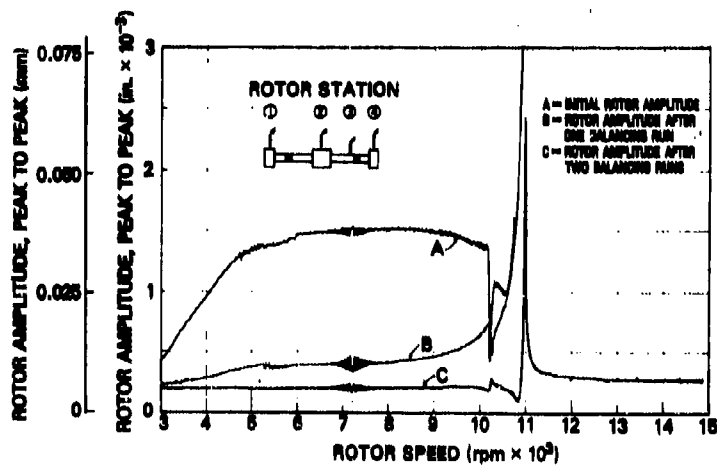
Fig. 7.27. Vertical amplitudes at station 2 before and after two consecutive balancing runs by the least squares method: rotor with in-plane, in-phase, unbalance [20]

Table 7.8. Rotor with in-plane, in-phase unbalance: results of least squares procedure [20]

Rotor speed (rpm)	Probe station	Peak-to-peak rotor amplitudes							
		Rotor amplitude before balancing*		After balancing Run 1*		Reduction (%) after balancing Run 1	After balancing Run 2*		Reduction (%) after balancing Run 2	Total reduction (%)
		μin.	μm	μin.	μm		μin.	μm		
6,000	1	1325	33.65	310	7.87	76.5	10	0.25	96.8	99.3
	2	1450	36.83	375	9.52	74.2	210	5.33	44.0	85.5
	3	1425	36.19	160	4.06	88.8	110	2.79	31.3	92.3
	4	1350	34.29	70	1.77	94.9	30	0.76	57.2	97.8
9,000	1	1600	40.64	210	5.33	86.9	5	0.12	97.6	99.7
	2	1480	37.59	460	11.68	68.9	200	5.08	56.5	86.5
	3	1475	37.46	175	4.44	88.1	125	3.17	28.6	91.5
	4	1650	41.91	100	2.54	93.9	0	0	100	100
10,670	1			525	13.33		100	2.54	81.0	
	2			1075	27.30		180	4.57	83.3	
	3			375	9.52		160	4.06	57.4	
	4			750	19.05		0	0	100	

*Because 3000 μin. was the maximum amplitude permitted in the test rig, the rotor was not actually run up to 10,670 rpm until after the second balancing run.

Rotor with in-plane, out-of-phase unbalance—least-squares balancing. As shown in Figs. 7.28 and 7.29, and in Table 7.9, only two trial balance runs were necessary for the rotor to pass smoothly through the third critical speed. The first correction run reduced amplitudes by almost 95 percent at 9000 rpm. These results are superior to those obtained with the exact-point-speed procedure of comparable conditions, in which three correction runs were needed.

Badgley and co-workers report two additional tests in which they investigated the effect of replacing one end disk of the rotor with an aluminum disk and unbalancing only the two steel disks. The rotor modes and excitation thereby lose their symmetry, and some bearing damping occurs to affect the rotor response. The rotor tends to orbit in a conical mode in the low range. Both exact-point-speed balancing and least-squares balancing were attempted, and results of comparable quality were achieved with both methods. No sharply defined resonant peak was observed, and both methods resulted in rapid (two trial runs) convergence to excellent balance quality.

The second of these tests dealt with the effects of the shaft being out of round on instrument readings and hence on balance quality. The end aluminum disk was machined 0.0022 in. out of round, which showed up as a two-per-revolution probe signal at that location. Badgley et al. report that the disk out-of-roundness was "ignored by the computer," and (evidently) calculations were based on the mean orbit radius. This corresponded to a heavy-disk unbalance (0.0011 in.),
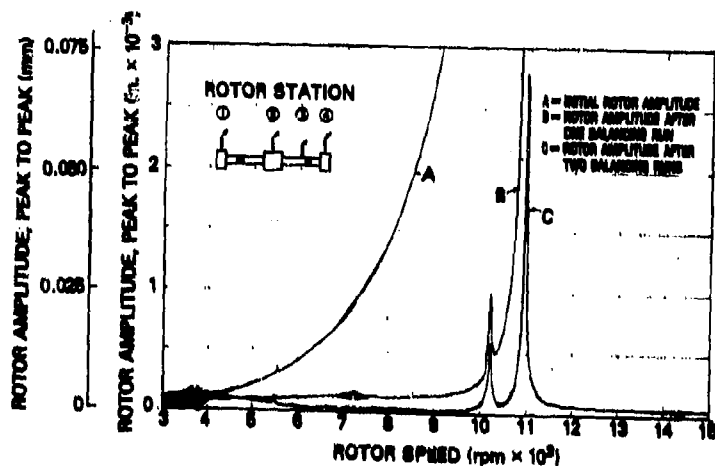
Fig. 7.28. Vertical amplitudes at station 1 before and after two consecutive balancing runs by the least squares method: rotor with in-plane, out-of-phase unbalance [20]
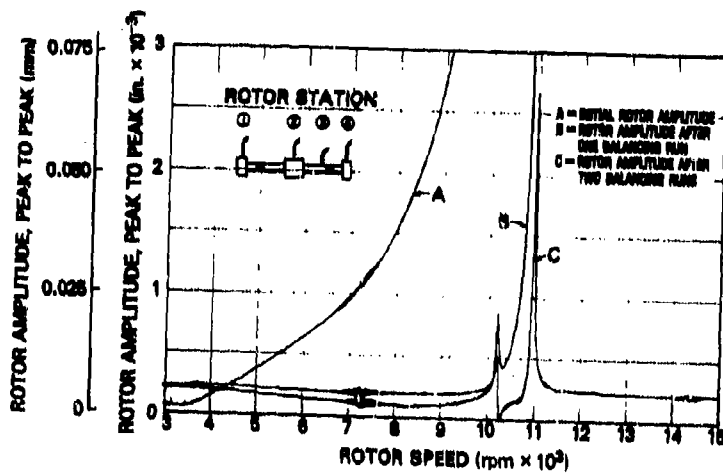
Fig. 7.29. Vertical amplitudes at station 2 before and after two consecutive balancing runs by the least squares method: rotor with in-plane, out-of-phase unbalance [20]

Table 7.9. Rotor with in-plane, out-of-phase unbalance: results of least squares procedure [20]

Rotor speed (rpm)	Probe station	Peak-to-peak rotor amplitudes								
		Rotor amplitude before balancing		After balancing Run 1*		Reduction (%) after balancing Run 1	After balancing Run 2'		Reduction (%) after balancing Run 2	Total reduction (%)
		μin.	μm	μin.	μm		μin.	μm		
6,000	1	460	11.68	125	3.17	73.0	50	1.27	60.0	89.2
	2	650	16.51	235	5.97	63.9	150	3.81	36.2	77.0
	3	700	17.78	80	2.03	88.6	40	1.01	50.0	94.3
	4	210	5.33	85	2.16	59.6	35	0.89	58.9	83.4
9,000	1	2925	74.29	150	3.81	94.9	25	0.63	83.4	99.2
	2	2800	71.12	210	5.33	92.5	125	3.17	40.5	94.4
	3	1875	47.62	100	2.54	94.7	75	1.90	25.0	96.0
	4	2700	68.58	60	1.52	97.8	50	1.27	16.7	98.2
10,670	1	1250	31.75				150	3.81	81.0	
	2	1000	25.4				160	4.06	84.0	
	3	525	13.33				175	4.44	66.6	
	4	1075	27.30				150	3.81	86.1	

*Because 3000 μin. was the maximum amplitude permitted in the test rig, the rotor was not actually run up to 10,670 rpm until the second balancing run.

which the computer attempted to remove by selecting a correction mass with enough centrifugal force to bend the shaft back to the zero position. The results suggest that the program was adversely affected by the shaft being out of round.

The overall result of this test series is that the least-squares approach appears to give results comparable in quality to those obtained by the exact-point-speed approach. In general, least-squares balancing also leads to more broadly acceptable balance conditions throughout the speed range with fewer balance iterations.

Balancing for Operation Through Several Bending Critical Speeds

Tessarzik conducted additional experiments to investigate the influence of the following conditions [22]:

1. Operation through several critical speeds, bending and torsional
2. Rigid and flexible bearings
3. Bearings with significantly different stiffness properties in the horizontal and vertical directions
4. Different balancing input data
5. Different initial unbalance configurations.

A special test rig was developed (Fig. 7.30) to permit observations through the third and fourth critical speeds (i.e., first and second flexural modes) and of the first and second torsional modes. The critical speed map for the rotor is shown in Fig. 7.31. An unbalance response chart for specified bearings and a specified unbalance distribution are shown in Fig. 7.32.

Rigid pedestals: in-plane, in-phase unbalance, seven displacement sensors. Trial-weight data were obtained at 3315 rpm to balance
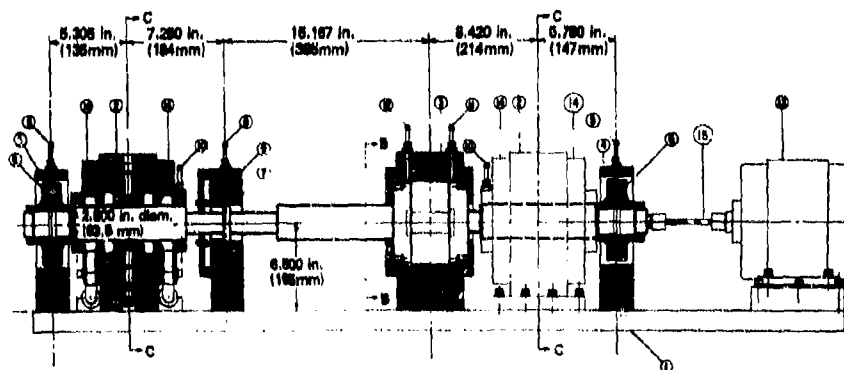
Fig. 7.30. Flexible-rotor test rig with rigid bearing supports used by Tessarzik [22]
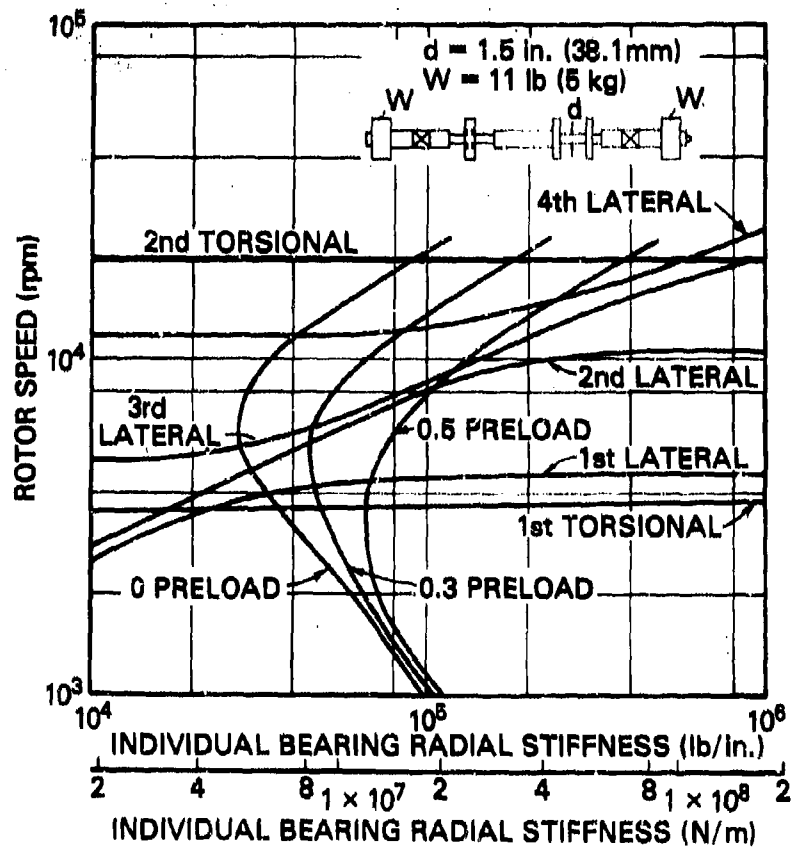
Fig. 7.31. Calculated critical speed map and bearing stiffnesses for shaft-bearing system used during high-speed multiplane flexible-rotor balancing tests [22]
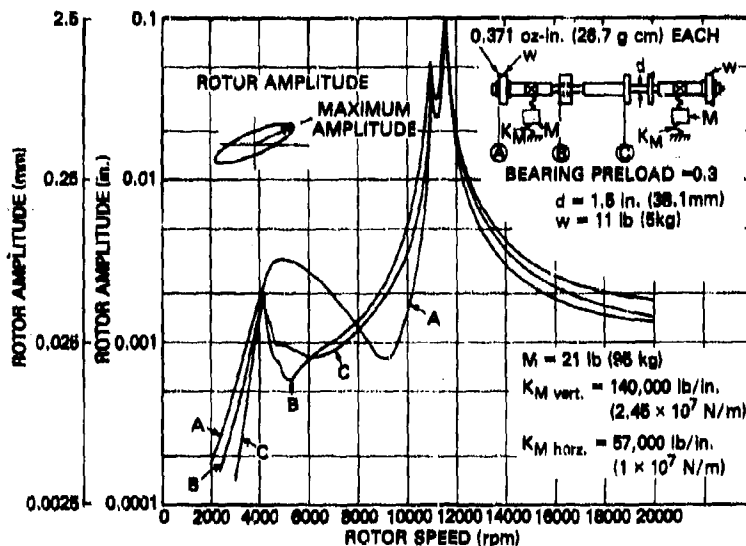
Fig. 7.32. Maximum damped rotor amplitudes (peak) at stations A, B, and C: rotor with in-line, alternating-phase unbalance and flexible bearing supports [22]

out the strong amplitude buildup at about 4000 rpm associated with the first bending critical speed. The result is shown as curve A in Fig. 7.32. Subsequent trial runs with balancing data taken at 4265 rpm (curve B) at 4395 rpm (curve C), and at 4345 rpm (curve D) reduced rotor amplitudes throughout the speed range to acceptable operational values.

Rigid pedestals: In-plane, in-phase unbalance, four displacement sensors. This experimental setup had one less balancing plane and three fewer sensors. The results were similar in quality to those reported for the preceding case, with similar economy of balancing runs. Another test of this type was attempted with two displacement sensors (i.e., adjacent to the bearings) under otherwise identical conditions. It proved to be inefficient, as the sensors were located adjacent to the nodes of the first bending mode. Three trial runs were required to achieve satisfactory balance.

Rigid pedestals: In-plane alternating-phase unbalance, four displacement sensors. Results indicated that a balance of comparable quality to that of the preceding case could be achieved with about one more trial run for each balance.

Flexible pedestals: In-plane, in-phase unbalance, four displacement sensors. For this test, bearings were not changed, only the

pedestal support flexibilities. The rotor was balanced with four vertical sensors throughout the operating-speed range with one set of trial runs per speed.

Flexible pedestals: in-plane alternating-phase unbalance, four displacement sensors. Two additional trial-weight runs were required to achieve smooth passage through the fourth critical speed. A final correction run was made with data acquired at 4200, 9600, and 10,600 rpm.

The tests described above further demonstrate the effectiveness of the influence coefficient method in balancing a lightly damped rotor in flexible bearings throughout an operating-speed range that contains two strong bending critical speeds.

Experimentally Demonstrated Status of Influence Coefficient Method

The experimental results described above show that the influence coefficient method is an effective procedure for balancing flexible rotors. It is not adversely influenced by the presence of one or several bending critical speeds within the operating-speed range. It has been shown to be capable of balancing rotors in damped, flexible bearings, with bearing supports that are either rigid or flexible, and hence by inference capable of balancing rotors whirling in elliptical orbits.

The experiments of Badgley and co-workers were conducted with two rotors only, but with similar success. Documentation of field trials is now needed to indicate the efficiency of the influence coefficient method when used by semiskilled technicians under diverse circumstances.

7.6 Laboratory Verification of the Influence Coefficient Method: Lund and Tonnesen

Two experimental studies of influence coefficient balancing have been made by Lund and Tonnesen [23] and by Tonnesen [24]. These studies provided additional independent data on the effectiveness of this method under carefully controlled experimental conditions.

The first of these studies investigated the application of the least-squares procedure in two and three planes to a rotor whose speed range involved a strong bending critical speed. The stated objectives of this study were (a) to examine the validity and accuracy of the influence coefficient method in determining balance correction weights and (b) to investigate the influences of various types of sensing and analysis instrumentation on the attainable accuracy.

The second study extended the objectives (a) to perform balancing simultaneously in up to five correction planes within a speed range containing three critical speeds and (b) to investigate the absolute minimum level of residual vibration that is attainable by the influence coefficient procedure.

In many respects these tests provide an independent viewpoint of many of the tests reported by Badgley and associates. A comparison of the findings of both studies and a review of results are given at the end of this section.

Experimental Apparatus and Instrumentation

The rotor used by Lund and Tonnesen (Fig. 7.33a) consisted of a shaft with a nominal diameter of 2.0 in. and an overall length of 46.0 in., with a 25.7-in. span between bearings. The shaft carried an integral central mass and two disks inboard of the bearings. Two additional disks were mounted outboard of the bearings, one at each end. The total weight of the shaft was 75.3 lb.

The central mass contained two rows of correction planes around its circumference, and each disk contained one correction plane. The two bearings were externally pressurized air bearings, mounted on flexible supports consisting of eight radial spokes. These bearings were found to be highly adaptable during testing and had low power consumption. The journal diameters were both 2.2 in., with similar bearing lengths and bearing radial clearances of 0.0011 in. Air was supplied at 100 psia (6.9×10^5 Pa). The calculated radial stiffness of each bearing, including the flexible pedestal, was 0.508×10^8 lb/in., and the damping was 9652 lb-s/in. With the bearings represented by their theoretical stiffness values, the critical speeds of the rotor system were 8060, 11,220, and 12,130 rpm. The maximum speed of the test rig was 16,000 rpm.

The test rig is shown schematically in Fig. 7.33c. The rotor was driven through a floating splined coupling. The transmission shaft was driven by a timing belt with a step-up speed ratio of 4:1. The pedestal supports were rigid and were mounted on a massive bedplate. Precise motor speed control was available. The rotor vibrations were measured by five inductance probes and four velocity pickups. Probes at the bearings measured relative displacements between the rotor and the pedestal housing. Other probes measured absolute displacements. Phase was measured with an electronic counter relative to a reference signal generated by a pin located near the middle of the rotor, which passed a magnetic pickup once per revolution.
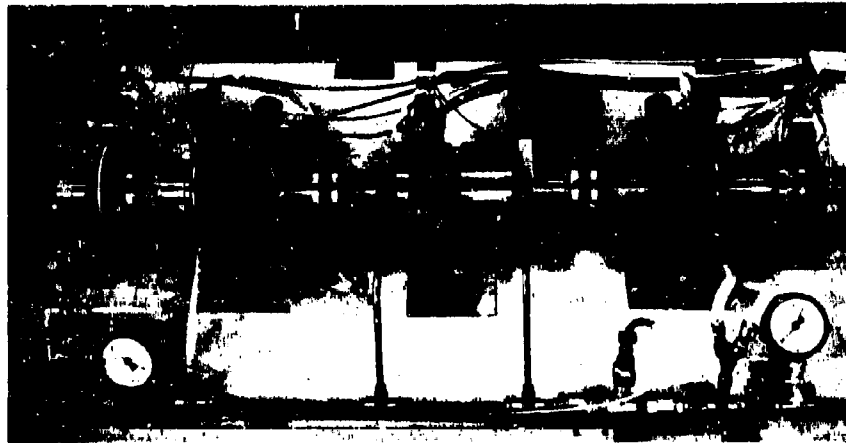
(a) Rotor assembly

(b) View of instrumentation

STATION NUMBERS. BRG.   BRG.

PROBE POSITIONS (INDUCTIVE)
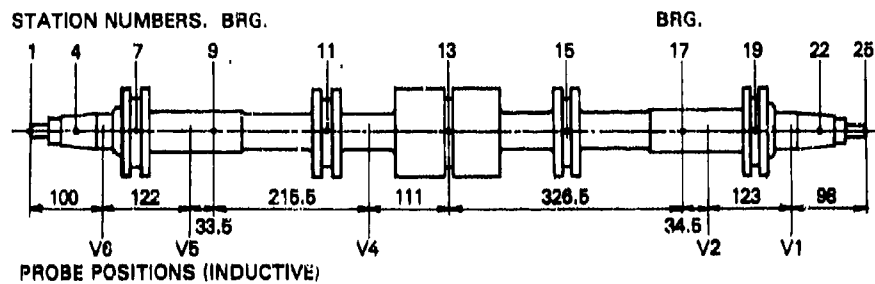
(c) Probe positions and rotor stations

Fig. 7.33. Experimental apparatus and instrumentation used by
Lund and Tonnesen [23]

The electronic counter measured the time elapsed from the passage, at increasing amplitude, of the probe signal. The phase angle ϕ—that is, the angle by which the amplitude leads the reference in the rotor in the direction of rotation—is defined as follows:

$$\phi = 270 - 6 \text{ (speed times measured time)}$$

where ϕ is in degrees, speed is in revolutions per minute, and the measured time is in seconds. The relationship assumes that the magnetic pickup is in the same vertical position as the probes. From this definition it follows that the angular locations of the unbalance weights and the trial weights are measured from the reference, fixed in the rotor, in the direction of rotation.

As all phase-angle measurements and position angles have a common reference, they are absolute quantities. Actually, this is unnecessary for balancing tests where only relative measurements are required, as in most conventional field balancing. It is, however, very convenient not to have to keep track of separate references for each balancing plane; furthermore, it makes it possible to subtract out any out-of-roundness of the rotor.

Test Program: Three Correction Planes, Single Critical Speed

The correction planes used by Lund and Tonnesen are numbered 7, 13, and 19 in Fig. 7.33c. Center plane 13 was not used. Trial-run measurements were taken at 6000, 7800, 8700, and 10,200 rpm, as required. The imposed unbalance distribution is shown in Table 7.10. The trial weights were 1.1 gms and were located at a 49-mm radius.

Lund and Tonnesen discuss at some length the accuracy of all measurements involved in the tests and calculations. The average errors which occurred are given in Table 7.11.

The following conclusions can be drawn from these experiments:

1. The influence coefficient method has been demonstrated to be capable of balancing a rotor through a speed range that contains a bending critical speed.

2. The quality of the balance obtained has been evaluated in terms of the sources of error inherent in the system. It is shown that, if the errors in the amplitude and phase-angle measurements do not exceed 3 to 4 percent, a satisfactory balance can be obtained.

3. Commercially available instrumentation can be used to balance a flexible rotor, provided it is carefully calibrated.

4. If sufficient measurements are taken, the influence coefficient method can be used for simultaneous balancing in more than two correction planes.

Table 7.10. Calculated correction weights, all tests* [23]

Test No.	Speed (rpm)	Probe	Plane 7 Weight (g)	Plane 7 Angle (degrees)	Plane 13 Weight (g)	Plane 13 Angle (degrees)	Plane 19 Weight (g)	Plane 19 Angle (degrees)	Average deviation Weight (%)	Average deviation Angle (%)	Average deviation (degrees)
Test weight			0.575	-135.0	0.929	115.0	0.650	-110.0			
12			0.542	-132.5			0.635	-93.9	4.1	16.1	9.3
22	6,000	Induction	0.459	-143.9			0.574	-98.0	16.2	18.2	10.5
32			0.472	-136.2			0.543	-103.2	17.3	7.5	4.2
42			0.490	-133.2			0.582	-100.4	12.7	9.9	5.7
52	7,800	V1, V2	0.496	-134.6			0.581	-100.2	12.3	8.9	5.1
13	8,700	V4, V5	0.647	-128.0	1.250	103.8	0.779	-93.9	22.2	19.8	11.4
23		V6	0.459	-145.9	0.982	114.0	0.557	-102.1	16.1	11.5	6.6
33	10,200		0.507	-136.3	0.805	110.9	0.566	-104.4	12.7	6.4	3.7
43			0.510	-128.1	0.818	102.4	0.565	-96.4	12.1	19.3	11.0
53			0.537	-125.8	0.839	102.7	0.570	-96.8	9.5	19.0	10.9
12		Induction	0.539	-134.0			0.655	-94.6	3.5	14.2	8.2
22	6,000		0.401	-161.7			0.606	-88.5	19.0	41.8	24.1
42		V1, V2	0.487	-135.4			0.574	-99.5	13.5	9.5	5.5
52			0.489	-137.6			0.569	-103.3	13.4	8.0	4.6
62			0.469	-132.5			0.568	-101.2	15.6	9.5	5.5
13	7,800	V4, V5	0.601	-129.3	1.268	104.3	0.749	-95.4	18.7	17.9	10.3
23	8,700	V6	0.398	-160.0	0.827	113.9	0.582	-97.5	17.5	11.7	18.2
43			0.450	-130.0	0.826	102.1	0.594	-93.6	13.8	19.8	11.4
53			0.493	-122.1	0.839	102.9	0.577	-101.0	11.7	19.8	11.3
63			0.427	-132.3	0.845	103.3	0.560	-95.3	16.2	16.8	9.7
12	7,800 8,700	Velocity V22, H22	0.555	-131.9			0.610	-94.1	3.3	16.1	9.2
13	10,280	V25, H25	0.606	-121.3	1.233	112.8	0.580	-96.9	20.5	14.5	8.3

*Common conditions: two trial runs per balancing plane, optimized influence coefficient, weight radius 49 mm.

Table 7.11. Details of average errors likely to occur during balancing [23]

Speed (rpm)	Number of planes	Average error (%)	Averages ranges of errors (%)
6000, 7800	2	3.7	7.1
8700, 10,200	3	5.3	9.0
6000, 7800	2	2.0	3.2
8700	3	4.2	7.1

5. The assumption of linearity on which the influence coefficient method is based was found to be valid for the rotor-and-bearing system tests.

Experiments to Determine Optimum Balancing Conditions

In a second series of experiments with the influence coefficient method, Tonnesen [24] sought an optimum balance condition for operation through three critical speeds of the rotor system. This optimum condition consists of determining the accuracy to which the test rotor could be balanced by use of a least-squares procedure with a minimum number of balancing runs, using four correction planes. Determination of the absolute minimum level of residual vibration for the conditions used was another objective.

The rotor-support system was the same as that used by Lund and Tonnesen [23] with minor modifications to the drive. Thorough details are given of the rotor vibration measurement system and its settings, which consisted of the original transducer system with additional capacitance distance probes and piezoelectric accelerometers mounted horizontally. Rotor motions were monitored continuously. In test runs an active filter (48 dB/octave) was used to obtain only the synchronous component. Corresponding amplitudes were measured with a digital voltmeter, and phase-angle measurements were made with an electronic counter used in the time-interval mode. All signals were time averaged over 100 periods. For tests with six and seven balancing planes a lock-in amplifier was used as a tracking filter. A photoelectric pickup was used to phase-lock the amplifier to the test rotor, and the amplifier outputs (amplitude and phase) were measured with digital voltmeters.

Experiments were conducted to determine the influence of number of correction planes, number of balance speeds, etc., on the quality of balance attainable. Influence coefficients were evaluated on the basis of two trial-weight runs per plane using the same trial weight. For each test run the deviation from the correct value is given for each

weight in each plane. Total average deviations are also given. The total average deviation for all tests was found to be 4.5 percent for the capacitance probes and 7.3 percent for the inductance probes with the same values of trial weight and phase angle.

Table 7.12 shows the calculated absolute average error of the system. Errors are given in percentages for the measured amplitudes and in degrees for the phase angles. Accuracy of the measuring equipment was fairly standard: 0.1 percent for amplitude measurements and 0.1° for phase angles.

Random distribution of unbalance was studied by placing unbalances at random locations in six planes along the rotor length (planes 4, 7, 11, 13, 15, and 19 in Fig. 7.34). Four planes were used for inserting correction weights (planes 7, 11, 15, and 19). It was required that the rotor be balanced to a minimum level of vibration over the entire speed range by simultaneous balancing in these four planes.

Curves A in Figs. 7.35 and 7.36 are plots of the synchronous response of the rotor with its initial unbalance acting. In this condition, it was just possible to operate through the entire speed range. The first critical speed was at 7850 rpm, the second at 9300 rpm, and the third at 10,400 rpm; the other peaks were due to drive effects. The rotor was then balanced to achieve a zero-rotor condition, and then the random unbalances were inserted into the six "unbalancing" planes. In this condition (curve A in Fig. 7.35) the rotor was so strongly unbalanced that the first critical speed could not be passed. After balancing at 5000, 7000, and 7500 rpm, the rotor ran safely through its first, second, and third critical speeds, with a whirl amplitude of less than half the bearing clearance (curve B in Fig. 7.35). The rotor was again balanced at 7500, 9500, and 11,000 rpm in the same correction planes. The results are shown as curves C in Figs. 7.35 and 7.36.

A second set of tests was undertaken by installing a disk in an end plane so that the rotor nodes in the strong bending critical speed at 7650 rpm occurred within both journal bearings. This gives a zero-damping rotor configuration. Unbalance was randomly distributed in seven planes. Four correction planes were again used, and four transducers were used for amplitude measurements at the bearings and at the overhangs. There was difficulty in passing through the bending critical speed because of the low bearing damping. The rotor was balanced both below and on passing through the critical speed and subsequently at 7300, 9000, and 11,000 rpm. It could then be operated smoothly throughout its entire operating-speed range.

Figures 7.37 and 7.38 show the amplitudes obtained after the first and second balancing operations. It is a testimony to the precision of

Table 7.12. Calculated average error on system—all tests, all transducers [24]

Test run No.	Five probes, H1C to H5C Amplitude (%)	Phase (deg)	Five probes, H1I to H5I Amplitude (%)	Phase (deg)	Two probes, H2C to H4C Amplitude (%)	Phase (deg)	Two probes, HB1IV and HB2IV Amplitude (%)	Phase (deg)	Two probes, HB1A and HB2A Amplitude (%)	Phase (deg)
16.2-1	1.46	1.21	1.13	0.86	1.42	0.96	2.10	1.52	2.44	1.91
16.2-2	2.00	0.79	1.85	0.67	2.46	0.64	3.52	1.29	3.16	1.07
16.3-1	1.56	1.08	1.58	0.94	1.73	1.23	2.74	1.73	2.41	1.66
16.3-2	1.62	0.73	1.60	0.83	1.86	0.81	2.13	1.94	1.82	1.53
16.4-1	1.76	0.86	1.51	0.76	2.74	1.22	2.32	1.14	2.24	1.11
16.4-2	1.69	0.80	1.49	0.87	1.82	1.00	1.27	0.71	1.51	0.79
16.5-1	1.54	0.88	1.54	0.95	1.52	1.00	2.12	1.05	2.26	1.26

PLANE NUMBERS
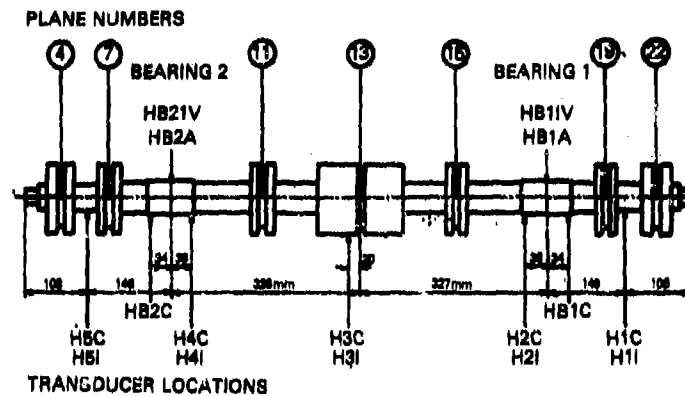
Fig. 7.34. Transducer locations and rotor planes
used in tests by Tonnesen [24]
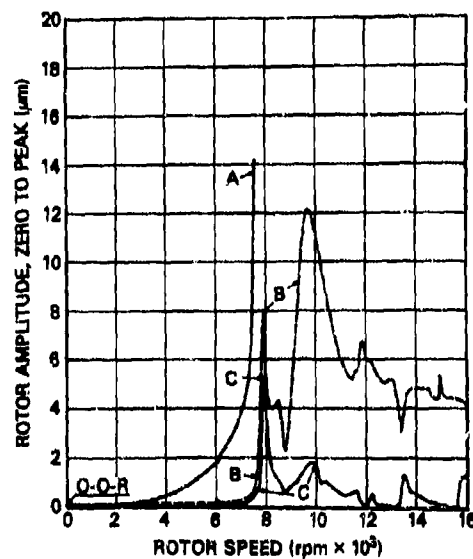
Fig. 7.35. Rotor amplitudes at bearing 2 after
balancing in six planes, using two transducers
and influence coefficients from initial balancing
[24]. A = unbalanced rotor, B = result of
first balancing, C = result of second balancing.
Recording probe: H4C.

Fig. 7.36. Rotor amplitudes at midspan after balancing in six planes with two transducers [24]. A = unbalanced rotor, B = result of first balancing, C = result of second balancing. Recording probe: H3C.
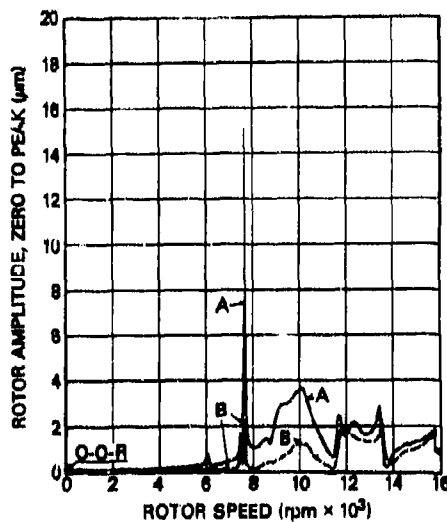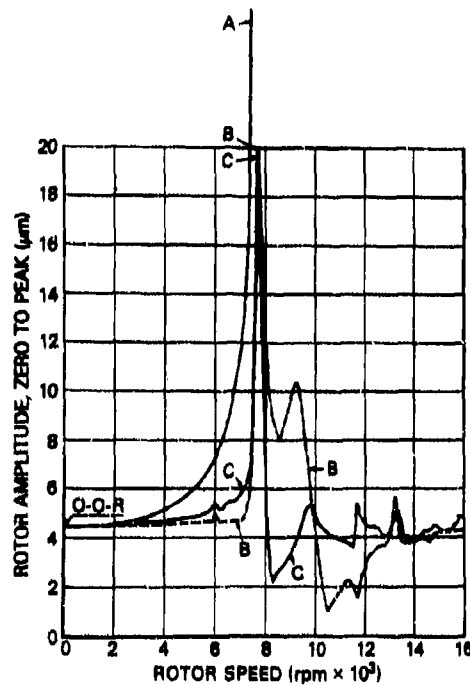
Fig. 7.37. Rotor amplitudes at bearing 2 after balancing in seven planes with four transducers [24]. A = unbalanced rotor, B = result of first balancing, C = result of second balancing. Recording probe: H4C.
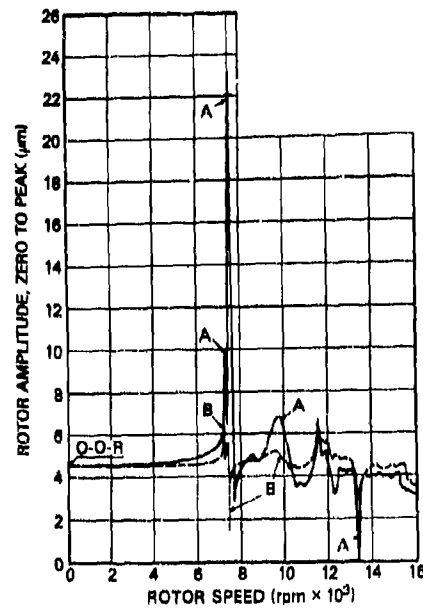
Fig. 7.38. Rotor amplitudes at midspan after balancing in seven planes with four transducers [24]. A = unbalanced rotor, B = result of first balancing, C = result of second balancing. Recording probe: H3C.

the balance achieved that the rotor could be held at the very peak of the first critical speed with minimal vibration. This condition was held for more than 1 hr without any change in amplitude.

The tests conducted by Tonnesen indicate that the influence coefficient method is perfectly capable of balancing a rotor through three flexible critical speeds with two to five transducers in up to five correction planes. The method was further found to be linear over wide ranges (as required by the theory), and the overall accuracy in determining the balance weights is 4.5 percent, for a measurement accuracy of 1.5 percent. The quality of the balance achieved is rated as ISO quality class 0.4 in terms of rigid-rotor residual unbalance levels. It is concluded that the minimum amplitude is a function of (a) number of balance planes and their axial location, (b) the operating-speed range, and (c) the number of measurement transducers and their axial positions. Tonnesen [24] states that balancing with a single transducer on or near a bearing is adequate for many applications, but, for ultraprecision balancing, transducers placed outside the immediate area of the bearings are mandatory.

7.7 Comparison of Flexible-Rotor Balancing Methods:
Kendig Computer Study

A comprehensive study of the principal flexible-rotor balancing methods in use has been made by Kendig [25]. This study was based on extensive computer calculations for two different rotor-bearing systems: a medium-size steam-turbine rotor in undamped fluid-film bearings with planar and spatial unbalance distributions, the same rotor in damped bearings, and a small high-speed gas-turbine rotor. Computer programs were developed for each of the following balancing methods: (a) the modal balancing method (Bishop), (b) the modal averaging method (Moore), (c) the simultaneous modal method (Kellenberger), (d) the comprehensive modal method (Federn), and (e) the exact-point-speed influence coefficient method. A variety of balance-plane combinations was tried. Details of the results obtained are discussed below.

Steam-Turbine Rotor in Flexible Undamped Bearings:
Planar Unbalance

The rotor system model used in this study (Fig. 7.39) was based on a medium-size steam-turbine unit operating in the speed range 0 through 12,000 rpm. The rotor weighs approximately 5000 lbf and operates in two tilting-pad journal bearings, 6 in. in diameter and 3 in. long, located close to the rotor ends. The dynamic stiffness properties of the tilting-pad bearings were obtained from tables given in Lund [26]. Bearing damping was neglected for this first comparison calculation, and no other system damping was included.

The rotor unbalance was taken as a planar set of mass distributions. In the absence of damping, the selected unbalance arrangement can be expected to excite the rotor translatory whirl mode, the conical mode, and the lowest flexural mode. Furthermore, in the absence of damping and with in-plane, in-phase unbalance, the mode shapes can be expected to appear as plane forms.
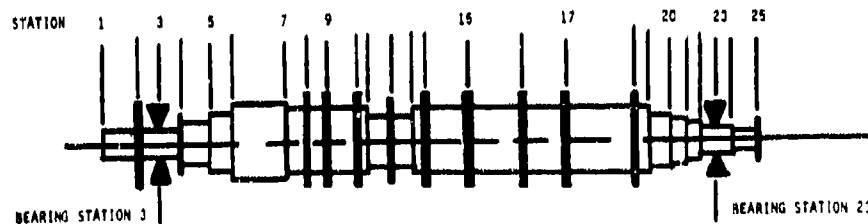
Fig. 7.39. Steam-turbine rotor model used by Kendig [25]
(©1975, J.R. Kendig; used by permission)

The selected planar distribution of weights was such that the first three flexural modes of vibration could be excited. The unbalance was taken to be a set of three masses of 5, 5, and 2.5 oz-in. at angular locations of 0°, 180°, and 0°, respectively, at rotor stations 8, 16, and 22 (see Fig. 7.40). The uncorrected rotor unbalance response, shown in Fig. 7.41, indicates the existence of three critical speeds, at 2300, 5500, and 10,000 rpm. The character of these criticals can be seen from the rotor deflection plots of Fig. 7.42. It is obvious that the prime factors in effect at these speeds are the first, second, and third flexural modes, respectively, with no apparent rigid-body effects.

Some general remarks about the balancing procedures are in order. No assumption of knowledge of the residual unbalance was made. The method of balancing-plane selection was to choose, for a given mode, the plane or planes that would have the greatest effect on that mode while minimizing effects on the other modes. The plane selection was based on the deflection shapes resulting from the unbalance response of the actual rotor. Similarly, all balancing operations were based on actual rotor deflection shapes at the critical speeds rather than on any characteristic deflection shapes derived from a solution of the eigenvalue problem. It was therefore assumed that the deflection at the critical speed corresponded to the characteristic mode at that speed.

During the actual modal balancing procedure, it was found that the balancing of a given mode affected the balance level achieved in the lower modes. The related weight distribution was applied to trim the lower modes, but this approach was found to produce results that adversely affected the balance levels in other modes. The method of correcting lower modes was thereafter combined with the usual weight-distribution calculations; thus, when a set of trial weights was determined for a given mode, sets of trial trim weights were also produced for any lower modes. In this way all lower modes could be trimmed without upsetting the higher modes, with very effective results.

In applying the N modal method of Bishop and Gladwell [27], the theoretical approach was used: a single mass was used to correct the first mode, two were used for the second, and so on. Although in actual use with industrial rotors this scheme might be altered to introduce multimass distributions in each mode to reduce the size of the required correction masses, no description of such a scheme appears to have been described in the subject literature. Similarly, in applying the N and $N + B$ methods of Kellenberger [5], discrete masses were used, based the procedure on theoretical formulations found in the literature.

The N modal method of Bishop and Gladwell gave the amplitude-vs-speed curve of Fig. 7.43 when the first mode was removed. Removal of the second and third modes resulted in the amplitude-vs-speed
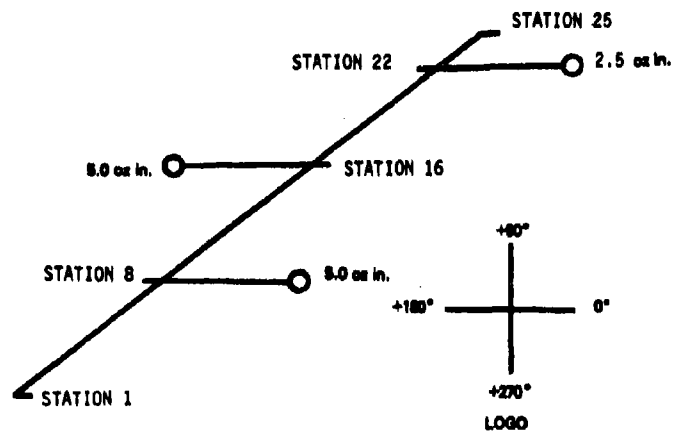
Fig. 7.40. Planar unbalance weight distribution in the steam-turbine rotor model used by Kendig [25] (©1975, J.R. Kendig; used by permission)
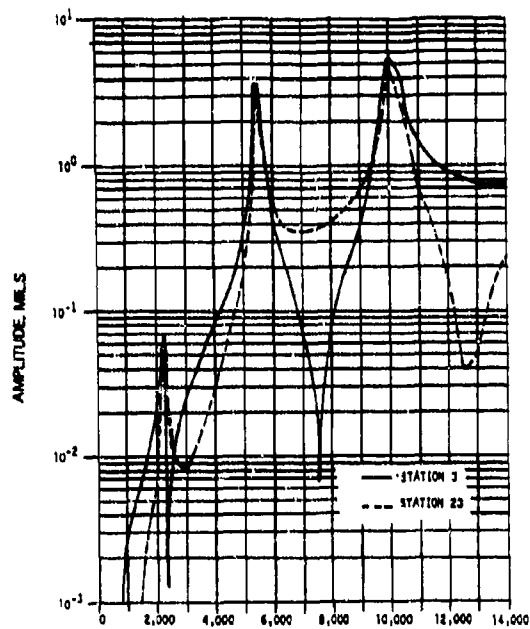
Fig. 7.41. Original unbalance response: Kendig's steam-turbine rotor in flexible undamped bearings [25] (©1975, J.R. Kendig; used by permission)

STATION 25

(a) 2300 rpm

STATION 1

STATION 25

(b) 5500 rpm

STATION 1

STATION 25

(c) 10,000 rpm

STATION 1
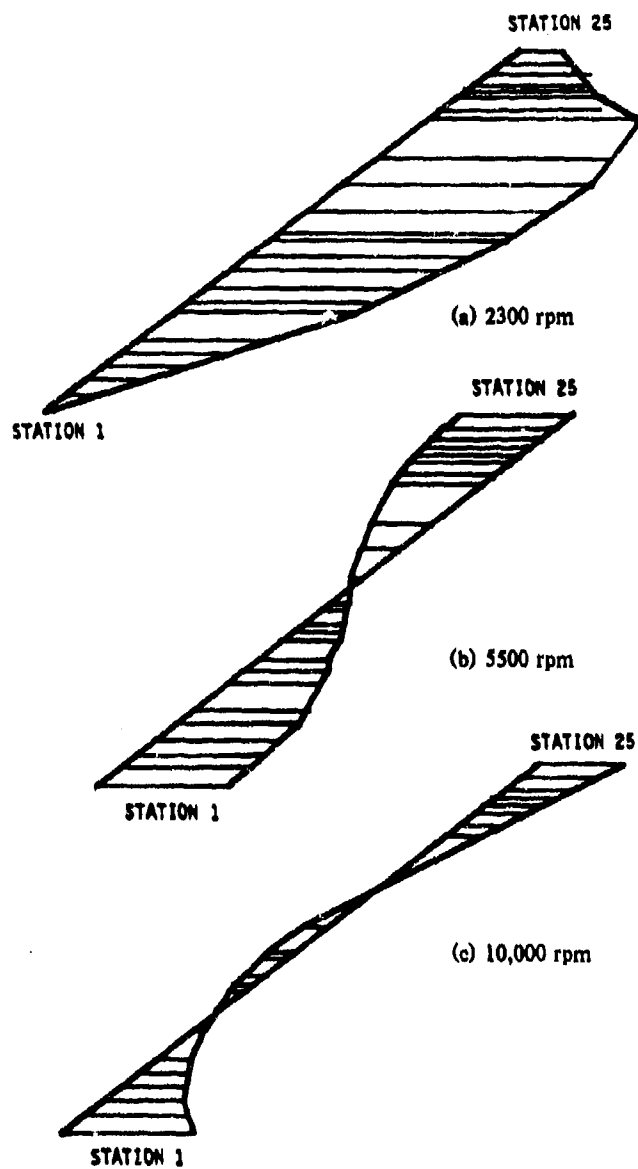
Fig. 7.42. Rotor mode shapes at the three critical speeds of 2300, 5500, and 10,000 rpm. Planar unbalance [25]. (©1975, J.R. Kendig; used by permission).

Fig. 7.43. Rotor amplitudes obtained with the N modal method: first mode removed [25] (©1975, J.R. Kendig; used by permission)
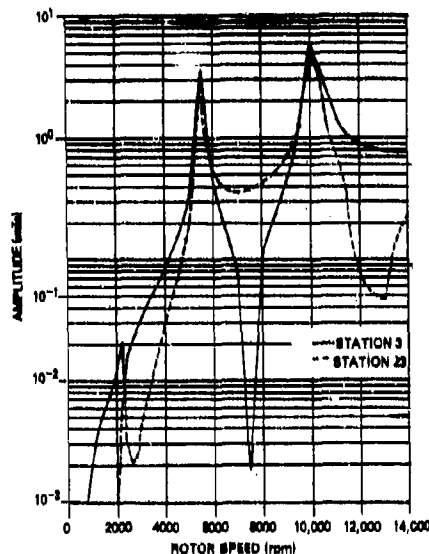
curves of Figs. 7.44 and 7.45, respectively. Final balancing resulted in the amplitude-vs-speed plots of Fig. 7.46. These diagrams provide insight into the stepwise modal method.

Application of the simultaneous N modal method of Kellenberger necessitated, by definition, the use of three balance planes. The three balancing distributions, one for each mode, resulted in the final balance demonstrated in Fig. 7.47.

The influence coefficient method was also applied to correct the original unbalance in the first three modes. The procedure used required three balancing speeds and five correction planes, i.e., an (N + 2) correction. The resulting balance obtained is shown in Fig. 7.48.

Steam-Turbine Rotor in Flexible Undamped Bearings: Spatial Unbalance

A second series of computer calculations was performed by Kendig [25], as in the preceding series, for a steam-turbine rotor in flexible undamped bearings (see Fig. 7.39), but a spatial unbalance weight distribution was used. It consisted of 5.0-oz-in. weights at stations 17, 18, and 19 at angular orientations of 0°, 90°, and 180° (Fig. 7.49). The weight distribution was selected for its ability to stimulate all three flexural vibration modes as well as to introduce a substantial asymmetrical rotor response. The original unbalance response of this rotor system, shown in Fig. 7.50, indicates that the critical speeds are still to be
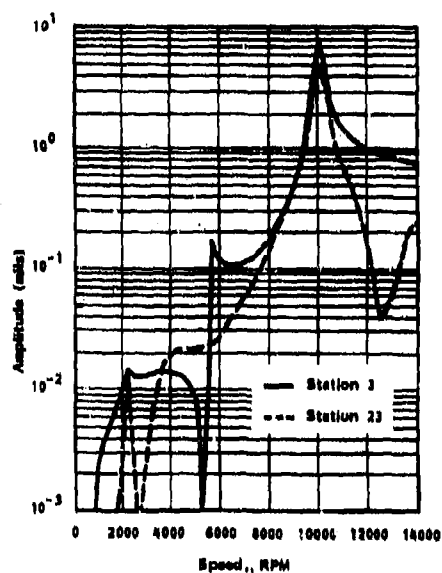
Fig. 7.44. Rotor amplitudes obtained with the N modal method: second mode removed [25] ([c]1975, J.R. Kendig; used by permission)

Fig. 7.45. Rotor amplitudes obtained with the N modal method: third mode removed [25] ([c]1975, J.R. Kendig; used by permission)

Fig. 7.46. Rotor amplitudes obtained after the final balance by the N modal method [25] ([c]1975, J.R. Kendig; used by permission)
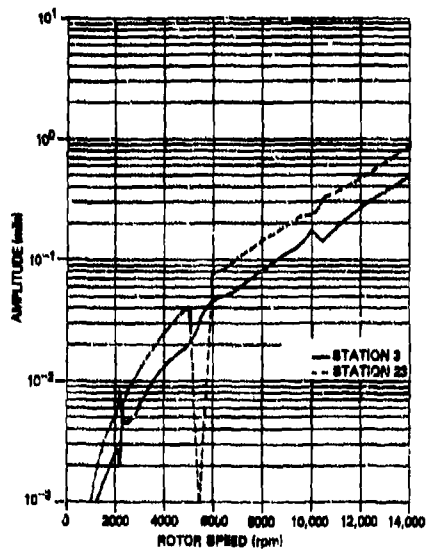
Fig. 7.47. Rotor amplitudes obtained after balancing by the Kellenburger simultaneous N modal method [25] ([c]1975, J.R. Kendig; used by permission)
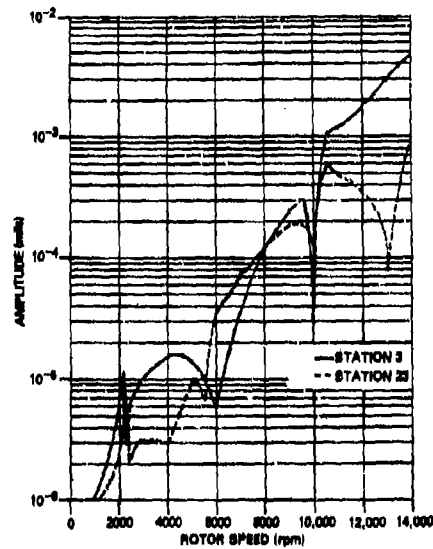
Fig. 7.48. Rotor amplitudes obtained
after balancing in five correction planes by
the influence coefficient method [25]
(©1975, J.R. Kendig; used by permission)
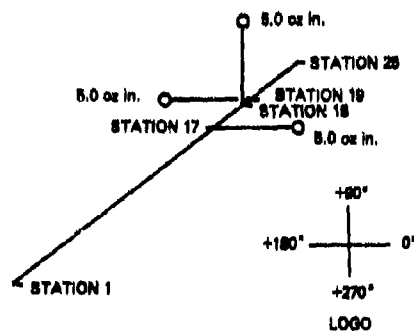
Fig. 7.49. Spatial unbalance distribution
in the steam-turbine rotor model [25]
(©1975, J.R. Kendig; used by permission)
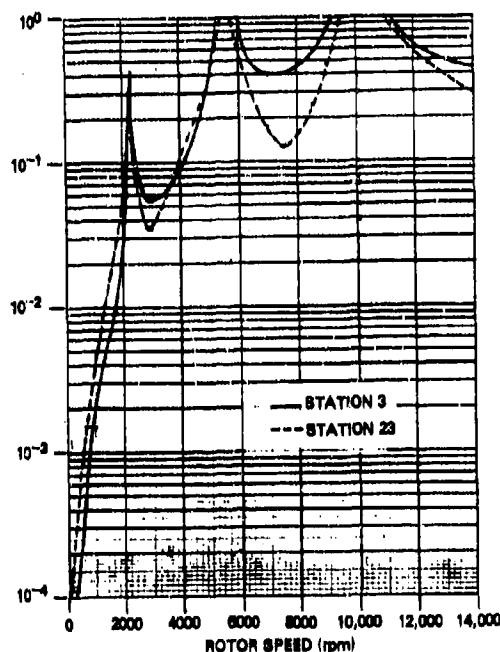
Fig. 7.50. Original unbalance response of steam-turbine rotor model with a spatial unbalance distribution [25] (©1975, J.R. Kendig; used by permission)

found at 2300, 5500, and 10,000 rpm. The corresponding deflection shapes (Fig. 7.51) show that no apparent rigid-body effects were experienced by the system, and so the rotor is functioning as a flexible system.

In applying the N modal method of Bishop and Gladwell [27], the procedure was the same as that used in the preceding example. A reduction of two orders of magnitude in the rotor unbalance condition was realized by this method. The critical speed peak amplitudes shown in Fig. 7.50 were all successfully suppressed. This demonstrates the effectiveness of the N modal balancing method in the absence of damping, for the case of a complex spatial distribution of rotor unbalance.

Use of the simultaneous N modal method of Kellenberger resulted in the amplitude-vs-speed plot of Fig. 7.52. Although an acceptable balance level was attained, it was impossible to reduce both bearing vibrations to levels below those attained in Fig. 7.52 (see Fig. 7.53). In an effort to reduce these vibration levels, two additional weight distributions were added; the results are shown in the amplitude-vs-speed
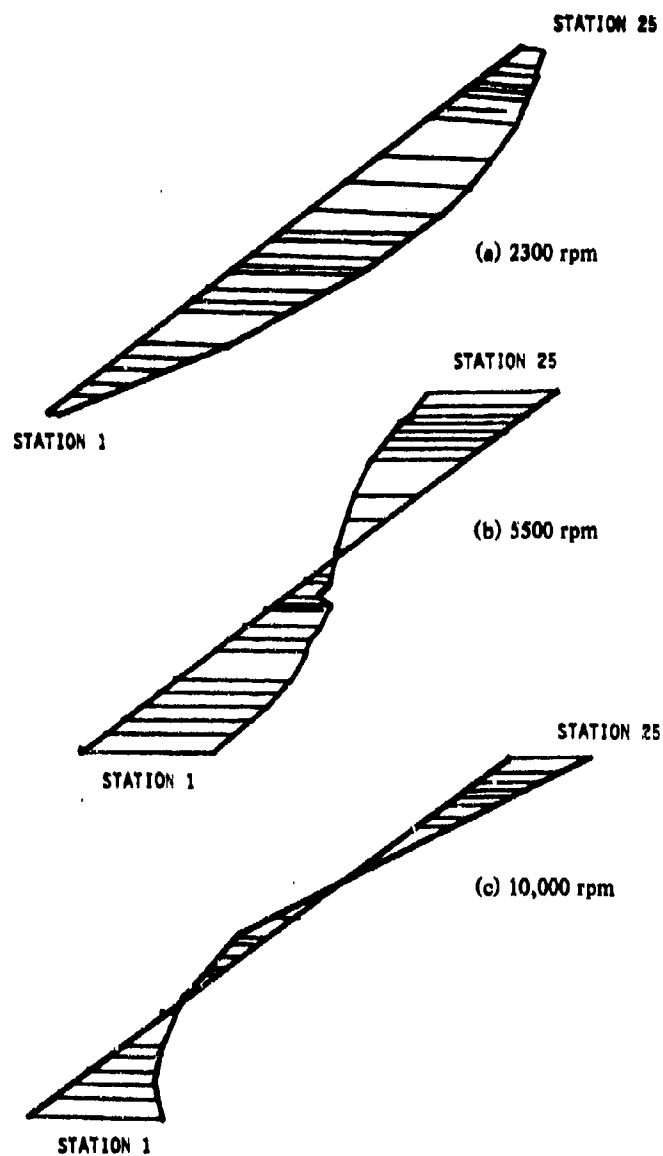
Fig. 7.51. Rotor mode shapes at the three critical speeds of 2300, 5500, and 10,000 rpm. Spatial unbalance [25] (©1975, J.R. Kendig; used by permission).
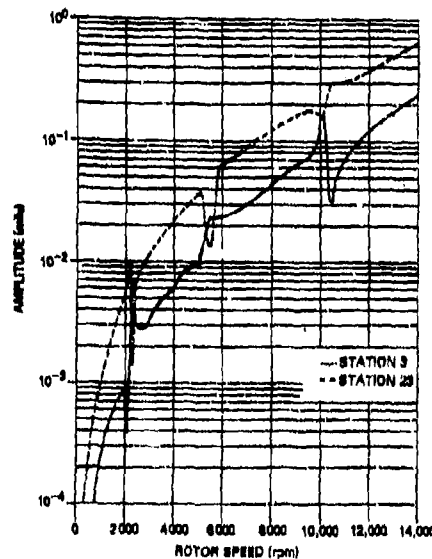
Fig. 7.52. Rotor amplitudes obtained after balancing by the simultaneous N modal method [25] (©1975, J.R. Kendig; used by permission)
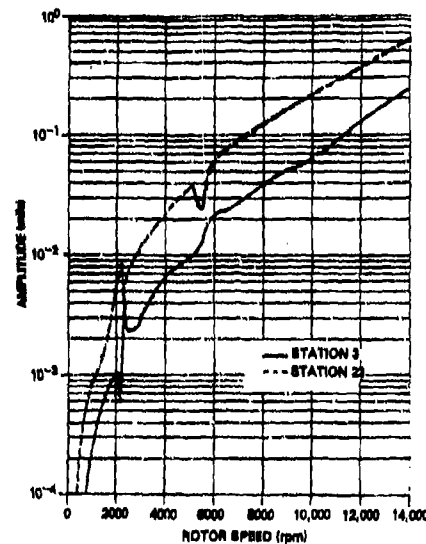
Fig. 7.53. Rotor amplitudes obtained after balancing by the simultaneous N modal method and applying a new N balance distribution [25] (©1975, J.R. Kendig; used by permission)

plot of Fig. 7.54. In this particular instance, it was decided to add two additional balance planes to the existing three-plane distributions; the objective was to provide two extra planes for two-plane trimming operations. The resulting five-plane weight distributions yielded the results shown in Fig. 7.55.

The two-plane trimming operations were conducted to investigate the possibilities of trimming the rotor response to more acceptable levels. Two of these operations were conducted: one at low speed (Fig. 7.55) and the other at 10,000 rpm (Fig. 7.56). Both trimming operations improved the rotor response only slightly throughout the operating-speed range.

Another application of the simultaneous N modal method was made after the rotor had been balanced at low speed in two planes. The weight distributions were then based on this rigid-body balanced rotor. Application of the simultaneous N modal procedure gave acceptable balance levels, as shown in Fig. 7.56.

The balance level of the rotor, though improvable by a two-plane balance, was of sufficiently low unbalance that it was considered to be previously balanced at low speeds. With this assumption, an attempt
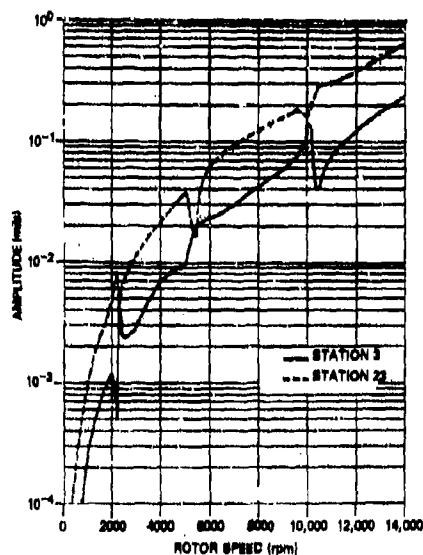
Fig. 7.54. Rotor amplitudes obtained after balancing by the simultaneous N modal method and applying a new $N + 2$ balance distribution [25] (©1975, J.R. Kendig; used by permission)
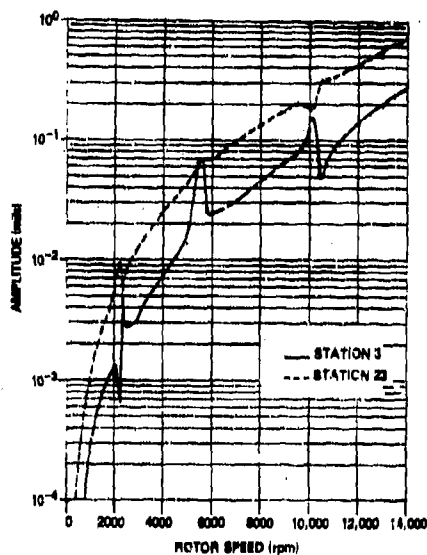
Fig. 7.55. Rotor amplitudes obtained after balancing by the simultaneous N modal method, adding two more balance planes, and two-plane trimming at low speed [25] (©1975, J.R. Kendig; used by permission)

Fig. 7.56. Rotor amplitudes obtained after balancing by the simultaneous N modal method, adding two more balance planes, and two-plane trimming at 10,000 rpm [25] (©1975, J.R. Kendig; used by permission)
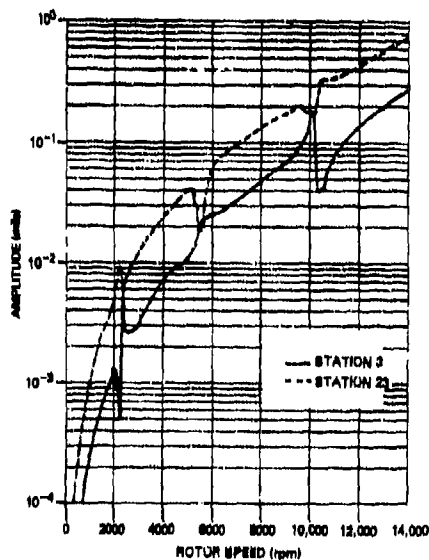
was made to balance the rotor by the simultaneous $N + B$ modal method. This required, by definition ($N = 3$, $B = 2$), five balance planes. Two distinct sets of five balance planes were used, one set using two of the planes to coincide with the bearings, and the other with the additional two planes distributed throughout the length of the rotor. Both $N + B$ modal approaches balanced the rotor, but did not result in a significant improvement over the previous procedures.

Influence coefficient balancing was performed using both sets of the five-plane combinations applied in the simultaneous $N + B$ test. The results are shown in Figs. 7.57 and 7.58. In both cases the influence coefficient method gave lower amplitudes than were achieved by any of the previous methods.

Steam-Turbine Rotor in Damped Flexible Bearings: Planar Unbalance

The rotor and unbalance distribution are the same as for the undamped rotor with planar unbalance (see Fig. 7.41), the only difference being the introduction of bearing damping to account for the viscous effects of the fluid-film bearings. The bearing damping coefficients were calculated, as were the bearing stiffness coefficients, from data presented in Ref. 28. In the first calculations each rotor residual unbalance was increased by two orders of magnitude, from 5 to 500 oz. in., to offset the effect of damping, and to increase the rotor response amplitudes. The results of this unbalance distribution are the amplitude-vs-speed curves in Fig. 7.59.

The effect of damping in suppressing the critical speed peaks is readily apparent when Fig. 7.59 is compared with Fig. 7.41. Also, the rotor amplitudes in Fig. 7.59 are generally more than ten times greater, because of the increased unbalance. Introduction of damping into the bearings also results in the rotor deflections becoming "twisted" in space, no longer exhibiting the planar response of the undamped system, shown in Fig. 7.60. The rotor deflection shapes are now those of Fig. 7.61. The effects observed are in agreement with results obtained by Last [29], who found that bearing damping produced rotor deflections that are helical. The deflection shapes shown in Figs. 7.60 and 7.61 also substantiate the statements of Meirovitch [30], cited previously, concerning the effects of nonnegligible system damping.

Another way of presenting the information of Fig. 7.61 is to show the rotor response as an Argand diagram, or a polar plot, as shown in Fig. 7.64. This diagram and the Kennedy-Pancu method for rotor dynamic analysis is described by Bishop and Parkinson [1].

Fig. 7.57. Rotor amplitudes obtained after three-speed balancing by the influence coefficient method in five planes: (stations 1, 9, 14, 17, and 25 in Fig. 7.39) [25] (©1975, J.R. Kendig; used by permission)
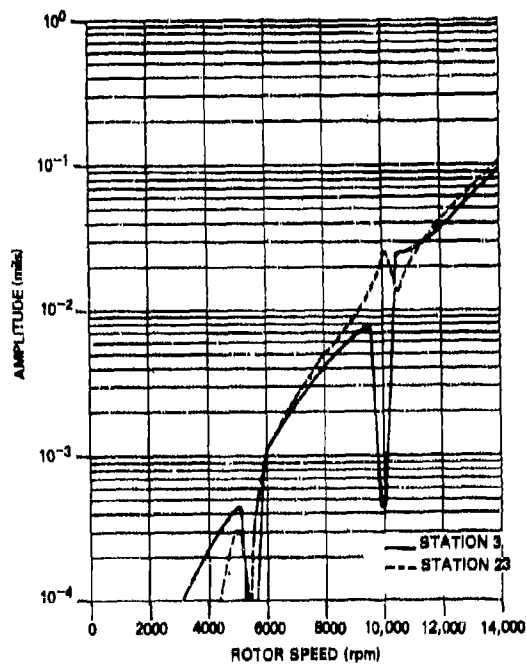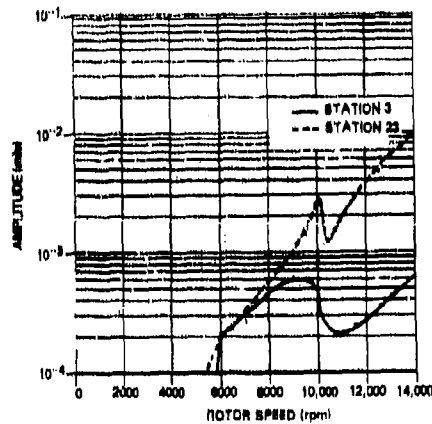
Fig. 7.58. Rotor amplitudes obtained after three-speed balancing by the influence coefficient method in five planes (stations 1, 3, 14, 23, and 25 in Fig. 7.39) [25] (©1975, J.R. Kendig; used by permission)
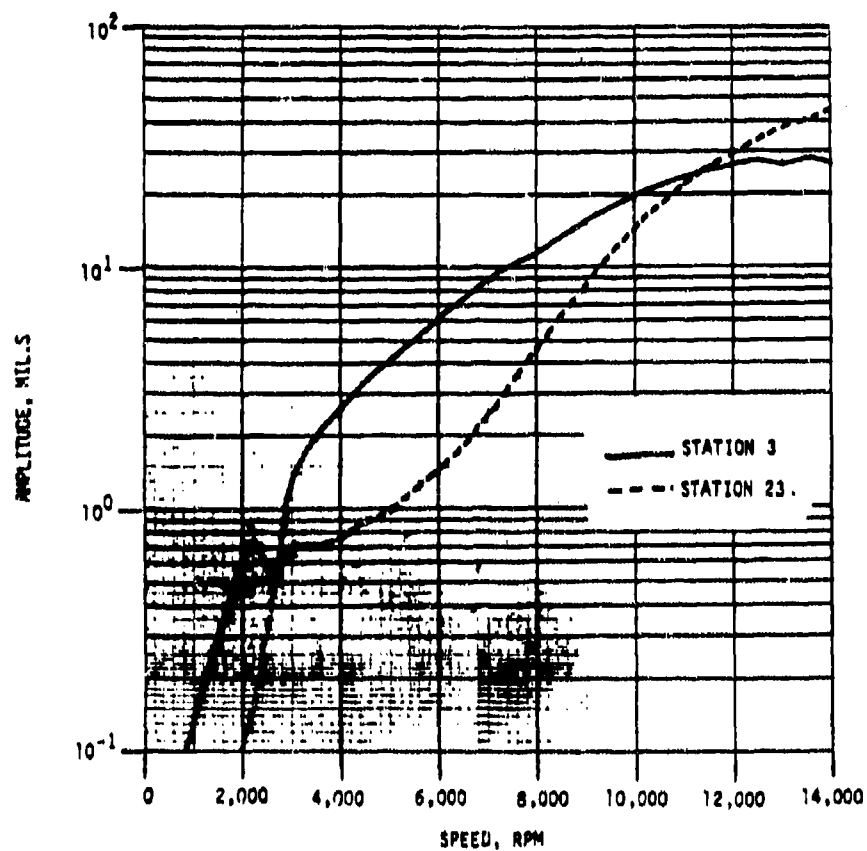
Fig. 7.59. Original unbalance response: steam-turbine rotor in damped flexible bearings, planar unbalance [25] (©1975, J.R. Kendig; used by permission.)
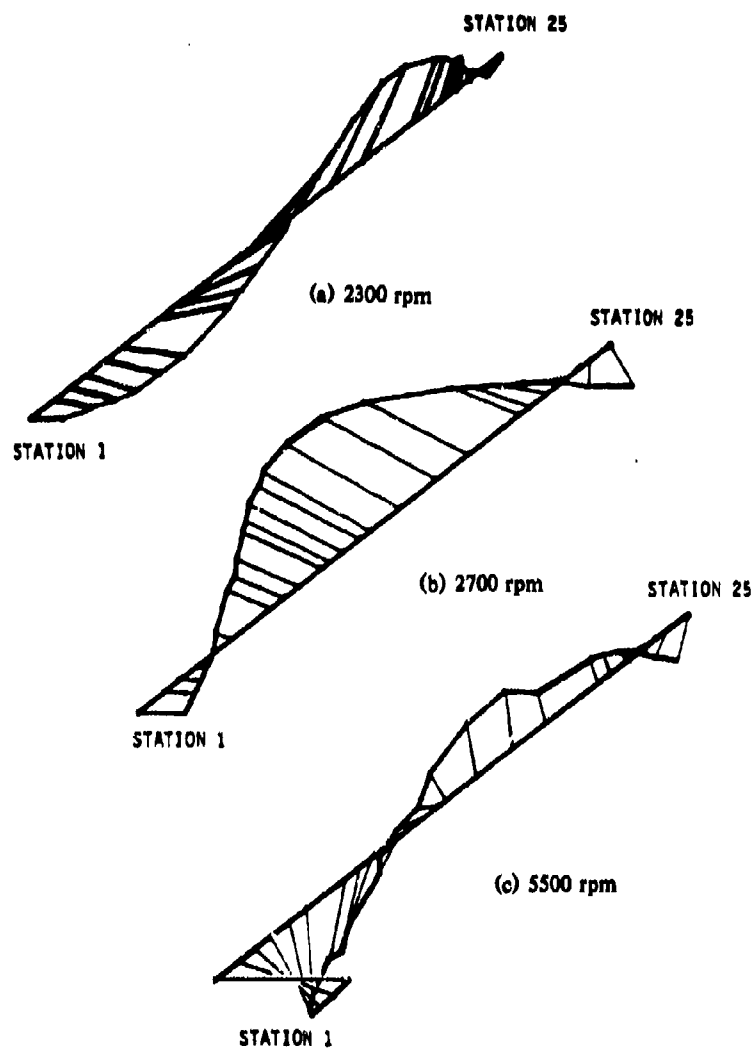
Fig. 7.60. Rotor deflections at 2300, 2700, and 5500 rpm. Planar
unbalance [25] (©1975, J.R. Kendig; used by permission).
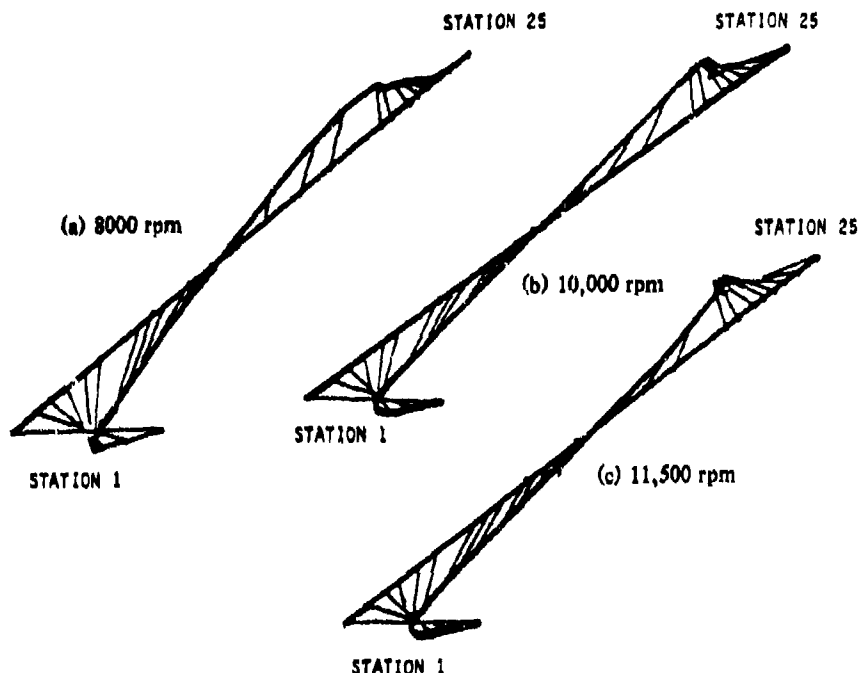
Fig. 7.61. Rotor deflections at 8000, 10,000, and 11,500 rpm. Planar unbalance [25] (©1975, J.R Kendig; used by permission).

From the amplitude-vs-speed diagram of Fig. 7.59, it can be deduced that critical speeds occur at 2300, 2700, and approximately 11,500 rpm. The deflection shape at 11,500 rpm (Fig. 7.61c) shows that this speed corresponds to a deflection primarily in the second mode. Therefore, it can be concluded that the first and the second modes are only two characteristics of importance in this case. It follows that these modes are the only ones for which balancing is necessary in this instance.

On the basis of these assumptions, the N modal method of Bishop and Gladwell was applied, with the results shown in Fig. 7.62. Likewise the simultaneous N modal method of Kellenberger was used, yielding the amplitude-vs-speed diagram of Fig. 7.63. It was noticed in applying these procedures that the methods both converged more slowly to an acceptable balance level, and at the expense of worsening the first-mode balance. Both procedures were halted at the balance levels demonstrated by Figs. 7.62 and 7.63, the results of which are moderately successful.

Fig. 7.62. Rotor amplitudes obtained after balancing by the N modal method [25] (©1975, J.R. Kendig; used by permission)
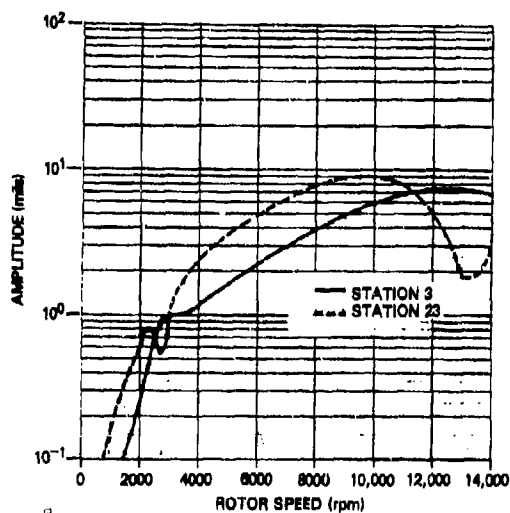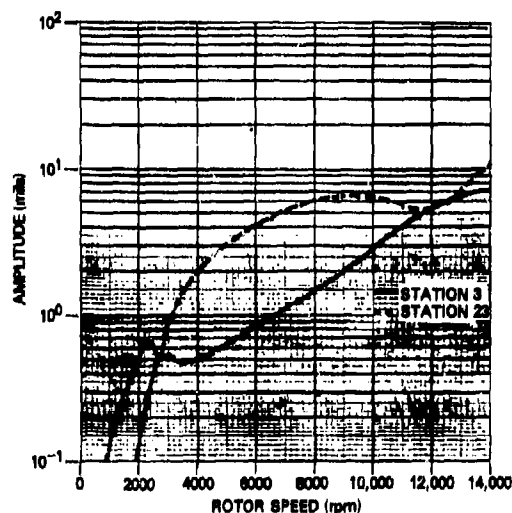
Fig. 7.63. Rotor amplitudes obtained after balancing by the simultaneous N modal method [25] (©1975, J.R. Kendig; used by permission)

The polar diagrams of Fig. 7.64, interpreted in the manner of Bishop and Parkinson [31], indicate why the above methods failed to achieve a better balance: the maximum phase-angle changes occur at approximately the undamped critical speeds of 2300, 5500, and 10,000 rpm. With use of the undamped deflection shapes of these speeds to balance the rotor at the corresponding speed, the N modal method of

(a)
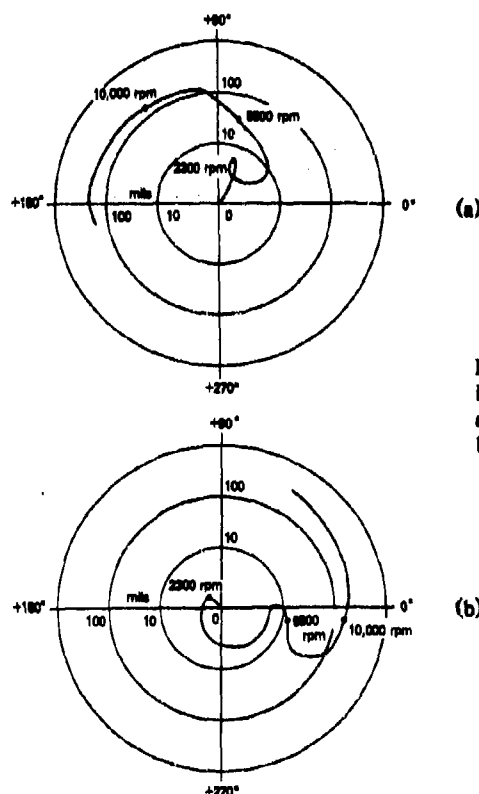
Fig. 7.64. Argand diagrams of the original response of bearings at stations 3 and 23 [25] (©1975, J.R. Kendig; used by permission)

(b)

Bishop and Gladwell was again applied. The results are shown in the amplitude-vs-speed diagram of Fig. 7.65.

Steam-Turbine Rotor in Damped Flexible Bearings: Spatial Unbalance

This series of balance comparisons was again based on a steam-turbine rotor in damped flexible bearings, but the unbalance distribution was spatial (see Fig. 7.49). The response of the unbalanced rotor (Fig. 7.66) indicated that critical speeds occurred at 2700 and 12,000 rpm. The corresponding deflection shapes are shown in Fig. 7.67. It is apparent from these deflection diagrams that the higher speed deflections are neither solely under the influence of the second mode nor solely under the influence of the third mode, but rather some combination of the two modes. The deflection shapes of the rotor are not, nor can they be approximated to be, planar in nature.

Fig. 7.65. Rotor amplitudes obtained after balancing by the *N* modal method at undamped critical speeds [25] (©1975, J.R. Kendig; used by permission)
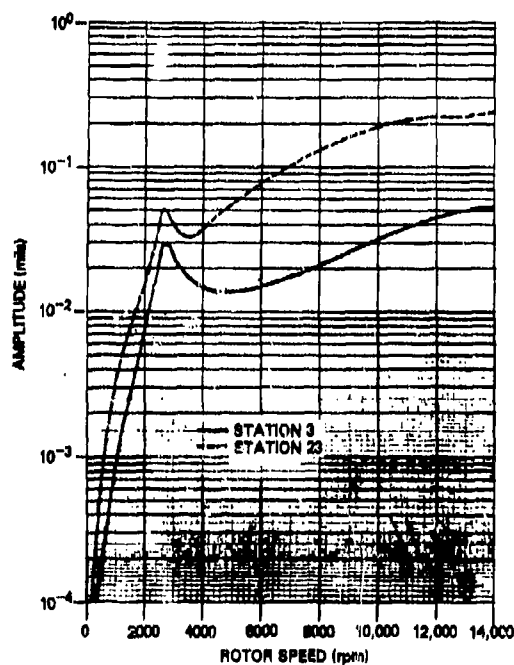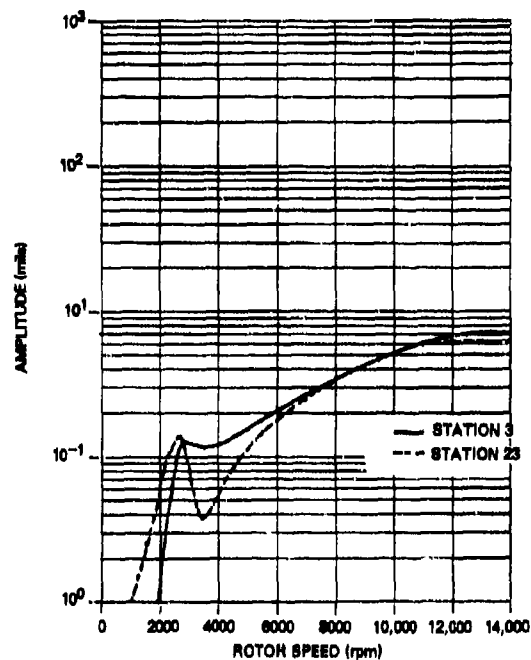
Fig. 7.66. Original unbalance response: steam-turbine rotor in damped flexible bearings, spatial unbalance [25] (©1975, J.R. Kendig; used by permission)
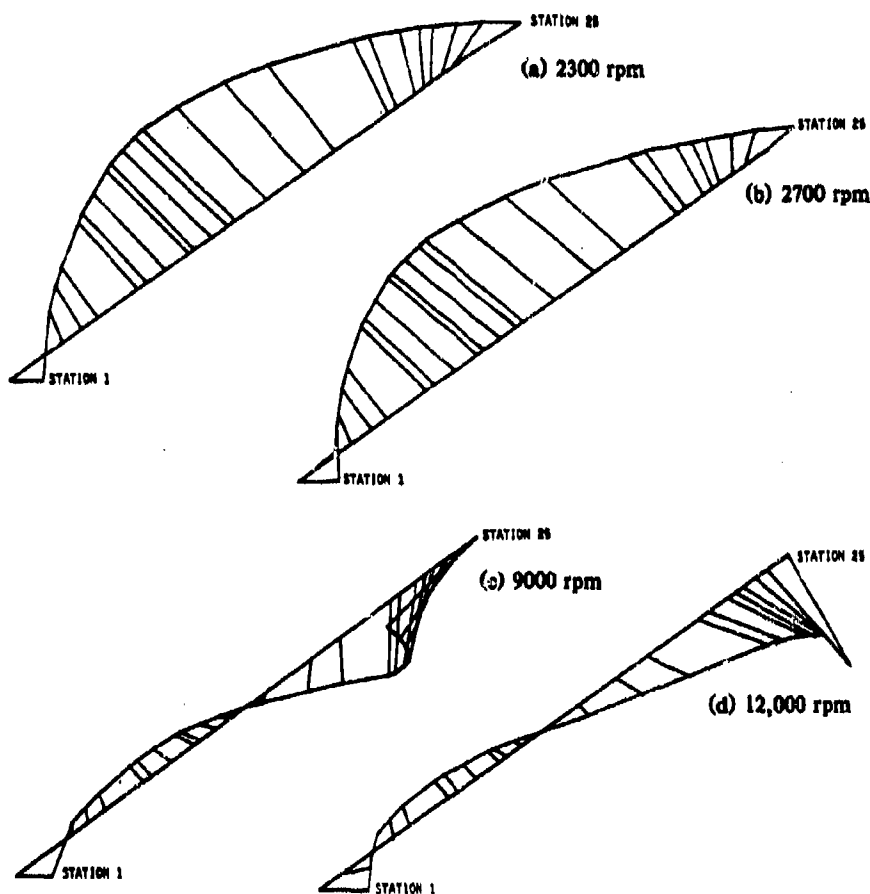
Fig. 7.67. Original rotor deflections at 2300, 2700, 9000, and
12,000 rpm [25] ([*]1975, J.R. Kendig; used by permission)

    Applying the N modal method and balancing in midplane for the
first critical speed at 2700 rpm yielded the amplitude-vs-speed curves of
Fig. 7.68. The deflection shape corresponding to this critical speed after
first-mode removal is illustrated in Fig. 7.69a; it shows the residual
unbalance starting to take the form of the second and/or third modes.
The use of end planes to remove the second mode at a speed of 12,000
rpm yielded the deflection shapes shown in Fig. 7.69b and c, in which a
third-mode deflection form is being assumed by the rotor. The N
method, applied at 270 0 and 12,000 rpm, did not achieve especially low
rotor response amplitudes. The use of a third balancing speed, 6500

rpm, was also tried to further assist in the removal of all three modes, but a modest additional improvement only was observed.

The application of the modal 'averaging' technique of Moore and Dodd is illustrated in Figs. 7.70 through 7.72, which show the results of four- and five-plane balancing at 2700 and 9000 rpm.

The results obtained with the influence coefficient technique are illustrated in Figs. 7.73 through 7.78, for a variety of speeds, planes, and numbers of planes. It can be seen that the most satisfactory results were obtained with a two-speed balance in four balancing planes (Fig. 7.78).
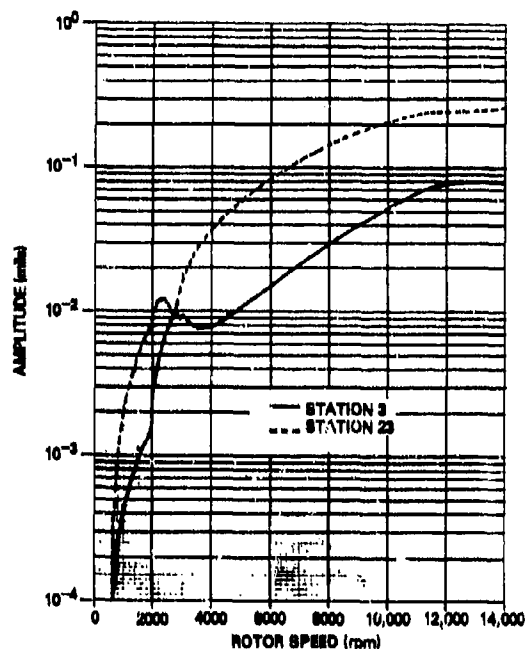
Fig. 7.68. Rotor amplitudes obtained after mid-plane balancing by the *N* modal method: first-mode removal at 2700 rpm using station 14 [25] (©1975, J.R. Kendig; used by permission)

(a) Deflection at 2700 rpm after first-mode removal

(b) Deflection at 2700 rpm after second-mode removal at 12,000 rpm using stations 1 and 25

(c) Deflection at 9000 rpm after second-mode removal at 12,000 rpm using stations 1 and 25
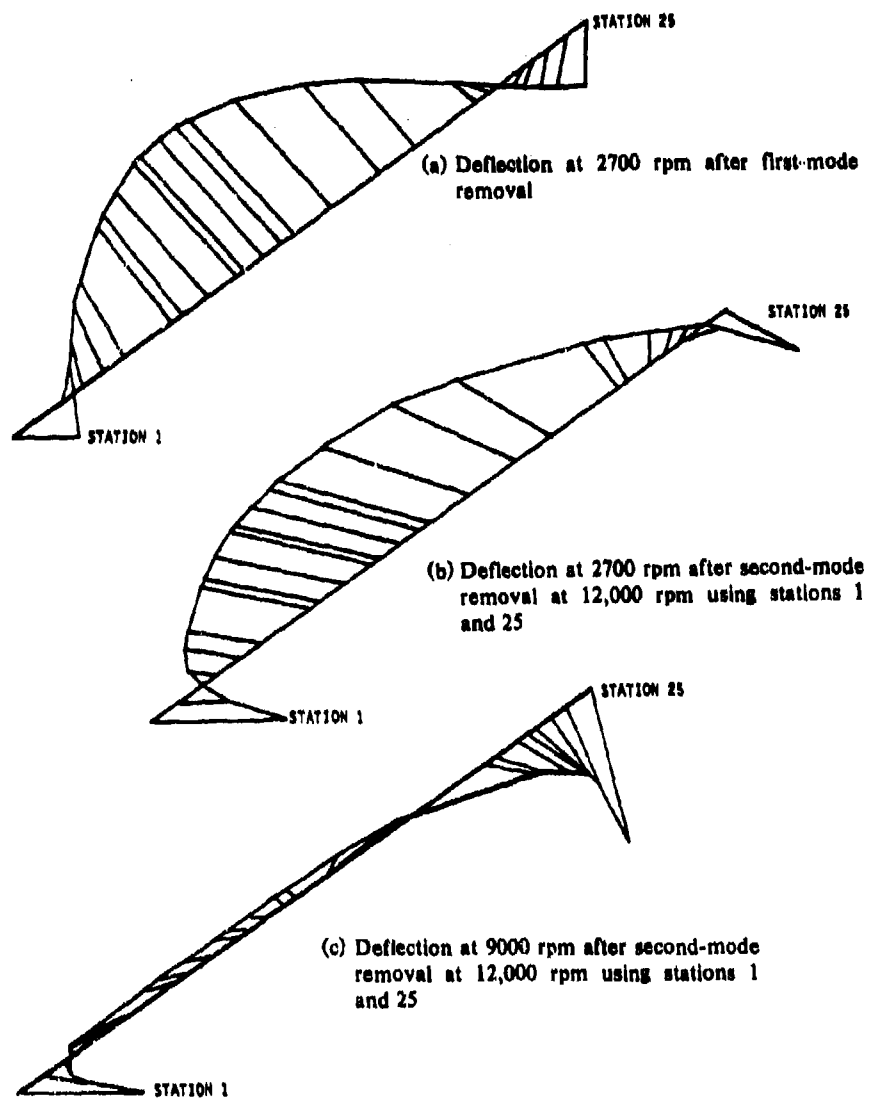
Fig. 7.69. Rotor deflections after first- and second-mode removal [25] (©1975, J.R. Kendig; used by permission)

Fig. 7.70. Rotor amplitudes obtained after balancing by the modal averaging method in four planes (stations 1, 7, 16, and 23) at 2700 rpm [25] (©1975, J.R. Kendig; used by permission)
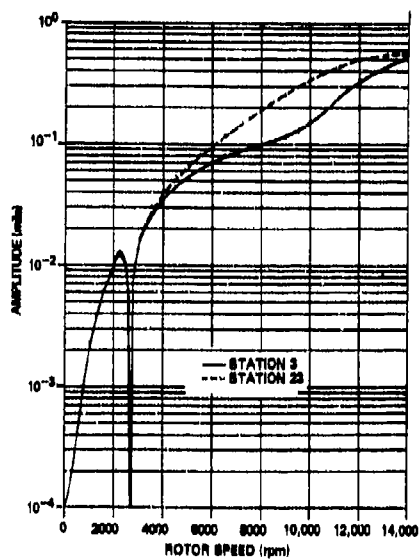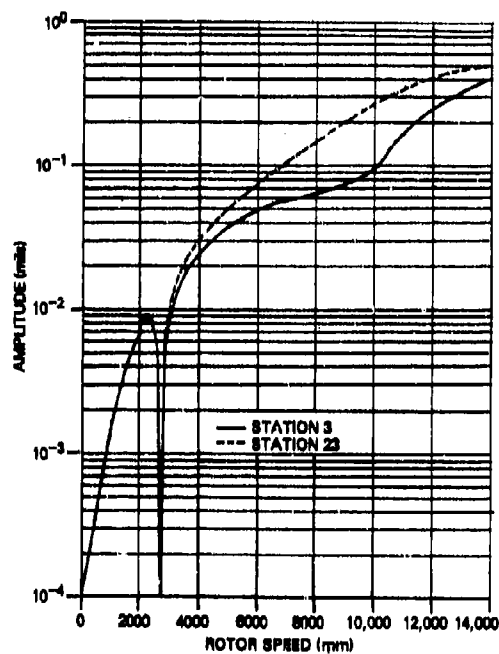
Fig. 7.71. Rotor amplitudes obtained after balancing by the model averaging method in five planes (stations 1, 7, 10, 16, and 23) at 2700 rpm [25] (©1975, J.R. Kendig; used by permission)
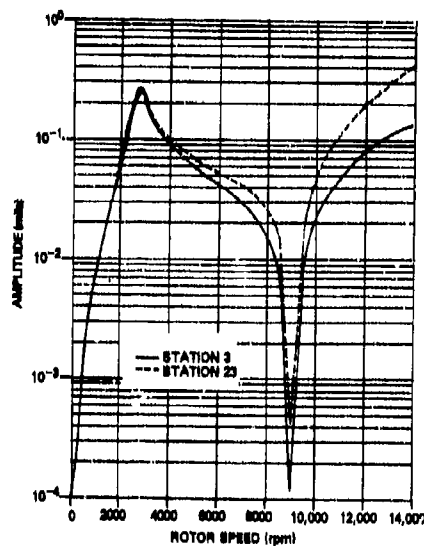
Fig. 7.72. Rotor amplitudes obtained after balancing by the modal averaging method in four planes (stations 1, 7, 16, and 23) at 9000 rpm [25] (©1975, J.R. Kendig; used by permission)
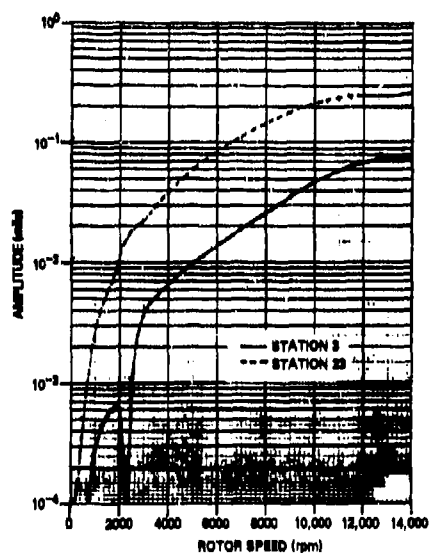
Fig. 7.73. Rotor amplitudes obtained after midplane balancing by the influence coefficient method: first-mode removal at 2300 rpm using station 14 [25] ([c]1975, J.R. Kendig; used by permission)

Fig. 7.74. Rotor amplitudes obtained after two-plane (stations 7 and 16) balancing by the influence coefficient method at 2700 rpm [25] ([c]1975, J.R. Kendig; used by permission)
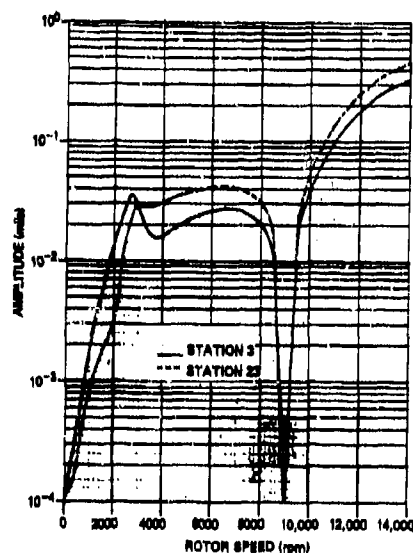
Fig. 7.75. Rotor amplitudes obtained after two-plane (stations 1 and 23) balancing by the influence coefficient method at 9000 rpm [25] (®1975, J.R. Kendig; used by permission)
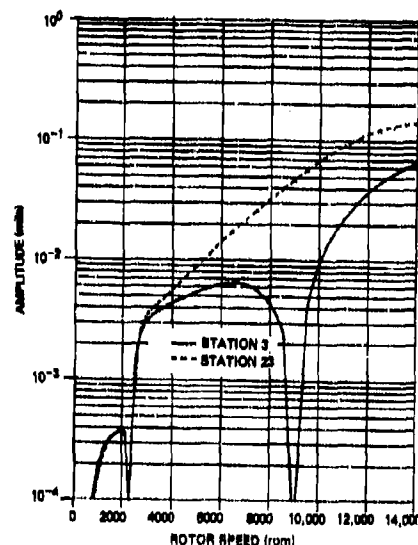
Fig. 7.76. Rotor amplitudes obtained after three-plane (stations 8, 14, and 21) balancing by the influence coefficient method at 2300 and 9000 rpm [25] (®1975, J.R. Kendig; used by permission)

Fig. 7.77. Rotor amplitudes obtained after three-plane (stations 8, 16, and 21) balancing by the influence coefficient method at 2300 and 9000 rpm [25] (®1975, J.R. Kendig; used by permission)
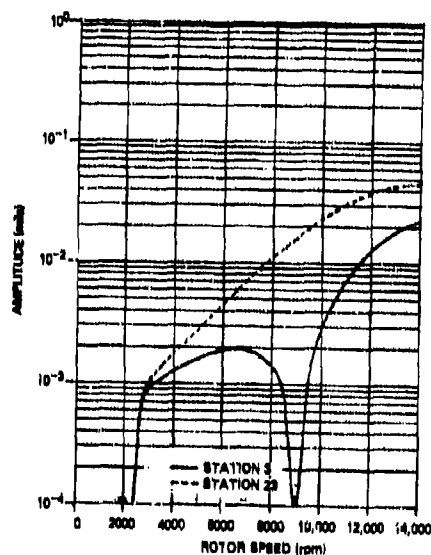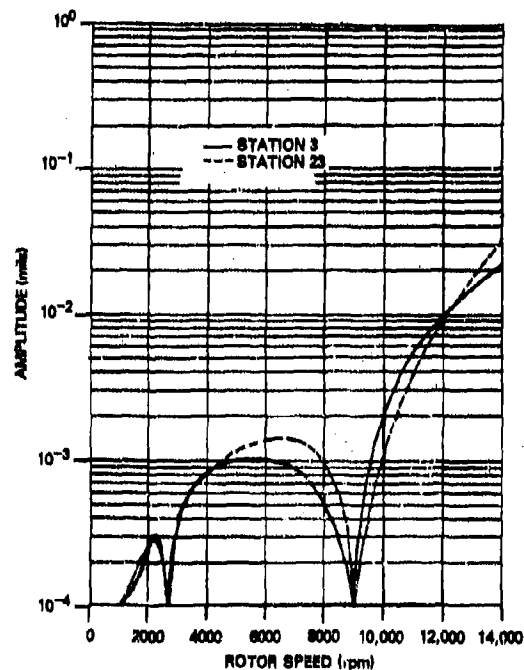
Fig. 7.78. Rotor amplitudes obtained after four-plane (stations 1, 7, 16, and 23) balancing by the influence coefficient method at 2700 and 9000 rpm [25] (©1975, J.R. Kendig; used by permission)

Gas-Turbine Rotor in Damped Flexible Bearings

Another series of computer calculations was performed by Kendig [25] using the small gas-turbine rotor shown in Fig. 7.79. The rotor is supported on two gas-lubricated tilting-pad bearings mounted, in turn, on flexible-bearing pedestals. The damping, though of a low level, is not negligible. The bearing stiffness and damping coefficients were obtained from the design data given by Rieger [33]. The pedestal stiffnesses were based on the design calculations of the rotor [32]. The rotor system was designed for a nominal operating speed of 66,000 rpm. It was assumed that unbalance forces of 1.0 oz-in. would act at each of the three rotor disks (stations 3, 9, and 19) and all unbalances would act in phase at zero degrees from the reference. The selection of this unbalance distribution was based on the fact that the rotor is a built-up unit, with the disks being shrunk onto the rotor shaft. Because of this mode of construction, the worst possible unbalance distribution would result from all unbalances operating in the same plane and direction.
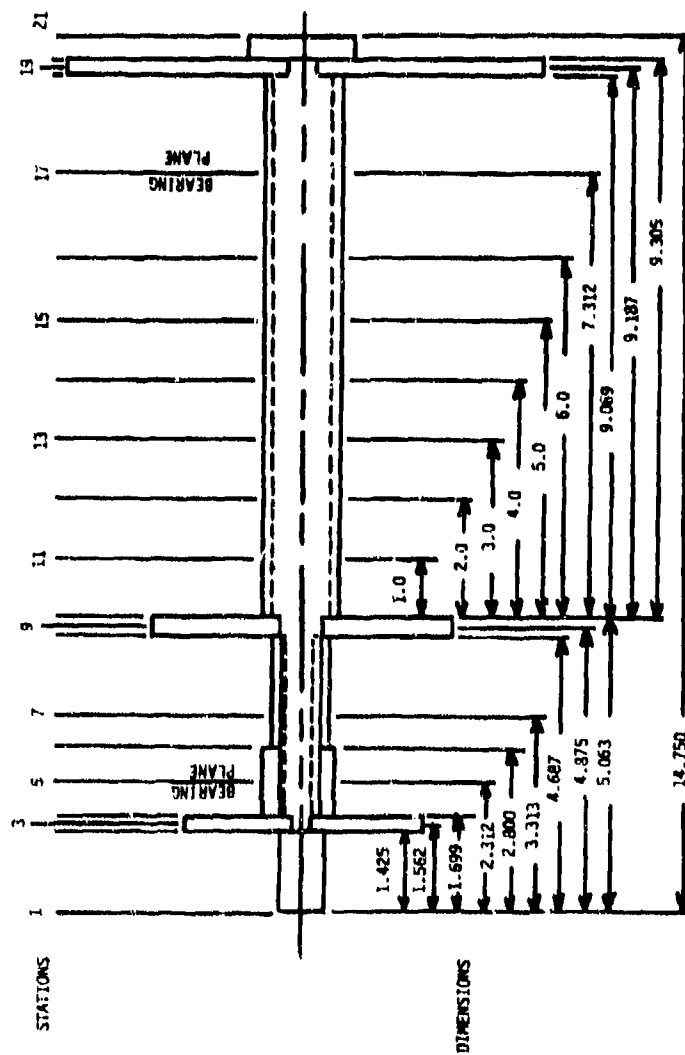
Fig. 7.79. Gas-turbine rotor model used by Kendig [25]

A critical speed calculation was made of this rotor system. This showed critical speeds occurring at 7052, 9593, and 24,946 rpm. The undamped rotor deflection shapes shown in Fig. 7.80 indicate that the first two speeds are rigid-body criticals and the third speed is the first flexural critical. Subsequent use of the unbalance distribution neglecting damping verified the critical speed results. Introducing the bearing damping into the rotor system altered the deflection shapes to those shown in Fig. 7.81. The basic mode shapes have been changed only slightly from the undamped mode shapes.

Plotting the amplitude of the damped rotor response as a function of speed gave the curves of Fig. 7.82, with critical speeds occurring at 7200, 10,400, and 25,450 rpm. The deflection shapes corresponding to these critical speeds are shown in Fig. 7.83. Comparison with the deflection shapes of Fig. 7.81 shows little difference between these two sets of deflection shapes.

(a) First critical speed at 7051.87 rpm

(b) Second critical speed at 9592.82 rpm

(c) Third critical speed at 24,946 rpm
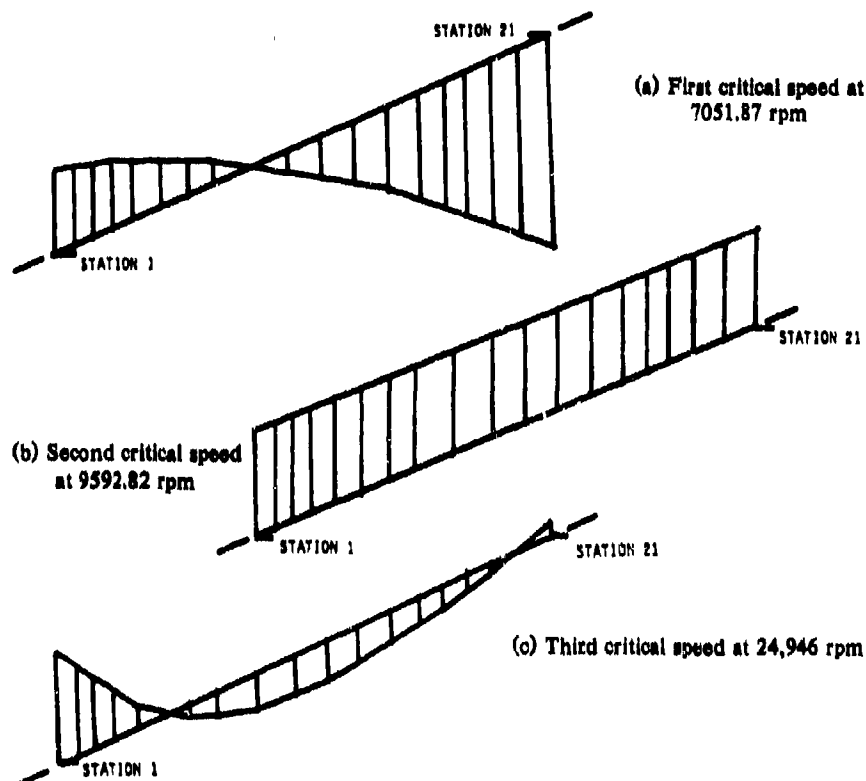
Fig. 7.80. Rotor deflections at the first, second, and third critical speeds (without damping) [25] (©1975, J.R. Kendig; used by permission)

(a) First critical speed at 7051.87 rpm

(b) Second critical speed at 9592.8 rpm

(c) Third critical speed at 24,946.6 rpm
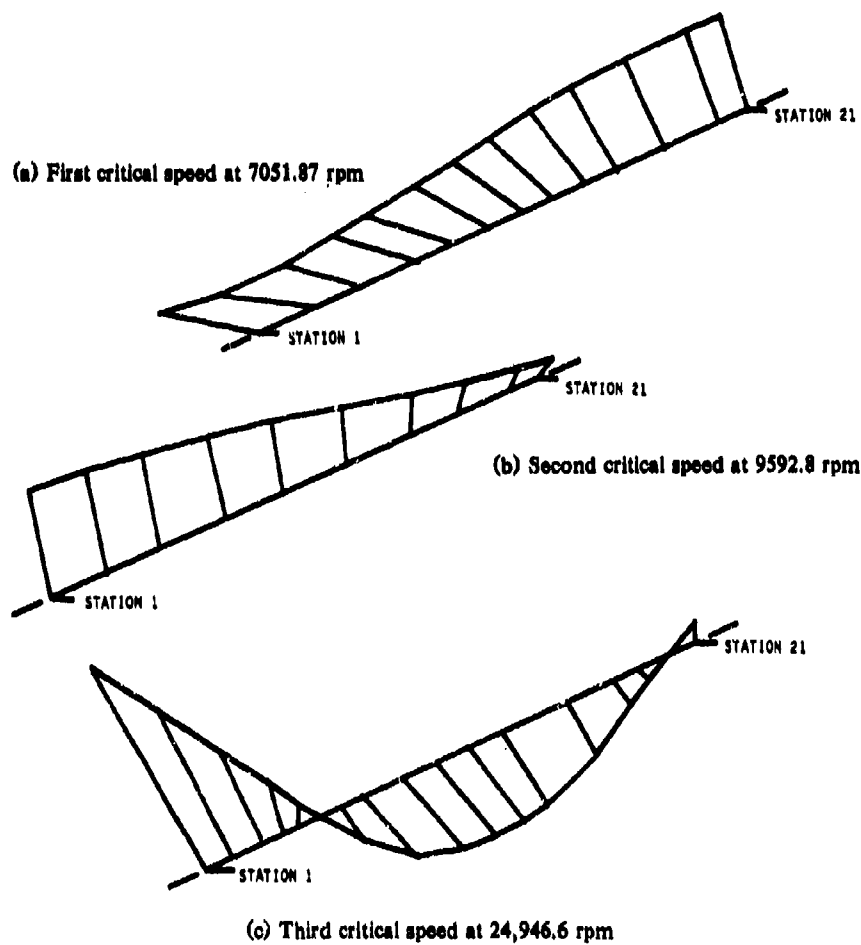
Fig. 7.81. Original rotor deflections at the first, second, and third critical speeds (with damping) [25] (©1975, J.R. Kendig; used by permission)
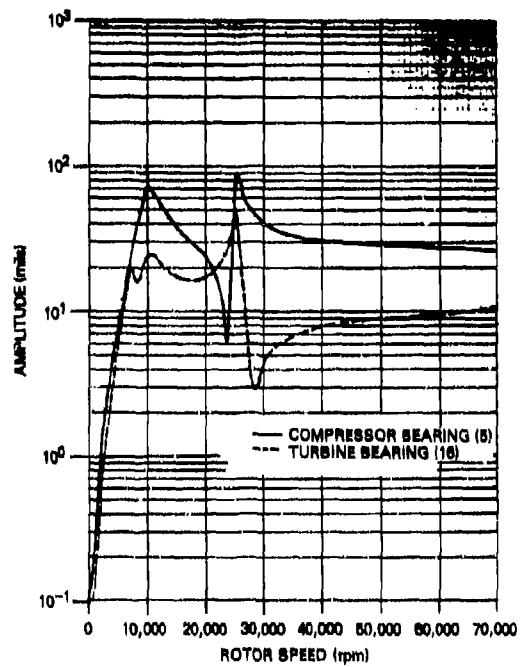
Fig. 7.82. Original response: gas-turbine rotor model
[25] (©1975, J.R. Kendig; used by permission)
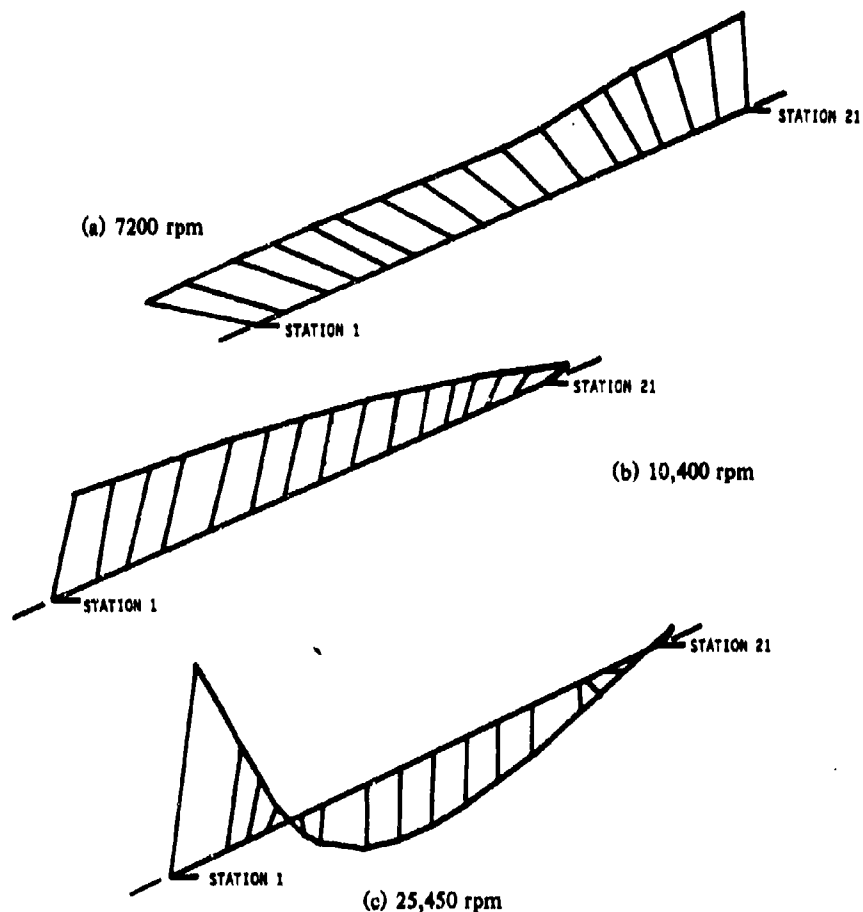
Fig. 7.83. Original damped rotor deflections at 7200, 10,400, and
25,450 rpm [25] (©1975, J.R. Kendig; used by permission)

The N modal method of Bishop and Gladwell was applied to bal-
ance this rotor, with one correction weight added at 7200 rpm, two at
10,250 rpm, and three at 25,450 rpm. It was soon found that the
rigid-body behavior at the two lower rotor-bearing critical speeds in-
hibited successful balancing of the rotor system, and it was therefore
necessary to resort to a two-plane, low-speed balance. The data in
Table 7.13 indicate the effect of the two-plane balances. After the
low-speed balancing performed with the planes of the bearings, the N
modal method was again applied. This resulted in large whirl ampli-
tudes at the third critical speed. An acceptable stepwise balance could
not be achieved in this manner.

Table 7.13. Gas-turbine rotor balancing results. Kendig [25]

| Condition or method | Response (μin.) | | | | | |
| | 7200 rpm | | 10,250 rpm | | 25,450 rpm | |
	Bearing at 5	Bearing at 17	Bearing at 5	Bearing at 17	Bearing at 5	Bearing at 17
Original response	23.7094	19.4391	70.4157	24.6123	90.2387	43.0197
Two-plane, Stations 1 and 21	3.25162	6.29162	9.34174	5.76853	528.517	296.470
Low-speed two-plane, Stations 1 and 21	0.507159	1.52682	1.06859	1.59700	8.68777	4.61221
N modal: First-mode removal (station 10) at 7200 rpm after low-speed two-plane balancing	1.14066	1.84779	2.2471	2.8090	44.892	36.021
N + 2 modal: First-mode removal after low-speed two-plane balancing	0.353475	0.470152	2.67149	1.07980	87.4333	52.9232
Second-mode removal	0.841874	1.13166	0.453592	0.453600	109.513	62.8802
First-mode trim	0.457521	0.579836	0.133233	0.871080	120.072	67.3487
Third-mode removal	4.10343	0.628429	11.5311	4.00038	31.4838	31.4816
Third-mode iteration	4.51295	0.641854	12.6423	4.27890	9.88247	10.0557

The next method tried was the stepwise $N + 2$ modal method. Acceptable amplitude reductions were achieved using this method, at the two rigid body criticals. The third mode amplitudes were reduced by successive trim corrections, as shown in Table 7.13. Further trim balancing would probably have lead to further amplitude reductions.

Amplitude results from a two-plane balance at 500 rpm are presented in Figs. 7.84 and 7.85. These charts show amplitude-vs-speed curves and the deflection shapes at the critical speeds, respectively. It is obvious that rotor amplitudes are reduced in region of the rigid-body critical speeds, but that the amplitudes are increased at higher speeds. Rotor mode shapes are shown in Fig. 7.85.

With the rotor balance condition of Fig. 7.83 as a basis, the modal averaging technique of Moore and Dodd was next applied at the 25,450-rpm flexural critical. The results of this balancing correction are shown in Fig. 7.86.

Figures 7.87 through 7.95 show the results obtained by use of the influence coefficient method in various combinations of balance planes and speeds to cope with the system response of Fig. 7.82. It can be seen from Figs. 7.87, 7.88, and 7.89 that, although the method requires only three balancing planes to provide a good two-speed balance, the addition of a fourth balance plane yields substantially superior results.

This extra correction plane further improves the balance level by between one and two orders of magnitude as shown in Figs. 7.90 and 7.91. Adding two balance planes allows a four-speed balance to be performed: see Figs. 7.92 and 7.93. In this instance the unbalance response level has been reduced by two orders of magnitude below those attained in Figs. 7.90 and 7.91.

The effects of low-speed prebalancing on results obtained with an influence coefficient balance in seven planes and using four balance speeds are shown in Figs. 7.92 and 7.93. These results can be compared directly with Figs. 7.94 and 7.95, which show the response to a similar influence coefficient procedure without prior low-speed balancing.
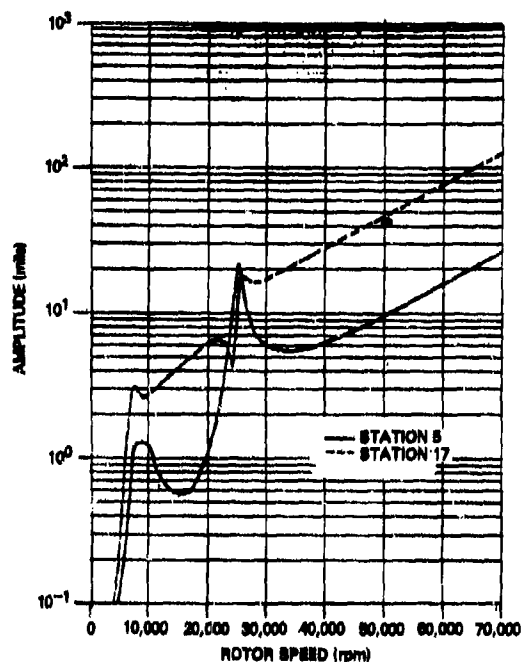
Fig. 7.84. Rotor amplitudes obtained after a rigid-body two-plane balance using stations 5 and 17 at 500 rpm [25] (©1975, J.R. Kendig; used by permission)

STATION 21

(a) 7200 rpm

STATION 1

STATION 21

STATION 1

(b) 10,400 rpm

STATION 21   (c) 25,450 rpm
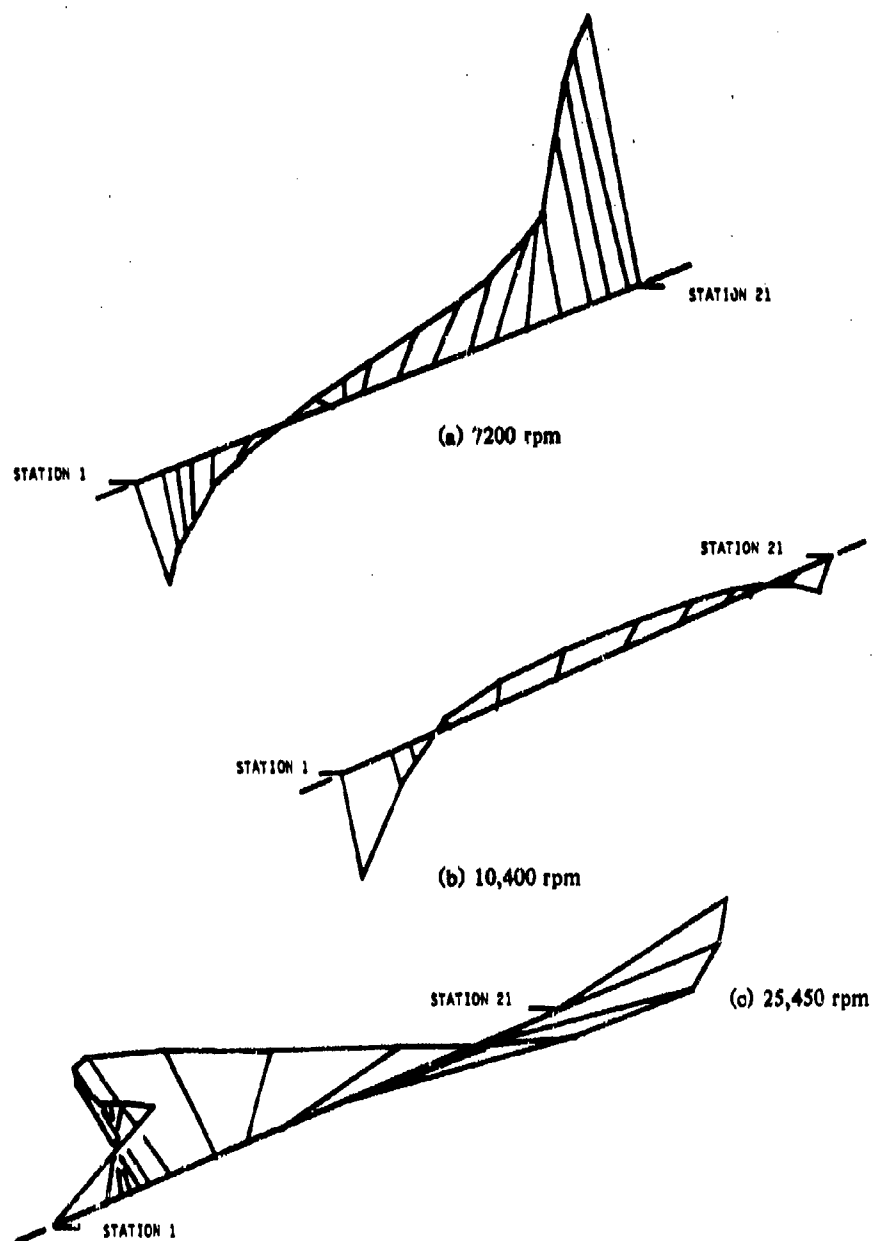
STATION 1

Fig. 7.85. Rotor deflections at 7200, 10,400, and 25,450 rpm [25]
(©1975, J.R. Kendig; used by permission)
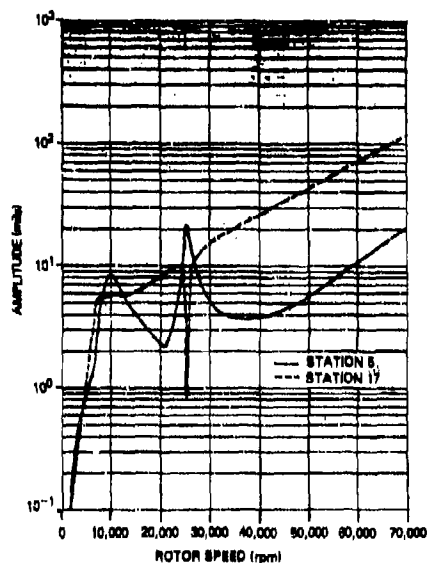
Fig. 7.86. Rotor amplitudes obtained after balancing the rigid-body-balanced rotor by the modal averaging method: 25,450 rpm, five planes (stations 1, 2, 13, 16, and 21) [25] (©1975, J.R. Kendig; used by permission)
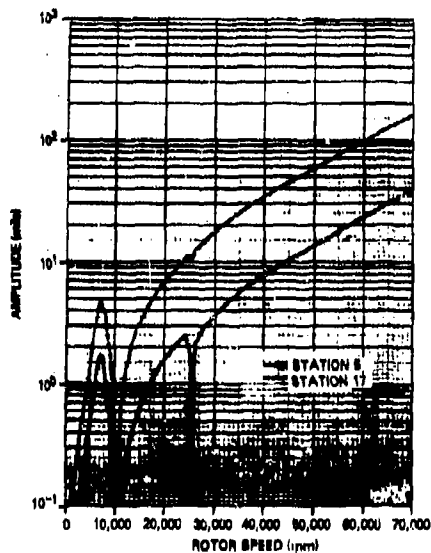
Fig. 7.87. Rotor amplitudes obtained after rigid-body balancing and subsequent influence coefficient balancing in three planes (stations 1, 2, and 16) at 10,400 and 25,450 rpm [25] (©1975, J.R. Kendig; used by permission)

Fig. 7.88. Rotor amplitudes obtained after rigid-body and subsequent influence coefficient balancing in three planes (stations 1, 2, and 21) at 10,400 and 25,450 rpm [25] (©1975, J.R. Kendig; used by permission)
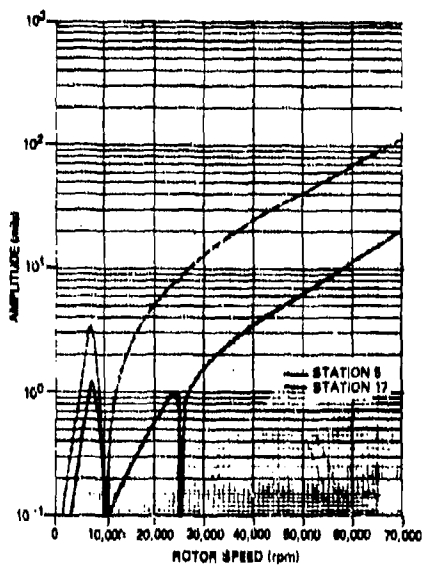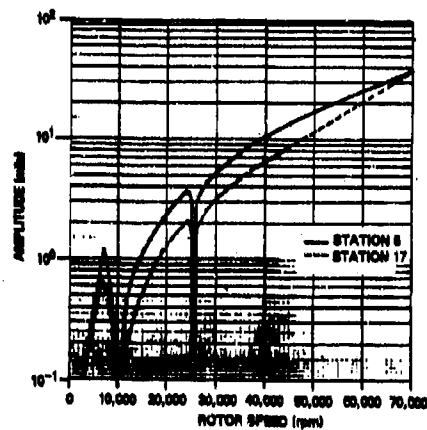
Fig. 7.89. Rotor amplitudes obtained after rigid-body and subsequent influence coefficient balancing in four planes (stations 1, 2, 15, and 21) at 10,400 and 25,450 rpm [25] (©1975, J.R. Kendig; used by permission)
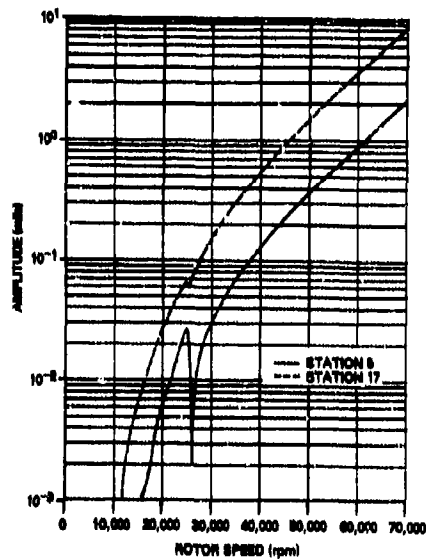
Fig. 7.90. Rotor amplitudes obtained after rigid-body and subsequent influence coefficient balancing in five planes (stations 1, 2, 13, 16, and 21) at 7200, 10,400, and 25,450 rpm [25] (©1975, J.R. Kendig; used by permission)
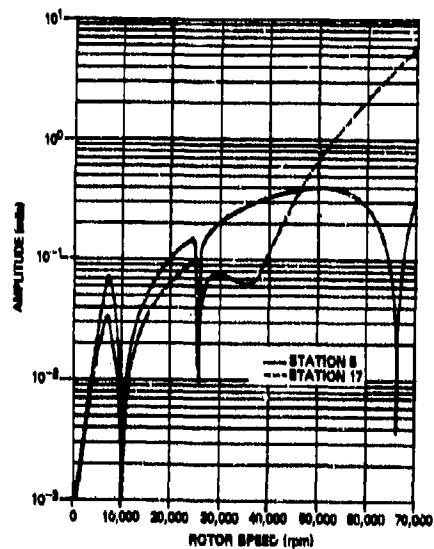
Fig. 7.91. Rotor amplitudes obtained after rigid-body and subsequent influence coefficient balancing in five planes (stations 1, 2, 13, 16, and 21) at 10,400, 25,450, and 66,000 rpm [25] (©1975, J.R. Kendig; used by permission)
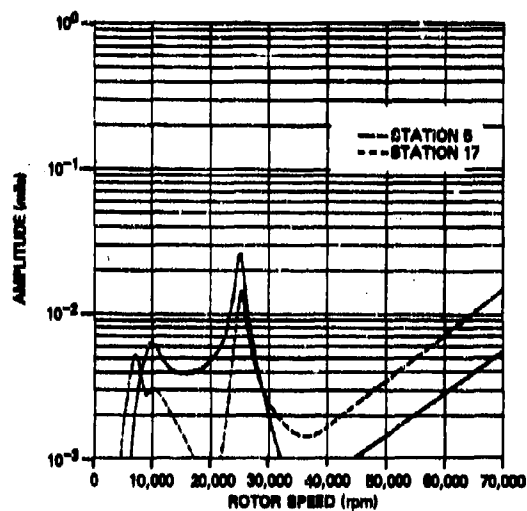
Fig. 7.92. Rotor amplitudes obtained after rigid-body and subsequent influence coefficient balancing in seven planes (stations 1, 2, 8, 11, 13, 16, and 21) at 10,400, 25,450, 50,000, and 66,000 rpm [25] (©1975, J.R. Kendig; used by permission)
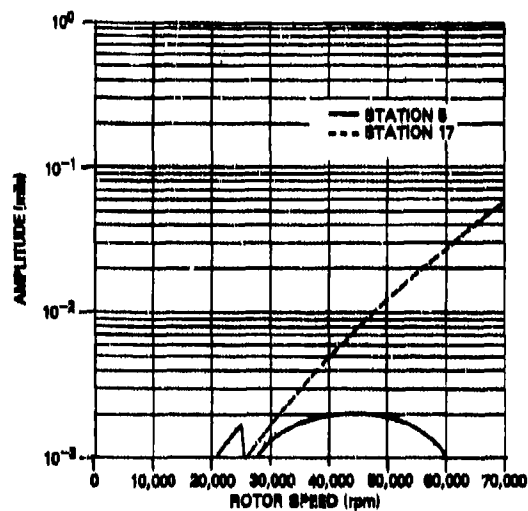
Fig. 7.93. Rotor amplitudes obtained after rigid-body and subsequent influence coefficient balancing in seven planes (stations 1, 2, 8, 11, 13, 16, and 21) at 7200, 10,400, 25,450, and 66,000 rpm [25] (©1975, J.R. Kendig; used by permission)
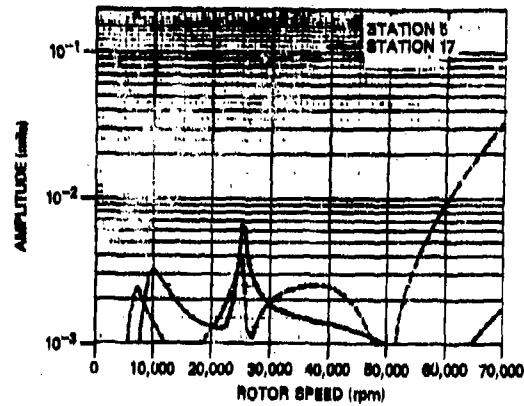
Fig. 7.94. Rotor amplitudes obtained after influence coefficient balancing in seven planes (stations 1, 2, 8, 11, 13, 16, and 21) at 10,400, 25,450, 50,000, and 66,000 rpm [25] (©1975, J.R. Kendig; used by permission)
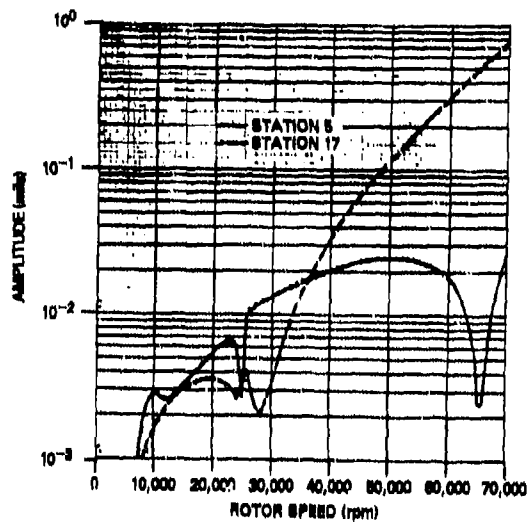
Fig. 7.95. Rotor amplitudes obtained after influence coefficient balancing in seven planes (stations 1, 2, 8, 11, 13, 16, and 21) at 7200, 10,400, 25,450, and 66,000 rpm [25] (©1975, J.R. Kendig; used by permission)

Conclusions from the Kendig Balancing Study

Kendig [25] has demonstrated a computer procedure that solves for a system of complex trial weights for either the modal formulations of Bishop and Gladwell or the modal formulations of Federn and Kellenberger. Kendig also demonstrated a program that solves for a system of modal correction weights based on trial-weight responses; the program is based on the general modal graphical constructions of Fig. 7.4 and is compatible with any modal balancing technique. In addition, Kendig demonstrated two programs that apply the modal averaging technique of Moore and Dodd to any rotor system, including those with asymmetrical bearing of rotor conditions. The results of this computer-based study of various balancing techniques can be summarized as follows:

1. The assumption that the deflection shape of a rotor in the vicinity of its critical speed is primarily a planar form is valid for undamped systems and for lightly damped systems.

2. The modal elimination process that forms the basis of the modal balancing techniques has been demonstrated using computer techniques. It has been shown that the modal methods are most readily applied to lightly damped rotor systems, i.e., on those rotors having planar mode shapes.

3. Inclusion of dissimilar and cross-coupled bearing stiffness or damping conditions the orthogonality between the principal modes of vibration.

4. The presence of bearing damping may complicate the modal balancing procedures if the actual rotor deflection shapes are used in the balancing operations.

5. The Moore and Dodd modal averaging procedure is applicable to both damped and undamped rotor-and-bearing systems.

6. If a rotor exhibits purely flexible behavior, the N modal and N simultaneous methods are both applicable, and produce similar results. The $N + B$ simultaneous method was found to give less satisfactory results.

7. If a rotor exhibits purely flexible behavior, the N modal and N simultaneous methods are both applicable, and produce similar results, but the $N + B$ simultaneous method does not always yield satisfactory results.

8. Use of two-plane low- or high-speed trim balance on a balanced flexible rotor gives negligible improvement in balance levels unless an increase in unbalance levels can be tolerated at speeds other than that for which the system is so trimmed.

9. The use of asymmetrical "corkscrew" unbalances has been shown to complicate the modal balancing procedures by introducing

nonplanar rotor response and by forcing the rotor axis to distort in space.

10. Flexible rotors that exhibit nonnegligible rigid-body effects cannot be balanced by pure flexural modal techniques, such as the N modal or N simultaneous modal methods. These rotors must be initially balanced as rigid bodies in two planes.

11. Additional flexible vibration modes may have to be considered in balancing rotors that are damped or exhibit rigid-body effects. Higher flexible modes which influence the balance quality may be obscured by damping effects or by rigid-body vibrations.

12. The influence coefficient method has been shown to be effective on undamped and damped flexible rotors and on damped rotors exhibiting both rigid and flexural behavior. This method appears to be the most effective, and most generally applicable, rotor-balancing technique.

13. Compared to the influence coefficient method, the modal methods required more effort, time, and trimming in this study to achieve a satisfactory balance, because of the requirement to apply the modal method iteratively: see Parkinson [2].

7.8. Experimental Comparison of Modal Balancing Procedures

Giers [4] made an experimental comparison of effectiveness between the comprehensive modal balancing method of Federn and Kellenberger and the modal averaging method of Moore. The essential difference is that the comprehensive modal method requires that the rigid-body modes be balanced out before flexible-rotor balancing, whereas the modal averaging method does not require the balancing of such modes on the grounds that they do not exist in the response of the actual flexible-rotor system.

The apparatus used for this comparison is shown in Fig. 7.96. The rotor consists of a uniform steel shaft with a diameter of 1.968 in., a 73.228-in. span between bearing supports, and an overall length of 98.425 in. The shaft is mounted on rollers at either end, which serve as bearing supports. The rollers and their axles are effectively rigid, and the surfaces have slight spherical contours. The rotor supports are mounted in a hard-support balancing machine—that is, on pedestals that are rigid in the vertical direction and have a calibrated stiffness exceeding 55,000 lb/in. in the horizontal direction. The rotor-and-bearing system is therefore a flexible rotor in rigid bearings; the modes are shown in Fig. 7.97. Giers indicates that the nodes of the modes did not quite coincide with the bearing supports.

The rotor is driven by the standard drive motor of the balancing machine, attached to the rotor by a lightweight universal drive shaft.

Fig. 7.96. Flexible test rotor used by Giers [4] on the balancing machine (©1971 VDI-Verlag GmbH; used by permission)

$f_{01} = 32$ Hz $G = 54$ kg
$f_{02} = 117$ Hz
$f_{03} = 238$ Hz
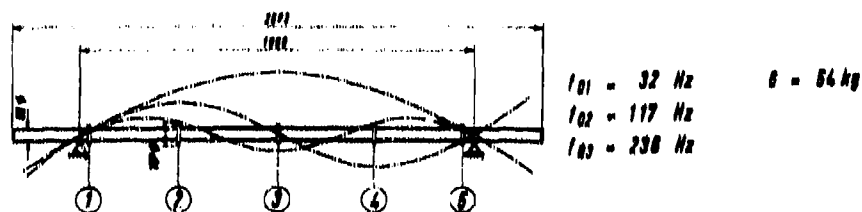
Fig. 7.97. Modes of test rotor used by Giers [4] (©1971 VDI-Verlag GmbH; used by permission)

The rotor has five balancing rings, suitable for the insertion of correction weights, equally spaced along its length (Fig. 7.97). The forces transmitted to the bearings because of rotor unbalance were sensed through the instrumented pedestals of the balancing machine. These measurements were displayed as vector points for either bearing by use of the balancing machine vectormeter equipment (see Section 3.5 for description).

The vibration response of the rotor in the original balance condition is shown in Fig. 7.98. A mass of 30 g was then added to plane 1 at 0° to unbalance the rotor.
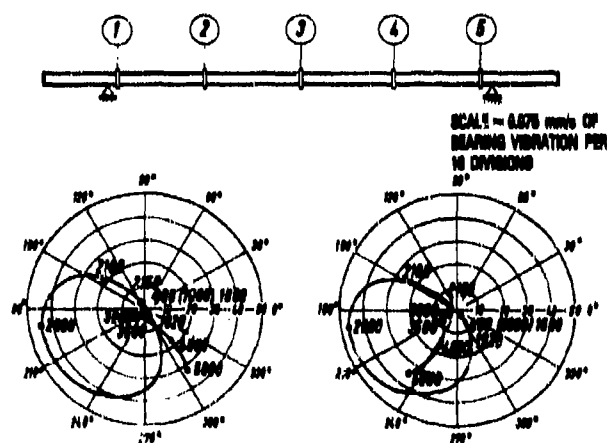
Fig. 7.98. Vibration velocity at the bearings, initial condition
Giers [4] (©1971 VDI-Verlag GmbH; used by permission)

The comprehensive modal balancing method was used first. No description of the procedure is given, except to indicate that this procedure was accommodated directly by the balancing-machine circuitry, presumably as part of the Schenck ABC dial-in procedure. The balancing machine indicated that a correction weight of 30 g at 180° was required in plane 1 (i.e., opposite the unbalance weight and of equal magnitude). No correction was required in any other plane. The resulting rotor response is shown in Fig. 7.99. It is evident that the prescribed correction has returned the rotor to the original unbalance condition shown in Fig. 7.98.

The modal averaging method was then applied as follows: the rotor was run close to the first critical speed at about 2100 rpm, where strong vibrations were encountered. These vibrations were diminished by placing a 5-g mass in plane 3 (angle not stated; presumably 180°).
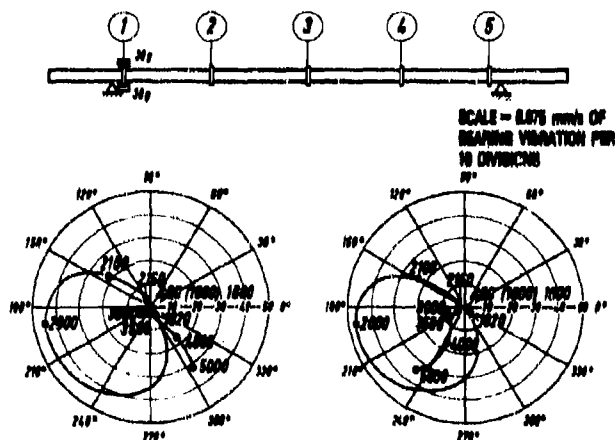
Fig. 7.99. Vibration velocity at the bearings, unbalance in plane
1, balanced by Federn's comprehensive modal method Giers [4]
(©1971 VDI-Verlag GmbH; used by permission)

Speed was then increased to 3000 rpm, where again heavy asymmetrical
vibrations were encountered. These asymmetrical vibrations were
assumed to be due to a combination of the second and third modes
(see Ref. 10 for discussion). Both modes were suppressed without
affecting the first (balancing) mode by insertion of a mass of 36 g at
180° in plane 2 and a mass of 36 g at 0° in plane 4. These masses
brought the rotor into a symmetrical vibration condition, but with
considerable amplitudes remaining.

The modal averaging method, applied next, calls for the third
mode to be balanced without disturbing the now-balanced first and
second modes. This was achieved by placing 63 g at 180° in plane 2,
63 g at 180° in plane 4, and 105 g at 0° in plane 3. After balancing the
first three modes in this manner, the residual vibrations were as shown
in Fig. 7.100 throughout the speed range. It is evident that the balance
achieved by the comprehensive modal balancing method in this
instance is superior to that achieved by the modal averaging method for
the steps taken.

A second test was attempted, with the original unbalance of 30 g at
0° located in plane 2. A comprehensive modal low-speed balance was
made at 400 rpm. This indicated that 22.5 g at 180° in plane 1 and
7.5 g at 180° in plane 5 were required to balance the rotor at this speed.
The rotor was then run at 1600 rpm, and a set of three balancing
weights found by a calibration run were added; 30 g at 0° in plane 1,
22 g at 180° in plane 3, and 11 g at 0° in plane 5. The rotor then ran
smoothly at 1600 rpm. It ran well at 1920 rpm (the first critical speed)
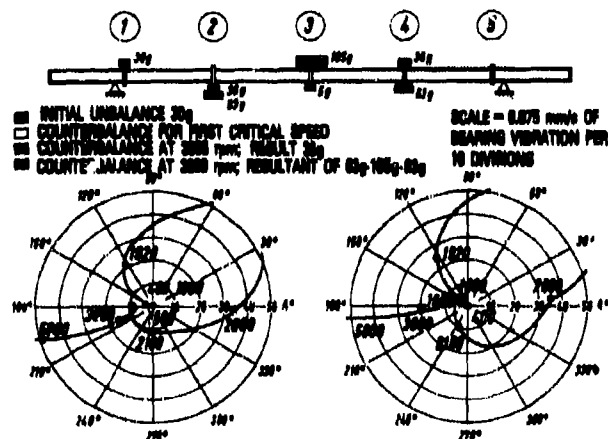
Fig. 7.100. Vibration velocity at the bearings, unbalance in plane
1, balanced by Moore's modal averaging method Giers [4]
(©1971 VDI-Verlag GmbH; used by permission)

and up to 5000 rpm "without any further correction." The corrected
response achieved by the comprehensive modal method for this case is
shown in Fig. 7.101.

The modal averaging method was then applied for the same origi-
nal unbalance condition of 30 g at 0° in plane 2. A mass of 21 g at
180° was first inserted in plane 3. This left a small asymmetrical result,
and the rotor speed was increased to 300 rpm, where rougher running
was experienced.

After 20 g at 180° in plane 2, 20 g at 0° in plane 4, and 20 g in
plane 3, followed by an additional 12 g at 180° in plane 2 and 12 g at
180° in plane 4 were added, the rotor was observed to run smoothly
from 200 up to 5000 rpm (see Fig. 7.102).

A third test was conducted with an initial unbalance of 30 g at 0°
in plane 3. The rotor was first balanced by the comprehensive modal
method at 400 and at 1800 rpm, and then by the modal averaging
method at 1800 and 3000 rpm; the results are shown in Figs. 7.103 and
7.104, respectively.

Further tests were then conducted for both methods, with known
unbalances inserted in planes 1, 2, and 3 simultaneously. The results
of these tests are shown in Figs. 7.105 and 7.106.

The major conclusions of this study by Giers [4] are as follows:

1. The comprehensive modal and modal averaging methods can
both be used to balance this flexible rotor up to 5000 rpm.
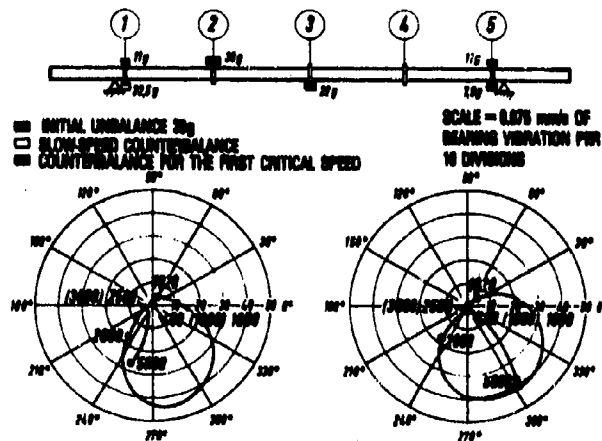
Fig. 7.101. Vibration velocity at the bearings, unbalance in plane 2, balanced by Federn's comprehensive modal method Giers [4] (©1971 VDI-Verlag GmbH; used by permission)
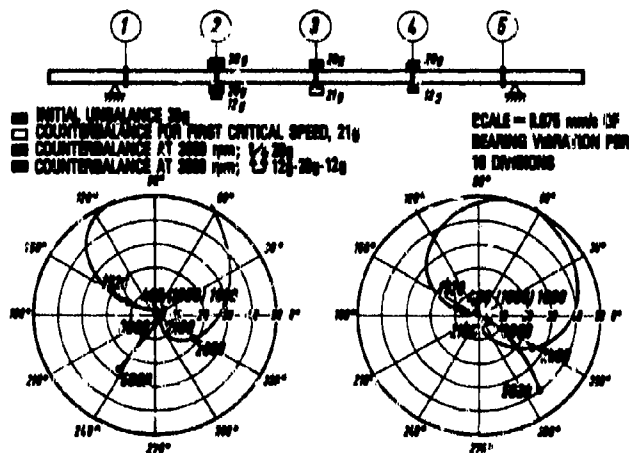
Fig. 7.102. Vibration velocity at the bearings, unbalance in plane 2, balanced by Moore's modal averaging method Giers [4] (©1971 VDI-Verlag GmbH; used by permission)
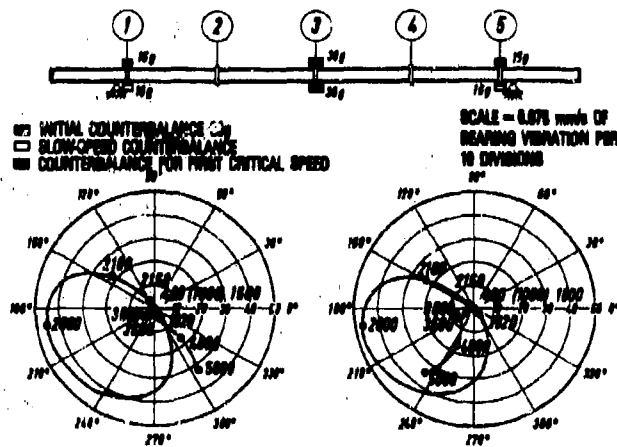
Fig. 7.103. Vibration velocity at the bearings, unbalance in plane 3, balanced by Federn's comprehensive modal method Giers [4] (©1971 VDI-Verlag GmbH; used by permission)
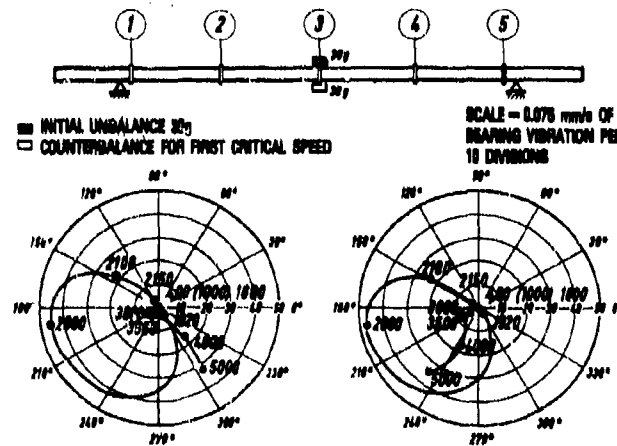
Fig. 7.104. Vibration velocity at the bearings, unbalance in plane 3, balanced by Moore's modal averaging method Giers [4] (©1971 VDI-Verlag GmbH; used by permission)
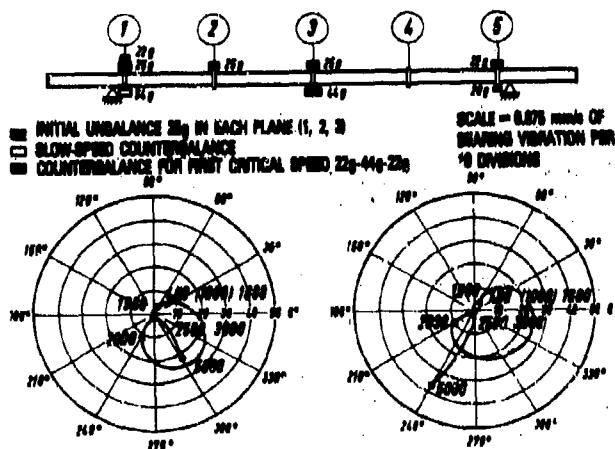
Fig. 7.105. Vibration velocity at the bearings, unbalance in planes 1, 2, and 3, balanced by Federn's comprehensive modal method Giers [4] (©1971 VDI-Verlag GmbH; used by permission)
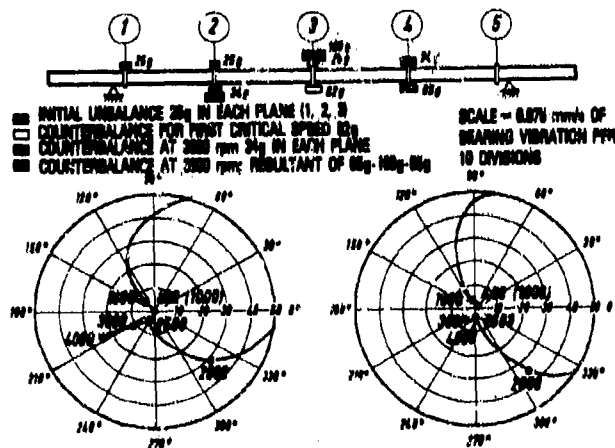
Fig. 7.106. Vibration velocity at the bearings, unbalance in planes 1, 2, and 3, balanced by Moore's modal averaging method Giers [4] (©1971 VDI-Verlag GmbH; used by permission)

2. For rotors with such little damping, it seems to be necessary to balance the portion of the unbalance that is in the nodes of the first mode. If the comprehensive modal method is used, this is done at low speed. If the modal averaging method is used, speeds higher than the

first critical speed are used, but this is not really modal balancing because the weight combinations added do not bend the rotor.

3. If the comprehensive modal method is used, the bearing forces are controlled from low speed through the first critical speed to the highest balancing speed. With the modal averaging method, an improvement close to the first critical speed can result in higher bearing force at low speed.

4. If the modal averaging method is applied to a rotor with little damping and substantial unbalance, the first correction for running through the first critical speed cannot be made at a speed close to first critical. Therefore it might be necessary to make a second correction between that first speed and the first critical speed.

5. The comprehensive modal method requires fewer corrections and smaller correction weights than does the modal averaging method. It has a disadvantage in requiring a measuring device that is capable of measuring very small unbalances at speeds where the rotor is certainly still rigid. However, the comprehensive modal method seems to be easier to use.

6. The modal averaging method seems to be applicable only if the bearing conditions are very close to service conditions. Therefore, this method might also be very good for balancing in situ.

7. Reapplication of flexible-rotor balancing to a balanced rotor produces only marginal improvement in the balance level.

Giers points out that these conclusions apply specifically to the rotor and the test conditions studied.

Giers does not make clear how the comprehensive modal method was applied: whether it was built into the high-speed balancing machine used or whether it was simply the Schenck ABC method common to all hard-bearing balancing machines. The rotor system under test was effectively without external damping. There were no fluid-film bearings, and the supports were very close to the nodes. As such, this was a stringent test of the two balancing methods in one sense and an incomplete test in that the complicating effects of modal damping were absent. The results should give guidance for the balancing of large two-bearing rotating equipment such as generator rotors, which commonly exhibit planar modes (see Ref. 13) in which damping plays only a small part. Having the shaft ends overhung beyond the bearings further makes this system a reasonable structural (i.e., modal) model for much related two-bearing rotating equipment with overhangs and/or end couplings.

There is one valid objection that could be raised: The modal averaging method can actually achieve a balance much superior to that

which has been shown in these results if a series of trim-balance runs is made. This is usually done in practice [1,2], but additional runs are needed.

This study appears to suggest that low-speed balancing of overhung rotors in rigid bearings can be accomplished with fewer overall balancing runs by making an initial low-speed balance. If this is generally true, it is obviously an important time- and cost-saving measure. No comparable study by proponents of either the modal averaging method or the modal method seems to have been made. Such a response appears to be warranted if the above general conclusion is not valid.

7.9 Flexible Balancing Optimization Studies

Combination of Modal Balancing and Influence Coefficient Balancing

Drechsler [33] has proposed a combined balancing method in which the intuitive optimizations of the modal method(s) are combined with the pragmatic efficiency of the influence coefficient method. He uses the least-squares version of the influence coefficient method, in which the squares of the residual vibration amplitudes over the rotor length are to be minimized throughout the operating-speed range. In Drechsler's paper this is stated as a general integral formulation into which the rotor modal shapes are introduced as approximate deflection functions. The usual variational procedure is then followed to obtain a weighted version of the influence coefficient matrix. The weighting matrix is said to depend on the number and the location of the measuring stations along the rotor length.

Drechsler has formulated the problem as follows: Since the unbalance normally cannot be removed entirely, a small vibration will persist after balancing. This residual vibration should be small for all speeds within the operating range and for all locations along the shaft axis. This can be stated mathematically as follows:

$$\int_{\omega=0}^{\omega_{max}} \int_{x=0}^{l} [\tilde{W}^R(z,\omega)]^T \tilde{W}^R(z,\omega)\, dz\, d\omega = \min, \qquad (7.1)$$

where T = transpose and $\tilde{W}^R(z,\omega)$ is the vector of the residual vibration. The tilde on the vector $\tilde{W}$ indicates that W is a function of z and ω. The components of the residual vibration normally are complex quantities:

$$\tilde{W}^R(z,\omega) = [\tilde{W}_x^R(z,\omega), \ \tilde{W}_y^R(z,\omega)]$$

$$= (\tilde{W}_{xc}^R + i\tilde{W}_{xs}^R, \ \tilde{W}_{yc}^R + i\tilde{W}_{ys}^R). \qquad (7.2)$$

Integral (7.1) is therefore composed of two parts that have to be considered at the same time:

$$\int \int (\tilde{W}^R)^T \tilde{W}^R \, dz \, d\omega = \int \int \tilde{W}_x^R \tilde{W}_x^R \, dz \, d\omega + \int \int \tilde{W}_y^R \, W_y^R \, dz \, d\omega.$$

For an isotropic rotor in isotropic bearings, both parts are identical and it is possible to consider one integral alone. When the bearing conditions are anisotropic, it is theoretically better to minimize the sum of both integrals, although they are more or less linearly dependent, so that even in this case it is practically sufficient to consider just one of the two integrals.

When the influence of N sets of balancing weights is introduced, the residual vibration vector takes the form

$$\tilde{W}^R(z,\omega) = W_0(z,\omega) + \sum_{i=1}^{N} u_i \, W_i(z,\omega). \qquad (7.3)$$

Substituting this relationship into integral (7.1) and differentiating with respect to the unknown balancing weights yield a system of linear equations for the balancing weights for minimizing the integral:

$$\sum_{i=1}^{N} \left[\int \int (\tilde{W}_k^T W_i \, dz \, d\omega) u_i \right] + \int \int \tilde{W}_k^T W_0 \, dz \, d\omega = 0,$$

$$(k = 1, 2, \ldots, N).$$

For numerical computation this formulation can be approximated by the summation

$$\sum_{i=1}^{N} \sum_{p=1}^{P} \sum_{q=1}^{Q} [\tilde{W}_k^T \, W_i(z_p, \omega_q)] u_i + \sum_{p=1}^{P} \sum_{q=1}^{Q} \tilde{W}_k^T \, W_u(z_p, \omega_q) = 0 \quad (7.4)$$

$$(k = 1, 2, \ldots, N),$$

in which it is assumed that there are p measuring stations along the length of the rotor and that q balancing speeds are used in the balancing process. This summation expression corresponds to a least-squares minimization of a set of $[2 \times p \times q]$ linear equations, as described in Section 6.6 for the influence coefficient method.

To obtain the above matrices in a form suitable for computation, the rotor deflection at any speed is represented as the sum of its normal modes;

$$\tilde{W}(z) = a_1 \tilde{\phi}_1(z) + \cdots + a_p \, \tilde{\phi}_p(z) \qquad (7.5)$$

or, in matrix notation, as

$$\tilde{W} = \tilde{\phi}^T a. \tag{7.5a}$$

This approximation is limited to a speed range $0 < \Omega < \Omega(p)$, where $\Omega(p)$ is a speed that is far enough below the $(p + 1)$st critical speed so that the $(p + 1)$st mode and all higher ones can be neglected. Since this approximation implies a reduction of the vibrating system to p degrees of freedom, it yields p linear independent equations only, which allow the determination of p sets of balancing weights.

If the coordinates of the measuring stations are introduced into Eq. (7.5), a linear relationship between the measured vibrations and the coefficients a can be established:

$$\begin{bmatrix} W(z_1) \\ \cdot \\ \cdot \\ \cdot \\ \cdot \\ W(z_p) \end{bmatrix} = \begin{bmatrix} \phi_1(z_1) \cdots & \cdots \phi_p(z_1) \\ \cdot & \cdot \\ \cdot & \cdot \\ \cdot & \cdot \\ \cdot & \cdot \\ \phi_1(z_p) \cdots & \cdots \phi_p(z_p) \end{bmatrix} \begin{bmatrix} a_1 \\ \cdot \\ \cdot \\ \cdot \\ a_p \end{bmatrix}$$

or, in matrix notation,

$$W = \Phi a, \tag{7.6}$$

which yields the unknown coefficients

$$a = \Phi^{-1} W. \tag{7.7}$$

When the approximation (7.4) is introduced into the integrals of Eq. (7.1) and Eq. (7.7) is substituted for the coefficients a, the integrals take the form

$$\int \int \tilde{W}_{xi} \tilde{W}_{xk} \, dz \, d\omega + \int \int \tilde{W}_{yi} \tilde{W}_{yk} \, dz \, d\omega$$

$$= \sum \tilde{W}_{xi}^T(\omega_q) \, [\Phi_x^{-1}]^T \int \int \phi_x \phi_x^T dx \, [\phi_x^{-1}] \, W_{xi}(\omega_1)$$

$$+ \sum \tilde{W}_{yi}^T(\omega_q) \, [\Phi_y^{-1}]^T \int \int \phi_y \tilde{\phi}_y^t \, dz \, [\phi_y^{-1}] \, W_{yk}(\omega_q)$$

$$= \sum_{q=1}^{q_p} [\tilde{W}_{xi}^T(\omega_q) W_x W_{xk}(\omega_q) + W_{yi}^T W_y W_{yk}(\omega_q)], \tag{7.8}$$

$$(1 \leqslant i; \, k \leqslant p),$$

where $\mathbf{W}_x$ and $\mathbf{W}_y$ are the weighting matrices, which weigh the measured vibration amplitudes in the x,z and the y,z plane with respect to the mode shapes corresponding to these planes in the speed range $0 < \omega < \omega_q(r)$. Normally there are enough sampling points in the speed range, and therefore the integral over the speed can be approximated by a sum in a straightforward manner, the index q_p indicating the last sampling point within the integration interval.

If there are more than p correction planes, a step-by-step procedure has to be adopted, as suggested by the modal theory. The first step yields p balancing weights, which makes it possible to calculate the residual vibration after the first step:

$$\mathbf{W}_0^1(x_p, \omega_q) = \mathbf{W}_0(x_p, \omega_q) + \sum_{l=1}^{p} \mathbf{W}(z_p, \omega_q) u_l. \qquad (7.9)$$

These residual vibrations are essentially composed of modal components of an order higher than p, since the modal components 1 to p ought to be negligible. In practice, the first modal component will be compensated for best of all, but the pth mode, which is much nearer to the neglected higher modes, might not be compensated for satisfactorily. This suggests a renewed approximation of Eq. (7.9), similar to Eq. (7.3), in which one of the compensated modes is now neglected, and one higher modal component, previously neglected, is taken into account:

$$W_0^1(z) = a_2\phi_2(z) + \cdots + a_{p+1}\phi_{p+1}(z). \qquad (7.10)$$

In order to not reintroduce the compensated mode shapes, which are neglected in this stage of the calculation, the set of unknown balancing weights determined in this step has to be orthogonal to all the lower modes, which are neglected in the renewed approximation. For the sake of clarity and simplicity, it is also assumed that each set is orthogonal to all modes of the order $l < p$. At this stage the speed range $0 < \omega < \omega(p + 1)$ can be considered, $\omega(p + 1)$ being a speed far enough below the $(p + 2)$nd critical speed, up to which the new approximation is valid. Repeating the procedure outlined above, we now obtain a set of balancing weights that compensate for the $(p + 1)$st mode and yield corrections to the state of balance of the reconsidered modes 2 to p. The magnitude of these corrections indicates the quality of the acquired data. Each step could be rounded off by calculating the root mean square of the residual vibration. After the rth step, the residual vibrations are given by

$$W_0^R(z_p, \omega_q) = W_0(z_p, \omega_q) + \sum_{s=1}^{r} \sum_{l=s}^{p+s-1} W_l(z_p, \omega_q) u_l^{(s)}. \qquad (7.11)$$

The process has to be interrupted as soon as the inaccuracy of the measured vibration data does not permit the calculation of further valid correction weights. At this stage the root mean square of the residual vibrations is stationary.

Drechsler has provided some results to demonstrate the functioning of the above procedure. The rotor model used was a typical generator rotor (see Fig. 7.107). Bearing—pedestal stiffnesses of 1.27×10^6 lb/in. and 3810 lb/in. were used for the calculations. To simulate the unbalance of this rotor, a uniform eccentricity of 60×10^{-3} mm was assumed along the generator armature section, with a 0.5-kPa/cm local coupling unbalance at either end of the rotor in phase with the main unbalance force. The results of these computations are given in Tables 7.14, 7.15 and 7.16. The influence of bearing stiffness on the various critical speeds of the generator is shown in Table 7.14.
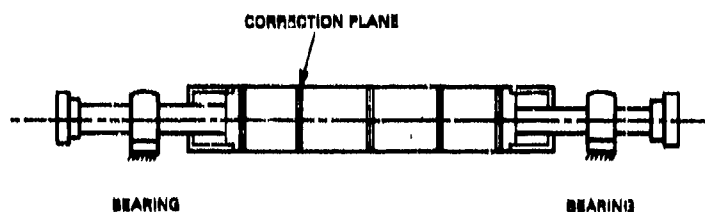
Fig. 7.107. Generator rotor type used by Drechsler for balancing tests [34] (©1976, Institution of Mechanical Engineers; used by permission)

Table 7.14. Critical speeds of a typical generator rotor in different bearing conditions

Pedestal stiffness (kPa/cm × 10⁶)	Critical speed (rpm)				
	1	2	3	4	5
0.5	583	1594	2874	3884	6467
1.5	635	1904	3978	4275	8011

Table 7.15. Correction weights for a pedestal stiffness of 0.5×10^6 kPa/cm [34]

Method	Balancing weight (cm kP)				
	Plane 1	Plane 2	Plane 3	Plane 4	Plane 5
I-2	0.47	85.23	117.3	97.45	5.31
W-3	0.10	85.19	116.7	97.23	5.32
I-4	0.51	84.81	117.1	97.11	5.25

Table 7.16. Balancing weights for a pedestal stiffness of
1.5×10^6 kPa/cm [34]

Method	Balancing weight (cm kPa)				
	Plane 1	Plane 2	Plane 3	Plane 4	Plane 5
I-2	4.04	79.59	122.9	94.47	7.18
W-S	1.04	83.99	118.5	96.71	6.07
W-M	2.80	79.82	120.2	92.55	7.28
I-4	4.04	78.79	122.5	93.34	7.53

7.10 Summary of Practical Experience with Balancing Methods

No doubt remains that the three primary methods of flexible-rotor
balancing—the modal, the influence coefficient, and the comprehensive
modal methods— are all capable of balancing a rotor to an acceptable
balance quality level. The modal method has been shown by Bishop
and used by Moore for many years. Influence coefficient balancing has
been demonstrated by Badgley, Lund, Tonnesen, and others to be a
versatile and sophisticated method under a wide variety of cir-
cumstances. Comprehensive modal balancing is widely used as a rou-
tine procedure in flexible-rotor balancing. The questions that remain
concern the application of each method to specific problems and
machine types. Room exists for additional development in this area.

7.11 References

1. R. E. D. Bishop, and A. G. Parkinson, "Vibration and Balancing
   of Flexible Shafts," *Appl. Mech. Rev.* May 1968 439—451.
2. A. G. Parkinson, "An Introduction to the Vibration of Rotating
   Flexible Shafts," *Bull. Eng. Educ.*, 6, 47 (1967).
3. N. F. Rieger, *Flexible Rotor-Bearing System Dynamics*, Part III,
   "Unbalance Response and Balancing of Flexible Rotors in Bear-
   ings," ASME, 1973.
4. A. Giers, "Comparison of the Balancing of Flexible Rotor Follow-
   ing the Methods of Federn-Kellenberger and Moore," *VDI Ber.*,
   161, 29—34 (1971).
5. W. Kellenberger, "Should a Flexible Rotor Be Balanced in N or
   $(N+2)$ Planes?," ASME Paper No. 71 Vibr-55, 1971.
6. A. G. Parkinson, K. L. Jackson, and R. E. D. Bishop, "Some
   Experiments on the Balancing of Small Flexible Rotors: Part I,
   Theory," *J. Mech. Eng. Sci.*, 5(1), 114—128 (1963).
7. A. G. Parkinson, K. L. Jackson, and R. E. D. Bishop, "Some
   Experiments on the Balancing of Small Flexible Rotors: Part II,
   Experiments," *J. Mech. Eng. Sci.*, 5(2), 133—145 (1963).

8. A. L. G. Lindley and R. E. D. Bishop, "Some Recent Research on the Balancing of Large Flexible Rotors," *Proc. Inst. Mech. Engrs.* 177(30), 811—825 (1963).

9. L. S. Moore, "The Significance of Anisotropy of Support Conditions When Balancing Very Large Flexible Rotors," in *Vibrations of Rotating Systems,* Institution of Mechanical Engineers, 1972, pp. 86—95.

10. L. S. Moore and E. G. Dodd, "Mass Balancing of Large Flexible Rotors," *GEC J. Sci. Technol.* 31(2), 74 (1964).

11. L. S. Moore and E. G. Dodd, "Mechanical Balancing of Large Rotors," *Parsons J.,* C. A. Parsons Co., Newcastle-upon-Tyne, England, June 1970, pp. 1—13.

12. L. S. Moore, "Balancing of Large Turbine Rotors," *Inst. Marine Eng. Trans.* 81 105—115 (Apr. 1969).

13. R. H. Badgley and N. F. Rieger, "The Effects of Multi-Plane Balancing on Flexible Rotor Whirl Amplitudes," paper presented at SAE Automotive Engineering Congress and Exposition, Jan. 8—12, 1973.

14. P. G. Morton, "Discussion of Paper by Lindley and Bishop, 'Some Recent Research on the Balancing of Large Flexible Rotors'," *Proc. Inst. Mech. Engrs.* 177(30), 811—825 (1963).

15. E. W. Consterdine, "Discussion of Paper by Lindley and Bishop 'Some Recent Research on the Balancing of Large Flexible Rotors'," *Proc. Inst. Mech. Engrs.,* 177(30), 830—833 (1963).

16. S. I. Mikunis, "Balancing Flexible Rotors in Turbine Generators," *Russian Eng. J.* 41(9), 10 (1961).

17. S. I. Mikunis, "Balancing Non-Rigid Rotors in Turbine Units," *Russian Eng. J.* 39(12), 21—26 (1959).

18. R. H. Badgley, J. M. Tessarzik, and D. Fleming, "Experimental Evaluation of Multiplane-Multispeed Rotor Balancing Through Multiple Critical Speeds," ASME Paper No. 75-DET-73, Design Engineering Technical Conference, Wash, D.C., 1975. Also *Trans. ASME,* Ser. B, *J. Eng. Ind.J* 94(1), 148—158 (1972).

19. J. M. Tessarzik, R. H. Badgley, and W. J. Anderson, "Flexible Rotor Balancing by the Exact Point-Speed Influence Coefficient Method," *J. Eng. Ind., Trans. ASME,* Ser. B, 94(1), 148—158, (1972). Also *Flexible Rotor Balancing by the Exact Point-Speed Influence Coefficient Method,* by J. M. Tessarzik, NASA-CR-72714, 1970.

20. R. H. Badgley and J. M Tessarzik, "Experimental Evaluation of the Exact Point-Speed and Least-Squares Procedures for Flexible Rotor Balancing by the Influence Coefficient Method," ASME Paper 73-DET-115, 1973. Also *Flexible Rotor Balancing by the*

Influence Coefficient Method, Part I: Evaluation of the Exact Point-Speed and Least Squares Procedures, by J. M. Tessarzik, NASA-CR-121107, 1972.

21. J. W. Lund and F. K. Orcutt, "Calculations and Experiments on the Unbalance Response of a Flexible Rotor," *Trans. ASME*, Ser. B, *J. Eng. Ind.* 89(4), 785—796 (1967). ASME Paper 67-Vibr-27.

22. J. M. Tessarzik, *Flexible Rotor Balancing by the Influence Coefficient Method—Multiple Critical Speeds With Rigid or Flexible Supports*, MTI Tech. Report MTI-75TR3, NASA CR-2553, 1975.

23. J. W. Lund and J. Tonnesen, "Analysis and Experiments on Multi-Plane Balancing of a Flexible Rotor," *Trans. ASME, J. Eng. Ind.* Ser. B, 94, 233—242 (1972).

24. J. Tonnesen, "Further Experiments on Balancing of a High-Speed Flexible Rotor," *ASME Paper*, No. 73-DET-99, 1973: *Trans. ASME*, Ser. B, J. Eng. Ind., 96(2), 431—440 (1974).

25. J. R. Kendig, "Current Flexible Rotor-Bearing System Balancing Techniques Using Computer Simulation," M.S. thesis, Rochester Institute of Technology, 1975. Advisor: N.F. Rieger.

26. J. W. Lund, "The Stability of an Elastic Rotor in Journal Bearings with Flexible Damped Supports," *Trans. ASME*, Ser. E, 32, 911—920.

27. R. E. D. Bishop and G. M. L. Gladwell, "The Vibration and Balancing of an Unbalanced Flexible Rotor," *J. Mech. Eng. Sci.* 1, 66.-67 (1959).

28. J. W. Lund, Mechanical Technology Inc., *Rotor-Bearing Dynamics Design Technology*, Part III," Design Handbook for Fluid Film Type Bearings, Report AFAPL-TR-65-45, May 1965.

29. B. P. Last, "The Balancing of Flexible Turbine and Generator Rotors," *Proc. Inst. Mech. Engrs.* 180(1), 1209—1222 (1965—66).

30. L. Meirovitch, *Analytical Methods in Vibrations* Macmillan Co., New York, 1967.

31. R. E. D. Bishop and A. G. Parkinson, "On the Isolation of Modes in the Balancing of Flexible Shafts," *Proc. Inst. Mech. Engrs.*, 177(16), 811—841 (1963).

32. J. R. Kendig, *Rotor-Bearing Dynamic Analysis and Balancing*, Project Report of Selected Machine Elements course, Rochester Institute of Technology, Rochester, N.Y., 1972.

33. N. F. Rieger, "Bearing-Rotor Dynamics," RPI-MTI Gas Bearing Design Course, Mechanical Technology Inc., Latham, N.Y., 1967.

34. J. Drechsler, "A Combination of Modal Balancing and the Influence Coefficient Method," *Proceedings of the Fourth World Congress on the Theory of Machines and Mechanisms*, Newcastle-on-Tyne, 1975.

CHAPTER 8
FUTURE DEVELOPMENTS IN BALANCING TECHNOLOGY

8.1 Overview of Recent Progress

The rapid growth of balancing technology in recent years has been closely related to a flow of new instrumentation and component developments, the rapid development of electronics technology, and the application of minicomputers and microprocessors. Equally important has been the practical adaptation of procedures for general flexible-rotor balancing, their industrial verification, and the development of balancing standards and criteria.

The objective of new developments in balancing technology is to provide more efficient procedures that will lead to higher balance quality. The attainment of this objective requires

1. Instrumentation capable of acquiring and recording the rotor amplitude and phase signals at convenient rotor locations and at prescribed speeds

2. Signal-processing equipment capable of extracting the needed amplitude and phase-angle data from the incoming sensor signals

3. Sequential procedures that, when programmed into a controlling minicomputer, will process suitable test signals into required balance-weight and phase-angle values

4. Convenient test facilities with drive capability (e.g., spin pit, test cell, machine casing, balance machine).

Instrumentation, software, computer hardware, and facilities for the balancing of rotors have developed rapidly over the past ten years as aspects of the general computer/electronics surge. Rotor balancing received a steady flow of patents for instrumentation from about 1930 onward. As the number of rotating machines placed in service continued to grow, selected patents were consolidated into balancing equipment. An example is the recent consolidation of universal hard-support machines with wattmeter filtering and plane separation, where soft-support machines were previously used. New patents for instrumentation have also brought about the development of ancillary equipment for existing balancer designs. The development of microprocessors for influence coefficient balancing is an example of this evolution. The next step in this process appears to call for an influence coefficient balancing machine. It can also be expected that future balancing machines will incorporate improved microprocessors and computer routines to permit the balancing of more complex rotating machinery (e.g.,

537

more flexible, multibearing rotors). Such instrumentation will likely be packaged in a machine frame, together with multiple readout locations and with readout instrumentation. Microprocessor units incorporating these items are now possible. What remains to be developed are product lines of such equipment for flexible rotors.

8.2 Need for Advanced Balancing Technology

The need for advanced balancing technology is exemplified by the development of aircraft jet engines over the past 20 years. In 1960 all jet engine rotors could be balanced as rigid rotors (class 1 or class 2 rotors): no bending modes occurred within the operating-speed range. Balancing consisted of component balancing, stack balancing with position marking, and final trim balancing in the engine test cell using the easily accessible end planes. Maintenance was straightforward: as the rotor required only two-plane balancing, any problems could be corrected in the end trim planes. Engine developments in the past 20 years have led to substantial power and thrust increases, significant size increases, and greatly increased complexity; an example is the multispool Rolls-Royce Olympus engine. The increased size tends to lower the critical speeds and to make the engine generally more flexible. This means that the modern engine will have mode shapes that involve more bending. There are also likely to be more critical speeds (and more structural vibration modes) in the operating range than for smaller, more rigid engines of the early 1960s.

The balancing of modern (and future) jet engines involves a change from rigid-rotor balancing to flexible-rotor balancing in at least three planes. With multishaft engines and flexible support structures, the point is being approached where *each shaft* will have to be balanced in three planes as a class 3 rotor. This fact will require that access to a midspan trim balancing plane be included in the engine design. This represents a major structural change that, to date, some engine designers have been reluctant to contend with.* As jet engines continue to increase in size and complexity, such changes are inevitable. It seems likely that future engines with multiplane balancing will run more smoothly and quietly, with longer periods between overhauls because of the superior balance quality attainable with multiplane balancing.

Computerization of the balancing process began in the 1960s. The full effect of this dramatic change has not yet been felt, but, as shown by the following examples, many significant developments have already occurred:

---

*The requirement for a midspan balance plane has been repeatedly emphasized by Badgley [1], who has also suggested a correlation between the incidence of engine component failures due to fatigue and the operating unbalance levels in the larger engines.

1. Hand calculators are now available as off-the-shelf items that can perform a two-plane rigid-rotor balance.

2. Online influence coefficient balancing is now available with terminal access to a remote computer. Multiplane flexible-rotor balancing in the field can be performed in this manner by dialing in with a code key.

3. Analog computer hardware has been incorporated into the signal-processing equipment of hard-bearing balancing machines; an example is wattmeter filtering.

4. A stand-alone minicomputer for flexible-rotor balancing is included with the influence coefficient balancing package now being marketed.

These important developments are evidently just the beginning of a basic movement to make rotor balancing a highly computerized procedure in which the operator sets the conditions (speed, vibration amplitude) for a particular balancing operation. The data-taking and storage with preinstalled instrumentation may eventually become a pushbutton procedure. However, the task still remains to manually install and reposition the trial weights and the final balance weights. This can amount to a serious, time-consuming operation, especially as it may involve substantial runup and rundown times. Where an evacuated spin pit must be used (e.g., in the balancing of bladed rotors), the time between runs is further increased by the pumpdown time required to evacuate the chamber. New developments are needed to shorten the times involved or eliminate such steps. Other possibilities may involve procedures in which the present type of trial-weight sequence and associated runup and rundown periods are not required. Such a development would constitute an important advance in flexible-rotor balancing. Procedures of this type are now in use for rigid rotors (the Schenck ABC method), as previously noted. Influence coefficient data banks from history or for rotor types are a further step in this direction: See Section 8.3.

The rapid increase in the size and power of turbine-generators in recent years has stimulated developments in balancing technology, rotor dynamics, and bearing technology. Generator centrifugal stress limitations have promoted rotors with longer spans and lower critical speeds, having more critical speeds within the operating range. Large U.S. generators commonly operate between their second and third criticals; large European machines frequently operate between their third and fourth criticals. Such machines could not have been developed without an improved understanding of shaft dynamics and the related development of multiplane balancing techniques.

The basic technology for multiplane balancing is available, but important refinements are still needed. For instance, dissimilar support

stiffness resulting from bearing stiffness asymmetry, support asymmetry, etc., can cause elliptical whirl orbits. Differences between the major axis mode and the minor axis mode cannot be accurately accommodated by present balancing programs. Moreover, wherever non-linear effects enter the dynamics (e.g., dissimilar shaft stiffness, non-linear foundation or bearing properties), subharmonic resonances enter the shaft dynamic response characteristics. These and other aspects of flexible-rotor balancing remain to be considered in the balancing process.

8.3 Developments in Balancing Techniques

In recent years the development of minicomputers for efficient balancing calculations has evolved concurrently with the development of efficient flexible-rotor balancing methods. Computer methods are now being increasingly incorporated into certain flexible balancing procedures (at least in the influence coefficient method), and, as computer balancing evolves further, it seems certain that special computers (and more efficient balancing computer programs) will also be evolved. This will decrease both the present complexity of the balancing process and the amount of time required to perform the balancing operations, i.e., decreasing the number of hands-on operations.

Modal balancing is a practical technique that, in the hands of a skilled operator, allows an effective rotor balance to be achieved with speed and simplicity. Pure modal balancing has not been adapted for computer calculation as far as is known, though Kendig [2] programmed the constructions given by Moore [3] and applied them to examine the efficiency of flexible-rotor balancing procedures. However, the major restriction in this process—the skill required of the operator—seems destined to keep the modal method from widespread use, when compared with the influence coefficient method. Influence coefficient methods can be applied by relatively unskilled personnel who follow routine instructions once certain basic decisions, such as the selection of balance planes and test speeds, have been made. Such decisions can now be made by the designer—analyst, guided by rotor-response data. Once such decisions have been made, the influence coefficient procedure can be made routine.

It is, however, apparent that the influence coefficient method can be optimized further through the incorporation of modal concepts, and progress in this direction has recently been made by Drechsler [4], and by Darlow et al. [20]. In fact, such optimization is being practiced each time a rotor is run up close to a critical speed and balanced. Although the influence coefficient method does not require the rotor to be run at or near its critical speeds to magnify the shaft modes, the ability to

acquire balancing data which facilitate the efficient suppression of the system principal modes will evidently assist the overall balancing process. Where the modes are lightly damped, this step is easily accomplished by observing the location of the sharp resonances. However, many rotors have heavily damped higher modes in which the amplitudes remain high and fairly constant. In such regions the modes can be difficult to discern, and modal methods can be difficult to apply. Improved procedures for the balancing of rotors operating in such regions are evidently needed.

The many additional flexible-rotor balancing techniques that have been proposed should be mentioned here, together with certain new techniques. New ideas and techniques for flexible-rotor balancing are proposed each year. Many of these propose that influence coefficients for the shaft should be obtained in some manner other than by rotating the shaft—for example, by vibrating the shaft [5] or by calculating the influence coefficients [6,7]. The latter technique can be employed successfully where many rotors of the same general shape and size are to be balanced. A general understanding of the significance of the influence coefficients of a particular configuration can be developed in this manner, and the actual numbers can also be stored in the computer for referral, together with experience gained during previous trial runs. This valuable background with similar rotors has been of use in attaining a satisfactory balance in many applications, sometimes with one trial-weight run. Procedures of this type are now being used and developed in industry.

The development of computer programs that optimize influence coefficient procedures through an understanding of the rotor modes is continuing e.g., [20]. In the long run it seems likely that the increased capabilities of next-generation computers are likely to dilute the effectiveness of such developments, as increases in computer and minicomputer technology appear likely to outstrip flexible-rotor technology demands by a wide margin. For the interim (e.g., five years), optimization of influence coefficient programs will probably continue. An improved understanding of modal methods should lead to further improvements in balancing procedures for flexible rotors. More widespread understanding of rotor modal properties should also lead to improved balancing design approaches and to improved test-stand procedures in selecting balance planes and balance speeds.

8.4 Developments in Balancing Hardware

Signal Processing Equipment

Existing signal-conditioning techniques such as wattmeter filtering, plane separation, etc., have now become necessary for all balancers,

except for certain simple industrial types. These procedures have been incorporated into most balancer consoles, and there are many signal-conditioner patents. Additional signal-processing concepts and equipment for multiplane balancing of flexible rotors remain to be developed, to permit faster and more efficient balancing. New developments are especially needed in the logic circuitry for conveying the additional input data to the central minicomputer of a flexible-rotor balancing machine.

Minicomputers

The minicomputer has become the heart of balancer signal processing. This device may range from a microprocessor for plane separation and digital data display (vectormeter) to a dedicated minicomputer that also serves for data storage, sequencing, digital matrix manipulation, and equation solving. It is now evident that minicomputers can function effectively for semiautomatic balancing, as in the Schenck ABC universal balancer. The effectiveness of a dedicated minicomputer for flexible-rotor balancing has also been demonstrated in the balancer console developed by Mechanical Technology Inc. Further developments are needed to incorporate a multiplane capability into a universal balancer for class 3 rotors and to aid in automating data acquisition and sequencing for multiplane balancing. Related circuit/minicomputer developments for multiplane onsite balancing in the field are also needed. It may be observed that, however efficient the field-balancing process becomes, measurement and correction-plane access along the whole rotor length must always be more convenient in the shop. This indicates that the present procedure of shop balancing followed by onsite trim and correction balancing seems likely to remain. Minicomputers and instruments to improve both shop and field balancing will therefore continue to be needed.

8.5 Advanced Studies in Rotor Dynamics

Linear analysis i now accepted as a reliable basis for rotor-dynamics calculations, and computer programs based on linear rotor analysis and on linearized bearing theory are widely used in the design of rotating machinery. It is, however, recognized that the linearizing assumptions used to make the bearing equations more amenable to analysis can, under certain conditions, give misleading results. The problem then is to anticipate which procedure is most suitable for a given set of circumstances. Apart from personal experience, there is no existing criterion for such a decision.

A general theory of linear rotor dynamics has recently been presented by Bishop and Fawzi [8]. Based on the complex fourth-order

rotor equation developed in Chapter 5 [9], rotor displacements are for-
mulated as modal expansions. This leads to a matrix equation of order
$2n$, where n is the modal number. The bearing properties are also
introduced as a matrix of modal coefficients and are applied at specified
points along the length of the rotor, using the Dirac delta function.
Solutions for unbalance response and stability are then sought from the
particular integral and the complementary function to these equations,
respectively. The formulation is elegant, but no applications to practice
are discussed by the authors.

Modal resolution has also been applied by Black and Nuttall [10] to
a generalized rotor in cross-coupled bearings. The nonconservative
equations of motion are separated by binormal orthogonalization and
solved by modal resolution. The modal resolution procedure is demon-
strated for unbalance response and balancing with a sample calculation.

Finite-element formulations of linear rotor-dynamics problems
have been introduced by Ruhl and Booker [11], Zorzi and Nelson [12],
Thomas and Rieger [13], and others. In general, these approaches have
been used to adapt the rotor problem for solution by advanced linear
structural matrix techniques (e.g., wavefront, QR algorithm). At
present, matrix methods are less efficient for solving rotor problems
because of the large and often nonsymmetrical matrices that must be
manipulated. Transfer matrix methods remain superior for multisec-
tion beam-type rotors. The finite-element method has excellent poten-
tial for nonlinear rotor analyses and for including complicated rotor-
support properties [14]. Steady-state, finite-element studies of journal
bearings with complex geometry have been made by Reddi [15] and by
Allaire [16], and the procedures involved could be adapted for calculat-
ing the dynamic properties of complex bearing shapes such as grooves,
pockets, and inlets.

Giberson [17] developed a nonlinear theory and a computer pro-
gram which solves the complete bearing equations for specified bearing
types from given initial conditions, which give nonlinear whirl orbit
results for the rotor. Such calculations require more computer time
than do corresponding linear system calculations. Calculations for a
general stepped cylindrical rotor in two multiarc bearings of any type
can be made in this manner. Results for unbalance-response spectra,
transmitted-force spectra, and stability orbit plots can be obtained with
this program. Rotor response to nonrotating forces is also available as
an option.

Advanced experimental studies of shaft dynamics and multiplane
balancing have been conducted at the high-speed shaft facility at
Mechanical Technology Inc. (MTI), Latham, New York. This device
consists of a power loop in which one leg is a shaft 28 ft long, 8.0 in. in
diameter, and having a 0.25-in. wall that is designed to rotate at speeds

up to 8500 rpm. This shaft is able to transmit up to 6000 hp and can run through seven critical speeds before reaching its maximum operating speed. Similar experiments were attempted by Baier and Mack [18] in 1969 with a long helicopter drive shaft. The MTI facility can test the capabilities of existing shaft technology and computer codes, applied in a highly advanced situation. For instance, the capabilities of the influence coefficient method are being tested by applying it to the practical balancing of a shaft in up to 10 planes simultaneously. It is evident that, because of the low damping of the rotor system, the balancing procedure must be effective throughout the full operating-speed range, as was observed by earlier experimenters (see, for example, Ref. 19). This test facility will also allow the development of rotor damping devices, together with studies of the practical durability of balance and of components in a shock-prone situation. This unique facility can therefore include each factor likely to influence smooth shaft operation in a general environment: response, stability, balancing, shock response, and damper technology.

8.6 Balance Criteria

Balance criteria and standards for rotating machinery are now available for both rigid and flexible rotors in a developmental form. An important achievement is ISO Document 1940-1973(E), which is now being used to guide rotor balancing and acceptance in member countries of ISO and elsewhere. Rigid rotors represent the majority of all rotors produced. This document therefore represents an important step in ensuring high-quality rotating machinery and in providing guidelines for the reduction of associated vibration and noise.

Provisional criteria for flexible-rotor balancing are now available in ISO Document TC 108/SC 1/18 (1976). Though the criteria values are preliminary, they provide a means for approaching this difficult question, and the values in the tables have been developed from broad practical experience. Flexible rotors frequently represent the most troublesome and time-consuming rotors for balancing. Tables in the flexible-rotor document give guidance for selecting the most suitable balancing procedure and for classifying the rotor. Rotors are classified in terms of machine function (e.g., grinding wheel, jet engine). Most flexible rotors can be suitably balanced for their function in two correction planes. Where two-plane balancing is an acceptable alternative to three-plane balancing, a considerable saving in production costs can be realized. ISO Document TC 108/SC 1/18 (1976) also gives guidance on the balancing techniques most suited to each particular class of rotor.

Work by the ISO Rotor Committee is continuing to devise more adaptable standards of broader scope, and with more general balance criteria values.

8.7 References

1. R. H. Badgley, "Modern Influence Coefficient Techniques for Multiplane Rotor Balancing in the Factory, Test Cell and Field," *Proc. Inst. Mech. Eng., Conference on Vibrations in Rotating Machinery,* Churchill College, Cambridge University, Sept. 15–17, 1976, Paper C189/76.

2. J. R. Kendig, "Comparison of Current Flexible Rotor-Bearing System Balancing Techniques Using Computer Simulation," M.S. thesis, Rochester Institute of Technology, Rochester, N.Y., Nov. 1975.

3. L. S. Moore, "Balancing of Large Turbine Rotors," *Inst. Mar. Engrs. Trans.* 81 (Apr. 1969).

4. J. Drechsler, "Systematic Combination of Experiments and Data Processing in Balancing of Flexible Rotors," *Proc. Inst. Mech. Eng., Conference on Vibrations in Rotating Machinery,* Churchill College, University of Cambridge, Sept. 15–17, 1976, Paper C179/76.

5. A. H. Church and R. Plunkett, "Balancing Flexible Rotors," *Trans. ASME,* Ser. B, *J. Eng. Ind.* 83, No. 4, 383–389 (1961),

6. S. Yanabe and A. Tamura, "Multi-plane Balancing of Flexible Rotor Consisting of Two Disks," *Bull. JSME,* 12, No. 54 (1969).

7. M. S. Hundal and R. T. Harker, "Balancing of Flexible Rotors Having Arbitrary Stiffness and Mass Distribution," *Trans. ASME, J. Eng. Ind.* 88, Ser. B, No. 2, 217–223 (1966); ASME Paper 65-MD-8, 1965.

8. R. E. D. Bishop and I. Fawzi, "A Strategy for Investigating the Linear Dynamics of a Rotor in Bearings," *Proc. Inst. Mech. Eng., Conference on Vibrations in Rotating Machinery,* Churchill College, Cambridge University, Sept. 15–17, 1976, Paper C219/76.

9. R. E. D. Bishop and G. M. L. Gladwell, "The Vibration and Balancing of an Unbalanced Flexible Rotor," *J. Mech. Eng. Sci.* 1, No. 1 (1959).

10. H. F. Black and S. M. Nuttall, "Modal Resolution and Balancing of Synchronous Vibrations in Flexible Rotors with Non-conservative Cross Coupling," *Proc. Inst. Mech. Eng., Conference on Vibrations in Rotating Machinery,* Churchill College, Cambridge University, Sept. 15–17, 1976, Paper C182/76.

11. R. L. Ruhl and J. F. Booker, "A Finite Element Model for Distributed Parameter Turborotor Systems," *Trans. ASME*, 94, Ser. B, *J. Engr. Ind.*, 126–132 (1972).

12. E. S. Zorzi and H. D. Nelson, "Finite Element Simulation of Rotor Bearing Systems with Internal Damping," ASME Paper 76-GT-89, Gas Turbine Conference, New Orleans, Mar. 1976.

13. C. B. Thomas and N. F. Rieger, "Dynamic Stiffness Matrix Approach for Rotor Bearing System Analysis," *Proc. Inst. Mech. Eng., Conference on Vibrations in Rotating Machinery*, Churchill College, Cambridge University, Sept. 15–17, 1976, Paper C187/76. See also C. B. Thomas, "A Unified Matrix Formulation for the Unbalanced Response of a Flexible Rotor in Fluid-Film Bearings," M.S. thesis, Rochester Institute of Technology, Rochester, N.Y., July 1974.

14. G. Diana, N. Bachsmid, B. Pizzigone, and F. Di Pasquantonio, "A Method for Investigating the Dynamic Behaviour of a Turbomachinery Shaft on a Foundation," ASME Paper 77-DET-16, Sept. 1977.

15. M. M. Reddi, "Finite Element Solution of the Steady-State Compressible Lubrication Problem," *Trans. ASME*, Ser. F, *J. Lubr. Technol.*, 91, No. 3 (1969).

16. P. E. Allaire, *Finite Element Analysis of Fluid Film Bearings*, Report ME-543-120-75, University of Virginia Research Laboratories of the Engineering Sciences, Charlottesville, Va., Aug. 1975.

17. M. F. Giberson, proprietary computer program, Turbo Research, Inc., Lionville, Pa., 1972.

18. R. Baier and J. Mack, *Design and Test Evaluation of a Supercritical Speed Shaft*, USAAVLABS Technical Report 66-49/R458, Boeing Co., Vertol Division, Morton, Pa., June 1966.

19. J. E. Voorhees, H. S. Meacham, J. B. Day, and D. E. Close, *Design Criteria for High-Speed Power-Transmission Shafts*, Part II, "Development of Design Criteria for Supercritical Shaft Systems," Technical Report ASD-TDR 62-728, Battelle Memorial Institute, Dec. 1964.

20. M. S. Darlow, A. J. Smalley, and A. G. Parkinson, "Demonstration of a Unified Approach to Balancing of Flexible Rotors," *J. Engrg. Power, Trans. ASME*, 103(1), pp 101-107 (Jan. 1981).

APPENDIX
STIFFNESS AND DAMPING COEFFICIENTS FOR
FLUID-FILM JOURNAL BEARINGS

General

Journal bearings frequently exert a significant influence on the dynamics of rotors. A useful procedure for representing the dynamic properties of fluid-film journal bearings is to replace the fluid film by an equivalent set of eight stiffness and damping coefficients, by which the small, linear motions of the journal may be related to the steady-state equilibrium position of the journal within the bearing clearance. This representation allows the fluid-film dynamic forces acting on the journal to be calculated. Other procedures also exist for examining the journal motion within the bearing, involving direct integration of the rotor-bearing equations in time.

This appendix describes procedures for obtaining the stiffness and damping coefficients of certain common types of journal bearings. Charts of bearing dynamic coefficients are included, together with sample calculations illustrating their use. Analytical procedures for obtaining bearing dynamic data have been described by Pinkus and Sternlicht [1], Lund and Sternlicht [2], Shapiro and Rumbarger [3], and others. Additional sources of data on dynamic coefficients are given in the text.

Principle of Operation

Hydrodynamic bearings operate by creating a convergent wedge of fluid between the bearing and journal surfaces, shown in Fig. 1. Consider the case of a plain cylindrical journal that rotates within a plain stationary bearing with an incompressible lubricant, under the following assumptions:

1. The fluid-film radial thickness is very small compared with the bearing length and breadth dimensions.
2. No pressure variation occurs across the lubricant film thickness, i.e., $\partial p / \partial h = 0$.
3. The lubricant flow within the film is laminar and continuous at all points (no cavitation or bubbles).
4. Inertia forces are negligible in comparison with the viscous forces within the film.

547

5. No slip occurs between the lubricant and the bearing or journal surfaces.

It has been shown by Pinkus and Sternlicht [1] that, subject to these assumptions, the flow of lubricant within the clearance is governed by the Reynolds equation. For the geometry of Fig. 1, this is

$$\frac{\partial}{\partial \theta}\left[h^3 \frac{\partial p}{\partial \theta}\right] + R^2 \frac{\partial}{\partial z}\left[h^3 \frac{\partial p}{\partial z}\right] = 6\mu R \frac{\partial h}{\partial \theta} U + 12\mu R^2 V$$

where

h = bearing film thickness at angle θ
    = $C + e \cos \theta = C(1 + \epsilon \cos \theta)$
ϵ = e/C, bearing eccentricity ratio
U = tangential velocity component of the journal surface
V = radial velocity component of the journal surface
e = eccentricity of the journal along the line of centers, OO'
C = machined *radial* clearance between the journal
    diameter and the bearing diameter
ϕ = attitude angle between vertical and line
    of centers
θ = angle from line of centers to position in film.
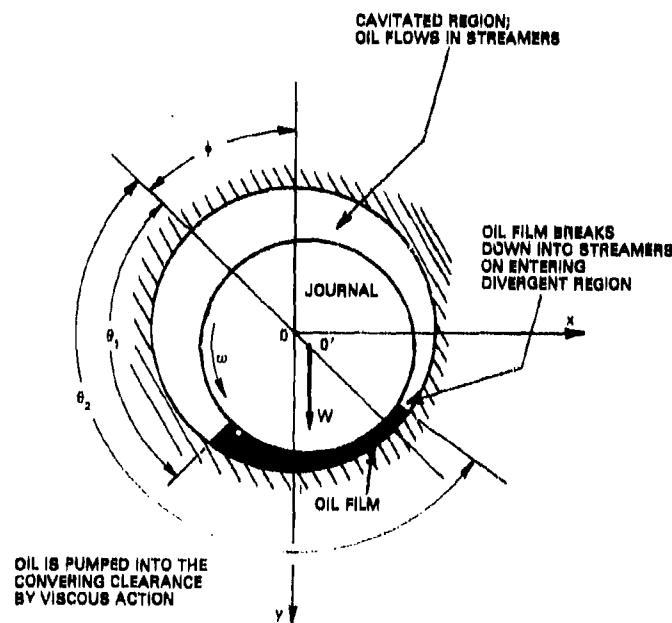
Fig. 1. Hydrodynamic action in plain cylindrical bearing

Bearing Dynamic Operation Conditions

Consider the dynamically loaded journal rotating in the bearing shown in Fig. 2. If the bearing surface is fixed and immovable, the shaft center alone will have the following instantaneous radial and tangential velocities under dynamic loading conditions:

$$V_r = C \frac{d\epsilon}{dt}$$

and

$$V_t = \epsilon \frac{d(\psi + \phi)}{dt}.$$
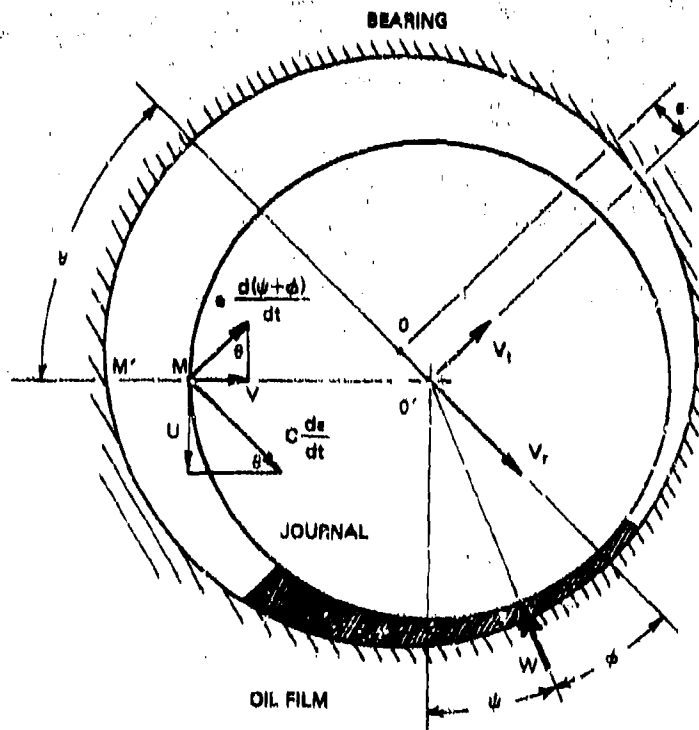
Fig. 2. Dynamically loaded journal bearing showing velocities and load vector. After Pinkus and Sternlicht [1].

At any point M on the bearing surface, a distance θ from the line 00', there will be tangential and normal velocities U, V relative to M' on the surface of the bearing. These velocities are made up of the shaft center velocity components given above plus the shaft surface velocity about its own center:

$$U = R\omega + C \frac{d\epsilon}{dt} \sin\theta - C\epsilon \frac{d(\psi + \phi)}{dt} \cos\theta$$

and

$$V = C \frac{d\epsilon}{dt} \cos\theta + C\epsilon \frac{d(\psi + \phi)}{dt} \sin\theta.$$

Now $(C/R) << 2$ (always) and $(\epsilon/R) << 2 \cos\theta$ (commonly). Write

$$2C\epsilon \frac{d(\psi + \phi)}{dt} \sin\theta = -2 \frac{d(\psi + \phi)}{dt} \frac{dh}{d\theta} = -2 \dot\alpha \frac{dh}{d\theta},$$

where $\alpha = \psi + \phi$, and

$$6U\mu R \frac{\partial h}{\partial\theta} = 6\mu R (R\omega + C\dot\epsilon \sin\theta - C\epsilon\dot\alpha \cos\theta)(-C\epsilon \sin\theta)$$

$$\approx 6\mu R (R\omega)(-C\epsilon \sin\theta),$$

and

$$12\mu R^2 V = 12\mu R^2 [C\dot\epsilon \cos\theta - \dot\alpha(-\epsilon C \sin\theta)]$$

$$= 6\mu R [2CR\dot\epsilon \cos\theta + 2\epsilon CR\dot\alpha \sin\theta].$$

The right-hand side of the time-dependent Reynolds equation can be written as

$$6\mu R \frac{\partial h}{\partial\theta} U + 12\mu R^2 V = 6\mu R^2 C[-\epsilon(\omega - 2\dot\alpha) \sin\theta + 2\dot\epsilon \cos\theta].$$

The total expression for the dynamic pressure distribution is then

$$\frac{\partial}{\partial\theta}\left[\frac{h^3}{C^3} \frac{\partial p}{\partial\theta}\right] + R^2 \frac{\partial}{\partial z}\left[\frac{h^3}{C^3} \frac{\partial p}{\partial z}\right]$$

$$= 6\mu\left(\frac{R}{C}\right)^2 [\epsilon(2\dot\alpha - \omega) \sin\theta + 2\dot\epsilon \cos\theta]$$

This expression holds throughout the bearing clearance, wherever the fluid film is continuous.

Linear Form of the Bearing Dynamic Equation

The time-dependent Reynolds equation can be written in the form

$$\frac{\partial}{\partial x}\left(\frac{h^3}{\mu}\frac{\partial p}{\partial x}\right) + \frac{\partial}{\partial z}\left(\frac{h^3}{\mu}\frac{\partial p}{\partial z}\right) = 6R\omega\left(1 - 2\frac{\dot{\alpha}}{\omega}\right)\frac{\partial h}{\partial x} + 12\dot{e}\cos\theta$$

$$(x = R\theta).$$

where $x = R\theta$. Introducing the dimensionless parameters

$$x = D\bar{x}, \quad z = L\bar{z}, \quad h = 2C\bar{h}, \quad h = \frac{1}{2}C(1 + \epsilon\cos\theta), \quad e = C\epsilon,$$

$$p = \frac{\mu\omega}{2\pi}\left(\frac{R}{C}\right)^3\bar{p},$$

and assume constant viscosity through the fluid film. The above parameters lead to the dimensionless Reynolds equation:

$$\frac{\partial}{\partial\bar{x}}\left(\bar{h}^3\frac{\partial\bar{p}}{\partial\bar{x}}\right) + \left(\frac{D}{L}\right)^2\frac{\partial}{\partial\bar{z}}\left(\bar{h}^3\frac{\partial\bar{p}}{\partial\bar{z}}\right) = 6\pi\frac{\partial\bar{h}}{\partial\bar{x}} + 12\pi\frac{\dot{e}/\omega}{(1 - 2\dot{\alpha}/\omega)}\cdot\cos\theta$$

The resulting fluid-film force is then the integral of the pressure over the load-carrying film in the α-direction:

$$F_\alpha = \mu N\left(1 - 2\frac{\dot{\alpha}}{\omega}\right)\left(\frac{R}{C}\right)^2 DL\int_0^1\int_0^\pi P\cos(\theta + \alpha)\,dx\,dz$$

$$= \lambda\omega\left(1 - 2\frac{\dot{\alpha}}{\omega}\right)f_\alpha\left(\frac{L}{D}, \epsilon, \alpha, \frac{\dot{e}/\omega}{(1 - 2\dot{\alpha}/\omega)}\right),$$

where

$$\lambda = \frac{\mu RL}{\pi}\left(\frac{R}{C}\right)^2.$$

Stiffness and Damping Coefficients

The required formulation of fluid-film dynamic properties in terms of displacement ("stiffness") coefficients and velocity ("damping") coefficients can be obtained by making a first-order Taylor-series expansion of the above force expression, above the journal steady-state ("static") equilibrium position:

$$dF_\alpha = \lambda\omega\left(1 - 2\frac{\dot\alpha}{\omega}\right)\left[\frac{\partial f_\alpha}{\partial\epsilon}\,d\epsilon + \frac{1}{\epsilon}\,\frac{\partial f_\alpha}{\partial\alpha}\,\epsilon\,d\alpha\right.$$

$$\left. + \frac{\partial f_\alpha}{\partial\left(\dfrac{\dot\epsilon}{\omega}\right)}\cdot d\left(\frac{\dot\epsilon}{\omega}\right) - \frac{2}{\epsilon}\,\frac{f_\alpha}{\omega}\,\epsilon\,d\dot\alpha\right]$$

To simplify, write

$$\frac{\partial f_\alpha}{\partial\left(\dfrac{\dot\alpha}{\omega}\right)} = \frac{\partial f_\alpha}{\partial\left[\dfrac{\dot\epsilon}{\omega}\,\Big/\,\left(1 - 2\dfrac{\dot\alpha}{\omega}\right)\right]}\;\frac{\partial\left[\dfrac{\dot\epsilon}{\omega}\,\Big/\,\left(1 - 2\dfrac{\dot\alpha}{\omega}\right)\right]}{\partial\left(\dfrac{\dot\alpha}{\omega}\right)}$$

$$= \frac{\partial f_\alpha}{\partial\left[\dfrac{\dot\epsilon}{\omega}\,\Big/\,\left(1 - 2\dfrac{\dot\alpha}{\omega}\right)\right]}\;\frac{2\dfrac{\dot\epsilon}{\omega}}{\left(1 - 2\dfrac{\dot\alpha}{\omega}\right)^2}.$$

At the equilibrium position $\dot\epsilon = 0$ and $\dot\alpha = 0$.

For a cylindrical bearing, the dynamic force is expressed in terms of radial and tangential components dF_r and dF_t. The required expressions are also obtained as Taylor-series expressions:

$$dF_r = \lambda\omega\left[\frac{\partial f_r}{\partial\epsilon}\,d\epsilon + \frac{\partial f_r}{\epsilon\,\partial r}\,\epsilon\,dr + \frac{\partial f_r}{\partial(\dot\epsilon/\omega)}\,d\left(\frac{\epsilon}{\omega}\right) - \frac{2f_r}{\epsilon\omega}\,\epsilon\,d\dot r\right]$$

and

$$dF_t = \lambda\omega\left[\frac{\partial f_t}{\partial\epsilon}\,d\epsilon + \frac{\partial f_t}{\epsilon\,\partial t}\,\epsilon\,dt + \frac{\partial f_t}{\partial(\dot\epsilon/\omega)}\,d\left(\frac{\dot\epsilon}{\omega}\right) - \frac{2f_t}{\epsilon\omega}\,\epsilon\,d\dot t\right].$$

To relate these expressions to Cartesian coordinates, write

$$F_x = -F_r\cos\alpha - F_t\sin\alpha$$

and

$$F_y = -F_r\sin\alpha + F_t\cos\alpha.$$
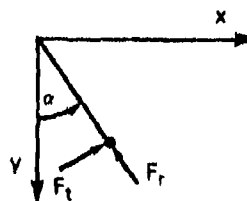
For small-amplitude motions,

$$dF_x = -dF_r \cos \alpha + F_r \sin \alpha \, d\alpha - dF_t \sin \alpha - F_t \cos \alpha \, d\alpha$$

and

$$dF_y = -dF_r \sin \alpha - F_r \cos \alpha \, d\alpha + dF_t \cos \alpha - F_t \sin \alpha \, d\alpha.$$

Furthermore,

$$x = C\epsilon \cos \alpha, \quad d\epsilon = \frac{1}{C} (\cos \alpha \, dx + \sin \alpha \, dy),$$

$$y = C\epsilon \sin \alpha, \quad \epsilon \, d\alpha = \frac{1}{C} (-\sin \alpha \, dx + \cos \alpha \, dy).$$

Substituting and simplifying give

$$dF_x = -K_{xx} \, dx - B_{xx} \, d\dot{x} - K_{xy} \, dy - B_{xy} \, d\dot{y}$$

and

$$dF_y = -K_{yx} \, dx - B_{yx} \, d\dot{x} - K_{yy} \, dy - B_{yy} \, d\dot{y},$$

where

$$K_{xx} = \frac{1}{C}\lambda\omega \left[\frac{\partial f_r}{\partial \epsilon} \cos^2 \alpha + \frac{f_r}{\epsilon} \sin^2 \alpha + \left(\frac{-f_t}{\epsilon} + \frac{\partial f_t}{\partial \epsilon} \right) \cos \alpha \sin \alpha \right],$$

$$\omega B_{xx} = \frac{1}{C}\lambda\omega \left\{ \frac{2f_r}{\partial(\dot{\epsilon}/\omega)} \cos^2 \alpha + \frac{2f_t}{\epsilon} \sin^2 \alpha + \left[\frac{2f_r}{\epsilon} + \frac{\partial f_t}{\partial(\dot{\epsilon}/\omega)} \right] \right.$$

$$\left. \times \cos \alpha \sin \alpha \right\},$$

$$K_{xy} = \frac{1}{C}\lambda\omega \left[\frac{-f_t}{\epsilon} \cos^2 \alpha - \frac{\partial f_t}{\partial \epsilon} \sin^2 \alpha + \left(\frac{f_r}{\epsilon} - \frac{\partial f_r}{\partial \epsilon} \right) \cos \alpha \sin \alpha \right],$$

$$\omega B_{xy} = \frac{1}{C}\lambda\omega \left\{ \frac{2f_r}{\epsilon} \cos^2 \alpha - \frac{\partial f_t}{\partial(\dot{\epsilon}/\omega)} \sin^2 \alpha + \left[\frac{2f_t}{\epsilon} - \frac{\partial f_r}{\partial(\dot{\epsilon}/\omega)} \right] \right.$$

$$\left. \times \cos \alpha \sin \alpha \right\},$$

$$K_{yx} = \frac{1}{C}\lambda\omega\left[\frac{\partial f_t}{\partial\epsilon}\cos^2\alpha + \frac{f_t}{\epsilon}\sin^2\alpha + \left(\frac{f_r}{\epsilon} - \frac{\partial f_r}{\partial\epsilon}\right)\cos\alpha\sin\alpha\right],$$

$$\omega B_{yx} = \frac{1}{C}\lambda\omega\left\{\frac{\partial f_t}{\partial(\dot\epsilon/\omega)}\cos^2\alpha - \frac{2f_r}{\epsilon}\sin^2\alpha + \left[\frac{2f_t}{\epsilon} - \frac{\partial f_r}{\partial(\dot\epsilon/\omega)}\right]\right.$$

$$\left.\times\cos\alpha\sin\alpha\right\},$$

$$K_{yy} = \frac{1}{C}\lambda\omega\left[\frac{f_r}{\epsilon}\cos^2\alpha + \frac{\partial f_r}{\partial\epsilon}\sin^2\alpha - \left(\frac{-f_t}{\epsilon} + \frac{\partial f_t}{\partial\epsilon}\right)\cos\alpha\sin\alpha\right],$$

$$\omega B_{yy} = \frac{1}{C}\lambda\omega\left\{\frac{2f_t}{\epsilon}\cos^2\alpha + \frac{\partial f_r}{\partial(\dot\epsilon/\omega)}\sin^2\alpha - \left[\frac{2f_r}{\epsilon} + \frac{\partial f_t}{\partial(\dot\epsilon/\omega)}\right]\right.$$

$$\left.\times\cos\alpha\sin\alpha\right\},$$

and where dF_x, dF_y, dx, dy, $d\dot{x}$, $d\dot{y}$ represent small harmonic forces, displacements, and velocities, respectively, about the journal equilibrium position. These expressions are calculated numerically with a digital computer, subject to specified fluid-film and geometric boundary conditions.

Numerical Solution of the Reynolds Equation

For finite-length bearings the customary procedure is to express the Reynolds equation as a set of finite difference equations each corresponding to a nodal point i, j in a mesh, as shown in Fig. 3. These equations are then solved on a computer. Local pressure is the unknown in each equation. The finite-difference formulation may include the pointwise variation of film thickness, viscosity, temperature, etc.

For an incompressible lubricant, the dimensionless steady-state Reynolds equation is:

$$\frac{\partial}{\partial\theta}\left(\bar{h}^3\frac{\partial\bar{p}}{\partial\theta}\right) + \left(\frac{D}{L}\right)^2\frac{\partial}{\partial\bar{z}}\left(\bar{h}^3\frac{\partial\bar{p}}{\partial\bar{z}}\right) = 6\pi\frac{\partial\bar{h}}{\partial\theta}$$

where

$$\bar{z} = \frac{z}{L}, \quad \bar{h} = \frac{h}{C} = 1 + \epsilon\cos\theta, \quad \epsilon = \frac{e}{C}, \quad \bar{p} = \frac{p}{\mu N}\left(\frac{C}{R}\right)^2,$$

(a) Finite-difference gridwork   (b) Typical node
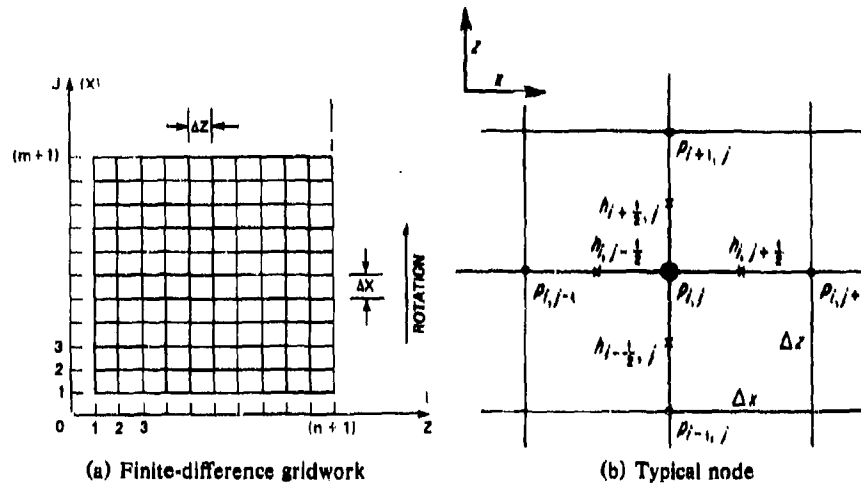
Fig. 3. Finite-difference grid for solving the Reynolds equation

In finite-difference form,

$$\frac{\partial}{\partial \theta}\left(\bar{h}^3 \frac{\partial \bar{p}}{\partial \theta}\right) = \frac{\bar{h}^3_{i,j+1/2}\dfrac{\bar{p}_{i,j+1} - \bar{p}_{i,j}}{R\Delta\theta} - \bar{h}^3_{i,j-1/2}\dfrac{\bar{p}_{i,j} - \bar{p}_{i,j-1}}{R\Delta\theta}}{R\Delta\theta},$$

$$\frac{\partial}{\partial \bar{z}}\left(\bar{h}^3 \frac{\partial \bar{p}}{\partial \bar{z}}\right) = \frac{\bar{h}^3_{i+1/2,j}\dfrac{\bar{p}_{i+1,j} - \bar{p}_{i,j}}{\Delta\bar{z}} - \bar{h}^3_{i,j-1/2}\dfrac{\bar{p}_{i,j} - \bar{p}_{i-1,j}}{\Delta\bar{z}}}{\Delta\bar{z}},$$

and

$$\frac{\partial \bar{h}}{\partial \theta} = \frac{h_{i,j+1/2} - h_{i,j-1/2}}{R\Delta\theta}.$$

Substituting gives

$$p_{ij} = \frac{\left\{6\pi\left[\dfrac{h_{i,j-1/2} - h_{i,j+1/2}}{R\Delta\theta}\right] + \left(\dfrac{D}{L}\right)^2\left[h^3_{i+1/2,j}\dfrac{p_{i+1,j}}{(\Delta\bar{z})^2} + h_{i-1/2,j}\dfrac{p_{i-1,j}}{(\Delta\bar{z})^2}\right] + h^3_{i,j+1/2}\dfrac{p_{i,j+1}}{(R\Delta\theta)^2} + h_{i,j-1/2}\dfrac{p_{i,j-1}}{(R\Delta\theta)^2}\right\}}{\left\{\left(\dfrac{D}{L}\right)^2\dfrac{h^3_{i+1/2,j} + h^3_{i-1/2,j}}{(\Delta\bar{z})^2} + \dfrac{h^3_{i,j+1/2} + h^3_{i,j-1/2}}{(R\Delta\theta)^2}\right\}}.$$

For any point i, j in the mesh shown in Fig. 3, the h-values are constant and the above expression has the form

$$p_{i,j} = a_0 + a_1 p_{i+1,j} + a_2 p_{i-1,j} + a_3 p_{i,j+1} + a_4 p_{i,j-1},$$

where a_0, a_1, a_2, a_3, and a_4 are constants. In this manner, the pressure at any location i, j is specified in terms of the pressures at the adjacent nodes in the mesh. The solution of the Reynolds equation is then reduced to the solution of a corresponding set of simultaneous equations. The time-dependent Reynolds equation can be handled in a similar manner.
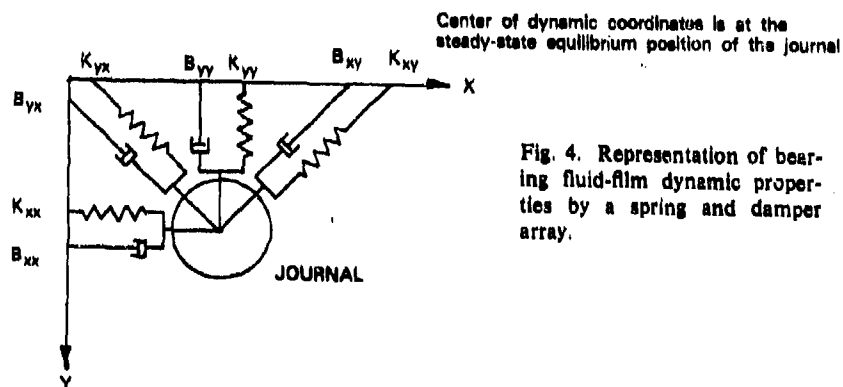
Fig. 4. Representation of bearing fluid-film dynamic properties by a spring and damper array.

Center of dynamic coordinates is at the steady-state equilibrium position of the journal

Charts of Bearing Stiffness and Damping Coefficients

The dynamic force acting on a journal that is displaced a small distance from its equilibrium position is related to the coordinate dynamic amplitudes and velocities of the journal motions by the expressions

$$- F_x = K_{xx} x + K_{xy} y + B_{xx} \dot{x} + B_{xy} \dot{y}$$

and

$$- F_y = K_{yx} x + K_{yy} y + B_{yx} \dot{x} + B_{yy} \dot{y},$$

F_x, F_y — dynamic force components acting in the directions shown in Fig. 4
x, y — journal dynamic displacements in the coordinate directions
$\dot{x}, \dot{y}$ — journal velocities in the coordinate directions.

The K terms are stiffness coefficients of the fluid film that relate journal displacement to force, and the B terms are velocity coefficients of the fluid film that relate journal velocity to force.

The cross-coupling terms K_{xy}, K_{yx}, B_{xy}, B_{yx} relate the journal displacement and velocity in one coordinate direction to the force that

occurs in the other coordinate direction. The total coordinate forces which result from journal motion within the bearing are obtained as the sum of the effects indicated above.

Figures 5 through 8 are charts of stiffness and damping coefficients vs Sommerfeld number for the plain cylindrical bearing and for the tilting-pad bearing. These charts are taken from design data given by Lund [4]. This reference contains stiffness and damping data on a variety of bearing types. The dynamic bearing coefficient charts given herein apply to bearings with an L/D ratio of 0.5. The tilting-pad bearing charts are for a four-pad bearing with an applied load acting on the bottom pad, and with an applied load acting between the lower pads. These charts represent typical dynamic coefficient data for each of the bearing types shown. Bearings with other proportions, other L/D values, pad preload, etc., would be represented by data of similar form but with different numerical values. The tilting-pad bearing charts shown are for the case of zero preload. The effect of pad preload is discussed by Lund [5].

$$s = \frac{\mu NDL}{W}\left(\frac{R}{C}\right)^2$$
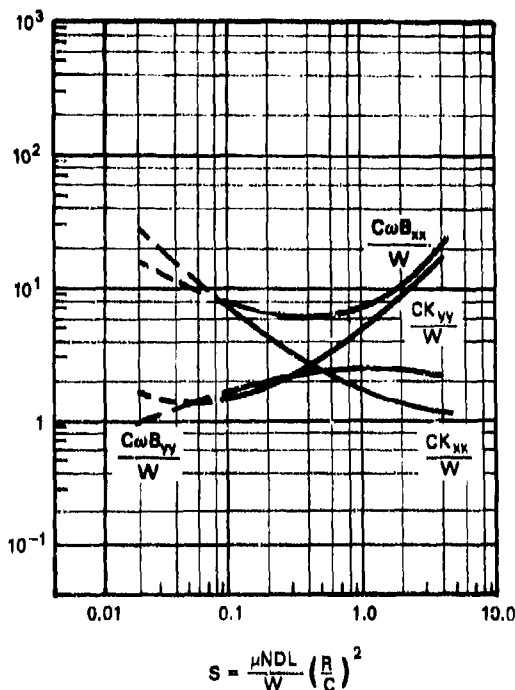
Fig. 5. Dimensionless stiffness and damping coefficients for a plain cylindrical bearing ($L/D = 0.5$). From Lund [4].

$$S = \frac{\mu NDL}{W} \left(\frac{R}{C}\right)^2$$
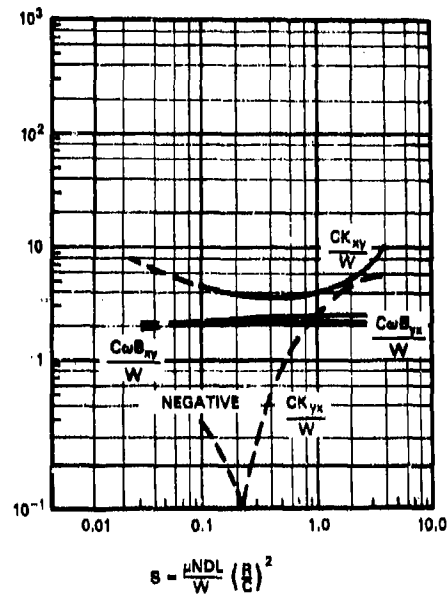
Fig. 6. Dimensionless stiffness and damping coefficients for a plain cylindrical bearing ($L/D = 0.5$). From Lund [4].

$$S = \frac{\mu NDL}{W} \left(\frac{R}{C}\right)^2$$
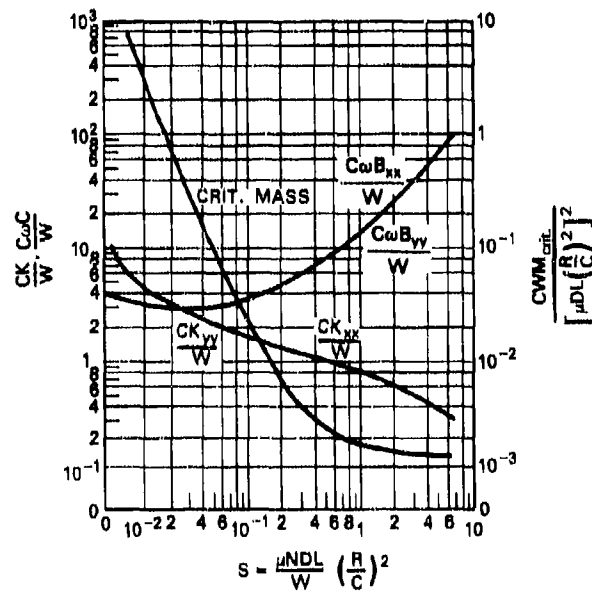
Fig. 7. Dimensionless stiffness and damping coefficients for a tilting-pad bearing ($L/D = 0.5$), load between lower pads. From Lund [4].
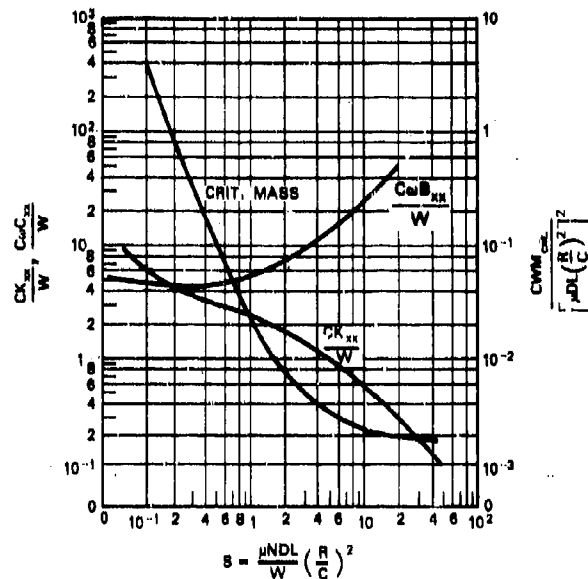
Fig. 8.   Dimensionless stiffness and damping coefficients for a tilting-pad bearing ($L/D = 0.5$), load on the lower pad. From Lund [4].

Most bearing types possess a full set of eight dynamic coefficients. This indicates that considerable cross-coupling exists between the coordinate motions (see, for example, the plain cylindrical bearing data in Figs. 5 and 6). An exceptional case is the tilting-pad bearing that has only four dynamic coefficients and zero cross-coupling effect, as indicated in Figs. 7 and 8.

This absence of cross-coupling between the coordinate motions of the tilting-pad bearing results from the freedom of each pad to "track" the shaft motions, virtually independently of the other pad motions. This absence of cross coupling confers a high instability threshold speed on the tilting-pad bearing.

Procedure for Calculating Bearing Dynamic Coefficients

Step 1 in the procedure is to calculate the Sommerfeld number $S = (\mu NLD/W)(R/C)^2$ for the specified bearing operating conditions. A lubricant viscosity appropriate to the bearing outlet temperature should be used.

Step 2 is to select the bearing-parameters chart that relates to the bearing type and L/D ratio. Allowance should be made for the effect of any bearing grooving on the L/D ratio.

In step 3, the appropriate Sommerfeld number values are entered into the charts, and the corresponding values of bearing dimensionless coefficients, $\bar{K}_{xx}$, etc., are read.

The required dimensional values of the bearing coefficients are then obtained as follows:

$$\bar{K}_{xx} = \frac{K_{xx}C}{W}, \quad K_{xx} = \bar{K}_{xx}\left(\frac{W}{C}\right), \text{ etc.}$$

and

$$\bar{B}_{xx} = \frac{B_{xx}\omega C}{W}, \quad B_{xx} = \bar{B}_{xx}\left(\frac{W}{C}\right)\frac{1}{\omega}, \text{ etc.,}$$

where K_{xx} is the bearing stiffness coefficient in the x-direction, etc., B_{xx} is the bearing velocity damping coefficient in the x-direction, etc., C is the bearing nominal radial clearance, W is the steady applied load on the journal, and ω is the circular rotational frequency (rad/s) of the journal.

Example

Find the stiffness and damping coefficients for a plain cylindrical bearing with a diameter of 4.00 in., a length of 2.0 in., and a machined diametrical clearance of 0.004 in. The journal operates at 3000 rpm with oil at a viscosity of 1.10^{-6} lb s/in.^{2}, an oil outlet temperature of 180°F, and an applied steady load of 1200 lb.

1. The Sommerfeld number is obtained from

$$S = \frac{\mu NLD}{W}\left(\frac{R}{C}\right)^2 = \frac{(10^{-6})(50)(2)(4)}{1200}\left(\frac{2}{2 \times 10^{-3}}\right)^2 = 0.333.$$

2. Figures 5 and 6 are parameter charts for an L/D ratio of 0.5.

3. The required dimensionless stiffness and damping coefficients for $S = 0.333$ and $L/D = 0.5$ are

$\bar{K}_{xx}$	$\bar{K}_{xy}$	$\bar{K}_{yx}$	$\bar{K}_{yy}$	$\bar{B}_{xx}$	$\bar{B}_{xy}$	$\bar{B}_{yx}$	$\bar{B}_{yy}$
3.35	3.75	−0.25	2.10	6.45	2.14	2.14	2.34

4. The dimensional stiffness and damping coefficient values are

$$K_{xx} = \bar{K}_{xx}\left(\frac{W}{C}\right) = (3.35)\frac{1200}{2 \times 10^{-3}} = 2.01 \times 10^6 \text{ lb/in.}$$

and

$$B_{xx} = \bar{B}_{xx}\left(\frac{W}{C\omega}\right) = (6.45)\left(\frac{1}{314.1}\right)\frac{1200}{2\times10^{-3}} = 12,320 \text{ lb s/in.}$$

$\dfrac{K_{xx}}{2.01\times10^6}$	$\dfrac{K_{xy}}{2.25\times10^6}$	$\dfrac{K_{yx}}{-0.15\times10^6}$	$\dfrac{K_{yy}}{1.25\times10^6}$

$\dfrac{B_{xx}}{12,320}$	$\dfrac{B_{xy}}{4087}$	$\dfrac{B_{yx}}{4087}$	$\dfrac{B_{yy}}{4469}$.

These values apply for given Sommerfeld number conditions *only*. If any change occurs in outlet temperature, load, speed, etc., the bearing dynamic coefficient values will also change from those given above.

Approximate Bearing Dynamic Coefficients

The Ockvirk short-bearing theory [6] can be extended to give approximate expressions for bearing stiffness and damping coefficients. Expressions for the plain cylindrical bearing developed by Morrison [7] and Smith [8] are given below. Operating parameters for a plain cylindrical bearing with a 180°F oil film, are given below.

The relation between Sommerfeld number and eccentricity ratio is:

$$C_n = S\left(\frac{L}{D}\right)^2 = \frac{(1-\epsilon^2)^2}{\pi\epsilon[\pi^2(1-\epsilon^2)+16\epsilon^2]^{1/2}}.$$

Static load capacity:

$$W = \frac{\pi}{4}\frac{\mu RNL^3}{C^2}\frac{\epsilon^2}{(1-\epsilon^2)^2}[\pi^2(1-\epsilon^2)+16\epsilon^2]^{1/2}.$$

Journal friction force:

$$F = \frac{2\pi\mu NR^2}{C}\frac{2\pi}{(1-\epsilon^2)^{1/2}}.$$

Oil flow-through clearance:

$$Q = 2\pi NRC\epsilon L.$$

Bearing stiffness coefficients:

$$K_{xx} = \frac{4[\pi^2(1-\epsilon^2)(1+2\epsilon^2)+32\epsilon^2(1+\epsilon^2)]}{(1-\epsilon^2)[\pi^2(1-\epsilon^2)+16\epsilon^2]^{3/2}},$$

$$K_{xy} = \frac{\pi[\pi^2(1 - \epsilon^2)(1 + 2\epsilon^2) + 32\epsilon^2(1 + \epsilon^2)]}{\epsilon(1 - \epsilon^2)^{1/2}[\pi^2(1 - \epsilon^2) + 16\epsilon^2]^{3/2}},$$

$$K_{yx} = \frac{-\pi[\pi^2(1 - \epsilon^2)^2 - 16\epsilon^4]}{\epsilon(1 - \epsilon^2)^{1/2}[\pi^2(1 - \epsilon^2) + 16\epsilon^2]^{3/2}},$$

$$K_{yy} = \frac{4[\pi^2(2 - \epsilon^2) + 16\epsilon^2]}{[\pi^2(1 - \epsilon^2) + 16\epsilon^2]^{3/2}}.$$

Bearing damping coefficients:

$$B_{xx} = \frac{2\pi[\pi^2(1 - \epsilon^2)^2 + 48\epsilon^2]}{\epsilon(1 - \epsilon^2)^{1/2}[\pi^2(1 - \epsilon^2) + 16\epsilon^2]^{3/2}},$$

$$B_{xy} = \frac{8[\pi^2(1 + 2\epsilon^2) - 16\epsilon^2]}{[\pi^2(1 - \epsilon^2) + 16\epsilon^2]^{3/2}},$$

$$B_{yx} = \frac{8[\pi^2(1 + 2\epsilon^2) - 16\epsilon^2]}{[\pi^2(1 - \epsilon^2) + 16\epsilon^2]^{3/2}},$$

$$B_{yy} = \frac{2\pi(1 - \epsilon^2)^{1/2}[\pi^2(1 + 2\epsilon^2) - 16\epsilon^2]}{\epsilon[\pi^2(1 - \epsilon^2) + 16\epsilon^2]^{3/2}}.$$

These expressions are based on the assumption that the lubricant viscosity is constant. Comparison shows that the results obtained with these coefficients are similar to those obtained from the finite bearing theory, for L/D ratios lower than 1.0 and for eccentricity ratios between $\epsilon = 0.2$ and 0.7. The required relationship between the Sommerfeld number and the eccentricity ratio is given above. A chart expressing this relationship for the 180° plain cylindrical bearing [8] is given in Fig. 9.

Example

Calculate the plain cylindrical bearing coefficients for the example given in the preceding section. Compare the results obtained using finite-difference theory and short-bearing theory. Assume that $S = 0.333$ and $L/D = 0.5$. The eccentricity ratio is then found from the expression

$$C_n = S\left(\frac{L}{D}\right)^2 = \frac{(1 - \epsilon^2)^2}{\pi\epsilon[\pi^2(1 - \epsilon^2) + 16\epsilon^2]^{1/2}} = 0.08325.$$

By iteration, $\epsilon = 0.548$.
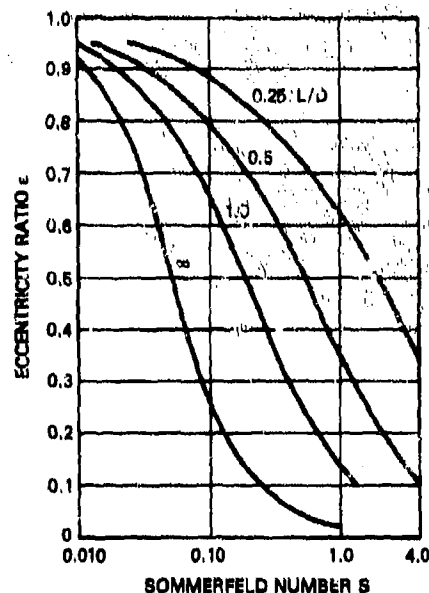
Fig. 9. Variation of eccentricity with the Sommerfeld number for a plain cylindrical bearing, 180° oil film. After Smith [8].

The next step is to evaluate K_{xx}:

$$K_{xx} = \frac{4[\pi^2(1 - \epsilon^2)(1 + 2\epsilon^2) + 32\epsilon^2(1 + \epsilon^2)]}{(1 - \epsilon^2)[\pi^2(1 - \epsilon^2) + 16\epsilon^2]^{3/2}}$$

$$= \frac{4[\pi^2(1 - 0.30)(1 + 0.60) + 32(0.30)(1.30)]}{(1 - 0.30)[\pi^2(1 - 0.30) + 16(0.30)]^{3/2}} = 3.356.$$

Similarly, the other coefficients are found.

Short-bearing coefficients:

$\bar{K}_{xx}$	$\bar{K}_{xy}$	$\bar{K}_{yx}$	$\bar{K}_{yy}$	$\bar{B}_{xx}$	$\bar{B}_{xy}$	$\bar{B}_{yx}$	$\bar{B}_{yy}$
3.356	4.027	−0.582	2.154	4.978	2.195	2.195	2.634

Finite-bearing coefficients [3]:

$\bar{K}_{xx}$	$\bar{K}_{xy}$	$\bar{K}_{yx}$	$\bar{K}_{yy}$	$\bar{B}_{xx}$	$\bar{B}_{xy}$	$\bar{B}_{yx}$	$\bar{B}_{yy}$
3.35	3.75	−0.25	2.10	6.45	2.14	2.14	2.34

The close correlation between these results is reasonably common, provided the L/D and ϵ restrictions mentioned above are not grossly exceeded. Short-bearing representations for partial-arc bearings and for tilting-pad bearings have also been obtained.

The following computer program listing calculates the plain cylindrical bearing dynamic coefficients. The input consists of the Sommerfeld number and the L/D ratio. The program first calculates bearing eccentricity from the Ockvirk parameter $S(L/D) = f(\epsilon)$ given above and then computes the bearing coefficients. The accuracy of typical results is shown above. Short-bearing coefficients were calculated with this program.

Program for Calculating Dynamic Coefficients for a 180° Plain Cylindrical Bearings Using the Short-Bearing Theory

```
1.000            REAL KXX,KXY,KYX,KYY
2.000            IR=105,IW=108
3.000            A1=3.14159265 4
4.000            A2=A1**2
5.000    100     READ(IR,10,END=999) S,ELEN,DIA
5.500            OUTPUT S,ELEN,DIA
6.000            E=0.02
7.000            GO TO 20
8.000    40      E=E-F/FP
9.000    20      A3=E**2
10.000           B1=1.-A3
11.000           B4=B1**2
12.000           C1=16.*A3
13.000           F1=SQRT(A2*B1+C1)
14.000           R=ELEN/DIA
15.000           F=(S*(R**2))-(B4/(A1*E*F1))
16.000           FP=((4.*F1*B1*A3)+(B4*(F1+(A3*6.13/F1))))/(A1*A3*(F1**2))
17.000           IF(ABS(F)-.00001) 30,30,40
18.000    30     SC=((1./R)**2)*((B1**2)/(A1*E*F1))
19.000           OUTPUT 'ENTERED',S,'COPUTED',SC,'ECC.',E,'L/D',R
20.000           B2=1+A3
21.000           B3=SQRT(B1)
22.000           C2=2.*C1
23.000           C3=3.*C1
24.000           D1=1.+2.*A3
25.000           D2=B1+1.
26.000           F2=F1**3.
27.000           G=A2*B1*D1+C2*B2
28.000           G1=E*B3*F2
29.000           G2=A2*D1-C1
30.000           KXX=4.*G/(B1*F2)
31.000           KYY=4.*(A2*D2+C1)/F2
32.000           KXY=A1*G/G1
33.000           KYX=-A1*(A2*B4-C1*A3)/G1
34.000           BXX=2.*A1*(A3*B4+C3)/G1
35.000           BYY=2.*A1*B3*G2/(E*F2)
36.000           BXY=8.*G2/F2
37.000           BYX=BXY
38.000           OUTPUT KXX,KXY,KYX,KYY,BXX,BXY,BYX,BYY
39.000           GO TO 100
39.500    10      FORMAT(3G)
40.000    999     STOP
41.000           END
```

Sample Calculation

$S = 0.333$

$L = 1.0$ in.

$D = 2.0$ in.

```
7.333,1.,2.,
 S = .333000000000000
ELEN = 1.00000000000000
DIA = 2.00000000000000
ENTERED
S = .333000000000000
COPUTED
SC = .333010831895641         Check calculation.
ECC.
E = .547648958337471          Eccentricity ratio
L/D                           joined by Newton's
K = .500000000000000   L/D    method.
KXX = 3.35580600618411
KXY = 4.02678544086108
KYX = -.58151293870671J
KYY = 2.15442321303017
BXX = 4.97745162174338        Results
BXY = 2.19479004851876        q
BYX = 2.19479004851876
BYY = 2.63362917785935
```

References

1. O. Pinkus and B. Sternlicht, *Theory of Hydrodynamic Lubrication*, McGraw-Hill, New York, 1961.
2. J. W. Lund and B. Sternlicht, "Rotor-Bearing Dynamics with Emphasis on Attenuation," *Trans. ASME, Basic Eng.*, 84, 491—502 (1962).
3. W. Shapiro and J. H. Rumbarger, "Bearing Influence and Representation in Rotor Dynamics Analysis," in *Flexible Rotor-Bearing System Dynamics*, New York, 1972.
4. J. W. Lund, *Rotor Bearing Dynamics Design Technology*, Part 3, "Design Handbook for Fluid-Film Type Bearings," Technical Report AFAPL TR-65-45, Air Force Systems Command, Wright-Patterson Air Force Base, Dayton, Ohio, May 1965.
5. J. W. Lund, "Spring and Damping Coefficients for the Tilting-Pad Bearing," *Trans. ASLE*, 7, 342—352 (1964).
6. F. W. Ockvirk, "Short-Bearing Approximation for Full Journal Bearings," N.A.C.A. Technical Note 2808, 1952.

7.   D. Morrison, "Influence of Plain Journal Bearings on Whirling Action of an Elastic Rotor," *Proc. Inst. Mech. Eng.* **176**, 542 (1962).

8.   D. M. Smith, *Journal Bearings in Turbomachinery,* Chapman and Hall Ltd., London, 1969.

BIBLIOGRAPHY

BALANCING

General Topics

Elonka, S., "Balancing Rotating Machinery," *Power* 103, No. 6, 213–226 (1959).

Fletcher, C. N., *The Balancing of Machinery*, Emmet and Co., Ltd., 1931.

Jung, I., "Gustaf De Laval, The High Speeds and the Gear," the Royal Swedish Academy of Engineering Sciences, printed by Stal-Laval Turbine AB, Vasteras, Sweden, De Laval Memorial Lecture, 1968.

Kiuchi, A., "On Vibration Characteristics of Elastically Supported Mechanical System With Non-Uniform Shaft Having Masses on It" (in English) *Bull. JSME* 2, No. 6, 318–323 (1959).

Kroon, R. P., "Balancing of Rotating Apparatus-I," *Trans. ASME, J. Appl. Mech.* 10, A-225 (1943).

Kroon, R. P., "Balancing of Rotating Apparatus-II," *Trans. ASME, J. Appl. Mech.* 11, A-47 (1944).

Last, B. P., "The Balancing of Flexible Turbine and Generator Rotors," *Proc. Inst. Mech. Eng.* Part 1, 180, 1209–1222 (1965–66).

Levit, M. Ye., "Theory and Practice of Balancing Turbomachines," (Teoriya i praktika uravnoveshivaniye turbomashin), in Uravno-veshivaniye mashin i priborov (Balancing of machinery and instruments), V. A. Shchepetil'nikov, ed., Izd-vo Mashinostroyeniye, 1965. In Russian.

Mills, B., Kaljszer, H., and Blader, F. B., "The Effect of Vibration Due to Rotating Unbalance in Machinery," Avery Symposium on Dynamic Balancing, University of Birmingham, Mar. 1964.

Muster, D., "Balancing of Rotating Machinery, Part I: Theory of Balancing," in *Shock and Vibration Handbook*, C. M. Harris and C. E. Crede, eds., 3, McGraw-Hill, New York, 1961, pp. 39-1 to 39-220.

Panfilov, Ye. A., "Some Peculiarities of Vibration and Balancing of High-Speed Rotors," *Balancing of Machinery and Instruments*, Izd-vo Mashinostroyeniye, Moscow, 1965, pp. 91–99.

567

Parkinson, A. G., "An Introduction to the Vibration of Rotating Flexi-
    ble Shafts," *Bull. Eng. Educ.* **6**, 47 (1967).

Pedermann, J. E., "Balancing Heavy Shafts and Rotors," *Allis-Chalmers
    Elec. Rev.* **23**, 30 (1958).

Rieger, N. F., "Unbalance Response and Balancing of Flexible Rotors
    in Bearings," *Flexible Rotor-Bearing System Dynamics*, ASME Mono-
    graph, New York, 1973.

Samarov, N. G., "Static-Dynamic Balancing of Elastically Deformable
    Rotors," (Statiko-dinamicheskoye uravnoveshivaniye uprugodefor-
    miruyemykh rotorov), in Uravnoveshivaniye mashin i priborov
    (Balancing of machinery and instruments), V. A. Shchepetil'nikov,
    ed., Izd-vo Mashinostroyeniye, Moscow, 1965. In Russian.

Senger, W. I., "Balancing of Rotating Machinery, Part III: Practice of
    Balancing," in *Shock and Vibration Handbook*, C. M. Harris and
    C. E. Crede, eds., 3, McGraw-Hill New York, 1961, pp. 39-23 to
    39-41.

Senger, W. I., "Specifying Dynamics Balance-Part I, Types of Unbal-
    ance," *Mach. Des.* **16**, 101 (Nov. 1944).

Senger, W. I., "Specifying Dynamic Balance-Part II, Sources of
    Unbalance," *Mach. Des.* **16**, 131 (Dec. 1944).

Senger, W. I., "Specifying Dynamic Balance-Part III, Methods of
    Correction," *Mach. Des.* **17**, 127 (Jan. 1945).

Senger, W. I., "Specifying Dynamic Balance-Part IV, Balancing Equip-
    ment," *Mach. Des.* **17**, 163 (Feb. 1945).

Shchepetil'nikov, V. A., "Current State of the Art of Balancing Tech-
    nology," in *Balancing of Machinery and Instruments*, Izd-vo Mashi-
    nostroyeniye, Moscow, 1956, pp. 7—16.

Rigid Rotors

International Organization for Standardization, "Balance Quality of
    Rotating Rigid Bodies," ISO Document 1940-1973(E). Available
    from the American National Standards Institute, New York.

Muster, D., "Basic Principles of Balancing," in *Proceedings-Balancing
    Seminar*, Vol. I, Report 58GL119, General Electric Co., Schenec-
    tady, N.Y., Apr. 1958.

Theory of Balancing, Schenck Trebel Corp., Deer Park, Long Island,
    N.Y., Oct. 1973.

Flexible Rotors

International Organization for Standardization, "Recommendation for
    Balancing Criteria for Flexible Rotors," proposed draft document
    ISO/TC 108/SC-1 (Secretariat-1), 1973. Available from the
    American National Standards Institute, New York.

Theory of Flexible Rotor Balancing, Schenck Trebel Corp., Deer Park, Long Island, N.Y., Dec. 1973.

Criteria (Rigid Rotors)

Chistyakov, A. A., "Determination of Permissible Unbalance of Aviation Gas Turbine Rotors," in Uravnoveshivaniye machin i priborov (Balancing of machinery and instruments), V. A. Shchepetil'nikov, ed., Izd-vo Machinostroyeniye, Moscow, 1965, pp. 478–496. In Russian.

Feldman, S., "Unbalance Tolerance and Criteria," Vol. IV of *Proceedings-Balancing Seminar,* GEC Report 58GL122, General Electric Co., Schenectady, N.Y., Apr. 1958.

International Organization for Standardization, "The Mechanical Balancing of Flexible Rotors," proposed draft document, ISO/TC 108/SC 1, 1976. Available from the American National Standards Institute, New York.

Mechanical Vibrations of Shipboard Equipment, MIL-STD-167-2 (Ships), Naval Ship Engineering Center, U.S. Navy, May 1974.

Muster, D., and Flores, B., "Balancing Criteria and Their Relationship to Current American Practice," *Trans. ASME,* Ser. B, *J. Eng. Ind.* **91**, 1035–1046 (1969).

National Electrical Manufacturers Association, Standard MG 1, par 12.05, Dynamic Balance of Motor, 1978.

National Electrical Manufacturers Association, Standard MG 1, par 12.06, Method of Measuring Dynamic Balance, 1978.

National Electrical Manufacturer's Association, Standard Document SM 23, Steam Turbines for Mechanical Drive Service, 1979.

Rathbone, T. C., "Turbine Vibration and Balancing," *Trans. ASME* **51**, 267 (1929).

Rathbone, T. C., "Vibration Tolerance," *Power Plant Eng.* **43**, 721–724 (1939).

Precision Components

Burmist, J., and Guins, S. B., "Precision Balancing of Rotating Machine Parts," *Mach. Des.* **24**, 121–126 (Dec. 1952).

Lawrie, G. C., "Precision Production Balancing," *Tool Eng.* **30**, 48 (Apr. 1953).

Satchwell, D. L., "More Accurate Balancing for High-Speed Rotors," *Mach. Des.* **37**, 183–184 (Sept. 1965).

Reciprocating Machinery

Johnson, W. E., "Method of Balancing Reciprocating Machines," *Trans. ASME* **57**, A-81 (1935).

Ker Wilson, W., *Balancing of Oil Engines*, C. Griffin & Co., Ltd., London, 1929.

Lowell, C. M., "Lateral Vibrations in Reciprocating Machinery," ASME Winter Meeting Nov. 30—Dec. 5, 1958, ASME Paper 58-A-79.

Unbalance Distribution

Lawrie, G. C. "Dynamic Unbalance—Its Cause, Effects and Correction," *Instruments* 15, 357 (Sept. 1942).

Steam Turbine Rotors

Fu, Ch.-F., "Possible Use of Flexible Rotors in Marine Steam Turbines," *Chung-kuo tsao ch'uan* 1, 75—89 (1964). In Chinese.

Grobel, L. P., "Balancing Turbine-Generator Rotors," *General Electric Rev.* 56, 22—25 (July 1953). (See Vol. 59, pp. 2—7, 1956.)

Lisitsyn, I. S., "Balancing Turbogenerator Rotors in Situ," *Russ. Eng. J.* 40 (11), 7—11 (1960).

Mikunis, S. I., "Balancing Flexible Rotors in Turbine Generators," *Russ. Eng. J.* 41 (9), 10 (1961).

Mikunis, S. I., "Balancing Non-Rigid Rotors in Turbine Units," *Russ. Eng. J.* 39 (19) 21—26 (1959).

Moore, L. S., "Balancing of Large Turbine Rotors," *Inst. Mar. Eng. Trans.* 81, 105—115 (Apr. 1969).

Gas Turbine Rotors

Dunaiski, R. M., Freeman, M. A., and Kennedy, G. R., "Gas Turbine Internal Inspection with Minimum Disassembly," ASME Paper 74-GT-15, 1974.

Erdmann, A. D., and Ludwig, G. A., "Gas Turbine Vibration Limits— A Fundamental View," ASME Paper 73-GT-48, 1973.

Levit, M. Ye., and Royzman, V. P., "Vibration and Oscillation of Aviation Engine Rotors," English translation from the Russian, Foreign Technology Division, Air Force Systems Command, Wright-Patterson AFB, Ohio, 1970.

Orlov, I. I., and Rayer, G. A., "Experimental Study of Dynamics of Cantilever Rotors of Gas-Turbine Engines," *Trudy TSKTI* (Tsentr. Nauch.-issled. i Proektno-konstruktorskiy Kotloturbinnyy in-t im. I. I. Polzunova 44, 141—154 (1964).

Ota, H., et al., "Elimination of the Unstable Region of the Major Critical Speed in a Rotating Shaft System Carrying an Unsymmetrical Rotor," *Bull. JSME* 12, 470—481 (June 1969).

Rieger, N. F., and Badgley, R. H., "Flexible Rotor Balancing of a High-Speed Gas Turbine Engine," SAE Paper 720-741, 1972.

Schnittger, V. R., "Development of a Smooth-Running Double-Spool
    Gas Turbine Rotor System," *ASME Trans.*, Ser. A, *J. Eng. Power*
    81, 151–160 (Apr. 2, 1959).

Aircraft Jet Engines, Helicopter Rotors, Gyroscopic Rotors, and Aerospace Bodies

Eroshkin, A. I., Maksimov, V. P., and Samylin, E. A., "Diagnostic
    Method of Rotating-Bearing Damage" (Metody diagnostiki povre-
    zhdeniya podshipnikov kacheniya), in Strength and dynamics of
    aircraft engines (Prochnost i dinamika aviatsionnykh dvigatelei),
    Izd-vo Mashinostroyeniye, Moscow, 1966, pp. 214–230. In Rus-
    sian.

Helicopter Shafts and Rotors

Hooper, W. E., "A Vibration Balancing Device for Helicopters," *J.
    Amer. Helicopter Soc.* **11**, 28–43 (1966).

Gyro Rotors

Kovalev, M. P., *Dynamic Balancing of Rotors of Gyroscopic Systems,*
    English translation from the Russian, Foreign Technology Divi-
    sion, Air Force Systems Command, Wright-Patterson AFB, Ohio,
    Nov. 1965.
Kovalev, M. P., Morzhakov, S. P., and Terekhova, K. S., *Dynamic and
    Static Balancing of Gyroscopic Devices* (Dinamicheskoe i sta-
    ticheskoe uravnoveshivaye giroskopicheskikh ustroistv), 2nd ed.,
    Izd-vo Mashinostroyeniye, Moscow, 1965. In Russian.

Aerospace Bodies

McQuery, D. E., and Stadelbauer, D. G., "Balancing Aerospace Bodies
    on Industrial Balancing Machines," Schenck-Trebel Corp., Paper
    929, presented at the 31st Annual Conference of the Society of
    Aeronautical Weight Engineers, Inc., Atlanta, Ga., May 22–25,
    1972.
Stadelbauer, D. G., "A New Aerospace Balancing System for Mass
    Properties Determination," Schenck Trebel Corp., Paper 737, for
    presentation at the 28th Annual Conference of the Society of
    Aeronautical Weight Engineers, Inc., at San Francisco, Calif., May
    5–8, 1969.

Field Balancing

"Balancing QE2's Problems," *Engineering* **207**, 7 (Jan. 1969).
Chen, Y. N., "Field Balancing of Turbomachine Rotors," *Sulzer Tech.
    Rev.* **48**, 222–228 (1966).

Duckwald, C. S., "Characteristics of IRD Balancing Equipment Model 600," GEC Report 61GL135, General Electric Co., Schenectady, N.Y., July 31, 1961.

Jackson, C., "Balance Rotors by Orbit Analysis," *Hydrocarbon Proc.* **50**, 73—79 (Jan. 1971).

Jackson, C., "Using the Orbit to Balance Rotating Equipment," *Mech. Eng.* **93**, 28—32 (Feb. 1971).

Keck, P., "Balancing in a Motor Car Plant," Avery Symposium on Dynamic Balancing, University of Birmingham, U.K., Mar. 1964.

Macinante, J. A., "Simple Way to Field Balance Rigid Rotors," *Engineer* **228**, 36—37 (May 1, 1969).

Matthew, G. D., "Field Balancing of a Rigid Rotor by Measurements of Vibration Amplitude Alone," *Engineer* **221**, 460—462 (Mar. 25, 1966).

Runov, B. T., *Balancing of Turbogenerators in Power Stations,* M. Gosenergoizdat, Moscow, 1963. In Russian.

Rushing, F. C., and Rose, B. A., "Balancing Rotating Machines in the Field," *Elec. J.* **34**, 441 (1937).

Stadelbauer, D. G., "Balancing of Fans and Blowers," *Vibration and Acoustic Measurement Handbook,* M. P. Blake and W. S. Mitchell, eds., Spartan Books, New York and Washington, D.C., 1972, p. 337.

Thearle, E. L., "Dynamic Balancing of Rotating Machinery in the Field," *Trans. ASME,* Ser. B, **56**, No. 3, 745 (1934); APM-56-19.

Calibration

Macinante, J. A., "Calibrating Dynamic Balancing Machines—Graphical Method Not Employing Previously Balanced Specimens," *Engineering* **182** (Aug. 10, 1956).

Rigid-Rotor Experiments

Orlov, I. I., and Rayer, G. A., "Experimental Study of Dynamics of Cantilever Rotors of Gas-Turbine Engines," *Tr. TSKTI* (Tsentr. Nauch.-issled. Proektno-konstruktorskiy Kotloturbinnyy in-t im. I. I. Polzunova) **44**, 141—154 (1964).

Parkinson, A. G., Jackson, K. L., and Bishop, R. E. D., "Some Experiments on the Balancing of Small Flexible Rotors: Part I—Theory," *J. Mech. Eng. Sci.* **5**, 114—128 (Mar. 1963).

Parkinson, A. G., Jackson, K. L., and Bishop, R. E. D., "Some Experiments on the Balancing of Small Flexible Rotors: Part II—Experiments," *J. Mech. Eng. Sci.* **5**, No. 2, 133—145, (June 1963).

Unbalance Determination

Baker, J. G., "Routine Method for Unbalance Correction Determination from Vibration Readings," Research Report R-94051-R, Westinghouse Research Laboratories, Dec. 6, 1937.

Baker, J. G., "Methods of Rotor-Unbalance Determination," *Trans. ASME* 61, A1–A6 (1939).

Becker, H., "Unbalances in Flexible Rotors," *Archiv. Technisches Messen*, Part I, Vol. 297, p. 209 (1960); Part II, Vol. 299, p. 257 (1960).

Goodman, T. P., "Correction of Unbalance by Force-Canceling Bearing Pedestals," Report 61GL110, General Electric Co., May 15, 1961.

Royzman, V. P., "Determining Imbalance When Balancing Elastically Deformed Rotors," in *Strength and dynamics of aircraft engines*, Izd-vo Mashnostroyeniye, Moscow, 1966, pp. 180–184. In Russian.

Samarov, N. G., "Determining the Location and Degree of Unbalance of Flexible, Multi-mode Rotor," *Energomashinostroyeniye* 8, 29–31 (1966). In Russian.

Schapker, R. L., *Program for Computing Balance Corrections*, Report R61FPD200, General Electric Co., Small Aircraft Engine Dept., Lynn, Mass., Apr. 1961.

BALANCING FUNDAMENTALS

Federn, K., "Analysis of Balancing Procedure," lecture held at the General Electric Co. Balancing Seminar, Schenectady, N.Y., May 3, 1956.

Federn, K., "Aktuelle Grundsatz- und Verfahrensfragen der Auswuchttechnik," *Deut. Ingen.*, Nos. 1 and 3 (1962). In German.

Federn, K., "Fundamentals of Systematic Vibration Elimination from Rotors with Elastic Shafts," *VDI Ber.* 24 (1957).

Federn, K., "Looking to the Future in Balancing," Avery Symposium on Dynamic Balancing, University of Birmingham, Mar. 1964.

"Le probleme de l'equilibrage," *Pratique des Industries Mecaniques* 39(10), 253–259; 39(11), 281–289 (1956). In French.

Rieger, N. F., "Balancing High-Speed Rotors to Reduce Vibration Levels," paper presented at ASME Design Conference, Chicago, Ill., May 11, 1972.

Dynamic Balancing of High-Speed Rotary Machinery, National Aeronautics and Space Administration, Technology Brief 70-10433, Washington, D.C., 1970.

Rathbone, T. C., "Vibration Tolerance," *Power Plant Eng.* 43, No. 11, 721–724 (1939).

Reiher, H., and Meister, F. J., "Die Empfindlichkeit des Menschen gegen Erschutterungen," *Forschung. Geb. Ingenieurw.* **2**, No. 11, 381—386 (Nov. 1931). In German.

BALANCING METHODS

Proposed Methods

Bishop, R. E. D., and Gladwell, G. M. L., "The Vibration and Balancing of an Unbalanced Flexible Rotor," *J. Mech. Eng. Sci.* **1**, 66—77 (1959).

Goodman, T. P., "A Least-Squares Method for Computing Balance Corrections," *Trans. ASME,* Ser. B, *J. Eng. Ind.* **86**, 273—279 (1964).

Hübner, E., "The Balancing of Flexible Rotors, A Problem of Structural Analysis," *Ingenierw. Arch.* **30**, 325 (1961).

Hundal, M. S., and Harker, R. J., "Balancing of Flexible Rotors Having Arbitrary Mass and Stiffness Distribution," *Trans. ASME* Ser. B, *J. Eng. Ind.* **88**, 217—223 (1966).

Julis, K., and Boruvka, V., "Results of Balancing Method Research of Flexible Rotors With Free Mass, Part I and II," *Dynamics of Machines,* Proceedings of the Conference on Machine Dynamics, Publ. House of the Slovakian Academy of Science, Bratislava, 1963, pp. 77—95.

Kascheev, V. M., "Dinamicheskaya balensirova rotorcv metodom kachanii," *Izv. AN SSSR, Otd. Tekh. Nauk,* No. 2, 51—57 (Feb. 1958). In Russian.

Kellenberger, W., "Balancing Flexible Turbo-Rotors With the Aid of the Theory of Orthogonal Functions," *CIGRE* (Conference Internationale des Grands Reseaux Electriques), Report 11-10, 1970.

Kendig, J. R., "Current Flexible Rotor-Bearing System Balancing Techniques Using Computer Simulation," M. S. thesis, Rochester Institute of Technology, Rochester, N.Y., Nov. 1975.

Kushul', M. Ya., and Shlyakhtin, A. V., "Balancing Flexible Rotors," *Izv. AN SSSR, Mekh. Mashinostr.* **2**, 61—77 (1964).

LeGrow, J. V., "Multiplane Balancing of Flexible Rotors—A Method of Calculating Correction Weights," ASME 3rd Vibration Conference, Sept. 1971, Toronto, Canada; ASME Paper 71-Vibr-52.

Matthieu, P., "Eine mathematische Theorie für die Auswuchtung elastischer Rotoren," *ZAMM-Sonderheft,* GAMM-Tagung, Part 94 (1967).

Meldahl, A., "Auswuchten elastischer Rotoren," *Z. angew. Math. u Mech.* **34**, 8—9 (1954).

Rastrigin, L. A., "Application of the Method of Self-adaptive Models in Automatic Rotor Balancing," in *Balancing of Machinery and Instruments*, Izd-vo Mashinostroyeniye, Moscow, 1965, pp. 45–51. In Russian.

Rieger, N. F., *Computer Program for Balancing of Flexible Rotors*, Technical Report 67TR68, prepared for NASA Lewis Research Center under Contract NAS 3-10926, Mechanical Technology Inc., Sept. 15, 1967.

Tang, T. M., and Trumpler, P. R., "Dynamics of Synchronous-Processing Turborotors With Particular Reference to Balancing. Part I, Theoretical Foundation," *Trans. ASME*, Ser. E, *J. Appl. Mech.* 31, 115–122 (Mar. 1964).

Tessarzik, J. M., Badgley, R. H., and Anderson, W. J., "Flexible Rotor Balancing by the Exact Point-Speed Influence Coefficient Method," *Trans. ASME*, Ser. B, *J. Eng. Ind.* 94, 148–158 (1972).

Influence Coefficient Method

Badgley, R. H., and Tessarzik, J. M., "Experimental Evaluation of the Exact Point-Speed and Least-Squares Procedures for Flexible Rotor Balancing by the Influence Coefficient Method," ASME Paper 73-DET-115, *Trans. ASME*, Ser. B, *J. Eng. Ind.* 96 (2), 633–643 (1974).

Kendig, J. R., "Current Flexible Rotor-Bearing System Balancing Techniques Using Computer Simulation," M.S. thesis, Rochester Institute of Technology, Rochester, N.Y., Nov. 1975.

Comprehensive Modal Method

Kellenberger, W., "Should a Flexible Rotor Be Balanced in N or $(N + 2)$ Planes?," *Trans. ASME*, Ser. B, *J. Eng. Ind.* 94, 548–560 (1972).

Kendig, J. R., "Current Flexible Rotor-Bearing System Balancing Techniques Using Computer Simulation," M.S. thesis, Rochester Institute of Technology, Rochester, N.Y., Nov. 1975.

Modal Methods

Bishop, R. E. D., "Shaft Balancing One-Shot Technique," *Engineering* 211, 430–431 (1971).

Bishop, R. E. D., and Parkinson, A. G., "On the Isolation of Modes in the Balancing of Flexible Shafts," *Proc. Inst. Mech. Eng.* 177, 407–423 (1963).

Christiansen, R. G., and Parmenter, W. W., "Recovery of Modal Information From a Beam Undergoing Random Vibration," ASME Paper 73-WA/DE-10, 1973.

Dodd, E. G., and Moore, L. S., "Mechanical Balancing of Large Rotors," *Parsons J.* 1–13, Summer 1970.

Fridman, V. M., "Balancing of Flexible Shafts According to Natural Vibration Modes," *Coll. Balancing Rotors of Power-Generating Machiner,* Moscow, Tsintielektroprom, 1962.

Kendig, J. R., "Current Flexible Rotor-Bearing System Balancing Techniques Using Computer Simulation," M.S. thesis, Rochester Institute of Technology, Rochester, N.Y., Nov. 1975.

Kushul', M. Ya., and Shlyakhtin, A. V., "Modal Approach to Balancing with Additional Constraints," *Izv. AN SSSR, Mekh. Mash.* No. 2 (1966).

Miwa, S., "Balancing of a Flexible Rotor by Means of Mode Separation," *VDI Ber.* 161, 53 (1971).

Parkinson, J., "Critical Speed Vibration—Modal Balance," Soc. Automotive Eng., National Transportation, Powerplant, and Fuels and Lubr. Meeting, Baltimore, Md., October 19–23, 1964, SAE Paper 928A.

Parkinson, A. G., and Bishop, R. E. D., "Residual Vibration in Modal Balancing," *J. Mech. Eng. Sci.* 7, No. 1, 33–39 (1965).

Least-Squares Procedures

Badgley, R. H., and J. M. Tessarzik, "Experimental Evaluation of the Exact Point-Speed and Least-Squares Procedures for Flexible Rotor Balancing by the Influence Coefficient Method," ASME Paper 73-DET-115, 1973.

Damon, E. P., Kneale, S. G., and Martin, M. A., *Minimizing the Maximum Error by Weighted Least Squares,* Report R59SD404, Technical Information Series, General Electric Co., Philadelphia, Pa., 1949.

Goodman. T. P., "Least Squares Method for Computing Balance Corrections," Report 61GL46, General Electric Co., Feb. 1961.

Goodman. T. P., "A Least-Squares Method for Computing Balance Corrections," *Trans. ASME,* Ser. B, *J. Eng. Ind.* 86, No. 3., 273–279 (1964).

Little, R. M., "The Application of Linear Programming Techniques to Balancing Flexible Rotors," Ph.D. dissertation, University of Virginia, 1973.

Multiplane Balancing

Antonov, I. L., "Random Search Method for Rotating Rotor Balancing," in *Vibrations and Stability Under Variable Stresses* (Kolebaniya i prochnost' pri peremennykh napryashcniyakh), Nauka Inst. Mash., Moscow, 1965, pp. 134–141. In Russian.

Badgley, R. H., "The Potential Impact of Multi-plane Multi-speed Balancing on Gas Turbine Production and Overhaul Costs," ASME Paper 74-GT-94, 1974.

Badgley, R. H., and Rieger, N. F., "The Effects of Multi-plane Balancing on Flexible Rotor Whirl Amplitudes," paper presented at Society of Automative Engineers Automotive Engineering Congress and Exposition, Jan. 8–12, 1973.

Dimentberg, F. M., "Present Status of Flexible Rotor Balancing Theory," Russ. Eng. J. 11, 7–14 (1964).

Federn, K., Multi-Plane Balancing of Elastic Rotors—Fundamental Theories and Practical Application,: GEC Technical Information Series, No. 58GL121, General Electric Co. (originally published in German, 1956).

Giers, A., "Comparison of the Balancing of a Flexible Rotor Following the Methods of Federn-Kellenberger and Moore," VDI Ber. 161 (1971).

Gusarov, A. A., "On Placing of Balancing Planes on Flexible Rotor," Proc. National Research Institute of Machinery of the Soviet Academy of Sciences, Scientific Publ. House Moscow, 1965, pp. 112–124.

Hill, H. N., Barker, R. S., and Murtland, J. B., "Dynamic Balancing of Hydroelectric Units," Trans. AIEE Power Apparatus and Systems 76, No. 32, 703–710 (1957).

LeGrow, J. V., "Multiplane Balancing of Flexible Rotors—A Method of Calculating Correction Weights," ASME 3rd Vibration Conference, Toronto, Canada, Sept. 1971, ASME Paper 71-Vibr-52.

Lund, J. W., and Tonnesen, J., "Analysis and Experiments on Multiplane Balancing of a Flexible Rotor," Trans. ASME, Ser. B, J. Eng. Ind. 94, 233–242 (1972).

Yanabe, S., and Tamura, A., "Multi-plane Balancing of Flexible Rotor Consisting of Two Disks," Bull. JSME 12, No. 54 (1969).

Rigid Rotors

Bromberg, J., "A Mathematical Solution of the Rotor-Balancing Problem," Trans. ASME 56, 707 (1934).

French. M. J., "Balancing High Speed Rotors at Low Speeds," Engineer 215, No. 5605 (June 1963).

Kuensch, W. G., "Quick Way to Balance Rotors," Iron Age 183, No. 3, 84–85 (Jan. 15, 1959).

Badgley, R. H., and Rieger, N. F., "Effects of Multi-plane Balancing on Flexible Rotor Whirl Amplitudes," SAE Automotive Congress and Exposition, Detroit, Mich., Jan. 8–12, 1973.

Baier, R. J., "Flight Test Evaluation of a Super-Critical-Speed Shaft," Boeing Co., Vertol Division, USAAVLABS Tech. Report 70-50,

U.S. Army Aviation Material Laboratories, Fort Eustis, Va., Sept. 1970.

Berger, Ye. G., "Self-alignment and Balancing of Coaxial Rotors," English translation from the Russian, Foreign Technology Division, Air Force Systems Command, Wright-Patterson AFB, Ohio, Trans. from *Vestn. Leningr. Univ., Mat. Mekh. Astron.* 3, 119–121 (1963).

Bishop, R. E. D., and Gladwell, C. M. L., "The Vibration and Balancing of an Unbalanced Flexible Rotor," *J. Mech. Eng. Sci.* 1, No. 1, 66– 77 (1959).

Bishop, R. E. D., and Parkinson, A. G., "Vibration and Balancing of Flexible Shafts," *Appl. Mech. Rev.* 21, 439–451 (1968).

Church, A. H., and Plunkett, R., "Balancing Flexible Rotors," *Trans. ASME,* Ser. B, *J. Eng. Ind.* 83, No. 4, 383–389 (1961).

Danek, O., "Auswuchten elastischer Rotoren," *Strojnicky Casopis* XXII, No. 6 (1971). In German.

Den Hartog, J. P., "The Balancing of Flexible Rotors," in *Air, Space and Instruments,* Stark Draper Commemoration Volume, McGraw-Hill, New York, 1963, p. 165.

Federn, K., "Überblick über die gegenwärtigen Betrachtungsweisen, die Richtlinien und Normen und die gebräuchlichen Wege zum Auswuchten wellenelastischer Rotoren," *VDI Ber.* 161 (1971).

Findlay, J. A., "Review of 'Balancing of Flexible Rotors,' by Hundal and Harker," ASME Paper 65-MD-8, 1965.

Gusarov, A. A., "Balancing Flexible Rotors with Two Weights," *Dynamika Strojov, Shornik Prac. z Konf. SAV,* Vydav. Slov. Akad. Vied, Bratislava, 1963. In Czechoslovakian.

Gusarov, A. A., and Dimentberg, F. M., "Balancing Flexible Shafts," *Vestn. Mashinostr.* 1 (1959).

Gusarov, A. A., and Dimentberg, F. M., "Balancing Flexible Rotors with Distributed and Concentrated Masses," *Coll. Problems of Strength in Engineering,* 6th ed., Moscow, Izd-vo AN SSSR, 1960.

Kellenberger, W., "Balancing Flexible Rotors on Two Generally Flexible Bearings," *Brown Boveri Rev.* 53, 603–617 (1967).

Kellenberger, W., "Should a Flexible Rotor be Balanced in N or $(N + 2)$ Planes?," *Trans. ASME,* Ser. B, *J. Eng. Ind.* 94, 548–560 (May 1972).

Kushul', M. Ya., and Shlyakhtin, A. V., "Balancing Flexible Rotors," *Izv. AN SSSR, Mekh. Mashinostr.* 2, 61–77 (1964).

Lindley, A. L. G., and Bishop, R. E. D., "Some Recent Research on the Balancing of Large Flexible Rotors," *Proc. Inst. Mech. Eng.* 177, 811–825 (1963).

Lindsey, J. R. "Significant Developments in Methods for Balancing High-Speed Rotors," ASME Paper 69-Vibr-53, presented at 2nd Vibrations Conference, Philadelphia, Pa., Mar. 30, 1969.

Miwa, S., "Theoretical Consideration in General Condition of Balancing a Flexible Rotor," *VDI Ber.* **161**, 49 (1971).

Moore, L. S., "Mechanical Balancing of Large Rotors," *Parsons J.,* C. A. Parsons and Co., Heaton Works, Newcastle-Upon-Tyne, England (Summer 1970).

Moore, L. S., "The Significance of Anisotropy of Support Conditions When Balancing Very Large Flexible Rotors," in *Vibrations of Rotating Systems,* Conf. Inst. Mech. Eng., Feb. 1972, pp. 86–95.

Moore, L. S., and Dodd, E. G., "Mass Balancing of Large Flexible Rotors," *GEC J.* **31**, No. 2, 74 (1964).

Parkinson, A. G., "Balancing of Flexible Shafts Rotating in Massive Flexible Bearings," *J. Mech. Eng. Sci.* **15**, 430–438 (1973).

Parkinson, A. G., "On the Balancing of Shafts with Axial Symmetry," *Proc. Royal Soc. (London)* **294**, Ser. A, 66 (1966).

Rieger, N. F., "Computer Program for Balancing of Flexible Rotors," Tech. Rept. 67TR68, prepared for NASA Lewis Research Center under Contract NAS 3-10926, Mechanical Technology Inc., Sept. 15, 1967.

Royzman, V. P., "Balancing Elastically Deformable Rotors," *Tr. Kuybyshevsk. Aviats. Instituta* **19**, 69–79 (1965). In Russian.

Theory of Flexible Rotor Balancing, Schenck Trebel Corp., Deer Park, Long Island, N.Y., Dec. 1973.

Simek, J., "Balancing of Rotors with Flexible Shafts," *Strojirenstvi* **4**, 707–711 (1954).

Multibearing Rotors

Julis, K., "Balancing of Rotors with Statically Indeterminate Supports," *Strojirenstvi* **14**, No. 1, 3–11 (1964).

Parkinson, A. G., and Bishop, R. E. D., "Vibration and Balancing of Rotating Continuous Shafts," *J. Mech. Eng. Sci.* **3**, 200–213 (1961).

Plainevaux, J. E., "Balancing of a Set of Rotors Mounted on a Straight Shaft Supported in Self-aligning Bearings," *Acad. Royal Belg. Bull. Cl. Sci.* **39**, No. 3 (1953).

Unequal Support Stiffnesses

Fryml, B., and Boruvka, V., "Balancing of Rotors with Unequal Shaft Stiffness," *Strojirenstvi* **9**, No. 8, 582–588 (1959).

Parkinson, A. G., "The Vibration and Balancing of Shafts Rotating in Asymmetric Bearings," *J. Sound Vib.* **2**, 477–501 (1965).

Instrumentation

Baker, J. G., and Rushing, F. C., "Balancing Rotors by Means of Electrical Networks," *J. Franklin Inst.* 222, 183 (1936).

Eubanks, R. A., "Development of Methods and Equipment for Balancing Flexible Rotors," Armour Research Foundation, Final Report ARF K-206, 2nd ed., Contract Nobs-78753, Jan. 1963.

Gross, W. A., "Use of Capacity-Controlled RF Energized Ionization Transducer for Balancing Rotors," *Rev. Sci. Instr.* 30, 522–523 (1959).

Haardt, H. H., "Messen und Beseitigen von Unwucht an Umaufenden Maschinenteilen mit Hilfe der Wattmeter Methode," in *Transactions of Instruments and Measurements Conference,* Stockholm, 1952, pp. 212–217.

Hack, H., "Auswuchten in der Serienfertigung," *Werkstatt Betr.* 92, 109–120 (1959).

Hauck, L. T., Kerfoot, R. E., and Palm, J. E., "Evaluation of Machinery Characteristics Through On-Line Vibration Spectrum Monitoring," ASME Paper 73-GT-68, 1973.

Jarvis, C. A., "Balancing Machine Instruments," *Avery Symposium on Dynamic Balancing,* University of Birmingham, Mar. 1964.

Maddox, V. V., "Vibration Monitoring and Diagnostic Instrumentation for Industrial and Marine Gas Turbines, ASME Paper 73-GT-50, 1973.

Rhodes, J. E., "Electronic Vibration Analysis," *Mach. Des.* 27, 193 (Nov. 1955).

Seale-Finch, V., "Automatic Position Indicator for Use with Dynamic Balancing Machines," *Machinery* (London) 92, 377–378 (Feb. 14, 1958).

Sensitivity

Baker, J. G., "Methods of Rotor-Unbalance Determination," *Trans. ASME* 61, A1–A6 (1939).

Frank, K. F., "Design of Supersensitive Balancing Equipment," *Mach. Des.* 18, 109 (Feb. 1946).

RIGID-ROTOR BALANCING

Akimoff, N. W., "Recent Developments in Balancing Apparatus," *Trans. ASME* 39, 779 (1918).

Alexander, J. D., "An Automatic Dynamic Balancer," in *Developments in Theoretical and Applied Mechanics,* Proc. 2nd Southeastern Conf., Georgia Institute of Technology, Atlanta, Ga., Mar. 5–6, 1964.

Cade, J. W., "Self-compensating Balancing in Rotating Mechanisms," *Design News* (Apr. 28, 1965).

"The Dynamic Balancing of Motor Car Engine Crankshafts," *Machinery* (London) **86**, 433 (Feb. 25, 1955).

"Dynamic Balancing for Small Parts," *Amer. Mach.* No. 26, 95—96 (Dec. 15, 1958).

Federn, K., "Bedeutung Elektrischer Mess- und Steuermittel für die Auswuchttechnik," *Z. Elektr. Austrustung,* No. 1, 31—38 (1960).

Feldman, S., "Unbalance Tolerances and Criteria," in *Proc. Balancing Seminar* IV, Rept. 58GL122, General Electric Co., Schenectady, N.Y., Apr. 1958.

International Organization for Standardization, "Mechanical Vibration of Machines with Operating Speeds from 10 to 200 rev/s—Basis for specifying evaluation standards," ISO 2372, 1974.

International Organization for Standardization, "Mechanical Vibration of Certain Rotating Electrical Machinery with Shaft Heights Between 80 and 400 mm; Measurement and evaluation of vibration severity," ISO 2373, 1974.

Maichin, V. E., "Dynamic Balancing of Rotors Used in Instrument Engineering," *Technology and Design of Gyroscopic Instruments,* Izd-vo Mashinostroyeniye, Moscow, 1964, pp. 40—53. In Russian.

Muster, D., "Basic Principles of Balancing," in *Proc. Balancing Seminar* 1, Rept. 58CL119, General Electric Co., Schenectady, N.Y., Apr. 17, 1958.

Somervaille, I. J., "Balancing a Rotating Disc, Simple Graphical Construction," *Engineering* 177 (Feb. 19, 1954).

Trumpler, W. E., "The Dynamic Balance of Small High-Speed Armatures," *Elec. J.* **22**, 34 (1925).

BALANCING MACHINES

Akimoff, B., "Balancing Apparatus," *Trans. ASME* **39**, 779 (1917). Described in A. Stodola, *Steam and Gas Turbines,* Vol. 1, McGraw-Hill, New York, 1927.

Akimoff, N. W., "Dynamic Balance," *Trans. ASME* **38**, 367 (1916).

Alexander, J. D., "An Automatic Dynamic Balancer," in *Developments in Theoretical and Applied Mechanics,* Proc. 2nd Southeastern Conf., Georgia Institute of Technology, Mar. 5—6, 1964.

"Dynamic Balancing for Small Parts," *Amer. Mach.* No. 26, 95—96 (Dec. 15, 1958).

Baker, J. G., and Rushing, F. C., "Balancing Rotors by Means of Electrical Networks," *J. Franklin Inst.* **222**, 183 (1936).

Bishop, R. E. D., and Parkinson, A. G., "On the Use of Balancing Machines for Flexible Rotors," *Trans. ASME,* Ser. B, *J. Eng. Ind.* **94**, 561—576 (1972).

Federn, K., "New Developments in Balancing Machines," *VDI Zeit.* **92**, No. 25, 702—710 (Sept. 1950).

International Organization for Standardization, ISC Standard 2953-1975(E), "Balancing machines--description and evaluation, 2d edit., 1981.

"Jackson and Bradwell Direct-Indicating Static and Dynamic Balancing Machines," *Machinery* (London) **93**, No. 2402, 1230–1232 (Nov. 26, 1958).

Landsnell, C., "Automatic Balancing on Gisholt Machines," *Machinery* (London) **89**, No. 2300, 1341–1347 (Dec. 14, 1956).

Laskin, I., "Study of the Stewart-Warner Industrial Balancing Machine," Rept. 66TR42, Mechanical Technology Inc., August 1966.

Liselius, E., "New Balancing Machines for Dynamic Balancing of Rotors," *Ericsson Rev.* No. 3, 87–100 (1948).

McQueary, D. E., "Understanding Balancing Machines," *Amer. Mach.* Special Rept. 656, June 11, 1973.

"R06 and R16 Schenck Balancers Designed for Small Parts," *Machinery,* **66**, 210 (May 1960).

Rose, F. D., "The Design of Balancing Machines," *Aircr. Eng.* **17**, 149 (May 1945).

Senger, W. I., "Performance Tests for Balancing Machines," *Machinery* (New York) **64** (No. 7, 8), 156–167 (Mar. 1958); 160–168 (Apr. 1958).

Soderberg, C. R., "Recent Developments in Balancing Machines," *Trans. ASME* **45**, 111 (1923).

Thearle, E. L., "A New Type of Dynamic Balancing Machine," *Trans. ASME* **54** (11), 131–140 (1932); APM-54-12.

Tobisch, K., "Die Grosse Auswucht- und Schleuderanlage der Maschinenfabrik Oerlikon," *Sonderdruck aus Energie und Technik* **1** (1968). In German.

Tung, Shih-yu, "The Measurement of the Performance of the Dynamic Balancer," *Shang hai chi hsieh* **9**, 39–41 (1963). In Chinese.

VDI 2059, "Measurement of Shaft Vibrations on Turbine Machines," ("Wellenschwingungen zur Überwachung von Turbomaschinen"). VDI-Verlag, Düsseldorf, 1977.

CRITICAL SPEED

General

Biezeno, C. B., and Grammel, R., *Engineering Dynamics,* Vol. 3, Part 3, English translation, 1954.

Brozens, P. J., and Crandall, S. H., "Whirling of Unsymmetrical Rotors," *J. Appl. Mech.* **28**, 355–362 (1961).

Craifaleanu, D., "On the Critical Speed of Shafts," *Rev. Roumaine Sci. Tech. Ser. Mech. Appl.* **9**, 843–850 (1964).

Eubanks, R. A., and Eshleman, R. L., *Dynamics of Flexible Rotors*, IITRI Final Report K-6056, Bureau of Ships Contract Nobs-88607, 1964.

Klompas, N., "Theory of Rotor Dynamics with Coupling of Disk and Blade Flexibility and Support Structure Asymmetry," ASME Paper 74-GT-159, 1974.

Rankine, W. J. Mc.Q., "Centrifugal Whirling of Shafts," *Engineer* 26 (Apr. 9, 1868).

Santini, P., "Dynamic Problems of Rotors," *L'Acrotecnia* 43, 199—215 (1963).

Stodola, A., *Steam and Gas Turbines*, Vol. I and II, McGraw-Hill, New York, 1927, pp. 491, 929, 1122, 1125.

Flexible-Rotor Systems

Downham, E., "The Critical Whirling Speeds and Natural Vibrations of a Shaft Carrying a Symmetrical Rotor," ARC Technical Report, R&M 2854, Aeronautical Research Council, National Physical Laboratory, Teddington, Middlesex, 1954.

Dunkerley, S., "Whirling and Vibration of Shafts," *Trans. Royal Soc. (London)*, Ser. A, 185 (1894).

Eshleman, R. L., and Eubanks, R. A., *Studies on Shaft Vibration*, IITRI Final Report K-6073, Contract Nobs-90475, Jan. 1966.

Federn, K., *Auswuchttechnik*, Bd. 1, *Allegemeine Grundlagen Messverfahren und Richtlinien*, Springer-Verlag, Berlin, 1977.

Jeffcott, H. H., "The Periods of Lateral Vibration of Loaded Shafts," *Phil. Mag.* 42, 635 (1921).

Lees, S., "Whirling of an Eccentrically Loaded Overhung Shaft," *Phil. Mag.* 37, 515—523 (1919).

Lees, S., "Whirling of an Overhung Eccentrically Loaded Shaft," *Phil. Mag.* 45, 689—708 (1923).

Petersen, P. T., "On Forward and Backward Precession of Rotors," Report No. 17, Danish Center for Applied Mathematics and Mechanics, Technical University of Denmark, Sept. 1971.

Rasmussen, S. B., "Practical Rotor Dynamics, Part 1, Geometric Properties of Rotors," *Mach. Des.* 41, 142—145 (Feb. 6, 1969).

Rasmussen, S. B., "Practical Rotor Dynamics, Part 2, Load/Deflection Relationship," *Mach. Des.* 41, 157—161 (Feb. 20, 1969).

Rasmussen, S. B., "Practical Rotor Dynamics, Part 3, Natural Frequencies and Critical Speeds," *Mach. Des.* 41, 158—162, Mar. 6, 1969).

Rodgers, C., "On the Vibration and Critical Speeds of Rotors," *Phil. Mag.* Ser. 6, 44, 122—156 (1922).

Stodola, A., "Neuere Beobachtungen über die kritischen Umlaufzahlen von Wellen," *Schweiz Bauzg.*, Oct. 1916. In German.

Supercritical Shafts

Battelle Memorial Institute, *Design Manual, Super-Critical-Speed Power-Transmission Shafts,* Columbus, Ohio, 1965.

Bellenot, C., Dzung, L. S., and Erni, E., "Determining Critical Speeds of Fast Running Shafts," *Brown Boveri Rev.* 44, No. 4–5, 234–238 (1957).

Day, J. B., Dubensky, R. G., Meacham, H. C., and Voorhees, J. E., *Design Criteria for High-Speed Power-Transmission Shafts, Phase II,* First Quarterly Report, Contract No. AF 33(657)-10330, for Wright-Patterson AFB, Ohio, Aug. 1963.

Dimentberg, F. M., "Certain Problems of High-Speed Shaft Bending Vibration," thesis, AN SSSR, Institut Mashinovedeniya, Moscow, 1955. In Russian.

Meacham, H. C., and Voorhees, J. E., *Design Criteria for High-Speed Power-Transmission Shafts,* Phase II, Third Quarterly Report, Contract No. AF 33(657)-10330, for Wright-Patterson AFB, Ohio, Nov. 1963.

Asymmetrical Shafts

Aiba, S., *On the Vibration and Critical Speeds of an Asymmetrical Rotating Shaft,* Report of the Faculty of Engineering, Yamanashi University, Kofu City, Yamanashi, Japan (Dec. 1962).

Banakh, L. Ya., and Dimentberg, F. M., "Flexural Vibrations of a Rotating Shaft Carrying a Component in Which the Values of the Principal Central Mass Moment of Inertia Are Unequal," *Izv. AN SSSR, Otd. Tekh. Nauk, Mekh. Mashinostr.* 6, 91–97 (1960).

Dimentberg, F. M., "Transverse Vibrations of a Rotating Shaft Having Dissimilar Principal Moments of Lateral Intertia" (Poperechnye kolebaniya vrashchayushchegosya vala, imeyushchego neodinakovye glavnye momenty inertsii secheniya), Second Symposium on Transverse Vibrations and Critical Speeds, Izd-vo AN SSSR, 1953. In Russian.

Hull, E. H., "Shaft Whirling as Influenced by Stiffness Asymmetry," *Trans. ASME,* Ser. B, *J. Eng. Ind.* 83, 219–226 (1961).

Robertson, D., "Static Balance of a Shaft with Skew Stiffness," *Engineer* 154, 126 (1932).

Robertson, D., "Whirling of Shaft with Skew Stiffness," *Engineer* 156, 152–153, 179–181, 213–214 (1933).

Calculation Procedures

Fehrle, L., "Kritische Drehzahlen gewisser Rotorformen," *Ing. Arch.* 25 (No. 5) 319–329 (1957). In German.

Prohl, M. A., "A General Method for Calculating Critical Speeds of Flexible Rotors," *Trans. ASME, J. Appl.. Mech.* 12, No. 3, A142–A148 (1945).

Ryder, G. H., "Determination of Critical Speeds by 'Exact' and 'Approximate' Methods," *Mech. World* 137, No. 3456, 294–297 (1957).

Tondl, A., "An Analysis of Resonance Vibrations of Nonlinear Systems with Two Degrees of Freedom," *Rozpr. Cesk. Akad. Ved.* (CSAV), Ser. TV, 74, No. 8 (1964).

Rotors on Multiple Supports

Bufler, H., and Hahn, H. B., "Critical Speeds and Bending Vibrations of Contentiously Loaded Shafts with Variable Supports," *Ing. Arch.* 26, 387–397 (1958). In German.

Bufler, H., and Hahn, H. G., "Der Einfluss der Trägheitsmomente einer gleichmässig kontinuierlich besetzten Welle konstanter Biegesteifigkeit auf die kritischen Drehzahlen und Biegeschwingungs-Eigenfrequenzen bei verschiedenen Randbedingungen," *Forsch. Geb. Ingenieurw.* 23, No. 1–2, 22–26, (1957). In German.

Ekong, I. E., Eshleman, R. L., and Bonthron, R. J., "Dynamics of Continuous Multimass Rotor Systems," ASME Paper 69-Vibr-51, pp. 1–8, 1969.

Eshleman, R. L., "On the Critical Speeds of a Continuous Shaft-Disk System," ASME Vibrations Conf., Boston, Mass., ASME Paper 67-Vibr-9, 1967. Also *Trans. ASME, J. Eng. Ind.* 89, 645-652 (1967).

Jeffcott, H. H., "Whirling Speeds of a Loaded Shaft Supported in Three Bearings," *Phil. Mag.* 42, 635–668 (1921).

Prohl, M. A., "Calculation of Gravity Sag and Lateral Vibration of Multispan Turbine-Generator Rotors," Report DF-66-MSD-2, General Electric Co., Jan. 13, 1966.

Torque and Gyroscopic Effects

Arnold, R. N., and Maunder, L., "Gyroscopic Effects in the Whirling of Shafts," Ch. 15 in *Gyrodynamics and Its Engineering Applications,* Academic Press, New York, 1961.

Bauer, V. O., "The Influence of the Structural Characteristics of the Fastening of Disks on the Critical Velocities of Rotors" (Vliianic konstruktivnykh osobrunostei krepleniia diskov na kriticheskic skorosti rotorov), Izd-vo Mashinostroyeniye, Moscow, 1966, pp. 117–131. In Russian.

Craifaleanu, D., "Lateral Vibrations of Whirling Bars Subjected to an Axial Force and to a Torque," *Rev. Roumaine Sci. Tech., Ser. Mec. Appl.* 111, 521–537 (1966).

Golumb, M., and Rosenberg, R. M., "Critical Speeds of Uniform Shafts Under Axial Torque," *Proc. Fourth U.S. National Congress Appl. Mech.*, New York, 1961.

Goloskokov, Ye. G., and Filippov, A. P., "Non-stationary Bending-Twisting Oscillations of a Motor-Rotor System," *Izv. AN SSSR Mehk. Mashinostr.* 2, 153–157 (1964).

Green, R. B., "Gyroscopic Effects of the Critical Speeds of Flexible Rotors," *Trans. ASME* 70, 369–376 (1948).

Huang, T. C., and Huang, C. C., "An Analysis of Precession and Critical Speeds of Rotor Systems," ASME Paper 69-Vibr-54, 1969.

Asymmetrical and Flexible Supports

Billet, R. A., "Effects of Symmetrical Nonlinear Flexibility on Shaft Whirl," *J. Mech. Eng. Sci.* 8, 234–240 (1966).

Cavicchi, R. H., "Critical-Speed Analysis of Rigid Rotors on Flexible Foundations," NASA TN D-4858, Oct. 1968.

Cavicchi, R. H., "Comparison of Flexible and Firm-Foundation Rotor Critical-Speed Analyses," ASME Paper 69-Vibr-49, 1969.

Foote, W. R., Poritsky, H., and Slade, J. J., Jr., "Critical Speeds of a Rotor with Unequal Shaft Flexibility, Mounted in Bearings of Unequal Flexibility—I," *Trans. ASME, J. Appl. Mech.*, A77–A84 (June 1943).

Gunter, E. J., "Influence of Flexibly Mounted Rolling Element Bearings on Rotor Response, Part I—Linear Analysis," *Trans. ASME, Ser. F, J. Lubr. Technol.* 92, 59–75 (Jan. 1970).

Kramer, E., "Kritische Drehzahlen von anisotrop gelagerten Wellen," Darmstadt, Federal Republic of Germany, Auszug im Sonderdruck ans. BBC-Nachrichten, Part 3, 1956. In German.

Linn, F. C., and Prohl, M. A., "The Effect of Flexibility of Support Upon the Critical Speeds of High-Speed Rotors," *Trans. Soc. Nav. Arch. Mar. Eng.* 59, 536–553 (Nov. 1951).

Lisitsyn, I. S., "On Transversal Vibrations of Revolving Rotors with Bearings of Different Elasticity and Mass," *Vestn. Mashinostr.* 8, 23–30 (1961). In Russian.

Lund, J. W., "Stability and Damped Critical Speeds of a Flexible Rotor in Fluid-Film Bearings," ASME Vibrations Conference, Cincinnati, Ohio, 1973, ASME Paper 73-DET-103. Also *ASME Trans.*, Ser. B, *J. Eng. Ind.*, 96, No. 2, 509-517 (1974).

Olimpiyev, V. I., "The Natural Frequencies of a Rotor Running in Journal Bearings," *Izv. AN SSSR, Otd. Tekh. Nauk* 3 (1960). In Russian.

Stodola, V. A., "Kritische Wellenstorung infolge der Nachgiebigkeit des Oelpolsters im Lager," *Schweiz. Bausg.* 85(21), 265 (1925).

Tondl, A., "Some Problems Concerning the Vibration and Stability of Elastically Mounted Rotors," *Rozpr. Cesk. Akad. Ved.* 65, Ser. TV, No. 5 (1955).

Tondl, A., "A Contribution to the Dynamics of Steel Foundations for Turbo-machinery," *Strojirenstvi* 12 (1960).

Tondl, A., "Some Results of Experimental Investigations into the Motion of a Rotor Supported in an Elastically Mounted Frame," *Strojnicky Casopis* 1 (1962).

Effect of Ball Bearings, Gears, and Construction

Gleyzer, S. I., "Critical Speeds of Shafts Fitted with Elliptical Gears," *Trudy Leningrads. Tekhnol. Inst. Tsellyulozno-Bumazhnoy Promyshlennosti,* 14 (1964). In Russian.

Kal'mens, V. Ya., "Effect of Web and Hub Placement on the Bending and Critical Speed of a Turbine Rotor," *Energomashinostroyenie* 4, 28—30 (1964). In Russian.

Yamamoto, T., "On Critical Speeds Induced by Ball Bearings at Lower Rotating Speeds," *Bull. JSME* 1 (1957). In Japanese.

TRANSIENT WHIRLING AND ACCELERATED MOTION

Baker, J. G., "Mathematical-Machine Determination of the Vibration of Accelerated Unbalanced Rotor," *Trans. ASME,* Ser. E, *J. Appl. Mech.* 61, A-145—A-150 (1939).

Bodger, W. K., "Deceleration of an Unbalanced Rotor Through a Critical Speed," First Vibrations Conference, ASME, Boston, Mass., May 1, 1967.

Gluse, M. R., "Acceleration of an Unbalanced Rotor Through Its Critical Speeds," *Naval Eng. J.* 791, 135—144 (1967).

Grobov, V. A., "Transverse Vibrations of a Shaft During Transition Through Critical Speed" (Poperechnye kolebaniya vala pri perekhode cherez kriticheskoe chislo oborotov), *T. Rizhskogo Kransnoznam Vysshego Inzhen. Aviats. Uchilishcha,* (Transactions of the Riga Red Flag Higher Engineering and Aviation College) 5 (1956). In Russian.

Howitt, F., "Accelerating a Rotor Through a Critical Speed," *Engineer,* 669—692 (Oct. 27, 1961).

Kapitza, P. L., "Stiffness and Transition Through a Critical Speed of a Rapidly Rotating Rotor, in the Presence of Friction," *J. Tech. Phys.* 9, 125—147 (1939).

Kimball, A. L., and Hull, E. H., "Vibration Phenomena of a Loaded Unbalanced Shaft While Passing Through Critical Speed," *Trans. ASME* 47, 673 (1926).

Lewis, F., "Vibrations During Acceleration Through a Critical Speed," *Trans. ASME* 54, No. 3 (1932).

Macchia, D., "Acceleration of an Unbalanced Rotor Through the Critical Speed," ASME Paper 63-WA-9, 1963.

Marples, V., "Transition of a Rotating Shaft Through a Critical Speed," Inst. Mech. Eng. Convent'on, Churchill College, Cambridge, England, Apr. 4–6, 1966.

McCann, G. D., Jr., and Bennett, R. R., "Vibration of Multifrequency Systems During Acceleration Through Critical Speeds," *Trans. ASME*, Ser. E, *J. Appl. Mech.* 16, 375–382 (1949).

Robertson, D., "Transient Whirling of a Rotor," *Phil. Mag.* 20, 793 (1935).

Shcheglyaev, A. V., and Kostyuk, A. G., "Effect of Sudden Loss of Balance on the Rotor of a Turbine Set," *Therm. Eng.* 16, No. 8, 7–13 (1969).

STABILITY

General

Badgley, R. H., and Booker, J. F., "Turbo Instability: Effect of Initial Transients on Plane Motion," *Trans. ASME*, Ser. F, *J. Lub. Technol.* 91, 625–633 (1969).

Baker, J. G., "Self-Induced Vibrations," *Trans. ASME* 55, 5–13 (1933).

Bautin, N. N., *The Behavior of Dynamic Systems in the Vicinity of the Boundaries of the Range of Stability*, Moscow, Tekhteoretizdat, 1949. In Russian.

Bogusz, W., "The Stability of Motion of Bars Rotating with Variable Angular Velocity," *Rozprawy Inzh.* 6, No. 4, 549–555 (1958). In Polish.

Broniarek, C., "On the Stability of Spring Pendulum Vibration with the Movable Suspension Point," *Nonlinear Vibration Problems*, Warsaw, Poland, 1969. In Polish.

Brooks, G. W., "The Mechanical Instability and Forced Response of Rotors on Multiple Degree of Freedom Supports," Ph.D. dissertation, Princeton University, Oct. 1961.

Childs, D. W., "A Simulation Model for Flexible Rotating Equipment," *Trans. ASME*, Ser. B, *J. Eng. Ind.* 94, 210–219 (1972).

Ehrich, F. F., "Dynamic Stability of Rotor/Stator Radial Rubs in Rotating Machinery," *ASME Trans.*, Ser. B, *J. Eng. Ind.* 91, 1025–1028 (1969).

Ehrich, F. F., *Identification and Avoidance of Instabilities and Self-Excited Vibrations in Rotating Machinery,* General Electric Co., Aircraft Engine Group, Lynn, Mass., Nov. 1971, pp. 1–28.

Guntor, E. J., and De Choudhury, P., *Rigid Rotor Dynamics,* Part V, "Stability and General Transient Analysis," NASA CR-1391, University of Virginia for NASA Lewis Research Center, Aug. 1969.

Kapitza, P. L., "Influence of Friction Forces on the Stability of High-Speed Rotors," *J. Phys.* (Inst. Phys. Probl., Moscow), 1, 29 (1939).

Lund, J. W., *Rotor-Bearing Dynamics Design Technology* Part V: "Computer Program Manual for Rotor Response and Stability," Tech. Report AFAPL-TR-65-45, Air Force Aero Propulsion Laboratory, Wright-Patterson AFB, Ohio, May 1965.

Poritsky, H., "Rotor Stability," 5th U.S. National Congress of Applied Mechanics, University of Minnesota, Minneapolis, June 14–17, 1966.

Scheffel, R., Steenbeck, J., and Zippe, G., *Device for Stabilization of the Rotor Movements of High-speed Centrifuges,* English translation from the German, Union Carbide Corp., Nuclear Div., Oak Ridge, Tenn., Sept. 1962; Patent Appl. No. 1,136,644, Oct. 22, 1958.

Tondl, A., "The Stability of Motion of a Rotor with Unsymmetrical Shaft on an Elastically Supported Mass Foundation," *Ing.-Arch.* 29, 410–418 (1960).

Tondl, A., *Some Problems of Rotor Dynamics,* Czechoslovak Academy of Sciences, Prague, 1965 (Chapman and Hall, Ltd., London).

Yamamoto, T., Ota, H., and Kono, K., "On the Unstable Vibrations of a Shaft with Unsymmetrical Stiffness Carrying an Unsymmetrical Rotor," Paper 68-APM-N; *Trans. ASME,* Ser. E, *J. Appl. Mech.* 35(2), 313–321 (1968).

Dry Friction Whirl

Billet, R. A., "Shaft Whirl Induced by Dry Friction," *Engineer* 220, 713–714 (Oct. 1965).

Ehrich, F. F., "Dynamic Stability of Rotor/Stator Radial Rubs in Rotating Machinery," *ASME Trans.,* Ser. B, *J. Eng. Ind.* 91, 1025–1028 (1969).

Hysteresis Whirl

Chayevski, M. I., "The Combined Effect of Eccentricity and Internal Friction on the Stability of Motion of Elastic Shafts" (Sovmestnoe vliianie ekstsentritsiteta i sil vnutrennego treniya na ustoichivost dvizheniya gibkogo vala), *Vopr. mashinoved.* 5, Izd-vo AN SSSR (1957).

Ehrich, F. F., "Shaft Whirl Induced by Rotor Internal Damping," ASME Paper 64-APM-7, 1963.

Gunter, E. J., Jr., "The Dynamic Stability of the Single Mass Rotor," Ph.D. dissertation, University of Pennsylvania, Philadelphia, June 1965.

Gunter, E. J., Jr., "The Influence of Internal Friction on the Stability of High-Speed Rotors," *J. Trans. ASME*, Ser. B, *J. Eng. Ind.* 89, 683-688 (1967).

Gunter, E. J., Jr., and Trumpler, P. R., "The Influence of Internal Friction on the Stability of High-Speed Rotors with Anisotropic Supports," *Trans. ASME*, Ser. B, *J. Eng. Ind.* 91, 1105-1113 (1969).

Kushul', M. Ya., "Transverse Vibrations of Rotating Shafts under the Effect of Internal and External Friction," *Izv. AN SSSR, Otd. Tekh. Nauk* 10 (1954).

Robertson, D., "Hysteretic Influences on the Whirling of Rotors," *Mech. Eng.* 57, 716-717 (1935).

Self-Excited Whirl

Alford, J. S., "Protecting Turbomachinery from Self-Excited Rotor Whirl," *Trans. ASME*, Ser. A, *J. Eng. Power* 87, 333-334 (1965).

Glienicke, J., "Schwingungs- und Stabilitätsuntersuchungen an gleitgelagerten Rotoren," *Motortech. Z.* 33 (4), 135-139 (1972).

Landzberg, A. H., "Stability of a Turbine-Generator Rotor Including the Effects of Certain Types of Steam and Bearing Excitations," *Trans. ASME*, Ser. E, *J. Appl. Mech.* 27, 410-416 (1960).

Olimpiyev, V. I., "The Problem of Self-Excited Vibrations in Elastic Turbomachinery Rotors," *Elektromashinostroenie* 10 (1959).

Rotor Whirl

Ehrich, F. F., "Shaft Whirl Induced by Rotor Internal Damping," ASME Paper 64-APM-7, 1964.

Grobov, V. A., "Unstable Vibrations of a Turbine Shaft in the Critical Speed Region" (Nestatsionarnye kolebaniya vala turbiny v oblasti kriticheskikh chisel oborotov), *Izv. AN Latv. SSR* (Journal of the Latvian Academy of Sciences) 8 (1957).

Ota, H., "On the Unstable Vibrations of a Shaft System Carrying an Unsymmetrical Rotor," Summer Conference, Boulder, Colo., ASME Paper 64-APM-32, 1964.

Ota, H., et al., "Elimination of the Unstable Region of the Major Critical Speed in a Rotating Shaft Carrying an Unsymmetrical Rotor," *Bull. JSME* 12, 470-481 (June 1969).

Someya, T., "Stabilität einer in zylindrischen Gleitlagern laufenden, unwuchtfreien Welle," *Ing. Arch.* 33, No. 2, 85 (1963). In German.

Someya, T., "Stability and Vibrational Behavior of an Unbalanced Shaft Running in Cylindrical Journal Bearings," *VDI-Forschungsh.* 510 (1965).

Bearing Whirl

Arwas, B., Sternlicht, B., and Poritsky, H., "Dynamic Stability Aspects of Cylindrical Journal Bearings Using Compressible and Incompressible Fluids," *Proc. First Intl. Symp. Gas-Lubricated Bearings, Washington, D.C., 1959.*

Badgley, R. H., "Turborotor Instability: Dynamic Unbalance, Gryoscopic and Variable Speed Effects with Finite-Length Cavitated, Fluid-Film Bearings," Ph.D. dissertation, Cornell University, Ithaca, N.Y., 1967.

Hagg, A. C., "The Influence of Oil-Film Journal Bearings on the Stability of Rotating Machines," *Trans. ASME, J. Appl. Mech.,* **68**, 221–222 (1946); see also Discussion, *J. Appl. Mech.* **69**, 77–78 (1947).

Jennings, U. D., "An Investigation of Oil Bearing Whirl by Electronic Analog Computer," Ph.D. thesis, Cornell University, Ithaca, N.Y., 1960.

Kushul', M. Ya., "Transverse Vibrations of Rotating Shafts Under the Effect of Internal and External Friction," *Izv. AN SSSR, Otd. Tekh. Nauk* **10** (1954).

Newkirk, B. L., "Shaft Whipping," *General Electric Rev.* **27**, 169–178 (1924).

Sternlicht, B., and Winn, L. W., "On the Load Capacity and Stability of Rotors in Self-acting Gas-Lubricated Plain Cylindrical Journal Bearings," American Society of Mechanical Engineers and American Society of Lubricating Engineers, Lubrication Conference, Pittsburgh, Pa., Oct. 16–18, 1962, Paper 62-LUB-8.

Fluid-Film Whirl

Bowman, R. M., Collingwood, L. C., and Midgley, J. W., "Some Factors Affecting the Whirl Instability of a Journal Bearing, Part I," Paper No. 2, Lubrication and Wear Group Convention, 1963.

Bowman, R. M., Collingwood, L. D., and Midgley, L. W., "Some Factors Affecting the Whirl Instability of Journal Bearing, Part 2," Paper No. 5, Lubrication and Wear Group Second Convention, Eastbourne, May 1974.

Cameron, A., "Oil Whirl in Bearings—Theoretical Deduction of a Further Criterion," *Engineering* **179**, 237–239 (1955).

Cameron, A., and Solomon, P. J. B., "Vibrations in Journal Bearings: Preliminary Observations," *Proc. Conf. Lubrication and Wear, 1957,* Institution of Mechanical Engineers, London, Paper 103, p. 191.

Gunter, E. J., Jr., "The Dynamic Stability of the Single Mass Rotor," Ph.D. dissertation, University of Pennsylvania, Philadelphia, June 1965.

Gunter, E. J., Jr., Dynamic Stability of Rotor-Bearing Systems, SP-113, National Aeronautics and Space Adminstration, Washington, D.C., 1966.

Iida, S., "Eccentric Rotation of Circular Cylinder in Fluid," Bull. JSME 2, 1–9 (Feb. 1959).

Lund, J. W., "Stability and Damped Critical Speeds of a Flexible Rotor in Fluid Film Bearings," ASME Vibrations Conference, Cincinnati, Ohio, 1973.

Robertson, D., "Whirling of a Journal in a Sleeve Bearing," Phil. Mag. 15 (1933).

Sternlicht, B., Poritsky, H., and Arwas, E., "Dynamic Stability Aspects of Cylindrical Journal Bearings Using Compressible and Incompressible Fluids," General Electric Company Eng. Report for contract Nonr 2844(00); Proc. First Intl. Symp. Gas-Lubricated Bearings, Washington, D.C., 1959.

UNBALANCE RESPONSE

Calculation Methods

Baker, J. G., "Methods of Rotor-Unbalance Determination," Trans. ASME 61, A1–A6 (1939).

Booker, J. F., and Ruhl, R. L., "A Finite Element Model for Distributed Parameter Turborotor Systems," Trans. ASME, Ser. B., J. Eng. Ind. 94, 126–132 (1972).

Guenther, T. G., and Lovejoy, D. C., "Analysis for Calculating Lateral Vibration Characterisitics of Rotating Systems with Any Number of Flexible Supports, Part 2–Application of the Method of Analysis," Trans. ASME, Ser. E, J. Appl. Mech. 28, 591 (1961).

Koenig, E. C., "Analysis for Calculating Lateral Vibration Characteristics of Rotating Systems with Any Number of Flexible Supports. Part 1–The Method of Analysis," Trans. ASME, Ser. E, J. Appl. Mech. 28, 585–590 (1961).

Koenig, E. C., "A Rotating Systems Analyzer for Balancing and Simulating Rotating Systems," Ph.D. dissertation, University of Wisconsin, 1956.

Lund, J. W., IBM 704 Computer Program: Unbalance Response and Critical Speeds of a Rotor with Flexible Bearing Supports, MTI-62TR3, Mechanical Technology Inc., Feb. 26, 1962.

Lund, J. W., Rotor-Bearing Dynamics Design Technology, Part V, "Computer Program Manual for Rotor Response and Stability," Tech.

Report AFAPL-TR-65-45, Air Force Aero Propulsion Laboratory, Wright-Patterson AFB, Ohio, May 1965.

Lund, J. W., "Modal Response of a Flexible Rotor in Fluid-Film Bearings," ASME Paper 73-DET-98, 1973; *Trans. ASME*, Ser. B., *J. Eng. Ind.* 96(2), 525–533 (1974).

Thomas, C. B., Jr., and Rieger, N. F., in "Dynamic Stiffness Matrix Approach for Rotor Bearing System Analysis," *Proc. Inst. Mech. Eng. Conf. on Vibrations in Rotating Machinery*, Churchill College, Cambridge University, Sept. 1976.

Thomas, C. B., Jr., "A Unified Matrix Formulation for the Unbalance Response of a Flexible Rotor in Fluid-Film Bearings," M.S. thesis, Rochester Institute of Technology, Rochester, N.Y., Aug. 1974.

Whirl Modes

Orbits, by the Engineering Staff of The Bently Nevada Corp., Minden, Nev., 1970.

Downham, E., "Theory of Shaft Whirling," *Engineering* 204, No. 5307, 518–522, (Oct. 11, 1957); No. 5308, 552–555 (Oct. 18, 1957); No. 5309, 588–591 (Oct. 25, 1957); No. 5310, 524–628 (Nov. 1, 1957); No. 5311, 660–665 (Nov. 8, 1957).

Powell, J. W., "Unbalance Whirl of Rotors Supported in Gas Journal Bearings," *Engineer* 216, 145–146 (July 26, 1963).

Shawki, G. S. A., "Whirling of a Journal Bearing—Experiments Under No-Load Conditions," *Engineering* 179, No 4648, 243–246 (Feb. 25, 1955).

Shen, F. A., *Sources of Rotor Dynamic Excitation*, literature survey, ASME Monograph, draft, 1972.

Smith, D. M., "The Motion of a Rotor Carried by a Flexible Shaft in Flexible Bearings," *Proc. Royal Soc. (London)*, Ser. A, 142, 92 (1933).

Rigid-Rotor Systems

Pan, C. H. T., and Sternlicht, B., "On the Translatory Whirl Motion of a Vertical Rotor in Plain Cylindrical Gas-Dynamic Journal Bearings," ASME Paper 61-LUB-4; *Trans. ASME*, Ser. D, *J. Basic Eng.* 84(1), 152–158 (1962).

Powell, J. W., "Unbalance Whirl of Rotors Supported in Gas Journal Bearings," *Engineer* 216, 145–146 (July 26, 1963).

Sternlicht, B., and Elwell, R. C., "Synchronous Whirl in Plain Journal Bearings," ASME Paper 62-LUBS-19, 1962.

Flexible-Rotor Systems

Arwas, E. B., and Orcutt, F. K., *An Investigation of Rotor Bearing Dynamics with Flexible Rotors and Turbulent Flow Journal Bearings, Part I,* Mechanical Technology Inc., Tech. Rept. 65TR12, prepared for U.S. Atomic Energy Commission, Contract AT(30-1)-3363, Mar. 1965.

Baier, R. J., and Mack, J., *Design and Test Evaluation of a Super-Critical-Speed Shaft,* USAAVLABS Tech. Report 66-49/R458, Boeing Co., Vertol Division, Morton, Pa., June 1966.

Cole, E. B., "Whirling of Light Shaft Carrying Two Eccentrically Loaded Disks," *Engineer* 197, 382–383 (1954).

Craifaleanu, D., "Lateral Vibrations of Whirling Bars Subjected to an Axial Force and to a Torque," *Rev. Roumaine Sci. Tech., Ser. Mec. Appl.* 11, 521–537 (1966).

Dawson, D. E., *Dynamics of Flexible Rotors,* Final Rept. N-86805, IIT Research Institute, Chicago, Ill., 1963.

Dimentberg, F. M., and Gusarov, A. A., "Bending Forces in Flexible Shafts Due to Unbalance Forces," *Coll. Problems of Strength of Materials and Structures,* Izd-vo AN SSSR, Moscow, 1959.

Downham, E., "Some Preliminary Model Experiments on the Whirling of Shafts," ARC Technical Report, R&M No. 2768, Aeronautical Research Council, National Physical Laboratory, Teddington, Middlesex, 1953.

Dubensky, R. G., Meacham, H. C., and Voorhees, J. E., *Design Criteria for High-Speed Power-Transmission Shafts, Phase II,* Second Quarterly Report, prepared for Wright-Patterson AFB, Contract No. AF 33(657)-10330, Aug. 1963.

Guenther, T. G., and Lovejoy, D. C., "Analysis for Calculating Lateral Vibration Characteristics of Rotating Systems with Any Number of Flexible Supports, Part 2—Application of the Method of Analysis," *Trans. ASME,* Ser. E, *J. Appl. Mech.* 28, 591 (1961).

Jeffcott, H. H., "The Lateral Vibration of Loaded Shafts in the Neighborhood of a Whirling Speed—The Effect of Want of Balance," *Phil. Mag.* 37, 304–314 (1919).

Koenig, E. C., "Analysis for Calculating Lateral Vibration Characteristics of Rotating Systems with Any Number of Flexible Supports. Part 1—The Method of Analysis," *Trans. ASME,* Ser. E, *J. Appl. Mech.* 28, 585–590 (1961).

Lund, J. W., and Orcutt, F. K., "Calculations and Experiments on the Unbalance Response of a Flexible Rotor," *Trans. ASME,* Ser. B, *J. Eng. Ind.* 89, 785–796 (1967).

Morton, P. G., "On the Dynamics of Large Turbo-Generator Rotors," *Proc. Inst. Mech. Eng. (London)* 180, Part 1, 295 (1965–66).

Morton, P. G., *Some Research on Rotor Vibrations in Large Turbosets*, English Electric Co. Ltd., Stafford, England.

Rieger, N. F., "Unbalance Response of an Elastic Rotor in Damped Flexible Bearings at Supercritical Speeds," ASME Paper 70-WA/Pwr-3, 1971; *Trans. ASME*, Ser. A, *J. Eng. Power* 93(2), 265–278 (1971).

Rieger, N. F., "Unbalance Response and Balancing of Flexible Rotors in Bearings," *Flexible Rotor-Bearing System Dynamics*, ASME Monograph, 1973.

Rieger, N. F., *Rotor-Bearing Dynamics, State-of-the-Art, 1976*, Report 76 WRL M4, Department of Mechanical Engineering, Rochester Institute of Technology, Rochester, N.Y., 1976.

Robertson, D., "The Whirling of Shafts," *Engineer* 158, 216–217, 228–331 (1934).

Segraves, W. A., "Dynamics of an Unbalanced Unsymmetrical Single Mass Rotor," Master's thesis, University of Pennsylvania, 1961.

Sternlicht, B., "Stability and Dynamics of Rotors Supported on Fluid Film Bearings," ASME Paper 62-WA-190; *Trans. ASME*, Ser. A, *J. Eng. Power* 85, 331 (1965).

Sternlicht, B., "Rotor Bearing Dynamics of High-Speed Turbomachinery," Society of Automotive Engineers, Automotive Engineering Congress, Jan. 9–13, 1967, Detroit, Mich., Paper 670059.

Damped Flexible Rotors

Artemov, Ye. A., "Oscillations of an Unbalanced Rotor with Hydraulic Dampers on Elastic Supports" (Kolebaniya neuravno-veshennogo rotor s gidravlicheskimi dempferami na uprugikh opurakh), *Izv. VUZ Aviats. Tekh.* 9, 100–107 (1966). In Russian.

Johnson, D. C., "Forced Vibration of a Rotating Elastic Body—A Study Applicable to Bodies Rotating About a Fixed Axis and Including the Effects of Damping," *Aircraft Eng.* 24, No. 283, 271–273 (Sept. 1952); see also *Aircraft Eng.* 24, No. 282, 234–236 (Aug. 1952).

Lund, J. W., and Sternlicht, B., "Rotor-Bearing Dynamics with Emphasis on Attenuation," ASME Paper 61-WA-68, 1961; *Trans. ASME*, Ser. D, *Basic Eng.* 84 (1962).

Morrison, D., "Influence of Plain Journal Bearings on the Whirling Action of an Elastic Rotor," *Proc. Inst. Mech. Eng.* 176, No. 22 (1962).

Effect of Supports

Chasman, M. R., and Dayton, R. D., "Experimental Rotor Unbalance Response Using Hydrostatic Gas Lubrication," ASME Paper 72-LUB-31, 1972.

Crook, A. W., and Grantham, F., "An Approach to the Prediction of the Vibrations of Turbine Generators on Undertuned Foundations," ASME Paper 67-Vibr-46, 1967.

Gladwell, G. M. L., and Bishop, R. E. D., "The Vibration of Rotating Shafts Supported in Flexible Bearings," *J. Mech. Eng. Sci.* 1, No. 3, 195–206 (1959).

Hagg, A. C., "Some Vibration Aspects of Lubrication," in *Lubric. Eng.* (Aug. 1948).

Kirk, R. G., and Gunter, E. J., "The Effect of Support Flexibility and Damping on the Dynamic Response of a Single-Mass Flexible Rotor," *Trans. ASME,* Ser. B, *J. Eng. Ind.* 94, 221–232 (1972). ASME Paper 71-Vibr-72.

Levitan, S. I., "Determination of the Amplitude-Frequency Characteristics of the Rotor in a High Speed Gas Turbine Engine, Taking the Effect of the Sleeve Bearing Oil Film Into Account," *Tr. Tsentr. n-i. Avtomob. i Avtomotorn. In-ta,* 63, 15–27 (1964).

Morton, P. G., "Influence of Coupled Asymmetric Bearings on the Motion of a Massive Flexible Rotor," *Proc. Inst. Mech. Eng.* 182, No. 13, Part I (1967–1968).

Morton, P. G., "Analysis of Rotors Supported Upon Many Bearings," *J. Mech. Eng. Sci.* 14, 25–33 (1972).

Poznyak, E. L., "Vibrations of Rotors Running in Elastic Mass Bearings with Regard to the Dynamic Properties of the Oil Film in Journal Bearings" (Kolebaniya rotorov na uprogmassivnykh oporakh s uchetom dinamicheskikh svoistv maslonoi plenki v podshipnikakh skolzheniya), *Izv. AN SSSR, Otd. Tekh. Nauk, Mekh. Mashinostr.* 4 (1960).

Sternlicht, B., "Influence of Bearings on Rotor Behavior," *Proc. International Symp. Lubrication and Wear,* University of Houston, Texas, June 1963, 529–699, Berkeley McGutchan Publ. Corp., 1965.

Shaft Experiments

Bishop, R. E. D., and Mahalingam, S., "Some Experiments in the Vibration of a Rotating Shaft," *Proc. Royal Soc. (London),* Ser. A, 292, 561 (1966).

Downham, E., "The Experimental Approach to the Problems of Shaft Whirling," Aero. Res. Council, London, 1951.

Holmes, R., and Parkins, D. W., "Assessing Unbalance Effects in a Small Turbo-rotor," ASME Paper 69-DE-9, 1969.

Kal'mens, V. Ya., "Dynamic Modeling of Self-excitation of Rotor Vibrations in Heavy-duty Turbine Machines on the Oil Films of the Sliding Bearing," *Trudy TSKTL* (Tsentr. Nauch-issled. i Proyektno-konstruktorsl iy Kotloturbinnyy in-t im. I. I. Polzunova) 44, 120–132 (1964).

Residual Unbalance

Kellenberger, W., "Magnetic Pull in Turbine-Generator Rotors as the Cause of a Mechanical Unbalance," *Forschung. Elek.* **50**, No. 4, 253–265 (1966).

Bent Shaft

Bishop, R. E. D., "Unbalanced and Initially Bent Shafts," *Engineering* **190**, 735–736 (Nov. 25, 1960); 848–849 (Dec. 23, 1960); **191**, 312–313 (Mar. 3, 1961).

BEARINGS

General

Bisson, E. E., and Anderson, W. J., "Stability," in *Advanced Bearing Technology*, NASA SP-38, National Aeronautics and Space Administration, 1964, p. 130.

Boyd. J., and Raimondi, A. A., "An Analysis of the Pivoted-Pad Journal Bearing," *Mech. Eng.* **75**, 380 (1953).

Burgvits, A. G., and Lysov, A. M., "Operation of a Magnetohydrodynamic Bearing," *Trudy TSKTI* (Tsentr. Nauch. Issled. i Proyektno-konstruktorskiy Kotloturbinnyy in-t im. I. I. Poltzunova) **44**, 133–140 (1964).

Static Properties

Missana, A., "An Analysis of Performance Characteristics of Large Journal Bearings Operating With Turbulent Oil Films," M.S. thesis, Union College, Schenectady, N.Y.

Orcutt, F. K., *Steady-State and Dynamic Properties of Journal Bearings in Laminar and Superlaminar Flow Regimes*, Part I, "Tilting-Pad Bearings," NASA CR-732 Apr. 1967, prepared by Mechanical Technology Inc., Latham, N.Y.

Smith, D. J., *Journal Bearings in Turbomachinery*, Chapman and Hall, Ltd., London, 1969.

Dynamic Properties

Hagg, A. C., and Sankey, G. O., "Elastic and Damping Properties of Oil-Film Journal Bearings for Application to Unbalance Vibration Calculations," *Trans. ASME, Ser. E, J. Appl. Mech.* **25**(1), 141 (1958).

Hagg, A. C., and Sankey, G. O., "Some Dynamic Properties of Oil-Film Journal Bearings With Reference to the Unbalance Vibration of

Rotors," *Trans. ASME,* Ser. E, *J. Appl. Mech.* 23(2), 302–306 (1956); *Appl. Mech. Rev.* 9, 1665 (1956).

Holmes, R., "Oil Whirl Characteristics of a Rigid Rotor in 360° Journal Bearings," *Proc Inst. Mech. Eng.* (London) 177, No. 11 (1963).

Kramer, E., "Der Einfluss des Olfilms von Gleitlagern auf die Schwingungen von Maschinenwellen," *VDI-Ber.* 35 (1959).

Lund, J. W., "The Effect of the 150 Degree Partial Bearing on Rotor-Unbalance Vibration," in Discussion, ASME Paper 63-LUBS-6, P. C. Warner and R. J. Thoman, pp. 1–4, 1963.

Mitchell, J. R., Holmes, R., and Van Ballegooyen, H., "Experimental Determination of a Bearing Oil-Film Stiffness," *Proc. Inst. Mech. Eng.* (London) 180, No. 2, Part 3K (1965–66).

Morton, P. G., "Measurement of the Dynamic Characteristics of a Large Sleeve Bearing," ASME Paper 70-LUB-14, 1970.

Orcutt, F. K., *Steady-State and Dynamic Properties of Journal Bearings in Laminar and Superlaminar Flow Regimes, Part I,* "Tilting-Pad Bearings," NASA CR-732, Apr. 1967, prepared by Mechanical Technology Inc., Latham, N.Y.

Smith, D. M., "Dynamic Characteristics of Turbine Journal Bearings," in *Proc. Lubrication and Wear Conference,* Bournemouth, Inst. Mech. Eng., London, 1963.

Smith, D. M., *Journal Bearings in Turbomachinery,* Chapman and Hall, Ltd., London, 1969.

Sternlicht, B., "Elastic and Damping Properties of Cylindrical Journal Bearings," *Trans. ASME,* Ser. D, *J. Basic Eng.* 81, 101–108 (1959).

Thomas, C. B., Jr., *Comparison of Dynamic Bearing Coefficients for a Plain Cylindrical Fluid-Film Bearing,* 1974 WRL M3, Rochester Institute of Technology, Rochester, N.Y., May 1974.

Turbulent Flow

Arwas, E. B. and Orcutt, F. K., *An Investigation of Rotor Bearing Dynamics with Flexible Rotors and Turbulent Flow Journal Bearings, Part I,* Mechanical Technology Inc., Tech. Rept. 65TR12, prepared for U.S. Atomic Energy Commission, Mar. 1965.

Arwas, E. B., and Sternlicht, B., *Analysis of Finite Length Bearings Operating in Turbulent Regime,* Mechanical Technology, Inc., Tech. Rept. 63TR10, prepared for Atomics International, July 1963.

Gas Bearings

Fuller, D. D., Gunter, E. J., Jr., and Hinkle, J. G., *Design Guide for Gas-Lubricated Tilting-Pad Journal and Thrust Bearings with Special Reference to High-Speed Rotors,* Franklin Institute, Philadelphia, Pa., Nov. 1964.

Gross, W. A., "Investigation of Whirl in Externally Pressurized Air-Lubricated Journal Bearings," *Trans. ASME,* Ser. D, *J. Basic Eng.* **84,** 132–138 (1962).

Gunter, E. J., Castelli, V., and Fuller, D. D., "Theoretical and Experimental Investigation of Gas-Lubricated Pivoted-Pad Journal Bearings," *Trans. ASLE* **6,** 346–357 (1963).

Gunter, E. J., and Fuller, D. D., "Recent Progress on the Development of Gas-Lubricated Bearings for High-Speed Rotating Machinery," *Proc. USAF Aerospace Fluids and Lubr. Conf.,* Apr. 1963, pp. 487–507.

Bearing Whirl

Boeker, G. F., and Sternlicht, B., "Investigation of Translatory Fluid Whirl in Vertical Machines," *ASME Trans.* **78(1)** Sect. 1 13–20 (Jan. 1956).

Downham, E., *The Influence of Plain Bearings on Shaft Whirling,* ARC Technical Report, R&M No. 3046, Aeronautical Research Council, National Physical Laboratory, Teddington, Middlesex, 1958.

PEDESTALS

Artemov, Ye. A., "Experimental and Mathematical Determination of the Pliancy of the Resilient Bearings of Turbo-Engines," *Izv. VUZ Aviats. Tekh.* **2,** 48–55 (1965).

Kramer, E., "Über den Einfluss des Fundamentes auf die Laufruhe von Turbogruppen," *Elektrizitätswirtschaft* **61,** No. 1 (1962).

VIBRATION FUNDAMENTALS

Biezeno, C. B., and Grammel, R., *Engineering Dynamics,* Vol. 3, Part 3, English translation, Blackie and Sons Publishers, London 1954.

Bishop, R. E. D., "The Analysis of Vibrating Systems Which Embody Beams in Flexure," *Proc. Inst. Mech. Eng.* **169,** 1031–1046 (1955).

Bishop, R. E. D., and Gladwell, G. M. L., "The Receptances of Uniform and Non-Uniform Rotating Shafts," *J. Mech. Eng. Sci.,* **1,** 78–91 (1959).

Bishop, R. E. D., and Johnson, D. C., *The Mechanics of Vibration,* Cambridge University Press, London, 1960.

Crossley, F. R. E., *Dynamics in Machines,* Ronald Press, New York, 1954.

Dalby, W. E., *Balancing of Engines,* Longmans, Greene & Co., New York, 1929.

Den Hartog, J. P., *Mechanical Vibrations,* 4th ed., McGraw-Hill, New York, 1956.

Jensen, J., Niordson, F., and Pedersen, P., *Author and KWIC Index on Rotor Dynamics*, Technical University of Denmark, Lyngby, 1974.

Loewy, R. G., and Piarulli, V. J., *Dynamics of Rotating Shafts*, Shock and Vibration Monograph No. 4, DOD Shock and Vibration Information Center; Naval Research Laboratory, Washington, D.C., 1969.

Meirovitch, L., *Analytical Methods in Vibrations*, Macmillan, New York, 1967.

Morris, J., *The Strength of Shafts in Vibration*, Crosby Lockwood, 1929.

Rieger, N. F., "Flexural Stiffness of a Rotor with Uniformly-Spaced Axial Slots," Mechanical Technology, Inc., Engineering Analysis Design Memorandum No. 6, Latham, N.Y., Dec. 1967.

Yamamoto, T., *Collected Works*, L. Wirt, ed., AiResearch Manufacturing Corp., Phoenix, Ariz., 1966.

APPLIED ASPECTS

Rotating Shafts

Aiba, S., *On the Vibration and Critical Speeds of an Asymmetrical Rotating Shaft*, Report of the Faculty of Engineering, Yamanashi University, Kofu City, Yamanashi, Japan, Dec. 1962.

Ariaratnam, S. T., "The Vibration of Unsymmetrical Rotating Shafts," ASME Winter Annual Meeting, Nov. 29–Dec. 4, 1964, Paper 64-WA/APM-4.

Bishop, R. E. D., "The Vibration of Rotating Shafts," *J. Mech. Eng. Sci.* 1, No. 1, 50–65 (June 1959).

Bishop, R. E. D., and Parkinson, A. G., "Vibration and Balancing of Flexible Shafts," *Appl. Mech. Rev.* 21, No. 5, 439–451 (1968).

Chree, C., "Whirling and Transverse Vibrations of Rotating Shafts," *Phil. Mag.* Ser. 6, 7, 504 (1904).

Dimentberg, F. M., *Flexural Vibrations of Rotating Shafts*, Butterworth and Co., Ltd., London, 1961. Translated from Russian by Production Engineering Research Association.

Dimentberg, F. M., "Transverse Vibrations of a Rod Carrying a Distributed Mass and Subject to Resistance" (O poperechnykh kolebaniyakh sterzhnya s raspredelennoi massoi pri nalichii soprotivleniya), *Prikl. Matem. Mekh. (Appl. Math. Mech.)* XIII, Leningrad, (1949).

Goodman, T. P., *Correction of Unbalance by Force-Canceling Bearing Pedestals*, Report 61GL110, General Electric Co., May 15, 1961.

Grobov, V. A., "Transverse Vibrations of a Shaft Rotating with Variable Angular Velocity" (O poperechnykh kolebaniyakh vraschchayushchegosya vala pri peremennoi uglovoi skorosti vrashcheniya), Izd-vo AN Latv. SSR, Symposium on Problems of Dynamics and Dynamic Stability, *Proc.* 1, 1953.

Grobov, V. A., "Transverse Vibrations at Variable Speed of a Rotor Carrying an Axially Distributed Mass" (Poperechnye kolebaniya rotora s raspredelennoi po dline massori pri skorosti vrashcheniya), *Izv. AN Latv. SSR* (Journal of the Latvian SSR Academy of Sciences) **5** (1955).

Holmes, R., "The Vibration of a Rigid Shaft on Short Sleeve Bearings," *J. Mech. Eng. Sci.* **2**, 337–441 (1960).

Howland, R. C. J., "Vibrations of Revolving Shafts," *Phil. Mag.* Ser. 7, **12**, 297–311 (1931).

Howland, R. C. J., "Whirling Speeds of Shafts Carrying Concentrated Masses," *Phil. Mag.* Ser. 6, **49**, 1131–1145 (1925).

Johnson, D. C., "Free Vibration of a Rotating Elastic Body—The General Theory and Some Examples of Practical Cases," *Aircr. Eng.* **24**, No. 282, 234–236 (Aug. 1952).

Kiuchi, A., "On Vibration Characterisitics of Elastically-Supported Mechanical System with Non-Uniform Shaft Having Masses on It," *Bull. JSME* **2**, 318–323 (May 1959).

Lewis, P., and Sternlicht, B., "Vibration Problems with High-Speed Turbomachinery," *Trans. ASME,* Ser. B, *J. Eng. Ind.* **90**, 174–186 (1968).

Marcelli, V., "Some Problems Related to the Vibration of Turbo-Alternators," in *Czechoslovak Heavy Industry, Part 1,* 1962, p. 32.

Marcelli, V., and Balda, M., "A Study on Vibrations of Large Turbines at Lenin Works in Plzen," Celostatna konferencie o problemoch dynamiky strojov. 2d, Smolenice, 1961; *Dynamika Strojov* (Dynamics of machines), sbornik prac z konferencie SAV, Bratislava, Vyd-vo SAV, 104–125 (1963).

Olimpiyev, V. I., "Investigation of the Influence of the Static Flexure on the Transverse Vibrations of Turbine-Type Rotors," *Ref. Zh., Mekh.* **9**, 160 (1958).

Petersen, S. R., "Vibration in Rotating Machinery," *Power Eng.* **64**, 70–72, 76 (July 1960).

Philbrick, D. C., Rashevsky, M., and Hawkshaw, P. J., "Vibrations in Rotating Systems," *Westinghouse Eng.* **19**, 178–181, diagrams (Nov. 1959).

Reeser, H. G., and Severud, L. K., *Analysis of the M-1 Liquid Hydrogen Turbopump Shaft Critical Whirling Speed and Bearing Loads,* Report NAS3-2555, Aerojet-General Corp., Sacramento, Calif., Dec. 1965.

Robertson, D., "The Vibrations of Revolving Shafts," *Phil. Mag.* Ser. 7, **13**, No. 82, 862 (1932).

Sergeyev, S. I., "Damping of Forced and Self-excited Oscillations," *Tr. Vses. N.-i. In-ta Kislo-rodn. Mashinostr.* **7**, 57–72 (1963).

Shimizu, H., and Tamura, H., "Vibration of Rotor Based on Ball Bearing," *Bull. JSME* **9**, 524–532 (1966).

Smith, D. M., "Vibrations in Turbomachinery," *Proc. Inst. Mech. Eng.* (London) **180**, Part 3 (1965–66).

Subharmonics

Bishop, R. E. D, and Parkinson, A. G., "Second Order Vibration of Flexible Shafts," *Phil. Trans. Royal Soc. (London)* Ser. A, **259**, 619–649 (1965).

Kellenberger, W., "Flexural Vibrations in Non-Circular Shaft Rotating About Horizontal Axis," *Brown Boveri Rev.* **46**, 182–193 (1959).

Kellenberger, W., "Forced, Double-Frequency, Flexural Vibrations in a Rotating, Horizontal, Cylindrical Shaft," *Brown Boveri Rev.* **42**, 79–85 (1955).

Effect of Bearings on Rotor

Burgvits, A. G., and Lysov, A. M., "On the Problem of Shaft Vibration in Journal Bearings" (K voprosu o kolebanii valov opirayushehik hsya na podshipniki skolzhashehego treniya), *Tr. Seminara po Teorii Mash. Mekh.* XIII, Ser. 50, 77 (1953).

Capriz, C., "On the Vibrations of Shafts Rotating on Lubricated Bearings," *Ann. Mat. Pura Appl.* IV, Ser. 50, 223 (1960).

Cameron, A., and Solomon, P. J. B., "Vibrations in Journal Bearings: Preliminary Observations," *Proc. Conf. Lubrication and Wear*, Institution of Mechanical Engineers, London, Paper 103, p. 191, 1957.

Glienicke, J., "Schwingungs- und Stabilitätsuntersuchungern an gleitgelagerten Rotoren," *Motortech. A.* **33**, 135–139 (Apr. 1972).

Newey, D. A., "Investigation of the Influence of the Static Flexure on the Transverse Vibrations of Turbine-type Rotors," *Ref. Zh. Mekh.* **9**, 150 (1958).

Ono, L. and Tamuri, A., "On the Vibrations of a Horizontal Shaft Supported in Oil-Lubricated Journal Bearings," *Bull. JSME* **11**, 813–824 (1968).

Tamura, A., "On the Vibrations Caused by Ball Diameter Differences," *Bull. JSME* **11**, No. 44 (1968).

Tamura, A., and Taniguchi, O., "On the Subharmonic Vibration of the Order One-half Caused by Passing Balls in a Ball Bearing," *Bull. JSME* **4**, 193–200 (1961).

Yamamoto, T., "Response Curves at the Critical Speeds of Sub-Harmonic and Summed and Differential Harmonic Oscillations," *Bull. JSME* **3**, No. 12 (1960).

Yamamoto, T., "On Subharmonic and Summed and Differential Harmonic Oscillations of Rotating Shaft," *Bull. JSME* **4**, No. 13, 51 (Feb. 1961).

Gyroscopic Effects

Bauer, V. O., "Forced Vibration of a System of Coaxial Rotors Taking Into Account the Gyroscopic Effect of Disks," in Prochnost' i dinamika aviatsionnykh dvigateley (Strength and Dynamics of Aircraft Engines); *Sbornik Statey* 2, 201–254, Moscow, Izd-vo Mashinostroyeniye (1965).

Dimentberg, F. M., "Transverse Vibrations of a Rotating Shaft Carrying Discs and Subject to Frictional Resistance" (Poperechnye kolebaniya vrashchayuschegosya vala s diskami pri nalichii soprotivleniya treniya), First Symposium on Transverse Vibrations and Critical Speeds, Izd-vo AN SSSR, 1952.

Passing Through Resonance

Filippov, A. P., "Forced Vibrations of a Linear System During Transition Through Resonance" (Vynuzhdennye kolebaniya lineinoi systemy pri perekhode cherez resonans), Symposium on Vibrations in Turbine Machinery, Institute of Machine Science of the USSR Academy of Sciences, Izd-vo AN SSSR, 1956.

VIBRATION SUPPRESSION

Bohm, R. T., "Designing Complex Turbo Rotor Systems with Controlled Vibration Characteristics," Soc. Automotive Eng., National Transportation, Powerplant, and Fuels and Lubricants Meeting, Baltimore, Md., Oct. 19--23, 1964, Paper 928B.

Mechanical Vibrations of Shipboard Equipment, MIL-STD-167-2 (Ships), Naval Ship Engineering Center, U.S. Navy, May 1974.

Dubensky, R. G., Mellor, C. C., Jr., and Voorhees, J. E., *Design Criteria for High-Speed Power-Transmission Shafts, Part 1*, "Analysis of Critical Speed Effects and Damper Support Location," Tech. Rept. ASD-TDR-62-728, Battelle Memorial Institute, Jan. 1963.

Goledzinowski, A., and Rabenda, M., "Constructional and Technological Conditions for Improving the Vibration Characteristic of Turbine Motors," *Techn. Lotnicza* 9, 225–234 (1964).

Katavev, F. P., "Reduction of Transverse Vibrations of Rotating Machine Shafts," *Tr. Soyuz.* (Gos. Vsewoyuz. Dor. Nauch. Issled. In-ta), 4 (1964).

Kel'zon, A. S. and Pryadilov, V. I., "Elimination of Dangerous Vibrations in High-Speed Vertical Rotors," AN SSSR, *Izv. Mekh.* 6, 42–48 (1965).

Lappa, J. J., Gusak, Ya. M., and Shoykhet, A. I., Vibrations of High-Speed Gas Turbine Installations," *Energomashinostroyeniye* 11, 28–32 (1965).

Snowdon, J. C., "Vibration of Resilient Isolators and Internally Damped Structures," in *Proc. Institute for Science and Engineering,* Vol. 2, Plenum Press, 1967, Ch. 13.

VIBRATION: DIAGNOSIS

Kennedy, C. C., and Pancu, D. D. P., "Use of Vectors in Vibration Measurements and Analysis," *J. Aero. Sci.* 14, 603 (1947).

SHAFTS

Ariaratnam, S. T., "The Vibration of Unsymmetrical Rotating Shafts," ASME Paper 64-WA/APM-4, 1964.

Armstrong, E. K., Christie, P. I., and Hunt, T. M., "Vibration in Cylindrical Shafts," Institution of Mechanical Engineers, Applied Mechanics Convention, Bristol, England, 1966.

Bert, C. W., "Deflections of Stepped Shafts," *Mach. Des.* 32, 128–133 (Nov. 1960).

Rieger, N. F., "Curves Aid in Determining Critical Speeds of Stepped Shafts Quickly and Easily," *Machine Design,* Sept. 10, 1964.

SUBJECT AND AUTHOR INDEX

Please note that the author entries appear in italics. The first number (in brackets) following the entry is the reference number. The subsequent numbers are the pages on which the references are cited.

605

610 SUBJECT AND AUTHOR INDEX